Author:
Han, Songlin

Title:
High temperature deformation modelling and finite element implementation for single crystal turbine blade materials.

HIGH TEMPERATURE DEFORMATION MODELLING AND FINITE ELEMENT IMPLEMENTATION FOR SINGLE CRYSTAL TURBINE BLADE MATERIALS

BY

Songlin Han

A thesis submitted to the University of Bristol
in accordance with the requirements of
the degree of Doctor of Philosophy
in the Department of Mechanical Engineering
in the Faculty of Engineering

March 2000

Advanced Engineering Materials and Structural Integrity Group
Department of Mechanical Engineering
University of Bristol
Bristol BS8 1TR

ABSTRACT

This thesis presents a theoretical and numerical investigation on the anisotropic viscoplastic deformation behaviour of single crystal nickel base superalloys under isothermal and thermomechanical loading. Two constitutive models, one phenomenological model and one crystallographic model, have been proposed and implemented into the finite element code ABAQUS using UMAT subroutines for structural analysis.

A consistent procedure to determine the material constants in the two models using the same experimental results is proposed. The procedure includes a number of local optimisation routines to determine several groups of material constants from experimental data associated with the deformation characteristics described by a given group of material constants. This allows a direct comparison to be made of the intrinsic characteristics of the phenomenological and crystallographic models.

The analytical procedures for transforming the differential anisotropic viscoplastic equations of the both models into numerical incremental equations suitable for finite element application have been developed. Also the techniques for implementing the equations in a UMAT subroutine for the ABAQUS finite element code have been developed. The closed form solutions achieved in the implementation procedure improve both the numerical calculation accuracy and FE analysis efficiency.

A comprehensive program has been carried out to verify the numerical implementation procedure, the UMAT subroutines and interfacing them with ABAQUS. The results obtained from the finite element analysis were found to be in good agreement with theoretical predictions. The UMAT and ABAQUS codes have been successfully used for structural stress analysis for different geometric shapes, including cylindrical bars, plates and tubes. The shapes were subjected to uniaxial tension, cyclic tension/compression, pure torsion and combined tension-torsion loading conditions.

There are two main significant findings, among the other findings, in this work. Firstly, a procedure has been developed and successfully used to determine the material constants in the anisotropic elasto-viscoplastic constitutive models. The procedure was consistent and common for both the phenomenological and the crystallographic models, and can provide necessary material data for direct comparison of the two models. Secondly, a novel method had been developed to achieve a closed form numerical implementation of the two models into FE codes. This provides the solid base for successful and efficient structural analysis of single crystal engineering components.

ACKNOWLEGEMENTS

I wish to express my sincere thanks to my supervisor, Prof. David J Smith, for his continuous guidance, advice and encouragement during the whole time of this research work.

The research project was funded by the Defence Evaluation and Research Agency (DERA), UK, and its financial support is gratefully acknowledged. I would like to thank Prof. George Harrison, Drs. Ashley Boyd-Lee and Tim Ward in DERA for their technical support of the project, and many perceptive comments and valuable suggestions for the research work.

I would also like to thank the members of the Advanced Engineering Materials and Structural Integrity Group, THEKOGS, for providing a warm and productive environment in which to work, and for their friendship, encouragement and good cheer.

Finally, I would like to thank my family, and to all my friend, old and new, for their continuous support and help in many different ways.

DECLARATION

The accompanying dissertation entitled "High Temperature Deformation Modelling and Finite Element Implementation for Single Crystal Turbine Blade Materials " is submitted in support of an application for the degree of Doctor of Philosophy in Engineering at the University of Bristol. The dissertation is based on independent work by the candidate - all contributions from others have been acknowledged fully in the text. This work has not been submitted for any other degree or diploma at this University or any other institution.

I declare that the above statements are true.

Songlin Han

March 2000

CONTENTS

LIST OF TABLES

LIST OF FIGURES

Chapter 2

Chapter 6

NOMENCLATURE

1. Operators

Operator	Meaning
X:	Scalar
X_i:	Components of vector $\vec{x}$
X_{ij}:	The matrix of second order tensor
$\dot{X}$:	Time derivative of X (=dX/dt)
X^t:	Transpose of X
X^{-1}:	Inverse of X
X':	Deviator of X
Sign(X):	+ or - sign of scalar X
<X>:	<X>=X if X>0, <X>=0 if X<0
δ_{ij}:	Kronecker delta, δ_{ij}=1 when i=j and δ_{ij}=0 when i≠j

2. Symbols

Symbol	Meaning
f^s:	The yielding function of slip system s (s=1,2,.....18)
τ^s:	The shear stress on slip plane s
x^s:	The back stress on slip plane s
$\dot{x}^s$:	The back stress rate on slip plane s
r^s:	The isotropic stress on slip plane s
$\dot{v}^s$:	Pseudo-multiplier
γ^s:	The plastic shear strain on slip plane s
$\dot{\gamma}^s$:	The plastic shear strain rate on slip plane s
σ_{ij}:	Stress matrix
σ_i:	Stress vector
σ_i':	The stress deviators
ε_{ij}^T:	Total strain tensor
ε_i^T:	Total strain vector
ε_{ij}^e:	Elastic strain tensor
ε_i^e:	Elastic strain vector
ε_{ij}^{in}:	Inelastic strain tensor
ε_i^{in}:	Inelastic strain vector
ε_{ij}^{th}:	Thermal strain tensor

ε_i^{th}	Thermal strain vector
m_{ij}^s:	Transformation matrix for slip system s, (i,j=1,2,3)
n_i^s:	The direction of slip plane s
l_i^s:	The slip direction of slip system s
A_{ij}:	Stress transformation matrix
$A^{-1}{}_{ij}$:	The inverse matrix of A_{ij}
B_{ij}:	Strain transformation matrix
$B^{-1}{}_{ij}$:	The inverse matrix of B_{ij}
C_{ij}:	Elastic stiff matrix
S_{ij}:	Elastic compliance matrix
X_{ij}:	Back stress matrix
X_i:	Back stress vector
X'_i:	The deviators of back stress vector X_i
R:	Isotropic stress
p:	Accumulated inelastic strain
α_i :	Thermal expansion vector

CHAPTER 1
INTRODUCTION

The design of advanced jet engines with improved efficiency and durability has placed increasing demands on materials that operate in the hot sections of gas turbine engines. Single crystal nickel base superalloys developed for gas turbine blade applications have superior thermal, fatigue and creep properties than conventional cast alloys. Though single crystal alloys are more expensive and difficult to produce and improvement is required to commercially achieve the superior properties, it is an important development for gas turbine material. The superior properties of single crystal alloys are attributed to the elimination of grain boundaries with only a single grain. However, the single grain material structure for single crystal alloys also leads to material anisotropy that produces orientation dependent material response. In order to fully utilise the advantages of single crystal alloys, new constitutive models have been developed to account for both the strong orientation dependent and the viscoplastic behaviour of single crystal alloys during high temperature operations. The material models should be available in a multiaxial form for use in conjunction with a finite element method, or a similar analysis, so that a component can be assessed for structural stability and integrity under the complex conditions representative of service.

There are two categories of constitutive models for anisotropic single crystal materials. One category is the phenomenological models that are developed from the continuum based approaches. The phenomenological models for single crystal alloys were based on modification of the isotropic constitutive models developed for polycrystalline materials. Another category is the crystallographic models that are developed from the physical based approaches. The crystallographic models for single crystal were based on the modification of the classical plasticity models of the crystalline slip theory. There have been a number of studies carried out to investigate the characteristics of a specific model, and to verify the model with various experimental data (Choi and Krempl [1989], Nouailhas [1990], Li [1993]), (Stouffer et al [1990], Meric et al [1991], Jordan and Walker [1992]). However there has been only very limited work that compares the different models, in particular with the

comparison of the general features of the phenomenological and crystallographic models to investigate the similarities and differences between the two categories of models.

Similar to all the modern constitutive models, both phenomenological and crystallographic include a larger number of material constants compared with the classical isotropic models. These material constants must be determined by some simple laboratory tests. It is well known that an appropriate procedure to determine the material constants is essential to successfully apply any modern constitutive model. There have been a number of studies on the development of procedures for determining material constants for isotropic constitutive models (James et al [1987], Agatonovic and Clorman [1987], Sherwood and Fay [1992], Schwertel et al [1992]). The procedure to determine the material constants for the constitutive models for single crystal materials are more complex compared with those for isotropic models. However, there has been no specific work that is dedicated to developing procedures for single crystal materials. Furthermore, in order to be able to compare phenomenological and crystallographic models, the material constants in both models must be determined using a consistent procedure using the same experimental data. If this is not done the approximations and errors introduced in the procedure for determining the material constants may override the characteristics of the models. Consequently, it will not be possible to explore the intrinsic features of different models.

Structural analysis of engineering components, such as turbine blades, under complex loading conditions is generally carried out using the displacement-based finite element method. The numerical differential formulation of this method comes from the principle of virtual work. Therefore, once a constitutive model has been developed, there are two steps required for its application for structural analysis. First, an identification process must be undertaken to obtain all the material parameters in the constitutive models; second, numerical implementation of the equations has to be performed (generally in finite element codes) in order to solve practical boundary value problems. For single crystal superalloys, both the

determination of the material constants and the numerical implementation of the anisotropic constitutive equations may be different from the approaches used for classical isotropic models. This is because account has to be taken on the significant anisotropic mechanical deformation characteristics.

The main objectives of this work are the development and comparison of the phenomenological and crystallographic models for single crystal materials, and numerical implementation of the models for finite element structural analysis. A literature review on single crystal nickel base superalloys is presented in Chapter 2. The review is carried out mainly on the material microstructural features, the anisotropic mechanical deformation characteristics induced by material anisotropy and the constitutive models to describe the anisotropic behaviour of single crystal alloys. The formulations of two constitutive models, one phenomenological and the other crystallographic model for both isothermal and thermomechanical applications, together with a consistent procedure to determine the material parameters in the models, are presented in Chapter 3. Numerical simulations are also carried out in Chapter 3 to compare the fundamental characteristics of the two different models. The numerical implementation procedures for the two models for FE analysis, and interfacing, through UMAT subroutines, with the ABAQUS finite element code are developed and verified in Chapter 5. The FE programs are used in Chapter 6 for structural stress analysis using different geometry specimens under various loading conditions. Finally, concluding remarks and recommendations for future work are presented in Chapter 7.

CHAPTER 2
LITERATURE REVIEW

2.1. Introduction

To utilise single crystal superalloys efficiently for structural components a full understanding of material behaviour under thermal mechanical loading is essential. Broad research investigations have been undertaken both experimentally and theoretically. This chapter provides a literature review of experimental investigations and developments in the modelling of nickel base single crystal superalloys used at high temperature. In section 2 a concise description on processing developments for single crystal superalloys is given. The microscopic structure and features of single crystal metallic alloys are described in section 3. Single crystal mechanical properties based on a wide range of experiments are presented in section 4. The review of aspects of isothermal anisotropic elastic viscoplastic deformation modelling is given in section 5, while the nonisothermal modelling is given in section 6. Finally a review on the implementation of material models into FE code for structural analysis is presented in section 7.

2.2 Development of Processing of Nickel Base Single Crystal Alloys

Nickel base single crystal superalloys have been developed over the last decades and are widely used for high temperature engine applications. Power generation and aerospace applications constitute the major field of use for nickel base superalloys, and applications include steam generator tubing, structural components of reactor cores, gas turbine parts such as blades, disks, rings shafts and various compressor and diffuser components. All these components are subjected high temperature, and therefore the material is required to have superior high temperature strength and resistance to oxidation and corrosion.

To improve the mechanical properties of an alloy various elements are added to perform one or more desirable functions. Nickel base superalloys are defined as those alloys that have nickel as the major constituent, with significant amounts of

chromium. The combination of nickel and chromium gives these alloys outstanding oxidation resistance. Nickel base superalloys are both solid solution and precipitation strengthened. Precipitation - strengthening nickel alloys contain aluminium, titanium or niobium to cause precipitation of a second phase during appropriate heat treatment. The precipitated phase, usually γ' or γ'' substantially increase the strength and hardness of the alloy (Pollock and Argon [1994]). Strengthening of the grain boundaries has been achieved by introducing titanium, tantalum, hafnium and niobium, which are used to form carbides, and these carbides play an effective role in the strengthening of the grain boundaries.

There are several disadvantages associated with the grain boundaries in a material for high temperature application. First, material strength is lowered because the grain boundaries are a source of weakness at high temperature particular those which lie perpendicular to the applied stress. Creep life and thermal fatigue life are both badly affected by these transverse boundaries. Micro damage along the grain boundaries is one of the main creep failure mechanisms. Second, alloying additions are required to strengthen grain boundaries and many of these additions lower the incipient melting temperature of the alloy. This limits the maximum allowable heat treatment temperature and prevents the realisation of the full strength potential of the alloy.

In order to eliminate the transverse boundaries, directionally solidified casting was introduced. In this way the grains can be made to grow in one preferred orientation (along the length of the blade) and have no transverse boundaries. The mechanical properties obtained from directionally solidified (DS) material show significant improvements in thermal fatigue resistance, creep life and ductility in the longitudinal direction, i.e. parallel to grain orientation. The Young's modulus along the major axis of DS material is reduced by 30%. The principal reasons for the improvement in creep and ductility properties lie in the absence of transverse grain boundaries and in the preferred crystallographic orientation of the grains (Kounitzky et al [1991]). However, the transverse properties tend to be unaffected.

Further development of directional solidification is the production of single crystal alloy which only has a single crystal grain, and therefore eliminates all the grain boundaries in the alloy. The absence of transverse grain boundaries in single crystal alloys further enhances creep properties compared with DS alloys, since damage along the grain boundaries is one of the main mechanisms of creep failure. Furthermore, since single crystal alloys contain no grain boundaries there is no need to add in the alloy elements that are traditionally used to strengthen these boundaries. When these elements (C, B, Zr, Hf) are excluded from nickel base alloys the melting point is raised appreciably. This allows high temperature heat treatments to be applied to single crystal alloys that cannot be used with conventionally cast (CC) or DS superalloys. The heat treatments optimise the microstructure of the alloy and allow the full strength potential to be achieved. The combination of these factors gives significant improvement for single crystal alloys in terms of creep and thermal fatigue properties compared with conventionally cast material (Kounitzky et al [1991]).

2.3 Material Anisotropy and Microstructure Features

2.3.1 Initial Material Structure

Nickel-base single crystals superalloys are produced by directional solidification and are both solid solution and precipitation strengthened. They have a face-centred cubic crystal structure, i.e. in a unit cubic cell, in addition to 8 atoms at 8 corners there is one atom in the centre of every cubic plane. Fig 2.1 shows a unit cell of the basic structure of a nickel base single crystal superalloy and the three principal cubic symmetry orientations [001]-[010]-[100]. The basic structure of single crystals consist of a γ matrix with a precipitated γ' phase. The γ matrix is a face centred cubic disordered phase and solid-solution strengthened by γ' precipitates phase which has an ordered face centred structure. γ' precipitates are coherent with the surrounding γ matrix. Therefore, there are two ways to describe a nickel base single crystal. At the micro-level, it can be described as a two-phase material, the overall material characteristics are determined by the material properties of the γ and γ' phases and their interface characteristics (Nouailhas [1995]). At the macro-level, it

can be described as a homogeneous material with a single material response reflecting the overall combined properties of γ and γ' phases and their interface. Since both γ and γ' phases have cubic symmetry, the initial structure of a single crystal nickel base superalloy exhibits an overall cubic symmetry response (Stouffer et al [1990], Li [1993]).

The γ' volume fraction has a strong influence on the material structure and characteristics of a single crystal superalloy (Pope and Ezz [1984]). The strength increases with increasing the volume fraction of the γ'. The new generation single crystal nickel base superalloys normally have a high γ' volume fraction of 55-70% (Li [1993]) with the single crystal SRR99 used in this study having a γ' volume fraction of 60%. Therefore, the elementary cell of the typical initial microstructure of a single crystal superalloy can be represented by a periodic pattern made from a cube (γ' phase) and surrounded with the matrix channels (γ phase). Also it was found that the microstuctural changes can be induced by internal stress due to the lattice misfit, (Nouailhas and Cailletaud [1995]).

2.3.2 Structure Change Induced by Internal Stress

One of the significant characteristics of structural change of single crystal alloys under high temperature deformation is the progressive coarsening of the cuboidal γ' precipitates into preferentially orientated plates or "rafts" structure. This phenomenon is caused by the internal stresses due to the lattice mismatch of γ matrix and γ' precipitates, and driven by external applied stress. Directional coarsening of γ' precipitates under the influence of an applied stress was first studied in detail by Tien and Copley [1971], and this phenomenon has been observed subsequently and investigated by many researchers (Nathal et al [1983,1985], Pollock and Argon [1994]). The morphological changes in the two phases of the microstructure of nickel base superalloys are of particular interest because it alters the creep resistance of the material in the stress and temperature range where these alloys are used (Pearson et al [1980], Nathal et al [1989]).

Two types of rafting behaviour in [001] oriented nickel-base single crystals have been identified by Fredholm et al [1984]. In type N, the elongated precipitates or "rafts" develop normal to the direction of an externally applied stress; in type P, elongated precipitates or "rafts" develop parallel to the direction of the externally applied stress. Under creep conditions, type N "rafts" occur under tensile stresses, whilst type P "rafts" develop under compressive stresses.

The development of the "rafted" structures in single crystal alloys under high temperature deformation changes the overall material microstructural characteristics, and consequently influences the material response. There have been also studies on the influence of rafting on creep deformation rupture behaviour of single crystal alloys (Schneider et al [1992], Pollock and Argon [1994]). However, only limited investigations have been conducted on the influence of the rafting structure on the fundamental material characteristics, such as material anisotropy, of single crystal superalloys. Some numerical simulation results show that the initial cubic symmetry, which is a basic material property of single crystal nickel base superalloys, may no longer exist when the rafting process takes place (Nouailhas [1995]).

2.4 Mechanical Deformation Characteristics

2.4.1. Anisotropic Elastic Behaviour

As discussed in section 2.3, the single crystal nickel base superalloy initially has a face centred cubic material microscopic structure (not considering microstructural change, e.g. rafting), which means that the material crystal lattices possess 3 axes of symmetry. Consequently, the anisotropic elastic deformation response of a single crystal alloy exhibits cubic symmetry characteristics. The elastic stress and strain relationship in the single crystal principal symmetry axes, i.e. [100]-[010]-[001], can be written as:

$$\begin{bmatrix}\varepsilon_{11}\\ \varepsilon_{22}\\ \varepsilon_{33}\\ \varepsilon_{23}\\ \varepsilon_{31}\\ \varepsilon_{12}\end{bmatrix}=\begin{bmatrix}\frac{1}{E} & \frac{-\nu}{E} & \frac{-\nu}{E} & 0 & 0 & 0\\ \frac{-\nu}{E} & \frac{1}{E} & \frac{-\nu}{E} & 0 & 0 & 0\\ \frac{-\nu}{E} & \frac{-\nu}{E} & \frac{1}{E} & 0 & 0 & 0\\ 0 & 0 & 0 & \frac{1}{2G} & 0 & 0\\ 0 & 0 & 0 & 0 & \frac{1}{2G} & 0\\ 0 & 0 & 0 & 0 & 0 & \frac{1}{2G}\end{bmatrix}\begin{bmatrix}\sigma_{11}\\ \sigma_{22}\\ \sigma_{33}\\ \sigma_{23}\\ \sigma_{31}\\ \sigma_{12}\end{bmatrix} \tag{2.1}$$

There are three independent material constants, Young's modulus E, Poisson's ratio ν, and shear modulus G in the [001] orientation. Using this stress-strain relationship, the orientation dependence in the elastic stress and strain can be modelled by transforming equation (2.1) into any given orientation (Li et al [1994]).

For uniaxial loading in a given crystal orientation [h, k, l], and using the transformation from the principal coordinate of the single crystal to the coordinates which coincide with [h, k, l], then the stress and strain relation in the loading direction can be expressed as:

$$\sigma_{11}=E_{[hkl]}\varepsilon_{11}=\left[S_{11}-2\left((S_{11}-S_{12})-\frac{S_{44}}{2}\right)\frac{h^2l^2+k^2l^2+h^2k^2}{(h^2+k^2+l^2)^2}\right]^{-1}\varepsilon_{11} \tag{2.2}$$

with

$$S_{11}=\frac{1}{E},\ S_{12}=\frac{\nu}{E},\ S_{44}=\frac{1}{G} \tag{2.3}$$

It can be seen that the elastic response will be different for specimens tested with different crystal orientations, since the longitudinal elastic modulus, $E_{[hkl]}$, is a function of the direction cosines [h, k, l].

Test results (Gabb et al [1986]) for the longitudinal elastic modulus of single crystal nickel base superalloy Rene N4 at 760°C and 980°C confirmed the orientation dependence behaviour. At 760°C, Young's modulus varies from 104 GPa in the most compliant [001] direction to 253 GPa in the stiffest [111] direction. At 980°C the trend is the same, but the elastic modulus decreases with increasing test temperature. A systematic study on the influence of crystal orientation on the elastic behaviour of single crystal SRR99 for different temperatures has been conducted by Li and Smith (1995b).

A number of studies have also been performed to investigate the transverse elastic anisotropy under a uniaxial loading for different crystal orientations (Yang [1985], Li et al [1996]). Both theoretical and experimental results indicate that the transverse strains induced by longitudinal stress, in general, varies sinusoidally around the longitudinal axis. Only for loading in the [111] and [001] directions is the transverse response isotropic. For all other loading directions, the transverse response shows various degrees of anisotropy. For the case of a nickel base single crystal, the highest degree of anisotropy is seen when loaded in the [011] crystallographic direction (Yang [1985]). This is attributed to the cubic symmetry structure of nickel base single crystal. When loaded in the [011] orientation, the lattice spatial distribution in the transverse directions is most irregular, and therefore produces the highest degree of material anisotropy.

2.4.2 Orientation Dependent Plastic Response

The basic microstructure of modern nickel base single crystal alloy consist of a γ matrix with a precipitated γ' phase. The cubic precipitates of the crystallographic γ' phase are in coherence with the crystallographic cubic matrix γ phase. Therefore the global deformation response of the microscopic two phases (composite) single crystal alloys exhibit general (pure) cubic single crystal characteristics (Nathal and Ebert [1985], Milligan and Antolovich [1987], Walker and Jordan [1989], Meric et al [1991], Nouailhas and Cailletaud [1995]).

The basic plastic deformation mechanism in a single crystal is slip, i.e. the sliding of blocks of material over one another along definite crystallographic planes, called slip planes. The extent of slip in a single crystal depends on the magnitude of the shear stress produced by external load, the geometry of the crystal structure and the orientation of the active slip planes with respect to the shearing stresses. Slip begins when the shearing stress on slip planes in a slip direction reaches a threshold value called the Critical Resolved Shear Stress (CRSS), which is defined by Schmid's Law [1931] for the uniaxial loading case as:

$$\tau_s = \sigma_y \cos\theta \cos\varphi \qquad (2.4a)$$

or

$$\tau_s = \sigma_y S_{\{l_2,m_2,n_2\}\{l_3,m_3,n_3\}} \qquad (2.4b)$$

where σ_y is the yield stress, θ is the angle between the applied tensile stress $[l_1,m_1,n_1]$ and the slip direction whilst the φ is the angle between the applied tensile stress $[l_1,m_1,n_1]$ and the slip plane normal direction $[l_3,m_3,n_3]$, which are illustrated in Fig. 2.2. $s=\cos\theta\cos\varphi$ is Schmid's Factor. The details on the derivation of the Schmid's law and the calculation of the Schmid factor are given in Appendix I.

Slip occurs most readily in specific directions on certain crystallographic planes. Generally the slip plane is the plane of greatest atomic density and the slip direction is the closest-packed direction within the slip plane. The slip plane together with the slip direction establishes the slip system. The active slip systems in fcc nickel base single crystal alloys depend upon crystal orientation with respect to the applied loads, temperature and strain rate, and could involve one or more types of slip. For a nickel base single crystal alloy, 30 possible slip systems have been identified and can be divided into 3 primary slip groups:

(a) 12 Octahedral {111}[110] slip

(b) 12 Octahedral {111}[112] slip

(c) 6 Cubic {001}[110] slip

The three slip groups are illustrated in Fig. 2.3. The flow behaviour of a single crystal alloy is determined by the active systems.

A number of investigations were carried out on various nickel base single crystal superalloys, such as PWA1480 (Milligan and Antolovich [1987], [1990]), AM1 (Guedou and Honnorat [1990], Poubanne [1990]), Rene N4 (Miner et al [1986a], [1986b]) and SRR99 (Ghosh et al [1992], Leverant et al [1971], Russell et al [1985], Sun and Hazzledine [1988], Li [1993]), to study the anisotropic plastic deformation

behaviour of single crystal alloys. The results indicated that temperature also has a strong influence on the orientation dependent plastic deformation response, because different slip systems can be active at different temperatures for a given crystal orientation.

2.4.3. Time and Temperature Dependent (Creep) Behaviour

Single crystal nickel base superalloys have been developed for high temperature applications, such as gas turbine blades operating at temperatures over 1000°C. At elevated temperature, single crystal superalloys also exhibit time dependent deformation (e.g. creep), although the creep resistance of single crystal alloy is improved compared with polycrystalline alloys. There has been a number of investigations on the time dependent deformation behaviour of single crystal nickel base superalloys (Kear and Piearcey [1967], Leverant et al [1971], [1973], Oblak and Rand [1974], Nathal and Ebert [1985], Fleury and Remy [1994], Pan et al [1994, 1997]). Most of the studies have been conducted to study the influence of crystal orientation and temperature on the creep deformation and creep rupture life of single crystal superalloys.

It was found that the major anisotropic effect is exhibited in the temperature range 750°C to 850°C. Kear and Piearcey [1967] were the first to study the creep behaviour of single crystal superalloys. Their results revealed that a substantial improvement in creep life of single crystal Mar-M20 occurs between 750°C to 850°C with orientations near [001] and [111], and very short lives were exhibited with orientations near [011]. At 980°C, crystallographic orientation was found to have much less of an influence on the creep life.

At a temperature of about 760°C, the degree of anisotropy in stress rupture lives is often large. Single crystals Mar-M20 (Kear and Piearcey [1967], Leverant et al [1971], [1973], Oblak and Rand [1974]) oriented near [011] have much shorter rupture lives than crystals oriented near [001]. Mar-M247 single crystal showed similar behaviour, and also very long rupture lives were observed for samples

orientated near [111]. Large differences in creep lives were found for differently orientated samples. In order to understand the orientation dependence of the extent and rate of creep, Leverant and Kear [1970] considered the Schmid factors and multiplicity of slip for the {111}[112] slip system. In general, crystals having orientations with high Schmid factors are more favourably orientated for slip than crystals with low Schmid factors. Thus, a crystal with an orientation near [111] should exhibit the highest stress rupture life. This, in part, is because the [111] orientation provides the lowest Schmid factor (0.31) for [112] slip, and strong work hardening may occur due to interactions between mobile dislocations gliding within several intersecting systems. In general, both [001] and [111] orientations showed better creep life behaviour compared with other orientations. However, there were contradictory experimental results regarding whether [001] or [111] crystal orientation has the longest creep life (Ghosh et al [1990], (Winstone [1989], Sun and Hazzledine [1988]).

In the temperature regime over 1000°C the effect of crystal orientation on creep properties of nickel base alloys is much less pronounced and the material behaviour appears to be isotropic in terms of creep life. The explanation for this is the thermal activation of the other slip systems at this temperature. For instance, slip on the {100} planes becomes energetically favourable. However, the increased mobility of dislocations due to thermally activated climb and cross slip processes enhances creep rates overall.

There have been also a number of investigations on the microstructural change, i.e. rafting, of single crystal nickel base superalloys under creep loading (Schneider et al [1992], Pollock et al [1994]). However, most of the studies are limited to creep deformation induced microstructural change in the [001] orientation.

2.4.4. Strain Rate Dependent Behaviour

Early experimental investigations on mechanical behaviour of single crystal superalloy CMS-X2, PWA1480 and AM1 by Milligan et al (1987), Jean-Yves

Guedou et al (1990) and Poubanne (1990) reported that at temperatures above 760°C strong strain rate dependent mechanical behaviour was observed in a wide range of orientations. Comparison of test results with strain rates of 0.008pct/s and 0.8pct/s were given by Milligan et al for single crystal PWA1480 (Milligan et al [1987]. At temperatures below 705°C there is no effect of strain rate in the range. At the lower strain rate the strength began to fall at 760°C, while at the higher strain rate the strength does not begin to drop until above 815°C. At constant temperature, the strength was significantly lower for the lower strain rate. The saturation stress at 950°C noticeably increases with strain rate. At the same strain, the higher the rate of strain is, the higher will be the stress, (Lemaitre and Chaboche, [1990]). A change in the strain rate during the test results in an immediate change in the stress-strain curve.

2.4.5. Yielding Behaviour

The yield behaviour for single crystal alloys under uniaxial and multiaxial loading has been investigated experimentally by many researchers (Li [1993], Milligan [1987] and Miner [1986], Nouailhas [1993]). It was reported that the yielding behaviour of single crystal is much more complex than conventional materials. The yield strength is generally temperature, strain rate and orientation dependent for uniaxial loading, and non-uniform yielding is observed for pure torsion and for the tension-torsion combined load.

For nickel-base superalloy PWA 1480 the yield strength was constant from 20°C to 760°C. Above 760°C the strength dropped rapidly and became a strong function of strain rate (Milligan [1987]). A similar trend was found for single crystal SRR99, i.e. all specimen orientations show a yield strength plateau between room temperature and 600°C, followed by an increase in yield strength with temperature between 600 to 750°C. A significant drop in strength occurs beyond 750°C, although the rate of decrease is less for temperatures beyond about 900°C (Li [1993]). Such behaviour is typical of high γ' volume fraction nickel base superalloy single crystals and has been documented for several similar nickel base single crystal systems (Nathal et al [1982], Shah and Duhl [1984], Walter et al [1987]).

The orientation dependence of yield strength was not significant for temperatures above 750°C with the yield strength slightly higher in the [111] orientation. Also the tension-compression asymmetry of yield strength was found in [001] and [111] orientations but no significant asymmetry of yield strength was found for specimens with intermediate orientations.

The yield behaviour of single crystal alloys depends on both temperature and loading conditions. Yielding and plastic deformation behaviour of single crystal alloy under multiaxial loading is more complex, since material anisotropy induces in non-uniform deformation. Only limited experiments had been conduced to investigated multiaxial yielding behaviour of single crystal alloys (Policella et al [1990], Nouailhas et al [1993]). A thin tube made in single crystal CMSX2 was submitted to tension-torsion loading (Nouailhas et al [1993]). The axis of the tube coincides with the [001] material orientation. Local strain measurement was made by means of strain gages, and the analysis of the slip traces was made by a replica technique. Both octahedral and cubic slips were observed in the tension-torsion tests, but only octahedral slip was active in tension for the [001] orientation. Cubic slip is predominant for pure torsion loading at room temperature and high temperature (Nouailhas et al [1993]). A strong strain localisation occurs in the four [011] zones at room and high temperatures. The [110] regions are more deformed than the [100] ones. The localisation of the shear bands in the [110] regions is more pronounced at high temperature (950°C) than at room temperature (Nouailhas et al [1993]).

Some experimental investigations on the effect of hydrostatic pressure on the plastic flow properties of single crystal were carried out by Spitzig (1978, 1981), and Richmond et al (1980). Their experimental results show that the assumption of constant volume remains reasonably valid for single crystal alloys, which means the material flow or plastic deformation is hydrostatic pressure independent as is assumed for conventional polycrystalline materials. The first stress invariant represents hydrostatic pressure, therefore the yield criterion and flow law should not

include the first invariant, and only be the functions of the second and higher stress invariants.

2.4.6. Cyclic Deformation and Fatigue Behaviour

The high temperature fatigue behaviour of a nickel base single crystal superalloy will be much more complex than tensile or creep behaviour, because at elevated temperatures, plastic flow, creep, and relaxation may occur simultaneously under cyclic loading. The fatigue deformation and life behaviour of single crystal alloys are strongly dependent on both temperature and crystal orientation as well as cyclic loading conditions.

The orientation and temperature dependence of the cyclic yield strength, tension - compression anisotropy and flow behaviour in fatigue tests are generally similar to those observed in tensile tests. Experimental results on PWA1480 (Milligan [1990]), Rene N4 (Gabb. et al [1989]), AM1 (Poubanne [1990]) and SRR99 (Li [993]) nickel base single crystal superalloys show that the magnitude and orientation dependence of tension-compression anisotropy is quite significant at lower temperatures (below 760°C-800°C), but generally not so at higher temperatures. A similar tension -compression anisotropy has been observed in single crystal Ni_3Al by Ezz et al [1982] and by Shah and Duhl [1984] for the single crystal PWA1480.

The cyclic and fatigue behaviour of SRR99 single crystal were studied by Li and Smith [1995] at 750°C, 950°C and 1050°C. Specimens with various orientations were subjected to various applied strain ranges. Dwell periods at constant applied tensile strain, compressive strain and balanced tension/compression strain were included in a number of experiments to study the combined creep-fatigue effect. The hardening and softening response was investigated by considering the resulting stress range over the life. At 750°C the stress range remained stable throughout the test, thus indicating that no hardening/softening behaviour was present. This was found even when dwell periods were included. At 950°C no hardening/softening was observed until dwell periods were introduced. Tensile, compressive and balanced tension/compression dwell cycles all induced cyclic softening during the first 10%

of fatigue life. At 1050°C continuous cyclic softening was observed for all tests, with or without dwell cycles. However tensile dwells induced the most softening, indicating more creep damage was introduced during tensile dwell period.

The temperature dependence of cyclic work-hardening behaviour has been observed for several other nickel base single crystal superalloys (Gabb et al [1986], Poubanne [1990]), At lower temperatures (below 760°C), only slight work-hardening was observed for Rene N4 (Gabb et al [1986]) and AM1 (Poubanne [1990]). The orientation dependence of work-hardening is also very small at lower temperatures. For example, the calculated hardening exponents for all orientations, including the [001], [011], [111], [236], [027] and [145] orientations, for Rene N4 is about 0.20. At higher temperatures, work hardening becomes large and strong work hardening anisotropy for different orientations is observed. Both Rene N4 and AM1 show the highest hardening in the [001] orientation compared with other orientations. It is quite surprising to note the markedly low hardening level of the [111] orientation.

The high temperature fatigue life behaviour of nickel base single crystal alloys was found to be significantly better than nickel base polycrystalline alloys. Li and Smith [1994] had compared the high temperature fatigue lives between single crystal SRR99 and polycrystalline Mar-M002 nickel base superalloys. A significant improvement in the fatigue life was observed for SRR99 single crystal alloy. At a given total strain range, the fatigue life of SRR99 was found to be nearly ten times longer that that of the polycrystalline nickel base superalloys Mar-M002 (Li [1993], Li and Smith [1994]).

The improved fatigue behaviour of single crystal alloys has been attributed to a change in the mode of crack propagation from intergranular in conventionally cast materials to transgranular in single crystals. High temperature fatigue tests on nickel base single crystal superalloys Mar-M200 (Chan et al [1987a,1987b])], Rene N4 (Poubanne [1990]) and PWA1480 (Millian [1990]) all show similar fatigue fracture modes. Fatigue crack initiation occurred at carbides or micro-pores, and subsequent crack growth takes place by either a stage I or stage II mode. Fracture behaviour is also strongly dependent on temperature, crystal orientation and cyclic frequency.

2.4.7 Material Deformation Mechanisms

The basic inelastic (plastic, creep and viscoplastic) deformation mechanism for a single crystal alloy is slip. There are a number of possible slip systems for a given single crystal material. The type and number of active slip systems observed from a particular test depend on microstructure of the single crystal, temperature, orientation and loading conditions.

Basic studies of the cyclic stress-strain behaviour of single crystals, devoted to pure copper (Mughrabi [1978], Vogel et al [1982] and aluminium alloys with a low volume fraction of fine precipitates (Vogel et al [1982], Reme [1984]), showed that f.c.c. crystals deform by octahedral {111}<110. slip. The behaviour of superalloy single crystals is much more complex since they bear out a high volume fraction of the γ' phase. Some studies have shown the role of cubic slip in the mechanical properties of and γ-γ' superalloys by in-situ experiments between 150°C and 900°C (Clement et al [1991]). A number of studies have been carried out to identify the active slip systems using various techniques, including photos, replica and interferometry (Hanriot et al [1991], Policella et al [1990], Nouailhas et al [1993]).

Single crystal nickel base superalloy AM1 was studied by Hanriot et al [1991]. Cyclic stress-strain tests were conducted at 650°C and 950°C. The orientations considered were [001], [101], [111] and [213]. Plastic replicas of the tested specimens were taken to study the characteristics of the slip bands, and for the identification of the active slip systems. It was found that AM1 deforms by both cubic and octahedral slip, even at intermediate temperature (Hanriot et al [1991]).

At 650°C plastic strains were accommodated by very localised slip bands. The slip band structure is heterogeneous at a macroscopic level, except for near the [111] orientation, which exhibited a more homogenous slip band structure. The [001] orientation gives rise to multiple octahedral slip, as shown in Fig.2.4. Slip occurred along the {111}<101> system and along several directions in the {111} plane. Near the [101] orientation, multiple cubic slip was also observed. The {001} slip plane

was predominant. This is the single plane visible at a low magnification on a surface replica, shown in Fig.2.5. Observation under a high magnification revealed short slip traces on a secondary cubic plane. Near the [111] orientation, deformation occurred only by multiple cubic slip with a {001} primary system. Near the [213] orientation, both multiple octahedral slip, on a {1 -11} slip plane, and cubic slip on {100} and {001} planes, were observed.

Experimental results for PWA 1480 single crystal alloy at intermediate temperatures (650°C - 760°C) also revealed cubic slip deformation for the [111] orientation (Gabb et al [1989]).

At 950°C, surface replicas taken by Hanriot et al [1991] are shown in Fig. 2.6 and 2.7. The [001] orientation gave rise to multiple octahedral slip. Slip occurred in the four octahedral {111} planes along two or three directions (Fig.2.6). Near the [111] orientation, deformation occurred only by cubic slip along the {001}[110] slip system (Fig. 2.7).

Active slip systems not only depend on temperature but also depend on loading conditions. Single crystal nickel base superalloys CMSX 2 was studied by Policella et al [1990] and Nouailhas et al [1993]. Mechanical tests using tube specimens were carried out a room temperature, 650°C, 950°C and 1100°C under various loading conditions, including torsion and combined tension-torsion loading. Different methods had been used to identify the active slip systems.

The experimental results showed a strong heterogeneity of deformation in torsion at both room temperature and at 950°C (Nouailhas et al [1993]). Figure 2.8 shows the slip traces observed on the outside surface of the specimen. It can be seen that horizontal and vertical traces, characteristic of cubic slip, are not evenly distributed along the circumference of the tube specimen. They are localised on four more deformed zones which were identified as the areas corresponding to the [110] region in the transverse direction (the axis of the specimen is along the [001] orientation). Similar slip traces have been observed by Policella et al [1990], as shown in Fig.2.9.

A detailed study of the traces on the specimen tested under torsion had been made by means of replicas and interferometry (Nouailhas et al [1993]). Typical results obtained by Nouailhas [1993] are reproduced in Fig 2.10. Fig.2.10a shows the horizontal slip lines taken with a scanning electron microscope at low magnification. The corresponding picture obtained by interferometry is shown in Fig.2.10b. The results confirmed the presence of slip bands at the surface of the specimen, with very small step (0.8μm) in the slip band. The same microstructural study has been made on the specimen under combined in-phase tension-torsion and followed by pure torsion test. The microstructure was found to be much more complex, due to the combined tension-torsion loading. Both octahedral and cubic lips were present (Nouailhas et al [1993]). A general view of the slip bands is given in Fig.2.11. The four octahedral planes were found to be active, together with the cubic ones. The traces of the octahedral planes have a sinusoidal form, while the cubic traces as fine horizontal lines.

A more detailed illustration of the surface is given in Fig.2.12. The first view (Fig.2.12a) shows that the cubic and octahedral systems were present simultaneously. Fig.2.12b and 2.12c correspond to increasing magnification of Fig.2.12a. They reveal the γ‘ structure and also the fact that several bands can be seen inside a large one. The interferometry (Fig.2.12d) demonstrated that the step corresponding to the octahedral planes was much larger than the step of the cubic planes.

From the above experimental results, it can be seen that among a number of possible slip systems, octahedral and cubic slip systems, are the basic slip systems that appear to operate during deformation of nickel base single crystal superalloys. Therefore, these fundamental slip systems should be considered in the constitutive models for single crystal nickel base superalloys.

2.5 Isothermal Anisotropic Viscoplastic Deformation Modelling

2.5.1. Overview

The elimination of grain boundaries in single crystal nickel base superalloys has led to superior thermal fatigue and creep properties compared to conventional cast alloys. However, as reviewed in section 2.3, the absence of grains in single crystal alloys also leads to material anisotropy which produces orientation dependent material responses. In order to fully utilise the advantages of single crystal alloys, new constitutive models must be developed to account for both strong orientation dependent and general viscoplastic behaviour for high temperature application. The models should be available in a multiaxial form for use in conjunction with a finite element method for structural stress analysis, or a similar analysis, so that a component can be assessed for structural stability and integrity under the complex conditions representative of service.

There has been significant progress on the development of isothermal anisotropic constitutive models to describe viscoplastic deformation behaviour of various materials in the last decades. A large number of different constitutive models have been proposed (Chaboche and Nouailhas [1989], Chan and Lindholm [1990], Chan et al [1989, 1990], Walker and Jordan [1989]) and their applicability to describe material response under various loading conditions have been reviewed by a number of investigators (Chaboche and Rousselier [1983], Ohno and Wang [1992], Ohno [1990]). Consequently, the review in the following sections will only limited to development of isothermal constitutive models for single crystal superalloys. In section 2.5.2 a brief summary of the general development of viscoplastic constitutive models is presented. Then two different approaches, i.e. the phenomenological and the crystallographic approaches, used to develop constitutive models for single crystal superalloys are reviewed in sections 2.5.3 and 2.5.4 respectively. In the final section, 2.5.5, other simple models developed for single crystal alloys are also briefly reviewed.

2.5.2. General Development of Constitutive Models

(i) Classical and Unified Models

In general, material deformation behaviour can be classified in three different categories: elastic, plastic and creep. Consequently, for small strain cases, a classical constitutive model is written as:

$$\dot{\varepsilon}_{ij}^{T} = \dot{\varepsilon}_{ij}^{e} + \dot{\varepsilon}_{ij}^{p} + \dot{\varepsilon}_{ij}^{c} \tag{2.5}$$

where the total strain rate tensor is decomposed into elastic strain rate $\dot{\varepsilon}_{ij}^{e}$, plastic strain rate $\dot{\varepsilon}_{ij}^{p}$ and creep strain rate $\dot{\varepsilon}_{ij}^{c}$ tensors.

However, a distinguishing feature in the development of modern constitutive models, such as the unified model, is to treat both plasticity and creep as one inelastic strain. The decomposition of the total strain rate tensor for small strain cases in a unified model is given as:

$$\dot{\varepsilon}_{ij}^{T} = \dot{\varepsilon}_{ij}^{e} + \dot{\varepsilon}_{ij}^{in} \tag{2.6}$$

where $\dot{\varepsilon}_{ij}^{in}$ is the inelastic strain rate tensor.

The primary motivation for using unified models is based on two aspects. Firstly, a modern constitutive model intends to include more important manifestations of inelastic behaviour in the same set of equations, e.g. strain rate dependent plastic flow, creep, stress relaxation. However, inelastic behaviour of solids is exceedingly complex and many aspects of the physics of polycrystalline, even single crystal, materials are far from being fully understood. Interaction of 'creep' and 'plasticity' is one such complication. Because creep-plasticity interactions and recovery of hardening may take place simultaneously, it is difficult to separate time-independent (plasticity) and time-dependent (creep) deformation.

Secondly, studies on the physical mechanisms of inelastic deformation also reveal that both 'plasticity' and 'creep' (at least creep due to slip) are controlled by the

motion of dislocations. This leads directly to unify 'plasticity' and 'creep' with a single set of equations, rather than taking the traditional engineering approach of using one set of equations to predict 'time-independent' plastic strains and a separate set of equations to predict 'time-dependent' creep strains.

(ii) Internal Variables and Evolution Laws

Another distinguishing feature of the development of modern constitutive models, particularly the unified models, is the use of internal variables to describe the influence of microstructural change on the mechanical response of materials, e.g. drag stress and back stress for isotropic and kinematic hardening. This is based on the physical knowledge of the role of internal structure (e.g. dislocation density, and the state of internal stress) in controlling the inelastic deformation. This leads directly to the use of internal structure variables, rather than only the external variables.

Consequently the strain rate equation, gives the inelastic strain rate $\dot{\varepsilon}_{ij}^{in}$ in terms of the deviatoric stress σ'_{ij} (where $\sigma'_{ij} = \sigma_{ij} - \delta_{ij}\sigma_{kk}$), internal variables (e.g., K and X_{ij} which are defined below), and the temperature T, i.e.

$$\dot{\varepsilon}_{ij}^{in} = \dot{\varepsilon}_{ij}^{in}(\sigma'_{ij}, K, X_{ij}, T) \tag{2.7}$$

The evolutionary equations describe the rate of change of the internal variables due to stress, current structure and temperature, i.e.

$$\dot{K} = \dot{K}(\sigma'_{ij}, X_{ij}, K, T) \tag{2.8}$$

and

$$\dot{X}_{ij} = \dot{X}_{ij}(\sigma'_{ij}, X_{ij}, K, T) \tag{2.10}$$

Typically, two internal variables are chosen as the minimum set. One internal variable which is associated with kinematic hardening or deformation-induced anisotropy, is often termed as the "back stress" and is given by a second-order tensor X_{ij}. Mechanically, back stress X_{ij} defines the centre of the loading or yield locus.

This back stress X_{ij} affects the magnitude of the superimposed applied stress needed to produce additional plastic flow and thus produces the Bauschinger effect i.e. the type of anisotropy associated with kinematic hardening. The other internal variable, K, is associated with isotropic hardening effects to describe cyclic hardening or softening.

2.5.3. Crystallographic Models

Modelling of the time-dependent behaviour of single crystal superalloys started with the crystallographic approach in conjunction with Schmid's law. It assumed that the overall behaviour of a single crystal under a given loading condition is controlled by the deformation characteristics of a certain number of active slip systems, and the contributions of each slip system are summed up by using established procedures of time-independent crystal plasticity theory. Early developments in the crystallographic approach are attributed to Taylor [1937], Bishop and Hill [1951], and Bishop [1952]. The application of the crystallographic approach to single crystal nickel base superalloys began with the work of Paslay et al [1970,1971], and recently by Shah [1983] to the γ' phase of these alloys. The classical constitutive assumption is Schmid's law, in which slip on a particular system is a function of the resolved shear stress on the slip plane in the direction of slip. However, the simple Schmid's law used in time-independent crystal plasticity theory does not apply for a L_{12} crystal, or for single crystal nickel base superalloys. This is because the deformation of these materials is time dependent. Modifications of the crystal plasticity theory have been carried out for describing the viscoplastic deformation behaviour of single crystal nickel base superalloys. More recently, the crystallographic approach has been developed by Dame and Stouffer [1988], Stouffer et al [1990], Walker and Jordan [1989], Cailletaud [1987,1988], Meric et al [1991]. The principal advantage of this approach is that a significant portion of the model is based on the physics of the deformation mechanism.

In general, the constitutive equations are introduced at the microscopic level which is the slip system and are similar to the form of the phenomenological unified

constitutive equations, e.g. Chaboche model (Chaboche [1989]). At the macroscopic level, the macroscopic strain is partitioned into an elastic and inelastic strain as in the unified theory. The elastic constitutive relations are written directly at the macroscopic level by using classical elasticity theory. The models include three distinct steps and two operating levels, i.e. a step that introduces localisation, a step that introduces constitutive equations at the local level and finally a step the sums the individual contributions (a homogenisation step), see Fig.2.4. In the first step, i.e. the localisation step, the macroscopic stress tensor is transformed or resolved to shear stresses at the microscopic level in the slip systems. In the second step, the constitutive equations, which are the relationship between the resolved shear stresses and the inelastic shear strain rates on the slip systems, i.e. $\dot{\gamma}^s = \dot{\gamma}^s(\tau^s,...)$, operate at the microscopic level, and the local shear strain rates can be obtained. In the third step, a transformation from the microscopic shear strain rate $\dot{\gamma}^s$ to the macroscopic strain rate tensor $\dot{\varepsilon}^{in}$ is carried out. Overall the fundamental requirement for the application of the crystallographic model is the identification of the active slip systems in the single crystal under a given loading condition.

The advantages of this type of model are:

(i) The concept is based on the physical deformation mechanisms in a single crystal;

(ii) The different microstructural changes and the deformation characteristics of the various slip systems can be taken into account.

The disadvantages are:

(i) It is difficult to accurately determine the number and type of active slip systems;

(ii) It is not easy to determine the material parameters in the model when written at the microscopic level for each slip system; and

(iii) A large number of equations are to be solved in the numerical implementation.

2.5.4. Phenomenological Models

Phenomenological constitutive models, especially the unified models, have been well developed and applied, with some success, to describe the cyclic plasticity and viscoplasticity behaviour of polycrystalline materials (Chaboche and Nouailhas [1989], Chan and Lindholm [1990], Chan et al [1989, 1990]). However, there are only limited studies on the applicability of these models to the single crystal superalloys. An attempt was made by Choi and Krempl [1989] to adopt the orthotropic unified theory of viscoplasticity based on overstress (VBO) (developed by Lee and Krempl [1991] for polycrystalline materials) for a cubic single crystal, and to describe the tension/compression tests in the [001], [110] and [111] directions. However, this was only a theoretical study with no experimental verification of the model.

The approach used in the phenomenological model was based on continuum mechanics framework, and modification of the isotropic constitutive models developed for polycrystalline materials. Therefore, the choice of the formations of the functions used in the model will determine the anisotropic features described by the model. In this context, the potential (yield) functions is expressed as a function of the invariants (I_1, I_2,.....I_n), which involve the function automatically invariant for the group of orthogonal transformations characterising the material symmetries required in continuum mechanics. The problem is then the determination of the integrity basis. For a f.c.c crystal, and for second-order stress tensor, σ_{ij}, one way to express the integrity basis is (Smith and Kiral [1978]):

$$I_1=(\sigma'_{11})+(\sigma'_{22})+(\sigma'_{33}) \qquad I_2=(\sigma'_{11})^2+(\sigma'_{22})^2+(\sigma'_{33})^2$$

$$I_3=(\sigma'_{11})^3+(\sigma'_{22})^3+(\sigma'_{33})^3 \qquad I_4=(\sigma'_{23})^2+(\sigma'_{31})^2+(\sigma'_{12})^2$$

$$I_5=(\sigma'_{11})(\sigma'_{23})^2+(\sigma'_{22})(\sigma'_{31})^2+(\sigma'_{33})(\sigma'_{12})^2 \qquad I_6=(\sigma'_{23})(\sigma'_{31})(\sigma'_{12})$$

$$I_7=(\sigma'_{11})^2(\sigma'_{23})^2+(\sigma'_{22})^2(\sigma'_{31})^2+(\sigma'_{33})^2(\sigma'_{12})^2 \qquad I_8=(\sigma'_{23})^4+(\sigma'_{31})^4+(\sigma'_{12})^4$$

$$I_9=(\sigma'_{11})(\sigma'_{23})^4+(\sigma'_{22})(\sigma'_{31})^4+(\sigma'_{33})(\sigma'_{12})^4$$

Where σ'_{ij} are the deviatoric components of the stress tensor σ_{ij}.

How many and what stress invariants are to be included in the potential (yield) function is a compromise among accuracy, complexity and practicability. This choice must be guided by material deformation characteristics and verified by the experimental results.

The Chaboche viscoplasticity model [1989] was modified by Nouailhas [1990] for modelling the cyclic mechanical behaviour of single crystal CMSX-2 at elevated temperature, and used for simple uniaxial cases under continuous cycling conditions. This model has been further developed by Li [1993] based on a comprehensive test programme involving combined creep and fatigue loading under isothermal conditions. The constitutive equations have been used with some degree of success to describe the cyclic viscoplastic deformation response and for predicting the fatigue and creep life of single crystal SRR99.

However, the previous studies have been limited to studies using simple specimens and uniaxial loading conditions. The characteristics of the constitutive model to describe a complex component geometry, e.g. a gas turbine blade, under three dimensional loading conditions have not been examined. This requires the use of the constitutive models with finite element analysis. Furthermore, complete structural analysis using the finite element method also makes it possible to directly compare the phenomenological and crystallographic models.

2.5.5. Other Models

There are also other models used to describe various deformation behaviours of single crystal superalloys. Some of the models are not developed in terms of the principles of continuum mechanics, but by fitting of empirical expressions to experimental observations. Graham and Walles (Graham and Walles, [1955])

proposed a set of creep equations, i.e. Graham-Walles model, to describe the creep deformation of metals and superalloys. This model was developed purely to fit the uniaxial creep curves. This model has been further developed by Harrison and Homewood [1994] for modelling the anisotropic creep deformation of single crystal SRR99 under simple loading conditions. In this model, the initial Graham and Walles equations are directly applied to the local slip systems.

For an isotropic material:

$$\varepsilon = \sum_{i=1}^{n} c_i \sigma^{\beta_i} t^{k_i} (T'-T)^{-20k_i} \tag{2.10}$$

where c_i, β_i and k_i are material constants.

For a single crystal at each slip plane:

$$\gamma = \sum c_i \tau^{\beta_i} t^{k_i} (T'-T)^{-20k_i} \tag{2.11}$$

The overall creep response of a single crystal alloy is determined by the summation of all the creep deformation of all the possible active slip systems in the way exactly same to the crystallographic model.

This model can be used, with some degree of success (Harrison and Homewood, [1994]), for modelling pure creep deformation of single crystal alloys. However, this model can not be generalised to a three-dimensional constitutive model to describe the viscoplastic deformation response including both plasticity and creep. This is because there is neither a yielding criterion nor a load/unload criterion in the model.

2.6 Nonisothermal Mechanical Behaviour Modelling

Over the last decade there has been substantial interest in developing elastic viscoplastic constitutive equations which are suitable for complex thermal and mechanical loading. A number of different approaches have been adopted to develop thermomechanical models to describe nonisothermal deformation behaviour of various engineering materials (Miller, [1976]; Bodner et al, [1978]; Merzer et al,

[1979]; Walker, [1981]; Moreno and Jordan, [1986]; Chan et al [1988, 1990]; Bhattachar et al, [1993]; Jordan and Walker, [1992]). In general, the effort has been devoted to developing nonisothermal models by extending and using isothermal models for predicting the nonisothermal response of materials. Two major different categories of nonisothermal models have been developed: explicit and implicit models.

The explicit models use temperature or temperature rate explicitly in the constitutive equation, i.e. using temperature or temperature rate as explicit variables in the constitutive equations. The Miller model (Miller [1976, 1987]) included the temperature in the flow equation and in the equation for the evolution of the back stress. The unified nonisothermal model by Ramaswamy and Stouffer model (Bhattachar and Stouffer, [1993]) has also included temperature in the flow equation. The flow equation is based on the Arrhenius theory for nonisothermal processes and the material parameters used in the flow equation and the evolution equations do not vary with temperature. This method uses an activation energy term to represent a dominant mode of deformation.

In the implicit models the temperature or temperature rate are included in the constitutive equation through the temperature dependent material parameters rather than as explicit variables. The Bodner model has been used to predict the nonisothermal response of the single crystal alloy B1900+Hf (Chan et al, [1988, 1990]) by the introduction of temperature rate terms in a procedure similar to a Taylor series expansion. The temperature derivatives of the flow, back stress evolution and isotropic hardening equations are included. Temperature rates have also been introduced in the elasticity equations by differentiating the modulus of elasticity with respect to temperature.

A number of investigators have compared the advantages and disadvantages of the implicit and explicit methods (Miller [1976], Bhattachar and Stouffer [1993], Thompson [1982]). The explicit method requires deformation data with temperature, i.e. stress and strain as functions of temperature. This requires complex

thermal mechanical deformation tests. Implicit methods are generally developed by extending the isothermal constitutive models, and consequently only isothermal test data are required to determine the temperature dependent material parameters.

There have been only limited studies using thermal mechanical models of single crystal alloys. The Walker (Jordan and Walker [1992]) crystallographic model uses an implicit method to carry out the prediction of thermomechanical response for single crystal superalloy PWA 1480 (Jordan and Walker [1992]). Here the implicit method will be used to extend the isothermal constitutive models developed to describe the thermomechanical deformation of nickel base single crystal superalloy SRR99. Consequently, only the implicit method is described briefly in the following section.

2.7 Implementation of Constitutive Models for Structural Analysis

2.7.1. Overview

The ultimate objective of any investigation into the material response, and subsequent development of constitutive models, is to be able to perform structural analysis to assess the structural integrity of engineering components, such as single crystal gas turbine blades. To achieve this objective, some appropriate numerical methods are required to implement the constitutive models into a formulation suitable for numerical simulation. Then the practical boundary problems of structural analysis are conducted by using a finite element code in the design and assessment of engineering components operating under complex conditions representative of service.

There has been a large number of investigations on the development of numerical methods to implement various constitutive models [Meric and Cailletaud [1991], [1994], Culie and Nouailhas [1993], Chan and Lindholm [1990]). The general theory of the finite element method has been well developed and details can be obtained

from standard text books. In this section, only a brief review is presented on the numerical method developed for stiff viscoplastic equations, and the basic features of the finite element code, i.e. ABAQUS, used in this work.

2.7.2. Numerical Implementation of Viscoplastic Equations

A common feature of the viscoplastic constitutive equations is the property of "high stiffness" due to their rate dependent nature. The primary numerical consideration is mathematical 'stiffness' arising from a coupling of the non-elastic and elastic strain to calculate the total strain. For example, assume the total strain rate $\dot{\varepsilon}^T$ is specified, and consider the prediction of the stress history directly from the compatibility equation

$$\dot{\sigma} = E[\dot{\varepsilon}^T - \dot{\varepsilon}^{in}(\sigma)] \tag{2.12}$$

Because $\dot{\varepsilon}^{in}(\sigma)$ is a strong function of σ, small numerical or truncation errors in σ are magnified through their effect on $\dot{\varepsilon}^{in}(\sigma)$. These errors feed back as larger errors in σ via the above differential equation for $\dot{\sigma}$. Small strain increments are therefore required to obtain reasonable accuracy and to prevent unstable numerical oscillations.

The procedure employed in the numerical analysis is the displacement-based finite element method. The exact solution for the problems involving approximate (finite element) solutions for stress, strain, deformation and force, etc. requires that both force and moment equilibrium be maintained at all times over any arbitrary volume of the body. The displacement finite element method is based on approximating this equilibrium requirement by replacing it with a weaker requirement, that equilibrium must be maintained in an average sense over a finite number of divisions of the volume of the body. The formulation used is small strain and small displacement, so that only material nonlinearities are taken into account. The integration of constitutive equations is carried out at the Gauss points for given total deformation

increments. There are generally two integration algorithms which can be used for transforming the constitutive rate equations into incremental equations: explicit and implicit algorithms. For explicit integration, e.g. forward Euler integration, the time increment needs to be controlled. For implicit integration, the algorithm is more complicated and often requires local iteration, but there is usually no stability limit.

The generalised trapezoidal rule and the midpoint-type rule are often used in implicit integration methods. At a temperature T and a temperature rate $\dot{T}$ ($\dot{T}$=dT/dt), all of the unified constitutive models for general nonisothermal mechanical deformation can be represented in the following temperature explicit form:

$$\dot{\varepsilon}^{in} = f(\sigma, x, T) \tag{2.13a}$$

$$\dot{x} = g(\sigma, x, T) \tag{2.13b}$$

$$\dot{\sigma} = D(\dot{\varepsilon} - \dot{\varepsilon}^{in}) + \eta(\alpha, D)\dot{T} \tag{2.13c}$$

with

$$\eta(\alpha, D) = [\varepsilon - \varepsilon^{in} + \alpha(T - T_0)]\frac{\partial D}{\partial T} - D[(T - T_0)\frac{\partial \alpha}{\partial T} + \alpha] \tag{2.13d}$$

where ε, ε^{in}, σ and x are the total strain, inelastic strain, stress and hardening variable vectors respectively; D is the elastic stiffness matrix and α is the coefficient of thermal expansion.

The implicit thermomechanical constitutive model contains temperature dependent material parameters. The model predicts nonisothermal deformation based on material constants determined from isothermal data and their derivatives of temperature. Using these constitutive models for thermomechanical loading requires a means of tracing and updating the current values of the hardening variables and the other materials parameters during temperature changes.

Following from the general description of the constitutive equations for the phenomenological model described in section 2.5.2, the general forms of thermal-mechanical constitutive equations are as follows:
The yield function is:

$$f = f(\sigma_{ij}, X_{ij}, M_{ij}(T), R, k(T)) \tag{2.14}$$

and the flow law is:

$$\dot{\varepsilon}_{ij}^{in} = F(\sigma_{ij}, X_{ij}, M_{ij}(T), n(T), K^*(T)) \tag{2.15}$$

The kinematic hardening rate equation is:

$$\dot{X}_{ij} = G(\sigma_{ij}, X_{ij}, N_{ij}(T), Q_{ij}(T)) \tag{2.16}$$

and to describe isotropic hardening:

$$\dot{R} = H(R, b(T), R_0(T)) \tag{2.17}$$

The material parameters M_{ij}, k, n, K^*, N_{ij}, Q_{ij}, b, R_0 are temperature dependent and expressed as functions of temperature. There is no explicit temperature variable in the constitutive equations.

In the trapezoidal rule, a linear interpolation is employed within the time increment Δt, so that for variable Z:

$$\Delta Z = [(1-\theta)\dot{Z}(t) + \theta\dot{Z}(t+\Delta t)]\Delta t \tag{2.18}$$

where $\Delta Z = \begin{pmatrix} \Delta\sigma \\ \Delta\varepsilon \\ \Delta\varepsilon^{in} \\ \Delta X \end{pmatrix}$ for phenomenological models; $\Delta Z = \begin{pmatrix} \Delta\sigma \\ \Delta\gamma_v^s \\ \Delta\alpha^s \end{pmatrix}$ for crystallographic models.

The implicit time operator θ has values ranging from zero to unity, i.e. $0 \le \theta \le 1$. It should be noted that the numerical scheme reduces to Euler's explicit method when $\theta = 0$ and to Euler's implicit method when $\theta = 1$.

The value of $\dot{\varepsilon}^{in}$, and $\dot{X}$, at time $t = t+\Delta t$ can be approximated by their previous values and their gradients at time t through the Taylor's expansion:

$$\dot{\varepsilon}^{in}(t+\Delta t) = \dot{\varepsilon}^{in}(t) + \frac{\partial \dot{\varepsilon}^{in}}{\partial \sigma}\Big|_t \Delta\sigma + \frac{\partial \dot{\varepsilon}^{in}}{\partial X}\Big|_t \Delta X + \frac{\partial \dot{\varepsilon}^{in}}{\partial T}\Big|_t \Delta T \tag{2.19}$$

$$\dot{X}(t+\Delta t) = \dot{X}(t) + \frac{\partial \dot{X}}{\partial \varepsilon^{p}}\Big|_t \Delta\varepsilon^{in} + \frac{\partial \dot{X}}{\partial X}\Big|_t \Delta X + \frac{\partial \dot{X}}{\partial T}\Big|_t \Delta T \tag{2.20}$$

Substituting constitutive equations for $\dot{\varepsilon}_t^{in}, \dot{X}_t, \dot{\sigma}_t$ and the above equations into the incremental equations for $\Delta\sigma, \Delta\varepsilon, \Delta\varepsilon^{in}, \Delta X$, then after rearranging terms leads to

$$[M]\begin{bmatrix} \Delta\sigma \\ \Delta\varepsilon^{in} \\ \Delta X \\ \Delta\varepsilon \end{bmatrix} = [\Delta V] + [\Delta V'] \tag{2.21}$$

and

$$\begin{bmatrix} \Delta\sigma \\ \Delta\varepsilon^{in} \\ \Delta X \\ \Delta\varepsilon \end{bmatrix} = [M]^{-1}[\Delta V] + [M]^{-1}[\Delta V'] \tag{2.22}$$

where

$$[M] = \begin{bmatrix} -\theta\Delta t \frac{\partial F}{\partial \sigma}\Big|_t & I & -\theta\Delta t \frac{\partial F}{\partial X}\Big|_t & 0 \\ 0 & -\frac{\partial G}{\partial \dot{\varepsilon}^{in}}\Big|_t & I - \theta\Delta t \frac{\partial G}{\partial X}\Big|_t & 0 \\ I & D & 0 & -D \end{bmatrix} \tag{2.23}$$

$$[\Delta V] = \begin{bmatrix} \Delta t\{F_t - \theta(\dot{\varepsilon}_t^{in} - F_t)\} \\ \Delta t\{\dot{X}_t - \frac{\partial G}{\partial \dot{\varepsilon}^{in}}\Big|_t \dot{\varepsilon}_t^{in}\dot{\varepsilon}^{in}) - \theta(\dot{X}_t - G_t)\} \\ 0 \end{bmatrix} \tag{2.24}$$

and

$$[\Delta V'] = \begin{bmatrix} \theta \Delta t \frac{\partial F}{\partial T}\Big|_t \dot{T} \\ \theta \Delta t \frac{\partial G}{\partial T}\Big|_t \dot{T} \\ \Delta t \eta(\alpha, D)\dot{T} \end{bmatrix} \tag{2.25}$$

where $[M]^{-1}[\Delta V]$ are the isothermal terms, $[M]^{-1}[\Delta V']$ are the nonisothermal terms, and I is the unit matrix.

2.7.3. FE Application Codes

Many FE application packages have been used in elastic-viscoplastic modelling (Meric and Cailletaud [1991], [1995], Culie and Nouailhas [1993], Chan and Lindholm [1990]). Different packages use different code and for different analysis purpose. For main frame computers, there are ABAQUS, ADINA, ANSYS, etc. For present research the ABAQUS code has been used.

The finite element program ABAQUS has been widely used in the deformation and stress analysis of solids. Besides a broad range of constitutive models, ABAQUS also provides an interface where by the user may write his or her own constitutive model in a subroutine (UMAT) in a very general way using the FORTRAN language (ABAQUS User's Manual, 1989). The stresses, strains and solution dependent state variables are solved incrementally by ABAQUS. When the subroutine UMAT is called, it is provided with the state at the start of the increment (stress, solution dependent state variables) and with the strain increments and the time increment. The subroutine UMAT performs two functions: it updates the stresses and the solution dependent state variables to their values at the end of the increment, and it provides the material Jacobian matrix, $\partial\Delta\sigma/\partial\Delta\varepsilon$, for the constitutive model as required for an iterative Newton-Rhapson solution. So any material constitutive model can be coded in ABAQUS by using UMAT.

2.8 Summary

From the literature review, it can be seen the absence of grain boundaries in single crsytal alloys also leads to material anisotropy which produces orientation dependent mechanical deformation responses. In order to fully utilise the advantages of single crystal alloys, new constitutive models must be developed to account for both strong orientation and time dependent elasto-viscoplastic behaviour of single crystal alloys during high temperature operations, in conjunction with new methods specifically developed to implement the anisotropic elasto-viscoplastic models. Even though a lot of work has been done for single crystal alloys, considerable work is still required in the following area:

1. Further development of constitutive models, including development of procedures for determining the material constants in the models.

   The two categories of models have been developed separately based on totally different principles. They have been used with some success to limited loading conditions. A comprehensive understanding of the intrinsic characteristics of the models is required to apply the models to general applications. One way to explore the features of the models is to directly compare the two models. The comparison results will provide information for further development of the models based on the characteristics of the models.

   Both constitutive models include a larger number of material constants. A consistent procedure to determine these material constants is vital for engineering application of the models. Furthermore, in order to be able to directly compare the two models, a consistent procedure must be developed for both models using the same experimental data. Otherwise, it will not be possible to explore the intrinsic features of different models.

2. Development of a robust method for implementation of the anisotropic models in FE code for structural analysis.

The literature review indicated that numerical implementation of the modern constitutive models, even for isotropic materials, is always a challenge due to the highly non-linear systems of equations with the property of mathematical 'stiffness'. For single crystal materials, it is much more difficult since the anisotropic constitutive models result in direction dependent deformation response during structural analysis. A novel method is required to be developed to implement both the phenomenological and the crystallographic models to a FE code, such as ABAQUS, to achieve stable and efficient structural calculations.

CHAPTER 3

ISOTHERMAL AND NONISOTHERMAL CONSTITUTIVE EQUATIONS FOR SINGLE CRYSTAL SUPERALLOY

3.1 Introduction

Two categories of constitutive models, i.e. phenomenological and crystallographic models have been proposed to describe the anisotropic viscoplastic deformation behaviour of single crystal nickel base superalloys. The two kinds of models have been developed based on different principles. The phenomenological models have been developed by modifying the unified isotropic models proposed initially for polycrystalline materials in terms of continuum mechanics theory. The crystallographic models have been developed in terms of the deformation mechanism of single crystal alloys, i.e. slip deformation on different slip systems. These two different types of material constitutive models have been employed in this research to simulate high temperature mechanical behaviour of nickel base single crystal superalloys under arbitrary loading and to carry out structural FE analysis.

The formulation of two isothermal constitutive models, phenomenological and crystallographic, is presented in section 3.2. Then modification of these isothermal constitutive equations for non-isothermal application is described in section 3.3. A general procedure for determining the material constants in both models using the same experimental data is proposed in sections 3.4 and 3.5. Finally in section 3.6 a comparison of the fundamental intrinsic characteristics of the two models is discussed.

3.2 Formulation of Isothermal Constitutive Equations

3.2.1. Phenomenological Model

The phenomenological model presented in this section is a generalisation of a unified model initially proposed by Chaboche [1989] for isotropic materials subjected to multiaxial cyclic loading. The anisotropic characteristics of single crystal superalloys are taken into account by modifying the model and introducing a number of anisotropic material parameters. The basic mathematical formulation of the anisotropic viscoplastic

model is developed in the material principal axis, i.e. crystallographic axes [100]-[010]-[001], Fig.3.1, for a cubic single crystal.

The components of the total strain rate tensor are decomposed into elastic and inelastic (plastic and creep) strain rates:

$$\dot{\varepsilon}_{ij}^{*T} = \dot{\varepsilon}_{ij}^{*e} + \dot{\varepsilon}_{ij}^{*in} \tag{3.1}$$

The elastic strain rate is expressed in terms of the anisotropic elastic theory:

$$\dot{\varepsilon}_{ij}^{*e} = S_{ijkl}\dot{\sigma}_{kl}^{*} \tag{3.2}$$

where S_{ijkl} represents the basic elastic compliance matrix of the single crystal alloy. Note that the * superscript denotes conditions corresponding to the crystallographic axes.

The yield function and yield criterion in Chaboche's isotropic model is generalised by introducing a fourth order material anisotropy tensor, M_{ijkl}, to describe the initial anisotropy and possibly deformation induced material anisotropy:

$$f = \sqrt{\tfrac{3}{2}(\sigma_{ij}^{*'} - X_{ij}^{*'})M_{ijkl}(\sigma_{kl}^{*'} - X_{kl}^{*'})} - R - k \le 0 \tag{3.3}$$

where $\sigma_{ij}^{*'}$ and $X_{ij}^{*'}$ are the deviatoric components of stress and back stress deviation tensors.

A viscoplastic potential is proposed using the same formulation as in Chaboche's [1989] model:

$$\Omega = \frac{K}{n+1}\left\langle \frac{f}{K} \right\rangle^{n+1} \tag{3.4}$$

where n and K are material constants to represent the effects of viscosity and are strongly temperature dependent. The bracket< > is defined as:

$$\langle u \rangle = \begin{cases} u & \text{if } u > 0 \\ 0 & \text{if } u \le 0 \end{cases} \tag{3.5}$$

The viscoplastic (or inelastic) strain rate is then obtained from the normality hypothesis, that is:

$$\dot{\varepsilon}_{ij}^{*in} = \frac{\partial \Omega}{\partial \sigma_{ij}^{*}} = \dot{p}\frac{\partial f}{\partial \sigma_{ij}^{*}} = \frac{3}{2}\left\langle \frac{f}{K} \right\rangle^{n} \frac{M_{ijkl}(\sigma_{kl}^{*'} - X_{kl}^{*'})}{\sqrt{\frac{3}{2}(\sigma_{mn}^{*'} - X_{mn}^{*'})M_{mnuv}(\sigma_{uv}^{*'} - X_{uv}^{*'})}} \tag{3.6}$$

with

$$\dot{p}^{*} = \sqrt{\tfrac{2}{3}\dot{\varepsilon}_{ij}^{*p} M_{ijkl}^{-1} \dot{\varepsilon}_{kl}^{*p}} = \left\langle \frac{f}{K} \right\rangle^{n} \tag{3.7}$$

which is the accumulated inelastic strain rate.

The evolutionary equation for the back stress, which describes non-linear kinematic hardening, is modified to the form:

$$\dot{X}_{ij}^{*} = \tfrac{3}{2} N_{ijkl} \dot{\varepsilon}_{kl}^{*in} - Q_{ijkl} X_{kl}^{*} \dot{p}^{*} \tag{3.8}$$

where two additional anisotropic material tensors, N_{ijkl} and Q_{ijkl}, are introduced to describe the anisotropic hardening induced by microstructural anisotropy.

The evolution of isotropic hardening is given by

$$\dot{R} = b(W - R)\dot{p}^{*} \tag{3.9}$$

where b and W are two material constants used to describe deformation induced isotropic material hardening.

The above constitutive equations (3.1) to (3.9) are only applied to the case when stress directions are coincide with single crystal symmetry axes, i.e. [100]-[010]-[001], Fig.3.1. For arbitrary general loading conditions, the constitutive equations can be modified by stress and strain transformations.

Using the Voigt vectorial notation for the strain and stress tensors, they can be written as:

$$[\sigma]^{t} = [\sigma_1 = \sigma_{11}, \sigma_2 = \sigma_{22}, \sigma_3 = \sigma_{33}, \sigma_4 = \sigma_{23}, \sigma_5 = \sigma_{31}, \sigma_6 = \sigma_{12}] \tag{3.10a}$$

$$[\varepsilon]^{t} = [\varepsilon_1 = \varepsilon_{11}, \varepsilon_2 = \varepsilon_{22}, \varepsilon_3 = \varepsilon_{33}, \varepsilon_4 = \varepsilon_{23}, \varepsilon_5 = \varepsilon_{31}, \varepsilon_6 = \varepsilon_{12}] \tag{3.10b}$$

The stress and strain transformation from the global loading to the crystal axes, Fig.3.1, can be written as:

$$[\sigma_i^*]_{crystal} = A_{ij}[\sigma_j]_{loading} \tag{3.10c}$$

$$[\varepsilon_i^*]_{crystal} = B_{ij}[\varepsilon_j]_{loading} \tag{3.10d}$$

where A_{ij} and B_{ij} are transformation matrices (see Appendix II), which can be expressed as a function of the crystal orientation direction, [hkl], associated with one of the co-ordinate axes of the stress tensor in a general loading condition.

Using the Voigt notation and the transformation from the loading to the crystal axes, the general constitutive equation based on the phenomenological model, for a single crystal nickel base superalloy, can be summarised as follows:

Total strain rate: $$\dot{\varepsilon}_i = \dot{\varepsilon}_i^e + \dot{\varepsilon}_i^{in} \tag{3.11a}$$

Elastic strain rate: $$\dot{\varepsilon}_e = B_{ij}^{-1} S_{jk} A_{kl} \dot{\sigma}_l \tag{3.11b}$$

Anisotropic yielding: $$f = \sqrt{\tfrac{3}{2}(\sigma_i' - X_i')^t A_{ij}^t M_{jk} A_{kl} (\sigma_l' - X_l')} - R - k = 0 \tag{3.11c}$$

Inelastic strain rate: $$\dot{\varepsilon}_i^{in} = \frac{\partial \Omega}{\partial \sigma_i} = \frac{3}{2}\left\langle \frac{f}{K^*} \right\rangle^n \frac{B_{ij}^{-1} M_{jl} A_{lk} (\sigma_k' - X_k')}{\sqrt{\tfrac{3}{2}(\sigma_i' - X_i')^t A_{ij}^t M_{jk} A_{kl} (\sigma_l' - X_l')}} \tag{3.11d}$$

Kinematic hardening: $$\dot{X}_i = \left(\tfrac{3}{2} A_{ij}^{-1} N_{jk} B_{kl} \dot{\varepsilon}_l^{in}\right) - \left(A_{ij}^{-1} Q_{jk} A_{kl} X_l \dot{p}\right) \tag{3.11e}$$

Isotropic hardening: $$\dot{R} = b\,(W - R)\,\dot{p} \tag{3.11f}$$

Accumulated inelastic strain rate: $$\dot{p} = \sqrt{\tfrac{2}{3}(\dot{\varepsilon}_i^{in})^t B_{ij}^t M_{jk}^{-1} B_{kl} \dot{\varepsilon}_l^{in}} \tag{3.11g}$$

where A_{ij}^{-1}, B_{ij}^{-1} and A_{ij}^t, B_{ij}^t represent the inverse and transposed matrices of A_{ij} and B_{ij} respectively.

There are total of 11 viscoplastic material constants in the model. Five constants, k, K*, n, W and b are similar to those included in the isotropic model developed by Chaboche, to describe the time dependent viscoplastic behaviour. The other six constants are from the matrices M_{ij}, N_{ij} and Q_{ij}. The anisotropic behaviour of a single crystal is described by the introduction of the three anisotropic material tensors M_{ij}, N_{ij} and Q_{ij}, and the three tensors, M_{ij}, N_{ij} and Q_{ij} are reduced to the identity matrix in the case of isotropy. If it is assumed that cubic symmetry is retained for the inelastic properties for a nickel base single crystal superalloy and assuming inelastic strain incompressibility (Richmond and Spitzig [1980]), the anisotropic material tensors can be expressed in the general form (Li, [1993]):

$$[]_{ij} = \begin{bmatrix} []_{11}-[]_{12} & 0 & 0 & 0 & 0 & 0 \\ 0 & []_{11}-[]_{12} & 0 & 0 & 0 & 0 \\ 0 & 0 & []_{11}-[]_{12} & 0 & 0 & 0 \\ 0 & 0 & 0 & []_{44} & 0 & 0 \\ 0 & 0 & 0 & 0 & []_{44} & 0 \\ 0 & 0 & 0 & 0 & 0 & []_{44} \end{bmatrix} \tag{3.12}$$

where [] can be replaced by M, N or Q respectively. Because the term $[]_{11}-[]_{12}$ can be treated as a single constant there are only 2 constants for each of matrices M, N and Q. these are the simple formulations for the M, N and Q matrices, which can describe the fundamental anisotropic deformation behaviour of single crystal alloys. For more complex deformation response, such as deformation induced anisotropy, the formulation of the matrices will be more sophisticated .

Therefore generally for this phenomenological approach there are 7 variables, $\varepsilon^T, \varepsilon^e, \varepsilon^{in}, \sigma$, X, R and p used with 14 associated material constants including 3 elastic constants, E, ν and G.

3.2.2. Crystallographic Model

The anisotropic viscoplastic crystallographic models for single crystal alloys are developed from the classical time-independent crystal plasticity theory. In a typical

crystallographic model the constitutive equations are established at two levels, i.e. macroscopic and microscopic levels.

At the macroscopic level, the model is also a unified model with the total strain rate decomposed into a elastic and an inelastic strain rates as phenomenological model:

$$\dot{\varepsilon}_{ij}^{*T} = \dot{\varepsilon}_{ij}^{*e} + \dot{\varepsilon}_{ij}^{*in} \tag{3.13}$$

The elastic strain rate is expressed at the macroscopic level which is identical to the phenomenological model,

$$\dot{\varepsilon}_{ij}^{*e} = S_{ijkl}\dot{\sigma}_{kl}^{*} \tag{3.14}$$

At the microscopic level, the model follows the general time-independent crystal plasticity theory. The overall inelastic strain is assumed to be the summation of the inelastic shear strain on a number of active slip systems.

Although there are 30 possible slip systems for nickel base single crystal superalloys, 18 slip systems are only generally considered in a crystallographic model. This was bsed on the experimental observations reviewed in section 2.4.7 in Chapter 2. These include 12 octahedral [110]{111} and 6 cubic [110]{001}, Fig.3.2. Slip in the [112]{111} slip system only occurs at some particular temperature and loading conditions and has insignificant effect on most of the cases (Stouffer et al [1990], Meric et al [1991], Jordan and Walker [1992]).

The macroscopic inelastic strain rate is calculated through three steps to connect the macroscopic and microscopic levels of the constitutive equations. For a general loading case, the applied stress, σ_{ij}, in the global coordinate system is transformed into crystallographic coordinate system, σ_{ij}^{*}, using equation (3.10c), similar to the phenomenological model.

The first step for the crystallographic model is then to resolve the macroscopic stress, σ_{ij}^{*}, into the resolved shear stress (RSS), τ^{s}, at each slip system using Schmid's law:

$$\tau^{s} = \sigma_{ij}^{*} m_{ij}^{s} \tag{3.15a}$$

with

$$m_{ij}^s = \frac{1}{2}(n_i^s l_j^s + n_j^s l_i^s) \quad (i,j = 1,2,3;\ s=1,2,3.....18) \qquad (3.15b)$$

where n_i^s and l_i^s are the slip plane normal vector and slip direction vector respectively, each associated with the s slip system. The formulation of matrix m_{ij}^s related to the 18 slip systems is given in Appendix III.

The second step is to develop constitutive equations for different slip systems. One approach is to use the equations which are generally identical to those used in the phenomenological model. In this crystallographic model the constitutive equations at the microscopic level have the same formulation as the Chaboche isotropic model [1989].

The yield criteria for octahedral and cubic slip systems are:

$$f_o^s = \left|\tau_o^s - x_o^s\right| - k_o - r_o^s \le 0 \qquad (s=1,2,3 \ldots 12) \qquad (3.16a)$$

$$f_c^s = \left|\tau_c^s - x_c^s\right| - k_c - r_c^s \le 0 \qquad (s=13,14 \ldots 18) \qquad (3.16b)$$

where x^s and r^s are kinematic hardening and isotropic hardening variable respectively associated with each slip plane, and k_o and k_c are the initial critical resolved shear stresses (CRSS) for octahedral and cubic slip systems respectively.

Using the approach as for the Chaboche [1989] model, the constitutive equations at the microscopic level describe the relationship between the inelastic shear strain rate, and the resolved shear stress, for the octahedral and cubic slip systems. The inelastic shear strain rates on the two slip systems are given by:

$$\dot{\gamma}_o^s = \left\langle \frac{\left|\tau_o^s - x_o^s\right| - k_o - r_o^s}{K_o} \right\rangle^{n_o} \operatorname{sign}(\tau_o^s - x_o^s) \qquad (s=1,2,3 \ldots\ldots 12) \qquad (3.17a)$$

$$\dot{\gamma}_c^s = \left\langle \frac{\left|\tau_c^s - x_c^s\right| - k_c - r_c^s}{K_c} \right\rangle^{n_c} \operatorname{sign}(\tau_c^s - x_c^s) \qquad (s=13,14 \ldots\ldots 18) \qquad (3.17b)$$

where the bracket $\langle\ \rangle$ is defined as: $\langle x\rangle = x$ if $x > 0, \langle x\rangle = 0$ if $x \le 0$.

The rate of kinematic hardening variable is:

$$\dot{x}_o^s = c_o \dot{\gamma}_o^s - d_o x_o^s \left|\dot{\gamma}_o^s\right| \qquad (s=1,2,3 \ldots\ldots 12) \qquad (3.18a)$$

$$\dot{x}_c^s = c_c \dot{\gamma}_c^s - d_c x_c^s \left|\dot{\gamma}_c^s\right| \qquad (s=13,14 \ldots\ldots 18) \qquad (3.18b)$$

The rate of isotropic hardening is:

$$\dot{r}_o^s = (q_o - b_o r_o^s)\left|\dot{\gamma}_o^s\right| \qquad (s=1,2,3 \ldots\ldots 12) \qquad (3.19a)$$

$$\dot{r}_c^s = (q_c - b_c r_c^s)\left|\dot{\gamma}_c^s\right| \qquad (s=13,14 \ldots\ldots 18) \qquad (3.19b)$$

The third step sums up the individual viscoplastic shear strain rates, $\dot{\gamma}^s$, for each of the slip systems to obtain the overall macroscopic viscoplastic strain rate, $\dot{\varepsilon}_{ij}^{*in}$, in the crystallographic coordinate system.

$$\dot{\varepsilon}_{ij}^{*in} = \sum_{s=1}^{12} m_{ij}^s \dot{\gamma}_o^s + \sum_{s=13}^{18} m_{ij}^s \dot{\gamma}_c^s \qquad (3.20)$$

Finally, the viscoplastic strain rate, $\dot{\varepsilon}_{ij}^{*in}$, in the crystallographic coordinate system is transformed into the global coordinate system using the reverse of equation (3.10d).

There are a total of 14 material constants, k_o, K_o, n_o, c_o, d_o, q_o and b_o for the octahedral slip system, and k_c, K_c, n_c, c_c, d_c, q_c and b_c for the cubic slip system, respectively.

Similar to the phenomenological model, equations (3.13) to (3.20) are only applied to crystallographic coordinate systems. For arbitrary loading conditions, the constitutive equations are modified with introducing the Voigt notation and using the stress and strain transformations in the same way as for the phenomenological model.

3.3 Formulation of Nonisothermal Constitutive Models

The thermomechanical constitutive equations for single crystal superalloys are developed by modification of the isothermal constitutive equations presented in section 3.2 using an implicit approach.

For a general thermomechanical loading condition, the components of the total strains ε_i^T (and the corresponding rates, $\dot{\varepsilon}_i^T$) are decomposed into three parts: elastic strains ε_i^e, inelastic strains ε_i^{in} and thermal strains ε_i^{th}:

$$\varepsilon_i^T = \varepsilon_i^e + \varepsilon_i^{in} + \varepsilon_i^{th} \tag{3.21}$$

In the material principal axes (i.e. [100]-[010]-[001]), the thermal strains are expressed as:

$$\dot{\varepsilon}_i^{th} = \alpha_i (T - T_o) \tag{3.22}$$

with $$\alpha_i = \begin{cases} \alpha(T) & \text{when } i = 1,2,3 \\ 0 & \text{when } i = 4,5,6 \end{cases}$$

and i=1,2,3 correspond to the direct (tensor diagonal) strains and i=4,5,6 correspond to shear strains. There are no shear thermal strains, since the three material principal axes have same material properties, i.e. thermal deformations in [100], [010] and [001] are the same.

In the implicit approach, temperature, T, is only included explicitly in the thermal strain equation. The influence of temperature on the elastic and inelastic deformation is modelled implicitly by including temperature in the constitutive equations through the temperature dependent material constants. Temperature rates have also been introduced in the thermal and elastic strain rate equations by differentiating the corresponding strain equations with temperature. Following this approach, the thermomechanical constitutive equations of the phenomenological model can be summarised as follows:

Total strain rate: $$\dot{\varepsilon}^{T}_{i\,i} = \dot{\varepsilon}^{e}_{i} + \dot{\varepsilon}^{in}_{i} + \dot{\varepsilon}^{th}_{i} \qquad (3.23a)$$

Elastic strain rate: $$\dot{\varepsilon}_{e} = B^{-1}_{ij}\, S_{jk}(T)\, A_{kl}\, \dot{\sigma}_{l} + \frac{\partial (B^{-1}_{ij}\, S_{jk}(T)\, A_{kl})}{\partial T}\, \dot{T}\, \sigma \qquad (3.23b)$$

Thermal strain rate: $$\dot{\varepsilon}^{th}_{i} = B^{-1}_{ij}\left[\frac{d\alpha_{j}(T)}{dT}(T - T_{o}) + \alpha_{j}(T)\right]\dot{T} \qquad (3.23c)$$

Inelastic strain rate: $$\dot{\varepsilon}^{in}_{i} = \frac{3}{2}\left(\frac{f}{K^{*}(T)}\right)^{n(T)} \frac{B^{-1}_{ij}\, M_{jl}(T)\, A_{lk}\,(\sigma'_{k} - X'_{k})}{\sqrt{\frac{3}{2}(\sigma'_{i} - X'_{i})^{t}\, A^{t}_{ij} M_{jk}(T)\, A_{kl}(\sigma'_{l} - X'_{l})}} \qquad (3.23d)$$

with temperature dependent yielding:

$$f = \sqrt{\frac{3}{2}(\sigma'_{i} - X'_{i})^{t} A^{t}_{ij} M_{jk}(T) A_{kl}(\sigma'_{l} - X'_{l})} \; - R(T) - k(T) = 0 \qquad (3.23e)$$

Kinematic hardening:

$$\dot{X}_{i} = \tfrac{3}{2} A^{-1}_{ij} N_{jk}(T) B_{kl}\, \dot{\varepsilon}^{in}_{l} - A^{-1}_{ij} Q_{jk} A_{kl}(T)\, X_{l}\, \dot{p} \qquad (3.23f)$$

Isotropic hardening: $$\dot{R} = b(T)\,(W(T) - R)\,\dot{p} \qquad (3.23g)$$

Accumulated inelastic strain rate: $$\dot{p} = \sqrt{\tfrac{2}{3}(\dot{\varepsilon}^{in}_{i})^{t} B^{t}_{ij} M^{-1}_{jk}(T) B_{kl} \dot{\varepsilon}^{in}_{l}} \qquad (3.23h)$$

where A_{ij} and B_{ij} , A^{-1}_{ij}, B^{-1}_{ij} and A^{t}_{ij}, B^{t}_{ij} are defined in section 3.2.1.

The material parameters, k (T), K*(T), n(T), W(T) , b(T) and the anisotropic material tensors $M_{ij}(T)$, $N_{ij}(T)$ and $Q_{ij}(T)$ are defined similar to those in the isothermal model, but now they are temperature dependent parameters rather than material constants.

A similar procedure is applied for the crystallographic model to modify the isothermal constitutive equations to describe thermomechanical deformation of single crystal superalloys.

3.4 Determination of Material Elastic Constants

3.4.1 Analytical Procedure

Nickel base single crystal superalloys have a cubic structure. Only three elastic constants are required to define its elastic response. The elastic stress strain relationship for the single crystal in the main symmetry axes, i.e. [100]-[010]-[100] is:

$$\begin{bmatrix} \varepsilon_{11} \\ \varepsilon_{22} \\ \varepsilon_{33} \\ \varepsilon_{23} \\ \varepsilon_{31} \\ \varepsilon_{12} \end{bmatrix} = \begin{bmatrix} S_{11} & S_{12} & S_{12} & 0 & 0 & 0 \\ S_{12} & S_{11} & S_{12} & 0 & 0 & 0 \\ S_{12} & S_{12} & S_{11} & 0 & 0 & 0 \\ 0 & 0 & 0 & S_{44} & 0 & 0 \\ 0 & 0 & 0 & 0 & S_{44} & 0 \\ 0 & 0 & 0 & 0 & 0 & S_{44} \end{bmatrix} \begin{bmatrix} \sigma_{11} \\ \sigma_{22} \\ \sigma_{33} \\ \sigma_{23} \\ \sigma_{31} \\ \sigma_{12} \end{bmatrix}$$

with $S_{11} = \frac{1}{E_{[001]}}$, $S_{12} = -\frac{\upsilon_{[001]}}{E_{[001]}}$, $S_{11} = \frac{1}{G_{[001]}}$

where $E_{[001]}$, $\nu_{[001]}$ and $G_{[001]}$ are the Young's modulus, Poisson's ratio and shear modulus respectively when the loading is coincident with the [001] direction.

There are a number of methods commonly used to obtain the elastic constants, such as the sonic resonance technique, dynamic measurement and mechanical testing. For polycrystalline isotropic materials, Young's modulus E, shear modulus G and Poisson's ratio ν are not independent, and measurement of any two of them is enough to determine the elastic behaviour. The Young's modulus E and shear modulus can be directly calculated from the flexural and torsional resonant frequencies measured from the sonic resonance technique. For mechanical testing, one axial and one diametrical strain measurement can determine E and ν. Alternatively, E and G can be determined by uniaxial loading and simple torsion tests. However, for single crystal superalloys, the three elastic constants $E_{[001]}$, $\nu_{[001]}$ and $G_{[001]}$ are independent. Therefore, the sonic resonance technique cannot determine all the three constants. Also the simple torsion

test can not be used for single crystal alloy to determine the shear modulus due to the anisotropic shear response around the circumference of the torsion specimen.

Consequently, measurement of the three elastic parameters of single crystal superalloys is relatively difficult compared with polycrystalline materials. A simple method to determine the three elastic constants has been proposed in this work through some theoretical analysis and only requires simple mechanical testing.

For loading in any orientation [l, m, n], the elastic strains can be expressed through stress and strain transformation matrices A_{ij} and B_{ij} described in Section 3.2 as:

$$\varepsilon_i^c = B_{ij}^{-1} S_{jk} A_{kl} \sigma_l \qquad (3.24a)$$

To investigate the anisotropic transverse elastic response around the circumference of the specimen, a transformation Q_{ij} from the global coordinate system X-Y-Z to the coordinate system rotated around Z axis is applied to the above equation:

$$\varepsilon'^c_i = Q_{ij} B^{-1}_{jk} S_{kl} A_{lp} \sigma_p \qquad (3.24b)$$

with the transformation matrix Q_{ij} as a function of rotation angle θ given by:

$$Q_{ij} = \begin{bmatrix} \cos^2\theta & \sin^2\theta & 0 & 0 & 0 & 2\sin\theta\cos\theta \\ \sin^2\theta & \cos^2\theta & 0 & 0 & 0 & -2\sin\theta\cos\theta \\ 0 & 0 & 1 & 0 & 0 & 0 \\ 0 & 0 & 0 & \cos\theta & -\sin\theta & 0 \\ 0 & 0 & 0 & \sin\theta & \cos\theta & 0 \\ -\sin\theta\cos\theta & \sin\theta\cos\theta & 0 & 0 & 0 & (\cos^2\theta - \sin^2\theta) \end{bmatrix} \qquad (3.24c)$$

So for uniaxial loading along [l, m, n], the mathematical expression for the local transverse strain, ε_{22}, as a function of orientation [l, m, n] and measurement angle, θ, given by:

$$\frac{\varepsilon_{22}(l,m,n,\theta)}{\sigma} = 2W(l,m,n,\theta)(S_{11} - 2S_{44}) + M(l,m,n,\theta)S_{12} \qquad (3.25a)$$

and the longitudinal strain, ε_{33}, along the loading direction is only a function of orientation [l,m,n]:

$$\frac{\varepsilon_{33}}{\sigma} = S_{11} - [2(S_{11} - S_{12}) - S_{44}]A(l,m,n) \qquad (3.25b)$$

The coefficients W, M, A and B are given by:

$$W(l,m,n,\theta) = B(l,m,n)[l^2(m^4 + m^2n^2 + n^4)\cos^2\theta + m^2n^2(l^2 + m^2 + n^2)\sin^2\theta - lmn(m^2 - n^2)\sqrt{l^2 + m^2 + n^2}\sin\theta\cos\theta]$$

$$M(l,m,n,\theta) = B(l,m,n)\{ (m^2 + n^2)^2 + l^2(l^2m^2 + 2m^2n^2 + l^2n^2)\cos^2\theta + (l^2 + m^2 + n^2)[(l^2 + n^2) + m^2(l^2 + m^2)]\sin^2\theta + 2lmn\sqrt{l^2 + m^2 + n^2}(m^2 - n^2)\sin\theta\cos\theta \}$$

$$A(l,m,n) = \frac{l^2m^2 + m^2n^2 + l^2n^2}{(l^2 + m^2 + n^2)^2}$$

$$B(l,m,n) = \frac{1}{(l^2 + m^2 + n^2)^2(l^2 + m^2)}$$

To solve the unknown values S_{11}, S_{12} and S_{44} three equations, i.e. equation (3.25a) and equation (3.25b) with different angles θ_1 and θ_2 are required. The loading orientation [l,m,n] can be any direction except orientations [001] and [111] because in these two orientations the transverse strains, $\varepsilon_{22}^c(l,m,n,\theta)$, are the same or uniform, which means there are only two equations for three unknown values.

3.4.2 Experimental Determination

In principle, the proposed method for determination of single crystal elastic constants presented in above section only requires one specimen to determine the elastic properties, i.e. uniaxial loading in [l,m,n] oriented specimen. The measurements for local axial and transverse strains are needed.

Local axial and transverse strain measurements can be made using a combination of axial and diametrical extensometers (Li, Han and Smith [1996]). Fig.3.2a shows the schematic of the testing set up. The local transverse strain measurements have been made at 15-degree increments by rotating the diameter extensometer around the main axis of the cylindrical specimen. Measurements were conducted for nickel base single crystal alloys SRR99 and SC16 to determine the temperature dependent elastic constants. The measurement results were then analysed using the method given in section 3.4.1. Fig.3.2b presents a comparison between measurement and calculation results for SRR99 at 450°C, 750°C, 850°C and 950°C. Similar comparisons, though not shown here, were also made for SC16 at different temperatures. A good agreement between the experimental and calculation results were obtained for all the temperatures. The calculated elastic constants for SRR99 at various temperatures are given in Table 3.1. It can be seen that both Young's modulus, E, and shear modulus, G, decrease with temperature, whilst Poisson ratio υ increases with temperature.

Since measurement of the elastic constants for single crystal alloys is relatively difficult compared with polycrystalline materials there are very limited data published including all the three elastic constants.

For single crystal alloy SC16, measurement of Young's modulus, E, at different temperatures has been performed using tensile tests, as well as using dynamic measurement (Toulios [1993]). These results are shown in Fig.3.2c and compared with the data obtained from this study. It can be seen that there is a general agreement between the results although the Young's modulus obtained from dynamic measurements is higher than those from static measurements. The results also indicate that there is an abrupt change of Young's modulus in the temperature range from 600°C to 750°C, which is in agreement of the results obtained for SRR99 single crystal alloy.

3.5 Determination of Inelastic Material Constants

3.5.1 Identification of Deformation Characteristics

The phenomenological and crystallographic models include a large number of material constants. These constants must be determined from simple mechanical tests. Theoretical analyses have been carried out to determine the deformation responses predicted by the phenomenological and crystallographic models under various simple loading conditions. Uniaxial mechanical tests using specimens with [001] and [111] orientations identified as the most simple tests which meet the requirements for determining the basic material properties.

(i) Phenomenological Model

The equations for uniaxial loading in the [001] and [111] orientations are derived from the general constitutive equations, and expressed as follows.

For uniaxial loading in the [001] direction, as shown in Fig.3.1.(1b), with the loading σ_3 applied along direction 3, the complete equations are:

$$\dot{\varepsilon}_3^{in} = \left\langle \frac{\left|\sigma_3 - \frac{3}{2}X_3\right|\sqrt{M_{11}-M_{12}} - R - k}{K^*} \right\rangle^n \sqrt{M_{11}-M_{12}}\,\mathrm{sign}(\sigma_3 - \tfrac{3}{2}X_3) \quad (3.26a)$$

$$\dot{\varepsilon}_1^{in} = \dot{\varepsilon}_2^{in} = -\tfrac{1}{2}\dot{\varepsilon}_3^{in}; \qquad \dot{\varepsilon}_4^{in} = \dot{\varepsilon}_5^{in} = \dot{\varepsilon}_6^{in} = 0 \quad (3.26b)$$

$$\dot{X}_3 = \tfrac{2}{3}(N_{11}-N_{12})\dot{\varepsilon}_3^{in} - (Q_{11}-Q_{12})\,X_3\,\dot{p} \quad (3.26c)$$

$$\dot{X}_1 = \dot{X}_2 = -\tfrac{1}{2}\dot{X}_3; \qquad \dot{X}_4 = \dot{X}_5 = \dot{X}_6 = 0 \quad (3.26d)$$

$$\dot{p} = \frac{\left|\dot{\varepsilon}_3^{in}\right|}{\sqrt{M_{11}-M_{12}}} \quad (3.26e)$$

$$\dot{R} = b(W-R)\,\dot{p} = b\,(W-R)\,\frac{\left|\dot{\varepsilon}_3^{in}\right|}{\sqrt{M_{11}-M_{12}}} \quad (3.26f)$$

For uniaxial loading in the [111] direction, as shown in Fig.3.1c with loading applied along direction 3, the complete equations are:

$$\dot{\varepsilon}_3^{in} = \left\langle \frac{\left|\sigma_3 - \frac{3}{2}X_3\right|\sqrt{M_{44}/2} - R - k}{K^*} \right\rangle^n \sqrt{M_{44}/2}\,\mathrm{sign}(\sigma_3 - \tfrac{3}{2}X_3) \qquad (3.27a)$$

$$\dot{\varepsilon}_1^{in} = \dot{\varepsilon}_2^{in} = -\tfrac{1}{2}\dot{\varepsilon}_3^{in}; \qquad \dot{\varepsilon}_4^{in} = \dot{\varepsilon}_5^{in} = \dot{\varepsilon}_6^{in} = 0 \qquad (3.27b)$$

$$\dot{X}_3 = \tfrac{4}{3}N_{44}\dot{\varepsilon}_3^{in} - Q_{44}X_3\dot{p} \qquad (3.27c)$$

$$\dot{X}_1 = \dot{X}_2 = -\tfrac{1}{2}\dot{X}_3; \qquad \dot{X}_4 = \dot{X}_5 = \dot{X}_6 = 0 \qquad (3.27d)$$

$$\dot{p} = \frac{\left|\dot{\varepsilon}_3^{in}\right|}{\sqrt{M_{44}/2}} \qquad (3.27e)$$

$$\dot{R} = b(W-R)\dot{p} = b\,(W-R)\,\frac{\left|\dot{\varepsilon}_3^{in}\right|}{\sqrt{M_{44}/2}} \qquad (3.27f)$$

It can be seen that for these two special orientations, i.e. [001] and [111], the transverse strains ($\dot{\varepsilon}_1^{in}$ and $\dot{\varepsilon}_2^{in}$) are equal and the loading does not produce any shear deformation ($\dot{\varepsilon}_4^{in} = \dot{\varepsilon}_5^{in} = \dot{\varepsilon}_6^{in} = 0$). This indicates that the overall deformation behaviour of the single crystal under uniaxial loading in either the [001] or the [111] orientation exhibits isotropic response.

Another interesting observation from equations (3.26) and (3.27) is that the material parameters $(M_{11}-M_{12})$, $(N_{11}-N_{12})$ and $(Q_{11}-Q_{12})$ are completely uncoupled from M_{44}, N_{44} and Q_{44} for these two crystal orientations. Therefore tests in the [001] and [111] orientations are sufficient to determine fully all the material constants in the phenomenological model.

(ii). Crystallographic Model

For the crystallographic model, derivation of the constitutive equations for uniaxial loading is more difficult compared with the phenomenological model. A brief description of the derivation is given in the following sections.

For uniaxial loading in the [001] direction, as shown in Figure 3.1.(1b), the loading stress is σ_3. To obtain the resolved shear stress τ^s on each of the 18 possible slip systems the stress transformation, described by equation (3.10), and Schmid's law is used. It is found that there are only 8 octahedral slip systems with non-zero resolved shear stresses. The shear stresses on the other 4 octahedral slip systems and all the 6 cubic slip systems are zero. Furthermore, the magnitude of the resolved shear stresses on the 8 octahedral slip systems are the same, and is:

$$\tau_o = \frac{1}{\sqrt{6}}\sigma_3 \tag{3.28}$$

From equation (3.17), it can be seen that the shear strain rate on each slip system is proportional to the resolved shear stress on that slip system. Therefore the inelastic shear strain rates on the 8 octahedral slip systems also have the same magnitude. To obtain the total inelastic strain rate in the crystallographic coordinate system all the inelastic shear strain rates on the 8 octahedral slip systems are summed. This summed strain is then transformed to the global coordinate system. The constitutive equations for uniaxial loading in the [001] orientation can be expressed as:

$$\dot{\varepsilon}_3^{in} = \frac{8}{\sqrt{6}} \left\langle \frac{\left|\frac{1}{\sqrt{6}}\sigma_3 - x_o^3\right| - k_o - r_o^3}{K_o} \right\rangle^{n_o} \operatorname{sign}\left(\frac{1}{\sqrt{6}}\sigma_3 - x_o^3\right) \tag{3.29a}$$

$$\dot{\varepsilon}_1^{in} = \dot{\varepsilon}_2^{in} = -\tfrac{1}{2}\,\dot{\varepsilon}_3^{in}; \qquad \dot{\varepsilon}_4^{in} = \dot{\varepsilon}_5^{in} = \dot{\varepsilon}_6^{in} = 0 \tag{3.29b}$$

$$\dot{x}_o^3 = c_o \frac{\sqrt{6}}{8}\dot{\varepsilon}_3^{in} - d_o\, x_o^3 \frac{\sqrt{6}}{8}\left|\dot{\varepsilon}_3^{in}\right| \tag{3.29c}$$

$$\dot{r}_o^3 = \frac{\sqrt{6}}{8}(q_o - b_o\, r_o^3)\ \left|\dot{\varepsilon}_3^{in}\right| \tag{3.29d}$$

Where x_o^3, and r_o^3 donate to the back stress and isotropic hardening parameter in the third octahedral slip system.

For uniaxial loading in the [111] orientation, as shown in Fig.3.1c, the loading stress is again σ_3. Since loading is not in the crystallographic coordinate system, the loading stress is transformed into crystallographic coordinate system. The transformed stress in crystallographic model is:

$$\sigma_1^* = \sigma_2^* = \sigma_3^* = \sigma_4^* = \sigma_5^* = \sigma_6^* = \frac{1}{3}\sigma_3 \tag{3.30}$$

Using Schmid's law it is found that there are 3 cubic slip systems, as well as 8 octahedral slip systems, with non-zero resolved shear stresses. The magnitude of the resolved shear stresses on the 3 cubic slip systems are the same, and the magnitude of the resolved shear stresses on the 8 octahedral slip systems are also the same. These stresses are:

$$\tau^1 = \tau^2 = \tau^3 = \tau^4 = \tau^8 = \tau^{12} = 0$$
$$\tau^5 = \tau^9 = \tau^{10} = -\tau_o\,,\ \tau^6 = \tau^7 = \tau^{11} = \tau_o$$
$$\tau^{14} = \tau^{16} = \tau^{18} = 0\,,\ \tau^{13} = \tau^{15} = \tau^{17} = \tau_c$$

with
$$\tau_o = \frac{\sqrt{6}}{9}\sigma_3; \qquad \tau_c = \frac{\sqrt{2}}{3}\sigma_3 \tag{3.31}$$

It can be seen that cubic shear stress, τ_c, is $\sqrt{3}$ times higher than the octahedral shear stress, τ_o. Therefore at low strains, the inelastic deformation is dominated by the cubic slip systems, and the octahedral slip systems may be not active due to the low resolved shear stress on these slip planes. However, when the shear stresses on the octahedral slip systems increase and reach the critical resolved shear stress, the octahedral slip systems become active and also produce inelastic deformation.

Since the shear strain rate on each slip system is proportional to the resolved shear stress on that slip system, the shear strain rates on the 8 octahedral slip systems, and those on the 3 cubic slip systems, have the same magnitude respectively. Summing up all the inelastic shear strain rates on the octahedral and cubic slip systems to obtain the

total inelastic strain rate in the crystallographic coordinate system using equation (3.20) gives:

$$(\dot{\varepsilon}_{ij}^{*in}) = \sum_{s=1}^{18}(m_{ij}^{s}\dot{\gamma}^{s}) = \sum_{s=1}^{12}(m_{ij}^{s}\dot{\gamma}_{o}^{s}) + \sum_{s=13}^{18}(m_{ij}^{s}\dot{\gamma}_{c}^{s}) = (\dot{\varepsilon}_{ijo}^{*in}) + (\dot{\varepsilon}_{ijc}^{*in}) \qquad (3.32a)$$

The total inelastic strain rate in the global coordinate system can be obtained by the strain transformation described by equation (3.10d), and expressed as:

$$\dot{\varepsilon}_{ij}^{in} = \dot{\varepsilon}_{ijo}^{in} + \dot{\varepsilon}_{ijc}^{in} \qquad (3.32b)$$

The inelastic strain rate contributed by octahedral slip and by cubic slip can be derived from equations (3.15) to (3.19). Using the Voigt notation given in (3.10a) and (3.10b), the constitutive equations associated with octahedral and cubic deformation can be expressed in the following.

Octahedral inelastic strain rate:

$$(\dot{\varepsilon}_{3}^{in})_o = \frac{2\sqrt{6}}{3}\left\langle \frac{\left|\frac{\sqrt{6}}{9}\sigma_3 - x_o\right| - k_o - r_o}{K_o} \right\rangle^{n_o} \operatorname{sign}\left(\frac{\sqrt{6}}{9}\sigma_3 - x_o\right) \qquad (3.33a)$$

$$(\dot{\varepsilon}_{1}^{in})_o = (\dot{\varepsilon}_{2}^{in})_o = -\tfrac{1}{2}(\dot{\varepsilon}_{3}^{in})_o; \qquad (\dot{\varepsilon}_{4}^{in})_o = (\dot{\varepsilon}_{5}^{in})_o = (\dot{\varepsilon}_{6}^{in})_o = 0 \qquad (3.33b)$$

$$\dot{x}_o = \frac{\sqrt{6}}{4}c_o\,(\dot{\varepsilon}_{1}^{in})_o - \frac{\sqrt{6}}{4}d_o\,x_o\left|(\dot{\varepsilon}_{3}^{in})_o\right| \qquad (3.33c)$$

$$\dot{r}_o = \frac{\sqrt{6}}{4}(q_o - b_o\,r_o)\ \left|(\dot{\varepsilon}_{3}^{in})_o\right| \qquad (3.33d)$$

Cubic inelastic strain rate:

$$(\dot{\varepsilon}_3^{in})_c = \sqrt{2}\left\langle \frac{\left|\frac{\sqrt{2}}{3}\sigma_3 - x_c\right| - k_c - r_c}{K_c} \right\rangle^{n_c} \text{sign}\left(\frac{\sqrt{2}}{3}\sigma_3 - x_c\right) \qquad (3.34a)$$

$$(\dot{\varepsilon}_1^{in})_c = (\dot{\varepsilon}_2^{in})_c = -\tfrac{1}{2}(\dot{\varepsilon}_3^{in})_c; \qquad (\dot{\varepsilon}_4^{in})_c = (\dot{\varepsilon}_5^{in})_c = (\dot{\varepsilon}_6^{in})_c = 0 \qquad (3.34b)$$

$$\dot{x}_c = \frac{\sqrt{2}}{2} c_c (\dot{\varepsilon}_3^{in})_c - \frac{\sqrt{2}}{2} d_c x_c \left|(\dot{\varepsilon}_3^{in})_c\right| \qquad (3.34c)$$

$$\dot{r}_c = \frac{\sqrt{2}}{2}(q_c - b_c r_c) \left|(\dot{\varepsilon}_3^{in})_c\right| \qquad (3.34d)$$

The total inelastic strain rate in the loading direction along the [111] orientation can be written as:

$$\dot{\varepsilon}_3^{in} = (\dot{\varepsilon}_3^{in})_o + (\dot{\varepsilon}_3^{in})_c \qquad (3.35)$$

It can be seen that the inelastic strain deformation caused by the octahedral and cubic slip systems exhibit isotropic characteristics. Consequently, the overall inelastic strain response under uniaxial loading in the [111] orientation will also be isotropic.

Similar to the phenomenological model, the crystallographic model predicts isotropic deformation characteristics under uniaxial loading along the [001] and [111] orientations. Anisotropic deformation is predicted for all other orientations using the crystallographic model. Therefore, the best way to determine material constants in the crystallographic model is by using uniaxial tests along the [001] and [111] orientations. For the [001] case, the global inelastic deformation is the summation of only the shear deformation of the octahedral slip systems and the material constants for the octahedral slip systems can be determined from the [001] uniaxial tests. For the [111] case, both octahedral and cubic slip systems contribute to the global inelastic deformation, a procedure is required to determine the material constants for the cubic slip systems.

3.5.2. Identification of Material Constants

In this section experimental results required to determine the material constants associated with different deformation responses are identified.

The stress response for monotonic uniaxial tensile loading in the [001] and [111] orientations for the phenomenological model can be obtained by rearranging equations (3.26) and (3.27) to give:

Uniaxial loading in the [001] orientation

$$\sigma_{[001]} = \tfrac{3}{2}X_{[001]} + \frac{k+R}{\sqrt{M_{11}-M_{12}}} + \frac{K^*}{(M_{11}-M_{12})^{(n+1)/2n}}(\dot{\varepsilon}^{in}_{[001]})^{\frac{1}{n}} \qquad (3.36a)$$

$$X_{[001]} = \frac{2}{3}\sqrt{M_{11}-M_{12}}\;\frac{N_{11}-N_{12}}{Q_{11}-Q_{12}}\left(1-\exp\{-\frac{Q_{11}-Q_{12}}{\sqrt{M_{11}-M_{12}}}\varepsilon^{in}_{[001]}\}\right) \qquad (3.36b)$$

$$R = W\left(1-\exp\{-b\frac{\left|\varepsilon^{in}_{[001]}\right|}{\sqrt{M_{11}-M_{12}}}\right) \qquad (3.36c)$$

Uniaxial loading in the [111] orientation

$$\sigma_{[111]} = \tfrac{3}{2}X_{[111]} + \frac{k+R}{\sqrt{M_{44}/2}} + \frac{K^*}{(M_{44}/2)^{(n+1)/2n}}(\dot{\varepsilon}^{in}_{[111]})^{\frac{1}{n}} \qquad (3.37a)$$

$$X_{[111]} = \frac{4}{3}\sqrt{\frac{M_{44}}{2}}\;\frac{N_{44}}{Q_{44}}\left(1-\exp\{-\sqrt{\frac{2}{M_{44}}}(Q_{44})\varepsilon^{in}_{[111]}\}\right) \qquad (3.37b)$$

$$R = W\left(1-\exp\{-b\frac{\left|\varepsilon^{in}_{[111]}\right|}{\sqrt{M_{44}/2}}\}\right) \qquad (3.37c)$$

For crystallographic model, similar expressions can also be obtained from equations (3.29), and equations (3.33) and (3.34) for uniaxial loading in the [001] and [111] orientations respectively.

Uniaxial loading in the [001] orientation

$$\sigma_{[001]} = \sqrt{6}x_o + \sqrt{6}k_o - \sqrt{6}r_o + (\frac{\sqrt{6}}{8})^{\frac{1}{n_o}}\sqrt{6}K_o(\dot{\varepsilon}^{in}_{[001]})^{\frac{1}{n_o}} \tag{3.38a}$$

$$x_o = \frac{c_o}{d_o}(1-\exp\{-d_o\frac{\sqrt{6}}{8}\varepsilon^{in}_{[001]}\}) \tag{3.38b}$$

$$r_o = \frac{q_o}{b_o}\left(1-\exp\{-\frac{\sqrt{6}d_o}{8}\varepsilon^{in}_{[001]}\}\right) \tag{3.38c}$$

Uniaxial loading in the [111] orientation

$$\varepsilon^{in}_{[111]} = (\varepsilon^{in}_{[111]})_o + (\varepsilon^{in}_{[111]})_c \tag{3.39}$$

From the octahedral slip systems contributions

$$\sigma_{[111]} = \frac{3\sqrt{6}}{2}x_o + \frac{3\sqrt{6}}{2}k_o + \frac{3\sqrt{6}}{2}r_o + \frac{3\sqrt{2}}{\left(\sqrt{6}/4\right)^{n_o}}K_o(\dot{\varepsilon}^{in}_{[111]})_o^{1/n_o} \tag{3.40a}$$

$$x_o = \frac{c_o}{d_o}(1-\exp\{-d_o\frac{\sqrt{6}}{4}\varepsilon^{in}_{[111]}\}) \tag{3.40b}$$

$$r_o = \frac{q_o}{b_o}\left(1-\exp\{-\frac{\sqrt{6}d_o}{4}(\varepsilon^{in}_{[111]})_o\}\right) \tag{3.40c}$$

From the cubic slip systems contributions

$$\sigma_{[111]} = \frac{3\sqrt{2}}{2}x_c + \frac{3\sqrt{2}}{2}k_c + \frac{3\sqrt{2}}{2}r_c + \frac{3}{\left(\sqrt{2}\right)^{n_c+1}}K_c(\dot{\varepsilon}^{in}_{[111]})_c^{1/n_c} \tag{3.40d}$$

$$x_c = \frac{c_c}{d_c}(1-\exp\{-\frac{\sqrt{2}}{2}d_c(\varepsilon^{in}_{[111]})_c\}) \tag{3.40e}$$

$$r_c = \frac{q_c}{b_c}\left(1-\exp\{-\frac{\sqrt{2}d_c}{2}(\varepsilon^{in}_{[111]})_c\}\right) \tag{3.40f}$$

It can be seen that a group of generic equations can be extracted for both the phenomenological and crystallographic models under uniaxial tension loading in either the [001] or [111] directions.

$$\sigma = X'+k'+R'+K'*(\dot{\varepsilon}^{in})^{1/n'} \tag{3.41a}$$

$$X = \frac{N}{Q}(1-\exp\{-Q'\varepsilon^{in}\}) \tag{3.41b}$$

$$R' = W'(1-\exp\{-b'\varepsilon^{in}\}) \tag{3.41c}$$

The experimental variables required to determine the material constants are σ, ε^{in}, and $\dot{\varepsilon}^{in}$. Since both phenomenological and crystallographic models can be expressed using generic equations, a universal procedure is available to determine the material constants in both models using the same experimental data.

The real material constants for each model under different loading direction are related to the generic material constants in the following way:

Phenomenological model:

Loading in [001]:

$$k' = \frac{k}{\sqrt{M_{11}-M_{12}}} \;;\quad K'* = \frac{K^*}{(M_{11}-M_{12})^{(n+1)/2n}} \;; \tag{3.42a}$$

$$N' = (N_{11}-N_{12}) \;;\quad Q' = \frac{(Q_{11}-Q_{12})}{\sqrt{M_{11}-M_{12}}} \;; \tag{3.42b}$$

$$W' = \frac{W}{\sqrt{M_{11}-M_{12}}} \;;\quad b' = \frac{b}{\sqrt{M_{11}-M_{12}}} \tag{3.42c}$$

Loading in [111]:

$$k' = \frac{k}{\sqrt{M_{44}/2}} \quad ; \quad K'^{*} = \frac{K^{*}}{(M_{44}/2)^{(n+1)/2n}} \quad ; \tag{3.43a}$$

$$N' = 2\,N_{44} \quad ; \quad Q' = \frac{Q_{44}}{\sqrt{M_{44}/2}} \quad ; \tag{3.43b}$$

$$W' = \frac{W}{\sqrt{M_{44}/2}} \quad ; \quad b' = \frac{b}{\sqrt{M_{44}/2}} \tag{3.43c}$$

Crystallographic model:

Loading in [001]:

$$k' = \sqrt{6}\,k_o \quad ; \quad K'^{*} = \left(\frac{\sqrt{6}}{4}\right)^{\frac{1}{n_o}} \sqrt{6}\,K_o \quad ; \quad n = n_o \tag{3.44a}$$

$$N' = \frac{3}{4}\,c_o \quad ; \quad Q' = \frac{\sqrt{6}}{8}\,d_o \quad ; \tag{3.44b}$$

$$W' = \sqrt{6}\,\frac{q_o}{b_o} \quad ; \quad b' = \frac{\sqrt{6}}{8} b_o \tag{3.44c}$$

Loading in [111]:

In this case, due to the combined contributions of both the octahedral and the cubic slip systems to the overall inelastic deformation, a procedure is required to determine the material constants associated with the cubic slip systems.

This is done in three parts, first the octahedral inelastic strains are determined, and second the cubic inelastic strains are found by subtracting the octahedral contribution from the total inelastic strain. Finally the material constants are found from the cubic contribution.

(i) Determination of the octahedral slip system contribution

The material constants for the octahedral slip systems will have been determined from the [001] orientation test data. The octahedral inelastic strain rate, $(\dot{\varepsilon}_3^{in})_o$, and other variables such as inelastic strain $(\varepsilon_3^{in})_o$ and back stress, x_o, as functions of applied stress, σ , can be determined by numerical simulation of equations (3.40a) to (3.40c).

(ii) Determination of the cubic slip system contribution

The cubic inelastic strain rate $(\dot{\varepsilon}_3^{in})_c$ and cubic inelastic strain, $(\varepsilon_3^{in})_c$, can be extracted from the total inelastic strain rate, $\dot{\varepsilon}_3^{in}$, and inelastic strain ε_3^{in}, using

$$(\dot{\varepsilon}_3^{in})_c = \dot{\varepsilon}_3^{in} - (\dot{\varepsilon}_3^{in})_o \ ; \qquad (\varepsilon_3^{in})_c = \varepsilon_3^{in} - (\varepsilon_3^{in})_o \qquad (3.45)$$

(iii) Determination of the material constants

The constitutive equations describing the cubic inelastic strain rate, equations (3.40), can also be written in the same formulation as for the generic equations. Finally the common procedure can be used directly to determine the material constants associated with the cubic slip systems using the relationships:

$$k' = \frac{3\sqrt{2}}{2} k_c \ ; \quad K'^* = \frac{3}{(\sqrt{2})^{n_c - 1}} K_c \ ; \qquad (3.46a)$$

$$N' = \frac{3}{4} c_c \ ; \quad Q' = \frac{\sqrt{2}}{4} d_c \ ; \qquad (3.46b)$$

$$W' \doteq \frac{3\sqrt{2}}{2} \frac{q_c}{b_c} \ ; \qquad b' = \frac{\sqrt{2}}{2} b_c \qquad (3.46c)$$

From above analysis, it can be seen that the two types of constitutive models become very similar to each other for uniaxial loading in the two specific orientations, i.e. [001] and [111]. Isotropic deformation responses have been predicted by both the phenomenological and crystallographic models. Also the basic constitutive equations for uniaxial loading in the [001] and [111] orientations can be expressed as a group of generic equations. These generic equations provide the background to determining the

material constants of both models using a single procedure and based on the same experimental data.

3.5.3. Procedure for Determining Material Constants

(i) Test Requirement and Data Reduction Scheme

From the generic Equations (3.41a) to (3.41c), it can be seen that three basic variables, σ, $\dot{\varepsilon}^{in}$ and ε^{in} are required from experimental results to determine the material constants. The procedure proposed here is based on the separation of the material constants into different groups. Each group provides the characteristics of the material, described by the relevant material constants. The three groups of constants are associated with equations (3.41a), (3.41b) and (3.41c); where in one group the viscosity parameters K* and n' are determined together with the initial yield stress k', in the second group the back stress parameters N' and Q' are evaluated and in the third group the isotropic hardening parameters W' and b' are determined.

The procedure requires a number of total strain controlled uniaxial tests subjected to different strain rates, $\dot{\varepsilon}^{T}$, for the [001] and [111] orientations (at least 3 for each orientation). The strain ranges should be large enough such that a saturated stress state is achieved, i.e. $\dot{\varepsilon}^{in}_{max} \approx \dot{\varepsilon}^{T}_{max}$. All the material constants, except for those used to describe isotropic hardening, are determined by these simple monotonic uniaxial tensile tests. In addition, cyclic tests may also be required to obtain the cyclic hardening data to determine the isotropic hardening material constants, W' and b'.

During each test, a continuous record of axial stress versus strain, $\sigma \sim \varepsilon^{T}$, is required. The stress and total strain results are used in the following data reduction scheme to obtain material constants in the generic equations. To obtain the inelastic material constants it is necessary to determine the inelastic strain and strain rate. These are determined by subtracting the elastic strain from the total strain.

(ii) Regression Analysis

Based on the generic equations obtained from the theoretical analysis, the material constants are determined by regression analysis using the different groups described earlier.

(a) Viscosity Parameters K^*, n

From equation (3.41a), a viscoplastic stress can be defined as :

$$\sigma_v = \sigma - k' - R' - X' = K' * (\dot{\varepsilon}^{in})^{1/n} \tag{3.47}$$

The back stress is a strong function of inelastic strain, and will reach its saturated state, i.e. X' =constant, very quickly at relatively large strains which are 2.5% and 1% for loading in orientations [001] and [111] respectively. On the other hand, the isotropic hardening parameter, R', is a weak function of accumulated inelastic strain, and is introduced in the models mainly to describe the cyclic hardening effect. In the case of monotonic uniaxial loading, the influence of R' is small and here it is neglected. This is discussed later. At large strains, the stress and strain response will reach a saturated state, with $\dot{\varepsilon}^{in} \approx \dot{\varepsilon}^{T}, X' \approx \text{constant}$, and k'+R' ≈ k'= constant.

Consequently, from a number of monotonic uniaxial tests with different strain rates, e.g. F tests, a group of equations can be obtained from equation (3.47) using the results for saturated stress at given total strain rates. For the ith and jth tests

$$(\sigma_v)_i = \sigma_i - k' - X' = K' * (\dot{\varepsilon}_i^{in})^{1/n'} = K' * (\dot{\varepsilon}_i^{T})^{1/n'} \tag{3.48a}$$

$$(\sigma_v)_j = \sigma_j - k' - X' = K' * (\dot{\varepsilon}_j^{in})^{1/n'} = K' * (\dot{\varepsilon}_j^{T})^{1/n'} \tag{3.48b}$$

Therefore

$$\sigma_i - \sigma_j = K'^{*} [(\dot{\varepsilon}_i^{T})^{1/n'} - (\dot{\varepsilon}_j^{T})^{1/n'}] \qquad (i, j = 1,2,3,.....F) \tag{3.49}$$

Letting

$$Y_m = \sigma_i - \sigma_j, \text{ and } x_m(n') = (\dot{\varepsilon}_i^{T})^{1/n'} - (\dot{\varepsilon}_j^{T})^{1/n'} \tag{3.50}$$

equation (3.47) becomes:

$$Y_m = K'^{*} x_m(n') \qquad (m = 1,2,3,.....F(F-1)/2) \tag{3.51}$$

From the test results of σ_i(i=1,2,3,.....F) and $\dot{\varepsilon}_i^T$(i=1,2,3,.....F), where F is the number of tests, the total of F(F-1)/2 non-linear equations, like equation (3.51), contain the unknown parameters K'* and n'.

For a given value of the visco-plastic constants n' (i.e. $n'=n_0$), the non-linear equations (3.51) reduce to a group of linear equations. Therefore, using a least squares regression method, the square of the errors R for the chosen n_0 and the subsequently calculated K'* are written as

$$R^2(n_0) = \sum_{i=1}^{m}(Y_i - K'^* x_i(n_0))^2 \qquad (3.52)$$

where K'* is calculated using:

$$K'^*(n_0) = \frac{\sum Y_i x_i(n_0)}{\sum (x_i(n_0))^2} \qquad (3.53)$$

Therefore, for a number of different values of n', the corresponding value of K'*(n'), as well as the square of the errors $R^2(n')$ can be calculated. Finally, K'* and n' are determined when the square of the error $R^2(n')$ attains a minimum.

(b) Back Stress Parameters N' and Q' and Yield Parameter k'

From equation (3.41a), it can be seen that the non-viscosity stress component can be written as (noting that it is assumed that R'=0)

$$\sigma - K'^*(\dot{\varepsilon}^{in})^{1/n'} = k'+X' \qquad (3.54)$$

Combining Equations (3.54) with (3.41b), we have

$$\sigma - K'^*(\dot{\varepsilon}^{in})^{1/n'} = k'+\frac{N'}{Q'}(1-\exp(-Q'\varepsilon^{in})) \qquad (3.55)$$

Letting

$$Y = \sigma - K'^*(\dot{\varepsilon}^{in})^{1/n'} \qquad (3.56)$$

and

$$\overline{Y} = k'+\frac{N'}{Q'}(1-\exp(-Q'\varepsilon^{in})) \qquad (3.57)$$

Since K'* and n' have been determined, then from the data pairs σ_i, $\dot{\varepsilon}_i^{in}$ and ε_i^{in} (i=1,2,3,.....G) from a given test (or tests), the overall non-viscosity stress component Y can be calculated. Consequently, a group of non-linear equations can be obtained in the form

$$Y_i = \sigma_i - K'^{*}(\dot{\varepsilon}_i^{in})^{1/n'}$$

$$\overline{Y}_i = k' + \frac{N'}{Q'}(1 - \exp(-Q'\varepsilon_i^{in})) \qquad (i=1, 2, 3,.....G) \qquad (3.58)$$

The non-linear problem is reduced to a linear problem by choosing an initial value of Q'_0. For a number of different Q' values, a least squares regression approach can be used to determine the optimum value of Q':

$$R^2 = \sum_{i=1}^{n}(Y_i - \overline{Y}_i)^2 = \sum_{i=1}^{n}[Y_i - k' - \frac{N'}{Q'}(1 - \exp(-Q'\varepsilon_i^{in}))]^2 \qquad (3.59)$$

$$\frac{\partial R^2}{\partial k'} = \sum_{i=1}^{n}[Y_i - k' - \frac{N'}{Q'}(1 - \exp(-Q'\varepsilon_i^{in}))] = 0 \qquad (3.60)$$

$$\frac{\partial R^2}{\partial N} = \sum_{i=1}^{n}[Y_i - k' - \frac{N'}{Q'}(1 - \exp(-Q'\varepsilon_i^{in}))] \ \frac{1}{Q'}(1 - \exp(-Q'\varepsilon_i^{in})) = 0 \qquad (3.61)$$

A group of linear equations are obtained from Equations (3.60) and (3.61). These equations are solved by using the Gaussian method to obtain the constants N' and k' corresponding to each chosen Q'. The final values of N', Q' and k' are determined when the square of the errors R^2 reaches the minimum value.

(c) Isotropic hardening parameters W' and b'

The isotropic hardening parameter, R', is introduced in the models mainly to describe the cyclic hardening effect. Therefore the material constants associated with the isotropic hardening parameter should be determined using the cyclic hardening data.

In the case of uniaxial loading the accumulated inelastic strain, p, can be simply expressed as:

$$p = \sum_{0}^{N} \Delta\varepsilon^{in} \tag{3.62}$$

where N is the number of cycles, and $\Delta\varepsilon^{in}$ is the inelastic strain range which will change slightly with cycle number. Then the isotropic hardening parameter can be expressed as:

$$R'(N) = W'\left[1-\exp(-b'\sum_{0}^{N}\Delta\varepsilon^{in})\right] \tag{3.63}$$

In the total strain controlled tests, the inelastic strain rate, $\dot{\varepsilon}^{in}$, is approximately the same at the maximum stress of each cycle. The back stress, X', will be also approximately same corresponding the maximum stress at each cycle. Therefore from equations (3.41a) and (3.41c), the isotropic hardening parameters can be related to the change of the maximum cycle stresses in the cyclic tests as:

$$\sigma_{max}(N_i)-\sigma_{max}(N_j)=R'(N_i)-R'(N_j)=\exp(-b'\sum_{0}^{N_j}\Delta\varepsilon^{in})-\exp(-b'\sum_{0}^{N_j}\Delta\varepsilon^{in}) \tag{3.64}$$

A similar non-linear regression method, as described in the previous sections, has been applied to Equations (3.63) and (3.64) to determine the isotropic hardening material constants W' and b'.

3.5.4 Numerical Calculations

There are no existing experimental data required for the proposed procedure. Therefore verification of the proposed method to determine the material constants has been carried out using a set of simulation data. The simulation data have been obtained by simulating the proposed uniaxial monotonic and cyclic tests using the phenomenological model. The material constants used in the simulation were determined from experimental results for SRR99 single crystal nickel base superalloys obtained by Li in an earlier study (Li, [1993]). The earlier studies (Li et al, [1994], Li and Smith, [1995]) also indicated that the mechanical deformation behaviour of a range of nickel base single crystal superalloys, such as SRR99, PWA1480, AM1,

CMSX 2 are very similar. The results presented here are therefore representative of generic nickel base single crystal superalloys. Further discussion about the SRR99 single crystal data used in this work is given in Chapter 6.

The monotonic uniaxial experiments were conducted at 950°C for total strain controlled tests along the [001] and [111] orientations respectively. Six different strain rates, with $\dot{\varepsilon}^T$=0.00004/s, 0.0004/s, 0.001/s, 0.004/s, 0.01/s, 0.04/s, were used in the simulations in this work. Figures 3.3a and 3.3b plot the stress and strain curves for [001] and [111] respectively. For each orientation, samples were strained to achieve saturated stresses. The saturated stresses are given in Table 3.2. It can be seen that both orientations exhibited strong strain rate dependent characteristics. Due to the higher elastic modulus of [111] orientation compared with the [001] orientation, the stress level for a given strain rate at low strain range is higher for the [111] orientation compared with that of the [001] orientation. However, the inelastic hardening rate is higher in the [001] orientation than for the [111] orientation, and consequently the stress level at the final stage of deformation in the [001] orientation is observed to higher than that in the [111] orientation. Also the total strain ranges where the stress response reached a saturated state were found to be higher for [001] orientation compared with [111] orientation.

Figures 3.4a and 3.4b plot the cyclic stress and strain response in the first few cycles for the [001] and [111] orientations respectively. It can be seen that the cyclic hardening effect for SRR 99 single crystal alloy at 950°C was not significant.

From the 'experimental results', which are a group of simulation results, shown in figures 3.3a and 3.3b, as well as 3.4a and 3.4b, the data reduction scheme was used. A number of FORTRAN programs were written to perform the non-linear regression analyses. The generic equations are applied to the [001] and [111] orientations to determine the generic material constants in the equations. Examples of the regression results are given in Fig.3.5, where the square of the errors R^2 is plotted as a function of various material parameters.

Using the material constants in the generic equations, determined from the numerical regression analysis, the material constants for the phenomenological and the crystallographic models were then determined from the relationships described in section 3.4.2 Table 3.3 shows the material constants for the phenomenological model. The material constants for crystallographic model were determined by the general procedure assuming that the [111] orientation has combined octahedral and cubic deformation, and are given in Table 3.4.

3.5.5 Material Parameters for Thermomechanical Model

The thermomechanical constitutive model has been developed by modification of the isothermal constitutive models. The material parameters in the thermomechanical equations are temperature dependent, and can be expressed as various functions of temperature. The formulation of the functions can be determined from the experimental data. For a given temperature, the thermomechanical equations are reduced to the isothermal equations. The values of the material parameter at this temperature can be determined using the procedure described in the previous sections. Therefore, from the results obtained from a number of isothermal experimental data over a sufficient temperature range, the temperature dependent material parameter functions can be determined by numerical regression or curve-fitting.

Without a comprehensive experimental program in this project to obtain the material constants from testing data, a literature survey has been carried out to find the necessary material data from earlier publications. It was found that only sufficient elastic constants and thermal expansion ratios of single crystal superalloys over specific temperature ranges can be obtained (Li et al, [1996] and Dandekar et al, [1990]). The functional formulations for the elastic constants and thermal expansion ratio have been established as cubic functions of temperature by curve-fitting. The temperature dependence of the elastic constants are:

$$E = a_1T^3 + b_1T^2 + c_1T + d_1 \qquad (3.65a)$$

$$\upsilon = a_2T^3 + b_2T^2 + c_2T + d_2 \qquad (3.65b)$$

$$G = a_3T^3 + b_3T^2 + c_3T + d_3 \quad (3.65c)$$

$$\alpha = a_4T^3 + b_4T^2 + c_4T + d_4 \quad (3.65d)$$

All the coefficients for the above equations are listed in Table 3.5.

To obtain material constants for viscoplastic behaviour it was necessary to review results given in the literature. Material constants for single crystal alloys SRR99, CMSX2, AM1 and PWA 1480 were obtained. For example, Hanriot et al [1991] showed that the viscoplastic constant n is 10 and 4.6 for 650°C and 950°C respectively. Similar constants were obtained for PWA1480 at 593°C and 871°C by Jordan and Walker [1992]. For temperatures below about 600°C the mechanical behaviour is essentially elastic-plastic with little or no evidence for strain rate effects. This is observed in the variation of yield stress as a function of temperature for SRR99 (Li and Smith [1995]). This variation is shown in Figure 3.6a. A similar variation in the material constant k, is also expected.

For temperatures above about 600°C, the variation of the viscoplastic constant K* is shown in Figure 3.6b. A number of studies have been carried out to investigate the cyclic deformation behaviour of single crystal superalloys (Milligan [1990], (Gabb. et al [1989]), Poubanne [1990], Li [993]). This has been reviewed in Chapter 2. However, there has been no experimental data available in the form of real hysteresis to determine the temperature dependent isotropic hardening behaviour of single crystal alloys. The variations of material constants b ad W with temperature can not be determined. Therefore based on a limited data set only an approximate thermo-elastro-viscoplastic analysis can be undertaken for temperature above 600°C. However, for temperatures below 600°C the material response is not time dependent and consequently it would be necessary to utilise two models. Further work is required to explore use of dual models.

3.6 Comparison of the Phenomenological and Crystallographic Models

The two categories of model have been developed separately based on totally different principles. The crystallographic models have been developed based on crystalline slip theory. On the other hand, the phenomenological models have been developed by modifying the isotropic constitutive models initially proposed for polycrystalline materials. A number of studies (Nouailhas [1990], Stouffer et al [1990], Meric et al [1991], Jordan and Walker [1992], Li [1993]) have been carried out to investigate the characteristics of a specific model, and to verify the model with various experimental data. However, there has been only very limited work that compares the different models.

The identification of the common generic equations, (3.41a) to (3.41c), for both phenomenological and crystallographic models in section 3.5 makes it possible to determine the material constants of both models using a single procedure and based on the same experimental data. This will provide a basis for direct comparison of the two models to explore intrinsic features of each model. In this section, numerical simulation results using the phenomenological and crystallographic models are compared. The simulations have been conducted by a number of FORTRAN programs. The FORTRAN programs were verified by comparison of the simulation results with those obtained from a commercial software code SIMNON (Elmquist et al, [1986]).

3.6.1. Orientation Dependent Deformation Response

The simulation results from the phenomenological and crystallographic model are first compared with the 'experimental results' in Figs. 3.3a and 3.3b for the [001] and [111] orientations respectively. The stable cyclic stress and strain responses for the [001] and [111] orientations are presented in Figs.3.4c and 3.4d. The material constants given in Tables 3.3 and 3.4 were used for the phenomenological model and the crystallographic model respectively. As expected, the results obtained from both the phenomenological

and the crystallographic models are in very good agreement with the 'experimental results'.

Using the material constants determined from the same experimental results with a common procedure, numerical simulations have been carried out for other orientations as shown in Fig.3.7. This allows direct comparison of the two different categories of constitutive models. Firstly the deformation responses of some particular orientations under uniaxial loading conditions have been simulated to examine the fundamental features of single crystal nickel base superalloys with a cubic symmetry structure. The simulation results indicated that both phenomenological and crystallographic models can describe the following uniaxial deformation characteristics.

(i) Specimens with orientations on the [001]-[011] side of the stereotriangle, i.e. orientations [0ab], Fig.3.7, exhibit no inelastic shear deformation in the XY and YZ directions when loaded in the Z direction.

(ii) Specimens with orientations on [011]-[111] side of the stereotriangle, i.e. orientations [abb], show no inelastic shear deformation in the XY and XZ directions when loaded in the Z direction.

(iii) These is no inelastic shear deformation for a specimen with the [011] orientation. However the two transverse inelastic strains are different.

(iv) As discussed before, specimens with orientations in either [001] or [111] show isotropic inelastic deformation response.

(v) For all other orientations, simple uniaxial loading induces a complex anisotropic inelastic deformation response. All the six strain components are not zero.

These features of the inelastic deformation predicted by both the phenomenological and crystallographic models are similar to the elastic deformation described by the anisotropic elasticity theory for cubic symmetry. Some of these features, e.g. (iv),

have been verified by experimental data (Milligan [1990], Gabb. et al [1989], Poubanne [1990], Li [993]), and further experiments are required to fully verify these deformation characteristics.

Another interesting observation from the simulation results is the orientation dependent inelastic strain hardening characteristics of single crystal nickel base superalloys. Both the phenomenological and crystallographic models predict that the influence of orientation on inelastic strain hardening is opposite to the effect of orientation on the elastic modulus. The inelastic strain hardening rate, $d\sigma / d\varepsilon^{in}$, as a function of inelastic strain for various orientations, is shown in Fig. 3.8. The simulation results of both models indicate that the lower the elastic modulus, the higher the inelastic strain hardening rate. The [001] orientation with the lowest elastic modulus exhibits the highest inelastic strain hardening. The [111] orientation with the highest elastic modulus shows the lowest inelastic strain hardening.

The phenomenological model and the crystallographic model exhibit similarities in terms of describing the above fundamental deformation characteristics of single crystal nickel base superalloys. However, significant differences are also observed when results for various orientations are directly compared. To explore the differences between the two models, simulation results of the two models for a large number of orientations on the three sides of the stereographic triangle, Fig.3.7, have been compared. The relative errors between stress levels at a total strain of 1.2% predicted by the two models for different orientations are summarised in Fig.3.9. The relative error is defined as $\frac{|\sigma_{phen.} - \sigma_{cry.}|}{\sigma_{phen}}$, where σ_{phen} and σ_{cry} are the stresses predicted by the phenomenological and crystallographic models. Some examples of direct comparisons of the stress and strain response are given in Fig.3.10.

A number of simulation results for orientations on the [001]-[011] side of the stereographic triangle, i.e. orientations [0ab], are plotted in Fig.3.10a. In this case, the differences between the simulation results of the two models increase as the orientation

moves away from [001] orientation, and significant differences are observed for orientations near the [011] orientation.

Comparison of the simulation results obtained from the two models for the orientations on the [011]-[111] side of the stereographic triangle is given in Fig.3.10b. Deformation responses predicted by both the phenomenological and crystallographic models for orientations near to [111] were found to be similar, and discrepancies have been observed as the orientation moves to [011].

The simulation results of a number of orientations on the [001]-[111] side of the stereographic triangle, i.e. orientation [aab], indicated that deformation responses predicted by the phenomenological and crystallographic models are very similar for the orientations near the [001] or the [111] orientations. The differences between the simulation results increase as the orientations move away from the two corners and significant difference is observed for the middle orientation. Some of simulation results are compared in Fig.3.10c.

3.6.2. Comparison of Yielding Behaviour

In both the phenomenological and crystallographic models, the yield function is used as an inelastic potential in the inelastic strain rate equations. Consequently, the yield function has a significant influence on the inelastic deformation behaviour described by the constitutive models (Nouailhas et al, [1995]). Further simulations have been carried out to investigate the yield characteristics described by the phenomenological and the crystallographic models.

Figure 3.11 plots the variation of the initial yield stresses, normalised by the yield stress of the [001] orientation, for different orientations under uniaxial loading conditions. It can be seen that yield stresses predicted by the phenomenological and the crystallographic models are the same for the [001] and [111] orientations. The differences between the simulation results increase as the orientations move away from

the two corners. Significant differences are observed for the middle orientations, with the largest discrepancy being observed for the [011] orientation. These observations in terms of yield stresses are similar to those for the stress strain responses presented in Fig.3.9.

3.6.3. Comparison of Deformation Mechanisms

The inelastic deformation predicted by the crystallographic model is the combination of the inelastic deformation produced by the octahedral and the cubic slip systems. The importance of each of the two slip systems changes with crystal orientation. Both the simulation and experimental results indicate that inelastic deformation is dominated by octahedral slip for orientations close to the [001] and by cubic slip for orientations close to the [111] (Walker and Jordan [1989], Hanriot et al [1991]). Further detailed simulations have been carried out to examine the importance of the octahedral and cubic slip deformation for various orientations. The percentage of the inelastic strain produced by the cubic slip systems and by the octahedral slip systems at total strains of 1.2% for different orientations are presented in Fig.3.12. It can be seen that importance of the two slip systems to inelastic deformation depends strongly on orientation. The region where cubic slip dominates is much larger than the region for octahedral slip. This can also be attributed to the significant difference of the inelastic strain hardening behaviour between the octahedral and the cubic slip systems. The octahedral slip systems (dominating [001] deformation) have the highest strain hardening and the cubic slip systems (dominating [111] deformation) the lowest, Fig.3.8. Therefore inelastic deformation is more easily caused by cubic slip than by octahedral slip.

CHAPTER 4
FINITE ELEMENT IMPLEMENTATION OF THE MODELS

4.1. Introduction

Structural analysis of engineering components under complex loading conditions, such as a turbine blade under combined fatigue and creep loading, is generally carried out using the finite element method. In order to use a constitutive model for structural analysis, numerical implementation of the constitutive equations is required in conjunction with a finite element code to solve the practical boundary value problems. The finite element package used in this work is ABAQUS. This package has an advantage of having an interface that allows the user to implement general constitutive equations. The user defined material model is implemented in the subroutine UMAT.

For the implementation of the anisotropic viscoplastic constitutive equations into UMAT, and interfacing with ABAQUS, there are two aspects of problems to be solved: (i) developing a methodology to transform the differential equations into numerical incremental equations for FE coding; and (ii) writing a FORTRAN program for the UMAT subroutine, and performing the interface with ABAQUS.

In this chapter, the numerical implementation procedures for the isothermal constitutive models, both the phenomenological and the crystallographic models, are presented in section 4.2. The procedures for implementing the nonisothermal constitutive models are described in section 4.3. The three dimensional (3D) UMAT subroutines for the procedures developed in sections 4.2. and 4.3 and their interfacing with the ABAQUS main finite element code are described in section 4.4. The verification results of the finite element implementation procedure and UMAT program are described in section 4.5. Finally, improvement of the computing efficiency of the numerical implementation is described in section 4.6.

4.2. Isothermal Numerical Implementation

4.2.1. Numerical Integration Method

To carry out structural FE stress analysis the constitutive rate equations need to be transformed to incremental equations for integration. An implicit time integration scheme, using the trapezoidal method, is used to implement both the phenomenological and crystallographic models in this work. Due to the complexities of the anisotropic 3D constitutive models, the numerical integration procedure involves a very large amount of mathematical derivations. Using the trapezoidal method, the increments of the stress and strain, as well as the state variables in the constitutive equations can be expressed in terms of the relative rates at both beginning and end of the time increment. In the following a brief description of the integral procedure is presented step by step.

For a variable z and its rate $\dot{z}$, the trapezoidal rule is presented as:

$$\Delta z = \Delta t[(1-\theta)\dot{z}(t) + \theta\dot{z}(t+\Delta t)] \qquad (4.1)$$

The general implicit operator θ can be chosen from the interval $0 \le \theta \le 1.0$. The value $\theta = 0$ reduces the scheme to the explicit integration, i.e. forward Euler while $\theta = 1$ leading to backward Euler integration. The method leads to unconditionally stable integration when θ varies in the interval $0.5 \le \theta \le 1.0$ (Hughes, [1983], Ortiz and Popov, [1985]).

To avoid complicated mathematical equations for the 3D case, the implicit time integration scheme is used for the following simple uniaxial phenomenological model to demonstrate the main characteristics of the scheme. The constitutive equations are written as:

$$\dot{\varepsilon}^{T} = \dot{\varepsilon}^{e} + \dot{\varepsilon}^{in} \qquad (4.2a)$$

$$\dot{\varepsilon}^{e} = E^{-1}\,\dot{\sigma} \qquad (4.2b)$$

$$\dot{\varepsilon}^{in} = g(\sigma, X, R) \qquad (4.2c)$$

$$\dot{X}=h(\dot{\varepsilon}^{in},X) \tag{4.2d}$$

$$\dot{R}=q(\dot{p},R) \tag{4.2e}$$

$$\dot{p}=r(\dot{\varepsilon}^{in}) \tag{4.2f}$$

Using the implicit time integration scheme, i.e. the trapezoidal rule, the increments of the stress and strain, as well as the state variables in the constitutive equations can be expressed in terms of the relative rates at both beginning and end of the time increment such as:

$$\Delta\varepsilon^{in}=\Delta t[(1-\theta)\dot{\varepsilon}_t^{in}+\theta\dot{\varepsilon}_{t+\Delta t}^{in}] \tag{4.3a}$$

$$\Delta X=\Delta t[(1-\theta)\dot{X}_t+\theta\dot{X}_{t+\Delta t}] \tag{4.3b}$$

$$\Delta R=\Delta t[(1-\theta)\dot{R}_t+\theta\dot{R}_{t+\Delta t}] \tag{4.3c}$$

In the FE analysis, the variables at time $t+\Delta t$ are unknown and need to be determined. The only known variables are the total strain ε^T and increment $\Delta\varepsilon^T$. Consequently, all increments of other variables should be expressed only as a function of $\Delta\varepsilon^T$.

The rates of each variable $\dot{\varepsilon}_{t+\Delta t}^{in}$, $\dot{X}_{t+\Delta t}$ and $\dot{R}_{t+\Delta t}$ are unknown values, and there are three methods to obtain these values and the increments of the variables.

Method 1

Using equations (4.2c) to (4.2e) to obtain $\dot{\varepsilon}_{t+\Delta t}^{in}$, $\dot{X}_{t+\Delta t}$ and $\dot{R}_{t+\Delta t}$ in the increment equations (4.3a) to (4.3c) gives:

$$\dot{X}_{t+\Delta t}=h(\dot{\varepsilon}_{t+\Delta t}^{in},X_{t+\Delta t}) \tag{4.4a}$$

$$\dot{R}_{t+\Delta t}=q(\dot{\varepsilon}_{t+\Delta t}^{in},R_{t+\Delta t}) \tag{4.4b}$$

$$\dot{\varepsilon}_{t+\Delta t}^{in}=g(\sigma_t+\Delta\sigma,X_t+\Delta X,R_t+\Delta R) \tag{4.4c}$$

Further substituting equation (4.4b) into equations (4.4a) and (4.4c) leads:

$$\dot{X}_{t+\Delta t} = h(g(\sigma_t + \Delta\sigma, X_t + \Delta X), X_t + \Delta X) \quad (4.4d)$$

$$\dot{R}_{t+\Delta t} = q(g(\sigma_t + \Delta\sigma, X_t + \Delta X), R_t + \Delta R) \quad (4.4e)$$

Then substituting equations (4.4c) to (4.4e) into equations (4.3a) to (4.3c) respectively results in the following:

$$\Delta\varepsilon^{in} = \Delta t[(1-\theta)\dot{\varepsilon}_t^{in} + \theta g(\sigma_t + \Delta\sigma, X_t + \Delta X, R_t + \Delta R)] \quad (4.5a)$$

$$\Delta X = \Delta t[(1-\theta)\dot{X}_t + \theta h(g(X_t + \Delta X, \sigma_t + \Delta\sigma, R_t + \Delta R), X_t + \Delta X)] \quad (4.5b)$$

$$\Delta R = \Delta t[(1-\theta)\dot{R}_t + \theta q(g(X_t + \Delta X, \sigma_t + \Delta\sigma, R_t + \Delta R), R_t + \Delta R)] \quad (4.5c)$$

From equation (4.2b), the stress increment equation is as:

$$\Delta\sigma = E(\Delta\varepsilon^T - \Delta\varepsilon^{in}) \quad (4.5d)$$

The total strain increment $\Delta\varepsilon^T$ is known in ABAQUS because it uses the displacement method, so there are four unknown values, ΔX, ΔR, $\Delta\varepsilon^{in}$ and $\Delta\sigma$ for four equations (4.5a) to (4.5d). Therefore the solutions for ΔX, ΔR, $\Delta\varepsilon^{in}$ and $\Delta\sigma$ are completely determined. This method leads to an **analytical solution or closed form solution** for the increments of inelastic strain and stress for the model used in this work. In general, a analytical or closed form solution may not be possible, and a numerical method is required to solve the group of equations.

However the flow function $g(\sigma,X,R)$ is a high order nonlinear function of stress σ and back stress X, so the equations (4.5a) to (4.5c) are nonlinear and a coupled equation set, therefore the solution procedure is very complex mathematically. To avoid this two other methods can be used.

Method 2

$\varepsilon^{in}_{t_0+\Delta t}$, $X_{t_0+\Delta t}$ and $R_{t_0+\Delta t}$ can be obtained by using a numerical solution method for the following nonlinear differential equations:

$$\varepsilon^{in}_{t_0+\Delta t} = \varepsilon^{in}_{t_0} + \Delta t(1-\theta)\dot{\varepsilon}^{in}_{t_0} + \Delta t\theta\dot{\varepsilon}^{in}_{t_0+\Delta t} \qquad (4.6a)$$

$$X_{t_0+\Delta t} = X_{t_0} + \Delta t(1-\theta)\dot{X}_{t_0} + \Delta t\theta\dot{X}_{t_0+\Delta t} \qquad (4.6b)$$

$$R_{t_0+\Delta t} = R_{t_0} + \Delta t(1-\theta)\dot{R}_{t_0} + \Delta t\theta\dot{R}_{t_0+\Delta t} \qquad (4.6c)$$

where $\Delta t=t-t_0$

There are many numerical solution methods for solving nonlinear differential equations, such as the Euler method and Runge-Kutta method. However, numerical solution results are highly time consuming and result in low accuracy.

Method 3

This method is similar to method 1 and an approximation is introduced to avoid a complex analysis. This approach provides an **approximate closed form solution** or a so-called linear solution.

Here the unknown inelastic strain rate $\dot{\varepsilon}^{in}_{t+\Delta t}$, $\dot{X}_{t+\Delta t}$ and $\dot{R}_{t+\Delta t}$ at $t+\Delta t$ are approximated by their previous values and their gradients at time t through a Taylor's expansion, so that:

$$\dot{\varepsilon}^{in}_{t+\Delta t} = \dot{\varepsilon}^{in}_{t} + \frac{\partial g(\sigma,X,R)}{\partial\sigma}\Big|_t \Delta\sigma + \frac{\partial g(\sigma,X,R)}{\partial X}\Big|_t \Delta X + \frac{\partial g(\sigma,X,R)}{\partial R}\Big|_t \Delta R \cdots\cdots (4.7a)$$

$$\dot{X}_{t+\Delta t} = \dot{X}_{t} + \frac{\partial h(\dot{\varepsilon}^{in},X)}{\partial\dot{\varepsilon}^{in}}\Big|_t \Delta\dot{\varepsilon}^{in} + \frac{\partial h(\dot{\varepsilon}^{in},X)}{\partial X}\Big|_t \Delta X + \cdots\cdots \qquad (4.7b)$$

$$\dot{R}_{t+\Delta t} = \dot{R}_{t} + \frac{\partial r(\dot{\varepsilon}^{in},R)}{\partial\dot{\varepsilon}^{in}}\Big|_t \Delta\dot{\varepsilon}^{in} + \frac{\partial r(\dot{\varepsilon}^{in},R)}{\partial R}\Big|_t \Delta R + \cdots\cdots \qquad (4.7c)$$

Equation (4.7a) leads:

$$\Delta\dot{\varepsilon}^{in} = \dot{\varepsilon}^{in}_{t+\Delta t} - \dot{\varepsilon}^{in}_{t} = \frac{\partial g(\sigma, X, R)}{\partial \sigma}\Big|_t \Delta\sigma + \frac{\partial g(\sigma, X, R)}{\partial X}\Big|_t \Delta X + \frac{\partial g(\sigma, X, R)}{\partial R}\Big|_t \Delta R \cdots (4.7d)$$

Combining equations (4.7b) to (4.3d) leads $\dot{X}_{t+\Delta t}$ and $\dot{R}_{t+\Delta t}$ to be functions of $\Delta\sigma, \Delta X$ and ΔR, then substituting $\dot{X}_{t+\Delta t}$ and $\dot{R}_{t+\Delta t}$ into equations (4.3b) and (4.3c) whilst combining equations (4.7a) and (4.3a) so that the inelastic strain increment, $\Delta\varepsilon^{in}$, and internal variable increments, ΔX and ΔR can be expressed as:

$$\Delta\varepsilon^{in} = \chi(\Delta\sigma, \Delta X, \Delta R) \quad (4.8a)$$

$$\Delta X = \psi(\Delta\varepsilon^{in}, \Delta X, \Delta\sigma) \quad (4.8b)$$

$$\Delta R = \eta(\Delta\varepsilon^{in}, \Delta R, \Delta\sigma) \quad (4.8c)$$

Combining equation (4.5c), i.e.

$$\Delta\sigma = E[\Delta\varepsilon^{T} - \Delta\varepsilon^{in}] \quad (4.8d)$$

It can be seen that there are only four unknown variables, $\Delta\sigma$, $\Delta\varepsilon^{in}$, ΔX and ΔR, in the four equations (4.8a) to (4.8d). Therefore it is sufficient to determine $\Delta\sigma$, $\Delta\varepsilon^{in}$, ΔX and ΔR using these equations.

Then all the variables at time $t+\Delta t$ can be updated so that:

$$\sigma_{t+\Delta t} = \sigma_t + \Delta\sigma \quad (4.9a)$$

$$\varepsilon^{in}{}_{t+\Delta t} = \varepsilon^{in}{}_t + \Delta\varepsilon^{in} \quad (4.9b)$$

$$X_{t+\Delta t} = X_t + \Delta X \quad (4.9c)$$

$$R_{t+\Delta t} = R_t + \Delta R \quad (4.9d)$$

The methods used to solve the nonlinear equations (4.8a) to (4.8d) depend on the complexity of the functions $\chi(\Delta X, \Delta\sigma, \Delta R)$, $\psi(\Delta\varepsilon^{in}, \Delta X, \Delta R)$ and $\eta(\Delta\varepsilon^{in}, \Delta X, \Delta R)$. If only a first order Taylor expansion is used for approximating

$\dot{\varepsilon}^{in}_{t+\Delta t}$, $\dot{X}_{t+\Delta t}$ and $\dot{R}_{t+\Delta t}$ in equations (4.7a) to (4.7c), then equations (4.8a) to (4.8d) are a set of linear equations. So all the increments of stress, inelastic strain and back stress can be solved easily.

In this work this method has been used and the approximate closed form solutions have been achieved for implementing both the phenomenological and crystallographic models. A outline of the implementation procedure is given in the next sections.

4.2.2 Numerical Implementation of Phenomenological Model

Now applying the trapezoidal rule to all the variables in phenomenological model leads to the following:

$$\Delta\varepsilon_i^T = \Delta t[(1-\theta)\dot{\varepsilon}^T_{i(t)} + \theta\dot{\varepsilon}^T_{i(t+\Delta t)}] \tag{4.10a}$$

$$\Delta\sigma_i = \Delta t[(1-\theta)\dot{\sigma}_{i(t)} + \theta\dot{\sigma}_{i(t+\Delta t)}] \tag{4.10b}$$

$$\Delta\varepsilon_i^{in} = \Delta t[(1-\theta)\dot{\varepsilon}^{in}_{i(t)} + \theta\dot{\varepsilon}^{in}_{i(t+\Delta t)}] \tag{4.10c}$$

$$\Delta X_i = \Delta t[(1-\theta)\dot{X}_{i(t)} + \theta\dot{X}_{i(t+\Delta t)}] \tag{4.10d}$$

$$\Delta R = \Delta t[(1-\theta)\dot{R}_t + \theta\dot{R}_{t+\Delta t}] \tag{4.10e}$$

where $i = 1,2,\cdots 6$.

In the FE analysis, the variables at time t+Δt are unknown and need to be determined. In the FE application software ABAQUS, which is based on the displacement method, the only known increment is the total strain increment $\Delta\varepsilon^T$. Consequently, all increments of other variables should be expressed only as a function of $\Delta\varepsilon_i^T$.

By introducing a short hand notation for the various transformations, the original 3D constitutive equations are rewritten for simplicity and given in Appendix IV.

From

$$\dot{\varepsilon}_i^T = \dot{\varepsilon}_i^e + \dot{\varepsilon}_i^{in} \quad : \qquad \dot{\sigma}_i = C_{ij}^I(\dot{\varepsilon}_j^T - \dot{\varepsilon}_j^{in})$$

where $i, j = 1,2,\cdots 6$.

The following equations can be obtained:

$$\Delta\varepsilon_i^T = \Delta\varepsilon_i^e + \Delta\varepsilon_i^{in} \tag{4.11a}$$

$$\Delta\sigma_i = C_{ij}^I[\Delta\varepsilon_j^T - \Delta\varepsilon_j^{in}] \tag{4.11b}$$

So only the incremental equations (4.10c) to (4.10e) need further analysis. The unknown rate variables at time $t+\Delta t$, inelastic strain rate, $\dot{\varepsilon}_{t+\Delta t}^{in}$, back stress rate, $\dot{X}_{t+\Delta t}$ and isotropic stress rate $\dot{R}_{t+\Delta t}$, are expressed approximately by their previous values and their gradients at time t using a Taylor expansion, so that

$$\dot{\varepsilon}_{i(t+\Delta t)}^{in} = \dot{\varepsilon}_{i(t)}^{in} + \frac{\partial\dot{\varepsilon}_i^{in}}{\partial\sigma_j}\Big|_t \Delta\sigma_j + \frac{\partial\dot{\varepsilon}_i^{in}}{\partial X_j}\Big|_t \Delta X_j + \frac{\partial\dot{\varepsilon}_i^{in}}{\partial R}\Big|_t \Delta R \tag{4.12a}$$

$$\dot{X}_{i(t+\Delta t)} = \dot{X}_{i(t)} + \frac{\partial\dot{X}_i}{\partial\dot{\varepsilon}_j^{in}}\Big|_t \Delta\dot{\varepsilon}_j^{in} + \frac{\partial\dot{X}_i}{\partial X_j}\Big|_t \Delta X_j + \frac{\partial\dot{X}_i}{\partial\dot{p}}\Big|_t \Delta\dot{p} \tag{4.12b}$$

$$\dot{R}_{(t+\Delta t)} = \dot{R}_{(t)} + \frac{\partial\dot{R}}{\partial\dot{p}}\Big|_t \Delta\dot{p} + \frac{\partial\dot{R}}{\partial R}\Big|_t \Delta R \tag{4.12c}$$

$$\dot{p}_{(t+\Delta t)} = \dot{p}_{(t)} + \frac{\partial\dot{p}}{\partial\dot{\varepsilon}_i^{in}}\Big|_t \Delta\dot{\varepsilon}_i^{in} \tag{4.12d}$$

From equation (4.12a):

$$\Delta\dot{\varepsilon}_i^{in} = \frac{\partial\dot{\varepsilon}_i^{in}}{\partial\sigma_j}\Big|_t \Delta\sigma_j + \frac{\partial\dot{\varepsilon}_i^{in}}{\partial X_j}\Big|_t \Delta X_j + \frac{\partial\dot{\varepsilon}_i^{in}}{\partial R}\Big|_t \Delta R \tag{4.13a}$$

From equation (4.12d):

$$\Delta\dot{p} = \frac{\partial\dot{p}}{\partial\dot{\varepsilon}_i^{in}}\Big|_t \Delta\dot{\varepsilon}_i^{in} \tag{4.13b}$$

Combining equations (4.10), (4.12) and (4.13), the inelastic strain increment, $\Delta\varepsilon^{in}$, back stress and isotropic stress increments, ΔX and ΔR, can be expressed as:

$$\Delta\varepsilon_i^{in} = \chi(\Delta\sigma_i,\ \Delta X_i,\ \Delta R) \tag{4.14}$$

$$\Delta X_i = \psi\ (\Delta\sigma_i,\ \Delta X_i,\ \Delta R) \tag{4.15}$$

$$\Delta R = \eta(\Delta\sigma_i, \Delta X_i, \Delta R) \tag{4.16}$$

Replacing $\Delta\sigma_i$ in above equations with equation (4.11b), there are only three unknown variables, $\Delta\varepsilon_i^{in}$, ΔX_i and ΔR, in the three equations (4.14) to (4.16). Therefore it is sufficient to determine $\Delta\varepsilon_i^{in}$, ΔX_i and ΔR using these three equations.

The partial differential expressions in each term of equations (4.12a) to (4.12d) and (4.13a) to (4.13b) are as follows:

$$\frac{\partial\dot{\varepsilon}_i^{in}}{\partial\sigma_j} = \frac{3}{4g}\left[\bar{\bar{f}}\frac{1}{g}W_{ik} + 2\bar{f}M_{ik}^2\right]\frac{\partial\sigma_k'}{\partial\sigma_j} \tag{4.17a}$$

$$\frac{\partial\dot{\varepsilon}_i^{in}}{\partial X_j} = -\frac{3}{4g}\left[\bar{\bar{f}}\frac{1}{g}W_{ik} + 2\bar{f}M_{ik}^2\right]\frac{\partial X_k'}{\partial X_j} \tag{4.17b}$$

$$\frac{\partial\dot{\varepsilon}_i^{in}}{\partial R} = -\frac{3n}{2K^*}\left(\frac{f}{K^*}\right)^{n-1}\frac{M_{ij}^2(\sigma_j' - X_j')}{g} \tag{4.17c}$$

$$\frac{\partial\dot{X}_i}{\partial\dot{\varepsilon}_j^{in}} = \frac{3}{2}N_{ij}^1 \tag{4.18a}$$

$$\frac{\partial\dot{X}_i}{\partial X_j} = -Q_{ij}^1\dot{p} \tag{4.18b}$$

$$\frac{\partial\dot{X}_i}{\partial\dot{p}} = -Q_{ij}^1 X_j \tag{4.18c}$$

$$\frac{\partial\dot{R}}{\partial R} = -b\dot{p} \tag{4.19a}$$

$$\frac{\partial \dot{R}}{\partial \dot{p}} = b(Q - R) \tag{4.19b}$$

$$\frac{\partial \dot{p}}{\partial \dot{\varepsilon}_i^{in}} = \frac{1}{3\dot{p}}(M_{ik}^3 \dot{\varepsilon}_k^{in} + \dot{\varepsilon}_k^{in} M_{ki}^3) \tag{4.20}$$

where

$$\bar{\bar{f}} = \frac{3}{2}\frac{n}{K^*}\left(\frac{f}{K^*}\right)^{n-1} - \frac{3}{2}\bar{f}\frac{1}{g}$$

$$g = \sqrt{\tfrac{3}{2}(\sigma_i' - X_i')' M_{ij}^1 (\sigma_j' - X_j')}$$

$$\bar{f} = \left(\frac{f}{K^*}\right)^n$$

$$W_{ik} = W_i\left[M_{kl}^1(\sigma_l' - X_l') + M_{lk}^1(\sigma_l' - X_l')\right]$$

$$W_i = M_{ik}^2(\sigma_k' - X_k')\frac{1}{g}$$

$$i, j, k, l = 1,2,\ldots 6$$

and M_{ij}^1, M_{ij}^2, M_{ij}^3, N_{ij}^1, Q_{ij}^1 and g are defined in Appendix IV.

Solving equations (4.14) to (4.16) results in an expression for the inelastic strain increment as a function of the total strain increment,

$$\Delta\varepsilon_i^{in} = F_i^0 + F_{ij}^1 \Delta\varepsilon_j^T \tag{4.21a}$$

The functions F_i^o and F_{ij}^1 are defined in Appendix IV.

Then the increments of stress $\Delta\sigma_i$, and state variable ΔX_i and ΔR can all be expressed as functions of the total strain increment $\Delta\varepsilon_i^T$,

$$\Delta\sigma_i = C_{ij}^1\left[\Delta\varepsilon_j^T - [F_j^0 + F_{jl}^1 \Delta\varepsilon_l^T]\right] \tag{4.21b}$$

$$\Delta X_i = (PF6)_i + (PF7)_{ij}\Delta\sigma_j \tag{4.21c}$$

$$\Delta R = d1 + d2_i\,\Delta\sigma_i \tag{4.21d}$$

where C^I_{ij} , $(PF6)_i$, $(PF7)_{ij}$,d1 and $d2_i$ are given in Appendix IV.

Equations (4.21a) to (4.21d) provide the complete set of equations for the integration of the equations in FE analysis.

Then all the variables at time t+Δt can be updated so that:

$$\sigma_{i(t+\Delta t)} = \sigma_{i(t)} + \Delta\sigma_i \tag{4.22a}$$

$$\varepsilon^{in}_{i(t+\Delta t)} = \varepsilon^{in}_{i(t)} + \Delta\varepsilon^{in}_i \tag{4.22b}$$

$$X_{i(t+\Delta t)} = X_{i(t)} + \Delta X_i \tag{4.22c}$$

$$R_{(t+\Delta t)} = R_{(t)} + \Delta R \tag{4.22d}$$

Furthermore, the interface of UMAT with the main program of ABAQUS (Standard UMAT only) also requires provision of the Jacobian matrix, D_{ij}, at each increment level. This can be obtained from equation (4.21b), so that:

$$D_{ij} = \frac{\partial\Delta\sigma_i}{\partial\Delta\varepsilon^T_j} = C^I_{ij} - C^I_{ik}F^I_{kj} \tag{4.23}$$

It can be seen that the second term in the Jacobian matrix is directly associated with the inelastic deformation. Since significant non-elastic strains are involved, the Jacobian matrix is a variable stiffness matrix and must be updated from one increment to the next increment.

4.2.3 Implementation of the Crystallographic Model

Some short hand notations have been introduced into the constitutive equations for the crystallographic model. The notations are given in Appendix IV.

Similar to the phenomenological model, the following incremental equations are obtained for the crystallographic model:

$$\Delta\sigma_i = Cl_{ij}(\Delta\varepsilon_j^T - \Delta\varepsilon_j^{in}) \qquad (i,j = 1,2,\cdots 6) \qquad (4.24a)$$

$$\Delta\varepsilon_j^{in} = M3_{jm}\Delta\gamma_m \qquad (j = 1,2,\cdots 6;\ m = 1,2,\cdots 18) \qquad (4.24b)$$

$$\Delta\tau_s = MM1_{sj}\Delta\sigma_j \qquad (j = 1,2,\cdots 6;\ s = 1,2,\cdots 18) \qquad (4.24c)$$

$$\Delta\gamma_m = [(1-\theta)\dot{\gamma}_{m(t)} + \theta\dot{\gamma}_{m(t+\Delta t)}]\Delta t \qquad (m = 1,2,\cdots 18) \qquad (4.24d)$$

$$\Delta x_s = \Delta t[(1-\theta)\dot{x}_{s(t)} + \theta\dot{x}_{s(t+\Delta t)}]\Delta t \qquad (s = 1,2,\cdots 18) \qquad (4.24e)$$

where $0 \le \theta \le 1.0$

The rates of $\dot{\gamma}_m$ and $\dot{x}_m$ at time $t + \Delta t$ can be expressed by a Taylor expansion in the following forms:

$$\dot{\gamma}_{s(t+\Delta t)} = \dot{\gamma}_{s(t)} + \frac{\partial\dot{\gamma}_s}{\partial\tau_m}\Big|_t \Delta\tau_m + \frac{\partial\dot{\gamma}_s}{\partial x_m}\Big|_t \Delta x_m \qquad (4.25a)$$

$$\dot{x}_{s(t+\Delta t)} = \dot{x}_{s(t)} + \frac{\partial\dot{x}_s}{\partial\dot{\gamma}_m}\Big|_t \Delta\dot{\gamma}_m + \frac{\partial\dot{x}_s}{\partial x_m}\Big|_t \Delta x_m \qquad (4.25b)$$

Substituting equations (4.25a) to (4.25b) into (4.24) leads to the following:

$$\Delta\gamma_s = \Delta t[\dot{\gamma}_{s(t)} + \theta\frac{\partial\dot{\gamma}_s}{\partial\tau_m}\Big|_t \Delta\tau_m + \theta\frac{\partial\dot{\gamma}_s}{\partial x_m}\Big|_t \Delta x_m] \qquad (4.26a)$$

$$\Delta x_s = \Delta t[\dot{x}_{s(t)} + \theta\frac{\partial\dot{x}_s}{\partial\dot{\gamma}_m}\Big|_t \Delta\dot{\gamma}_m + \theta\frac{\partial\dot{x}_s}{\partial x_m}\Big|_t \Delta x_m] \qquad (4.26b)$$

Equation (4.25a) leads to:

$$\Delta\dot{\gamma}_s = \dot{\gamma}_{s(t+\Delta t)} - \dot{\gamma}_{s(t)} = \frac{\partial\dot{\gamma}_s}{\partial\tau_m}\Big|_t \Delta\tau_m + \frac{\partial\dot{\gamma}_s}{\partial x_m}\Big|_t \Delta x_m \qquad (4.26c)$$

where the partial differential expressions in each term of above equations are as follows:

$$\frac{\partial\dot{\gamma}_s}{\partial\tau_m} = AA1_{sm}\,,\ \frac{\partial\dot{\gamma}_s}{\partial x_m} = AA2_{sm} \qquad (4.26d)$$

$$\frac{\partial\dot{x}_s}{\partial\dot{\gamma}_m} = BB1_{sm}\,,\ \frac{\partial\dot{x}_s}{\partial x_m} = BB2_{sm} \qquad (4.26e)$$

where s,m =1,2,...18;

$$AA1_{sm} = \begin{cases} 0, & \text{when } s \neq m \\ \dfrac{n_i}{k_i}\left\langle\dfrac{f_m}{k_i}\right\rangle^{n_i-1}\dfrac{\tau_m - x_m}{|\tau_m - x_m|}, & \text{when } s = m \end{cases} \qquad (4.26f)$$

$$AA2_{sm} = -AA1_{sm} \qquad (4.26g)$$

$$BB1_{sm} = \begin{cases} 0, & \text{when } s \neq m \\ c_i - d_i\dfrac{x_m\dot{\gamma}_m}{|\dot{\gamma}_m|}, & \text{when } s = m \end{cases} \qquad (4.26h)$$

$$BB2_{sm} = \begin{cases} 0, & \text{when } s \neq m \\ -d_i|\dot{\gamma}_m|, & \text{when } s = m \end{cases} \qquad (4.26i)$$

The suffix i in the above matrices has two values, i.e. o and c and representing octahedral slip and cubic slip systems respectively. Equations (4.26f) to (4.26i) implies that there is no cross slip or interaction between slip systems, which is consequence of no interaction between slip systems introduced in the constitutive equations.

Combining equations (4.24a) to (4.24c), (4.26a) to (4.26c), the increments of $\Delta\tau_s$, $\Delta\gamma_s$ and Δx_s can be obtained as functions of the known values of variables at time t and total strain increment $\Delta\varepsilon_j^T$. Using the additional short hand notations, given in Appendix IV the increments of the variables can bé expressed as:

$$[\Delta\tau]_s = MM1_{sj} Cl_{jk}(\Delta\varepsilon_k^T - \Delta\varepsilon_k^v) = MM1_{sj} Cl_{jk}[\Delta\varepsilon_k^T - M3_{km}(\Delta\gamma)_m] \quad (4.27a)$$

$$(\Delta\gamma)_m = E4_m + E5_{mk}\Delta\varepsilon_k^T \quad (4.27b)$$

$$[\Delta x]_s = CCl_s + aCC3_{sk}\Delta\varepsilon_k^T - aCC4_{sm}(\Delta\gamma)_m \quad (4.27c)$$

where, s,m=1,2,...18; j,k=1,2,...6.

The matrices $E4_m$, $E5_{mk}$, CCl_s, $CC3_{sk}$, $CC4_{sm}$ and parameter a are also given in Appendix IV.

Then the increment of all the other variables can be solved, to give

$$\Delta\varepsilon_j^{in} = M3_{jim}(\Delta\gamma)_m \quad (4.28)$$

$$\Delta\sigma_i = Cl_{ij}(\Delta\varepsilon_j^T - \Delta\varepsilon_j^{in}) \quad (4.29)$$

Finally, the Jacobian matrix at each increment level required by the ABAQUS interfacing with the UMAT subroutine can be expressed as:

$$D_{ij} = \frac{\partial\Delta\sigma_i}{\partial\Delta\varepsilon_j^T} = Cl_{ij} - Cl_{ik}\frac{\partial\Delta\varepsilon_k^{in}}{\partial\Delta\varepsilon_j^T} = Cl_{ij} - Cl_{ik}M3_{km}\frac{\partial(\Delta\gamma)_m}{\partial\Delta\varepsilon_j^T} \quad (4.30)$$

Similar to the phenomenological model, the second term in the Jacobian matrix is directly associated with the inelastic deformation. Since significant non-elastic strain are involved, the Jacobian matrix is a variable stiffness matrix and must be updated from one increment to the next increment.

4.3 Nonisothermal Numerical Implementation

The thermomechanical constitutive model developed in this work is based on modifying the isothermal constitutive model. Consequently the implementation procedure described in the previous sections can be directly used for the thermomechanical model.

For a given time increment, Δt, the total strain increment includes elastic, inelastic strain and thermal strain increments

$$\Delta\varepsilon_i^T = \Delta\varepsilon_i^e + \Delta\varepsilon_i^{in} + \Delta\varepsilon_i^{th} \qquad (i=1, 2, \ldots 6) \tag{4.31}$$

However, the thermal strain increment can be directly calculated by the temperature increment corresponding to the time increment as:

$$\dot{\varepsilon}_i^{in} = \frac{d\alpha_i}{dT}\dot{T}(T - T_0) + \alpha_j\dot{T} \tag{4.32}$$

So that

$$\Delta\varepsilon_j^{th} = \alpha_{i(t+\Delta t)}(T_{t+\Delta t} - T_0) - \alpha_{i(t)}(T_t - T_0) = \alpha_{i(t+\Delta t)}\Delta T + \Delta\alpha_i(T_t - T_0) \tag{4.33}$$

Since the constitutive equations for the elastic and inelastic strain and strain rates in the thermomechanical model have the same formulation as those in the isothermal model, the implementation procedure described in the previous sections can be directly used for the thermomechanical model.

In the single crystal material principal axes system Hooke's law is:

$$\sigma_i = C_{ij}\varepsilon_j^e = C_{ij}(\varepsilon_j^T - \varepsilon_j^{in} - \varepsilon_j^{th}) \tag{4.34a}$$

Differentiating this equation with respect to time leads to the following:

$$\dot{\sigma}_i = C_{ij}(\dot{\varepsilon}_j^T - \dot{\varepsilon}_j^{in} - \dot{\varepsilon}_j^{th}) + \frac{dC_{ij}}{dT}(\varepsilon_j^T - \varepsilon_j^{in} - \varepsilon_j^{th})\dot{T} \tag{4.34b}$$

The equations (4.31) to (4.34) are the same for both the phenomenological model and crystallographic model for the nonisothermal numerical implementation procedure. Only the calculations of inelastic strain and strain rate involve the

constitutive equation of the material models. To demonstrate the parts of viscoplastic deformation integral for nonisothermal condition, the integration process of phenomenological model is given in the following.

Applying the trapezoidal rule to the equations of stress rate, inelastic strain rate, back stress rate and isotropic stress rate .

$$\Delta\sigma_i = \Delta t[(1-\theta)\dot{\sigma}_{i(t)} + \theta\dot{\sigma}_{i(t+\Delta t)}] \tag{4.35a}$$

$$\Delta\varepsilon_i^{in} = \Delta t[(1-\theta)\dot{\varepsilon}_{i(t)}^{in} + \theta\dot{\varepsilon}_{i(t+\Delta t)}^{in}] \tag{4.35b}$$

$$\Delta X_i = \Delta t[(1-\theta)\dot{X}_{i(t)} + \theta\dot{X}_{i(t+\Delta t)}] \tag{4.35c}$$

$$\Delta R = \Delta t[(1-\theta)\dot{R}_t + \theta\dot{R}_{t+\Delta t}] \tag{4.35d}$$

The increment of stress is obtained as:

$$\Delta\sigma_i = [C_{ij}+\theta\Delta t\frac{dC_{ij}}{dT}\dot{T}]_{t+\Delta t}(\Delta\varepsilon_j^T - \Delta\varepsilon_j^{in} - \Delta\varepsilon_j^{th}) + \Delta C_{ij}[(\varepsilon_{jt}^T - \varepsilon_{jt}^{in} - \varepsilon_{jt}^{th}) - \Delta t(1-\theta)(\dot{\varepsilon}_{jt}^T - \dot{\varepsilon}_{jt}^{in} - \dot{\varepsilon}_{jt}^{th})] \tag{4.36}$$

Using the first order Taylor expansion to approximate the variables at time $t+\Delta t$: $\dot{\varepsilon}_{i(t+\Delta t)}^{in}$, $\dot{X}_{i(t+\Delta t)}$ and $\dot{R}_{t+\Delta t}$ leads to the following:

$$\dot{\varepsilon}_{i(t+\Delta t)}^{in} = \dot{\varepsilon}_{i(t)}^{in} + \frac{\partial\dot{\varepsilon}_i^{in}}{\partial\sigma_j}\Big|_t\Delta\sigma_j + \frac{\partial\dot{\varepsilon}_i^{in}}{\partial X_j}\Big|_t\Delta X_j + \frac{\partial\dot{\varepsilon}_i^{in}}{\partial R}\Big|_t\Delta R + \frac{\partial\dot{\varepsilon}_i^{in}}{\partial T}\Big|_t\Delta T \tag{4.37a}$$

$$\dot{X}_{i(t+\Delta t)} = \dot{X}_{i(t)} + \frac{\partial\dot{X}_i}{\partial\dot{\varepsilon}_j^{in}}\Big|_t\Delta\dot{\varepsilon}_j^{in} + \frac{\partial\dot{X}_i}{\partial X_j}\Big|_t\Delta X_j + \frac{\partial\dot{X}_i}{\partial\dot{p}}\Big|_t\Delta\dot{p} + \frac{\partial\dot{X}_i}{\partial T}\Big|_t\Delta T \tag{4.37b}$$

$$\dot{R}_{t+\Delta t} = \dot{R}_t + \frac{\partial\dot{R}}{\partial\dot{p}}\Big|_t\Delta\dot{p} + \frac{\partial\dot{R}}{\partial R}\Big|_t\Delta R + \frac{\partial\dot{R}}{\partial T}\Big|_t\Delta T \tag{4.37c}$$

$$\Delta\dot{p} = \dot{p}_{t+\Delta t} - \dot{p}_t = \frac{\partial\dot{p}}{\partial\dot{\varepsilon}_i^{in}}\Big|_t\Delta\dot{\varepsilon}_i^{in} \tag{4.37d}$$

$$\Delta\dot{\varepsilon}_i^{in} = \dot{\varepsilon}_{i(t+\Delta t)}^{in} - \dot{\varepsilon}_{i(t)}^{in} = \frac{\partial\dot{\varepsilon}_i^{in}}{\partial\sigma_j}\Big|_t \Delta\sigma_j + \frac{\partial\dot{\varepsilon}_i^{in}}{\partial X_j}\Big|_t \Delta X_j + \frac{\partial\dot{\varepsilon}_i^{in}}{\partial R}\Big|_t \Delta R + \frac{\partial\dot{\varepsilon}_i^{in}}{\partial T}\Big|_t \Delta T \qquad (4.37e)$$

The partial differential expressions in each term of Equations (4.37a) to (4.37e) are the same as in the isothermal implementation procedure with the exception of the temperature differential terms, which are expressed as:

$$\frac{\partial\dot{\varepsilon}_i^{in}}{\partial T} = \dot{\varepsilon}_i^{in}\left[\frac{dn}{dT}\ln\left(\frac{f}{K^*}\right) - \frac{n}{f}\frac{dk}{dT} - \frac{n}{K^*}\frac{dK^*}{dT}\right] \qquad (4.38a)$$

$$\frac{\partial\dot{X}_i}{\partial T} = \frac{3}{2}\frac{dN_{ij}}{dT}\dot{\varepsilon}_i^{in} - \frac{dQ_{ij}}{dT}X_j\dot{p} \qquad (4.38b)$$

$$\frac{\partial\dot{R}}{\partial T} = \frac{db}{dT}(W-R)\dot{p} + b\frac{dW}{dT}\dot{p} \qquad (4.38c)$$

Replacing $\Delta\dot{p}$ and $\Delta\dot{\varepsilon}_i^{in}$ with equations (4.37d) and (4.37e) into equations (4.37b) and (4.37c), then combining equations (4.35b), (4.35c), (4.35d), (4.37a), (4.37b) and (4.37c) leads to the following equation set:

$$\Delta\varepsilon_i^{in} = F_1(\Delta\sigma, \Delta X, \Delta R, \Delta T) \qquad (4.39a)$$

$$\Delta X_i = F_2(\Delta\sigma, \Delta X, \Delta R, \Delta T) \qquad (4.39b)$$

$$\Delta R = F_3(\Delta\sigma, \Delta X, \Delta R, \Delta T) \qquad (4.39c)$$

Equation (4.36) can be expressed as:

$$\Delta\sigma_i = F_4(\Delta\varepsilon^T, \Delta\varepsilon^{in}, \Delta\varepsilon^{th}) \qquad (4.39d)$$

$\Delta\varepsilon^T$ is a known value provided by ABAQUS, and $\Delta\varepsilon^{th}$ and ΔT can be calculated at the start of the time increment. Therefore the four unknown increments of the variables can be solved from the four equations (4.39a) to (4.39d) which are linear equations. The rest of the procedure is similar as the one for the isothermal implementation procedure.

It can be seen from above equations that it is necessary to calculate

$$\frac{\partial \dot{\varepsilon}_i^{in}}{\partial T}, \frac{\partial \dot{X}_i}{\partial T}, \frac{\partial \dot{R}}{\partial T}, \frac{dC_{ij}}{dT} \text{ and } \frac{d\alpha_i}{dT},$$

To determine these differentials the thermal expansion ratio, elastic constants and viscoplastic constants as functions of temperature must be established based on test data for nonisothermal conditions.

4.4. UMAT Programs and Interfacing ABAQUS

4.4.1 UMAT Coding

Two, 3D UMAT subroutine programs to implement the above numerical procedures for the phenomenological and the crystallographic model have been written in FORTRAN particularly for the finite element code ABAQUS. The subroutine will be called at each material calculation point to define the anisotropic mechanical constitutive behaviour of single crystal material.

The interface card between the subroutine UMAT and ABAQUS is *USER SUBROUTINE. This is then followed by the common subroutine header defined in ABAQUS. The stresses, strains and solution dependent state variables are solved incrementally by ABAQUS. When the subroutine UMAT is called, it is provided with the state at the start of the increment (stress and solution dependent state variables, temperature) and with the strain increments, temperature increment and the time increment. The subroutine UMAT performs two functions: it updates the stresses and the solution dependent state variables to their values at the end of the increment, and it provides the material Jacobian matrix, $\partial \Delta\sigma / \partial \Delta\varepsilon$, for the constitutive model as required for an iterative Newton-Rhapson solution in ABAQUS.

All the material parameters for subroutine UMAT follow the card *USER MATERIAL in the *.INP file of ABAQUS. All data in ABAQUS data cards must be real variables.

The only way to output values of any variables from UMAT is by using the solution dependent state variables, STATEV. The number of solution dependent state variables can be defined by the user using the card *DEPVAR in the .INP file of ABAQUS. The format of the output for the solution dependent state variables in ABAQUS followed the card *EL PRINT is

	SDV	for all solution dependent state variables
or		
	SDVn	for the nth solution dependent state variable

The detailed FORTRAN programs for the UMAT subroutine are given in Appendix IX, where comments have been provided in the subroutine to explain, step by step, the programming procedure.

For coding UMAT for nonisothermal mechanical conditions, the formulations of the functions for elastic material constants presented in section 4.3 and the appropriate temperature derivatives of the constants in the constitutive model have been coded in an ABAQUS subroutine UMAT. So for a nonisothermal mechanical simulation by ABAQUS, in the input file under the input card "*USER MATERIAL, CONSTANTA=number of constants" the data given are the coefficients of material constants functions with respect to temperature rather than material constants as for isothermal conditions. For nonisothermal simulations all material constants are variables of time or temperature and have to be determined at each time increment.

4.4.2 Thermal and Mechanical Loading Input Coding

The thermomechanical loading is generally very complicated. There are many different types of thermal and mechanical combinations. For thermal fatigue loading the phasing of strain and temperature can be arbitrarily varied. Most investigations have been using two basic mechanical strain versus temperature cycles: 1, the "in-phase" cycle, where the mechanical strain is maximum at maximum temperature; and 2, the "out-of-phase" cycle, where the mechanical strain is maximum at the minimum temperature.

To be able to simulate the thermomechanical loading and carry out the structural FE analysis, it is very important that the FE program can cope with the complex thermal mechanical loading combination. In this aspect, ABAQUS provides some facilities to allow the user to code the loading condition in the program for both thermal and mechanical conditions. These aspects of the facilities are described in the following sections.

(i). Temperature Input

There are three possible ways for a user to define temperature at the nodes of elements in the model. ABAQUS then interpolates between the material points. Method (1): the temperature may be defined using the data which is put on the input card directly; method (2) the temperature may be read from a ABAQUS results file generated during a previous heat transfer analysis; method (3) the temperature may be specified using user subroutine UTEMP. More detailed descriptions of the above three methods are given in Appendix V.

For the calculations in this thesis, it was determined that method 1 is the most appropriate method for defining the temperature loading in the ABAQUS program. Consequently this method has been used to code a linear increase of temperature with time in the ABAQUS input cards.

(ii). Mechanical Loading Input

In ABAQUS there are some facilities for loading input and these facilities can describe various loading conditions, such as displacement control and stress control. Both displacement control and stress control can be input by using input cards *BOUNDARY with *AMPLITUDE or *USER SUBROUTINE. The detailed description of the syntax for using these cards is given in Appendix IX. The syntax 1 is used in current research program for linear variation of displacement input.

4.5. Verification

4.5.1 Isothermal Verification

A comprehensive procedure was carried out to verify the numerical implementation procedures, using the UMAT subroutines and their interface with the ABAQUS programs. The material parameters used in the both models were those identified in chapter 3. The verification included two main stages:

(i) Simulation of the elastic mechanical response

These studies were carried out to verify that the stress and strain transformation formulations in the UMAT subroutines were correct in describing the anisotropic mechanical response of single crystal alloys.

(ii) Simulation of the elastic-viscoplastic mechanical response

These studies were carried out to verify the incremental formulation and time integration schemes in the UMAT subroutines were correct in describing the time dependent behaviour of single crystal alloys.

Single element and cylindrical bar specimens were used in the verification calculations. The material constants identified in Chapter 3 were used in the FE calculations. Only the results obtained from the single element will be summarised in this section. The results obtained from cylindrical bar specimen will be presented

in Chapter 5. The single cubic element used in the verification calculations is the ABAQUS C3D20 type, i.e. 20-node quadratic brick element. The implicit operator θ was set to 0.5 for the implicit integration procedures coded in UMAT.

The boundary condition of the specimen is one end fixed and loading at the other end. The loading condition is displacement control at a constant strain rate to simulate the strain controlled laboratory tests.

The verification for both models is achieved mainly by comparing the results from the finite element results with results from theoretical simulations obtained using a FORTRAN program. The FORTRAN programs provide a purely mathematical simulation of the stress and strain response predicted by the constitutive models. The accuracy of the theoretical simulation results are verified and compared with experimental results in Chapter 6. Therefore, the simulation results can be used then to verify the finite element calculation results. The comparisons indicated that there is generally good agreement between the two sets of results. Some examples are given in the following sections.

Figure 4.1 shows the stress and total strain curves predicted by the finite element calculations using the phenomenological model. Four different orientations [001], [111], [011] and [123] were studied to examine the influence of crystal orientation on deformation behaviour of the single crystal alloy. Strain rate of 0.004/s was used in the simulation. It can be seen that crystal orientation has a strong influence on the mechanical behaviour of single crystal alloy. The [111] orientation has the highest elastic modulus, whilst [001] the lowest. Consequently, the [111] orientation exhibits higher stress compared other orientations at elastic region, and the inelastic strain component is higher compared than other orientations for a given total strain level. This can be seen more clearly in Fig.4.2a and Fig.4.2b, where comparison between FE calculations and theoretical simulations has been given in terms of stress and inelastic strain response. It is observed that with the same total strain $\Delta\varepsilon^T$= 0.5%, the inelastic strain for the [111] orientation is about 10 times higher compared to the [001] orientation. It is also noticed that the axial stress and strain responses for

the [011] and [123] orientations were found to be same in terms of both total strain and inelastic strain.

The comparison indicated that the strong orientation dependent stress and strain response, calculated by FE, agrees well with the theoretical results which were found to be in good agreement with experimental results (Li, [1993], Li and Smith [1995]). Further comparisons of the theoretical results and experimental results are given in Chapter 6.

The material anisotropy of single crystal induces significant anisotropic mechanical response. Even under simple uniaxial loading condition, the single crystal material, for most orientations, exhibits three dimensional deformation, i.e. the six strain components will be all non-zero. As an example, Fig.4.3a and 4.3b show the transverse and shear strain response as a function of axial strain for the [123] and [011] orientations. Although the axial stress and strain response for the [011] and [123] orientations are exactly same, as shown in Fig.4.1, the two transverse strains ε_{11} and ε_{22} for the [011] and [123] orientations are not same, and change with axial strain ε_{33} in different ways. Also for simple uniaxial loading, there are no shear strains induced for the [011] orientation in the given global coordinate system, but three shear strain components, $\varepsilon_{12}, \varepsilon_{13}$, and ε_{23} are all non-zero for the [123] orientation.

Another important feature of the constitutive equations that describe the high temperature mechanical behaviour of single crystal alloys, is the strain rate dependent response. The ability of the UMAT subroutine to calculate the strain rate effect has also been examined. Figures 4.4a and 4.4b plot the stress as a function of total strain and inelastic strain respectively for the [123] orientation at three different total strain rates, 0.4, 0.04 and 0.004 s^{-1}. It can be seen that both the FE calculations and the theoretical simulations indicate the same results, with a higher strain rate producing higher stress.

The comparison of the FE calculation results using the crystallographic model with the theoretical simulation results are presented in Figs. 4.5 and 4.6, in which the material parameters were those identified in chapter 3 for the crystallographic model. Strain rate of 0.004/s was used in the finite element calculations. Again there is excellent agreement between the theoretical and FE results. Further detailed simulations using the FE code and UMAT routines using the crystallographic model are given in the following chapter.

4.5.2 Nonisothermal Verification

The verifications carried out at this stage are mainly to demonstrate that the numerical integration procedure developed in this work is an appropriate approach. The UMAT program developed for the implementation of the numerical integration and its interface with ABAQUS program was also verified. This is achieved by comparing the ABAQUS results with those obtained from a FORTRAN program. The FORTRAN program is a numerical simulation of the thermal mechanical constitutive equations. This is a purely mathematical simulation of the stress and strain response without the deformation compatibility and overall load equilibrium. On the other hand, deformation compatibility, overall load equilibrium and boundary constrain are all required in the stress-strain calculations using ABAQUS. Therefore the results from the FORTRAN calculation can be used as benchmark for the stress-strain response from the ABAQUS calculation.

Two typical cases were studied.

Case 1:

Single element (a brick) loaded in [001], subjected to total strain rate of 0.004/s, with a fixed-time increment of 0.001, with a temperature range from 50°C to 762.5°C. Total time of the simulation was 1.125s. This corresponds to an in-phase thermomechanical loading condition is in-phase.

Case 2:

Single element (a brick) loaded in [111], with conditions which were the same as case 1.

The temperature dependent elastic properties, such as Young's modulus, E(T), and shear modulus G(T), exhibit nonlinear variation with temperature. These parameters were fitted using cubic curve functions with temperature in Chapter 3. Consequently, the thermal elastic deformation is nonlinear. The time stepping in finite element calculation is important for this case. Even for elastic deformation steps the loading speed has to be kept the same as for a viscoplastic deformation step, which is different compared to the isothermal simulation. For isothermal simulation the amplitude of displacement for elastic response step can be different with the one for viscoplastic response step, since the elastic response in the isothermal case is linear.

The results from the ABAQUS and FORTRAN calculations are compared in Figures 4.7 and 4.8. The good agreement of the results demonstrates that the UMAT coding for thermal-mechanical simulation and thermal mechanical loading input in the program were successful. It is recognised that there are only vary limited results for the thermal mechanical simulations, due to lack of experimental data for thermal mechanical loading. Further experiments, in particular of multiaxial and thermal mechanical tests, are vital for further development of the models and numerical methods for single crystal alloys. The studies conduced in this work will provide fundamental information the next stage development.

4.6 Improvement of Computing Efficiency of FE Implementation

The efficiency of a FE program computation depends on the UMAT coding. In this study many efforts were made to achieve maximum computational efficiency. The following describes the steps taken to improve efficiency.

4.6.1. Integration Scheme Application

The quality of the UMAT coding depends on the stability of the integration scheme coded and the convergence rate. In most cases the accuracy of the definition of the Jacobian matrix, $\frac{\partial \Delta\sigma}{\partial \Delta\varepsilon}$, is the most important factor governing the convergence rate. The definition of Jacobian matrix, $\frac{\partial \Delta\sigma}{\partial \Delta\varepsilon}$, depends on the integration scheme used if the constitutive model is in rate form. For any nontrivial constitutive model these are challenging tasks. So the Jacobian matrix must be determined properly using an appropriate integration procedure.

The integration scheme used in this study is an implicit integration method. It enables the integration scheme to be stable. This is because the Jacobian matrix determined by the implicit integration scheme is more accurate than by an explicit integration scheme. In a preliminary study for implementing the numerical models into UMAT, both implicit and explicit integration schemes were used in the same procedure, in which the implicit scheme was applied to the inelastic strain rate, whilst explicit integration was applied to other variables, i.e.

$$\Delta\varepsilon_i^{in} = \Delta t[(1-\theta)\dot{\varepsilon}_{i(t)}^{in} + \theta\dot{\varepsilon}_{i(t+\Delta t)}^{in}]$$

$$\Delta X_i = \Delta t\dot{X}_{i(t)}$$

$$\Delta R = \Delta t\dot{R}_t$$

In the preliminary procedure of implementing models into UMAT, all the rate equations were transformed to incremental equations and the implicit integration scheme was applied to stress, elastic strain and inelastic strain rates. However, an explicit integration scheme, i.e. forward Euler, was applied to back stress rate $\dot{X}$ and isotropic stress rate $\dot{R}$. This simplified the analysis but resulted in very time consuming solutions and very small time increments. The time increments had to be fixed to 0.001 second in the integration procedure and the facility of automatic time increment determination provided by ABAQUS could not be used, otherwise the integration procedure would crash. These are caused by the explicit integration scheme application involved because the explicit integration method has a stability

limit. To improve the computational efficiency of the integration procedure, the implicit integration scheme was then applied to all variables. This increased time increment to a wide range between 0.01 and 0.1 second for different strain rate controlled simulation and allowed the facility of automatic time increment determination to be used. The speed of computation was greatly increased by more than 5 times. The equations and analysis for this fully implicit scheme are described in section 4.2.2.

4.6.2. Further Improvements in Accuracy

To further improve the accuracy of the calculation, a non-linear iteration routine was coded in the UMAT. Even though the approximate closed form solution was achieved, using the Taylor expansion with limited terms still reduced the accuracy of the solutions. The solutions obtained from the procedure described in sections 4.2 and 4.3 are taken as the initial estimated values for the nonlinear iterative procedure described here. The solutions from the nonlinear iterative procedure are more precise than the approximate closed form solutions.

The non-linear iteration procedure coded into the UMAT is the Newton-Rhapson solution procedure. To demonstrate the iteration procedure, a procedure for uniaxial loading alone is described in the following:

In the phenomenological model subjected to uniaxial loading, the rate variables are:

$$\dot{\varepsilon}^{in} = f(\sigma, X, R) \tag{4.40a}$$

$$\dot{X} = g(\dot{\varepsilon}^{in}, X) \tag{4.40b}$$

$$\dot{R} = h(\dot{\varepsilon}^{in}, R) \tag{4.40c}$$

and the incremental equations are:

$$\Delta\varepsilon^{in} = \Delta t[(1-\theta)\dot{\varepsilon}_t^{in} + \theta\dot{\varepsilon}_{t+\Delta t}^{in}] \tag{4.41a}$$

$$\Delta X = \Delta t[(1-\theta)\dot{X}_t + \theta\dot{X}_{t+\Delta t}] \tag{4.41b}$$

$$\Delta R = \Delta t[(1-\theta)\dot{R}_t + \theta\dot{R}_{t+\Delta t}] \tag{4.41c}$$

Substituting

$$\dot{\varepsilon}^{in}_{t+\Delta t} = f(\sigma_{t+\Delta t}, X_{t+\Delta t}, R_{t+\Delta t}) \tag{4.42}$$

into equation (4.41a), and noting that $\sigma_{t+\Delta t} = \sigma_t + \Delta\sigma$, etc, then

$$\Delta\varepsilon^{in} = \Delta t[(1-\theta)\dot{\varepsilon}^{in}_t + \theta f(\sigma_t + \Delta\sigma, X_t + \Delta X, R_t + \Delta R)] \tag{4.43}$$

So the iteration equation is:

$$\Delta\varepsilon^{in}_{(i+1)} = \Delta t[(1-\theta)\dot{\varepsilon}^{in}_t + \theta f(\sigma_t + \Delta\sigma_{(i)}, X_t + \Delta X_{(i)}, R_t + \Delta R_{(i)})] \tag{4.44}$$

with

$$\Delta\sigma_{(i)} = Cl[\Delta\varepsilon^{T}_{(i)} - \Delta\varepsilon^{in}_{(i)}] \tag{4.45}$$

For i =0, the values of the all increments are the solutions carried out by the approximate closed form solution procedure. Combining with equations (4.41a) to (4.41c) and the constitutive equations (4.40a) to (4.40c), the iterative procedure will continue until the specific precision is satisfied. A larger time increment is therefore allowed for the nonlinear solution procedure since the incremental relations are more stable. This nonlinear iterative procedure was coded in the subroutine called ITERATION.

Also the Jacobian matrix for the nonlinear solution was determined from the theoretical analysis procedure to correspond to the nonlinear procedure. The Jacobian matrix and the procedure are briefly presented in the following:

$$\Delta\sigma_i = C^l_{ij}[\Delta\varepsilon^{T}_j - \Delta\varepsilon^{in}_j] \tag{4.46a}$$

$$\Delta\varepsilon^{in}_i = \Delta t[(1-\theta)\dot{\varepsilon}^{in}_{i(t)} + \theta\dot{\varepsilon}^{in}_{i(t+\Delta t)}] \tag{4.46b}$$

$$\Delta X_i = \Delta t[(1-\theta)\dot{X}_{i(t)} + \theta\dot{X}_{i(t+\Delta t)}] \tag{4.46c}$$

$$\Delta R = \Delta t[(1-\theta)\dot{R}_t + \theta\dot{R}_{t+\Delta t}] \tag{4.46d}$$

$$\dot{\varepsilon}^{in}_{j(t+\Delta t)} = \dot{\varepsilon}^{in}_{j(t+\Delta t)}(\sigma_{j(t)} + \Delta\sigma_j, X_{j(t)} + \Delta X_j, R_t + \Delta R) \tag{4.46e}$$

$$\dot{X}_{j(t+\Delta t)} = \dot{X}_{j(t+\Delta t)}(\dot{\varepsilon}^{in}_{j(t+\Delta t)}, X_{j(t)} + \Delta X_j) \tag{4.46f}$$

$$\dot{R}_{t+\Delta t} = \dot{R}_{t+\Delta t}(\dot{p}(\dot{\varepsilon}^{in}_{j(t+\Delta t)}), R_t + \Delta R)] \qquad (4.46g)$$

where, Equations (4.46e) to (4.46g) indicate that $\dot{\varepsilon}^{in}_{j(t+\Delta t)}$, $\dot{X}_{j(t+\Delta t)}$ and $\dot{R}_{t+\Delta t}$ are the functions of values of σ_j, X_j, R and $\dot{\varepsilon}^{in}_j$ at time $t+\Delta t$.

Substituting Equations (4.46e) to (4.46g) in Equations (4.46b) to (4.46d) respectively then combining with (4.46a) lead to the solution of the Jacobian matrix:

$$D_{ij} = \frac{\partial \Delta \sigma_i}{\partial \Delta \varepsilon^T_j} = (C\Omega MA1)^{-1}_{ik} C^1_{kj} \qquad (i,j,k = 1,2,...6) \qquad (4.47)$$

where $(C\Omega MA1)^{-1}_{ik}$ is the inverse matrix of $(C\Omega MA1)_{ik}$ and

$$(C\Omega MA1)_{ik} = [\delta_{ik} + a \cdot C^1_{ij}(\Omega MA)_{jk}]$$

$$a = \theta \Delta t$$

δ_{ik} is unit matrix and C^1_{ij} and $(\Omega MA)_{jk}$ are given in Appendix IV. The non-linear iteration procedure was based on the Newton Raphson scheme. The details of Newton Raphson method can be referred to most of numerical analysis books [Burden and Faires [1997], Constantinide and Mostoufi [1999]).

The calculation procedure of Jacobian matrix for the nonlinear solution was coded in the subroutine called NONLINJ. In the new version of UMAT, the approximate closed form solution procedure is first run to determine the solutions of all variables and the corresponding Jacobian matrix, then an option is provided to decide if switching on the nonlinear solution procedure or not by the value of a control parameter. If the nonlinear solution procedure is needed, the ITERATION subroutine will be called and the all values of variables from the approximate closed form solution procedure will be initial iteration values for nonlinear solution procedure. Consequently, the subroutine, NONLINJ, will be called to provide the Jacobian matrix corresponding to nonlinear solution. The new version of UMAT program is presented in Appendix IX. It is not clear that solution procedure is the best option although the non-linear solution is theoretically better. Further work is required to assess the best option.

CHAPTER 5

RESULTS OF FINITE ELEMENT STRUCTURAL ANALYSIS

5.1. Introduction

The constitutive models and the numerical implementation procedure, as well as the UMAT and ABAQUS interfacing codes, have been developed for general multiaxial 3-D stress analyses. The results from structural FE analyses can provide the characteristics of the material deformation for complex loading which may not be obtained easily from tests. These analyses can guide further experimental investigations and provide further improvements in predicting the integrity of a component. A number of specimens with different shapes have been used to assess the performance of the codes.

This chapter presents the results from finite element structural calculations obtained from both the phenomenological and the crystallographic models. Since a large number of calculations have been performed, only some important cases are presented in the following sections. The finite element calculation results will be compared with the theoretical simulations and some experimental results obtained from other sources (Li [1993], Li and Smith [1995a, 1995b]). Also the various results obtained from the phenomenological and the crystallographic models will be compared to examine further the intrinsic characteristics of different models.

In section 5.2, a detailed description of each geometry and element type, as well as the loading condition used in the FE analysis is presented. The FE results using both the phenomenological and crystallographic models for uniaxial loading are given in section 5.3. For multiaxial loading, the results from the two models are compared in section 5.4. Finally a comparison between the FE results for different loading conditions is given in section 5.5.

5.2. Specimen Geometry and Loading Conditions

5.2.1.Specimen Geometry

The specimens and various element types used in the structural stress analysis are as follows:

(i) Cylindrical Bar

A cylindrical bar was divided into 540 elements. It had 3 layers distributed along the radius. The central layer, which was a thinner cylinder, consisted of the C3D15 type element, i.e. 15-node quadratic triangular prism. Other layers consisted of the C3D27 type element, i.e. 27-node brick elements. All layers had 18 rows, with every row having 10 elements.

The cylindrical mesh requires a special ABAQUS functional option *MPC which allows constraints to be imposed to deal with the generation of the node numbers. The nodes which are at both the start and the end of the layers and located along the longitudinal direction have two numbers because the nodal distribution is around a circle. For the nodes in the longitudinal axial there are 18 numbers for a single node because 18 elements share a single node in the centre of a circle on cross section. The initial mesh of the cylindrical bar is plotted in Fig.5.1a.

(ii) Column with a Square Section

A bar with a square section was modelled with 8 layers of elements along its longitudinal axis and each layer had 16 elements. There were a total of 128 elements in the column bar. A simple 8-node linear brick element, i.e. type C3D8, was used for the bar. The initial mesh is plotted in Fig.5.1b.

(iii) Plate

The plate specimen had a rectangular shape which was divided into 40 elements. The element type was also a 20-node quadratic brick, element type C3D20. The initial mesh of the plate is plotted in Fig.5.1c.

(iv) Uniform Tube Specimen

The tube specimen had an inner radius of 4mm, outer radius of 8mm and with a length of 100mm. The tube was modelled using 100 solid elements of type C3D27 with 4 layers of elements parallel to its longitudinal axis. The initial or undeformed mesh of the tube specimen is plotted in Fig.5.2a.

(v) Nonuniform Tube Specimen

The nonuniform tube specimen had larger sections at both ends to model the practical test specimen more realistically. The inner radius along the length of the specimen was 6 mm. The outer radius of the middle section was 8mm and the other radius of end section was 14mm. The specimen was modelled using 832 elements of type C3D20R. The geometry and the initial mesh of the DERA specimen is plotted in Fig.5.2 b. This specimen was used for simulating the deformations of single crystal surperalloys under different loading condition carried out in real tests.

5.2.2. Loading Condition Applied

The loading conditions applied in the analyses included the following different cases:

(i) Uniaxial loading

Monotonic tension with either strain control or stress control. Different strain rates have been applied in strain control simulations to study the orientation dependence of the deformation of the single crystal superalloys.

(ii) Cyclic loading

Uniaxial cyclic loading with strain control was used in the simulations.

(iii) Torsion loading

Both force and displacement control methods were used in torsion simulations. Torque was applied in the force control method whilst a twist angle was imposed increasing linearly with time in the displacement control method.

(iv) Combined tension-torsion loading

Force control method was used. The ratio of axial stress to shear stress was varied to simulate different working loads.

5.3. Results of Uniaxial Loading

Uniaxial loading has been applied to specimens with different shapes using both the phenomenological and crystallographic models. The results for the single element under uniaxial loading were presented in Chapter 4 and verified the coded UMAT subroutines. Since a large number of calculations for various specimens have been carried out, only the important examples will be presented to illustrate the deformation characteristics of engineering components made of single crystal materials. The FE results from the column and cylindrical bar under uniaxial loading were found to be similar so here only the FE results of cylindrical bar and the plate using the two models, as well as single element under cyclic loading are presented and discussed in what follows.

5.3.1 Cylindrical Bar

The FE calculations for the cylindrical bar specimen have been carried out under displacement control. The bottom end of the cylindrical bar was fixed, and the top end was free, but with same displacement in the Z* direction which is the same as axis 3, shown in Fig. 5.1. Therefore, except for the elements near the fixed end, the strain distribution along the Z* direction of the cylindrical bar were the same for all the other elements. A number of cases for various crystal orientations have been calculated. The results for the cases in which loading direction Z* was along [001],

[111] and [123] orientation, which represents the most complex case, are given as the examples in the following sections.

(i) Global Stress and Strain Response

As mentioned above, for the given constraint and loading conditions, the global stress and strain response of the cylindrical bar is uniform along the Z* direction. Therefore, the stress and strain response can be compared with the single element and the theoretical results. Results in terms of total strain and inelastic strain for the different calculation results obtained from the phenomenological model are compared in Fig.5.3 and Fig. 5.4 respectively. It can be seen that the FE results for single element and cylindrical bar were both in good agreement with the theoretical simulation results, which are also found to be in agreement with experimental data (Li [1993]).

Similar comparisons are also made for the transverse and shear strain response in Fig.5.5 and 5.6 respectively. The good agreements demonstrate that the numerical implementation procedure and the UMAT program had been appropriately interfaced with ABAQUS. The anisotropic deformation induced interaction among the elements has also been well described in the procedure and the UMAT program. Consequently, the results were found to be independent to the number of elements. If the UMAT program and the interface with ABAQUS were not appropriate, the calculation results will show dependence with element number.

(ii) Local Stress and Strain Behaviour

To demonstrate more clearly the anisotropic deformation characteristics, an additional subroutine, LOCTRANS, was included in UMAT subroutine. This subroutine was used to transform the global strain response into the local coordinate system, i.e. the cylindrical coordinate system R-T-Z*, as shown in Fig.5.7, where R represents the local radial direction and T the tangential direction, (see Appendix VI)

Figures 5.8 and 5.9 show the axial, transverse and shear strain contours for the [123] orientation in the local coordinate system. Similar plots have also been made for the local inelastic strain distribution in the cylindrical bar in Figures 5.10 and 5.11. The specimen was fixed at the bottom end and consequently will show local constraint effect. It can be seen that, except at the bottom end, where constraint effects dominate the deformation response, all the strain components did not vary along Z*. The longitudinal strain ($\varepsilon_{ZZ} = \varepsilon_{Z^*Z^*}$) has a uniform distribution. The two transverse strain components, radial strain, ε_{RR}, and tangential strain, ε_{TT}, showed sinusoidal variations around the longitudinal axis, with two maximum strain and two minimum strain peaks 180 degrees apart. However, there was a 90 degree phase shift between radial strain, ε_{RR}, and tangential strain, ε_{TT}. The transverse shear strain, ε_{RT}, also showed a sinusoidal variation around the longitudinal axis, but the two longitudinal shear strain, ε_{RZ} and ε_{TZ}, showed different variation patterns with only one maximum and one minimum strain peak around the circumference of the cylindrical bar.

Figure 5.12 plots the output from ABAQUS of the axial strain, transverse strain and shear strain distributions around the circumference of the cylindrical bar. It is apparent that all the strain components, except of the strain in the loading direction, showed sinusoidal variation around the longitudinal axis. Consequently, the initial circular section of the cylindrical bar will become an ellipse section due to the anisotropic deformation. The results obtained from the cylindrical bar and the single element specimen are compared in Fig.5.13. It can be seen that the strain variations obtained from the cylindrical bar and those from single element are essentially identical.

The longitudinal, transverse and shear strain distribution contours of the cylindrical bar with a [123] orientation obtained from the crystallographic model are plotted in Figs. 5.14 and 5.15. The variation of the strains around the circumference of the cylindrical bar is plotted in Fig.5.16a. It can be seen that the main anisotropic deformation characteristics of single crystal nickel base superalloys predicted by the

crystallographic model are similar to those predicted by the phenomenological model.

However direct comparison of the strain responses predicted by the two models, Fig.5.16b, indicated the differences between the two models. For a given axial strain, the tangential and the shear strains predicted by the crystallographic model are generally higher than those predicted by the phenomenological model. This observation is in agreement to that obtained from the comparison of the two models in Chapter 3. The two models predicted similar deformation features, but quantitatively direct comparison showed the difference between the two models.

The results for single element given in Chapter 4 have demonstrated deformation features of the [011] and [123] orientations. It was indicated that the axial stress and strain responses for the two orientations are exactly the same, as shown in Fig.4.1. The transverse deformation, in terms of transverse and shear strains, are significantly different for the two orientations. These deformation characteristics have been further examined through the results obtained from the cylindrical bar. The axial, transverse and shear strain distribution contours of the cylindrical bar with the [011] orientation are plotted in Fig.5.17. Compared with the strain distributions for the [123] orientation, shown in Figs.5.14 and 5.15, it can be seen that deformation contours for all the transverse and shear strain components obtained from the [011] and [123] orientations are totally different.

5.3.2 Plate

The plate specimen was used to represent a simplified gas turbine blade component. The deformation response of the plate specimen is expected to illustrate the main deformation characteristics of a turbine blade with different orientations.

The general stress and strain responses of the plate specimen were found to be similar to those obtained from the cylindrical bar and the single element specimen. However, a striking feature was observed in terms of the geometrical shape change

caused by the anisotropic deformation of the single crystal alloy. The original mesh and the deformed mesh for the plate specimen with the [123] orientation are compared in Fig.5.18. It is apparent that significant out-of-plane deformation was induced even under the uniaxial loading. The three displacements along the longitudinal direction of the plate are shown in Fig.5.19. It can be seen that not only the displacements, U3, in the loading direction, but also the two transverse displacements, U1 and U2, change along the longitudinal axis. This result showed that the anisotropic deformation of single crystal material induces geometrical distortion of single crystal component. Therefore, not only the stress and strain, but also the geometrical change should be assessed for single crystal components.

In industrial applications of single crystal material for gas turbine blades, the orientation along the main direction of blade is normally expected to be within 10 degrees of the [001] orientation. However, it is not clear whether misorientation of about 10 degrees from [001] produces significant influence on the deformation behaviour of a turbine blade. Further calculations for two plate specimens, one with the loading direction in the [011] and another within 10 degrees from [001], have been carried out to examine the effect of misorientation, Both specimens were subjected to uniaxial loading under displacement control with a total strain of 0.12%.

The original and the deformed mesh of the plate with the [001] orientation are compared in Fig. 5.20. It can be seen that there is no out-of-plane deformation, i.e. the plate remains plane after deformed. The only deformation in the two transverse directions is the uniform deformation induced by Poisson's effect. The original mesh deformed with uniform deformation in the three directions and deformed mesh are parallel to the original mesh. For loading of the plate with an orientation [0.125,0.125,1], which is 10 degrees away from [001], the original and the deformed mesh of the plate are compared in Fig. 5.21. This is just one of the orientations on the 10 degree cone to demonstrate the misorientation effect. It can be seen that considerable out-of-plane deformation was induced even for misorientation of 10 degrees from the [001]. The deformed plate was observed with a twisted shape, and

the deformed mesh was no longer parallel to the original mesh. The maximum ratio of the out-of-plane deformation to the in-plane deformation, i.e. U_1/U_3 , was found to be about 0.22.

5.3.3 Cyclic Loading

The FE calculations for cyclic loading were carried out to demonstrate the abilities of the numerical implementation procedure, the UMAT and the finite element programmes to deal with the transition from elastic domain to the non-elastic domain. The analysis was carried out for single element to reduce the calculation time, since it was demonstrated in previous sections that the deformation behaviour obtained from the simulations are independent to the element numbers. In ABAQUS input file, the card *AMPLITUDE was used to define load by giving tabular data and the load curve will be named via optional input, NAMT= "name of loading curve", then under *STEP card, the card *BOUNDARY, AMPLITUDE= "name of loading curve" is used for loading control. Both the phenomenological and the crystallographic models have been used in the calculations.

The cyclic strain-stress responses obtained from the two models for the [001] and the [111] orientations are presented in Fig.5.22. The specimens were subjected to total strain control with a strain rate of 0.004/s at temperature of 950°C. The results indicated that the constitutive equations for the both models have been integrated well despite the repeated changes in straining direction. The results also illustrated that two models' capabilities to describe the cyclic deformation features such as the Bauschinger effect.

The differences of stress and strain responses for the other orientations under cyclic loading predicted by the two models were found to be similar to those described in Chapter 3 for the monotonic loading. For a given total strain range, the relative errors of the stress ranges predicted by the two models showed the similar orientation dependent feature as given in Fig.3.9. This is because for a given orientation, the deformation mechanisms in the monotonic and cyclic loading are the

same. The only difference in the calculations for cyclic loading is to modelling the loading and unloading conditions. The simulation results given in Fig.5.22 have demonstrated the ability of the modelling and the FE programme developed in this work to simulate the cyclic loading conditions.

5.4. Results for Multiaxial Cyclic Loading

5.4.1 Torsion

The tube specimens, either with a uniform cross section or with a with non-uniform cross section were analysed to study the deformation characteristics of single crystal alloy under pure torsion loading. The FE simulation results of tube specimens under pure torsion loading have been carried out using both the phenomenological and the crystallographic models. The tube with one end fixed was subjected to torsion by imposing a twisting angle or a torque around the longitudinal direction that coincides with the [001] orientation. The initial shear strain rates used in both the stress (torque) control and strain (twisting angle) control are 0.001 s^{-1}. For the geometry of the specimen used in the calculation, the rates applied in terms of torque and twisting angle were 5.55NM/s and 0.0296 radian/s respectively.

The deformation responses in terms of twist angle and torque are plotted in Fig.5.23a and Fig.5.23b for stress and strain control respectively. It was observed that the global deformation responses predicted by the two models are not the same for both the cases. Though the initial global responses (torque and twisting angle relationship), that were dominated by elastic deformation, were observed to be the same for the two models under both the stress and strain control loading conditions, considerable differences were observed in the final stage of the curves, where inelastic deformation became important. For a given torque in stress control, the crystallographic model predicted higher twist angle than that predicted by the phenomenological model under stress control case. Whilst for a given twist angle in the strain control, the crystallographic model predicted lower torque than that predicted by phenomenological model. The simulation results in terms of global

responses for stress and strain control showed the similar features for the two models. In both cases, the simulation results indicted that the global hardening predicted by the crystallographic model is lower than that predicted by the phenomenological model. This may be attributed to the higher inelastic strain zones predicted by the crystallographic model as discussed below.

The equivalent inelastic strain, i.e. $\varepsilon_{eq}^{in} = \sqrt{\frac{2}{3}\varepsilon_{ij}^{in}\varepsilon_{ij}^{in}}$, distributions obtained from the specimen with a non-uniform cross section are plotted in Fig. 5.24a and 5.24b for the phenomenological and crystallographic models respectively. Similar results were also observed from the uniform cross-section specimen, Fig.5.25a and Fig.5.25b, where non-uniform inelastic strain distributions across the thickness of the tube have been shown. In both specimens significant differences were observed between the inelastic strain distribution predicted by the two models. The phenomenological model predicted a uniform equivalent inelastic strain around the circumference of the specimen, whilst a non-uniform inelastic strain distribution was predicted by the crystallographic model.

Figure 5.26 plots the variation of the equivalent inelastic strains, $\varepsilon_{eq}^{in} = \sqrt{\frac{2}{3}\varepsilon_{ij}^{in}\varepsilon_{ij}^{in}}$, around the circumference of the tube. It clearly shows that the phenomenological model predicted a constant equivalent inelastic strain around the circumference of the tube. The distribution of the equivalent inelastic strain predicted by the crystallographic model exhibits periodical variations around the circumference of the tube. Four higher and four lower inelastic strain zones were observed around the circumference of the tube. The main direction of the tube specimen was in the [001] orientation. The secondary orientation of the specimen varies with the position around the circumference of the tube. The high inelastic strain zones were found to correspond to the vicinity of the [011] secondary orientations.

5.4.2. Combined Tension and Torsion

Combined tension and torsion loading was achieved using total strain control with equal amounts of total normal and shear strain rates, i.e. $\dot{\varepsilon}_{zz}^{T} = \dot{\varepsilon}_{\theta z}^{T} = 0.001/s$. Then the overall imposed displacement rate in the Z direction and the twist angle rate around the Z direction were calculated from the specimen dimensions, i.e. imposing displacement of 0.5mm and angle of 0.1radian in 5 seconds for the tube specimen with a length of 100mm and outer radius of 5mm. Both the phenomenological and the crystallographic models were used in the FE calculations. The results were then compared.

The tensile force and displacement response and the torque and twist angle response obtained from the calculations using the two models are compared in Fig.5.27a and 5.27b. It can be seen that the global deformation responses predicted by the two models are not significantly different. However significant differences were observed in terms of the local inelastic strain distributions around the circumference around the specimen, Fig.5.28 and Fig.5.29. Similar to the pure torsion case, a uniform equivalent inelastic strain distribution was predicted by the phenomenological model, whilst a non-uniform inelastic strain distribution was obtained using the crystallographic model. However, due to the interaction between the tension and torsion, the global deformation responses predicted by the two models were found to be different for pure torsion and combined tension torsion cases. For the pure torsion the phenomenological model exhibited greater hardening in terms of global loads and displacement compared with crystallographic model. This is because crystallographic model predicted four weak zones where larger deformation was generated.

5.5. Comparisons for Different Loading Conditions

To demonstrate the deformation characteristics under different loading conditions, the equivalent inelastic strain versus the von-Mises equivalent stress curves obtained

from the FE calculations were compared for tension, torsion and combined tension-torsion loading cases. The simulations were conducted under stress control, with a same equivalent strain rate of 0.001 s^{-1} at the beginning of the simulations.

Fig.5.30 plots the comparison of the results obtained using the phenomenological model. These curves are taken for the point on the surface of the middle part of the tube. Similar results were also observed using the crystallographic model. Significant differences have been observed from Fig.30. For a given von-Mises equivalent stress, the equivalent inelastic strain produced in the tension loading is much less than that produced by the torsion loading. The equivalent inelastic strain produced by the combined tension-torsion loading is between those generated by the simple tension and pure torsion loading cases. This indicated that inelastic strain hardening was higher for the tension loading compared with the torsion loading.

The main direction of the specimen is along the [001] orientation. In the simple tension loading case, the equivalent stress and equivalent strain were found to be a function of the stress and strain in the loading direction respectively. Therefore, the material constants included in the calculation are M_{11}-M_{22}, N_{11}-N_{22} and Q_{11}-Q_{22} only. In the pure torsion loading case, the equivalent stress and equivalent strain were found to be a function of the shear stress and shear strain respectively. Therefore, the material constants included in the calculation are M_{44}, N_{44} and Q_{44} only. As indicated in Chapter 3, the materials constants M_{11}-M_{22}, N_{11}-N_{22} and Q_{11}-Q_{22} are associated with the octahedral slip systems, whilst material constants M_{44}, N_{44} and Q_{44} are associated with the cubic slip system. Therefore, the simple tension is dominated by octahedral slip mechanism and the pure torsion is dominated by cubic slip mechanism.

Comparison of the deformation mechanisms in Chapter 3 (section 3.6.3) has revealed the differences between the octahedral and cubic slip deformation mechanisms. These differences were reflected in the material constants in the phenomenological model. Materials constants M_{11}-M_{22}, N_{11}-N_{22} and Q_{11}-Q_{22} associated with the octahedral slip systems were different to material constants M_{44},

N_{44} and Q_{44} associated with the cubic slip system. This was attributed to the significant difference of the inelastic strain hardening behaviour between the octahedral and the cubic slip systems. The octahedral slip systems (dominating [001] deformation, Fig.3.8) have the highest strain hardening and the cubic slip systems (dominating [111] deformation, Fig.3.8) the lowest. Therefore inelastic deformation is more easily caused by cubic slip than by octahedral slip. The results given in Fig.5.30 are in agreement with the deformation mechanism analysis results. The simple tension loading is dominated by octahedral slip systems that have higher strain hardening, and showed higher stress response. The pure torsion loading is dominated by cubic slip systems that have lower strain hardening, and showed lower stress response. The combined tension-torsion loading includes both octahedral and cubic slip systems, and exhibited stress response between the simple tension and pure torsion loading cases.

CHAPTER 6
GENERAL DISCUSSION

In this chapter, a general discussion is presented for the various issues raised from the previous chapters. The discussion is divided into 6 sections. In section 6.1 the influence of internal material structure of single crystal on mechanical properties is examined. The features of the analytical and numerical procedures developed in this work to determine the material constants in the constitutive models are discussed in section 6.2. The similarities and differences between the phenomenological and the crystallographic models are further examined in section 6.3 to explore the inherent characteristics of the two types of models. Consequently the possible modifications and further development of the constitutive models for single crystal materials are discussed in section 6.4. Section 6.5 is concerned with the numerical implementation of constitutive models and interfacing with finite element structural analysis. The effect of misorientation on the stress and strain response of single crystal materials, and on overall geometrical changes of the structure of single crystals is examined in section 6.6. Finally, the convergence and accuracy of the numerical calculations are analysed in section 6.7

6.1 Influence Of Internal Material Structure on Mechanical Properties

The constitutive models presented in previous Chapters are based on the initial material features and the main deformation characteristic, i.e. cubic symmetry. The influence of the change in the internal structure reviewed in Chapter 2 has not been included in the models in this stage. In order to highlight the possible influence of the internal material structure on the mechanical behaviour, a simple analysis is performed on the effect of 'rafting' on the elastic properties of a single crystal alloy.

In this analysis, a simple material mechanics method is adopted. The material is assumed to be completely 'rafting' with no misfit between γ and γ'. The two phases material is treated as a composite material. It is assumed that the overall Young's

modulus of the two phases material is E, and the Young's moduli of γ and γ' phase are E_γ and $E_{\gamma'}$ respectively. Then under uniaxial loading:

$$\sigma = E\varepsilon = Ef(\varepsilon_\gamma, \varepsilon_{\gamma'}) = Ef(E_\gamma\sigma_\gamma, E_{\gamma'}\sigma_{\gamma'}) \tag{6.1}$$

$$\sigma = g(\sigma_\gamma, \sigma_{\gamma'}) \tag{6.2}$$

where function f and g are defined in Appendix VII.

Thus

$$E = \frac{g(\sigma_\gamma, \sigma_{\gamma'})}{f(E_\gamma\sigma_\gamma, E_{\gamma'}\sigma_{\gamma'})} = h(E_\gamma, E_{\gamma'}) \tag{6.3}$$

The details of the analysis are given in Appendix VII. The results indicate that there is no significant influence of 'rafting' on the principal elastic properties of single crystal alloy since the basic elastic properties of γ and γ' are very similar. However, this is only a very simple analysis, further investigation on 'rafting' phenomenon and its influence on mechanical behaviour of single crystal nickel base superalloys is required. For inelastic deformation the rafting effect will have more significant and complex influence. There have only been very limited studies (Schneider et al [1992], Pollock and Argon [1994]) on the mechanisms of rafting and its influence on inelastic deformation behaviour of single crystal alloys. Consequently, there is no enough information for modelling of the rafting effect on inelastic deformation. This important issue will be subject to further extensive investigations and is beyond the scope of this work.

6.2 Determination of Material Constants

It is well known that appropriate procedures to determine the material constants are essential. There have been studies on the development of procedures for determining material constants for isotropic constitutive models (James et al [1987], Agatonovic and Clorman [1987], Sherwood and Fay [1992], Schwertel et al [1992]). The procedure to determine the material constants for the constitutive models for single crystal materials are more complex compared with those for isotropic models.

However, there has been no specific work that is dedicated to developing procedures for single crystal materials. Furthermore, in order to be able to compare phenomenological and crystallographic models, the material constants in both models must be determined using a consistent procedure using the same experimental data. If this is not done the approximations and errors introduced in the procedure for determining the material constants may override the characteristics of the models. Consequently, it will not be possible to explore the intrinsic features of different models. One of the main objectives of this work is to develop a consistent method to determine the material constants for both the phenomenological and the crystallographic models based on the same experimental data. Since the elastic equations for the both models are identical and the elastic constants are the same for the two models, the discussion concentrates on the features of the procedure for the inelastic material constants.

6.2.1 General Procedure

The procedure to determine the material constants for both phenomenological and crystallographic models has been developed in terms of a group of generic equations for uniaxial loading in the [001] and [111] orientations. This made it possible to determine the material constants in the two models from same experimental data with same analytical and numerical procedure. The general methodology used in the procedure is different to the methods for determination of the material constants in many plasticity and viscoplasticity models (James et al [1987], Agatonovic and Clormann [1987], Sherwood and Fay [1992], Schwertel et al [1992]). Most of the methods have been developed based on a numerical iteration scheme. Assumptions are often made in the iteration scheme to produce initial estimates of the material parameters. These initial material constants are used to integrate the plasticity or viscoplasticity equations of a given model to predict stress and strain response and compared with the experimental data. An iteration scheme is then used to change one or several material parameters to improve the predicted deformation response. For each change of a parameter the resulting predicted curves must be compared with the corresponding experimental data. These 'trial and error' procedures have

the disadvantage that the number of experimental curves that can be used for the fitting procedure is limited.

Another problem associated with the procedure is the determinations of the initial values of the material parameters, which have often not been presented (Dunne et al [1992]). One of the main features of the procedure is using a global optimisation routine to determine the material parameter simultaneously from a number of different tests, such as creep, constant strain rate, strain-controlled cyclic and relaxation tests without identifying the deformation characteristics associated with each of the material parameters. It is well known that the influence of a particular material parameter on the deformation response of one type of experimental test, or one stage of a given test, may be important. However, its influence can be neglected for another experimental test, or another stage of a given test. For example, the material constants included in the isotropic hardening equation only have significant influence for a cyclic test. Consequently, difficulties arise in providing the correct weighting for each type of experimental test with respect to each of the material parameters (Schwertel et al [1992]). Otherwise, the overall optimisation may produce a better fit for a given group of experiment tests using a combination of both over and under weighted material parameters (Schwertel et al [1992]). Since the real material parameters associated with the deformation characteristics have not been optimised, large errors may be induced in the prediction of other experimental tests.

The procedure developed in this work is based on the identification of the deformation characteristics associated with the material constants. Consequently characteristic experimental data have been extracted and used for determining a group of material constants, which have significant influence of the corresponding deformation characteristics. The local optimisation routine overcomes the above disadvantages of the global optimisation procedures, and provides physically reasonable material constants that are associated with the various deformation characteristics. The application of the procedure to pseudo-experimental data illustrated that there were no methodological and numerical errors induced by the

procedure. The square of the errors obtained from then non-linear regression analysis for various material parameters was close to zero.

To minimise the overall errors, global optimisation can be introduced using the common iteration scheme. In this case, the local optimisation routines will provide the initial values of the material constants for further iteration to improve the predicted deformation response.

6.2.2. Simplified Procedure

In terms of the observation of the slip traces on specimen surfaces, a number of investigations have indicated that the inelastic deformation of [111] orientation under uniaxial loading may be dominated by the cubic slip systems (Hanriot et al [1991], Meric et al [1991]). Consequently it has been assumed by some investigators (Walker and Jordan [1989], Nouailhas et al [1995]) that only the cubic slip systems are active for uniaxial loading in the [111] orientation and the material constants determined on this basis. Using this assumption, the constitutive equations for uniaxial loading in the [111] orientation can be simplified and expressed in terms of macroscopic stress and strain as:

$$\dot{\varepsilon}_3^{in} = \sqrt{2}\left\langle \frac{\left|\frac{\sqrt{2}}{3}\sigma_3 - x_c\right| - k_c - r_c}{K_c} \right\rangle^{n_c} \operatorname{sign}\left(\frac{\sqrt{2}}{3}\sigma_3 - x_c\right) \tag{6.4a}$$

$$\dot{\varepsilon}_1^{in} = \dot{\varepsilon}_2^{in} = -\tfrac{1}{2}\dot{\varepsilon}_3^{in}; \qquad \dot{\varepsilon}_4^{in} = \dot{\varepsilon}_5^{in} = \dot{\varepsilon}_6^{in} = 0 \tag{6.4b}$$

$$\dot{x}_c = \frac{\sqrt{2}}{2} c_c \dot{\varepsilon}_3^{in} - \frac{\sqrt{2}}{2} d_c x_c \left|\dot{\varepsilon}_3^{in}\right| \tag{6.4c}$$

$$\dot{r}_c = \frac{\sqrt{2}}{2}(q_c - b_c r_c) \left|\dot{\varepsilon}_3^{in}\right| \tag{6.4d}$$

If this assumption is applicable, the complex procedure presented in Chapter 4 to extract the inelastic deformation contributed by the cubic slip systems from the total inelastic deformation, is no longer required. A simplified procedure can be developed from the direct comparison of the uniaxial equations obtained from the crystallographic and the phenomenological models. The material constants of the two models are linked using the following.

$$\begin{cases} n_o = n \\ c_o = \frac{4}{3}(N_{11} - N_{12}) \\ d_o = \frac{8}{\sqrt{6}}(Q_{11} - Q_{12}) \\ K_o = \frac{1}{\sqrt{6}}(\frac{\sqrt{6}}{8})^{-\frac{1}{n_o}} K^* \\ k_o = \frac{1}{\sqrt{6}}k \\ b_o = \frac{8\sqrt{6}}{6\sqrt{M_{11} - M_{12}}}b \\ \frac{q_o}{b_o} = \frac{\sqrt{6}}{\sqrt{M_{11} - M_{12}}}W \end{cases} \qquad \begin{cases} n_c = n \\ c_c = \frac{4}{3}N_{44} \\ d_c = \frac{2}{\sqrt{M_{44}}}Q_{44} \\ K_c = \frac{1}{3}(\frac{2}{\sqrt{M_{44}}})^{\frac{n_c+1}{n_c}} K^* \\ k_c = \frac{2}{3\sqrt{M_{44}}}k \\ b_c = \frac{b}{\sqrt{M_{44}}} \\ \frac{q_c}{b_c} = \frac{2}{3\sqrt{M_{44}}}W \end{cases} \tag{6.5}$$

However this assumption has been proposed based on limited experimental observations. There has been no direct verification for this assumption in terms of mechanical deformation analysis and constitutive modelling.

The material constants for crystallographic model obtained from the above simplified determination procedure are presented in Table 6.1.

Numerical simulations have been carried out for the crystallographic model using the material constants obtained from the full and the simplified procedures, i.e. using the material constants given in Tables 3.4 and 6.1 respectively. The results are shown in Fig.6.1. It can see that the difference between the results is not significant. Simulations have also been performed for other orientations. The results obtained

were found to be similar to Fig.6.1, and no significant differences were found to using material constants given in Table 3.3 and 6.1. This indicated that the contribution of the octahedral slip systems, though 8 of them may be active, to the inelastic deformation of [111] orientation under uniaxial loading is very small.

Simulations were also carried out for other orientations using the crystallographic model with the material constants given in Tables 3.4 and 6.2 respectively. The simulation results were found to be very close using material constants either in Table 3.4 or in Table 6.1. Therefore it is possible to neglect the octahedral slip systems for the case of uniaxial loading in the [111] orientation to simplify the procedure of determination of the material constants for the cubic slip systems.

6.3 Characteristics of the Constitutive Models

The two categories of model have been developed separately based on totally different principles. The crystallographic models have been developed based on crystalline slip theory. On the other hand, modifying the isotropic constitutive models initially proposed for polycrystalline materials has developed the phenomenological models. The comparison of the simulation results given in Chapter 3 has revealed the similarities and the differences between the two models.

The analysis in Chapter 3 indicated that the two types of constitutive models were essentially identical to each other for uniaxial loading in the two specific orientations, i.e. [001] and [111]. Isotropic deformation response have been predicted by both the phenomenological and crystallographic models, and the basic constitutive equations for uniaxial loading in the [001] and [111] orientation can be expressed as a group of generic equations. Therefore, the material constants introduced into the two models are connected directly. The material constants, M_{11}-M_{12}, Q_{11}-Q_{12} and N_{11}-N_{12}, are associated to the deformation mechanisms of octahedral slip, whilst material constants, M_{44}, Q_{44} and N_{44} are mainly associated with cubic slip deformation mechanisms.

The results presented in Chapter 3 indicated that the differences between the two models in terms of stress and strain responses, initial yield stresses, as well as the contribution of the two slip systems to the inelastic strain, are all strongly dependent on crystal orientation. Further comparison is carried out to examine the orientation dependent characteristics of these deformation properties.

The results presented in Fig.3.9, Fig.3.11 and Fig.3.12 are plotted together in Fig.6.2 to illustrate the significant features of the different results. By comparing Fig.6.2a and 6.2b, it can be seen that the orientations where the two models give the closest simulation results coincide with the orientations where the inelastic deformation is dominated by either octahedral or cubic slip. The closer the contributions of the two slip systems to the inelastic deformation, the larger the difference between the phenomenological and crystallographic models. The orientations where the relative error in stress, shown in Fig.6.2a, between the two models are less than 5% corresponds approximately to the regions where 90% of the inelastic strain is produced by either octahedral or cubic slip (Fig.6.2b). The difference between the yield stresses obtained from the two models also shows the similar orientation dependence feature, Fig.6.2c. The yield stresses are the same for the phenomenological and the crystallographic models for the [001] and [111] orientations. The differences between the simulation results increase as the orientations move away from the two corners. Significant differences are observed for the middle orientations, with the largest discrepancy being observed for the [011] orientation. These observations, in terms of yield stresses, are similar to those shown in Fig.6.2a and Fig.6.2b for the difference in peak stresses and the contribution of the two slip systems respectively.

Numerical simulations were carried in Chapter 3 for the orientations along the three sides of the stereographic triangle. More simulations have been carried out for orientations inside the stereographic triangle. Consequently, the stereographic triangle can be divided into different regions, Fig.6.3. The regions in the stereographic triangle where the two models agree, and also where the deformation is 90% dominated either by octahedral or cubic slip, are identified in Fig.6.3. This

indicated that the anisotropic frameworks used in the two models at their present formulations are essentially the same. In the intermediate region the differences between the two models are larger, but as shown in Fig.6.2a the largest error in stress is only about 18%, and coincides approximately with [011].

The above results indicated that the large differences occur at the region when both octahedral and cubic slip systems are important for the deformation response. The results also demonstrate that the major difference between the phenomenological and the crystallographic models is how they deal with the combination of the two deformation mechanisms. The phenomenological model follows the continuum mechanics theory of stress and strain tensor transformation, whilst the crystallographic model is based on the classical slip theory of material science.

6.4 Further Development of Constitutive Models

Although extensive studies have developed constitutive models, both phenomenological and crystallographic types, for these single crystal alloys further improvement of the models is required.

6.4.1 Modification of Yield Function

From the finite element calculation results for the pure torsion and combined tension and torsion cases presented in Chapter 5, an important feature has been observed, particularly when the deformation predicted by the phenomenological and crystallographic models. The phenomenological model predicted a uniform yield and deformation around the circumference of the tube, whilst crystallographic model predicted non-uniform yielding and deformation. Similar features were also observed by Nouailhas et al [1995] for the case of a tube with [001] orientation loaded in pure torsion.

Non-uniform deformation has been observed in the experiments at room temperature (Nouailhas et al [1995]). To minimise the differences in the yield stresses predicted

by the phenomenological and crystallographic models for this particular case, the yield function of the phenomenological model has been modified by Nouailhas et al [1995] to include higher order stress invariants. This modification was based on the comparison of the phenomenological model and the crystallographic model predictions for pure torsion cases. It is necessary to provide a closer prediction between the two models to describe the deformation behaviour in the pure torsion. The modified yield function in terms of initial yielding is expressed as:

$$f = \left\{ \left[\left(\frac{2}{3}(I_2 + 2a_4 I_4) \right)^2 - a_8 I_8 \right]^3 - (a_6 I_6)^4 \right\}^{1/12} - k \qquad (6.6a)$$

The high order stress invariants are given by:

$$I_2 = (\sigma'_{11})^2 + (\sigma'_{22})^2 + (\sigma'_{33})^2 \qquad (6.6b)$$

$$I_4 = (\sigma'_{23})^2 + (\sigma'_{31})^2 + (\sigma'_{12})^2 \qquad (6.6c)$$

$$I_6 = (\sigma'_{23})(\sigma'_{31})(\sigma'_{12}) \qquad (6.6d)$$

$$I_8 = (\sigma'_{23})^4 + (\sigma'_{31})^4 + (\sigma'_{12})^4 \qquad (6.6e)$$

where σ'_{ij} are the deviatoric components of the stress tensor σ_{ij} , and the k is the initial yield stress, and a_4, a_6 and a_8 are material constants with the values of 4.456, 195 and 153 respectively (Nouailhas [1995]). The material constants were obtained from CMSX2 single crystal alloy that is very similar to SRR99 single crystal alloy (Li [1994b]). This modified yield function reduces to the yield function used in this work when the additional material constants a_4, a_6 and a_8 are set to zero.

It was demonstrated by Nouailhas et al [1995] that the modified phenomenological model gave a closer prediction of the yield stresses with those predicted by crystallographic model in the particular case of pure torsion. However, a general comparison between the two models had not been carried out by Nouailhas et al [1995].

Therefore, further calculations of the yield stresses for different orientations under uniaxial and bi-axial loading conditions have been carried out to examine the feasibility of modifying the yield function. The results of yield stresses under uniaxial loading predicted by different models are compared in Fig.6.4. The results based on the yield surface given by equation (6.6) are called the modified phenomenological model results. It can be seen that there is no significant improvement of the yield behaviour predicted by the modified yield function (8^{th} order) compared with the simple yield function (2^{nd} order).

The yield loci for tension-torsion loading and tension-tension loading are plotted in Fig.6.5 and Fig.6.6 respectively. For the bi-axial loading cases, the yield loci predicted by the modified yield function (8^{th} order) remain an ellipse similar to the simple yield function (2^{nd} order). The yield stresses predicted by the modified yield function for some stress states are closer to those predicted by the crystallographic model, but exhibit even larger discrepancies for other stress states. The corners in the hexagon yield loci predicted by the crystallographic model imply the change of yield mechanism from one slip system to another. For the phenomenological model, the continuous mathematical yield function will always generate smooth yield loci. This indicates that the differences between the phenomenological and crystallographic models can be attributed to the intrinsic characteristics of the two types of models. In this sense, there will always be differences in terms of yield behaviour predicted by the phenomenological and the crystallographic models. These differences will return unless the crystallographic model modified to eliminate discontinuities from one slip system to another. This may be achieved by include the interaction of different slip systems.

6.4.2. Interaction of Slip Systems

The orientation dependent features for the various deformation properties presented in Fig.6.3 show that large differences occur at the region when both octahedral and cubic slip systems are important for the deformation response. This indicates that some kind of interaction between the two slip systems may occur when both slip

systems are active. In fact the interactions of different slip systems, such as cross slip, have been studied (Pope and Ezz [1984]) for single crystal nickel base superalloys. The influence of cross slip on mechanical behaviour has been reported in the literature (Takeuchi and Kuramoto [1973], Lall et al [1979], Paidayr et al [1984]). Walker and Jordan [1989] included the non-Schmid shear stresses, i.e. the resolved shear stresses normal to the slip planes of octahedral or cubic slip systems, in a crystallographic model to describe the tension-compression asymmetry caused by cross slip. However the general influence of interactions of octahedral and cubic slip systems on the deformation behaviour of single crystal superalloys has not been investigated. Meric et al [1991] introduced an 'interaction matrix' in the isotropic hardening equations of a crystallographic model to describe the cross hardening effect caused by interactions of different slip systems. However due to the lack of information on the mechanism of slip system interactions on mechanical deformation behaviour, the coefficients in the 'interaction matrix' were selected to obtain a best fit to the uniaxial experimental data. Both Walker and Jordan [1989] and Meric et al [1991] introduced the interaction of slip systems in the isotropic hardening equations. There have been no studies that examine the influence of interaction of slip systems for kinematic hardening and further work is required. Nevertheless, the numerical implementation scheme developed in Chapter 3 for the crystallographic model has been presented in using a generalised formulation, i.e. Equations (4.26f) to (4.26i), which have the ability to include interaction of slip systems. Further work is required to investigate the mechanisms of interactions between slip systems and their influence on mechanical behaviour of single crystal alloys.

6.4.3 Modelling Of Anisotropy and Further Improvements

One of the important deformation characteristics of single crystal alloys is their orientation dependence. For elastic deformation, anisotropic elasticity theory was used for both the phenomenological and the crystallographic model, and the anisotropic elastic responses predicted by both models are identical. In terms of

inelastic deformation, two fundamental different approaches were used in the phenomenological and crystallographic models.

The approach used in the phenomenological model was based on a continuum mechanics framework. Anisotropic tensors, such as M_{ij}, Q_{ij} and N_{ij} discussed in chapter 3, were introduced to modify the isotropic constitutive models to describe the anisotropic deformation behaviour of single crystal alloys. On the other hand, the approach used in the crystallographic model was based on the classical slip theory. Different slip systems, such octahedral and cubic slip systems, were included in the models based on experimental observations. The global anisotropic inelastic deformation is the sum of the shear deformation on each of the active slip systems. Due to the directional feature of the slip systems, the global anisotropic inelastic material response is generated as a result of the shear strains on each of the slip systems. The fundamental different approaches used in the phenomenological and the crystallographic models determine the intrinsic characteristics of the two types of models.

For the phenomenological model, the choice of the functions used in the model will determine the anisotropic features described by the model. These functions must satisfy the principles of continuum mechanics. In this context, the potential (yield) functions are expressed as a function of the invariants (I_1, I_2, ..., I_n). For a f.c.c. crystal, and for the second-order stress tensor, σ_{ij}, one way to express the invarants are (Smith and Kiral [1978]):

$$I_1=(\sigma'_{11})+(\sigma'_{22})+(\sigma'_{33})$$

$$I_2=(\sigma'_{11})^2+(\sigma'_{22})^2+(\sigma'_{33})^2$$

$$I_3=(\sigma'_{11})^3+(\sigma'_{22})^3+(\sigma'_{33})^3$$

$$I_4=(\sigma'_{23})^2+(\sigma'_{31})^2+(\sigma'_{12})^2$$

$$I_5=(\sigma'_{11})(\sigma'_{23})^2+(\sigma'_{22})(\sigma'_{31})^2+(\sigma'_{33})(\sigma'_{12})^2$$

$$I_6=(\sigma'_{23})(\sigma'_{31})(\sigma'_{12})$$

$$I_7=(\sigma'_{11})^2(\sigma'_{23})^2+(\sigma'_{22})^2(\sigma'_{31})^2+(\sigma'_{33})^2(\sigma'_{12})^2$$

$$I_8=(\sigma'_{23})^4+(\sigma'_{31})^4+(\sigma'_{12})^4$$

$$I_9=(\sigma'_{11})(\sigma'_{23})^4+(\sigma'_{22})(\sigma'_{31})^4+(\sigma'_{33})(\sigma'_{12})^4$$

where σ'_{ij} are the deviatoric components of the stress tensor σ_{ij}.

How many and what stress invariants are to be included in the potential (yield) function is a compromise among accuracy, complexity and practicability. This choice must be guided by material deformation characteristics and verified by the experimental results.

The quadratic potential function had been used widely for polycrystalline materials and has been successful in describing the general deformation behaviour of a large range of isotropic materials (Chan and et al [1989], Chaboche et al [1983, 1989], Mroz and Niemunis [1990]). The phenomenological model for single crystal alloys was developed based on the modification of the isotropic model for polycrystalline materials. Naturally, the quadratic function was used and modified using the tensor M_{ij} to describe the anisotropic deformation behaviour of single crystal alloys. It has been demonstrated by a number of studies (Nouailhas [1990], Nouailhas and Freed [1992], Li [1993], Li and Smith [1995, 1998]) that the quadratic function can describe the fundamental anisotropic deformation behaviour observed from mechanical experiments, mostly under uniaxial loading, for single crystal nickel base superalloys.

However, the quadratic function is the very basic function and further modification may be required based on more complex (multiaxial) experimental results. The torsion and tension-torsion test of a tube specimen showed non-uniform deformation which can not be predicted by the phenomenological model using the quadratic function [Nouailhas et al [1995]). Consequently, the function was modified by Nouailhas et al [1995] to include higher order stress invariants. It was demonstrated by Nouailhas et al [1995] that the modified phenomenological model gave a better prediction for the particular case of pure torsion. However, a general comparison between the two models in this work indicated that there was no overall improvement in the yield behaviour predicted by the modified phenomenological

model when compared to the crystallographic model. Due to lack of experimental data, it is not easy to judge how to further modify the model to include or exclude different stress variants. Experiments have always provided the impetus for seeking more sophisticated constitutive models. These models are quite difficult to develop owing to highly nonlinear features. Consequently, countless purely theoretical conjectures have not withstood the scrutiny of experimentation. Further modification only can be made based on new experimental findings.

For a crystallographic model, the anisotropic features of the model depend on the choice of the type and number of slip systems to be included in the model. For nickel base single crystal alloys, experimental observations, as described in chapter 2 indicated that octahedral and cubic slip systems are the most basic slip systems and should be included in the crystallographic model. However, there are not enough experimental results to determine clearly how many slip systems will be active for various loading conditions under different temperature. Some experiments also showed the possibility of interaction between the two slip systems (Pope and Ezz [1984], Takeuchi and Kuramoto [1973], Lall et al [1979], Paider et al [1984]). However, the mechanisms of interaction between octahedral and cubic slip systems have not been clearly identified from experiments by material scientists. Consequently, the general influence of interactions between slip systems on mechanical deformation behaviour of single crystal superalloys has not been fully understood and included in the crystallographic models. Further work is required to investigate the mechanisms of interactions between slip systems and their influence mechanical behaviour of single crystal alloys.

Similar to isotropic materials, the subject of modelling anisotropic viscoplastic deformation of single crystals cannot be tackled by application of a single discipline in isolation to others. The interdisciplinary character of the subject has been well demonstrated by the past studies involving experimental, analytical and modelling work undertaken by scientists from material science, engineering and solid mechanics areas. Each discipline makes its own contributions, but further improvement of the model requires the collective contributions from a wide range of

disciplines. In general, a model development will always be through the following routines:

Basic experimental observation - Primary model development - Model simulation and predictions - Feature experiments guided by simulations - Model modification - Further experimental verification - Further model modification.

It is clear that both phenomenological and crystallographic models for single crystal alloys are still in the early development stage. Fundamental experiments, most under uniaxial loading and isothermal conditions had been carried out. Primary models had been developed and compared with the fundamental experimental results. Model simulations, such as the extensive work carried out in this thesis, revealed further deformation features for tests under more complex loading conditions although currently without experimental results. The simulations provide information about defining further feature experiments. Only after comparison of the experimental results with the simulations can it be possible to modify the models. Therefore, more experimental work is vital for further development of models for single crystal superalloys.

6.5. Numerical Implementation and Finite Element Analysis

It is well known that numerical implementation for the modern unified constitutive models is always a challenge since the unified formulations generally lead to highly non-linear systems of equations with the property of mathematical 'stiffness'. The constitutive models, both phenomenological and crystallographic models, developed in this work for describing the anisotropic elasto-viscoplatic deformation behaviour of single crystal materials are much more complicated compared with the constitutive models for the isotropic polycrystalline materials. Consequently, numerical implementation of these constitutive models for structural analysis with finite element method is considerably more difficult. Various numerical methods have been developed and combined with the finite element code ABAQUS in the

previous chapters. A general discussion will be presented here to illustrate the main characteristics of the different numerical methods.

The principle concept for finite element analysis is discretisation. The structure is divided into small finite elements whose stress-strain behaviour response is described by a constitutive law. The local information of the stress-strain behaviour is assembled at a global level so that equilibrium equations are satisfied throughout the elements of the whole structure. This procedure results in a large system of linear and nonlinear equations at both the local and global levels. Mathematically speaking, the prime objective of the numerical implementation is the development of incremental solution methods for the system of equations at both levels to achieve stability and convergence, as well as economical computation for structural analysis.

In this work, ABAQUS finite element code is used for the global level analysis. Consequently, the discussion will be concentrated on the numerical solution methods for the local level, i.e. the implementation of the anisotropic elastic time-dependent viscoplastic constitutive models for single crystal materials, and the interface with finite element analysis code, e.g. ABAQUS.

6.5.1 Local Constitutive Model Implementation

There are two distinguishing features of the numerical methods developed in this work.

(i) The numerical incremental algorithms for the numerical solution of the constitutive models used in this work have the general feature of an implicit integration algorithm.

(ii) Approximate **closed form solutions** for stress and strain, as well as the internal variables in the incremental equations have been achieved using a complex mathematical derivation. In addition, an approximate **closed form solution** for the Jacobian matrix that is required in the ABAQUS global level

numerical calculation is also obtained from the numerical integration schemes for the constitutive equations.

The progressive development of the numerical methods has been driven to achieve the accuracy and efficiency of numerical computing. A preliminary numerical incremental integration scheme was firstly developed to demonstrate the feasibility of application of the implicit numerical algorithm for the anisotropic elasto-viscoplastic constitutive models, and to achieve an approximate close form solution. Consequently, simplifications were introduced in the numerical method to reduce the level of difficulty in the mathematical derivation. In this preliminary numerical method, a full implicit scheme was applied to the inelastic strain rate which is the primary variable in the constitutive model, whilst a semi-implicit scheme was used to the back stress and isotropic hardening variables. Consequently, although approximate **closed form solutions** for the increments of stress and strain and the internal variables, as well as the Jacobian matrix have been obtained from the preliminary numerical method, the computing accuracy and efficiency were very low. The finite element calculation can only be carried out with very small time increment. When time step is increased, the numerical error caused by the additional approximation in the implicit scheme of the constitutive level generated a large accumulated error in the global level, the ABAQUS program was terminated since the calculation error was greater than the pre-specified tolerance in the ABAQUS code.

To improve the computational efficiency of the numerical method, the full implicit incremental integration scheme was applied to all the variables in the constitutive equations. Consequently, the mathematical derivation of the numerical implementation procedure is much more complicated, and great effort was required to obtain the **closed form solutions** for the two constitutive models with the full implicit schemes. However, when the numerical scheme was fully implemented and coded into the UMAT, the computation speed was greatly increased due to the relative large time increment step that can be used in the ABAQUS program.

A further improvement of the numerical method was to introduce iteration at the constitutive level. This is because utilisation of Taylor expansion in the implicit numerical integration scheme will always introduce some degree of error. The iteration routine is called when the local constitutive level error for each of the element is greater that a pre-specified tolerance. A combination of the non-linear iteration routine and the approximate closed form solutions obtained from the implicit numerical scheme has a significant advantage compared to the direct iteration method, since the approximate closed form solutions provide much more accurate estimation of the initial values for the iteration routine.

6.5.2 Interface with Global Finite Element Code

In the ABAQUS program, numerical implementation of the constitutive models is coded in the UMAT subroutine. When UMAT is called, it is provided with the state at the start of the increment (stress, solution dependent state (internal) variables) and with the strain increments and the time increment. The subroutine UMAT performs two functions: it updates the stresses and the solution dependent state (internal) variables to their values at the end of the increment, and it provides the material Jacobian matrix, $\partial\Delta\sigma/\partial\Delta\varepsilon$, obtained from the local constitutive level. The Jacobian matrix is then used in the global level to form the global stiffness matrix in the global equilibrium equations.

Since the material non-linearity appears directly in the Jacobian matrix, the global stiffness matrix will be a variable stiffness matrix, and must be updated from one increment to the next increment. The global ABAQUS system requires the Jacobian matrix at the current increment to determine the strain increments and provides the strain increments to the UMAT subroutine. On the other hand, the Jacobian matrix at the current increment can only be determined from the local constitutive level via UMAT when the strain increments were known. Therefore the strain increments in the ABAQUS global level could be only estimated on a previous strain history, e.g. based on the Jacobian matrix of the previous increment. Consequently, the global

iteration process in ABAQUS is carried out to keep the global error within a certain pre-specified tolerance.

From the interface process between global level and local level, e.g. ABAQUS and UMAT, it is apparent that the accuracy and efficiency of the numerical implementation schemes for the local constitutive equations is vitally important for the stable, convergence and economical computation of the overall finite element structural analysis. This is because the local errors introduced to the Jacobian matrix will be directly fed back to the global system. The errors not only effect the global numerical solution errors for the current time increment and also influence the estimation of the next step strain increments. The global errors introduced in the strain increment estimation will then further effect the local errors for the next increment solutions including the Jacobian matrix. Therefore, the global errors of the finite element analysis are the accumulated errors from the local constitutive level, and the possible errors induced in the global numerical procedure to solve the global equilibrium equations.

The progressive improvement of the local numerical implementation methods carried out in this work clearly demonstrated the above interface features between local and global levels in the finite element analysis. In the preliminary numerical method, relative large local errors were caused by the simplification of implicit numerical scheme. Consequently, the computing speed of the ABAQUS program was slow and only a small time increment was allowed in the ABAQUS program. When the time increment was increased, the ABAQUS program was terminated and terminating message indicated that the global error was over the error tolerance in the ABAQUS program. The improved full implicit numerical scheme for the incremental integration of local constitutive equations reduced the local errors and consequently increased the computing speed of the ABAQUS program. The time increment was increased and the global iteration was reduced. It was observed that overall computing efficiency was further improved by introducing local iteration routine in the constitutive level.

Finally, it can be seen that there is a strong interface between the local and global systems in the finite element method. To improve the overall stability, convergence and efficiency of the finite element computation, the global system and the local system must, in essence, be solved simultaneously. This requires the formulation (mathematical formulation rather than numerical formulation) of the Jacobian matrix for the complete system of equilibrium equations and the corresponding set of equations that govern the non-linear state of each element. This can not be achieved by using ABAQUS with UMAT since the local and global systems are separated. However, the methods developed in this work to obtain approximate closed form solutions (expressed in the mathematical formulation) at the local constitutive level provide the possibility to develop an alternative approach that solves the complete system of equations for all elements simultaneously. This alternative method (with the new FE code) may therefore further improve the efficiency of the finite element analysis.

6.6 Misorientation Effect

The manufacturing process for single crystal material is extremely complicated. It is very difficult to control the process to obtain the exact orientation of the turbine blade. In industrial applications, the orientation along the main direction of the turbine blade is normally controlled to be within 10 degrees of the required orientation, i.e. the [001] orientation. The [001] orientation, as demonstrated in Chapter 3, has an isotropic stress and strain response similar to the polycrystalline materials. Consequently the structural analysis for the single crystal turbine blade is usually carried out in industry using the isotropic stress and strain equations for the [001] orientation with the program developed for isotropic materials. However, there has been no detailed investigation on the effects of misorientation on the stress and strain response of single crystal materials, and more importantly, on the deformation behaviour of a single crystal structure, such as a turbine blade.

Further numerical simulations and finite element analysis have been carried out in this work to examine the overall effect of misorientation on the material and structure deformation characteristics.

The numerical simulations were conducted for the single element specimens with main direction 10 degree away from the [001] orientation and with various secondary orientations. Table 6.2 gives the details of the specimen orientations studied. The simulation was carried out at strain rate of 0.4% with a total strain range of $\pm 2.5\%$. The cyclic stress and strain responses in the main direction for the different specimens are shown in Fig.6.7, and the stresses and the strains at the maximum strain of 2.5% are presented in Table 6.3. It can be seen that there is only a small difference in terms of the peak stress in tension and compression in the main direction for various specimens compared to the [001] orientation. This is because θ is only 10 degrees and variation in ρ only had a small influence on the stress in the loading direction. However, there was a considerable difference in terms of the transverse strain and shear strain response. The [001] orientation has an isotropic strain response with two equal transverse strains and no shear strains. For all the specimens with misorientation, the two transverse strains were not equal and different shear strains were induced due to the anisotropic deformation. Since the shear strains will cause distortion deformation, there are fundamental differences in terms of the deformation feature of the misorientation specimens compared with the [001] specimen.

The finite element analysis was conducted with a plate specimen, which was used to represent the simplified turbine blade structure. The details of the finite element analysis have been given in Chapter 5. The results indicated that the magnitude of the anisotropic transverse strains and the shear strains in each element was found to be small. This is in agreement with the numerical simulation results. However, the accumulated anisotropic effect on the overall deformation of the plate was found to be significant. The contour of the displacements of the plate, in Fig.5.21, showed a significant out-of-plane deformation. A distortion was induced in the plate due to the anisotropic stress and strain response caused by the misorientation.

It is well know the efficiency of a gas turbine engine is strongly dependent on the profile of the turbine blades. . The distortion and profile changes of turbine blade during operation will significantly reduce the gas turbine efficiency. Since the shape and the profile of turbine blades are optimised during design to achieve the maximum efficiency. The simple method using the isotropic stress and strain relationship for the [001] orientation to predict the deformation behaviour of turbine blades with misorientation will generate considerable error in terms of the overall profile of the blades. Therefore, the anisotropic constitutive models and the finite element program developed in this work could be used in the design and assessment of single crystal turbine blades to improve the efficiency gas turbine engines.

6.7. Convergence and Accuracy Analysis

For numerical calculations of the nonlinear problems, such as the one studied in this work, the main concern is always to obtain a convergent and accurate solution at a minimum cost. In terms of numerical calculation of the stress and strain response, there are two important topics concerning convergence and accuracy. One is between the numerical results and analytical solution of the model, another is between the model predictions and the real material behaviour, i.e. experimental results. The first one is dependent on how good the numerical method was developed and implemented in the numerical codes whilst the second one is attributed to how good the model was developed based on the material deformation characteristics.

The first topic on numerical accuracy is discussed in section 6.7.1. The second topic, an accuracy of modelling is discussed in section 6.7.2.

6.7.1. Numerical Accuracy

A number of numerical calculation programs, such as SIMNON, in-house FORTRAN programs, and the FE programs (ABAQUS and UMAT) have been used in this work. The convergence and accuracy assessments will be carried out for the numerical simulation and the finite element (FE) calculation respectively.

(i) Numerical Simulations

SIMNON:

SIMNON is a commercial software developed by SSPA, Sweden, and a registered trademark of Department of Automatic control, Lund Institute of Technology, Sweden. SIMNON was developed for numerical simulation of nonlinear differential equations. The numerical integration methods used in SIMNON include the following:

Runge-Kutta-Fehlberg 4^{th} and 5^{th} (4^{th} with variable and fixed step size)

Rung-Kutta-Fehlberg 2^{nd} /3^{rd}

Euler Dormand – Prince 4^{th}/5^{th}

The first method was used in this research to achieve the appropriate accuracy.

SIMNON has been used by thousands of people all over the world as an efficient tool for numerical simulations. Universities and research centres in more than 40 countries have found SIMNON to be a useful program for interactive simulation. However, SIMNON program is only useful for simple one-dimensional problems.

For a commercial software, the stability, convergence and accuracy of SIMNON has been well studied and verified by numerous applications. As an example, Fig.6.8 and Fig.6.9 present comparisons between the SIMNON simulation results and the analytical results for the [001] and [111] orientations under uniaxial loading. The details about the analytical solution are given in the following section. It can be seen

that the numerical simulation results almost exactly agree with the analytical solutions.

Therefore, SIMNON was used in this work as benchmark to verify the in-house written FORTRAN simulation program, and then the FE calculation results.

FORTRAN Program:

The in-house FORTRAN program was developed to carry out the numerical integration of the nonlinear differential equations that describe the anisotropic viscoplastic deformation behaviour of single crystal alloys. Since it is only a simple numerical simulation, the running cost of the in-house FORTRAN program is very cheap. Consequently, it is possible to use very small time increments in the program to achieve stable, convergence, and highly accurate results. Therefore, the main concern when writing the program was to chose a simple convergence numerical integration scheme with small time increment in the simulations.

The numerical scheme used for the numerical integration is a classical predictor-corrector implicit (midpoint) method (Burden and Faires [1997], Constantinidal and Mostoufi [1999]). The main features of the numerical procedure are outlined as follows:

From ith step the output from the analysis is:

$$\sigma_i, \varepsilon_i^e, \varepsilon_i^{in}, X_i \;\; ; \qquad \dot{\sigma}_i, \dot{\varepsilon}_i^e, \dot{\varepsilon}_i^{in}, \dot{X}_i$$

i+1 step:

Input: $\dot{\varepsilon}_{i+1}^T, \quad \Delta t_{i+1}$

$$(\Delta\varepsilon_{i+1}^T)_{input} = \dot{\varepsilon}_{i+1}^T \Delta t_{i+1}$$

Predictor: $$(\dot{\sigma}_{i+1})_{pre.} = E(\dot{\varepsilon}_{i+1}^T - \dot{\varepsilon}_i^{in})$$

$$(\sigma_{i+1})_{pre.} = \sigma_i + (\dot{\sigma}_{i+1})_{pre.} \Delta t_{i+1}$$

Calculation corrector: $\dot{\varepsilon}_{i+1}^e, \;\; \dot{\varepsilon}_{i+1}^{in}, \;\; \dot{X}_{i+1}, \;\; \dot{\sigma}_{i+1}, \;\; \dot{\varepsilon}_{i+1}^T$

Midpoint scheme for increments:

$$\Delta\varepsilon^{e}_{i+1} = \tfrac{1}{2}\left(\dot{\varepsilon}^{e}_{i} + \dot{\varepsilon}^{e}_{i+1}\right)\Delta t_{i+1}$$

$$\Delta\varepsilon^{in}_{i+1} = \tfrac{1}{2}\left(\dot{\varepsilon}^{in}_{i} + \dot{\varepsilon}^{in}_{i+1}\right)\Delta t_{i+1}$$

$$\Delta X_{i+1} = \tfrac{1}{2}\left(\dot{X}_{i} + \dot{X}_{i+1}\right)\Delta t_{i+1}$$

$$\Delta\sigma_{i+1} = \tfrac{1}{2}\left(\dot{\sigma}_{i} + \dot{\sigma}_{i+1}\right)\Delta t_{i+1}$$

$$\Delta\varepsilon^{T}_{i+1} = \tfrac{1}{2}\left(\dot{\varepsilon}^{T}_{i} + \dot{\varepsilon}^{T}_{i+1}\right)\Delta t_{i+1}$$

Up date the variables:

$$\varepsilon^{e}_{i+1} = \varepsilon^{e}_{i} + \Delta\varepsilon^{e}_{i+1}; \qquad \varepsilon^{in}_{i+1} = \varepsilon^{in}_{i} + \Delta\varepsilon^{in}_{i+1}$$

$$X_{i+1} = X_{i} + \Delta X_{i+1}; \qquad \sigma_{i+1} = \sigma_{i} + \Delta\sigma_{i+1}$$

i+1 step output: $\sigma_{i+1}, \varepsilon^{e}_{i+1}, \varepsilon^{in}_{i+1}, X_{i+1}$; $\dot{\sigma}_{i+1}, \dot{\varepsilon}^{e}_{i+1}, \dot{\varepsilon}^{in}_{i+1}, \dot{X}_{i+1}$

The above is repeated for next step.

Note: for the first step, the explicit Euler method was used, e.g. $\Delta\varepsilon^{e}_{1} = \dot{\varepsilon}^{e}_{1}\ \Delta t_{1}$, and then followed the implicit method was followed.

It is well known that the implicit midpoint method is a stable, convergence numerical scheme within the time increment limits (Burden and Faires [1997], Constantinidal and Mostoufi [1999]). When the time increment approaches the zero, the numerical integration results will be close to the theoretical solution. Here theoretical solution is used to refer to the 'accurate' solution of the differential equations.

To demonstrate the numerical characteristics of the in-house FORTRAN program, the simulation results with different time increments are shown in Fig. 6.10. The simulation was carried out for the [111] orientation under uniaxial loading with constant total strain rate of 0.0004/s. It can be seen that using a large time

increment, dt=0.5s, simulation results exhibited an oscillatory feature. Decreasing the time increments (e.g. dt=0.05, 0.005, 0.0005), the simulation results reached to a stable and convergent solution.

The accuracy of the numerical simulations can be further verified by comparing the simulation results with the results from a closed form analytical solution for a time independent case. This is achieved by changing the material constants in the model to reduce the time dependent form to a time independent form. The details of the study are outlined as follow.

From Chapter 3, the generic constitutive equations for uniaxial loading are expressed as

$$\sigma = X'+k'+R'+K'*(\dot{\varepsilon}^{in})^{1/n'} \tag{6.7a}$$

$$X' = \frac{N'}{Q'}(1-\exp(-Q'\varepsilon^{in})) \tag{6.7b}$$

$$R' = W'(1-\exp(-b'\varepsilon^{in})) \tag{6.7c}$$

It can be seen that the last term in equation (6.7a), $K'*(\dot{\varepsilon}^{in})^{1/n'}$, changes with inelastic strain rate, and therefore represent the time dependent stress contribution. When this term is equal to zero, the stress will not depend on strain rate, and the deformation response becomes time independent.

Since X' and R' can be expressed analytically as a function of inelastic (plastic) strain, an analytical solution for the stress can be obtained for the time independent case.

$$\sigma_{analysis} = X'+k'+R' = k' + \frac{N'}{Q'}(1-\exp(-Q'\varepsilon^{in})) + W'(1-\exp(-b'\varepsilon^{in})) \tag{6.8}$$

where k', N', Q', W' and b are materials constants (defined in Chapter3). These constants depend on the crystal orientation.

Loading in [001]:

$$k'=\frac{k}{\sqrt{M_{11}-M_{12}}} \quad ; \quad K'^{*}=\frac{K^{*}}{(M_{11}-M_{12})^{(n+1)/2n}} \quad ; \quad n'=n \tag{6.9a}$$

$$N'=(N_{11}-N_{12}) \; ; \quad Q'=\frac{(Q_{11}-Q_{12})}{\sqrt{M_{11}-M_{12}}} \; ; \tag{6.9b}$$

$$W'=\frac{W}{\sqrt{M_{11}-M_{12}}} \quad ; \quad b'=\frac{b}{\sqrt{M_{11}-M_{12}}} \tag{6.9c}$$

Loading in [111]:

$$k'=\frac{k}{\sqrt{M_{44}/2}} \quad ; \quad K'^{*}=\frac{K^{*}}{(M_{44}/2)^{(n+1)/2n}} \quad ; \quad n'=n \tag{6.10a}$$

$$N'=2\,N_{44} \; ; \quad Q'=\frac{Q_{44}}{\sqrt{M_{44}/2}} \; ; \tag{6.10b}$$

$$W'=\frac{W}{\sqrt{M_{44}/2}} \quad ; \quad b'=\frac{b}{\sqrt{M_{44}/2}} \tag{6.10c}$$

The material constants k, K*, n, W, b, M_{11}-M_{12}, M_{44}, N_{11}-N_{12}, N_{44}, Q_{11}-Q_{12} and Q_{44} are given in Table 3.3.

In the numerical simulation, the time independent case can be approximately calculated using the FORTRAN program written for time dependent case with material constant K* chosen to be close to zero.

The results for simulations corresponding to the [001] and [111] orientations with different material constants K* are shown in Figures 6.11 and 6.12. The simulations were carried out under total strain control with a very slow strain rate of 0.00004/s. It can be seen that stress response decreases with decreasing values of K*, i.e. the time dependent stress contribution decreases by reducing K*. There is no significant stress difference between the simulation results with K* =16.968 and K*=1.6968, in Figs.6.11. and 6.12. This indicates that with K*=1.6968 the stress and strain

response is approximately time independent. Furthermore, the time dependent stresses with K* =1.6968 can be estimated from a simple calculation.

For strain rate of 0.00004/s, the maximum inelastic strain rate will be less than 0.00004/s. Therefore assuming that:

$$\dot{\varepsilon}^{in} = \dot{\varepsilon}^{T} = 0.00004\ /s$$

Then for the [001] orientation: $K'^{*}(\dot{\varepsilon}^{in})^{1/n'} = 0.102$ MPa

and for the [111] orientation: $K'^{*}(\dot{\varepsilon}^{in})^{1/n'} = 0.09$ MPa

It can be seen that there is only a minor influence on the stress response from the time (rate) dependent term. Therefore the simulation results can be compared with the analytical solution for the time independent cases.

The results from the simulations and the analytical solution are compared in Fig.6.8 and Fig.6.9 for the [001] and [111] orientations respectively. It can be seen that the numerical simulations almost exactly agree with the analytical solutions. The relative error in terms of stress is defined as

$$\sigma_{error} = \left| \frac{\sigma_{analysis} - \sigma_{simulation}}{\sigma_{analysis}} \right| \qquad (6.11)$$

It was found that the maximum σ_{error} during all the calculations for both the [001] and [111] orientations was less than 0.2%.

Further simulations were carried out for different strain rates to assess the numerical accuracy for time dependent deformation response. Figures 6.13 and 6.14 show results for the [001] and [111] orientations. Different K* values were used in the simulations to represent the time independent (K*=1.6968) and time dependent (K*=1696.8) cases. It can be seen that for the time independent cases, there is hardly any strain rate effect on the stress and strain response, Fig.6.13b and Fig.6.14b,

whilst a strong strain rate effect was observed for the time-dependent case, Fig.6.13a and Fig.6.14a.

The calculations indicated that the stress reaches to a saturated level at large strain level for a given strain rate. Then at large strain level, the inelastic strain rate is very close to the total strain rate, i.e. $\dot{\varepsilon}^{in} \approx \dot{\varepsilon}^{T}$. At the same time, the back stress, X', will also reaches to its saturated value. Therefore, the stress at the maximum strain can be calculated as:

$$\sigma = k' + X' + R' + K'*(\dot{\varepsilon}^{in})^{1/n'} = \sigma_p + \sigma_v \tag{6.12}$$

$$\sigma_p = k' + X' + R' \approx constant \tag{6.13}$$

$$\sigma_v = K'*(\dot{\varepsilon}^{in})^{1/n'} \approx K'*(\dot{\varepsilon}^{T})^{1/n'} \tag{6.14}$$

For a given strain rate, the stress difference between the time dependent form (σ_a) and the approximate time independent form (σ_b) can be analytically calculated as

$$\Delta\sigma_{ana.} = \sigma_a - \sigma_b \approx \{K'*\dot{\varepsilon}^{T})^{1/n'}\}_a - \{K'*\dot{\varepsilon}^{T})^{1/n'}\}_b \tag{6.15}$$

The stress difference between the numerical simulation results, $\Delta\sigma_{cal.}$, can be directly obtained from the simulation output files. Comparison between $\Delta\sigma_{ana.}$ and $\Delta\sigma_{cal.}$ can further verify the accuracy of the numerical simulations.

Analytical and numerical calculations have been carried out for the [001] and [111] orientations under total strain control loading with strain rates of 0.004/s, 0.0004/s and 0.00004/s respectively.

The results were summarised and compared in the following tables.

[001]	Analytical Results	Numerical Results	Relative Error
$\dot{\varepsilon}^T$	$\Delta\sigma_{ana.}$ (MPa)	$\Delta\sigma_{cal.}$ (MPa)	$\left\|\frac{\Delta\sigma_{ana.}-\Delta\sigma_{cal.}}{\Delta\sigma_{ana.}}\right\|$ %
0.004	**366.30**	**366.38**	***0.02%***
0.0004	**193.31**	**193.47**	***0.08%***
0.00004	**102.09**	**102.18**	***0.09%***

[111]	Analytical Results	Numerical Results	Relative Error
$\dot{\varepsilon}^T$	$\Delta\sigma_{ana.}$ (MPa)	$\Delta\sigma_{cal.}$ (MPa)	$\left\|\frac{\Delta\sigma_{ana.}-\Delta\sigma_{cal.}}{\Delta\sigma_{ana.}}\right\|$ %
0.004	**327.17**	**326.84**	***0.02%***
0.0004	**172.73**	**172.56**	***0.01%***
0.00004	**91.18**	**91.19**	***0.11%***

It can be seen that the relative stress errors are less that 0.2% for all the assessment cases.

The above assessment has demonstrated that the in-house FORTRAN program is a reliable program that produces stable convergence and accurate numerical results. These simulation results can then be used as benchmark to verify the finite element calculation results. The comparisons given in Chapters 4 and 5 showed very good agreement between simulation and FE calculation results.

Finite Element Calculations

The principle concept for finite element analysis is discretisation. The structure is divided into small finite elements whose stress-strain behaviour response is described by a constitutive law. The local information of the stress-strain behaviour

is assembled at a global level so that equilibrium equations are satisfied throughout the elements of the whole structure. The finite element program used in this work is a combination of the commercial software (ABAQUS) with in-house developed program (UMAT). The global numerical calculation of the nonlinear equilibrium equations is performed by ABAQUS, whilst the local numerical calculation of the nonlinear stress and strain is carried out by the UMAT subroutine.

For problems involving history dependent response, the solution in ABAQUS is usually obtained as a series of increments, with iteration within each increment to obtain the global equilibrium (ABAQUS User Manual [1995]). Therefore, the objective is to obtain a convergent solution at a minimum cost. The nonlinear procedures in ABAQUS offer two approaches to this. Direct user control of increment size is one choice, whereby the user specifies the incrementation scheme. This is sometimes useful in repetitive analysis, where the user has a good "feel" for the problem. Automatic control is the alternative approach, whereby ABAQUS automatically selects the increments as it develops the response in the step. This approach is usually more efficient, because the user cannot predict the response ahead of time. Ultimately, automatic control allows nonlinear problems to be run with confidence without extensive experience with the problem (ABAQUS User Manual [1995]).

Since automatic control was used in this work for the finite element calculations, the overall convergence and accuracy of the calculation results were controlled by ABAQUS procedures. The local numerical calculation (using UMAT) only influences the speed of the convergence and the efficiency of the finite element calculation.

ABAQUS incorporates an empirical algorithm designed to provide accurate, and at the same time economical, solution of the equilibrium equations of nonlinear systems. The algorithm controlling the criteria used to establish convergence of nonlinear increments, as well as the automatic adjustment of increment size based on the rate of convergence. There are numerous parameters associated with these

algorithms. These parameters are assigned default values, chosen to optimise the accuracy and efficiency of the solution for a wide spectrum of nonlinear problems. These default values need not be adjusted for most cases (ABAQUS User Manual [1995]).

These default control parameters are designed to provide reasonable optimal solution of complex problems involving combinations of nonlinearities, and efficient solution of simpler nonlinear cases. However, the most important consideration in the choice of the controls and of the default values assigned to the control parameters is that any solution that is accepted as "convergence" is a close approximation to the exact solution of the nonlinear equations (ABAQUS User Manual [1995]).

Since the automatic time incrementation scheme provided in ABAQUS will ensure convergence and accuracy solution for global numerical calculation, the main objective of this work is to develop a local numerical implementation scheme to improve the overall efficiency of the finite element calculations. This was achieved by selecting a stable implicit numerical integration scheme and obtaining approximate closed form solutions for the stress and strain, as well as the internal variables in the incremental equations. An approximate solution for the Jacobian matrix required in the ABAQUS global level equilibrium equations was also obtained from complex mathematical analysis.

The progressive development of the local level numerical schemes and their interaction with the global level ABAQUS calculations has been discussed in section 6.5 of Chapter 6. Two numerical integration algorithms have been progressively developed. One is a partial implicit integration scheme and one is a full implicit integration scheme. The partial implicit integration scheme was developed firstly to demonstrate the feasibility of application of the implicit numerical algorithm for the anisotropic elasto-viscoplastic constitutive models, and to achieve an approximate closed form solution. Consequently, simplifications were introduced in the numerical method to reduce the level of difficulty in the mathematical derivation. In this algorithm, a full implicit scheme was applied to the inelastic strain rate which

is the primary variable in the constitutive model. A semi-implicit scheme was used to the back stress and isotropic hardening variables. The full implicit algorithm was developed to improve the computational efficiency. In this algorithm, the full implicit incremental integration scheme was applied to all the variables in the constitutive equations. Consequently, the mathematical derivation of the numerical implementation procedure is much more complicated, and great effort was devoted to obtaining the closed form solutions.

The full implicit algorithm provided more accurate stresses, strains, and the Jacobian matrix, at each integration point to the global equilibrium equation. Consequently, the rate of convergence in global level calculation is improved and less iterations required. The improvement of the calculation efficiency can be demonstrated by the comparison of the computing time used in the calculations with partial implicit and full implicit algorithms. An example is given in the following table using the UMAT routine for the phenomenological model. The comparison includes results using a simple single element and the more complex cylindrical specimen.

Calculation Case	Computing time (minutes)		Improvement
	Partial implicit	Full implicit	
Single element	10	2	5 times
Cylindrical specimen (540 elements)	450	80	5 times

It can be seen that the local numerical integration method had a significant influence on the computational efficiency of the overall finite element calculations.

6.7.2. Modelling Consideration

The nickel based material used in this thesis is SRR99 single crystal superalloy developed for gas turbine blade applications. Extensive experimental studies (Li [1993], Li and Smith [1995a, b]) have been carried out to for this material at Bristol

University. However the main objective of the experimental work was to determine the fatigue life of single crystal SRR99 under combined fatigue and creep loading conditions. Consequently, the experimental results obtained from the earlier studies (Li [1993], Li and Smith [1995a,b]) can not be used directly to determine the material constants with a consistent procedure such as the procedure proposed in this work.

A trial and error method had been used by Li [1993] to fit the material constants for the phenomenological model. This method involved manual adjustment of the material constants to obtain the best fit of the experimental data. It was found that the trial and error method was very time consuming and non-repeatable. It is not possible to use the trail and error method to fit the material constants in two different models and then compare the models, since the errors induced by the method will override the characteristics of the models and the intrinsic features can not be explored. However, the extensive work carried out in the earlier work using the trial and error method did provide a reasonable good fit for the phenomenological model with the experimental results (Li [1993], Li and Smith [1995a,b]). Therefore, the simulation results generated by the phenomenological model with the material constants from earlier work will provide reasonable data similar to the real experimental data. These results can then be used to determine the material constants in both the phenomenological and crystallographic models with the proposed consistent procedure. This will provide the basis for direct comparison of the two models.

The method proposed in this work has identified suitable tests to determine the material constants for both models. A consistent procedure was established to determine the material constants for the two models using the same experimental data. The calculations demonstrated that this method can produce the exact material constants determined in the earlier work for the phenomenological model. Therefore, the accuracy of the consequent numerical simulation and finite element calculation results will be the same as in the earlier work (Li [1993], Li and Smith [1995a,b]).

As an example, Figs.6.15 and 6.16 compare experimental and simulation results generated by the phenomenological model (Li [1993]). The comparison includes continuous cyclic fatigue tests (Fig.6.15) and cyclic fatigue tests with time dwell at maximum and/or minimum strains, i.e. combined fatigue and creep tests (Fig.6.16). It can be seen that the simulations are in good agreement with the experimental results. This demonstrated that constitutive model was well developed based on the material deformation characteristics, and the accuracy of the model is reasonable good, at least based on the limited experimental evidence.

The finite element (FE) calculations for cylindrical bar specimen which represent the test specimens have been carried out using both the phenomenological and crystallographic models. The specimen orientations are given in Fig.6.17. The loading conditions used in the finite element simulation were exactly the same as those used in the experimental testing. The stress ranges calculated from the finite element simulations are compared with the experimental results (Li [1993], Li and Smith [1995a,b]) in the following table.

Specimen No	**Experimental Results**	**FE Results Phenomenological Model**		**FE Results Crystallographic Model**	
	$(\Delta\sigma)_T$, MPa	$(\Delta\sigma)_{FE}$, MPa	***Relative Error, %***	$(\Delta\sigma)_{FE}$, MPa	***Relative Error, %***
A	539	544	***0.93***	545	***1.11***
B	533	506	***-5.07***	534	***0.19***
C	368	393	***6.79***	406	***10.33***
D	338	330	***-2.37***	334	***-1.18***
E	212	226	***6.60***	226	***6.60***
F	429	414	***-3.50***	415	***-3.26***

Note: Relative Error $= \dfrac{(\Delta\sigma)_P - (\Delta\sigma)_{FE}}{(\Delta\sigma)_{FE}} \times 100\%$

The results are also plotted in Fig. 6.18. It can be seen that both the phenomenological and the crystallographic models provide good results when compared with the experimental results. Based on the limited available experimental data, it is difficult to draw definite conclusions to indicate which model is better. Further experiments, in particular multiaxial loading experiments, are required to verify the models. These experiments also are needed to provide information for further modification and improvement of the models.

CHAPTER 7
CONCLUDING REMARKS

7.1. Conclusions

1. Two constitutive models, one phenomenological and the other crystallographic, have been presented to describe the anisotropic viscoplastic deformation behaviour of single crystal nickel base superalloys under isothermal loading. These models have also been developed further for thermomechanical applications.

2. The two models are then applied to the simple uniaxial loading cases to identify the suitable tests for determining the material constants. A group of generic equations have been identified for both models for uniaxial loading in the [001] and [111] orientations. Consequently a consistent procedure to determine the material constants in the two models using same experimental results is proposed. This allows a direct comparison of the intrinsic characteristics of the phenomenological and crystallographic models.

3. A common numerical procedure to determine the material constants in the two models has been developed. The procedure includes a number of local optimisation routines to determine several group of material constants from experimental data associated with the deformation characteristics described by a given group of material constants. The procedure has been utilised successfully to determine the material constants in the two models for single crystal SRR99 at 950°C.

4. Using the material constants determined from same experimental results and using a consistent procedure, the intrinsic characteristics of the two models are compared. The simulation results indicate that both models can describe the fundamental deformation features of single crystal alloys. However, differences are observed when the stress and strain curves predicted by the two models are compared. Further investigations indicated that the difference between the two

models is dependent on crystal orientation. The orientations where the two models predict similar deformation behaviour are consistent with the orientations where either octahedral or cubic slip dominates the inelastic deformation.

5. A numerical implementation procedure, based on the implicit time integration scheme, has been developed to transform the differential anisotropic viscoplastic constitutive equations of both the phenomenological and the crystallographic models. Closed form approximate analytical solutions for nonlinear incremental equations have been achieved for the two models for both isothermal and thermomechanical applications. The closed form solutions improve both the numerical calculation accuracy and FE analysis efficiency, and reduce computer running costs.

6. The numerical implementation procedure has been successfully coded into UMAT subroutines in the ABAQUS FE code. A comprehensive program has been carried out to verify the numerical implementation procedure, the UMAT subroutines and their interface with ABAQUS. The results obtained from the finite element analysis were found to be in good agreement with theoretical predictions.

7. The UMAT and ABAQUS codes have been used successfully for structural stress analysis. Different shaped specimens, including cylindrical bar, plate and tube, have been analysed under uniaxial tension, cyclic tension/compression, pure torsion and combined tension-torsion loading conditions. The structural stress analysis further explored the anisotropic deformation characteristics of the single crystal superalloys, and examined the similarities and differences between the phenomenological and crystallographic models.

8. From the FE results using the two models for complex loading, the structural deformation response has been examined in detail. As an example it was found that under torsion loading, the two models gave very similar predictions for the

global response, i.e. torque versus twist angle. However, predicted local deformations using the two models were found to be very different.

7.2. Recommendations for Future Work

The results from the research have revealed that the two models provide significantly different results particularly in terms of the transverse response of single crystal structural components. Direct verification using a complex geometry, such as a notched bar to explore the transverse behaviour is required. However, the measured strains would be very low and difficult to measure.

Models have been developed and implemented here without cross-slip. It is evident from Chapter 4 that the formulation for the crystallographic model allows cross slip to be introduced.

The models explored in this work are for cyclic loading with limited creep effects. The material behaviour for longer duration is dominated by creep. Nevertheless, we would expect interactions between creep and plasticity. This is demonstrated in the current models. Further work is required in integrate the short term creep and plasticity effects with longer term creep behaviour.

Finally, further work is required to be able to simulate non-linear material response for a range of temperatures. Preliminary work has revealed that a single model for a range of temperature is difficult to implement.

REFERENCES

Agatonovic P. and Clormann U.H., [1987], "Application of an improved constitutive model to practical engineering problems with creep-fatigue behaviour", Int. Conf. on Computational Plasticity, Models, Software and Applications, Barcelona, Spain.

Bhattachar V. S. and Stouffer D. C., [1993a],"Constitutive equations for the thermomechanical response of Rene 80: Part 1-development from isothermal data", Jnl. of Eng. Mat. & Tech., October 1993, Vol. 115

Bhattachar V. S. and Stouffer D. C., [1993b],"Constitutive equations for the thermomechanical response of Rene 80: Part 2-effects of temperature history", Jul. of Eng. Mat. & Tech., October 1993, Vol. 115

Bodner S. R. and Merzer A. [1978], "Viscoplastic constitutive equations for copper with strain rate history and temperature effects", ASME Journal of Engineering Materials and Technology, Vol.100, pp.388-394.

Bondner S. R. and Partom Y., [1975], "Constitutive equation for elastic-viscoplastic strain-hardening materials", ASTM J. App. Mech., Vol.42, pp.385-389.

Burden R.L and Faires J.D., [1997], <Numerical Methods> 6th edition, Brooks/Cole Publishing Company, CA UAS.

Chaboche J. L. and Nouailhas D., [1989], "A Unified constitutive model for cyclic viscoplasticity and its applications to various stainless steels", transactions of the ASME October 1989 424/Vol.111, pp.424-430.

Chaboche J. L., [1989], "Constitutive equations for cyclic plasticity and cyclic viscoplasticity", International Journal of Plasticity, Vol.5 pp 247-302.

Chaboche J. L. and Rousselier G., [1983], "On the plastic and viscoplastic constitutive equations-part I: Rules developed with internal variable concept", Journal of pressure vessel technology, May 1983, Vol.105, pp.153-158.

Chaboche J. L. and Rousselier G., [1983], "On the plastic and viscoplastic constitutive equations-part II: Application of internal variable concepts to the 316 stainless steel", Journal of pressure vessel technology, May 1983, Vol.105, pp.159-164.

Chan K. S. and Lindholm U. S., [1990], "Inelastic deformation under nonisothermal loading", Journal of engineering material and technology, January 1990, Vol.112.

Chan K. S., Lindholm U. S. and Bodner S. R., [1988], "Constitutive modeling for isotropic materials (final report)", NASA CR-182132.

Chan K. S., Lindholm U. S., Bodner S. R. and Walker K. P., [1989], "High temperature inelastic deformation under uniaxial loading: theory and experiment", ASME J. Eng. Meter. Tech., Vol.111, pp.345-353.

Chan K. S., Lindholm U. S., Bodner S. R. and Nagy A., [1990], "High temperature inelastic deformation of the B1900+Hf alloy under multiaxial loading: theory and experiment", ASME J. Eng. Meter. Tech., Vol.112, pp.7-14.

Choi S. H. and Krempl E., [1989], "Viscoplasticity theory based on overstress applied to the modeling of cubic single crystals", Eur. J. Mech. A/Solids, Vol.8, pp.219-233.

Clement N,, Couret A and Caillard D., [1991], "An in-situ study of cube glide in the γ' phase of a superalloy: I The controlling mechanism – II. The anomalous stress-temperature dependence" Phil. Mag. Pp.231-267.

Constantinide A. and Mostoufi N., [1999], <Numerical Methods for Chemical Engineers with MATLAB Application>, Prentice Hall PTR, Upper Saddle River, New Jersey, UAS.

Culie J. P. and Nouailhas D., [1993], "New constitutive equations for single-crystal alloys: implementation in the SAMCEF code, and application", Rech. Aerosp.

Dandekar D. P. and Martin A. G., [1989],"single crystal elastic constants of two nickel based superalloys", Jnl. of Mat. Science Letters 8, 1989

Dandekar D. P. and Martin A. G., [1990], "Temperature dependence of flexural and torsional elastic constants of two nickel-based superalloys", Journal of Materials Science, 25, p3321-3326

Dunne F. P. E. Makin J. and Hayhurst D. R., [1992], "Automated procedures for the determination of high temperature viscoplastic damage constitutive equations" , Proc. R. Soc. Lond. A (1992) 437, 527-544.

Elmquist H., Astrom K.J. and Schonthal T., [1986], *SIMNON User's Guide for MS-DOS Computer*, Studentlitteratur AB, Lund.

Fleury E. and Remy L., [1994],"Behaviour of nickel base superalloys single crystals under thermal-mechanical fatigue", Matellurgical and Materials Transaction, Vol 25A, pp.99-109.

Freed, A.D., Chaboche, J.L. and Walker, K.P., [1991],"a viscoplastic theory with thermodynamic considerations", ACTA mechanica, 1991, vol.90, no.1-4, pp.155-174

Gabb T. P., Gayda J. and Miner R. V., [1986], "Orientation and temperature dependent of some mechanical properties of the single crystal nickel base superalloy Rene 4 Part II: low cycle fatigue behaviour", Metall. Trans. A, Vol.17A, pp.497-505.

Ghosh R.N., Curtis R.V. and Mclean M., [1992] " High temperature deformation in engineering alloys - modelling for strain or load control", Acta. Metall.,. Vol.40, pp.3075-3083.

Goodall I.W., Hales R. and Walters D.J., [1980], "On constitutive relation and failure criteria of an austenitic steel under cyclic loading under high temperature", IUTAM Symp., Leicester, Springer-Verlag.

Graham A. and Walles K. F. A., [1955], "Relationships between long- and short-time creep and tensile properties of a commercial alloy", J. of the Iron and Steel Institute, pp.105-120.

Guedou J.Y. and Honnorat Y., [1990], " Mechanical behaviour modeling of a nickel base single crystal superalloy" , in Constitutive Laws of Plastic Deformation and Fracture, (Eds. Krausz A.S. et al), Kluwer Academic Publishers, pp.35-41.

Hanriot F., Cailletaud G. and Remy L., [1991], "Mechanical Behaviour of a nickel-base superalloy single crystal", in<High Temperature Constitutive Modelling

– Theory and Application), (Editors: A.D. Freed and K.P. Walker) ASME, pp.139-150.

Harrison G.F. and Homewood T., [1994], "The application of the Graham and Walles creep equation to aeroengine superalloys", Journal of Strain Analysis vol. 29, No 3.

Hibbitt, Karlson & Sorenson, Inc., *ABAQUS Users Manual*, Pawtucket, USA, 1995

Hill, R., [1950], "The Mathematical Theory of Plasticity", Oxford Press.

Hughes, T.J.R., *Compu. Methods for Transient Analysis*, North-Holland, Amsterdam, 1983.

James G.H., Imbrie P.K., Hill P.S., [1987], "An experimental comparison of several current viscoplastic constitutive models at elevated temperatures", J. of Eng. Mater. Technol. Vol.109, pp130-139.

Jordan E. H. and Walker K. P., [1992], "A viscoplastic model for single crystals", Journal of Engineering Materials and Technology, vol.114, pp 19-26

Kear B.H. and Piearcey B.J, [1967], " Tensile and creep properties of single crystals of the nickel -base superalloy Mar-M200", Trans. AIME, Vol.239, p.1209.

Kounitzky A., Wortmann J. and Agarwal P.N., [1991], "A single crystal casting process for high-temperature components", Mater. Design, Vol.12, pp323-330.

Krempl E. and Yao D., [1987], " The viscoplasticity theory based on overstress applied to ratchetting and cyclic hardening", in Low-cycle Fatigue and Elasto-plastic Behaviour of Materials, (Ed. Rie K.T.), Elsevier Applied Science, pp.137-148.

Krieg R.D., Swearengen J.C. and Rohde, R.W., [1978], "A physical based internal variable model for rate-dependent plasticity", in Inelastic Behavior of Pressure Vessel and Piping Components. PVP-PB-028, (Eds. Chang T.Y and Kremple E.) ASME, New York, pp.15-28.

Lall C., Chin S. and Pope D., [1979], "The orientation and temperature dependence of the yield stress of Ni3[Al,Nb] single crystals", Metall. Trans A, Vol.10A, P.1323-1332.

Lee D. and Zaverl F., [1978], "A generalized strain rate dependent constitutive equation for anisotropic metals", Acta. Mechanica, Vol.29, pp.1771-1780.

Lee K.D. and Krempl E., [1991], "An orthotropic theory of viscoplasticity based on overstress for thermomechanical deformations", Int. J. Solids Struct., Vol.27, pp.1445-1459.

Lemaitre J. and Chabche J.-L., [1990], "Mechanics of Solid Materials"

Leverant G.R., Gell W. and Hopkins S.W., [1971], "The effect of strain rate on the flow stress and dislocation behavior of precipitation-hardened nickel base alloy ", Mater. Sci. Engng., Vol.8, p.125-133.

Leverant G.R. and Kear B.H., [1970], "The mechanism of creep in gamma prime precipitation-hardened nickel base alloys at intermediate temperature", Metall. Trans., Vol.1A[i], pp.491-518

Leverant R., Kear B.H. and Oblak J.M, [1973], "Creep of precipitation-hardened nickel-base alloy single crystals at high temperature", Metall. Trans., V.4, 355-362.

Li S. X., [1993], "High Temperature Creep-fatigue and Crack Growth Behaviour of a Single Crystal Nickel Base Superalloy", Ph.D thesis, University of Bristol, UK.

Li S.X. and Smith D.J., [1994] " Physical interpretation of unified elastic-visco-plastic models with particular reference to single crystal alloys", Report N0. 94/2, Department of Mechanical Engineering, University of Bristol.

Li S.X. and Smith D.J., [1995a] "Elevated temperature fatigue-creep behaviour of single crystal SRR99 nickel base superalloy:I Cyclic mechanical response", submitted to Fract. Fatig. Engng. Mater. Struct.

Li S.X. and Smith D.J., [1995b] "Temperature and orientation dependence of the elastic and yield properties of a single crystal nickel base superalloy", submitted to Materials Science and Technology.

Li S.X. and Smith D.J., [1995c] "Elevated temperature fatigue-creep behaviour of single crystal SRR99 nickel base superalloy:II Creep-Fatigue Life Behaviour", Fract. Fatig. Engng. Mater. Struct, Vol.18, No.5, pp.631-643

Li S.X. and Smith D.J., [1995d], "Modelling of Anisotropic Creep Deformation and Damage in Single Crystal Superalloys", Scripta Metall. et Mater., Vol.33, pp.711-718.

Li S. X., Han S and Smith D. J., [1996], "Measurement of the transverse local strain response of single crystal superalloys", <Local Strain and Temperature Measurements in Non-uniform Fields at Elevated Temperatures>, The Proceedings of the Symposium held at Berlin, Germany, 14-15 March 1996

Mackay R.A. and Maier R.D., [1982], "Influence of orientation on the stress rupture properties of nickel-base superalloy single crystals", Metall. Trans., Vol.13A, pp.1747-1754.

MacKay R.A. and Ebert L.J., [1983], "The development of directional coarsening of the γ' precipitate in superalloy single crystals", Scripta Metall., **17,** 1217.

Meric L. and Cailletaud G., [1991], " Single crystal modelling for structural calculation: Part 2-finite element implementation", J. Eng. Mater. and Tech., vol.113, pp.171-182

Meric L., Poubanne P. and Cailletaud G., [1991], "Single crystal modelling for Structure calculations. part 1. model presentation", J. Appl. Mechanics, Vol.113, pp.156-170.

Meric L., Cailletaud G and Gasperini M., [1994], "F.E. calculations of copper bicrystal specimens submitted to tension-compression tests", Acta metall. mater. Vol.42, No. 3, pp 921-935

Merzer A. and Bodner S. R., [1979], " Analytical formulation of a rate and temperature dependent stress-strain relation", ASME Journal of Engineering Materials and Technology, Vol. 101, pp.254-257

Miller, A., [1976a], "An inelastic constitutive model for monotonic, cyclic and creep deformation: Part1-equations development and analytical procedures", Jnl. of Eng. Materials and Technology, April 1976, pp97-105

Miller, A., [1976b], "An inelastic constitutive model for monotonic, cyclic and creep deformation: Part2-application to type 304 stainless steel", Jnl. of Eng. Materials and Technology, April 1976, pp106-113

Milligan W.W. and Antolovich S.D., [1987], "Yielding and deformation behavior of the single crystal superalloy PWA1408", Metall. Trans. A, Vol.18A, pp.85-95.

Milligan W.W. and Antolovich S.D., [1990], "The cyclic deformation of PWA1408 single crystal as a function of temperature, strain rate and orientation", in Constitutive Laws of Plastic Deformation and Fracture, (Eds. Krausz A.S. et al), Kluwer Academic Publishers, pp.43-48.

Miner R.V., Gabb T.P, Gayda J. and Hemker K.J., [1986a], "Orientation and Temperature dependence of some mechanical properties of the single crystal nickel base superalloy Rene N4: part III. Tension-Compression Anisotropy", Metall. Trans. A, 17A, pp.507-512.

Miner R.V., Voigt R.C., Gayda J. and Gabb T.P., [1986b], "Orientation and temperature dependence of some mechanical properties of the single - crystal nickel - base superalloy Rene N4: part I. Tensile behaviour", Metall. Trans. A, Vol.17A, pp.491-496.

Moreno V. and Jordan E.H., [1986], " Prediction of material thermomechanical response with a unified viscoplastic constitutive model", International Journal of Plasticity, vol. 2, pp. 223-245

Mroz Z. and Niemunis A., [1990], "On the description of deformation anisotropy of materials", in <Yielding, Damage and Fatigue of Anisotropic Solids> EGF5 (Edited by J.P. Boehler), Mechanical Engineering Publications, London, pp.171-186.

Mughrabi H. , [1978], "The cyclic hardening and saturation behaviour of copper single crystal", Mater. Sci. Engng. Vol.33, pp.207-233.

Nathal M. V., Maier R. D. and Ebert E.J., [1982], " The influence of coblat on the tensile and stress-temperature properties of the nickel-base superalloy", Metall. Trans. A, Vol.13A, pp.1767-1774.

Nathal M.V. and Ebert L.J., [1983], Scripta Metall. Vol.17, pp.11151.

Nathal M.V. and Ebert L.J., [1985], "Elevated temperature creep-rupture behaviour of the single crystal nickel base superalloy NASAIR 100", Metall. Trans., Vol.16A.

Nathal M.V., MacKay R.A and Miner R.V., [1989], "The Influence of Precipites Morphology on Intermediate Temperature Creep Properties of a Nickel-Base Superalloy single Crystal", Metall. Trans., Vol.20A, pp.133-141.

Nouailhas D., [1990] "Anisotropic constitutive equations for cyclic viscoplasticity: Application to the case of materials with cubic symmetry" Rech. Aerosp., No.3, pp11-28.

Nouailhas D. and Chaboche J. L., [1991],"Anisotropic constitutive modeling for single-crystal superalloys using a continuum phenomenological approach", 3rd International conference on "constitutive laws for engineering materials, theory and applications", Tucson (Arizona, USA), January 7-12, 1991.

Nouailhas D., Pacou D. and Cailletaud G., [1993], "Tension-torsion behavior of single-crystal superalloys: experiment and finite element analysis", 4th International Symposium on Plasticity and its Current Applications, Baltimore, MD (USA), July 19-23, 1993.

Nouailhas D., Pacou D. and Cailletaud G., Hanriot F. and Remy L, [1993], "Experimental study of the anisotropic behaviour of the CMSX2 single crystal

superalloy under tension-torsion loadings"", 4in Advances in Multiaxial fatigue (edition M Dowell and Ellis) ASTM, pp.244-258.

Nouailhas D. and Cailletaud G., [1995], "Tension-Torsion behaviour of Single-crystal surperalloys: experiment and finite element analysis", International Journal of Plasticity, Vol. 11, No.4, pp. 451-470, 1995.

Nouailhas D., Culie J.-P., Cailletaud G. and Meric L., [995], "Finite element analysis of the stress-strain behavior of single crystal tubes", European Journal of Mechanics, A/Solids, Vol.14, No.1, pp 137-154

Nouailhas D., [1995], "Microscopic and Macroscopic Behaviour of Two-Phased Single Crystal Superalloys", Presented in Seminar on Mechanical Behaviour of Superalloys, 4-5 October, 1995, Berlin.

Nye J.F., [1957], Physical Properties of Crystals, Clarendon Press, Oxford, London

Oblak J.M. and W.H. Rand, [1974], in 'Proc. 32nd Annual Meeting of Electron Microscopy Society of America' [ed C.J. Arceneauk], 502-503.

Ohno N., [1990], "Recent topics in constitutive modeling of cyclic plasticity and viscoplasticity", Appl. Mech. Rev., Vol. 43, pp. 283-295.

Ohno N. and Wang J., [1992], "Nonisothermal constitutive modelling of inelastic based on bounding surface", Nuclear Engng. & Design, Vol.133, pp.369-381

Ortiz M. and Popov E.P.,[1985], "Accuracy and stability of integration algorithms for elastoplastic constitutive relations", *Int. J. Numer. Methods Eng.*, **21**, 1561.

Pan L.M. et al, [1994], "Asymmetric creep deformation of a single crystal superalloy", Act Metall., Vol.43, pp.1375-1384.

Paider V., Pope D.P., and Vitek V., [1984], "A theory of the anomalous yield behaviour of LI order alloys", Act Metall., Vol.32, pp.435-449.

Paslay P., Wells C., and Leverant G., [1970], "An analysis of primary creep of nickel based superalloy single crystals", J. Appl. Mech., Vol.37, p.759.

Paslay P., Wells C., Leverant G. and Burke L., [1971], "Creep of single crystal nickel-based superalloy tubes under biaxial tension", J. Appl. Mech, Vol.38, p.623.

Pearson D.D., Lemkey R.D. and Kear B.H., in Superalloys 1980, Proc. 4th Int. Symp. on Superalloys, Am. Soc. Metals, Metals Park, Ohio, p.513

Plumbridge W.J., and Ellison E.G., [1987], "Low-cycle fatigue behaviour of superalloy blade materials at elevated temperature", Mater. Sci. Tech., Vol.3, pp.706-715.

Pollock T.M. and Argon A.S., [1994], "Directional Coarsening in Nickel-Base Single Crystal with High Volume Fraction of Coherent Precipitates", Acta Metall. Mater., 42, pp.1859-1874.

Policella H., Paulmier P. and Pacou D., [1990], "High temperature properties of single crystal CMSX2 alloy: Experimental results", Rech. Aerosp.., 4, pp.47-63.

Pope D.P. and Ezz S.S, [1984], "Mechanical properties of Ni_3Al and nickel-base alloys with high volume fraction of γ' ", Int. Metals Reviews, Vol.29, no.3, pp.136-167.

Poubanne P., [1990], "Anisotropic mechanical behaviour modeling of a nickel base single crystal superalloy" in Constitutive Laws of Plastic Deformation and Fracture, (Eds. Krausz A.S. et al), Kluwer Academic Publishers. pp.49-55.

Ramaswamy V.G., Stouffer D.C., and Laflen J.H., [1990], "A constitutive model for the inelastic uniaxial response of Rene 80 at temperature between 538C and 982C", J. Engineering Materials and Tech., Vol.112, pp.280-286.

Remy L., [1993], High temperature fatigue of superalloys" in Fatigue '93, (Eds. Bailon J P and Dickson J I) EMAS U.K vol.II, pp825-834.

Remy L., [1984], "Cyclic deformation and crack initiation processes" in Fatigue 84 (edition C.J. Beerers) E.M.A.S. London pp.15-30.

Richmond O. and Spitzig A., [1980], "Pressure dependence and dilatancy of plastic flow", IUTAM, 1980.

Russell R., Jenson and John, K. Tien, [1985], "Temperature and strain rate dependence of stress-strain behaviour in a nickel-base superalloy", Metall. rans. A, Vol.16A, pp.1049-1068.

Scherwood J. A. and Fay E. M., [1992], "Application of a unified constitutive theory to the nonproportional multiaxial strain deformation of 1045 steel", Journal of Eng. Mater. And Tech., April 1992, Vol.114.

Schmid E. and Siebel G., [1931], I Electrachew, Vol.37, p.447.

Schmidt C.G. and Miller A.K., [1981], "A unified phenomenological model for non-elastic deformation of type 316 stainless steel, Parts I and II", Res. Mechanica, Vol3, pp109-129, PP175-193.

Schneider W., Hammer J. and Mughrabi H., [1992], "Creep Deformation and Rupture Behaviour of the Monocrystalline Superalloys CMSX-4 - A Compaison with the Alloy SRR99", in Superalloys 1992, (Eds. Antolovich et al), The Miner. Metals Mater. Soc. pp.589-598.

Schwertel J., Diegele E., Schinke B. and Munz D., [1992], "Efficient algorithms for the evaluation of material parameters of viscoplastic constitutive equations", Proc. on Computational Plasticity III, Barcelona, Spain.

Shah D., [1983], "Orientation dependence of creep behaviour of single crystal (Ni_3Al)", Scripta Metall., Vol.17, p.997-1002.

Shah D.M. and Buhl D.N., [1984], "The effect of orientation, temperture and gamma prime size on the yield strength of a single crystal nickel base superalloy", in Superalloys 1984, Proc. 5th Int. Symposium on Superalloys, (Eds. Gell M. et al), AiME Warrendale PA. Pp.105-14.

Sheh, M.Y. and Stouffer, D.C., [1990], " A crystallographic model for the tensile and fatigue response for Rene N4 at 982 C", J. Appl. Mech, Vol.57, pp.52-31.

Smith G.F. and Kiral E., [1969], "Integrity basis of N symmetry second-order tensors, the crystal classes", Rend Circ. Mat. Palemo II, Ser. 18, pp.5-22.

Spitzig W. A., [1978], "Effect of hydrostatic pressure on plastic-flow properties of iron single crystals", Acta Metallurgica, Vol.27, pp. 523 to 534.

Spitzig W. A., [1981], "deformation Behavior of nitrogenated Fe-Ti-Mn and Fe-Ti single crystals", Acta Metallurgica, Vol.29, pp. 1359 to 1377.

Stouffer D.C., Sheh M.Y. and Dam L.T., [1990], "Anisotropic constitutive model of a single crystal superalloy at elevated temperature " , Appl. Mech Rev., Vol.43, no.5, pp.345-352.

Sun Y.Q. and Hazzledine P.M., [1988],"A TEM weak-beam study of dislocation in r' in a deformed Ni-based superalloy", Phil. Mag., A58, p.603-618.

Takenchi S. and Kuramoto E., [1973], "Temperature and orientation dependence of the yield stress in Ni_3Ga single crystals", Acta Met., vol.21, pp.415-425.

Tanaka T. G. and Miller A. K., [1988], "Development of a method for integrating time-dependent constitutive equations with large, small or negative strain rate sensitivity", international journal for numerical methods in engineering, Vol. 26, 2457-2485, 1988

Taylor G., [1937], "Plastic strains in metals", J. Inst. Metals, Vol.62, p.307.

Thompson, R.L., [1989], "Structural analysis method development for turbine hot section components", J. Engng. for Gas Turbines and Power, Vol.111, pp.286-300.

Thompson R. L., [1982], "Nonlinear constitutive theory for turbine engine structural analysis", NASA CP-2245

Tien J.K and Copley S.M., [1971], Metall. Trans. Vol.2, pp.543.

Toulios M., [1993], European Gas Turbine Ltd, Private communication.

Umakoshi Y., Pope D. and Vitek V., [1984], "The asymmetry of the flow stress in $Ni_3(Al,Ta)$ single crystals", Acta Metall., Vol.32, No.3, p.449-456.

Vogel W., Wilhelm M. and Gerold V., [1982], "Persistent slip bands in fatigue peak aged Al-Zn-Mg single crystal", Acta Metall., Vol.30, pp.21-35.

Walker K. P., [1981], "Research development program for non-linear structural modeling with advanced time-temperature dependent constitutive relationship", NASA CR-165533

Walker K.P. and Jordan E.H., [1989], "Biaxial constitutive modeling and testing of a single crystal superalloy at elevated temperatures", in Biaxial and Multiaxial Fatigue, EGF3, (Eds. M W. Brown and K.J. Miller), Mechanical Engineering Publications, London, pp.145-170

Walter W., Milligan and Antolovich D.A., [1987], "Yielding and deformation behaviour of the single crystal superalloy PWA 1480", Metall. Trans. A, Vol.18A, pp.85-95.

Winstone M., [1989], in Proc. of MTU Seminar on Single Crystals, Munich.

Yang S.W., [1985], "Elastic constants of a monocrystalline nickel base superalloy", Metall. Trans. A, Vol.16A, pp.661-665.

Zirin R.M. and Krempl E., [1982], "A finite element time integration method for the theory of viscoplasticity based on infinitesimal total strain", J. Pressure Vessel Tech., Vol.104, pp130-136.

APPENDIX I

SCHMID'S LAW AND SCHMID'S FACTORS

Consider a cylindrical single crystal with cross-section A and a crystal orientation $[l_1,m_1,n_1]$ loaded by a uniaxial load P. The direction of the normal to the slip plane is $[l_2,m_2,n_2]$ and the slip direction is $[l_3,m_3,n_3]$. The angle between the tensile axis and the normal to the slip plane is φ, and the angle which the slip direction makes with the tensile axis is θ. Hence, the area of the slip plane inclined at the angle φ will be $A/\cos\varphi$, and the component of the axial load acting in the slip plane in the slip direction is $P\cos\theta$. Therefore, the resolved shear stress, τ, is given by

$$\tau = \frac{P\cos\theta}{A/\cos\varphi} = \frac{P}{A}\cos\varphi\cos\theta \qquad \text{(A1.1)}$$

Schmid's Law states that yielding occurs when the resolved shear stress reaches the value of the **Critical Resolved Shear Stress (CRSS), τ_s ;**

$$\tau_s = \frac{P_y\cos\theta}{A/\cos\varphi} = \frac{P_y}{A}\cos\varphi\cos\theta = \sigma_y\cos\varphi\cos\theta \qquad \text{(A1.2)}$$

or

$$\sigma_y = \tau_s/\cos\varphi\cos\theta = \tau_s/S_{[l_2,m_2,n_2]\{l_3,m_3,n_3\}} \qquad \text{(A1.3)}$$

where σ_y is the uniaxial yield stress, $S_{[l_2,m_2,n_2]\{l_3,m_3,n_3\}} = \cos\varphi\cos\theta$ is called **Schmid's Factor.** For a given slip system and loading direction, **Schmid's Factor** can be calculated using the following equations.

$$\cos\theta = \frac{l_1l_3 + m_1m_3 + n_1n_3}{\sqrt{l_1^2 + m_1^2 + n_1^2}\sqrt{l_3^2 + m_3^2 + n_3^2}} \qquad \text{(A1.4)}$$

$$\cos\varphi = \frac{l_1l_2 + m_1m_2 + n_1n_2}{\sqrt{l_1^2 + m_1^2 + n_1^2}\sqrt{l_2^2 + m_2^2 + n_2^2}} \qquad \text{(A1.5)}$$

where l_i, m_i and n_i are direction cosines (i=1,2,3).

Appendix II

Global Loading to Crystallographic Coordinate System Transformation

The global and crystallographic coordinate systems are illustrated in Fig.3.1. The loading direction Z is set to be along orientation (l,m,n) in the crystallographic coordinate system, X*-Y*-Z*. Direction Z can then be written in a vector form as:

$$\vec{Z}=\frac{l}{\sqrt{l^2+m^2+n^2}}\vec{i}+\frac{m}{\sqrt{l^2+m^2+n^2}}\vec{j}+\frac{n}{\sqrt{l^2+m^2+n^2}}\vec{k} \qquad (A2.1)$$

The direction X, which is at 90° to Z, can be assigned arbitrarily by $\vec{X}=a\vec{i}+b\vec{j}+d\vec{k}$, and the third direction Y which is at 90° to both Z and X can be described as $\vec{Y}=d\vec{i}+e\vec{j}+f\vec{k}$. The values of a, b, c, d, e and f can be determined by the scalar products and vectorial products between the vectors $\vec{X}$, $\vec{Y}$ and $\vec{Z}$:

$$\vec{X}\cdot\vec{Y}=0$$
$$\vec{Y}\cdot\vec{Z}=0$$
$$\vec{Z}\cdot\vec{X}=0$$
$$\vec{X}\times\vec{Y}=\vec{Z}$$

These lead to:

$$\begin{cases} ad+be+cf=0 \\ ld+me+nf=0 \\ al+bm+cn=0 \\ bf-ce-\dfrac{l}{\sqrt{\Delta_l}}=0 \\ cd-af-\dfrac{m}{\sqrt{\Delta_l}}=0 \\ ae-bd-\dfrac{n}{\sqrt{\Delta_l}}=0 \end{cases} \qquad (A2.2)$$

With $\Delta_l=l^2+m^2+n^2$.

The solution of equation (A1.2) gives the direction cosines between the crystallographic directions, X*-Y*-Z* ([100]-[010]-[001]) and the loading directions, X-Y-Z, and one solution based on $m^2+n^2\neq 0$ is presented in the following table:

	X*: [100]	Y*: [010]	Z*: [001]
X	$\frac{m^2+n^2}{\sqrt{\Delta_1\Delta_2}}$	$-\frac{ml}{\sqrt{\Delta_1\Delta_2}}$	$-\frac{ln}{\sqrt{\Delta_1\Delta_2}}$
Y	0	$\frac{n}{\sqrt{\Delta_2}}$	$-\frac{m}{\sqrt{\Delta_2}}$
Z	$\frac{l}{\sqrt{\Delta_1}}$	$\frac{m}{\sqrt{\Delta_1}}$	$\frac{n}{\sqrt{\Delta_1}}$

with $\Delta_1 = l^2+m^2+n^2$, $\Delta_2 = m^2+n^2$

The stress and strain transformation matrices A_{ij} and B_{ij} are defined to transform the global stress and strain in the loading system to the crystallographic Coordinate system as

$$[\sigma_i^*]_{crystal} = A_{ij}[\sigma_j]_{loading}$$

$$[\varepsilon_i^*]_{crystal} = B_{ij}[\varepsilon_j]_{loading}$$

Consequently, matrices A_{ij} and B_{ij} have the following formulation.

$$A_{ij} = \frac{1}{\Delta_1\Delta_2}\begin{bmatrix} \Delta_2^2 & 0 & l^2\Delta_2 & 0 & 2l\Delta_2\sqrt{\Delta_2} & 0 \\ m^2l^2 & n^2\Delta_1 & m^2\Delta_2 & 2mn\sqrt{\Delta_1\Delta_2} & -2m^2l\sqrt{\Delta_2} & -2lmn\sqrt{\Delta_1} \\ l^2n^2 & m^2\Delta_1 & n^2\Delta_2 & -2mn\sqrt{\Delta_1\Delta_2} & -2ln^2\sqrt{\Delta_2} & 2lmn\sqrt{\Delta_1} \\ l^2mn & -mn\Delta_1 & mn\Delta_2 & (n^2-m^2)\sqrt{\Delta_1\Delta_2} & -2lmn\sqrt{\Delta_2} & l(m^2-n^2)\sqrt{\Delta_1} \\ -ln\Delta_2 & 0 & ln\Delta_2 & -lm\sqrt{\Delta_1\Delta_2} & (\Delta_2-l^2)n\sqrt{\Delta_2} & -m\Delta_2\sqrt{\Delta_1} \\ -lm\Delta_2 & 0 & lm\Delta_2 & ln\sqrt{\Delta_1\Delta_2} & (\Delta_2-l^2)m\sqrt{\Delta_2} & n\Delta_2\sqrt{\Delta_1} \end{bmatrix}$$

$$B_{ij} = \frac{1}{\Delta_1\Delta_2}\begin{bmatrix} \Delta_2^2 & 0 & l^2\Delta_2 & 0 & l\Delta_2\sqrt{\Delta_2} & 0 \\ m^2l^2 & n^2\Delta_1 & m^2\Delta_2 & mn\sqrt{\Delta_1\Delta_2} & -m^2l\sqrt{\Delta_2} & -lmn\sqrt{\Delta_1} \\ l^2n^2 & m^2\Delta_1 & n^2\Delta_2 & -mn\sqrt{\Delta_1\Delta_2} & -ln^2\sqrt{\Delta_2} & lmn\sqrt{\Delta_1} \\ 2l^2mn & -2mn\Delta_1 & 2mn\Delta_2 & (n^2-m^2)\sqrt{\Delta_1\Delta_2} & -2lmn\sqrt{\Delta_2} & l(m^2-n^2)\sqrt{\Delta_1} \\ -2ln\Delta_2 & 0 & 2ln\Delta_2 & -lm\sqrt{\Delta_1\Delta_2} & (\Delta_2-l^2)n\sqrt{\Delta_2} & -m\Delta_2\sqrt{\Delta_1} \\ -2lm\Delta_2 & 0 & 2lm\Delta_2 & ln\sqrt{\Delta_1\Delta_2} & (\Delta_2-l^2)m\sqrt{\Delta_2} & n\Delta_2\sqrt{\Delta_1} \end{bmatrix}$$

For loading in [001], i.e. l=m=0 and n=1, the stress and strain trasformation matrices A_{ij} and B_{ij} are unit matrices; for loading in [111], i.e.l=m=n=1, $\Delta_1 = 3$ and $\Delta_2 = 2$, the stress and strain transformation matrices A_{ij} and B_{ij} are:

$$A_{ij} = \begin{bmatrix} \frac{2}{3} & 0 & \frac{1}{3} & 0 & \frac{2\sqrt{2}}{3} & 0 \\ \frac{1}{6} & \frac{1}{2} & \frac{1}{3} & \frac{\sqrt{6}}{3} & -\frac{\sqrt{2}}{3} & -\frac{\sqrt{3}}{3} \\ \frac{1}{6} & \frac{1}{2} & \frac{1}{3} & -\frac{\sqrt{6}}{3} & -\frac{\sqrt{2}}{3} & \frac{\sqrt{3}}{3} \\ \frac{1}{6} & \frac{1}{2} & \frac{1}{3} & 0 & -\frac{\sqrt{2}}{3} & 0 \\ -\frac{1}{3} & 0 & \frac{1}{3} & -\frac{\sqrt{6}}{6} & \frac{\sqrt{2}}{6} & -\frac{\sqrt{3}}{3} \\ -\frac{1}{3} & 0 & \frac{1}{3} & \frac{\sqrt{6}}{6} & \frac{\sqrt{2}}{6} & -\frac{\sqrt{3}}{3} \end{bmatrix}$$

$$B_{ij} = \begin{bmatrix} \frac{2}{3} & 0 & \frac{1}{3} & 0 & \frac{\sqrt{2}}{3} & 0 \\ \frac{1}{6} & \frac{1}{2} & \frac{1}{3} & \frac{\sqrt{6}}{6} & -\frac{\sqrt{2}}{6} & -\frac{\sqrt{3}}{6} \\ \frac{1}{6} & \frac{1}{2} & \frac{1}{3} & -\frac{\sqrt{6}}{6} & -\frac{\sqrt{2}}{6} & \frac{\sqrt{3}}{6} \\ \frac{1}{3} & 1 & \frac{2}{3} & 0 & -\frac{\sqrt{2}}{3} & 0 \\ -\frac{2}{3} & 0 & \frac{2}{3} & -\frac{\sqrt{6}}{6} & \frac{\sqrt{2}}{6} & -\frac{\sqrt{3}}{3} \\ -\frac{2}{3} & 0 & \frac{2}{3} & \frac{\sqrt{6}}{6} & \frac{\sqrt{2}}{6} & -\frac{\sqrt{3}}{3} \end{bmatrix}$$

Appendix III

Slip Systems and Stress Localisation to Slip Systems

The basic inelastic deformation mechanism in a single crystal alloy will be slip. Inelastic flow occurs by slip on certain planes in particular slip directions. For single crystal nickel base alloy, with a fcc crystal structure, two types of primary slip systems have been identified from experimental observation and included in the crystallographic models. The two types of slip systems are octahedral and cubic slip systems as shown in Fig.3.2. There are total of 18 possible slip systems, with 12 octahedral and 6 cubic slip systems. The unit vector of the slip plane normal direction and slip direction in each of the slip systems are summarised in Table A3.1.

Table A3.1. Slip Plane Normal Directions and Slip Directions

Octahedral Slip System	$[l_1, l_2, l_3]$	$\{n_1, n_2, n_3\}$	Cubic Slip System	$[l_1, l_2, l_3]$	$\{n_1, n_2, n_3\}$
1	$[\frac{1}{\sqrt{2}}, 0, \frac{-1}{\sqrt{2}}]$	$\{\frac{1}{\sqrt{3}}, \frac{1}{\sqrt{3}}, \frac{1}{\sqrt{3}}\}$	13	$[\frac{1}{\sqrt{2}}, \frac{1}{\sqrt{2}}, 0]$	$\{0, 0, 1\}$
2	$[\frac{-1}{\sqrt{2}}, \frac{1}{\sqrt{2}}, 0]$	$\{\frac{1}{\sqrt{3}}, \frac{1}{\sqrt{3}}, \frac{1}{\sqrt{3}}\}$	14	$[\frac{-1}{\sqrt{2}}, \frac{1}{\sqrt{2}}, 0]$	$\{0, 0, 1\}$
3	$[0, \frac{-1}{\sqrt{2}}, \frac{1}{\sqrt{2}}]$	$\{\frac{1}{\sqrt{3}}, \frac{1}{\sqrt{3}}, \frac{1}{\sqrt{3}}\}$	15	$[\frac{1}{\sqrt{2}}, 0, \frac{1}{\sqrt{2}}]$	$\{0, 1, 0\}$
4	$[0, \frac{1}{\sqrt{2}}, \frac{-1}{\sqrt{2}}]$	$\{\frac{-1}{\sqrt{3}}, \frac{1}{\sqrt{3}}, \frac{1}{\sqrt{3}}\}$	16	$[\frac{-1}{\sqrt{2}}, 0, \frac{1}{\sqrt{2}}]$	$\{0, 1, 0\}$
5	$[\frac{-1}{\sqrt{2}}, \frac{-1}{\sqrt{2}}, 0]$	$\{\frac{-1}{\sqrt{3}}, \frac{1}{\sqrt{3}}, \frac{1}{\sqrt{3}}\}$	17	$[0, \frac{1}{\sqrt{2}}, \frac{1}{\sqrt{2}}]$	$\{1, 0, 0\}$
6	$[\frac{1}{\sqrt{2}}, 0, \frac{1}{\sqrt{2}}]$	$\{\frac{-1}{\sqrt{3}}, \frac{1}{\sqrt{3}}, \frac{1}{\sqrt{3}}\}$	18	$[0, \frac{-1}{\sqrt{2}}, \frac{1}{\sqrt{2}}]$	$\{1, 0, 0\}$
7	$[\frac{-1}{\sqrt{2}}, 0, \frac{-1}{\sqrt{2}}]$	$\{\frac{-1}{\sqrt{3}}, \frac{-1}{\sqrt{3}}, \frac{1}{\sqrt{3}}\}$			
8	$[\frac{1}{\sqrt{2}}, \frac{-1}{\sqrt{2}}, 0]$	$\{\frac{-1}{\sqrt{3}}, \frac{-1}{\sqrt{3}}, \frac{1}{\sqrt{3}}\}$			
9	$[0, \frac{1}{\sqrt{2}}, \frac{1}{\sqrt{2}}]$	$\{\frac{-1}{\sqrt{3}}, \frac{-1}{\sqrt{3}}, \frac{1}{\sqrt{3}}\}$			
10	$[0, \frac{-1}{\sqrt{2}}, \frac{-1}{\sqrt{2}}]$	$\{\frac{1}{\sqrt{3}}, \frac{-1}{\sqrt{3}}, \frac{1}{\sqrt{3}}\}$			
11	$[\frac{1}{\sqrt{2}}, \frac{1}{\sqrt{2}}, 0]$	$\{\frac{1}{\sqrt{3}}, \frac{-1}{\sqrt{3}}, \frac{1}{\sqrt{3}}\}$			
12	$[\frac{-1}{\sqrt{2}}, 0, \frac{1}{\sqrt{2}}]$	$\{\frac{1}{\sqrt{3}}, \frac{-1}{\sqrt{3}}, \frac{1}{\sqrt{3}}\}$			

For a general loading case, the global stress, σ_{ij}, is first transformed into the crystallographic coordinate system, σ^*_{ij}, using procedure given in Appendix II. Then the stress, σ^*_{ij}, is resolved into each of the slip systems using the localisation equation based on Schmid's law as

$$\tau^s = \sigma^*_{ij} m^s_{ij} \qquad \text{(A3.1)}$$

with

$$m^s_{ij} = \frac{1}{2}(n^s_i l^s_j + n^s_j l^s_i) \quad (i,j = 1,2,3;\ s = 1,2,3.....18) \qquad \text{(A3.2)}$$

APPENDIX IV

NOTATION OF THE CONSTITUTIVE EQUATIONS

In the following, the original 3D constitutive equations are rewritten by introducing a short hand notation for the various transformations, i.e. coordinate transformation and incremental transformations of variables.

(IV.i) The Phenomenological Model

(1) Notation of Basic Equations

Total stress rate given by:

$$\dot{\sigma}_i = A^{-1}_{ij} C^{-1}_{jk} A_{kl} \dot{\varepsilon}^e_l = C^1_{ij} \dot{\varepsilon}^e_j = C^1_{ij} (\dot{\varepsilon}^T_j - \dot{\varepsilon}^{in}_j) \tag{A4.1}$$

with

$$C^1_{ij} = A^{-1}_{ik} C_{kl} B_{lj} \tag{A4.2}$$

$$i, j, k, l = 1,2,\ldots 6$$

The yield function f is

$$f = \sqrt{\tfrac{3}{2}(\sigma'_i - X'_i)^t A^t_{ij} M_{jk} A_{kl} (\sigma'_l - X'_l)} \; - R - k$$
$$= \sqrt{\tfrac{3}{2}(\sigma'_i - X'_i)^t M^1_{ij} (\sigma'_j - X'_j)} - R - k \tag{A4.3a}$$

where

$$M^1_{ij} = A^t_{ik} M_{kl} A_{lj} \tag{A4.3b}$$

The inelastic strain is given as

$$\dot{\varepsilon}^{in}_i = \frac{3}{2}\left(\frac{f}{K^*}\right)^n \frac{B^{-1}_{ij} M_{jl} A_{lk} (\sigma'_k - X'_k)}{\sqrt{\tfrac{3}{2}(\sigma'_i - X'_i)^t A^t_{ij} M_{jk} A_{kl} (\sigma'_l - X'_l)}}$$
$$= \frac{3}{2}\left(\frac{f}{K^*}\right)^n \frac{M^2_{ij} (\sigma'_j - X'_j)}{g} \tag{A4.4a}$$

where

$$M^2_{ij} = B^{-1}_{ik} M_{kl} A_{lj} \tag{A4.4b}$$

The internal variable X is

$$\dot{X}_i = \left(\tfrac{3}{2} A^{-1}_{ij} N_{jk} B_{kl} \dot{\varepsilon}^{in}_l\right) - \left(A^{-1}_{ij} Q_{jk} A_{kl} X_l \dot{p}\right)$$
$$= \left(N^1_{ij} \dot{\varepsilon}^{in}_j\right) - \left(Q^1_{ij} X_j \dot{p}\right) \tag{A4.5a}$$

where

$$N_{ij}^{1} = \frac{3}{2} A_{ik}^{-1} N_{kl} B_{lj}$$
$$Q_{ij}^{1} = A_{ik}^{-1} Q_{kl} A_{lj} \qquad \text{(A4.5b)}$$

and the total accumulated strain rate is

$$\dot{p} = \sqrt{\frac{2}{3}\left(\dot{\varepsilon}_i^{in}\right)^t B_{ij}^t M_{jk}^{-1} B_{kl}\left(\dot{\varepsilon}_l^{in}\right)} = \sqrt{\frac{2}{3}\left(\dot{\varepsilon}_i^{in}\right)^t M_{ij}^{3}\left(\dot{\varepsilon}_j^{in}\right)} \qquad \text{(A4.6a)}$$

where

$$M_{ij}^{3} = B_{ik}^t M_{kl}^{-1} B_{lj} \qquad \text{(A4.6b)}$$

(2) Notation of Incremental Equations

$$F_i^0 = (PG4)_{ij}^{-1}(PG1)_j$$
$$F_{ij}^1 = \Delta t\theta (PG4)_{ik}^{-1}(PG3)_{kj}$$
$$(PF6)_k = (\delta_{kl} - (PF2)_{kl} - (PE2)_{kl})^{-1}(\Delta t \cdot \dot{X}_{lt} + c1 \cdot (PE3)_l)$$
$$(PF7)_{ij} = (PF4)_{ik}^{-1}(PF5)_{kj}$$
$$d1 = c1 + c2\frac{\partial \dot{p}}{\partial \dot{\varepsilon}_i^{in}}(PA2)_{ij}(PF6)_j$$

where $(PG1)_j = \Delta t \dot{\varepsilon}_{jt}^{in} + \theta \Delta t \cdot \frac{\partial \dot{\varepsilon}_j^{in}}{\partial X_k}(PF6)_k + \theta \Delta t \cdot d1 \frac{\partial \dot{\varepsilon}_k^{in}}{\partial R}$ and i, j, k, l =1,2,...6.

The definitions of matrices PG4, PF2, PE2, PE3, PA2, PF4, PF5, d2 , etc. are in the following:

EELAS(6): ε_i^e, i=1,2,...6

EPLAS(6): ε_i^{in}or ε_i^p, i=1,2,...6

ALPHA(6): X_i, i=1,2,...6

OLDS(6): σ_{i0}, i=1,2,...6; initial stresses of the time increment

OLDEL(6): ε_{i0}^e, i=1,2,...6; initial strains of the time increment

OLDPL(6): ε_{i0}^{in}or ε_{i0}^p, i=1,2,...6; initial inelastic strains of the time increment

ORN(3): [l,m,n]; orientation vector

C0(6,6): elastic modular matrix C_{ij} at crystalline coordinate system

ZM0(6,6): anisotropy matrix M_{ij} at crystalline coordinate system

ZN0(6,6): back stress parameter matrix N_{ij} at crystalline coordinate system

Q0(6,6): back stress parameter matrix Q_{ij} at crystalline coordinate system

C1(6,6): $C_{ij}^1 = A_{ik}^{-1} C_{kl} B_{lj}$

ZM1(6,6): $M_{ij}^1 = A_{ik}^t M_{kl} A_{lj}$

ZN1(6,6): $N_{ij}^1 = \frac{3}{2} A_{ik}^{-1} N_{kl} B_{lj}$

Q1(6,6): $Q^1_{ij} = A^{-1}_{ik} Q_{kl} A_{lj}$

ZM2(6,6): $M^2_{ij} = B^{-1}_{ik} M_{kl} A_{lj}$

ZM3(6,6): $M^3_{ij} = B^{-1}_{ik} M_{kl} B_{lj}$

XXX0(6): X_{i0} initial back stresses of the time increment

DDSTRESS(6): stress deviator σ'_i

DDOLDS(6): σ'_{i0} initial stress deviator of the time increment

DSX(6): $\sigma'_i - X'_i$

DSXOLD(6): initial vector $\sigma'_{i0} - X'_{i0}$ of the time increment

DDSDS(6,6): $\dfrac{\partial \sigma'_i}{\partial \sigma_j}$

WW1(6): $M^1_{ij}(\sigma'_{j0} - X'_{j0}) + M^1_{ji}(\sigma'_{j0} - X'_{j0})$

WW2(6): $M^2_{ij}(\sigma'_{j0} - X'_{j0})$

DEINDR(6): $\dfrac{\partial \dot{\varepsilon}^{in}_i}{\partial R}$

WW(6,6): $M^2_{ij}(\sigma'_{j0} - X'_{j0})\,[\,M^1_{ij}(\sigma'_{j0} - X'_{j0}) + M^1_{ji}(\sigma'_{j0} - X'_{j0})\,]$

FFG: $\dfrac{3}{2}\left[\dfrac{n}{K^*}\left(\dfrac{f}{K^*}\right)^{n-1} - \left(\dfrac{f}{K^*}\right)^{n} \dfrac{1}{\sqrt{\frac{3}{2}(\sigma'_{i0} - X'_{i0})^t A^t_{ij} M_{jk} A_{kl} (\sigma'_{l0} - X'_{l0})}}\right]$

G0: $G0 = \sqrt{\frac{3}{2}(\sigma'_{i0} - X'_{i0})^t A^t_{ij} M_{jk} A_{kl} (\sigma'_{l0} - X'_{l0})}$

WWW(6,6): $\dfrac{3}{4G0}\left[\dfrac{FFG}{G0} WW(I,J) + 2.0\left(\dfrac{f}{K^*}\right)^{n} M^2_{ij}\right]$

DEINDS(6,6): $\dfrac{\partial \dot{\varepsilon}^{in}_i}{\partial \sigma_j}$

DEINDX(6,6): $\dfrac{\partial \dot{\varepsilon}^{in}_i}{\partial X_j}$

EIN0(6): $\dot{\varepsilon}^{in}_{i0}$, initial inelastic strain rate of time increment

DELTA(6,6): unit matrix

EIN(6): $\dot{\varepsilon}^{in}_i$, final inelastic strain rate of time increment

DEEIN1(6): $\Delta t \dot{\varepsilon}^{in}_{i0} + [\,b(Q - R_0)\Delta t\theta \dfrac{\partial \dot{\varepsilon}^{in}_i}{\partial R} - \Delta t\theta \dfrac{\partial \dot{\varepsilon}^{in}_i}{\partial X_j} Q^1_{jk} X_{k0}\,]\Delta p$

DEEIN(6): $\Delta \varepsilon^{in}_i$

DEEE(6): $\Delta \varepsilon^{e}_i$

DSTRESS(6): $\Delta \sigma_i$

DXXX(6): ΔX_i

C1II(6,6): $(C^1_{ij})^{-1}$

PB1(6,6): $\dfrac{\partial \dot{X}_i}{\partial \dot{\varepsilon}^{in}_j}$

PB2(6): $\frac{\partial \dot{X}_i}{\partial \dot{p}}$

PB3(6,6): $\frac{\partial \dot{X}_i}{\partial X_j}$

PD(6,6): $\frac{\partial \dot{X}_i}{\partial \dot{\varepsilon}_j^{in}} + \frac{\partial \dot{X}_i}{\partial \dot{p}} \frac{\partial \dot{p}}{\partial \dot{\varepsilon}_j^{in}}$

PE1(6,6): $\theta \Delta t \, PD(i,j) \frac{\partial \dot{\varepsilon}_j^{in}}{\partial \sigma_k}$

PE2(6,6): $\theta \Delta t \, (PD(i,j) \frac{\partial \dot{\varepsilon}_j^{in}}{\partial X_k} + PB3(i,k))$

PE3(6): $\theta \Delta t \, PD(i,j) \frac{\partial \dot{\varepsilon}_j^{in}}{\partial R}$

PD1(6): $\frac{\partial \dot{p}}{\partial \dot{\varepsilon}_i^{in}}$

PF1(6,6): $CC2*PE3(i)PD1(j) \frac{\partial \dot{\varepsilon}_j^{in}}{\partial \sigma_k}$

PF2(6,6): $CC2*PE3(i)PD1(j) \frac{\partial \dot{\varepsilon}_j^{in}}{\partial X_k}$

PF3(6): $\Delta t \cdot \dot{X}_{it} + CC1 \cdot PE3(i)$

PF4(6,6): DELTA(i,j)-PF2(i,j)-PE2(i,j)

PF4I(6,6): inverse of PF4(i,j)

PF5(6,6): PE1(i,j)+PF1(i,j)

PF6(6): PF4I(i,j)PF3(j)

DD2(6,6): DEINDX(i,j)(PF4I(i,j)PF5(j,i))

D2(6): CC2*PD1(j)*(DEINDS(j,i)+DD2(j,i)

PG1(6): $\Delta t \dot{\varepsilon}_{it}^{in} + \theta \Delta t \cdot \frac{\partial \dot{\varepsilon}_i^{in}}{\partial X_j} PF6(j) + \theta \Delta t \cdot d1 \frac{\partial \dot{\varepsilon}_i^{in}}{\partial R}$

PG2(6,6): $\frac{\partial \dot{\varepsilon}_i^{in}}{\partial \sigma_j} + \frac{\partial \dot{\varepsilon}_i^{in}}{\partial X_j} PF5(j) + \frac{\partial \dot{\varepsilon}_i^{in}}{\partial R} D2(j)$

PG3(6,6): PG2(i,j)C1(j,k)

PG4(6,6): DELTA(i,j)+$\theta \Delta t$ PG2(i,j)

PG5(6): PG4I(i,j)PG1(j)

PG4I(6,6): inverse of PG4(i,j)

(3) Notation of matrices for nonlinear procedure Jacobian matrix

$$\Omega MA_{jk} = \Omega 3^{-1}_{ml} \, WWM_{lp} A^{\bullet}_{pk}$$

$$\Omega 3_{ml} = \delta_{ml} + \Omega 1_{ml} + \Omega 2_{ml}$$

$$\text{with } \Omega 1_{ml} = a \cdot WWM_{mk} ANQ_{kl}$$

$$\Omega 2_{ml} = (a \cdot b \cdot c^{\bullet}(Q-R)/(1 + a \cdot b \cdot \dot{p}_{(t)})) W_m MMM_l$$

$$WWM_{lp} = \frac{3b^*}{4g} W_l WM_p + d^* M_{lp}^2$$

$$W_l = \frac{M_{lk}^2(\sigma_k^{'} - X_k^{'})}{g}$$

$$WM_p = M_{pl}^1(\sigma_l^{'} - X_l^{'})$$

$$A_{pk}^* = \frac{\partial(\sigma_p^{'} - X_p^{'})}{\partial\sigma_k}$$

$a = \theta\Delta t$; b is material constant;

where,

$$b^* = \frac{3}{2}[\frac{n}{K^*}(\frac{f}{K^*})^{n-1} - \frac{1}{g}(\frac{f}{K^*})^n]$$

$$c^* = \frac{3}{2}\frac{n^{'}}{K^*}(\frac{f}{K^*})^{n-1}$$

$$d^* = \frac{3}{2}\frac{1}{g}(\frac{f}{K^*})^n$$

(III.ii) The Crystallographic Model

(1) Notation of the Basic Equations

Using the Voigt vectorial notation for stress and strain tensors

$$[\sigma]^t = [\sigma_1 = \sigma_{11}, \sigma_2 = \sigma_{22}, \sigma_3 = \sigma_{33}, \sigma_4 = \sigma_{23}, \sigma_5 = \sigma_{13}, \sigma_6 = \sigma_{12}]$$
$$[\varepsilon]^t = [\varepsilon_1 = \varepsilon_{11}, \varepsilon_2 = \varepsilon_{22}, \varepsilon_3 = \varepsilon_{33}, \varepsilon_4 = 2\gamma_{23}, \varepsilon_5 = 2\gamma_{13}, \varepsilon_6 = 2\gamma_{12}]$$

The stress localisation and strain homogenisation between the crystallographic and the macroscopic levels can be obtained

Stress localisation:

$$\tau^s = \sigma_{ij} m_{ij}^s = m_{11}^s\sigma_{11} + m_{22}^s\sigma_{22} + m_{33}^s\sigma_{33} + 2m_{23}^s\sigma_{23} + 2m_{13}^s\sigma_{13} + 2m_{12}^s\sigma_{12}$$

or

$$[\tau]_s = Ml_{si}\sigma_i \qquad \text{(A4.7a)}$$

with

$$ml_{s1} = m_{i1}^s, ml_{s2} = m_{22}^s, ml_{s3} = m_{33}^s,$$
$$ml_{s4} = 2m_{23}^s, ml_{s5} = 2m_{i3}^s, ml_{s6} = 2m_{12}^s \qquad \text{(s=1,2,...18; i=1,2,...6)} \qquad \text{(A4.7b)}$$

$$m_{ij}^s = \frac{1}{2}(n_i^s l_j^s + n_j^s l_i^s) \qquad \text{(s=1,2,...18, i=1,2,3)}$$

Strain homogenisation:

$$\dot{\varepsilon}_{ij}^{in} = \sum_{s} \dot{\gamma}^{s} m_{ij}^{s}$$

or
$$\dot{\varepsilon}_{j}^{in} = M2_{js}[\dot{\gamma}]_{s} \tag{A4.8a}$$

$$m2_{1s} = m_{11}^{s}, m2_{2s} = m_{22}^{s}, m2_{3s} = m_{33}^{s}$$
$$m2_{4s} = 2m_{23}^{s}, m2_{5s} = m_{13}^{s}, m2_{6s} = m_{12}^{s} \quad (j=1,2,...6;\ s=1,2,...18) \tag{A4.8b}$$

Under general loading conditions, stress and strain transformations are performed by matrix A and B:

$$[\sigma_i]_{crystal} = A_{ij}[\sigma_j]_{loading}$$
$$[\varepsilon_i]_{crystal} = B_{ij}[\varepsilon_j]_{loading}$$

The total stress rate is given as:

$$\dot{\sigma}_i = A_{ij}^{-1} C_{jk}^{-1} A_{kl} \dot{\varepsilon}_l^e = Cl_{ij} \dot{\varepsilon}_j^e = Cl_{ij}(\dot{\varepsilon}_j^T - \dot{\varepsilon}_j^{in}) \tag{A4.9a}$$
$$Cl_{ij} = A_{ik}^{-1} C_{kl} B_{lj} \tag{A4.9b}$$

then
$$[\tau]_s = MM1_{si}\sigma_i \tag{A4.10a}$$

$$MM1_{sj} = M1_{si}\ A_{ij} \tag{A4.10b}$$

and
$$\dot{\varepsilon}_i^{in} = M3_{is}[\dot{\gamma}]_s \tag{A4.11a}$$

$$M3_{is} = B_{ij}^{-1} M2_{js} \tag{A4.11b}$$

(2) Some notations used in incremental equations

$$[\Delta\tau]_s = C2_{sj}\Delta\varepsilon_j^T - M4_{sn}(\Delta\gamma)_n \tag{A4.12a}$$

$$C2_{sj} = MM1_{si}\,Cl_{ij} \qquad i,j=1,2,...6;\ s,n=1,2,...18 \tag{A4.12b}$$
$$M4_{sn} = C2_{si}\,M3_{in}$$

$$[\Delta x]_s = CCl_s + aCC3_{sj}\Delta\varepsilon_j^T - aCC4_{sm}(\Delta\gamma)_m \tag{A4.13a}$$

$$\Delta\gamma_m = E4_m + E5_{mk}\Delta\varepsilon_k^T \tag{A4.13b}$$

with
$$CCl_s = DBA_{sl}^{-1}\Delta t\dot{x}_{lt}\ ,\ CC3_{sj} = CC2_{sn}(MAC)_{nj}$$
$$CC2_{sn} = DBA_{sl}^{-1}BA11_{ln}\ ,\ CC4_{sm} = CC2_{sn}(ABM)_{nm}$$
$$E4_m = E3_{ms}^{-1}El_s\ ,\ E5_{mk} = E3_{ms}^{-1}E2_{sk}$$

where $a = \Delta t\theta$, and the definitions of matrices, DBA, MAC, BA11 ,ABM, E1, E2, E3 are given below.

$$DBA_{sl} = \delta_{sl} - a \cdot BA12_{sl} - a \cdot BB2_{sl}$$
$$BA12_{sl} = BB1_{sm}\, AA2_{ml}$$
$$MAC_{sk} = MM2_{si}\, A_{ij} C^{t}_{jk}$$
$$BA11_{sn} = BB1_{sm}\, AA1_{mn}$$
$$ABM_{sm} = MAC_{sk}\, BM_{km}$$
$$BM_{km} = B^{-1}_{kj} MM1_{jm}$$
$$E1_{m} = DD1_{m} + a \cdot DD4_{m}$$
$$DD1_{m} = \Delta t\dot{\gamma}_{m(t)}$$
$$DD4_{m} = AA2_{ms}\, CC1_{s}$$
$$E2_{mk} = a \cdot DD2_{mk} + a^{2} DD5_{mk}$$
$$DD2_{mk} = AA1_{ms}\, MAC_{sk}$$
$$DD5_{mk} = AA2_{ms}\, CC3_{sk}$$
$$E3_{ms} = \delta_{ms} + a \cdot DD3_{ms} + a^{2} DD6_{ms}$$
$$DD3_{ms} = AA1_{ml}\, ABM_{ls}$$
$$DD6_{ms} = AA2_{ms}\, CC4_{sl}$$

Where, k, j=1,2,...6; s, l, m=1,2, ...18, and matrices AA2, BB1 and BB2 and a are defined in Chapter 4.

APPENDIX V

THERMOMECHANICAL LOADING INPUT FOR FE ANAYSIS

1. Temperature Input

1) Method 1: This method is suitable for the case where the temperature distribution is only a function of time, i.e. the whole structure has the same temperature. The syntax for this method is as follows:

*INITIAL CONDITIONS, TYPE=TEMPERATURE

node set, initial temperature value at the node, additional temperature values

*AMPLITUDE, NAME=TEMP

t_1(time), a_1(amplitude at time t_1), t_2, a_2

*....

*STEP

....

*TEMPERATURE, AMPLITUDE=TEMP

node set name, a(reference temperature values)

*...

*END STEP

2)Method 2

ABAQUS provides a simple interface which uses the temperatures at the nodes stored on the ABAQUS results file from the heat transfer analysis to define the temperature field at different times in the stress analysis. This interface assumes that the node numbers are the same for corresponding nodes in the stress analysis mesh and the heat transfer analysis mesh. So a typical sequentially coupled thermal-stress analysis consists of two ABAQUS runs: a heat transfer analysis, and a subsequent stress analysis. The procedure of the method is as the follow:

First run: Heat transfer analysis (program: HEAT.INP)

*HEADING

...

*ELEMENT, TYPE=DC3D20

choose the heat transfer element type

**

...

...

*STEP

*HEAT TRANSFER, STEADY STATE

time step, time period, minimum time increment allowed

apply thermal loads and boundary conditions

...

*NODE FILE, NSET=NALL (create a results file for late use)

NT (give the identifying keys for the variables to be written to the results file for this node set. NT: all temperature values at a node)

write all nodal temperatures to the results file, HEAT.FIL

*END STEP

Second run: The subsequent thermal-stress structural analysis (program:STRESS.INP)

*HEADING

...

*ELEMENT, TYPE=C3D20

choose the continuum element type compatible with the heat transfer element type used

**

...

*STEP

*STATIC

apply structural loads and boundary conditions

...

*TEMPERATURE, FILE=HEAT

read in all nodal temperatures from the results file, HEAT.FIL

...

*END STEP

It is often convenient to set the period of the stress analysis step equal to the time period of the files being read in.

3.Method 3

This method provides temperatures at each time increment using the subroutine UTEMP which allows the user to prescribe the temperature at the nodes of a model. It will be called whenever a current value of temperature is needed for a node listed under a *TEMPERATURE option which includes the parameter USER. The syntax is as the follow:

*TEMPERATURE, USER (indicate that user subroutine UTEMP will be used to define temperature values)

...

*USER SUBROUTINES

SUBROUTINES UTEMP (TEMP, NSECPT,KSTEP,KINC,TIME,NODE,COORDS)

...

END

2. Mechanical Loading Input

Both displacement control and stress control can be input by using input cards *BOUNDARY with *AMPLITUDE OR *USER SUBROUTINE, the syntax for using these cards is as the following:

1)Syntax 1: for boundary condition defined by data lines to describe the variation of the loading amplitude

*HEADING

.....

*AMPLITUDE, NAME=PULL1, (DEFINITION=TABULAR(default), EQUALLY SPACED, PERIODIC, MODULATED, DECAY....which can describe sinusoidal, exponent type amplitude functions of time)

t_1, a_1, t_2, a_2, t_3, a_3,.....(tabular data)

.....

*STEP

.....

*BOUNDARY, AMPLITUDE=PULL1

node number of node set label, first degree of freedom constrained, last degree of freedom constrained, actual magnitude of the variable

.....

*END STEP

2)Syntax 2: for using prescribed loading condition defined by user subroutine to describe complex loading condition, such as sinusoidal surge motion, cyclic loading

,

etc.

*HEADING

.....

*STEP

.....

*BOUNDARY, USER

node number of node set label, first degree of freedom constrained, last degree of freedom constrained, actual magnitude of the variable(displacement, velocity, or acceleration) which may be redefined in user subroutine DISP or left blank and defined by user subroutine.

.....

*END STEP

*USER SUBROUTINE

```
      SUBROUTINE DISP(U, KSTEP, KINC,TIME, NODE, JDOF)
C
      INCLUDE 'ABA-PARAM.INC'
C
      DIMENSION U(3), TIME(2)
C
```

user coding to define U

RETURN

END

Variables to be defined:

U(1): total value of the prescribed variable(displacement, rotation, pore pressure, temperature, etc. depending on the degree of freedom constrained) at this point. U(1) will be passed into the routine as the value defined by any magnitude and /or amplitude specification on the data lines.

U(2):du/dt

U(3):d^2u/d^2t

3)Syntax 3:for distributed loads input

*HEADING

.....

*AMPLITUDE, NAME=PULL2,

giving all data needed by related option of DEFINITION)

.....

*STEP

.....

*DLOAD, AMPLITUDE=PULL2

element number or element set label, distributed load type label, actual magnitude of the load which can be modified by the use of the *AMPLITUDE option. For nonuniform loads, the magnitude must be defined in user subroutine DLOAD.

.....

*END STEP

4)Syntax 4: for nonuniform distributed loads input

*HEADING

.....

*STEP

.....

*DLOAD

element number or element set label, distributed load type label

.....

*END STEP

*USER SUBROUTINE

SUBROUTINE DLOAD (F, KSTEP, KINC, TIME, NOEL, NPT, LAYER, KSPT, COORDS, JLTYP)

.....

RETURN

END

Variable to be defined:

F: magnitude of the distributed load. Units are FL^{-2} for surface loads, FL^{-3} for body forces.

Syntax 1 has been used in current research program for linear variation of displacement input.

APPENDIX VI

STRAIN TRANSFORMATION IN THE CYLINDRICAL BAR CALCULATIONS

(i) Strain Transformation

In ABAQUS and UMAT subroutine, the stress and strain are all expressed in the global system, which can be referred as $X^* - Y^* - Z^*$. To investigate the anisotropic transverse and shear strain response in the cylindrical bar specimen, a local co-ordinate system, R-T-Z is introduced for each element, as shown in Fig.5.7. This system represents a local cylindrical co-ordinate system, with Z direction parallel with Z^* in the global system, and R is the radial direction and T is the tangential direction.

The strain tensors in the global system $X^* - Y^* - Z^*$ are denoted by ε_{ij}^*, and the strain tensors in the local cylindrical system by ε_{ij}. The transformation of the global strain to local strain can be expressed as

$$\varepsilon_{ij} = Q_{ik}^T \varepsilon_{kl}^* Q_{lj} \tag{A6.1}$$

The transformation tensor Q_{ij} is determined using the current coordinates, X^* and Y^* in the form

$$Q_{ij} = \begin{bmatrix} \frac{X^*}{\sqrt{X^*+Y^*}} & \frac{Y^*}{\sqrt{X^*+Y^*}} & 0 \\ -\frac{Y^*}{\sqrt{X^*+Y^*}} & \frac{X^*}{\sqrt{X^*+Y^*}} & 0 \\ 0 & 0 & 1 \end{bmatrix} \tag{A6.2}$$

In the FE calculations, when UMAT is called, ABAQUS provides the current coordinates for each integration point. These information is used in the UMAT as input to a sub-subroutine, TRANS1, to transforms the global strain into local strain.

(ii) Output of Local Strain

The calculated local strain components in the UMAT subroutine were then stored as solution dependent variables and can be printed out or used in post processing using RESTART file.

The local elastic and inelastic strain component stored in the array STATEV are in the order:

STATEV(3*NTENS+2)	STATEV(4*NTENS+1)	elastic strain ε_i^e (i=1,6)
STATEV(4*NTENS+2)	STATEV(5*NTENS+1)	inelastic strain ε_i^{in} (i=1,6)

APPENDIX VII

RAFTING EFFECT ON THE ELASTIC PROPERTIES OF SINGLE CRYSTAL SUPERALLOYS

Assuming γ'=60% (volume fraction of γ' phase)

1. The Young's Modulus of Original Structure

The original structure of a cubic single crystal is presented in Fig.A7.1a.

The volume fraction of γ' phase leads to the following, where a_1 is length of the γ' cube, and a is the length of the γ cube.

$$a_1^3 = 0.6a^3$$
$$a_1 = \sqrt[3]{0.6}\, a \approx 0.8434a$$
$$a_1^2 = 0.71138a^2$$

Then the change in length Δa of a associated with external load P is :

$$\Delta a = 2\varepsilon_I \frac{a - a_1}{2} + \varepsilon_{II} a_1 = 0.1566a\frac{\sigma_I}{E_I} + 0.8434a\varepsilon_{II}$$

$$\sigma_I = \frac{P}{a^2}, \varepsilon_{II} = \frac{\sigma_\gamma}{E_\gamma} = \frac{\sigma_{\gamma'}}{E_{\gamma'}} \text{ and}$$
$$\sigma_{\gamma'} a_1^2 + \sigma_\gamma (a^2 - a_1^2) = P$$

and

$$\sigma_\gamma = \frac{PE_\gamma}{a^2(0.71138E_{\gamma'} + 0.28862E_\gamma)}$$

$$\varepsilon_{II} = \frac{\sigma_\gamma}{E_\gamma} = \frac{P}{a^2(0.71138E_{\gamma'} + 0.28862E_\gamma)}$$

$$\Delta a = 0.1566a\frac{P}{a^2 E_\gamma} + 0.8434a\frac{P}{a^2(0.71138E\gamma' + 0.28862E_\gamma)}$$

Since

$$\varepsilon = \frac{\Delta a}{a} = \frac{\sigma}{E_{11}}$$

then

$$E_{11} = \frac{E_\gamma(0.71138E_{\gamma'} + 0.28862E_\gamma)}{0.1114E_{\gamma'} + 0.8886E_\gamma}$$

2. The Young's Modulus of a Rafting Structure

Two cases of rafting structure have been studied here.

(i) α case

The 'rafting" structure is shown as Fig.A7.1b, and the two phases are all parallel to loading direction.

The volume of γ' phase: $a^2 a_1 = 0.6a^3$

therefore

$$a_1 = 0.6a$$

$$\Delta a = \varepsilon a = \varepsilon_\gamma a = \varepsilon_{\gamma'} a$$

$$\sigma_{\gamma'} a_1 a + \sigma_\gamma a(a - a_1) = P$$

$$0.6\sigma_{\gamma'} + 0.4\sigma_\gamma a = \frac{P}{a^2} \qquad \text{(A7.1)}$$

Due to: $$\varepsilon_{\gamma'} = \varepsilon_\gamma, \frac{\sigma_{\gamma'}}{E_{\gamma'}} = \frac{\sigma_\gamma}{E_\gamma}, \sigma_\gamma = \frac{\sigma_{\gamma'}}{E_{\gamma'}} E_\gamma \qquad \text{(A7.2)}$$

Substituting equation (A7.2) into (A7.1) leads to the following result:

$$\sigma_{\gamma'} = \frac{PE_{\gamma'}}{a^2(0.6E_{\gamma'} + 0.4E_\gamma)}$$

$$\varepsilon = \frac{\Delta a}{a} = \frac{\sigma_{\gamma'}}{E_{\gamma'}} = \frac{P}{a^2(0.6E_{\gamma'} + 0.4E_\gamma)}$$

and $$E_\alpha = 0.6E_{\gamma'} + 0.4E_\gamma$$

(ii) β case

The structure is shown as Fig.A7.1c, the two phases are transverse to the loading direction.

$$\Delta a = 2\varepsilon_I 0.2a + \varepsilon_{II} 0.6a$$

$$\varepsilon_I = \frac{\sigma_I}{E_I} = \frac{P}{a^2 E_\gamma}, \varepsilon_{II} = \frac{\sigma_{II}}{E_{II}} = \frac{P}{a^2 E_{\gamma'}}$$

$$\Delta a = 0.4a\frac{P}{a^2E_\gamma} + 0.6a\frac{P}{a^2E_{\gamma'}} = \frac{P}{a}\left(\frac{0.4}{E_\gamma} + \frac{0.6}{E_{\gamma'}}\right)$$

$$\varepsilon = \frac{\Delta a}{a} = \frac{P}{a^2}\left(\frac{0.4}{E_\gamma} + \frac{0.6}{E_{\gamma'}}\right)$$

$$E_\beta = \frac{E_\gamma E_{\gamma'}}{0.4E_{\gamma'} + 0.6E_\gamma}$$

3. Examples of Young's Modulus

The calculation results for the two different temperature range are presented in following table:

T (°C)	E_γ (GPa)	$E_{\gamma'}$ (GPa)	$E_{//}$ (GPa)	E_α (GPa)	E_β (GPa)
1050°C	68.26	77.882	73.944	74.0332	73.7251
25°C	136.43	104.188	116.56	117.0848	115.0652

APPENDIX VIII
NON-LINEAR REGRESSION PROGRAMS FOR DETERMINING MATERIAL CONSTANTS

Non-Linear Regression Programs

(1) SLH01

This program is for the determination of K*, n and M_{ij} in the constitutive model for single crystal superalloys.

Data Input Files :

ZS10.in	data set for [001] orientation
ZS11.in	data set for [111] orientation

These files input the experimental data of strain rate and saturated stress $W(I)=\dot{\varepsilon}_i^T$, $S(I)=\sigma_i$, (I=1,2,3,.....F), with data format: (F10.5, F10.5)
The data number F will be inputted directly from the keyboard

Data Output Files:

ZS10.out	data output for [001] orientation
ZS11.out	data output for [111] orientation

These files output the regression results, including K*(i), n(i) and corresponding square error R^2(i), at each regression steps, and also the final results of the material constants optimised from the regression process.

Screen Output: The final results of K*, n and M_{44} are also shown on the screen

(2) SLH02

This program is for the determination of Q_{ij}, N_{ij} and k in the constitutive model for single crystal superalloys.

Data Input Files :

WZ10.in	data set for [001] orientation
WZ11.in	data set for [111] orientation

These files input the data $W(I)=\varepsilon^{in}$, $Z(I)=\sigma-\sigma_v=\sigma-K^{'*}(\dot{\varepsilon}^{in})^{1/n}$, (I=1,2,3,.....G), with data format: (F10.7, F10.5)
The data number G will be inputted directly from the keyboard

Data Output Files:

WZ10.out	data output for [001] orientation
WZ11.out	data output for [111] orientation

These files output the regression results, including Q(i), N(i), k(i) and corresponding square error R^2(i), at each regression steps, and also the final results of the material constants optimised from the regression process.

Screen Output: The final results of Q_{ij}, N_{ij} and k are also shown on the screen.

```
********* PROGRAM SLH01 **********
********
**@@@@@@@@@@@@@@@@@@@@@@@@@@@@@@@@@@@@
** Program Developed in:
** Engineering Materials and Structural Integrity Group
**        University of Bristol
**        May, 1996
** @@@@@@@@@@@@@@@@@@@@@@@@@@@@@@@@@@@@@
****
****
C ***********  The Calculation OF K*, n and Mij for  *********
c ***********   SINGLE CRYSTAL MODEL                ***********

      REAL X(100), Y(100), K(50), RN(40), KU, KD, RR(40), RR1
      REAL RRR,K1,RN1,W(50),S(50),NRN1,KK
      INTEGER N, I, J, NN,NNNN,M,IIII
      REAL OK(3),ON(3),M44

      OPEN(UNIT=1, FILE='ZS10.IN')
      OPEN(UNIT=11, FILE='ZS11.IN')
      OPEN(UNIT=10, FILE='ZS10.OUT')
      OPEN(UNIT=22, FILE='ZS11.OUT')
      OPEN(UNIT=33, FILE='FINAL.OUT')

      DO 10000 IIII=1,2

       IF (IIII.EQ.1) THEN
         PRINT *, '"data number for [001] NNNN="'
          READ *, NNNN
       ELSE
         PRINT *, '"data number for [111] NNNN="'
          READ *, NNNN
       END IF

      DO 50 I=1, NNNN
       IF (IIII.EQ.1) THEN
         READ(1, 70) W(I), S(I)
         WRITE (10,70) W(I),S(I)
       ELSE
         READ(11, 70) W(I), S(I)
         WRITE (22,70) W(I),S(I)
       END IF
50     CONTINUE

      DO 100  I=1,  NNNN
       DO 110 J=I+1, NNNN
      IF (I.EQ.1 .AND. J.EQ.2 ) THEN
           M=1
       ELSE
           M=M+1
        END IF
      Y(M)=S(I)-S(J)
C       WRITE (2,70) Y(M)
110      CONTINUE
100      CONTINUE

      DO 10 N=1,35
      RN(N)=0.2+(N-1)*0.005
```

```
      KU=0.0
      KD=0.0
      RNN=RN(N)
C *****************************************************
      CALL REGRES (RNN,KU,KD,KK,W,Y,X,NNNN)

      K(N)=KK
      RR1=0.0
      DO 30 J=1, M
      RR1=RR1+(Y(J)-K(N)*X(J))**2.0
30    CONTINUE
      RR(N)=RR1
      NRN1=1.0/RN(N)
      IF (IIII.EQ.1) THEN
        WRITE (10,60) RN(N),NRN1,K(N),RR1,KU,KD
      ELSE
        WRITE (22,60) RN(N),NRN1,K(N),RR1,KU,KD
      END IF
10    CONTINUE

      DO 40 NN=1, 20
      IF (NN.EQ.1) THEN
      RRR=RR(NN)
      RN1=RN(NN)
      K1=K(NN)
      ELSE IF (RR(NN).LE.RRR) THEN
      RRR=RR(NN)
      RN1=RN(NN)
      K1=K(NN)
      END IF
40    CONTINUE

      NRN1=1.0/RN1
      IF (IIII.EQ.1) THEN
       OK(1)=K1
       ON(1)=NRN1
      ELSE
       OK(2)=K1
       ON(2)=NRN1
      END IF

      IF (IIII.EQ.1) THEN
         WRITE (10,600)
         WRITE (10, 60) RRR, RN1,NRN1,K1
      ELSE
         WRITE (22,600)
         WRITE (22, 60) RRR, RN1,NRN1,K1
      END IF
60    FORMAT (8E15.6)
600   FORMAT (15X,' RRR=', 15X, ' n= ', 15X, ' K*=')
70    FORMAT (3F10.5)
10000 CONTINUE
      CLOSE (UNIT=1, STATUS='KEEP')
      CLOSE (UNIT=11, STATUS='KEEP')


      ON(3)=(ON(1)+ON(2))/2.0
      RNN=1.0/ON(3)
```

```
      CALL FINAL (RNN,OK,ON,M44)
c        M44=2.0*(OK(1)/OK(2))**(ON(3)*2.0/(ON(3)+1.0))

       WRITE (*,700)
       WRITE (*,60)  OK(1),ON(1)
700    FORMAT (8X, ' K*=', 8X, ' n=',10X,  'Orintation [001]')
       WRITE (*,800)
      WRITE (*,60)  OK(2),ON(2)
800    FORMAT (8X, ' K*=', 8X, ' n=', 10X, 'Orintation [111]')
       WRITE (*,900)
      WRITE (*,60)  OK(3),ON(3), M44
900    FORMAT (8X,'K*=',8X, 'n=',10X,'M44=',10X,'FINAL RESULTS')
       WRITE (33,700)
       WRITE (33,60)  OK(1),ON(1)
      WRITE (33,800)
     WRITE (33,60)  OK(2),ON(2)
      WRITE (33,900)
     WRITE (33,60)  OK(3),ON(3), M44


         END

SUBROUTINE REGRES (RNN,KU,KD,KK,W,Y,X,NNNN)
 REAL RNN,KU,KD,KK, W(100),X(100),Y(100)
 INTEGER NNNN
  KU=0.0
  KD=0.0
 DO 200  I=1,  NNNN
       DO 210 J=I+1, NNNN
      IF (I.EQ.1 .AND. J.EQ.2 ) THEN
            M=1
       ELSE
            M=M+1
       END IF
      X(M)=W(I)**RNN-W(J)**RNN
210      CONTINUE
200      CONTINUE

     OPEN (UNIT=213, FILE='TRY.OUT')

      DO 20 I=1,M
           KU=KU+Y(I)*X(I)
            KD=KD+X(I)*X(I)
20    CONTINUE
500     FORMAT (2X,6E15.6)
      KK=KU/KD
      WRITE (213,500) KU,KD,KK

      END


SUBROUTINE FINAL (RNN,OK,ON,M44)
REAL X(100), Y(100), KU, KD,RNN
REAL W(50),S(50),KK
INTEGER NNNN,M,IIII
REAL OK(3),ON(3),M44,OOK(3)

OPEN(UNIT=1, FILE='ZS10.IN')
```

```
      OPEN(UNIT=11, FILE='ZS11.IN')
      OPEN (UNIT=50, FILE='OUT.OUT')

      DO 1000  IIII=1,2
       IF (IIII.EQ.1) THEN
         PRINT *, '"data number for [001] NNNN="'
          READ *, NNNN
       ELSE
         PRINT *, '"data number for [111] NNNN="'
          READ *, NNNN
       END IF

          DO 50 I=1, NNNN
           IF (IIII.EQ.1) THEN
             READ(1, 70) W(I), S(I)
           ELSE
             READ(11, 70) W(I), S(I)
           END IF
   50     CONTINUE
   70     FORMAT (3F10.5)
          DO 100  I=1,  NNNN
          DO 110 J=I+1, NNNN
          IF (I.EQ.1 .AND. J.EQ.2 ) THEN
               M=1
          ELSE
               M=M+1
           END IF
          Y(M)=S(I)-S(J)
         WRITE (50,500)  Y(M)
  110     CONTINUE
   100    CONTINUE

   C ***************************************************
         CALL REGRES (RNN,KU,KD,KK,W,Y,X,NNNN)
          OOK(IIII)=KK
               DO 560  I=1,M
               WRITE (50,500) Y(I),X(I),KU,KD,KK
   560    CONTINUE
   1000   CONTINUE

         ON(3)=1.0/RNN
         OK(3)=OOK(1)
          M44=2.0*(OOK(1)/OOK(2))**(ON(3)*2.0/(ON(3)+1.0))
             WRITE (50, 500) RNN,OK(3),ON(3),M44
   500    FORMAT (2X,8E15.6)

          END
```

```
********* PROGRAM SLH02 **********
********
**@@@@@@@@@@@@@@@@@@@@@@@@@@@@@@@@@@@@
** Program Developed in:
** Engineering Materials and Structural Integrity Group
**        University of Bristol
**        May, 1996
** @@@@@@@@@@@@@@@@@@@@@@@@@@@@@@@@@@@@
****
****
C ******* Determination of Qij, Nij and k in the SINGLE CRYSTAL Model *****
c ***************  Based on [001] and [111] Orienation Deformation ********
      REAL  WWW(200),Z(200),X(200),Y(200),Q(200),AA(2),Q1,R(200),RR
      REAL QQ,AAA(200,2),QMIN,RMIN,M44,ZC(200),FNN(200),KK(200)
      REAL K10,K11,N10,N11,Q10,Q11
            INTEGER NN,IMIN,IIII
C          EXTERNAL REGS

         OPEN (UNIT=1, FILE='WZ10.IN')
         OPEN (UNIT=11, FILE='WZ11.IN')
         OPEN (UNIT=2, FILE='WZ10.OUT')
         OPEN (UNIT=22, FILE='WZ11.OUT')
          OPEN (UNIT=10, FILE='QR10.OUT')
           OPEN (UNIT=101, FILE='QR11.OUT')

      DO 10000  IIII=1,2
      IF (IIII.EQ.1) THEN
         PRINT *, '"data number for [001], NN=? (Nmax=200)"'
          PRINT *, '"NN= "'
           READ *,  NN
      ELSE
         PRINT *, '"data number for [111], NN=? (Nmax=200)"'
          PRINT *, '"NN="'
               READ *, NN
         PRINT *, '"for [111],  M44=?"'
           PRINT *, '"M44="'
                READ *, M44
      END IF
c .....(input data) .....
        DO 10 I=1,NN
        IF (IIII.EQ.1) THEN
         READ (1,20)  WWW(I), Z(I)
         WRITE (2,20) WWW(I), Z(I)
        ELSE
         READ (11,20)  WWW(I), Z(I)
         WRITE (22,20) WWW(I), Z(I)
        END IF
10      CONTINUE
20      FORMAT  (F10.7, F10.5)

C********** cycle for adjust Q variabl
                Q1=400.0
                QQ=Q1-10.0
C  cycle calculation of different Q

          DO  1000  II=1, 50
```

```
          WRITE (*,25) II
25      FORMAT (I10)
            Q(II)=QQ+10.0
          DO 30  I=1, NN
            X(I)=(1.0-EXP(-Q(II)*WWW(I)))
            Y(I)=1.0
30       CONTINUE

c ..... call subroutine for regression .....
          CALL  REGS (NN,X,Y,Z,ZC,DS,AA,RR)
c ..................................................
             R(II)=RR
             QQ=Q(II)
           DO 40 J=1,2
             AAA(II,J)=AA(J)
c ..... AAA(II,1)=N/Q, AAA(II,2)=k' .....
40       CONTINUE
          IF (IIII.EQ.1)  THEN
            FNN(II)=AAA(II,1)*Q(II)
            KK(II)=AAA(II,2)
           WRITE (10,50) R(II),Q(II),FNN(II),KK(II)
          ELSE
           Q(II)=Q(II)*SQRT(M44/2.0)
           KK(II)=AAA(II,2)*SQRT(M44/2.0)
           FNN(II)=AAA(II,1)*Q(II)*(1.0/2.0)/SQRT(M44/2.0)
           WRITE (101,50) R(II),Q(II),FNN(II),KK(II)
          END IF
50      FORMAT  (2X,5E15.6)
1000     CONTINUE

            QMIN=Q(1)
           RMIN=R(1)
           IMIN=1
          DO  2000  II=1, 50
           IF (R(II).LT.RMIN) THEN
            RMIN=R(II)
            QMIN=Q(II)
            IMIN=II
           END IF
2000     CONTINUE
2001     FORMAT (I10)

           IF (IIII.EQ.1) THEN
         WRITE (10,60) RMIN,KK(IMIN),FNN(IMIN),Q(IMIN), IMIN
           K10=KK(IMIN)
           N10=FNN(IMIN)
            Q10=Q(IMIN)
          ELSE
         WRITE (101,60) RMIN,KK(IMIN),FNN(IMIN),Q(IMIN), IMIN
           K11=KK(IMIN)
           N11=FNN(IMIN)
           Q11=Q(IMIN)
          END IF
60      FORMAT (2X, 4E15.6,2X, I10)

10000     CONTINUE
```

```
          WRITE (*,65)
65      FORMAT (15X, 'k=', 10X, 'Q11-Q12=', 5X, 'N11-N12=')
          WRITE (*,60) K10,Q10,N10
         WRITE  (*,70)
70      FORMAT (15X, 'k=', 10X, 'Q44=', 10X, 'N44=')
         WRITE (*,60)  K11,Q11,N11

        END



cccc  This is a REGRESSION programe for calculating
CC      A and B in the linear Eq. A*Xi+B*Yi=Zi

         SUBROUTINE REGS(NN,X,YY,Z,ZC,DS,XX,R)
              REAL AB(2,3),B(2),XX(2),A(2,2),X(200),Z(200),YY(200)
              REAL WW,ZC(200), DS(200),R
              INTEGER NN
3301      FORMAT (I10,10X,I10,10X,I10)

         OPEN  (UNIT=20, FILE='Z.OUT')
        DO 303  I=1, 2
              B(I)=0.0
        DO 304  J=1,2
              A(I,J)=0.0
304     CONTINUE
303     CONTINUE
         DO 305  I=1, NN
              A(1,1)=A(1,1)+X(I)*X(I)
              A(1,2)=A(1,2)+X(I)*YY(I)
              A(2,2)=A(2,2)+YY(I)*YY(I)
              B(1)=B(1)+X(I)*Z(I)
              B(2)=B(2)+YY(I)*Z(I)
305      CONTINUE
              A(2,1)=A(1,2)
C------ form  AB = ( A B)
                    DO 911 II=1,2
           DO 912  J=1,2
            AB(II,J)=A(II,J)
912      CONTINUE
911       CONTINUE
           DO 913  II=1,2
            AB(II,3)=B(II)
913     CONTINUE
                    M = 2
                    N = 3

c-----  write out AB(6,7)
          DO 210  I=1, M
           WRITE (20,1120)  (AB(I,J), J=1,N)
1120    FORMAT (2X,7F10.2)
210     CONTINUE
          DO 30, K = 1, M
           DO 40 Q = K, N
                    IF (AB(K, Q).GT.0.001)  GO TO 110
40      CONTINUE
                    WRITE(*,45)
45      FORMAT(' NO SOLUTION')
```

```
            GOTO 290
110         DO 50 P = 1, N
                S = AB(K, P)
                AB(K, P) = AB(Q, P)
                AB(Q, P) = S
50           CONTINUE
           T = 1 / AB(K, K)
            DO 60 R = 1, N
            AB(K, R) = T * AB(K, R)
60      CONTINUE
          DO 70  I = 1,M
           WW = -AB(I, K)
           IF (I.EQ.K)  GO TO 70
            DO 80 J = 1, N
                AB(I, J) = AB(I, J) + WW * AB(K, J)
80        CONTINUE
70      CONTINUE
30       CONTINUE
C-----seperate solution XX(i) from AB(i,n)

            DO 901 I=1,2
             XX(I)=AB(I,N)
901     CONTINUE

            DO 2510  I=1, 2
            WRITE (20,1520)  (AB(I,J), J=1,N)
1520    FORMAT (2X,7E15.6)
2510     CONTINUE
            WRITE (20, 1000)  XX(1), XX(2)
1000     FORMAT (2X, 6E15.5)

c calculation results of Zi (SS12(II)) and the relative errors
            R=0.0
            DO 10001  II=1, NN
              ZC(II)=0.0
              ZC(II)=XX(1)*X(II)+XX(2)*YY(II)
            DS(II)=ZC(II)-Z(II)
            R=R+DS(II)*DS(II)
10002   FORMAT (2X, 4E15.6)
10001    CONTINUE
290     END
```

APPENDIX IX

UMAT SUBROUTINES AND ABAQUS INTERFACE PROGRAMS

1. UMAT Subroutine for the Phenomenological Model

Program: GUMAT

2. UMAT Subroutine for the Crystallographic Model

Program: CUMAT

3. An Example of Interfacing ABAQUS Input File

Program: NUMAT.INP

```
********* PROGRAM GUMAT.INP **********
********
**@@@@@@@@@@@@@@@@@@@@@@@@@@@@@@@@@@@@
** This UMAT is a modified version for the phenomenological model
**Program Developed by Songlin Han
** Engineering Materials and Structural Integrity Group
**  University of Bristol, April, 1998
** @@@@@@@@@@@@@@@@@@@@@@@@@@@@@@@@@@@@
****

SUBROUTINE UMAT(STRESS,STATEV,DDSDDE,SSE,SPD,SCD,
    1 RPL,DDSDDT,DRPLDE,DRPLDT,
    2 STRAN,DSTRAN,TIME,DTIME,TEMP,DTEMP,PREDEF,DPRED,CMNAME,
    3 NDI,NSHR,NTENS,NSTATV,PROPS,NPROPS,COORDS,DROT,PNEWDT,
    4 CELENT,DFGRD0,DFGRD1,NOEL,NPT,LAYER,KSPT,KSTEP,KINC)


          INCLUDE 'ABA_PARAM.INC'
C       IMPLICIT REAL*8 (A-H, O-Z)


          CHARACTER*8 CMNAME


C       IMPLICIT REAL*8 (A-H,L-Z)
                .

C       EXTERNAL MATCA, INVERS
      DIMENSION STRESS(NTENS),STATEV(NSTATV),
     1 DDSDDE(NTENS,NTENS),DDSDDT(NTENS),DRPLDE(NTENS),
     2 STRAN(NTENS),DSTRAN(NTENS),TIME(2),PREDEF(1),DPRED(1),
     3 PROPS(NPROPS),COORDS(3),DROT(3,3),DFGRD0(3,3),DFGRD1(3,3)


C
      DIMENSION EELAS(6),EPLAS(6),ALPHA(6),OLDS(6),OLDEL(6),OLDPL(6)
C (dimension adding )
      DIMENSION ORN(3), C0(6,6),ZM0(6,6),ZN0(6,6),Q0(6,6),C1(6,6),
     1  ZM1(6,6),ZN1(6,6),Q1(6,6),ZM2(6,6),ZM3(6,6),XXX0(6),
     2  DSX(6),DSXOLD(6),DDSDS(6,6),XXXR(6),XXXR0(6),
     3  WW1(6),WW2(6),DEINDR(6),WW(6,6),WWW(6,6),DEINDS(6,6),
     4  DEINDX(6,6),EIN0(6),DELTA(6,6),EIN(6),
     5  DEEIN(6),DEEE(6),DSTRESS(6),DXXX(6),C1II(6,6),
     6  PB1(6,6),PB2(6),PB3(6,6),PD(6,6),PE1(6,6),PE2(6,6),
     7  PE3(6),PD1(6),PF1(6,6),PF2(6,6),PF3(6),PF4(6,6),PF5(6,6),
     8  PF6(6), DD2(6,6),D2(6),PG1(6),PG2(6,6),PG3(6,6),
     9  PG4(6,6),PG5(6),PG4I(6,6),PF4I(6,6),PF7(6,6),PG6(6,6)

      .

      PARAMETER(ZERO=0.D0,ONE=1.D0,TWO=2.D0,THREE=3.D0,SIX=6.D0,
     1       ENUMAX=.4999D0,NEWTON=10,TOLER=1.0D-6)


C       NTENS=6
C       NDI=3
          THETA=0.6
c
```

```
C-------------------------------------------------------------
C PROPS(1) - YOUNG'S MODULUS
C PROPS(2) - POISSON'S RATIO
C PROPS(3) - SHEAR MODULUS
C PROPS(4) - ORIENTATION  L
C PROPS(5) - ORIENTATION M
C PROPS(6) - ORIENTATION N
C PROPS(7) - K*
C PROPS(8) - n
C PROPS(9) - M11-M12
C PROPS(10) - M44
C PROPS(11) - N11-N12
C PROPS(12) - N44
C PROPS(13) - Q11-Q12
C PROPS(14) - Q44
C PROPS(15) -  b
C PROPS(16) - Q
C PROPS(17) - k
C-------------------------------------------------------------
C STATEV(1, NTENS) = elastic strain EELAS
C STATEV(NTENS, NTENS*2) = plastic strain EPLAS
C STATEV(NTENS*2, NTENS*3) = back stress  ALPHA (i.e. XXX)
C STATEV(NTENS*3+1) =  insotropic hardening  RRR
C STATEV(NTENS*3+2) =  accumulated plastic strain PPP
c -------------------------------------------------------------
c -------------------------------------------------------------
C +++++++++++++++++++++++++++++++++++++++++++++++++++++++++++++++
c---- input material constants  PROPS from file DPROPS.in
c +++++++++++++++++++++++++++++++++++++++++++++++++++++++++++++++
C     PROPS(3)=PROPS(1)/(2.0*(1.0+PROPS(2)))
C       OPEN(UNIT=1,FILE='CONS.IN')
C       READ (1,2) (PROPS(I),I=1,17)
C       READ (1,2) (DSTRAN(I),I=1,6)
C       READ (1,2) (STRAN(I),I=1,6)
C2      FORMAT(6F10.6)
          SSS11=1.0/PROPS(1)
          SSS12=-1.0*PROPS(2)/PROPS(1)
          SSS44=1.0/PROPS(3)
          CCC11=((1.0/(SSS11+2.0*SSS12))+(2.0/(SSS11-SSS12)))/3.0
          CCC12=CCC11-(1.0/(SSS11-SSS12))
          CCC44=1.0/SSS44
          ORN(1)=PROPS(4)
          ORN(2)=PROPS(5)
          ORN(3)=PROPS(6)


C  ELASTIC STIFFINESS IN THE [001]-[010]-[001] SYSTEM
C  set initial stiffness to zero
DO K1=1,6
DO K2=1,6
C0(K1,K2)=0.0
ZM0(K1,K2)=0.0
ZN0(K1,K2)=0.0
Q0(K1,K2)=0.0
END DO
END DO
 DO K1=1,3
    DO K2=1,3
```

```
          C0(K1,K2)=CCC12
            END DO
          C0(K1,K1)=CCC11
          ZM0(K1,K1)=PROPS(9)
          ZN0(K1,K1)=PROPS(11)
          Q0(K1,K1)=PROPS(13)
         END DO
         DO K1=4,6
          C0(K1,K1)=CCC44
         ZM0(K1,K1)=PROPS(10)
          ZN0(K1,K1)=PROPS(12)
          Q0(K1,K1)=PROPS(14)
END DO

C Elastic stiffness and other basic transformation
          CALL MATCA(ORN,C0,ZM0,ZN0,Q0,C1,ZM1,ZN1,Q1,ZM2,ZM3)
          CALL INVERS(C1,C1II)


C Recover elastic strain,plastic strain and shift tensor and rotate
C Use code 1 for (tensor) stress, code 2 for(engineering) strain
C DROT is the identity tensor if *ORIENTATION is used


C     CALL ROTSIG(STATEV(    1),DROT,EELAS,2,NDI,NSHR)
C     CALL ROTSIG(STATEV( NTENS+1),DROT,EPLAS,2,NDI,NSHR)
C     CALL ROTSIG(STATEV(2*NTENS+1),DROT,ALPHA,1,NDI,NSHR)


C +++++++
```

```
      END DO
C       RRR0=RRR
C       PPPR0=PPPR
C       RRATE0=RRATE
C       PPP0=PPP
C calculate predictor stress increment and "stress"
c ++++++++++++++++++++++++++++++++++++++++++++++++++++++++++++++++++++++++

          DO K1=1, NTENS
           DSTRESS(K1)=0.0
           DO K2=1,NTENS
          DSTRESS(K1)=DSTRESS(K1)+C1(K1,K2)*DSTRAN(K2)
           END DO
           END DO


            DO K1=1, NTENS
              STRESS(K1)=OLDS(K1)+DSTRESS(K1)
            END DO
     CALL SONGLIN(OLDS,XXX0,RRR0,NDI,NTENS,DSXOLD,ZM1,
    1          G0,FFF0,PROPS)
     CALL SONGLIN(STRESS,XXX0,RRR0,NDI,NTENS,DSX,ZM1,
    1          G1,FFF1,PROPS)
c ++++++++++++++++++++++++++++++++++++++++++++++++++++++++++++++++++++++++


c **************************************************
c determine if actively yielding
          IF (FFF1.GT.TOLER .AND. FFF0.GT.TOLER)  THEN
c actively yielding
c calculate dDSTRESS/dSTRESS
          DO K1=1, NDI
            DO K2=1, NDI
           DDSDS(K1,K2)=-(1.0/3.0)
            END DO
           DDSDS(K1,K1)=(2.0/3.0)
            END DO
           DO K1=NDI+1, NTENS
            DO K2=NDI+1, NTENS
           DDSDS(K1,K2)=0.0
             END DO
           DDSDS(K1,K1)=1.0
             END DO
c calculate derivation of inelastic starin rate with stress
          FKN=(FFF0/PROPS(7))**PROPS(8)
FFG0=(PROPS(8)/PROPS(7))*(FFF0/PROPS(7))**(PROPS(8)-1.0)
FFG=(3.0/2.0)*(FFG0-FKN/G0)


  DO K1=1, NTENS
    WW1(K1)=0.0
    WW2(K1)=0.0
    DEINDR(K1)=0.0
   DO K2=1, NTENS
    WW(K1,K2)=0.0
    WWW(K1,K2)=0.0
         DEINDS(K1,K2)=0.0
```

```
            DEINDX(K1,K2)=0.0
          END DO
        END DO
      DO K1=1, NTENS
       DO K2=1, NTENS
      WW1(K1)=WW1(K1)+ZM1(K1,K2)*DSXOLD(K2)+ZM1(K2,K1)*DSXOLD(K2)
      WW2(K1)=WW2(K1)+ZM2(K1,K2)*DSXOLD(K2)
       END DO
      END DO

       DO K1=1, NTENS
        DO K2=1, NTENS
        WW(K1,K2)=WW1(K1)*WW2(K2)
        END DO
       END DO


      DO K1=1, NTENS
       DO K2=1, NTENS
        WWW(K1,K2)=(FFG/G0)*WW(K1,K2)+2.0*FKN*ZM2(K1,K2)
            WWW(K1,K2)=(3.0/(4.0*G0))*WWW(K1,K2)
       END DO
      END DO
     DO K1=1, NTENS
     DO K2=1, NTENS
     DEINDS(K1,K2)=0.0
     DO K3=1, NTENS
     DEINDS(K1,K2)=DEINDS(K1,K2)+WWW(K1,K3)*DDSDS(K3,K2)
      END DO
        DEINDX(K1,K2)=-1.0*WWW(K1,K2)
         END DO
        DEINDR(K1)=(-3.0/(2.0*G0))*FFG0*WW2(K1)
         END DO
       DO K1=1,NTENS
       DO K2=1,NTENS
       DELTA(K1,K2)=0.0
       END DO
       DELTA(K1,K1)=1.
       EIN0(K1)=FKN*1.5/G0*WW2(K1)
CCC    XXXR0(K1)=0.0
CCC    XXX0(K1)=0.0
        END DO
CCC    XXXR0(3)=0.000001
CCC    XXXR0(1)=-0.0000005
CCC    XXXR0(2)=-0.0000005
CCC    XXX0(3)=0.000001
CCC    XXX0(1)=-0.0000005
CCC    XXX0(2)=-0.0000005
        PPPR0=FKN
        RRATE0=PROPS(15)*(PROPS(16)-RRR0)*PPPR0
CCC    RRATE0=RRATE0+0.0000001
CCC    RRR0=RRR0+0.0000001


       DO K1=1,NTENS
       PB2(K1)=0.0
       DO K2=1,NTENS
```

```
      PB1(K1,K2)=ZN1(K1,K2)
      PB3(K1,K2)=-PPPR0*Q1(K1,K2)
      PB2(K1)=PB2(K1)-Q1(K1,K2)*XXX0(K2)
      END DO
      END DO
C
      P1=PROPS(15)*(PROPS(16)-RRR0)
      P2=-PROPS(15)*PPPR0
      A1=THETA*DTIME
C
      DO K1=1,NTENS
      PD1(K1)=0.0
        DO K2=1,NTENS
        PD1(K1)=PD1(K1)+(1./(3.*PPPR0))*(ZM3(K1,K2)*EIN0(K2)
     1  +EIN0(K2)*ZM3(K2,K1))
        END DO
        END DO
C
        DO K1=1,NTENS
        DO K2=1,NTENS
        PD(K1,K2)=PB1(K1,K2)+PB2(K1)*PD1(K2)
        END DO
        END DO
C
        DO K1=1,NTENS
        DO K2=1,NTENS
        PE1(K1,K2)=0.0
        PE2(K1,K2)=0.0
        DO K3=1,NTENS
        PE1(K1,K2)=PE1(K1,K2)+A1*PD(K1,K3)*DEINDS(K3,K2)
        PE2(K1,K2)=PE2(K1,K2)+A1*PD(K1,K3)*DEINDX(K3,K2)
        END DO
        PE2(K1,K2)=PE2(K1,K2)+A1*PB3(K1,K2)
        END DO
        END DO
C
        DO K1=1,NTENS
        PE3(K1)=0.0
        DO K2=1,NTENS
        PE3(K1)=PE3(K1)+A1*PD(K1,K2)*DEINDR(K2)
        END DO
        END DO
C
        BB=1.-A1*P2
        B1=DTIME*RRATE0/BB
        B2=A1*P1/BB
        CC=0.0
        DO K1=1,NTENS
        CC=CC+PD1(K1)*DEINDR(K1)
        END DO
        CCC=1.-B2*CC
        CC1=B1/CCC
        C2=B2/CCC
C
        DO K1=1,NTENS
        DO K2=1,NTENS
        PF1(K1,K2)=0.0
        PF2(K1,K2)=0.0
```

```
      DO K3=1,NTENS
      PF1(K1,K2)=PF1(K1,K2)+C2*PE3(K1)*PD1(K3)*DEINDS(K3,K2)
      PF2(K1,K2)=PF2(K1,K2)+C2*PE3(K1)*PD1(K3)*DEINDX(K3,K2)
      END DO
      END DO
      END DO
C
      DO K1=1,NTENS
      PF3(K1)=DTIME*XXXR0(K1)+CC1*PE3(K1)
      END DO
      DO K1=1,NTENS
      DO K2=1,NTENS
      PF4(K1,K2)=DELTA(K1,K2)-PF2(K1,K2)-PE2(K1,K2)
      PF5(K1,K2)=PE1(K1,K2)+PF1(K1,K2)
      END DO
      END DO
      CALL INVERS(PF4,PF4I)
C
      DO K1=1,NTENS
      PF6(K1)=0.0
      DO K2=1,NTENS
      PF6(K1)=PF6(K1)+PF4I(K1,K2)*PF3(K2)
      END DO
      END DO
CCC    PF7=0.0
      DO K1=1,NTENS
      DO K2=1,NTENS
      PF7(K1,K2)=0.0
      DO K3=1,NTENS
      PF7(K1,K2)=PF7(K1,K2)+PF4I(K1,K3)*PF5(K3,K2)
      END DO
CCC   PF7=PF7+PF4I(K1,K2)*PF5(K2,K1)
      END DO
      END DO
      D1=0.0
      DO K1=1,NTENS
      DO K2=1,NTENS
      D1=D1+C2*PD1(K1)*DEINDX(K1,K2)*PF6(K2)
CCC   D1=D1+PD1(K1)*DEINDX(K1,K2)*PF6(K2)
      END DO
CCCCCC D1=D1+C2*PD1(K1)
      END DO
      D1=D1+CC1
C
      DO K1=1,NTENS
      DO K2=1,NTENS
      DD2(K1,K2)=0.0
      DO K3=1,NTENS
      DD2(K1,K2)=DD2(K1,K2)+DEINDX(K1,K3)*PF7(K3,K2)
      END DO
CCC    DD2(K1,K2)=DEINDX(K1,K2)*PF7
      END DO
      END DO
      DO K1=1,NTENS
      D2(K1)=0.0
      DO K2=1,NTENS
      D2(K1)=D2(K1)+C2*PD1(K2)*DEINDS(K2,K1)+
     1  C2*PD1(K2)*DD2(K2,K1)
```

```
      END DO
      END DO
C
      DO K1=1,NTENS
      PG1(K1)=0.0
      DO K2=1,NTENS
      PG1(K1)=PG1(K1)+A1*DEINDX(K1,K2)*PF6(K2)
      END DO
      PG1(K1)=PG1(K1)+DTIME*EIN0(K1)+D1*A1*DEINDR(K1)
      END DO
C
      DO K1=1,NTENS
      DO K2=1,NTENS
      PG2(K1,K2)=0.0
      DO K3=1,NTENS
      PG2(K1,K2)=PG2(K1,K2)+DEINDX(K1,K3)*PF7(K3,K2)
      END DO
CCC   PG2(K1,K2)=PG2(K1,K2)+DEINDX(K1,K2)*PF7
      PG2(K1,K2)=PG2(K1,K2)+DEINDS(K1,K2)+
     1     DEINDR(K1)*D2(K2)
      END DO
      END DO
C
      DO K1=1,NTENS
      DO K2=1,NTENS
      PG3(K1,K2)=0.0
      DO K3=1,NTENS
      PG3(K1,K2)=PG3(K1,K2)+PG2(K1,K3)*C1(K3,K2)
      END DO
      END DO
      END DO
C
      DO K1=1,NTENS
      DO K2=1,NTENS
      PG4(K1,K2)=DELTA(K1,K2)+A1*PG3(K1,K2)
      END DO
      END DO
      CALL INVERS(PG4,PG4I)
C
CCC    PG6=0.0
      DO K1=1,NTENS
      PG5(K1)=0.0
      DO K2=1,NTENS
      PG6(K1,K2)=0.0
      DO K3=1,NTENS
      PG6(K1,K2)=PG6(K1,K2)+PG4I(K1,K3)*PG3(K3,K2)
      END DO
      PG5(K1)=PG5(K1)+PG4I(K1,K2)*PG1(K2)
      END DO
      END DO
C
      DO K1=1,NTENS
CCC    DEEIN(K1)=PG5(K1)+A1*PG6*DSTRAN(K1)
      DEEIN(K1)=0.0
      DO K2=1,NTENS
      DEEIN(K1)=DEEIN(K1)+A1*PG6(K1,K2)*DSTRAN(K2)
      END DO
      DEEIN(K1)=DEEIN(K1)+PG5(K1)
```

```
      END DO
      DO K1=1,NTENS
      DSTRESS(K1)=0.0
      DO K2=1,NTENS
      DSTRESS(K1)=DSTRESS(K1)+C1(K1,K2)*(DSTRAN(K2)-DEEIN(K2))
      END DO
      END DO·
      DRRR=0.0
      DO K1=1,NTENS
      DRRR=DRRR+D2(K1)*DSTRESS(K1)
      END DO
      DRRR=DRRR+D1
      DO K1=1,NTENS
      DXXX(K1)=0.0
      DEEE(K1)=0.0
      DO K2=1,NTENS
      DXXX(K1)=DXXX(K1)+PF7(K1,K2)*DSTRESS(K2)
      DEEE(K1)=DEEE(K1)+C1II(K1,K2)*DSTRESS(K2)
      END DO
CCC   DXXX(K1)=PF7*DSTRESS(K1)+PF6(K1)
      DXXX(K1)=DXXX(K1)+PF6(K1)
      END DO
      DO K1=1,NTENS
      STRESS(K1)=OLDS(K1)+DSTRESS(K1)
      ALPHA(K1)=XXX0(K1)+DXXX(K1)
      EPLAS(K1)=OLDPL(K1)+DEEIN(K1)
      EELAS(K1)=OLDEL(K1)+DEEE(K1)
      END DO
      PPP=PPP0+DPPP
      RRR=RRR0+DRRR
C*************************
CCC   DO K1=1,NTENS
CCC   EIN(K1)=DEEIN(K1)/A1-(1.-THETA)*DTIME/THETA*EIN0(K1)
CCC   XXXR(K1)=DXXX(K1)/A1-(1.-THETA)*DTIME/THETA*XXXR0(K1)
CCC   END DO
CCC   RRATE=DRRR/A1-(1.-THETA)*DTIME/THETA*RRATE0
CCC   PPPR=DPPP/A1-(1.-THETA)*DTIME/THETA*PPPR0
      IF(PROPS(18).EQ.0.0)THEN
      CALL SONGLIN (STRESS,ALPHA,RRR,NDI,NTENS,DSX,ZM1,G,FFF,
     1      PROPS)
C     CALL SONGLIN(STRESS,ALPHA,KNDI,KNTENS,DSX,ZM1,G)
        DO K1=1,NTENS
        WW2(K1)=0.0
        END DO
        DO K1=1, NTENS
        DO K2=1, NTENS
          WW2(K1)=WW2(K1)+ZM2(K1,K2)*DSX(K2)
        END DO
       END DO
C      FFF=G-RRR-PROPS(17)
C      FFF=G-PROPS(17)
       FKN=(FFF/PROPS(7))**PROPS(8)
       DO K1=1,NTENS
       EIN(K1)=(1.5/G)*FKN*WW2(K1)
       END DO
       PPPR=FKN
CCC    PPPR=0.0
       DO K1=1,NTENS
```

```
          XXXR(K1)=0.0
          DO K2=1,NTENS
CCC        PPPR=PPPR+EIN(K1)*ZM3(K1,K2)*EIN(K2)
          XXXR(K1)=XXXR(K1)+ZN1(K1,K2)*EIN(K2)-
     1      Q1(K1,K2)*ALPHA(K2)*PPPR
          END DO
          END DO
CCC       PPPR=SQRT((2./3.)*PPPR)
C
CCCCC     DO K1=1,NTENS
CCCCC     XXXR(K1)=0.0
CCCCC     DO K2=1,NTENS
CCCCC     XXXR(K1)=XXXR(K1)+ZN1(K1,K2)*EIN(K2)-
CCCCC    1      Q1(K1,K2)*ALPHA(K2)*PPPR
CCCCC     END DO
CCCCC     END DO
          RRATE=PROPS(15)*(PROPS(16)-RRR)*PPPR
          DO K1=1,NTENS
          DO K2=1,NTENS
          DDSDDE(K1,K2)=0.0
          DO K3=1,NTENS
          DDSDDE(K1,K2)=DDSDDE(K1,K2)-A1*C1(K1,K3)*PG6(K3,K2)
          END DO
          DDSDDE(K1,K2)=DDSDDE(K1,K2)+C1(K1,K2)
          END DO
          END DO
C
          ELSE
          CALL ITERATION(STRESS,ALPHA,RRR,PPP,EPLAS,
     1   PROPS,EIN0,RRR0,XXX0,OLDS,PPP0,OLDPL,ZM1,ZM2,ZM3,ZN1,
     2   Q1,EIN,NTENS,NDI,THETA,DTIME,C1,DSTRAN,PPPR,DSX,G,FFF,
     3   XXXR,RRATE,PPPR0,XXXR0,RRATE0)
      CALL TENSORW(FFF,PROPS,G,ZM1,ZM2,DSX,WW1,WW2,FKN1,FFG01,
     1       FFG1,NTENS)
C
          DO K1=1,NTENS
           DSTRESS(K1)=STRESS(K1)-OLDS(K1)
C        DEEE(K1)=DSTRAN(K1)-(EPLAS(K1)-OLDPL(K1))
          DEEE(K1)=0.0
          END DO
          DO K1=1,NTENS
          DO K2=1,NTENS
          DEEE(K1)=DEEE(K1)+C1II(K1,K2)*DSTRESS(K2)
          END DO
C        EELAS(K1)=OLDEL(K1)+DEEE(K1)
          END DO
          DO K1=1,NTENS
          EELAS(K1)=OLDEL(K1)+DEEE(K1)
          END DO
           CALL NONLINJ (PPPR,G,FKN1,FFG01,FFG1,THETA,PROPS,
     1  EIN,ALPHA,RRR,WW1,WW2,Q1,ZM2,ZM3,ZN1,C1,DTIME,NTENS,
     2  DDSDDE,DDSDS)
C
          END IF
c ***************************************************************
c***************************************************************
c if not yielding, JACOBIN matrix same as elastic stiffness C1
      ELSE
```

```
                DO K1=1, NTENS
                      DO K2=1, NTENS
                 DDSDDE(K1,K2)=C1(K1,K2)
                      END DO
                       END DO
CCC              RRR=RRR0
CCC              PPP=PPP0
               RRR=0.0
               PPP=0.0
              DO K1=1, NTENS
                       DXXX(K1)=0.0
                        DEEIN(K1)=0.0
                       EIN(K1)=0.0
                       XXXR(K1)=0.0
                END DO
                RRATE=0.0
                PPPR=0.0
c update shift tensor, elastic, inelastic strain, stress and STATEE's
C       CALL INVERS(C1,C1II)
                DO K1=1, NTENS
                  DEEE(K1)=0.0
                 DO K2=1, NTENS
                  DEEE(K1)=DEEE(K1)+C1II(K1,K2)*DSTRESS(K2)
                END DO
                 END DO
                DO K1=1, NTENS
                 EELAS(K1)=OLDEL(K1)+DEEE(K1)
                 EPLAS(K1)=OLDPL(K1)+DEEIN(K1)
                 STRESS(K1)=OLDS(K1)+DSTRESS(K1)
                 ALPHA(K1)=XXX0(K1)+DXXX(K1)
               END DO

C ********************
                 END IF
C ***************************************************************************
C***************************************************************************
C Store elastic strains, plastic strains and shift tensor
C in state variable array
                EQE=0.0
                DO K1=1,NTENS
                DO K2=1,NTENS
                EQE=EQE+EPLAS(K1)*DELTA(K1,K2)*EPLAS(K2)
                END DO
                END DO
                EQE=(2./3.)*EQE
                 EQE=SQRT(EQE)
              DO K1=1,NTENS
                 STATEV(K1)=EELAS(K1)
                 STATEV(K1+NTENS)=EPLAS(K1)
                 STATEV(K1+2*NTENS)=ALPHA(K1)
C      DSTRAN(K1)=DEEE(K1)+DEEIN(K1)
                 STATEV(K1+3*NTENS)=EIN(K1)
                 STATEV(NTENS*4+K1)=XXXR(K1)
                   END DO
                 STATEV(NTENS*5+1)=RRR
                 STATEV(NTENS*5+2)=PPP
                 STATEV(NTENS*5+3)=RRATE
```

```
          STATEV(NTENS*5+4)=PPPR
          STATEV(NTENS*5+5)=EQE
            RETURN
             END
C
C ********************
C**************************************************
          SUBROUTINE SONGLIN(SS,X0,RRR,KNDI,KNTENS,DDSX,A,G,F,
     1          PROPS)
C
          IMPLICIT REAL*8 (A-H, L-Z)
          DIMENSION SS(6), X0(6), DDSX(6),A(6,6),
     1  DDSTRESS(6),PROPS(18)
C
C
C calculate deviatoric stress
C         VVSTRESS=0.0
C         VXXX=0.0
             VVSTRESS=(SS(1)+SS(2)+SS(3))/3.0
             VXXX=(X0(1)+X0(2)+X0(3))/3.0


              DO K1=1, KNDI
              DDSTRESS(K1)=SS(K1)-VVSTRESS
               DDSX(K1)=DDSTRESS(K1)-(X0(K1)-VXXX)
               END DO
              DO K1=KNDI+1, KNTENS
                   DDSTRESS(K1)=SS(K1)
                    DDSX(K1)=DDSTRESS(K1)-X0(K1)
                  END DO
c calculate yielding function f
                  G11=0.0
       DO K1=1,KNTENS
            DO K2=1, KNTENS
           G11=G11+DDSX(K1)*A(K1,K2)*DDSX(K2)
             END DO
             END DO
           G=SQRT((3.0/2.0)*G11)
           F=G-RRR-PROPS(17)
C         G=120.
C
           RETURN
           END
C**************************************************************
      SUBROUTINE MATCA(ORN,C0,ZM0,ZN0,Q0,C1,ZM1,ZN1,Q1,ZM2,ZM3)
C transformation of elastic and other basic matrix
            IMPLICIT REAL*8 (A-H,L-Z)
          DIMENSION ORN(3), C0(6,6),ZM0(6,6),ZN0(6,6),Q0(6,6),C1(6,6),
     1  ZM1(6,6),ZN1(6,6),Q1(6,6),ZM2(6,6),ZM3(6,6),ZM0I(6,6)
          DIMENSION A(6,6),B(6,6),BT(6,6),AT(6,6),AI(6,6),BI(6,6)


C         EXTERNAL  INVERS,MATAB, MATRA, MULMAT
           ALI=ORN(1)
           AMI=ORN(2)
           ANI=ORN(3)
c         MMMM1=ZM0(1,1)
c         MMMM4=ZM0(4,4)
```

```
c
c      IF(ALI.LE.1E-6) THEN
c        WRITE (*,1145)
c      ELSE IF(AMI.LE.1E-6) THEN
c        WRITE (*,1245)
c      ELSE IF (ANI.LE.1E-6) THEN
c         WRITE(*,1345)
c1145   FORMAT ('L=0')
c1245   FORMAT ('M=0')
c1345   FORMAT ('N=0')
c       END IF
c      IF(MMMM1.LE.1E-6) THEN
c        WRITE (*,1445)
c      ELSE IF(MMMM4.LE.1E-6) THEN
c        WRITE (*,1545)
c1445   FORMAT ('M1=0')
c1545   FORMAT ('M4=0')
c      END IF
C-----calculats  matrix A and B
          CALL MATAB (ALI,AMI,ANI,A,B)
C------computes transpose matrix AT, BT,
          CALL MATRA  (A,AT)
          CALL MATRA  (B,BT)
C----- computes inverse matrix AI, BI
          CALL INVERS (A, AI)
          CALL INVERS (B, BI)
          CALL INVERS (ZM0,ZM0I)
C------- computes material matrix
          CALL MULMAT (AI,C0,B,C1)
          CALL MULMAT (AT,ZM0,A,ZM1)
          CALL MULMAT (BI,ZM0,A,ZM2)
          CALL MULMAT (BT,ZM0I,B,ZM3)
          CALL MULMAT (AI,ZN0,B,ZN1)
          CALL MULMAT (AI,Q0,A,Q1)
           DO I=1,6
            DO J=1,6
          ZN1(I,J)=(2.0/3.0)*ZN1(I,J)
           END DO
            END DO
          RETURN
          END


C .....
          SUBROUTINE  MATAB (ALI, AMI, ANI, A, B)
C-------This subroutine calculates MATRIX Aij and Bij
          IMPLICIT REAL*8 (A-H,L-Z)
          DIMENSION  A(6,6), B(6,6)
               DD1=(ALI*ALI+AMI*AMI+ANI*ANI)
               DD2=(AMI*AMI+ANI*ANI)
               DD1D=(DD1)**0.5
               DD2D=(DD2)**0.5
               A(1,1)=DD2*DD2
               A(1,2)=0.0
               A(1,3)=ALI*ALI*DD2
               A(1,4)=0.0
```

```
A(1,5)=2.0*ALI*DD2*DD2D
A(1,6)=0.0
A(2,1)=ALI*ALI*AMI*AMI
A(2,2)=ANI*ANI*DD1
A(2,3)=AMI*AMI*DD2
A(2,4)=-2.0*ALI*AMI*ANI*DD1D
A(2,5)=-2.0*ALI*AMI*AMI*DD2D
A(2,6)=2.0*AMI*ANI*DD1D*DD2D
A(3,1)=ALI*ALI*ANI*ANI
A(3,2)=AMI*AMI*DD1
A(3,3)=ANI*ANI*DD2
A(3,4)=2.0*ALI*AMI*ANI*DD1D
A(3,5)=-2.0*ALI*ANI*ANI*DD2D
A(3,6)=-2.0*AMI*ANI*DD1D*DD2D
A(4,1)=-1.0*ALI*AMI*DD2
A(4,2)=0.0
A(4,3)=ALI*AMI*DD2
A(4,4)=ANI*DD2*DD1D
A(4,5)=(DD2-ALI*ALI)*AMI*DD2D
A(4,6)=ALI*ANI*DD1D*DD2D
A(5,1)=-1.0*ALI*ANI*DD2
A(5,2)=0.0
A(5,3)=ALI*ANI*DD2
A(5,4)=-1.0*AMI*DD2*DD1D
A(5,5)=(DD2-ALI*ALI)*ANI*DD2D
A(5,6)=-1.0*ALI*AMI*DD1D*DD2D
A(6,1)=ALI*ALI*AMI*ANI
A(6,2)=-AMI*ANI*DD1
A(6,3)=AMI*ANI*DD2
A(6,4)=(AMI*AMI-ANI*ANI)*ALI*DD1D
A(6,5)=-2.0*ALI*AMI*ANI*DD2D
A(6,6)=(ANI*ANI-AMI*AMI)*DD1D*DD2D
B(1,1)=DD2*DD2
B(1,2)=0.0
B(1,3)=ALI*ALI*DD2
B(1,4)=0.0
B(1,5)=ALI*DD2*DD2D
B(1,6)=0.0
B(2,1)=ALI*ALI*AMI*AMI
B(2,2)=ANI*ANI*DD1
B(2,3)=AMI*AMI*DD2
B(2,4)=-1.0*ALI*AMI*ANI*DD1D
B(2,5)=-1.0*ALI*AMI*AMI*DD2D
B(2,6)=AMI*ANI*DD1D*DD2D
B(3,1)=ALI*ALI*ANI*ANI
B(3,2)=AMI*AMI*DD1
B(3,3)=ANI*ANI*DD2
B(3,4)=ALI*AMI*ANI*DD1D
B(3,5)=-1.0*ALI*ANI*ANI*DD2D
B(3,6)=-1.0*AMI*ANI*DD1D*DD2D
B(4,1)=-2.0*ALI*AMI*DD2
B(4,2)=0.0
B(4,3)=2.0*ALI*AMI*DD2
B(4,4)=ANI*DD2*DD1D
B(4,5)=(DD2-ALI*ALI)*AMI*DD2D
B(4,6)=ALI*ANI*DD1D*DD2D
B(5,1)=-2.0*ALI*ANI*DD2
B(5,2)=0.0
```

```
B(5,3)=2.0*ALI*ANI*DD2
B(5,4)=-1.0*AMI*DD2*DD1D
B(5,5)=(DD2-ALI*ALI)*ANI*DD2D
B(5,6)=-1.0*ALI*AMI*DD1D*DD2D
B(6,1)=2.0*ALI*ALI*AMI*ANI
B(6,2)=-2.0*AMI*ANI*DD1
B(6,3)=2.0*AMI*ANI*DD2
B(6,4)=(AMI*AMI-ANI*ANI)*ALI*DD1D
B(6,5)=-2.0*ALI*AMI*ANI*DD2D
B(6,6)=(ANI*ANI-AMI*AMI)*DD1D*DD2D


DO I=1,6
  DO J=1,6
    A(I,J)=A(I,J)/(DD1*DD2)
    B(I,J)=B(I,J)/(DD1*DD2)
  END DO
END DO


RETURN
END


C.....
          SUBROUTINE MATRA ( AA, AAT)
C------ this is for matrix transpose i.e AATij=AAji

    IMPLICIT REAL*8 (A-H, L-Z)
  DIMENSION AA(6,6), AAT(6,6)
  DO  I=1,6
  DO  J=1,6
     AAT(I,J)=AA(J,I)
   END DO
    END DO
     RETURN
      END


C .....
          SUBROUTINE MULMAT (A,B,C,D)
C------this subroutine is for three matrix multplication A.B.C=D
          IMPLICIT REAL*8 (A-H, L-Z)
        DIMENSION A(6,6), B(6,6), C(6,6), D(6,6), AB(6,6)
        DO I=1, 6
  DO J=1,6
     AB(I,J)=0.0
  DO K=1,6
     AB(I,J)=AB(I,J)+A(I,K)*B(K,J)
    END DO
    END DO
     END DO
  DO I=1, 6
  DO J=1,6
    D(I,J)=0.0
  DO K=1,6
    D(I,J)=D(I,J)+AB(I,K)*C(K,J)
```

```
      END DO
       END DO
      END DO
      RETURN
      END


C .....
            SUBROUTINE  INVERS (A, AI)
C ===== this subroutine computes the INVERSE of a Matrix AI=A-1
             IMPLICIT REAL*8 (A-H, L-Z)
             DIMENSION  A(6,6),AI(6,6), AB(6, 12)

C------ form  AB = ( A II )
            DO   I=1, 6
            DO  J=1,12
             IF·((I+6).EQ.J) THEN
                    AB(I,J)=1.0
             ELSE
                    AB(I,J)=0.0
             END IF
               END DO
              END DO
            DO   I=1,6
            DO  J=1,6
              AB(I,J)=A(I,J)
             END DO
              END DO
               KM = 6
                 KN = 12
              DO 30, K = 1, KM
              DO 40, KQ = K, KM
               IF (ABS(AB(KQ,K)).GT.1E-18)  GO TO 110
40       CONTINUE
              WRITE(*,45)
45        FORMAT(' NO SOLUTION')
            GOTO 290
110    DO 50, KP = 1, KN
                    S = AB(K, KP)
                    AB(K, KP) = AB(KQ, KP)
                    AB(KQ, KP) = S
50     CONTINUE
                     T = 1 / AB(K, K)
            DO 60, KR = 1, KN
                    AB(K, KR) = T * AB(K, KR)
60     CONTINUE
              DO 70,  I = 1,KM
                       Y = -AB(I, K)
               IF (I.EQ.K)  GO TO 70
              DO 80, J = 1, KN
              AB(I, J) = AB(I, J) + Y * AB(K, J)
80       CONTINUE
70       CONTINUE
30       CONTINUE


C-----seperate solution AI from AB
```

```
      DO 901, I=1,6
      DO 902, J=7,12
            JJ=J-6
            AI(I,JJ)=AB(I,J)
902  CONTINUE
901  CONTINUE
290    RETURN
        END
C*************************************************************
      SUBROUTINE ITERATION(STRESS,ALPHA,RRR,PPP,EPLAS,
     1 PROPS,EIN0,RRR0,XXX0,OLDS,PPP0,OLDPL,ZM1,ZM2,ZM3,ZN1,
     2 Q1,EIN,KNTENS,KNDI,THETA,DTIME,C1,DSTRAN,PPPR,DSX,G,FFF,
     3 XXXR,RRATE,PPPR0,XXXR0,RRATE0)
      IMPLICIT REAL*8 (A-H, L-Z)
      DIMENSION STRESS(6),ALPHA(6),EPLAS(6),EIN0(6),XXX0(6),
     1 OLDS(6),OLDPL(6),ZM1(6,6),ZM2(6,6),ZM3(6,6),ZN1(6,6),
     2 Q1(6,6),WW2(6),DSX(6),EIN(6),XXXR0(6),XXXR(6),DEEIN(6),
     3 DXXX(6), DSTRESS(6),PROPS(17),C1(6,6),DSTRAN(6)
C
C calculate accumulated inelastic strain rate at start of time
c increment
C calculate isotropic stress rate at start of time increment and
C back stress rate at start of time increment
C
C do iteration loop
C     DO 121 K=1,3
      DO K=1,3
C calculate inelastic strain rate
      CALL SONGLIN (STRESS,ALPHA,RRR,KNDI,KNTENS,DSX,ZM1,G,FFF,
     1      PROPS)
C     CALL SONGLIN(STRESS,ALPHA,KNDI,KNTENS,DSX,ZM1,G)
      DO K1=1,KNTENS
      WW2(K1)=0.0
      END DO
      DO K1=1, KNTENS
       DO K2=1, KNTENS
        WW2(K1)=WW2(K1)+ZM2(K1,K2)*DSX(K2)
       END DO
      END DO
C     FFF=G-RRR-PROPS(17)
C     FFF=G-PROPS(17)
      FKN=(FFF/PROPS(7))**PROPS(8)
      DO K1=1,KNTENS
      EIN(K1)=(1.5/G)*FKN*WW2(K1)
      XXXR(K1)=0.0
      END DO
C  calculate acumulated inelastic strain rate dp/dt at t+dt
      PPPR=FKN
C calculate back stress rate dx/dt
      DO K1=1, KNTENS
      DO K2=1,KNTENS
      XXXR(K1)=XXXR(K1)+ZN1(K1,K2)*EIN(K2)-
     1       Q1(K1,K2)*ALPHA(K2)*PPPR
      END DO
      END DO
C isotropic stress rate
```

```
            RRATE=PROPS(15)*(PROPS(16)-RRR)*PPPR
C calculate the increments of inelastic strain by using implicite method,
C back stress, and update the values of variables
            DO K1=1,KNTENS
            DEEIN(K1)=DTIME*((1.-THETA)*EIN0(K1)+THETA*EIN(K1))
            DXXX(K1)=DTIME*((1.-THETA)*XXXR0(K1)+THETA*XXXR(K1))
           EPLAS(K1)=OLDPL(K1)+DEEIN(K1)
           ALPHA(K1)=XXX0(K1)+DXXX(K1)
           DSTRESS(K1)=0.0
            END DO
C calculate stress increment and the increments of scalor stress
C and accumulated inelastic strain,then update the variables
            DO K1=1,KNTENS
             DO K2=1,KNTENS
            DSTRESS(K1)=DSTRESS(K1)+C1(K1,K2)*(DSTRAN(K2)-DEEIN(K2))
             END DO
             END DO
             DRRR=DTIME*((1.-THETA)*RRATE0+THETA*RRATE)
             DPPP=DTIME*((1.-THETA)*PPPR0+THETA*PPPR)
C       DRRR=DTIME*(THETA*RRATE0+(1.-THETA)*RRATE)
C       DPPP=DTIME*(THETA*PPPR0+(1.-THETA)*RRATE)
             RRR=RRR0+DRRR
             PPP=PPP0+DPPP
             DO K1=1,KNTENS
            STRESS(K1)=OLDS(K1)+DSTRESS(K1)
             END DO
C121         CONTINUE
           END DO
            RETURN
            END
C++++++++++++++++++++++++++++++++++++++++++++++++++++++++++++++++++++++++++++++++
            SUBROUTINE TENSORW (FFF,PROPS,G,ZM1,ZM2,DSX,WW1,WW2,
     1                 FKN,FFG0,FFG,KNTENS)
C
            IMPLICIT REAL*8 (A-H, L-Z)
            DIMENSION PROPS(18),ZM1(6,6),ZM2(6,6),DSX(6),
     1   WW1(6),WW2(6)
C
c calculate derivation of inelastic starin rate with stress
            FKN=(FFF/PROPS(7))**PROPS(8)
            FFG0=(PROPS(8)/PROPS(7))*(FFF/PROPS(7))**(PROPS(8)-1.0)
            FFG=(3.0/2.0)*(FFG0-FKN/G)
C
              DO K1=1, KNTENS
                WW1(K1)=0.0
                WW2(K1)=0.0
              END DO
             DO K1=1, KNTENS
              DO K2=1, KNTENS
          WW1(K1)=WW1(K1)+ZM1(K1,K2)*DSX(K2)+ZM1(K2,K1)*DSX(K2)
             WW2(K1)=WW2(K1)+ZM2(K1,K2)*DSX(K2)
              END DO
             END DO
             RETURN
             END
C++++++++++++++++++++++++++++++++++++++++++++++++++++++++++++++++++++++++++++++++
      SUBROUTINE NONLINJ (PPPR,G,FKN,FFG0,FFG,THETA,PROPS,
     1  EIN,ALPHA,RRR,WW1,WW2,Q1,ZM2,ZM3,ZN1,C1,DTIME,KNTENS,
```

```
     2  DDSDDE,DDSDS)
C
          IMPLICIT REAL*8 (A-H,L-Z)


          DIMENSION EIN(6),ALPHA(6),PROPS(17),WW1(6),WW2(6),Q1(6,6),
     1  ZM2(6,6),ZM3(6,6),C1(6,6),ZN1(6,6),DDSDDE(6,6),
     2  M(6),W1(6,6),W(6,6),Y(6,6),DELTA(6,6),AQ(6,6),AQI(6,6),
     3  QX(6),QXM(6,6),NQ(6,6),ANQ(6,6),YY(6,6),YYY(6,6),YYYI(6,6),
     4  YMA1(6,6),YMA(6,6),CYMA(6,6),CYMAI(6,6),DDSDS(6,6)
C
          DO K1=1,KNTENS
          M(K1)=0.0
          DO K2=1,KNTENS
          M(K1)=M(K1)+ZM3(K1,K2)*EIN(K2)+EIN(K2)*ZM3(K2,K1)
          END DO
          END DO
C
          DO K1=1,KNTENS
          M(K1)=M(K1)/(3.0*PPPR)
          END DO
C
          A=DTIME*THETA
          AA=(3.0/2.0)*FKN/G
          BB=(3.0/2.0)*FFG0
          C=(3.0/4.0)*FFG/G
          CC=1.0+A*PROPS(15)*PPPR
          DD=A*PROPS(15)*BB*(PROPS(16)-RRR)/CC
          DO K1=1,KNTENS
          DO K2=1,KNTENS
          W1(K1,K2)=WW1(K1)*WW2(K2)/G
          END DO
          END DO
          DO K1=1,KNTENS
          DO K2=1,KNTENS
          W(K1,K2)=C*W1(K1,K2)+AA*ZM2(K1,K2)
          END DO
          END DO
C
          DO K1=1,KNTENS
          DO K2=1,KNTENS
          Y(K1,K2)=DD*WW2(K1)*M(K2)/G
          END DO
          END DO
C
          DO K1=1,KNTENS
          DO K2=1,KNTENS
          DELTA(K1,K2)=0.0
          END DO
          END DO
          DO K1=1,KNTENS
          DELTA(K1,K1)=1.0
          END DO
C
          DO K1=1,KNTENS
          DO K2=1,KNTENS
          AQ(K1,K2)=DELTA(K1,K2)+A*PPPR*Q1(K1,K2)
          END DO
```

```
      END DO
      CALL INVERS(AQ,AQI)
C
      DO K1=1,KNTENS
      QX(K1)=0.0
      DO K2=1,KNTENS
      DO K3=1,KNTENS
      QX(K1)=QX(K1)+Q1(K1,K3)*ALPHA(K3)
      END DO
      QXM(K1,K2)=QX(K1)*M(K2)
      END DO
      END DO
C
      DO K1=1,KNTENS
      DO K2=1,KNTENS
      NQ(K1,K2)=ZN1(K1,K2)-QXM(K1,K2)
      ANQ(K1,K2)=0.0
      YY(K1,K2)=0.0
      END DO
      END DO
C
      DO K1=1,KNTENS
      DO K2=1,KNTENS
      DO K3=1,KNTENS
      ANQ(K1,K2)=ANQ(K1,K2)+AQI(K1,K3)*NQ(K3,K2)
      END DO
      END DO
      END DO
C
      DO K1=1,KNTENS
      DO K2=1,KNTENS·
      DO K3=1,KNTENS
      YY(K1,K2)=YY(K1,K2)+A*W(K1,K3)*ANQ(K3,K2)
      END DO
      END DO
      END DO
C
      DO K1=1,KNTENS
      DO K2=1,KNTENS
      YMA1(K1,K2)=0.0
      YMA(K1,K2)=0.0
      CYMA(K1,K2)=0.0
      DDSDDE(K1,K2)=0.0
      YYY(K1,K2)=DELTA(K1,K2)+YY(K1,K2)+Y(K1,K2)
      END DO
      END DO
      CALL INVERS(YYY,YYYI)
      DO K1=1,KNTENS
      DO K2=1,KNTENS
      DO K3=1,KNTENS
      YMA1(K1,K2)=YMA1(K1,K2)+YYYI(K1,K3)*W(K3,K2)
      END DO
      END DO
      END DO
C
      DO K1=1,KNTENS
      DO K2=1,KNTENS
      DO K3=1,KNTENS
```

```
      YMA(K1,K2)=YMA(K1,K2)+YMA1(K1,K3)*DDSDS(K3,K2)
      END DO
      END DO
      END DO
      DO K1=1,KNTENS
      DO K2=1,KNTENS
      DO K3=1,KNTENS
      CYMA(K1,K2)=CYMA(K1,K2)+A*C1(K1,K3)*YMA(K3,K2)
      END DO
      CYMA(K1,K2)=CYMA(K1,K2)+DELTA(K1,K2)
      END DO
      END DO
      CALL INVERS(CYMA,CYMAI)
C
      DO K1=1,KNTENS
      DO K2=1,KNTENS
      DO K3=1,KNTENS
      DDSDDE(K1,K2)=DDSDDE(K1,K2)+CYMAI(K1,K3)*C1(K3,K2)
      END DO
      END DO
      END DO
      RETURN
      END
```

```
********* PROGRAM CUMAT.INP **********
********
**@@@@@@@@@@@@@@@@@@@@@@@@@@@@@@@@@@@@
** This UMAT is a modified version for crystallographic model
** Program Developed in:
** Engineering Materials and Structural Integrity Group
**       University of Bristol, June, 1998
** @@@@@@@@@@@@@@@@@@@@@@@@@@@@@@@@@@@@
------------------------------------------------------------

      SUBROUTINE UMAT(STRESS,STATEV,DDSDDE,SSE,SPD,SCD,
     1 RPL,DDSDDT,DRPLDE,DRPLDT,
     2 STRAN,DSTRAN,TIME,DTIME,TEMP,DTEMP,PREDEF,DPRED,CMNAME,
     3 NDI,NSHR,NTENS,NSTATV,PROPS,NPROPS,COORDS,DROT,PNEWDT,
     4 CELENT,DFGRD0,DFGRD1,NOEL,NPT,LAYER,KSPT,KSTEP,KINC)

      INCLUDE 'ABA_PARAM.INC'
CCC
      CHARACTER*8 CMNAME

C     IMPLICIT REAL*8 (A-H,L-Z)

C     EXTERNAL MATCA, INVERS
      DIMENSION STRESS(NTENS),STATEV(NSTATV),
     1 DDSDDE(NTENS,NTENS),DDSDDT(NTENS),DRPLDE(NTENS),
     2 STRAN(NTENS),DSTRAN(NTENS),TIME(2),PREDEF(1),DPRED(1),
     3 PROPS(NPROPS),COORDS(3),DROT(3,3),DFGRD0(3,3),DFGRD1(3,3)
C
C     DIMENSION STRESS(6),STATEV(90),
C    1 DDSDDE(6,6),
C    2 DSTRAN(6),STRAN(6),
C    3 PROPS(17)

      DIMENSION EELAS(6),EPLAS(6),OLDS(6),OLDEL(6),OLDPL(6)
C (dimension adding )
      DIMENSION ORN(3),C0(6,6),C1(6,6),C1I(6,6),WN(18,3),WL(18,3),
     1 DEIN(6),DEE(6),DSTRESS(6),DX(18),DR(18),TS0(18),
     2 TTR0(18),X0(18),WM1(6,18),WM2(18,6),BIM(6,18),TS(18),X(18),
     3 AA1(18,18),WMAC(18,6),WMA(18,6),ABM(18,18),
     4 BB1(18,18),BA11(18,18),DBA(18,18),A(6,6),
     5 CC1(18),CC2(18,18),CC3(18,6),CC4(18,18),
     6 DD1(18),DD2(18,6),DD3(18,18),DD4(18),DD5(18,6),DD6(18,18),
     7 E1(18),E2(18,6),E3(18,18),E4(18),E5(18,6),E3I(18,18),
     8 F1(6,18),F3(6,6),DBAI(18,18),BI(6,6),B(6,6)
      DIMENSION F(18),PK(18),PN(18),XR0(18),XR(18),
     1 PC(18),PD(18),PR(18),TTR(18),DX1(18),
     2 TEELAS(6),TEPLAS(6),TTEEE(6),DELTA(6,6),STRESS1(6)
      COMMON TTR0,XR0,TS0,TTR,XR,WMAC,ABM,PK,PN,PC,
     1  PD,PR,X,TS,X0,DR,DX,C1,C1I,WM2,BIM,WMA
C
C
      SSS11=1.0/PROPS(1)
      SSS12=-1.0*PROPS(2)/PROPS(1)
      SSS44=1.0/PROPS(3)
      CCC11=((1.0/(SSS11+2.0*SSS12))+(2.0/(SSS11-SSS12)))/3.0
      CCC12=CCC11-(1.0/(SSS11-SSS12))
      CCC44=1.0/SSS44
      ORN(1)=PROPS(4)
```

```
      ORN(2)=PROPS(5)
      ORN(3)=PROPS(6)
      ALI=ORN(1)
      AMI=ORN(2)
      ANI=ORN(3)
      THETA=0.6
C      NTENS=6
C      DO K1=1,6
C      DSTRAN(K1)=0.0
C      END DO
C      DSTRAN(3)=0.004*0.001
C      DTIME=0.001
C      OPEN(UNIT=1,FILE='ALL.OUT')
C
C
C  ELASTIC STIFFINESS IN THE [001]-[010]-[001] SYSTEM
C  set initial stiffness to zero
C      OPEN (UNIT=1010, FILE='C00.OUT')
       DO K1=1,6
       DO K2=1,6
       C0(K1,K2)=0.0
       END DO
       END DO
       DO K1=1,3
       DO K2=1,3
        C0(K1,K2)=CCC12
       END DO
         C0(K1,K1)=CCC11
       END DO
      DO K1=4,6
       C0(K1,K1)=CCC44
      END DO

 C Elastic stiffness and other basic transformation

       CALL MATCA(ORN,C0,C1)
       CALL MATAB(ALI,AMI,ANI,A,B)
       CALL INVERS(B,BI)
       CALL INVERS(C1,C1I)

 C Recover elastic strain,plastic strain and shift tensor and rotate
 C Use code 1 for (tensor) stress, code 2 for(engineering) strain
 C DROT is the identity tensor if *ORIENTATION is used

 C      CALL ROTSIG(STATEV(     1),DROT,EELAS,2,NDI,NSHR)
 C      CALL ROTSIG(STATEV( NTENS+1),DROT,EPLAS,2,NDI,NSHR)
 C      CALL ROTSIG(STATEV(2*NTENS+1),DROT,ALPHA,1,NDI,NSHR)

 C ++++++
```

```
      END DO
      DO I=4,9
      WN(I,1)=-WN1
      WN(I+3,2)=-WN1
      END DO
      DO I=13,18
      DO J=1,3
      WN(I,J)=0.0
      END DO
      END DO
      END DO
      DO I=1,2
      WN(I+12,3)=1.0
      WN(I+14,2)=1.0
      WN(I+16,1)=1.0
      END DO
C
      DO I=1,18
      DO J=1,3
      WL(I,J)=WL1
      END DO
      END DO
      WL(1,2)=0.0
      WL(1,3)=-WL1
      WL(2,1)=-WL1
      WL(2,3)=0.0
      WL(3,1)=0.0
      WL(3,2)=-WL1
      WL(4,1)=0.0
      WL(4,3)=-WL1
      WL(5,1)=-WL1
      WL(5,2)=-WL1
      WL(5,3)=0.0
      WL(6,2)=0.0
      WL(7,1)=-WL1
      WL(7,2)=0.0
      WL(7,3)=-WL1
      WL(8,2)=-WL1
      WL(8,3)=0.0
      WL(9,1)=0.0
      WL(10,1)=0.0
      WL(10,2)=-WL1
      WL(10,3)=-WL1
      WL(11,3)=0.0
      WL(12,1)=-WL1
      WL(12,2)=0.0
      WL(13,3)=0.0
      WL(14,1)=-WL1
      WL(14,3)=0.0
      WL(15,2)=0.0
      WL(16,1)=-WL1
      WL(16,2)=0.0
      WL(17,1)=0.0
      WL(18,1)=0.0
      WL(18,2)=-WL1
c********
c calculating m* and m-*
      DO II=1,18
       DO I=1,3
```

```
          WM2(II,I)=WN(II,I)*WL(II,I)
          END DO
         WM2(II,6)=WN(II,2)*WL(II,3)+WN(II,3)*WL(II,2)
         WM2(II,5)=WN(II,1)*WL(II,3)+WN(II,3)*WL(II,1)
         WM2(II,4)=WN(II,1)*WL(II,2)+WN(II,2)*WL(II,1)
         END DO
        DO I=1,6
         DO J=1,18
          WM1(I,J)=WM2(J,I)
         END DO
        END DO
c ###########################################################
 C Save stress and plastic strains and STATVE
 C      RRR0=STATEV(NTENS*3+1)
 C      PPP0=STATEV(NTENS*3+2)
 CC       DO K1=1,NTENS
 CC       STRESS(K1)=0.0
 CC       STATEV(K1)=0.0
 CC       STATEV(NTENS+K1)=0.0
 CC       STRAN(K1)=0.0
 CC       END DO
 CC      DO K1=1,18
 CC       STATEV(NTENS*2+K1)=0.0
 CC       STATEV(NTENS*2+18+K1)=0.0
 CC       STATEV(NTENS*2+36+K1)=0.0
 CC       STATEV(NTENS*2+54+K1)=0.0
 CC       STATEV(NTENS*2+72+K1)=0.0
 CC      END DO
 C     WRITE(*,45)
 CC45   FORMAT('OK-ONE')
 C--CALCULATION OF MATRICES:BIM(I,J)
       DO K1=1,6
       DO K2=1,18
       BIM(K1,K2)=0.0
       DO K3=1,6
       BIM(K1,K2)=BIM(K1,K2)+BI(K1,K3)*WM1(K3,K2)
       END DO
       END DO
       END DO
       DO K1=1,18
       DO K2=1,6
       WMA(K1,K2)=0.0
       DO K3=1,6
       WMA(K1,K2)=WMA(K1,K2)+WM2(K1,K3)*A(K3,K2)
       END DO
       END DO
       DO K1=1,18
       DO K2=1,6
       WMAC(K1,K2)=0.0
       DO K3=1,6
       WMAC(K1,K2)=WMAC(K1,K2)+WMA(K1,K3)*C1(K3,K2)
       END DO
       END DO
       END DO
C
CC     DO III=1,1000
CC     DSTRAN(3)=0.004*0.001
```

```
C     STRAN(3)=STRAN(3)+DSTRAN(3)
      DO K1=1,NTENS
       OLDS(K1)=STRESS(K1)
       OLDEL(K1)=STATEV(K1)
       OLDPL(K1)=STATEV(NTENS+K1)
       END DO
      DO K1=1,18
       TTR0(K1)=STATEV(NTENS*2+K1)
       TS0(K1)=STATEV(NTENS*2+18+K1)
       X0(K1)=STATEV(NTENS*2+36+K1)
       XR0(K1)=STATEV(NTENS*2+54+K1)
C      TR0(K1)=STATEV(NTENS*2+72+K1)
      END DO
C-----------------------------
      DO K1=1,NTENS
      DSTRESS(K1)=0.0
      END DO
      DO K2=1,NTENS
      DSTRESS(K1)=DSTRESS(K1)+C1(K1,K2)*DSTRAN(K2)
      END DO
C       END DO
      DO K1=1,NTENS
      STRESS(K1)=OLDS(K1)+DSTRESS(K1)
      END DO
CC       STRESS(3)=OLDS(3)+DSTRESS(3)
CC       WRITE(*,55)STRESS(3)
C--CARRY OUT (TAU-X) AND GRADIENTS IN TAYLOR EXPENSON OF SHERE STRAIN
RATE,
C--BACK STRESS RATE:AA1(I,J),AA2(I,J),BB1(I,J),BB2(I,J)
      DO K1=1,18
       DO K2=1,18
        AA1(K1,K2)=0.0
C        AA2(K1,K2)=0.0
       BB1(K1,K2)=0.0
C        BB2(K1,K2)=0.0
       END DO
      END DO
C-----------------------------------------
CC       WRITE(*,46)
CC46     FORMAT('OK-TWO')
C-----------------------
C CALCULATE SHERE STRESS
      DO K1=1,18
      TS(K1)=0.0
      DO K2=1,6
      DO K3=1,6
      TS(K1)=TS(K1)+WM2(K1,K2)*A(K2,K3)*STRESS(K3)
      END DO
      END DO
CC       WRITE(*,55)TS(K1)
      END DO

C
C-------------------------------
C       DO K1=1,18
C       FF(I)=ABS(TSX(I)-
C-------------
     DO K1=1,18
```

```
C       TSX0=TS0(K1)-X0(K1)
        IF(K1.LE.12)THEN
        PK(K1)=PROPS(7)
        PN(K1)=PROPS(9)
        PR(K1)=PROPS(11)
        PD(K1)=PROPS(13)
        PC(K1)=PROPS(15)
        ELSE
        PK(K1)=PROPS(8)
        PN(K1)=PROPS(10)
        PR(K1)=PROPS(12)
        PD(K1)=PROPS(14)
        PC(K1)=PROPS(16)
        END IF
        END DO
C-------------------------
        DO I=1,18
        TSX0=TS0(I)-X0(I)
        F0=ABS(TSX0)-PR(I)
        IF (F0.LE.0.0)THEN
        FKN0=0.0
        AA1(I,I)=0.0
        BB1(I,I)=0.0
        ELSE
        FKN0=(PN(I)/PK(I))*(F0/PK(I))**(PN(I)-1.)
C       AA1(I,I)=FKN0*TSX0(I)/ABS(TSX0(I))
        AA1(I,I)=FKN0
C       AA2(I,I)=-AA1(I,I)
        BB1(I,I)=PC(I)-PD(I)*X0(I)*TSX0/ABS(TSX0)
C
        END IF
CCC     AA1(I,I)=FKN0*TSX0(I)/ABS(TSX0(I))
C       AA2(I,I)=-AA1(I,I)
CCC     BB1(I,I)=PC(I)-PD(I)*X0(I)*TTR0(I)/ABS(TTR0(I))
C       BB2(I,I)=-PD(I)*ABS(TTR0(I))
C
        END DO
CC      WRITE(*,47)
47      FORMAT('OK-THREE')
C-----------------------------------
        DO K1=1,18
        DO K2=1,18
        BA11(K1,K2)=0.0
C       BA12(K1,K2)=0.0
        DO K3=1,18
        BA11(K1,K2)=BA11(K1,K2)+BB1(K1,K3)*AA1(K3,K2)
C       BA12(K1,K2)=BA12(K1,K2)-BB1(K1,K2)*AA1(K3,K2)
        END DO
        END DO
        END DO
C----------------------
        DO K1=1,18
        DO K2=1,18
C       DELTA(K1,K2)=0.0
        END DO
C       DELTA(K1,K1)=1.0
        END DO
        A1=DTIME*THETA
```

```
      DO K1=1,18
      DO K2=1,18
      DBA(K1,K2)=0.0
      END DO
      DBA(K1,K1)=1.0-A1*(-BA11(K1,K1)-PD(K1)*ABS(TTR0(K1)))
      END DO
      CALL INVERS1(DBA,DBAI)
CC       WRITE(*,50)
50     FORMAT('OK-4')
C-------------------------
C-------------------------------
      DO K1=1,18
      DO K2=1,18
      ABM(K1,K2)=0.0
      DO K3=1,6
      ABM(K1,K2)=ABM(K1,K2)+WMAC(K1,K3)*BIM(K3,K2)
      END DO
      END DO
      END DO
C-------------------------

      DO K1=1,18
      CC1(K1)=0.0
      DO K2=1,18
      CC1(K1)=CC1(K1)+DTIME*DBAI(K1,K2)*XR0(K2)
      END DO
      END DO
      DO K1=1,18
      DO K2=1,18
      CC2(K1,K2)=0.0
      DO K3=1,18
      CC2(K1,K2)=CC2(K1,K2)+DBAI(K1,K3)*BA11(K3,K2)
      END DO
      END DO
      END DO
C-------------------------
      DO K1=1,18
      DO K2=1,6
      CC3(K1,K2)=0.0
      DO K3=1,18
      CC3(K1,K2)=CC3(K1,K2)+CC2(K1,K3)*WMAC(K3,K2)
      END DO
      END DO
      END DO
      DO K1=1,18
      DO K2=1,18
      CC4(K1,K2)=0.0
      DO K3=1,18
      CC4(K1,K2)=CC4(K1,K2)+CC2(K1,K3)*ABM(K3,K2)
      END DO
      END DO
      END DO
C-------------------------
      DO K1=1,18
      DD1(K1)=DTIME*TTR0(K1)
      DO K2=1,6
      DD2(K1,K2)=0.0
      DD5(K1,K2)=0.0
```

```
      DO K3=1,18
      DD2(K1,K2)=DD2(K1,K2)+AA1(K1,K3)*WMAC(K3,K2)
      DD5(K1,K2)=DD5(K1,K2)-AA1(K1,K3)*CC3(K3,K2)
      END DO
      END DO
      END DO
      DO K1=1,18
      DD4(K1)=0.0
      DO K2=1,18
      DD3(K1,K2)=0.0
      DD6(K1,K2)=0.0
      DO K3=1,18
      DD3(K1,K2)=DD3(K1,K2)+AA1(K1,K3)*ABM(K3,K2)
      DD6(K1,K2)=DD6(K1,K2)-AA1(K1,K3)*CC4(K3,K2)
      END DO
      DD4(K1)=DD4(K1)-AA1(K1,K2)*CC1(K2)
      END DO
      END DO
C-------------------------
      DO K1=1,18
      E1(K1)=DD1(K1)+A1*DD4(K1)
       DO K2=1,6
       E2(K1,K2)=A1*DD2(K1,K2)+A1*A1*DD5(K1,K2)
      END DO
      DO K3=1,18
C       E3(K1,K3)=DELTA(K1,K3)+A1*DD3(K1,K3)+A1*A1*DD6(K1,K3)
       E3(K1,K3)=A1*DD3(K1,K3)+A1*A1*DD6(K1,K3)
      END DO
      E3(K1,K1)=1.+A1*DD3(K1,K1)+A1*A1*DD6(K1,K1)
     END DO
      CALL INVERS1(E3,E3I)
CC      WRITE(*,51)
51     FORMAT('OK-5')
      DO K1=1,18
       E4(K1)=0.0
       DO K2=1,18
        E4(K1)=E4(K1)+E3I(K1,K2)*E1(K2)
       END DO
      DO K2=1,6
      E5(K1,K2)=0.0
       DO K3=1,18
        E5(K1,K2)=E5(K1,K2)+E3I(K1,K3)*E2(K3,K2)
       END DO
      END DO
      END DO
C---------------------
      DO K1=1,6
C      F2(K1)=0.0
      DO K2=1,18
       F1(K1,K2)=0.0
        DO K3=1,6
        F1(K1,K2)=F1(K1,K2)+C1(K1,K3)*BIM(K3,K2)
        END DO
C       F2(K1)=F2(K1)+F1(K1,K2)*E4(K2)
      END DO
      END DO
      DO K1=1,6
      DO K2=1,6
```

```
      F3(K1,K2)=0.0
       DO K3=1,18
       F3(K1,K2)=F3(K1,K2)+F1(K1,K3)*E5(K3,K2)
       END DO
      END DO
      END DO
C-----------------------------------
      DO K1=1,18
      TSX=TS(K1)-X0(K1)
CC       WRITE(*,55)TSX
55     FORMAT(F20.10)
C
       F(K1)=ABS(TSX)-PR(K1)
      IF(F(K1).LE.0.0)THEN
       TTR(K1)=0.0
       XR(K1)=0.0
       DR(K1)=0.0
      ELSE

C CARRY OUT ALL VARIABLES INCREMENT
C       DO K1=1,18
      TTR(K1)=(F(K1)/PK(K1))**PN(K1)*(TSX/ABS(TSX))
       DR(K1)=0.0
       DO K2=1,6
       DR(K1)=DR(K1)+E5(K1,K2)*DSTRAN(K2)
       END DO
       DR(K1)=DR(K1)+E4(K1)
      END IF
      END DO
C-----------------------------------
      DO K1=1,18
       DX(K1)=0.0
       DX1(K1)=0.0
       DO K2=1,6
      DX(K1)=DX(K1)+A1*CC3(K1,K2)*DSTRAN(K2)
       END DO
       DO K2=1,18
      DX1(K1)=DX1(K1)+A1*CC4(K1,K2)*DR(K2)
       END DO
      DX(K1)=DX(K1)+CC1(K1)-DX1(K1)
      X(K1)=X0(K1)+DX(K1)
      XR(K1)=PC(K1)*TTR(K1)-PD(K1)*X(K1)*ABS(TTR(K1))
      END DO
      DO K1=1,18
C      X(K1)=X0(K1)+DX(K1)
C      XR(K1)=PC(K1)*TTR(K1)-PD(K1)*X(K1)*ABS(TTR(K1))
C      TR(K1)=TR0(K1)+DR(K1)
      TS(K1)=0.0
      DO K2=1,6
      DO K3=1,6
C      TS(K1)=TS(K1)+WMAC(K1,K2)*STRESS(K2)
      TS(K1)=TS(K1)+WM2(K1,K2)*A(K2,K3)*STRESS(K2)
      END DO
      END DO
      END DO

C----------------------------
      FIT=PROPS(17)
```

```
CC      WRITE(*,57)FIT
CC57    FORMAT(F12.5)
C       FITER=ITER+0.0
        IF(FIT.GT.0.)THEN
C       KIT=PROPS(17)
        ITER=INT(PROPS(17))
C
CC      WRITE(*,56)III,ITER
C       CALL NONLIN(TTR0,XR0,DSTRAN,TS0,TTR,XR,DTIME,THETA,
C     1 X0,WMAC,ABM,PK,PN,PC,PD,PR,ITER)
        CALL NONLIN(DTIME,THETA,ITER,DSTRAN,DDSDDE)
CC      WRITE(*,56)III
CC56    FORMAT(2I5)
C       END IF
        ELSE
        DO K1=1,6
        DO K2=1,6
        DDSDDE(K1,K2)=C1(K1,K2)-F3(K1,K2)
        END DO
        END DO
        END IF
C
        DO K1=1,6
        DEIN(K1)=0.0
        DSTRESS(K1)=0.0
        DO K2=1,18
        DEIN(K1)=DEIN(K1)+BIM(K1,K2)*DR(K2)
        END DO
        END DO
        DO K1=1,6
        DO K2=1,6
        DSTRESS(K1)=DSTRESS(K1)+C1(K1,K2)*(DSTRAN(K2)-DEIN(K2))
        END DO
C       DSTRESS(3)=DSTRESS(3)+C1(3,K1)*(DSTRAN(K1)-DEIN(K1))
        END DO
        DO K1=1,6
        DEE(K1)=0.0
        DO K2=1,6
        DEE(K1)=DEE(K1)+C1I(K1,K2)*DSTRESS(K2)
        END DO
        DSTRAN(K1)=DEE(K1)+DEIN(K1)
        END DO
C-----------------------------------
        DO K1=1,NTENS
        EELAS(K1)=OLDEL(K1)+DEE(K1)
        EPLAS(K1)=OLDPL(K1)+DEIN(K1)
        STRESS(K1)=OLDS(K1)+DSTRESS(K1)
        STRAN(K1)=STRAN(K1)+DSTRAN(K1)
        END DO
C-----------------------------
C-----------------------------------
C STORE ALL VARIABLES
        DO K1=1,NTENS
        STATEV(K1)=EELAS(K1)
        STATEV(K1+NTENS)=EPLAS(K1)
        END DO
        DO K1=1,18
```

```
      STATEV(NTENS*2+K1)=TTR(K1)
      STATEV(NTENS*2+18+K1)=TS(K1)
      STATEV(NTENS*2+36+K1)=X(K1)
      STATEV(NTENS*2+54+K1)=XR(K1)
C       STATEV(NTENS*2+72+K1)=TR(K1)
      END DO
          DO K1=1,NTENS
          DO K2=1,NTENS
          DELTA(K1,K2)=0.0
          END DO
          DELTA(K1,K1)=1.
          END DO
C
          EQE=0.0
          DO K1=1,NTENS
          DO K2=1,NTENS
          EQE=EQE+EPLAS(K1)*DELTA(K1,K2)*EPLAS(K2)
          END DO
          END DO
          EQE=(2./3.)*EQE
          EQE=SQRT(EQE)
          STATEV(109)=EQE
C ***********************************************************
C !!!!
```

```
CC      IF(WMM.EQ.0.0)THEN
CC      WRITE(1,1000)STRESS(3),STRAN(3),STRAN(1)
CC1000   FORMAT(F10.5,2F10.7)
CC      END IF
CC      END DO
      END
C*******************************************************
     SUBROUTINE  MATCA(ORN,C0,C1)
C transformation of elastic and other basic matrix
        IMPLICIT REAL*8 (A-H,L-Z)
      DIMENSION ORN(3), C0(6,6),C1(6,6)
      DIMENSION A(6,6),B(6,6),BT(6,6),AT(6,6),AI(6,6),BI(6,6)

         EXTERNAL   INVERS,MATAB, MATRA, MULMAT
        ALI=ORN(1)
        AMI=ORN(2)
        ANI=ORN(3)
C-----calculats  matrix A and B
       CALL MATAB (ALI,AMI,ANI,A,B)
C------computes transpose matrix AT, BT,
      CALL MATRA  (A,AT)
      CALL MATRA  (B,BT)
C----- computes inverse matrix AI, BI
      CALL INVERS (A, AI)
      CALL INVERS (B, BI)
C       CALL INVERS (ZM0,ZM0I)
C------- computes material matrix
      CALL MULMAT (AI,C0,B,C1)
       RETURN
       END
C .....
      SUBROUTINE  MATAB (ALI, AMI, ANI, A, B)
C-------This subroutine calculates MATRIX Aij and Bij

       IMPLICIT REAL*8 (A-H,L-Z)
       DIMENSION  A(6,6), B(6,6)
          DD1=(ALI*ALI+AMI*AMI+ANI*ANI)
          DD2=(AMI*AMI+ANI*ANI)
          DD1D=(DD1)**0.5
          DD2D=(DD2)**0.5
          A(1,1)=DD2*DD2
          A(1,2)=0.0
          A(1,3)=ALI*ALI*DD2
          A(1,4)=0.0
          A(1,5)=2.0*ALI*DD2*DD2D
          A(1,6)=0.0
          A(2,1)=ALI*ALI*AMI*AMI
          A(2,2)=ANI*ANI*DD1
          A(2,3)=AMI*AMI*DD2
          A(2,4)=-2.0*ALI*AMI*ANI*DD1D
          A(2,5)=-2.0*ALI*AMI*AMI*DD2D
          A(2,6)=2.0*AMI*ANI*DD1D*DD2D
          A(3,1)=ALI*ALI*ANI*ANI
          A(3,2)=AMI*AMI*DD1
          A(3,3)=ANI*ANI*DD2
          A(3,4)=2.0*ALI*AMI*ANI*DD1D
          A(3,5)=-2.0*ALI*ANI*ANI*DD2D
```

```
A(3,6)=-2.0*AMI*ANI*DD1D*DD2D
A(4,1)=-1.0*ALI*AMI*DD2
A(4,2)=0.0
A(4,3)=ALI*AMI*DD2
A(4,4)=ANI*DD2*DD1D
A(4,5)=(DD2-ALI*ALI)*AMI*DD2D
A(4,6)=ALI*ANI*DD1D*DD2D
A(5,1)=-1.0*ALI*ANI*DD2
A(5,2)=0.0
A(5,3)=ALI*ANI*DD2
A(5,4)=-1.0*AMI*DD2*DD1D
A(5,5)=(DD2-ALI*ALI)*ANI*DD2D
A(5,6)=-1.0*ALI*AMI*DD1D*DD2D
A(6,1)=ALI*ALI*AMI*ANI
A(6,2)=-AMI*ANI*DD1
A(6,3)=AMI*ANI*DD2
A(6,4)=(AMI*AMI-ANI*ANI)*ALI*DD1D
A(6,5)=-2.0*ALI*AMI*ANI*DD2D
A(6,6)=(ANI*ANI-AMI*AMI)*DD1D*DD2D
B(1,1)=DD2*DD2
B(1,2)=0.0
B(1,3)=ALI*ALI*DD2
B(1,4)=0.0
B(1,5)=ALI*DD2*DD2D
B(1,6)=0.0
B(2,1)=ALI*ALI*AMI*AMI
B(2,2)=ANI*ANI*DD1
B(2,3)=AMI*AMI*DD2
B(2,4)=-1.0*ALI*AMI*ANI*DD1D
B(2,5)=-1.0*ALI*AMI*AMI*DD2D
B(2,6)=AMI*ANI*DD1D*DD2D
B(3,1)=ALI*ALI*ANI*ANI
B(3,2)=AMI*AMI*DD1
B(3,3)=ANI*ANI*DD2
B(3,4)=ALI*AMI*ANI*DD1D
B(3,5)=-1.0*ALI*ANI*ANI*DD2D
B(3,6)=-1.0*AMI*ANI*DD1D*DD2D
B(4,1)=-2.0*ALI*AMI*DD2
B(4,2)=0.0
B(4,3)=2.0*ALI*AMI*DD2
B(4,4)=ANI*DD2*DD1D
B(4,5)=(DD2-ALI*ALI)*AMI*DD2D
B(4,6)=ALI*ANI*DD1D*DD2D
B(5,1)=-2.0*ALI*ANI*DD2
B(5,2)=0.0
B(5,3)=2.0*ALI*ANI*DD2
B(5,4)=-1.0*AMI*DD2*DD1D
B(5,5)=(DD2-ALI*ALI)*ANI*DD2D
B(5,6)=-1.0*ALI*AMI*DD1D*DD2D
B(6,1)=2.0*ALI*ALI*AMI*ANI
B(6,2)=-2.0*AMI*ANI*DD1
B(6,3)=2.0*AMI*ANI*DD2
B(6,4)=(AMI*AMI-ANI*ANI)*ALI*DD1D
B(6,5)=-2.0*ALI*AMI*ANI*DD2D
B(6,6)=(ANI*ANI-AMI*AMI)*DD1D*DD2D

DO I=1,6
DO J=1,6
```

```
      A(I,J)=A(I,J)/(DD1*DD2)
      B(I,J)=B(I,J)/(DD1*DD2)
    END DO
    END DO

    RETURN
    END

C.....
      SUBROUTINE MATRA ( AA, AAT)
C------ this is for matrix transpose i.e AATij=AAji
      IMPLICIT REAL*8 (A-H, L-Z)
    DIMENSION AA(6,6), AAT(6,6)
    DO  I=1,6
    DO  J=1,6
      AAT(I,J)=AA(J,I)
     END DO
      END DO
       RETURN
        END

C .....
      SUBROUTINE MULMAT (A,B,C,D)
C------this subroutine is for three matrix multplication A.B.C=D
       IMPLICIT REAL*8 (A-H, L-Z)
     DIMENSION A(6,6), B(6,6), C(6,6), D(6,6), AB(6,6)
     DO I=1, 6
     DO J=1,6
      AB(I,J)=0.0
    DO K=1,6
      AB(I,J)=AB(I,J)+A(I,K)*B(K,J)
     END DO
     END DO
      END DO
    DO I=1, 6
    DO J=1,6
      D(I,J)=0.0
    DO K=1,6
      D(I,J)=D(I,J)+AB(I,K)*C(K,J)
      END DO
       END DO
      END DO
     RETURN
     END

C .....
      SUBROUTINE  INVERS (A, AI)
C ===== this subroutine computes the INVERSE of a Matrix AI=A-1
       IMPLICIT REAL*8 (A-H, L-Z)
       DIMENSION  A(6,6),AI(6,6), AB(6, 12)

C------ form  AB = ( A II )
      DO  I=1, 6
      DO  J=1,12
       IF ((I+6).EQ.J) THEN
          AB(I,J)=1.0
       ELSE
```

```
      AB(I,J)=0.0
    END IF
     END DO
    END DO
DO   I=1,6
DO  J=1,6
   AB(I,J)=A(I,J)
  END DO
   END DO
    KM = 6
    KN = 12
DO 30, K = 1, KM
      DO 40, KQ = K, KM
       IF (ABS(AB(KQ,K)).GT.1E-18)  GO TO 110
40     CONTINUE
C         WRITE(*,45)
45      FORMAT(' NO SOLUTION')
      GOTO 290
110   DO 50, KP = 1, KN
          S = AB(K, KP)
          AB(K, KP) = AB(KQ, KP)
          AB(KQ, KP) = S
50    CONTINUE
          T = 1 / AB(K, K)
      DO 60, KR = 1, KN
          AB(K, KR) = T * AB(K, KR)
60    CONTINUE
      DO 70,  I = 1,KM
          Y = -AB(I, K)
       IF (I.EQ.K)  GO TO 70
      DO 80, J = 1, KN
      AB(I, J) = AB(I, J) + Y * AB(K, J)
80     CONTINUE
70     CONTINUE
30     CONTINUE

C-----seperate solution AI from AB
      DO 901, I=1,6
      DO 902, J=7,12
          JJ=J-6
          AI(I,JJ)=AB(I,J)
902   CONTINUE
901   CONTINUE
290     RETURN
       END

      SUBROUTINE  INVERS1 (A, AI)
C ===== this subroutine computes the INVERSE of a Matrix AI=A-1
       IMPLICIT REAL*8 (A-H, L-Z)
       DIMENSION  A(18,18),AI(18,18), AB(18, 36)
C
C------ form  AB = ( A II )
      DO  I=1, 18
      DO  J=1,36
       IF ((I+18).EQ.J) THEN
          AB(I,J)=1.0
       ELSE
          AB(I,J)=0.0
```

```
      END IF
        END DO
       END DO
    DO   I=1,18
    DO  J=1,18
      AB(I,J)=A(I,J)
     END DO
      END DO
       M = 18
       N = 36
    DO 30, K = 1, M
    DO 40, Q = K, M
     IF (ABS(AB(Q,K)).GT.1E-18)  GO TO 110
    40     CONTINUE
    C          WRITE(*,45)
    45       FORMAT(' NO SOLUTION')
           GOTO 290
    110   DO 50, P = 1, N
              S = AB(K, P)
              AB(K, P) = AB(Q, P)
              AB(Q, P) = S
    50    CONTINUE
              T = 1 / AB(K, K)
          DO 60, R = 1, N
              AB(K, R) = T * AB(K, R)
    60    CONTINUE
          DO 70,  I = 1,M
              Y = -AB(I, K)
           IF (I.EQ.K)  GO TO 70
          DO 80, J = 1, N
          AB(I, J) = AB(I, J) + Y * AB(K, J)
    80     CONTINUE
    70     CONTINUE
    30     CONTINUE

    C-----seperate solution AI from AB
          DO 901, I=1,18
          DO 902, J=19,36
              JJ=J-18
              AI(I,JJ)=AB(I,J)
    902   CONTINUE
    901   CONTINUE
    290     RETURN
          END
    C*****************************************
          SUBROUTINE NONLIN(DTIME,THETA,KTER,DSTRAN,DDSDDE)
    C       SUBROUTINE NONLIN(TTR0,XR0,DSTRAN,TS0,TTR,XR,DTIME,THETA,
    C     1  X0,WMAC,ABM,PK,PN,PC,PD,PR,ITER)
    C
          IMPLICIT REAL*8 (A-H,L-Z)
          DIMENSION  TTR0(18),XR0(18),DSTRAN(6),TS0(18),TTR(18),
         1  XR(18),WMAC(18,6),ABM(18,18),PK(18),PN(18),PC(18),PD(18),
         2  PR(18),F(18),DXX(6,18),DRR(6,18),ERO1(18),ERO2(18),
         3  DTS(18),DR(18),DX(18),X(18),TS(18),X0(18),DDSDDE(6,6),
         4  WMA(18,6),CBIM(6,18),CBIM1(6,6),CBIM11(6,6),C1(6,6),
         5  C11(6,6),A2(18),A3(18),A4(18),A5(18),A6(18),
         6  WM2(18,6),BIM(6,18)
           COMMON TTR0,XR0,TS0,TTR,XR,WMAC,ABM,PK,PN,PC,
```

```
     1  PD,PR,X,TS,X0,DR,DX,C1,C11,WM2,BIM,WMA
C
C       OPEN(UNIT=22,FILE='FITER.OUT')
CC        WRITE(*,552)999,KTER
552     FORMAT(2I5)
C       KITER=INT(ITER)
C       KIT=INT(FITER)
C       KIT=FITER
        DO K1=1,KTER
CC        OPEN(UNIT=22,FILE='FITER.OUT')
CC        WRITE(*,553)K1
CC553     FORMAT(I3)
          DO K2=1,18
          DR(K2)=DTIME*((1.-THETA)*TTR0(K2)+THETA*TTR(K2))
          DX(K2)=DTIME*((1.-THETA)*XR0(K2)+THETA*XR(K2))
          END DO
          DO K2=1,18
          DTS(K2)=0.0
           DO K3=1,6
           DTS(K2)=DTS(K2)+WMAC(K2,K3)*DSTRAN(K3)
           END DO
          DO K3=1,18
          DTS(K2)=DTS(K2)-ABM(K2,K3)*DR(K3)
          END DO
         END DO
         DO K2=1,18
         X(K2)=X0(K2)+DX(K2)
         TS(K2)=TS0(K2)+DTS(K2)
         END DO
C-------------------------
          DO K2=1,18
          TSX=TS(K2)-X(K2)
          F(K2)=ABS(TSX)-PR(K2)
          IF(F(K2).LT.0.0)THEN
          TTR(K2)=0.0
          XR(K2)=0.0
          ELSE
CC          WRITE(*,554)K2,TSX
          TTR(K2)=(F(K2)/PK(K2))**PN(K2)*TSX/ABS(TSX)
          XR(K2)=PC(K2)*TTR(K2)-PD(K2)*X(K2)*ABS(TTR(K2))
          END IF
          END DO
CC        WRITE(*,553)K1
C-----------------------------
          DO K2=1,18
          DXX(K1,K2)=DX(K2)
          DRR(K1,K2)=DR(K2)
          END DO
          FK1=REAL(K1)
          IF(FK1.GT.1.)THEN
          KK1=K1-1
          ERO1(K1)=0.0
          ERO2(K1)=0.0
          DO K2=1,18
          DDR12=DRR(K1,K2)-DRR(KK1,K2)
          DDX12=DXX(K1,K2)-DXX(KK1,K2)
          ERO1(K1)=ERO1(K1)+ABS(DDR12)
          ERO2(K1)=ERO2(K1)+ABS(DDX12)
```

```
      END DO
CC       WRITE(*,554)K1,ERO1(K1),ERO2(K1)
      IF(ERO1(K1).LT.1.E-10.AND.ERO2(K1).LT.1.E-8)THEN
      GO TO 555
      END IF
      END IF
C-----------------------------------
CC       WRITE(22,554)K1,ERO1(K1),ERO2(K1)
554    FORMAT(I2,2F20.12)
      END DO
C-----------------------------------------
555       A1=DTIME*THETA
          DO K1=1,18
          F(K1)=ABS(TS(K1)-X(K1))-PR(K1)
          IF(F(K1).LE.0.)THEN
          A2(K1)=0.0
          A3(K1)=1.
          A4(K1)=PC(K1)
          ELSE
          A2(K1)=A1*PN(K1)/PK(K1)*(F(K1)/PK(K1))**(PN(K1)-1.)
C         WRITE(*,554)K1
          A3(K1)=1.+A1*PD(K1)*ABS(TTR(K1))
          A4(K1)=PC(K1)-PD(K1)*X(K1)*(TS(K1)-X(K1))/ABS(TS(K1)-X(K1))
          END IF
CC        WRITE(*,554)88
          A5(K1)=A2(K1)*A4(K1)/A3(K1)
          A6(K1)=A2(K1)/(1.+A5(K1))
          END DO
C         DO K1=1,18
C         DO K2=1,6
C         WMA(K1,K2)=0.0
C         DO K3=1,6
C         WMA(K1,K2)=WMA(K1,K2)+WM2(K1,K3)*A(K3,K2)
C         END DO
C         END DO
C         END DO
C
          DO K1=1,6
          DO K2=1,18
          CBIM(K1,K2)=0.0
          DO K3=1,6
          CBIM(K1,K2)=CBIM(K1,K2)+C1(K1,K3)*BIM(K3,K2)
          END DO
          CBIM(K1,K2)=CBIM(K1,K2)*A6(K2)
          END DO
          END DO
C
          DO K1=1,6
          DO K2=1,6
          CBIM1(K1,K2)=0.0
          DO K3=1,18
          CBIM1(K1,K2)=CBIM1(K1,K2)+CBIM(K1,K3)*WMA(K3,K2)
          END DO
          END DO
          CBIM1(K1,K1)=1.+CBIM1(K1,K1)
          END DO
          CALL INVERS(CBIM1,CBIM11)
C
```

```
      DO K1=1,6
      DO K2=1,6
      DDSDDE(K1,K2)=0.0
      DO K3=1,6
      DDSDDE(K1,K2)=DDSDDE(K1,K2)+CBIM1I(K1,K3)*C1(K3,K2)
      END DO
      END DO
      END DO
     RETURN
      END
C**********************************
      SUBROUTINE TRANS1(ALI1,AMI1,ANI1,STRAN,TTSTRAN)

IMPLICIT REAL*8 (A-H,O-Z)

DIMENSION Q(6,6),QT(6,6),E(6,6),ET(6,6),ETT(6,6)
DIMENSION STRAN(6),TTSTRAN(6)

      Q(1,1)=ALI1
      Q(1,2)=AMI1
      Q(2,1)=-AMI1
      Q(2,2)=ALI1
      Q(3,3)=1.0
      Q(1,3)=0.0
      Q(2,3)=0.0
      Q(3,1)=0.0
      Q(3,2)=0.0

      DO  K1=1,3
      DO  K2=1,3
        QT(K1,K2)=Q(K2,K1)
      END DO
      END DO

      E(1,1)=STRAN(1)
      E(1,2)=0.5*STRAN(4)
      E(2,1)=E(1,2)
      E(2,2)=STRAN(2)
      E(3,3)=STRAN(3)
      E(1,3)=0.5*STRAN(5)
      E(2,3)=0.5*STRAN(6)
      E(3,1)=E(1,3)
      E(3,2)=E(2,3)

DO 1200 II=1,3
      DO 1300 JJ=1,3
       ET(II,JJ)=0.0
      DO 1400 KK=1,3
C transformation of stress to crystallographic axes system
       ET(II,JJ)=ET(II,JJ)+E(II,KK)*QT(KK,JJ)
1400     CONTINUE
1300     CONTINUE
1200     CONTINUE

      DO 1600 II=1,3
      DO 1700 JJ=1,3
       ETT(II,JJ)=0.0
      DO 1800  KK=1,3
```

```
      ETT(II,JJ)=ETT(II,JJ)+Q(II,KK)*ET(KK,JJ)
1800     CONTINUE
1700     CONTINUE
1600     CONTINUE

         TTSTRAN(1)=ETT(1,1)
         TTSTRAN(2)=ETT(2,2)
         TTSTRAN(3)=ETT(3,3)
         TTSTRAN(4)=2.0*ETT(1,2)
         TTSTRAN(5)=2.0*ETT(1,3)
         TTSTRAN(6)=2.0*ETT(2,3)

       RETURN
        END
```

```
**********************************NUMAT.INP*************************************
**@@@@@@@@@@@@@@@@@@@@@@@@@@@@@@@@@@@@@@@@@@@@@@@@@@@@@@@@@@@@@@@@@@@@@@@@@@@@
**@Program developed in:                                                      @
**@Engineering Materials and Structural Integrity Group                       @
**@March, 1998 By Songlin Han                                                 @
**@@@@@@@@@@@@@@@@@@@@@@@@@@@@@@@@@@@@@@@@@@@@@@@@@@@@@@@@@@@@@@@@@@@@@@@@@@@@

** one element test: for cubic SX using Chaboche model
**  (via 'UMAT' procedure)
* HEADING
1-EL ELASTICITY OF CUBIC SX UNDER UNIAXIAL LOAD
*NODE, NSET=NODEALL
1,  0.,   0.,   0.
2,  0.,  10.,   0.
3,  0.,  10.,  10.
4,  0.,   0.,  10.
5,  10.,  0.,   0.
6,  10.,  10.,  0.
7,  10.,  10.,  10.
8,  10.,  0.,  10.
9,  0.,  5.,   0.
10,  0.,  10.,   5.
11,  0.,  5.,  10.
12,  0.,  0.,   5.
13, 10.,  5.,   0.
14, 10.,  10.,  5.
15, 10.,  5.,  10.
16, 10.,  0.,   5.
17,  5.,  0.,   0.
18,  5.,  10.,   0.
19,  5.,  10.,  10.
20,  5.,  0.,   10.
**
*ELEMENT, TYPE=C3D20
1,1,5,6,2,4,8,7,3,17,13,18,9,20,15,19,11,12,16,14,10
*ELSET, ELSET=ONE
1
*BOUNDARY
1, PINNED
2,3
2,1
5,3
6,3
9,3
17,3
13,3
18,3
**
*SOLID SECTION, ELSET=ONE, MATERIAL=CRYSTAL
*MATERIAL, NAME=CRYSTAL
***USER MATERIAL, CONSTANTS=17
*USER MATERIAL, UNSYMM, CONSTANTS=18
0.8606E5,0.3883,0.8811E5,1.0,1.0,1.0,1700.0,3.6,
**1.0, 2.39,3.1E5,5.05E4,600.0,700.0,50.0,60.0,
1.0, 2.39, 3.1E5, 5.05E4, 600.0, 700.,0.,0.,
110.0, 0.0
** ELASTIC MODULUS, POISSON RATIO, SHEAR MODEULS
```

```
** ORIENTAION [L,M,L]
*DEPVAR
34
*NSET, NSET=LI1
8,19,7,3,11,4,20,15
*AMPLITUDE, NAME=PULL1
0.0, 0.0, 0.4,0.16
*AMPLITUDE, NAME=PULL2
0.0, 0.16, 0.4, 0.32
*AMPLITUDE, NAME=PULL3
0.0, 0.32, 0.6, 0.56
*RESTART, WRITE, FREQUENCY=10
 *STEP,INC=400
 PULL
 *STATIC
 0.02, 0.4, 0.0001, 0.02
 *BOUNDARY, AMPLITUDE=PULL1
 LI1,3, , 0.1
 *NODE PRINT, SUMMARY=NO,FREQUENCY=1
 U1,U2,U3,RF1,RF2,RF3
 *EL PRINT, POSITION=CENTROIDAL,SUMMARY=NO,FREQUENCY=1
 S
 E
 *EL PRINT,POSITION=CENTROIDAL, SUMMARY=NO,FREQUENCY=1
 SDV
 ***EL FILE,POSITION=CENTROIDAL, FREQUENCY=1
 **S
 **E
 *MONITOR, NODE=14, DOF=3
 *END STEP
 **
 *STEP,INC=700
 PULL
 *STATIC
 .001, 0.4, 0.000001, 0.01
 *BOUNDARY, AMPLITUDE=PULL2
 LI1,3, ,0.1
 *NODE PRINT, SUMMARY=NO,FREQUENCY=50
 U1,U2,U3,RF1,RF2,RF3
 *EL PRINT, POSITION=CENTROIDAL,SUMMARY=NO,FREQUENCY=50
 S
 E
 *EL PRINT, POSITION=CENTROIDAL,SUMMARY=NO,FREQUENCY=50
 SDV
 **S
 **E
 *MONITOR, NODE=14, DOF=3
 *END STEP
 *STEP,INC=1000
 PULL
 *STATIC
 0.001,0.6, 0.00001,0.01
 *BOUNDARY, AMPLITUDE=PULL3
 LI1, 3, , 0.1
 *NODE PRINT, SUMMARY=NO, FREQUENCY=100
 U1,U2,U3,RF1,RF2,RF3
 *EL PRINT, SUMMARY=NO, FREQUENCY=100
 S
```

```
E
*EL PRINT, POSITION=CENTROIDAL, SUMMARY=NO, FREQUENCY=100
SDV
**S
**E
*MONITOR, NODE=14, DOF=3
*END STEP
*USER SUBROUTINE
```

Table 3.1 Temperature Dependent Elastic Constants for SRR99 Single Crystal Alloy

Temperature ^{o}C	25	450	750	850	950
E (Mpa)	140750	123160	103030	95571	86000
G (Mpa)	137660	129670	119210	105030	88100
ν	0.3569	0.3612	0.3712	0.3805	0.388

Table 3.2. Saturated Stresses at Various Strain Rates

$\dot{\varepsilon}^{T}$ (1/s)	σ (MPa) [001]	σ (MPa) [111]
0.00004	726.67	350.52
0.0004	825.33	432.99
0.001	880.0	483.51
0.004	993.33	588.66
0.01	1100.0	687.63
0.04	1317.33	890.72

Table 3.3 Material Constants for the Phenomenological Model

Parameters	K* $MPa.s^{-1}$	n	M_{11}-M_{12}	M_{44}	N_{11}-N_{12} MPa	N_{44} MPa
	1696.8	3.604	1.0	2.385	309936.0	50384.3
Parameters	Q_{11}-Q_{12}	Q_{44}	k MPa	W MPa	b	
	600.0	699.62	110.20	61.3	50.9	

Table 3.4 Material Constants for the Crystallographic Model

Parameters	K_o (MPa)	n_o	k_o (MPa)	c_o (MPa)	d_o	b_o	q_o (MPa)
Octahedral slip	964.17	3.60	44.91	413333.3	1959.59	163.30	24000.1
Parameters	K_c (MPa)	n_c	k_c (Mpa)	c_c (MPa)	d_c	b_c	q_c (MPa)
Cubic slip	787.45	3.60	47.44	67333.0	905.59	42.52	1143.21

Table 3.5 Coefficients for Temperature Dependent Elastic Constants

a_1	-7.039×10^{-6}	a_2	5.4628×10^{-11}	a_3	-2.1886×10^{-4}	a_4	3.934×10^{-10}
b_1	-0.025	b_2	-2.9043×10^{-8}	b_3	0.2407	b_4	-5.6964×10^{-7}
c_1	-28.155	c_2	1.1731×10^{-5}	c_3	-85.7957	c_4	6.3035×10^{-4}
d_1	141480	d_2	0.3567	d_3	139640	d_4	1.0934

Table 6.1 Material Constants for the Crystallographic Model Using Simplified Procedure

Parameters	K_o (MPa)	n_o	k_o (MPa)	c_o (MPa)	d_o	b_o	q_o (MPa)
Octahedral slip	964.17	3.60	44.91	413333.3	1959.59	163.30	24000.1
Parameters	K_c (MPa)	n_c	k_c (MPa)	c_c (MPa)	d_c	b_c	q_c (MPa)
Cubic slip	792.72	3.60	53.08	67456.3	1020.58	45.73	1182.95

Table 6.2. Crystal Orientations Close to [001] - Misorientation Effect

(with θ =10 degree from [001] orientation)

Crystal Orientation	θ (degree)	ρ (degree)	l	m	n
001	0	0	0.0	0.0	1.0
b	10	0	0.176	0.0	1.0
c	10	15	0.174	0.031	1.0
d	10	30	0.153	0.088	1.0
e	10	45	0.125	0.125	1.0

Table.6.3 Orientation Dependent Stress and Strain Response for Specimens around (10 degree away from) [001] Orientation

Orientation	Normalised Transverse and Shear Strain ($\varepsilon_{33} = 2.5\%$)					Stress
	$\frac{\varepsilon_{11}}{\varepsilon_{33}}$	$\frac{\varepsilon_{22}}{\varepsilon_{33}}$	$\frac{\varepsilon_{13}}{\varepsilon_{33}}$	$\frac{\varepsilon_{23}}{\varepsilon_{33}}$	$\frac{\varepsilon_{12}}{\varepsilon_{33}}$	σ_{33} (MPa)
[001]	-0.445	-0.445	0.0	0.0	0.0	1046.31
b (θ=10, ρ=0)	-0.454	-0.444	0.0	0.0	0.056	978.63
c (θ=10, ρ=15)	-0.454	-0.444	-0.002	0.010	0.056	978.08
d (θ=10, ρ=30)	-0.452	-0.446	-0.004	0.029	0.050	977.89
e (θ=10, ρ=45)	-0.449	-0.449	-0.005	0.041	0.041	977.54

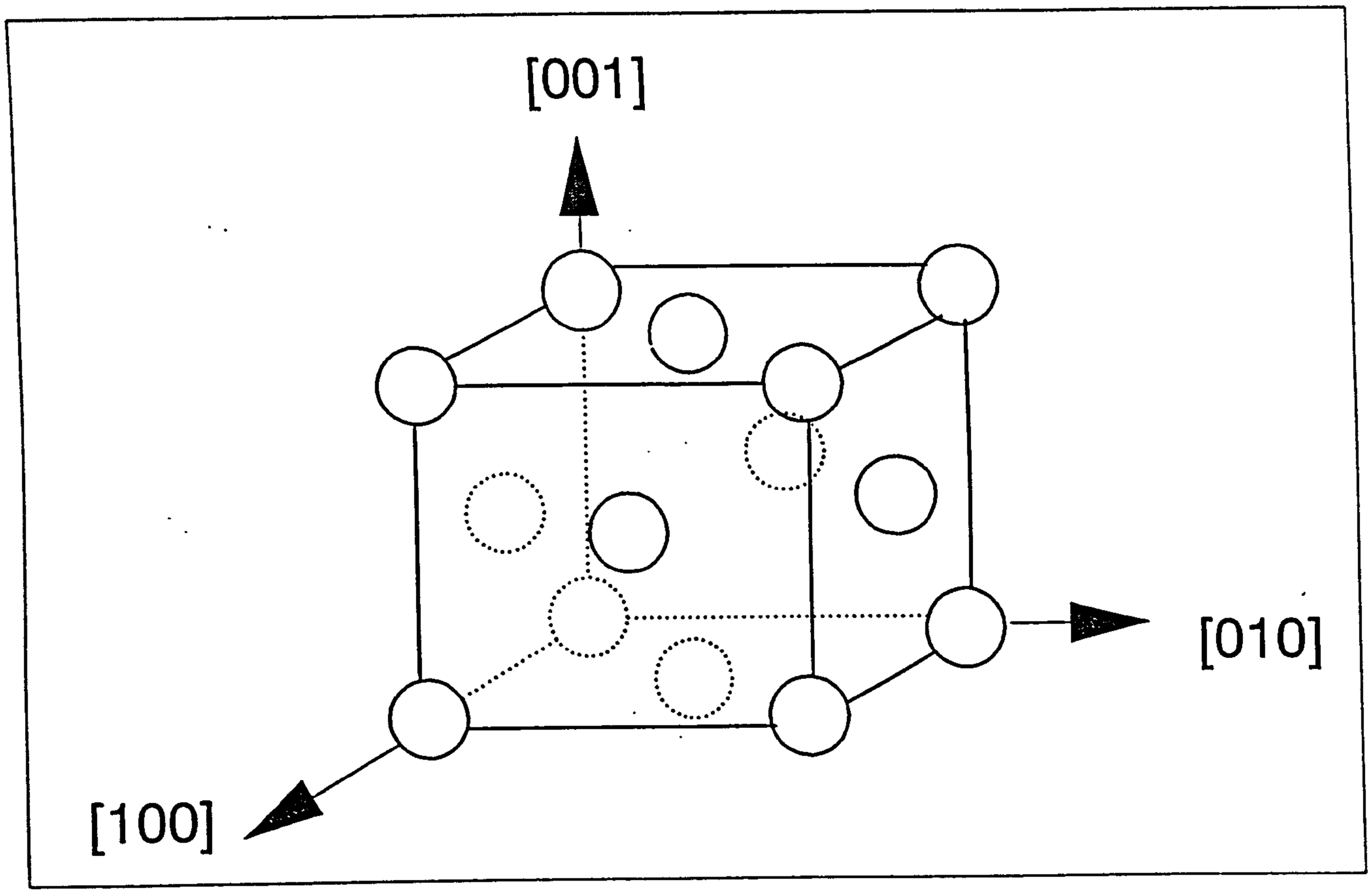

Fig.2.1. The Unit Cell of the Basic Structure of a Single Crystal Nickel Base Superalloy

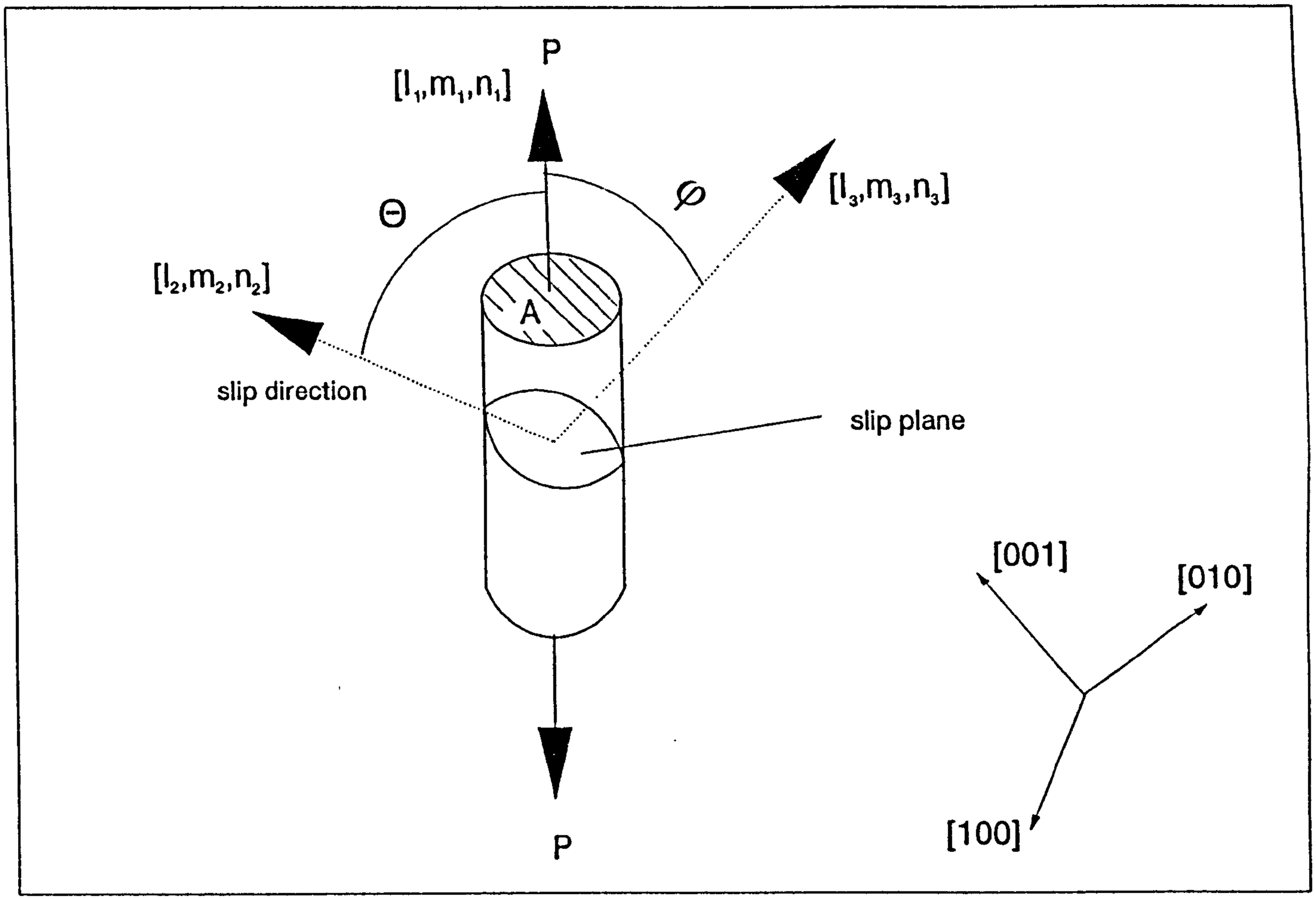

Fig.2.2. Diagram for Calculating Critical Resolved Shear Stress

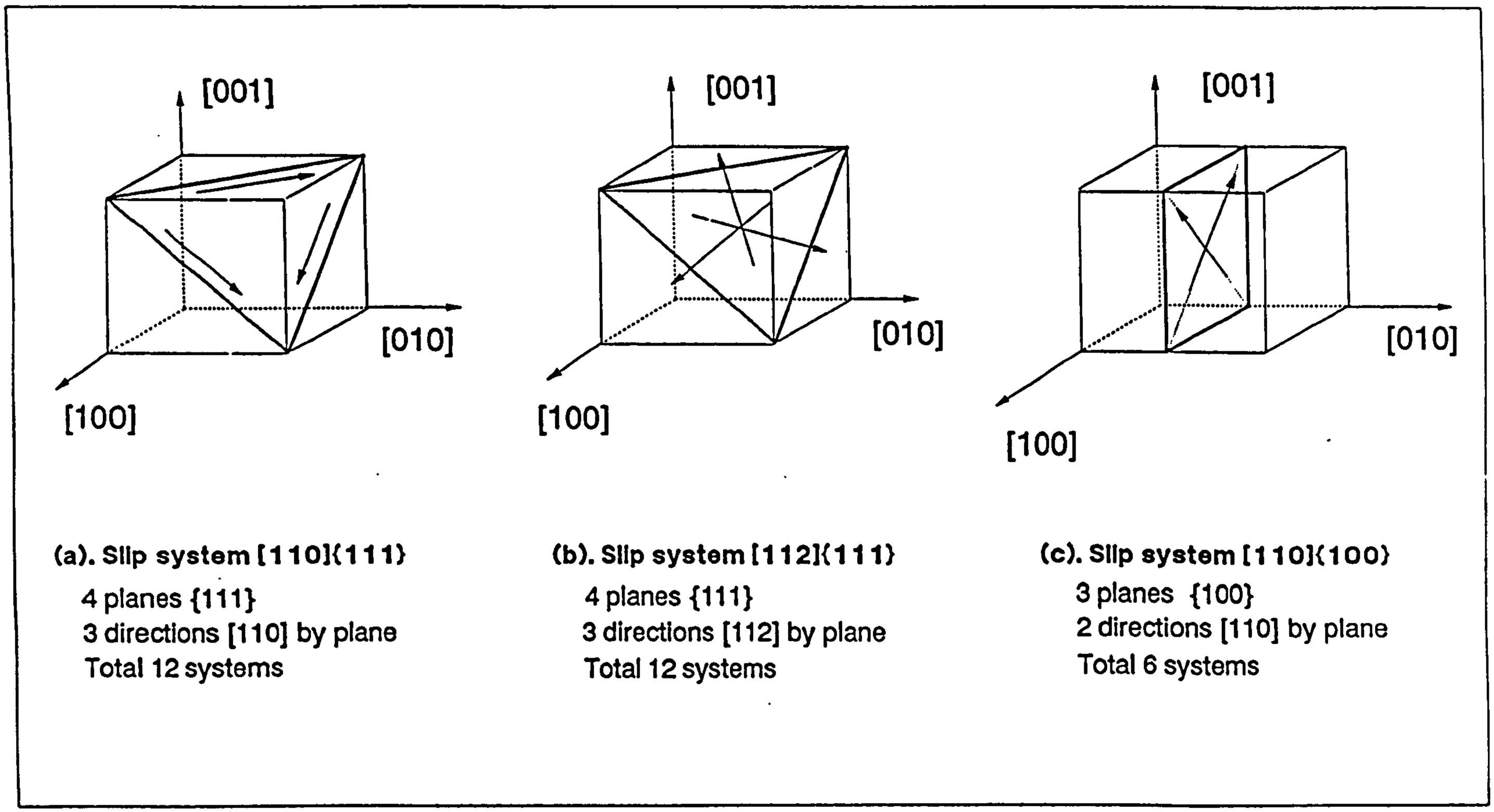

Fig.2.3 Schematic of the Slip Systems in Single Crystal Nickel Base Superalloys

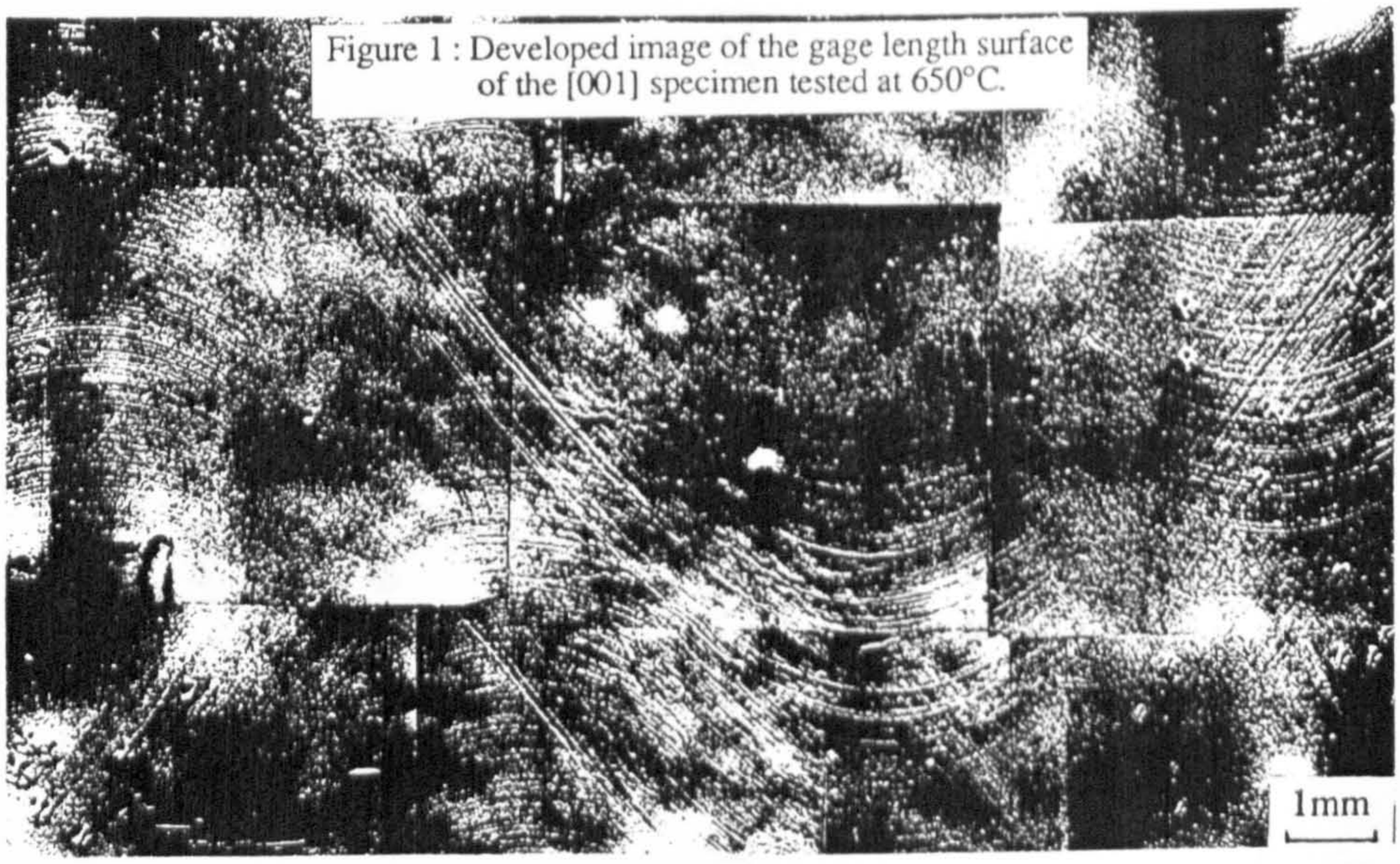

Fig.2.4 Slip Bands Observed for [001] Specimen Tested at 650°C
(After Hanriot et al [1991])

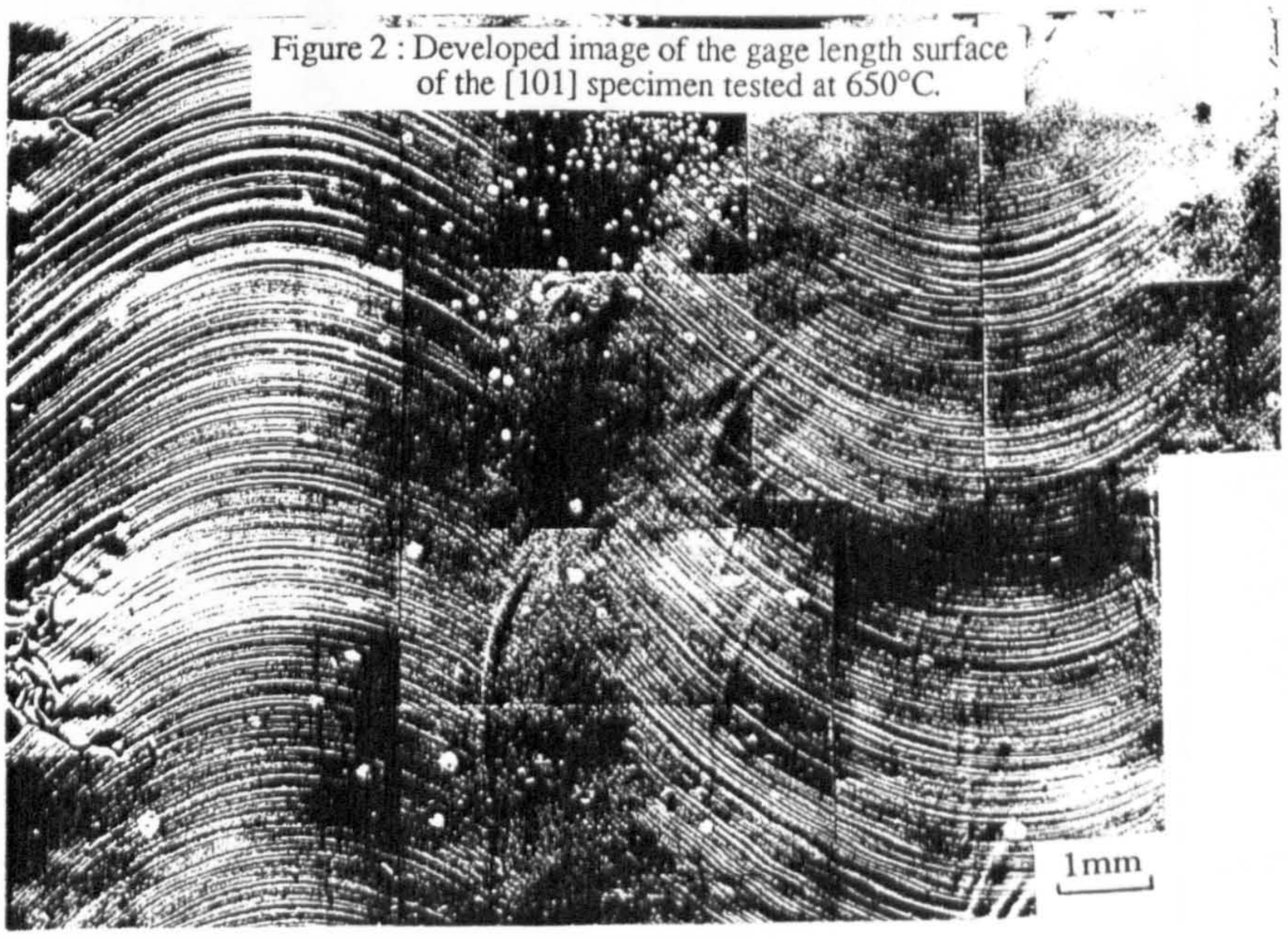

Fig.2.5 Slip Bands Observed for [101] Specimen Tested at 650°C
(After Hanriot et al [1991])

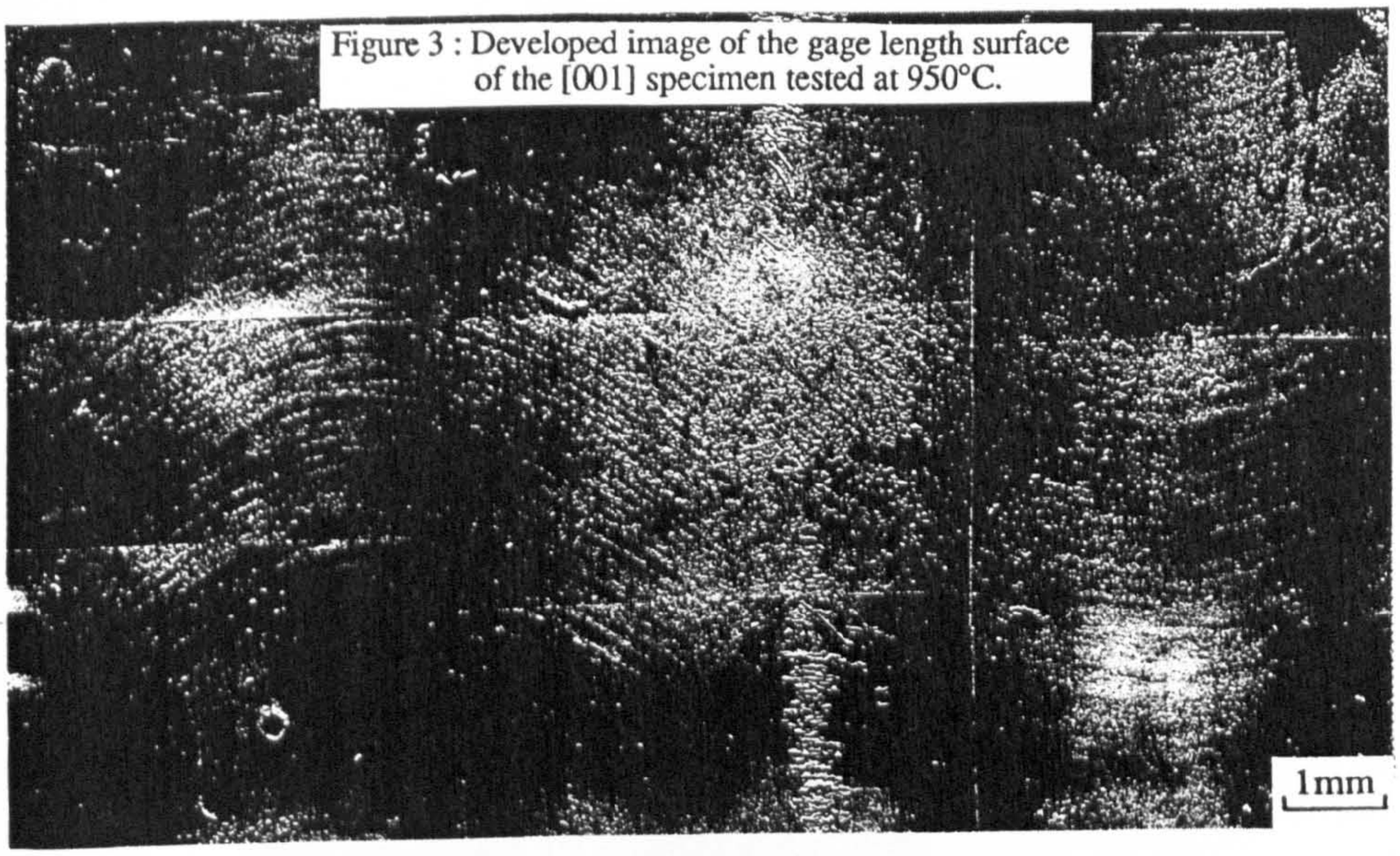

Fig.2.6 Slip Bands Observed for [001] Specimen Tested at 950°C
(After Hanriot et al [1991])

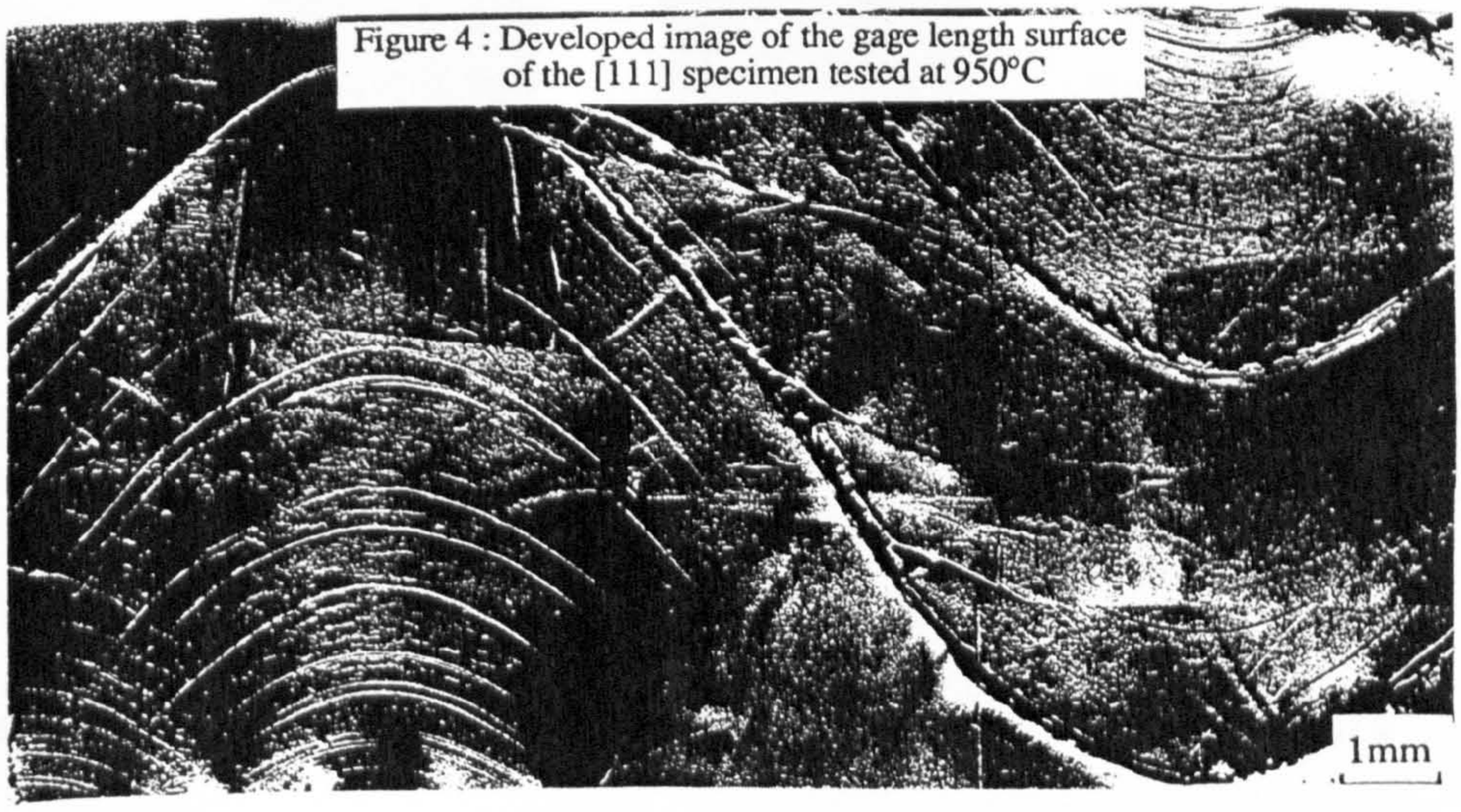

Fig.2.7 Slip Bands Observed for [101] Specimen Tested at 950°C
(After Hanriot et al [1991])

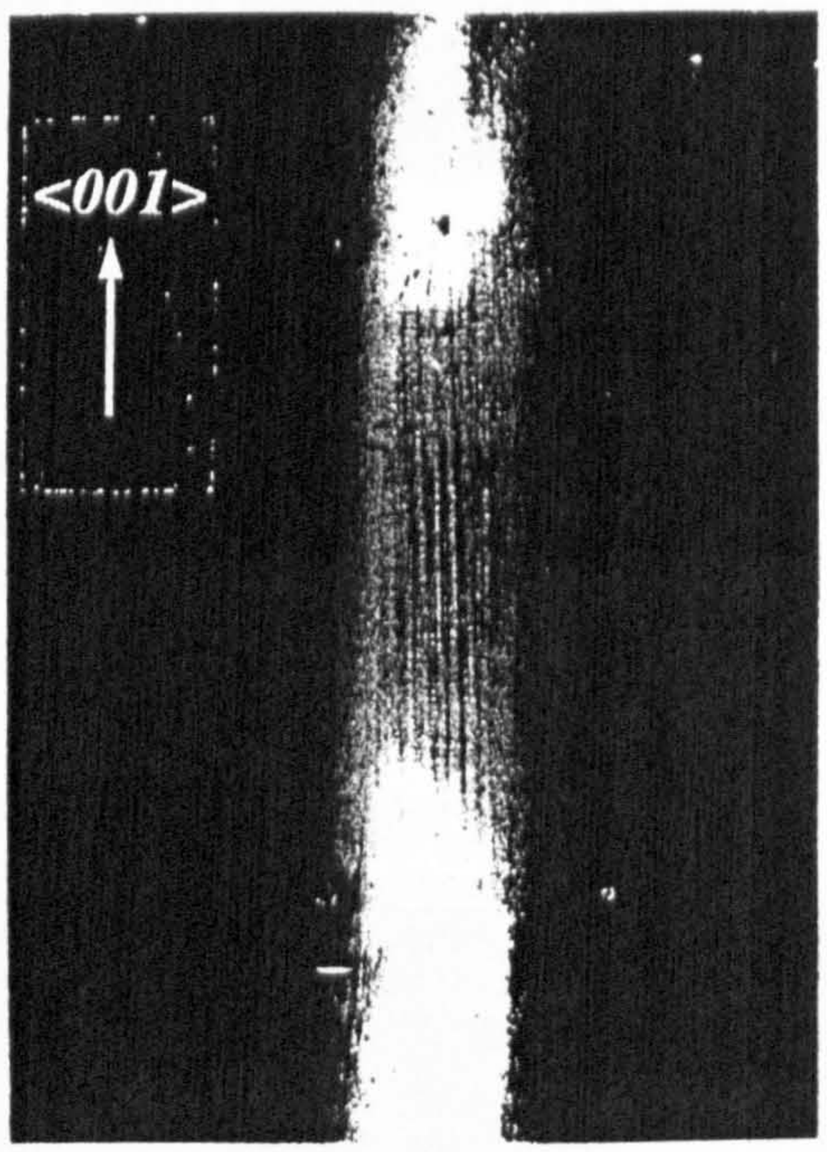

Fig.2.8 Slip Traces Observed on Specimen after Torsion Test at 950°C
(After Nouailhas et al [1993])

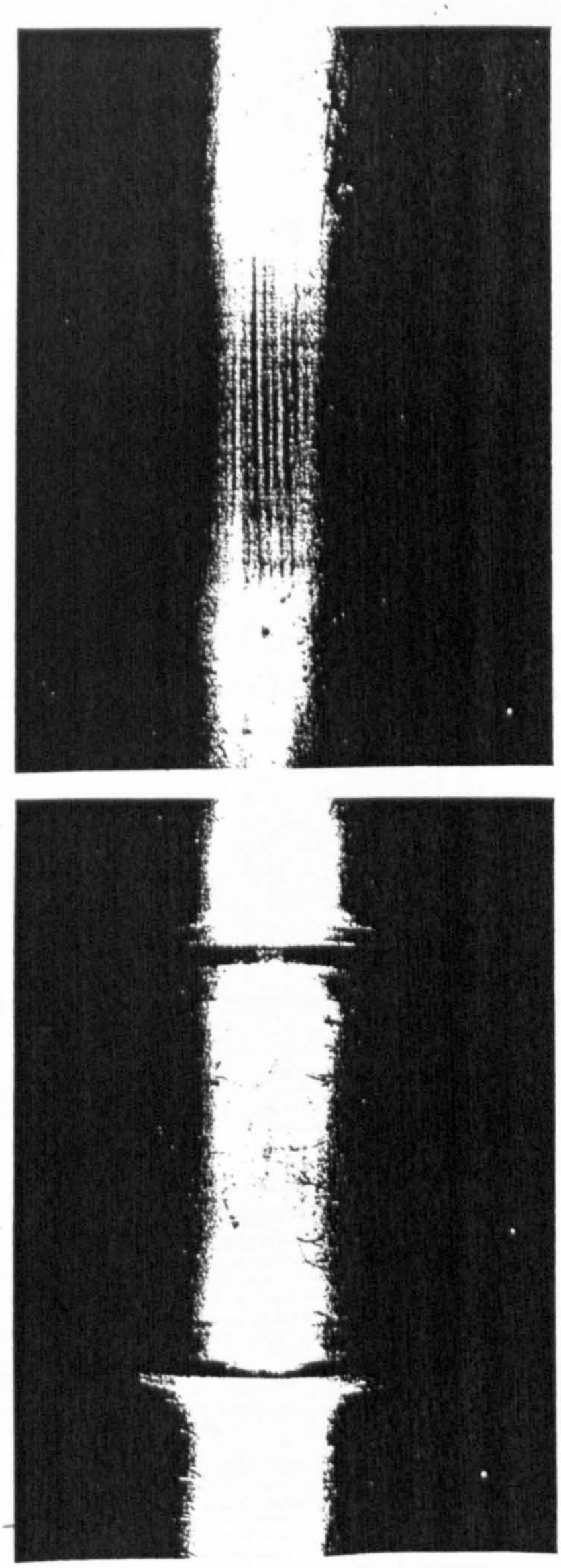

Fig.2.9 Traces Cubic Slip Observed after Torsion Test at 950°C
(After Policella et al [1990])

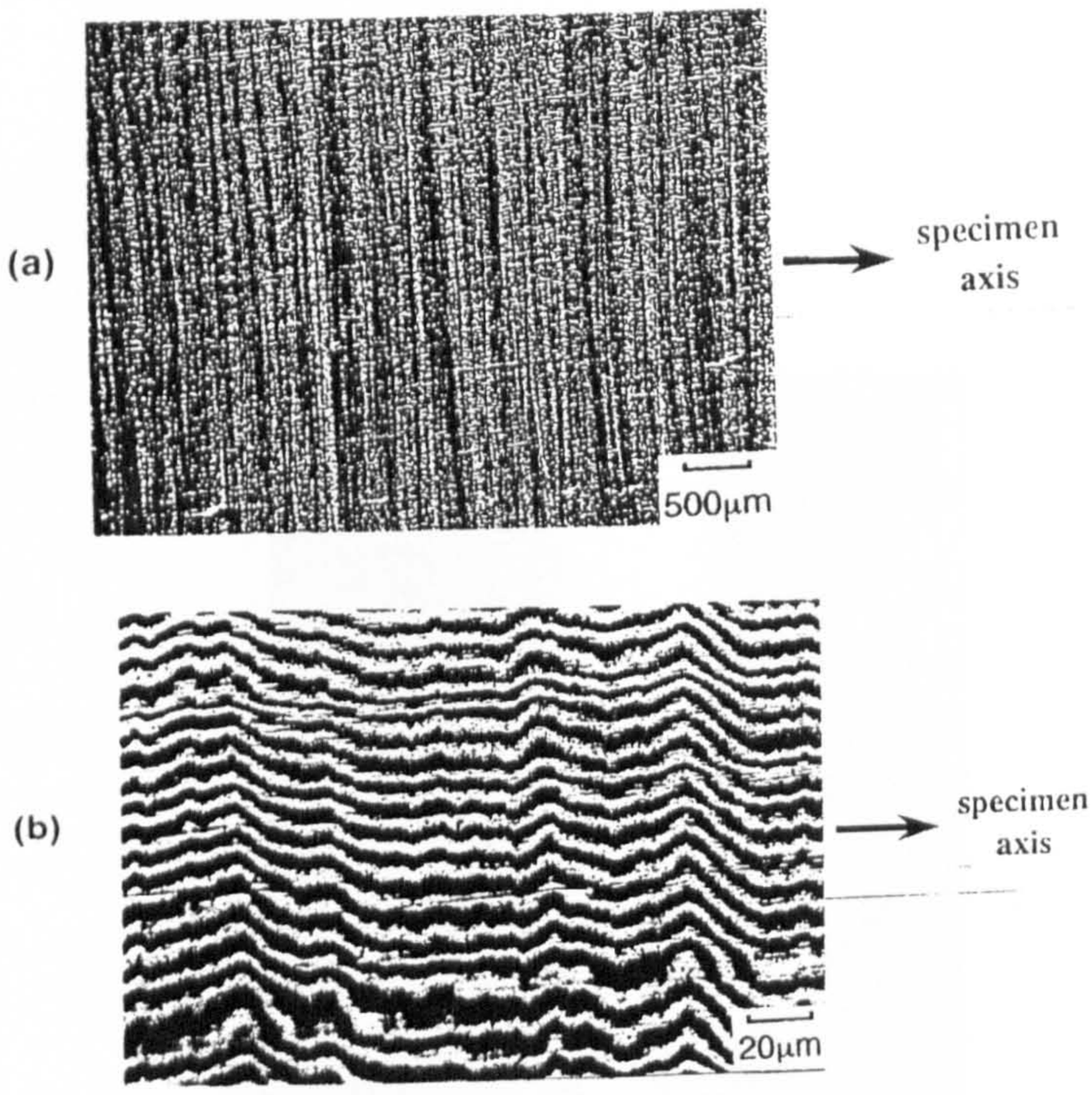

Fig.2.10 Shear Bands in Pure Torsion in the [110] areas
(a) SEM View of the Surface; (b) Image Obtained by Interferometry (λ=548nm)
(After Nouailhas et al [1993])

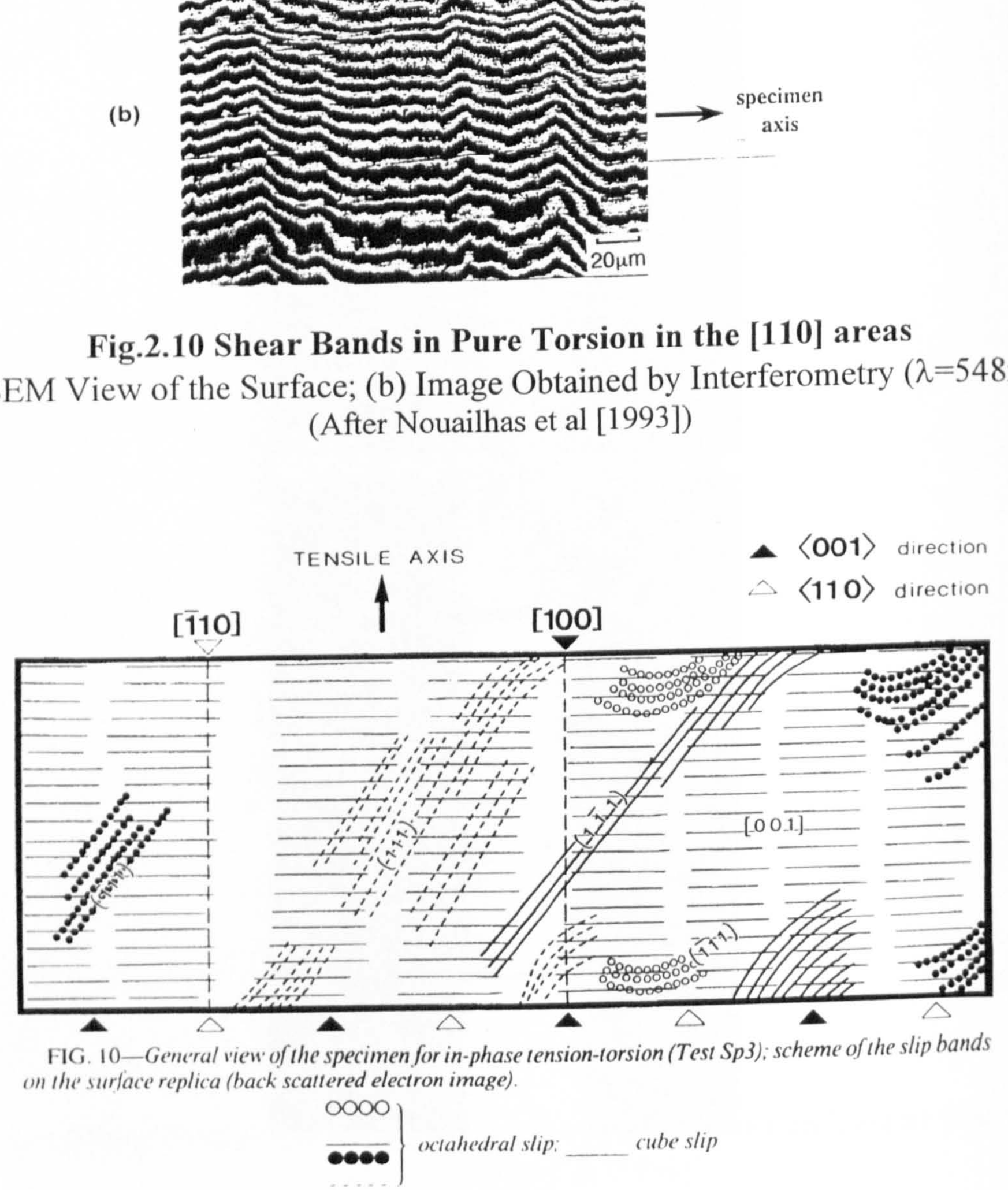

FIG. 10—*General view of the specimen for in-phase tension-torsion (Test Sp3); scheme of the slip bands on the surface replica (back scattered electron image).*

octahedral slip; _____ cube slip

Fig.2.11 General View of the Specimen after In-phase Tension-Torsion Test
Scheme of the Slip Bands on the Surface Replica
(After Nouailhas et al [1993])

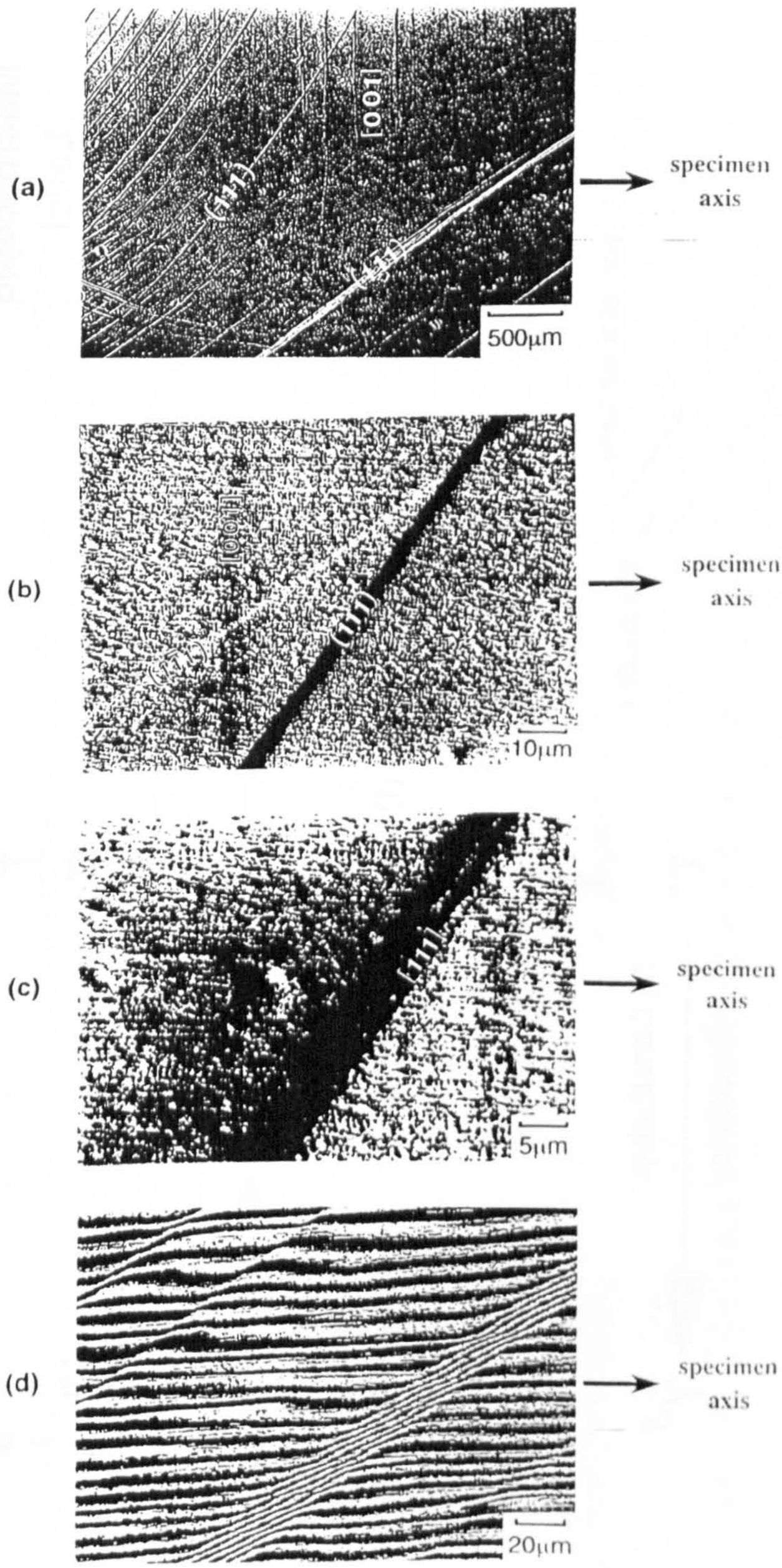

Fig.2.12 Shear Bands for In-phase Tension-Torsion in the [110] areas
(b) SEM View of the Surface; (b) Image Obtained by Interferometry (λ=548nm)
(After Nouailhas et al [1993])

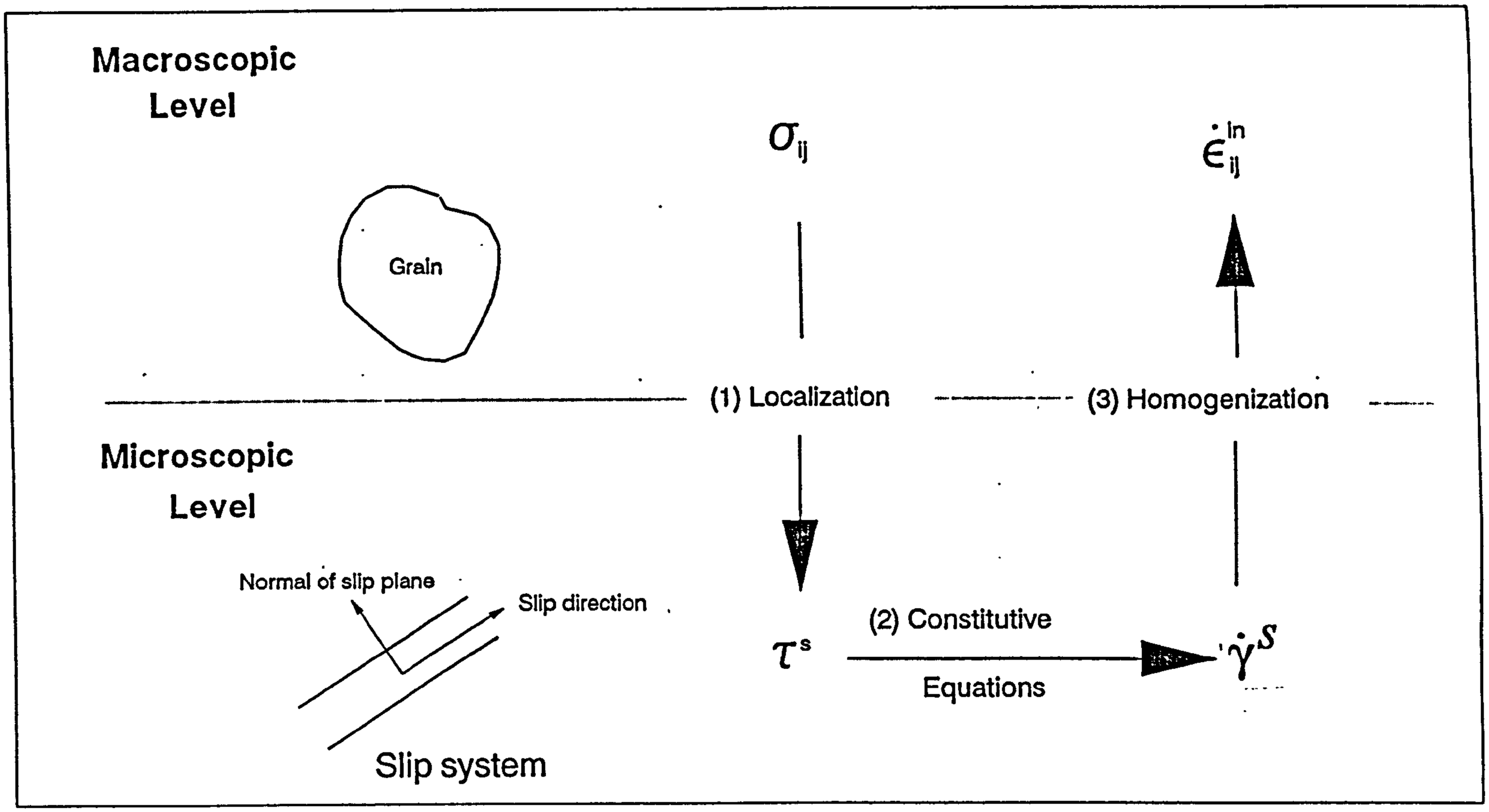

Fig.2.13The General Procedure in Developing a Crystallographic Model

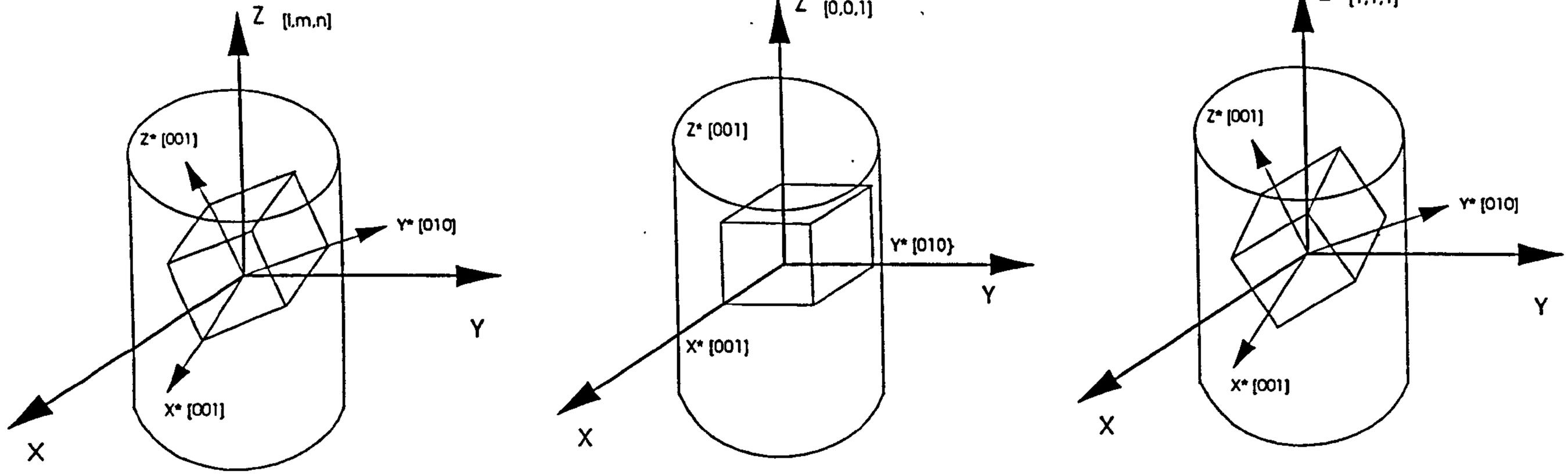

(1a). General Loading (1b). Loading in [001] (1c). loading in [111]

Fig.3.1. Coordinates Systems for Stress and Strain Transformation

X-Y-Z : Global Coordinate Systems
X* -Y* -Z* : Crystallographic Coordinate Systems

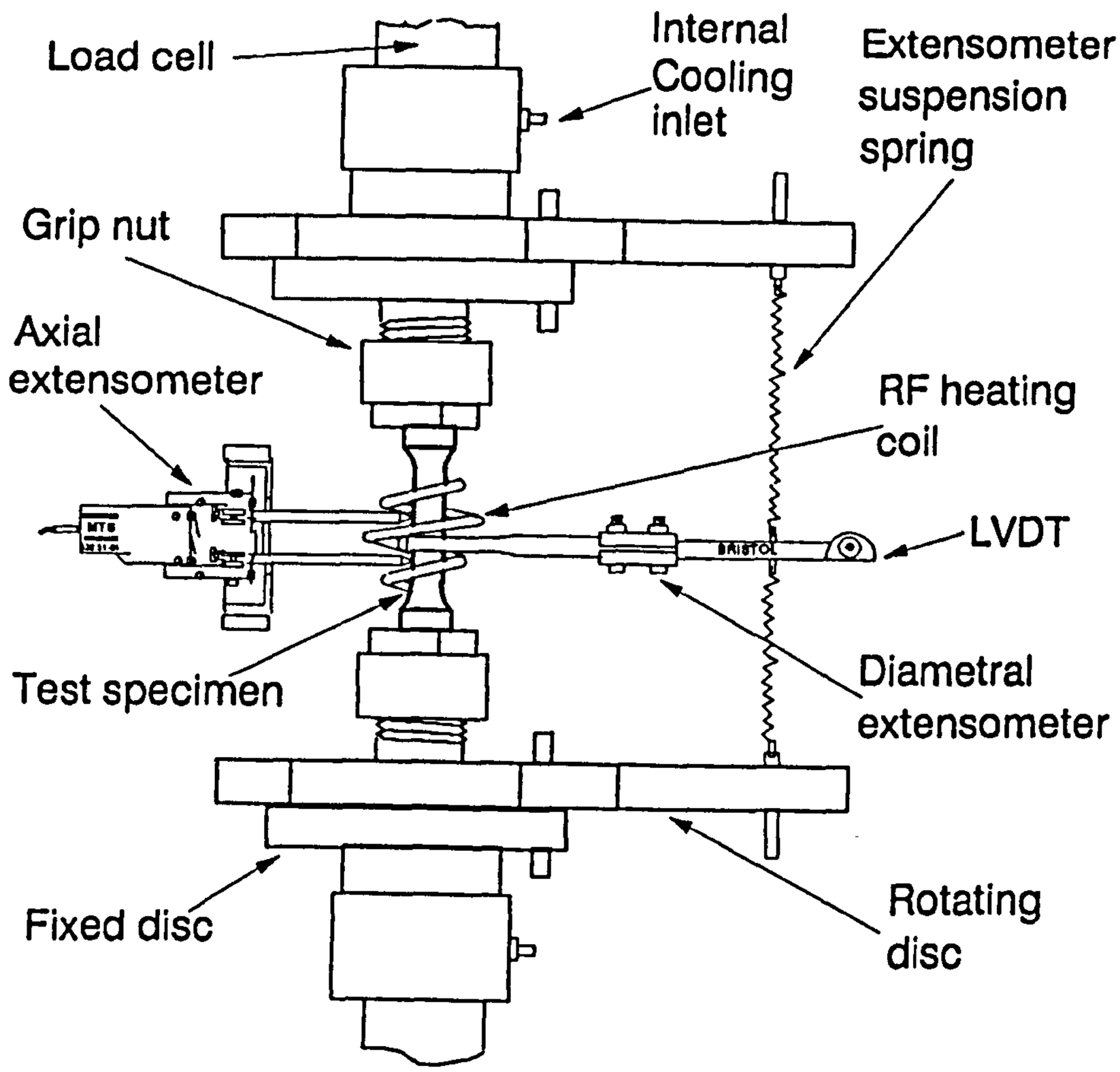

Fig.3.2a Schematic of Testing Set up for Axial and Transverse Local Strain Measurement

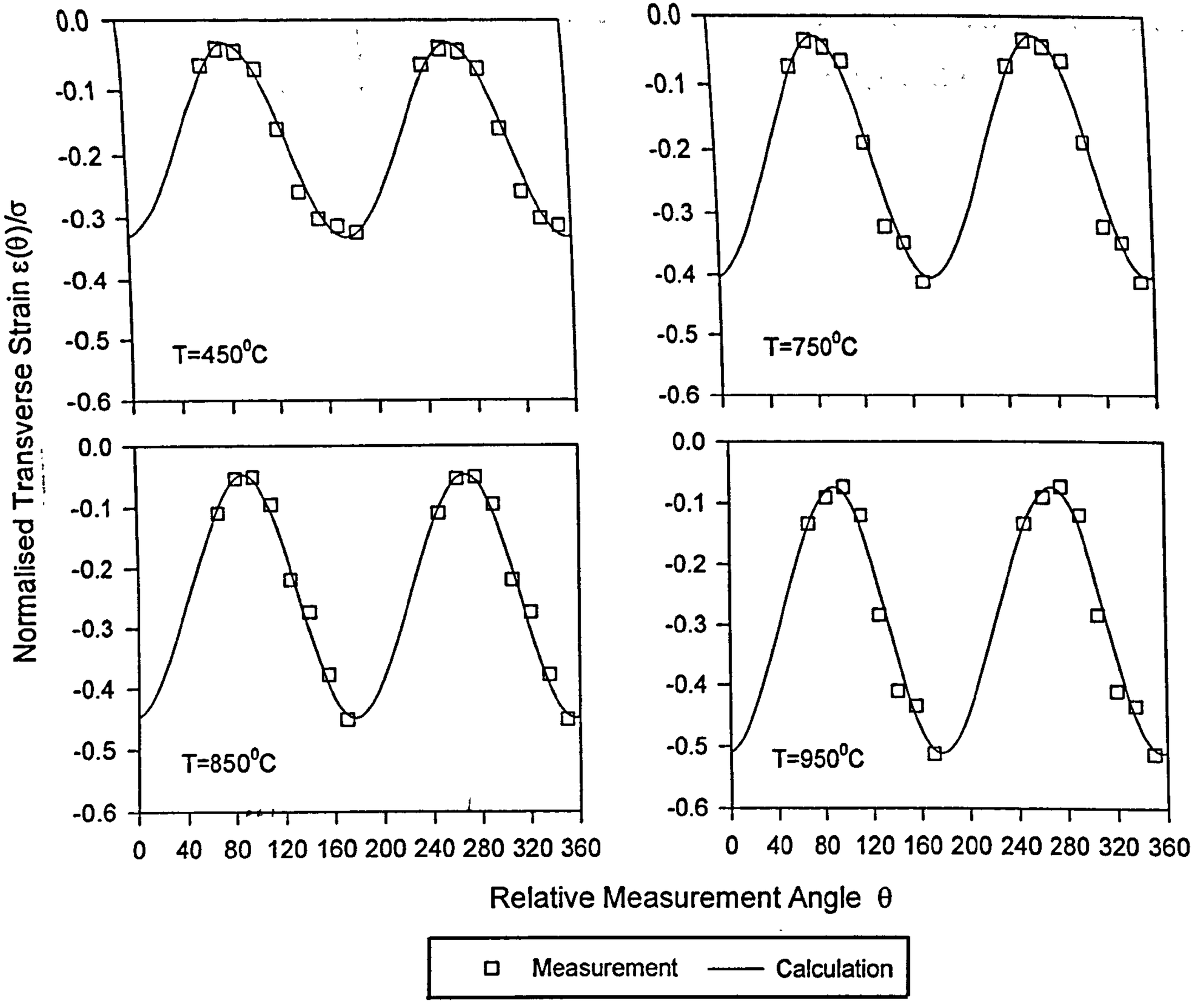

Fig.3.2b Comparison of Measurement and Calculation Results at Various Temperatures

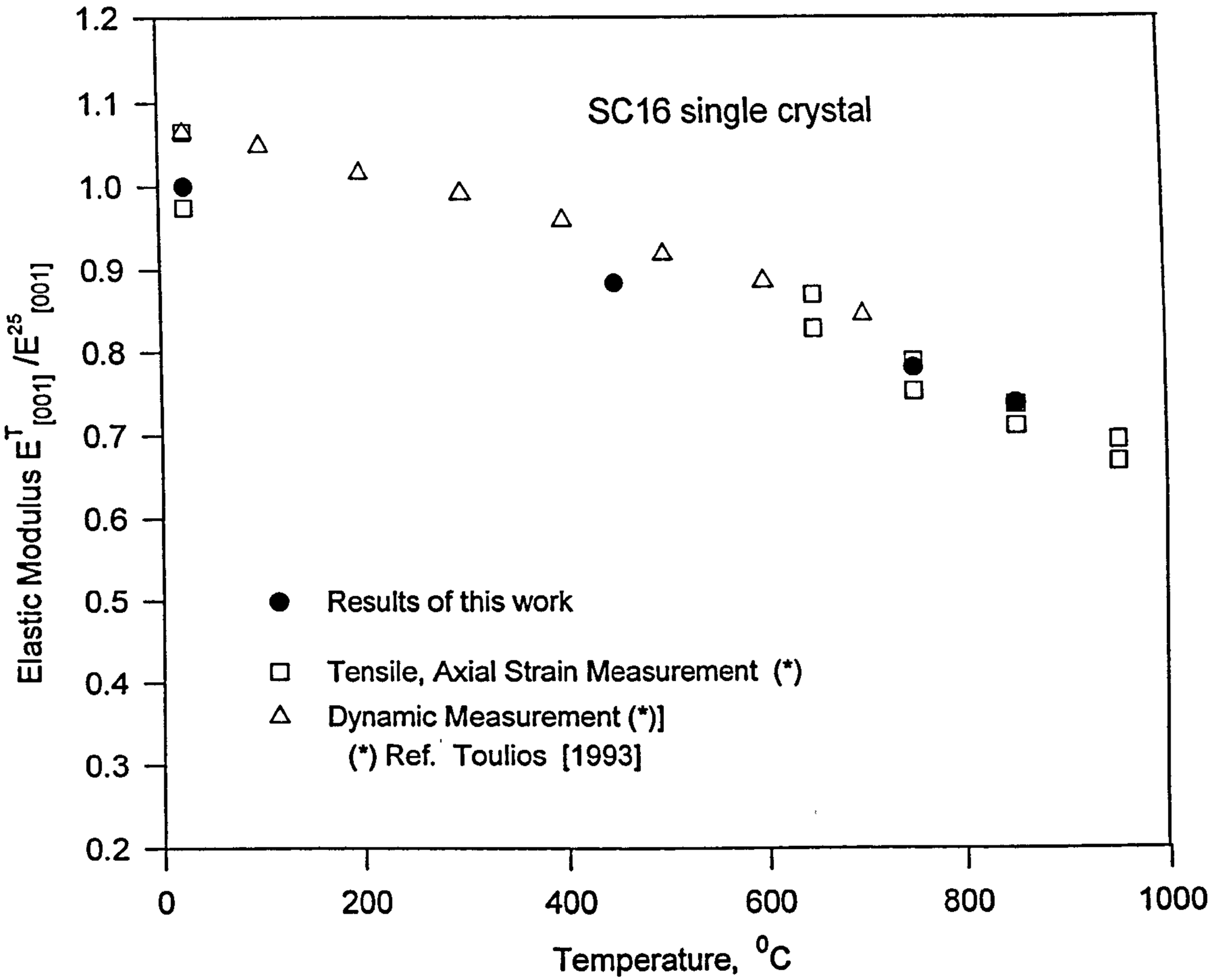

Fig.3.2c Comparison of Elastic Modulus by Different Measurements

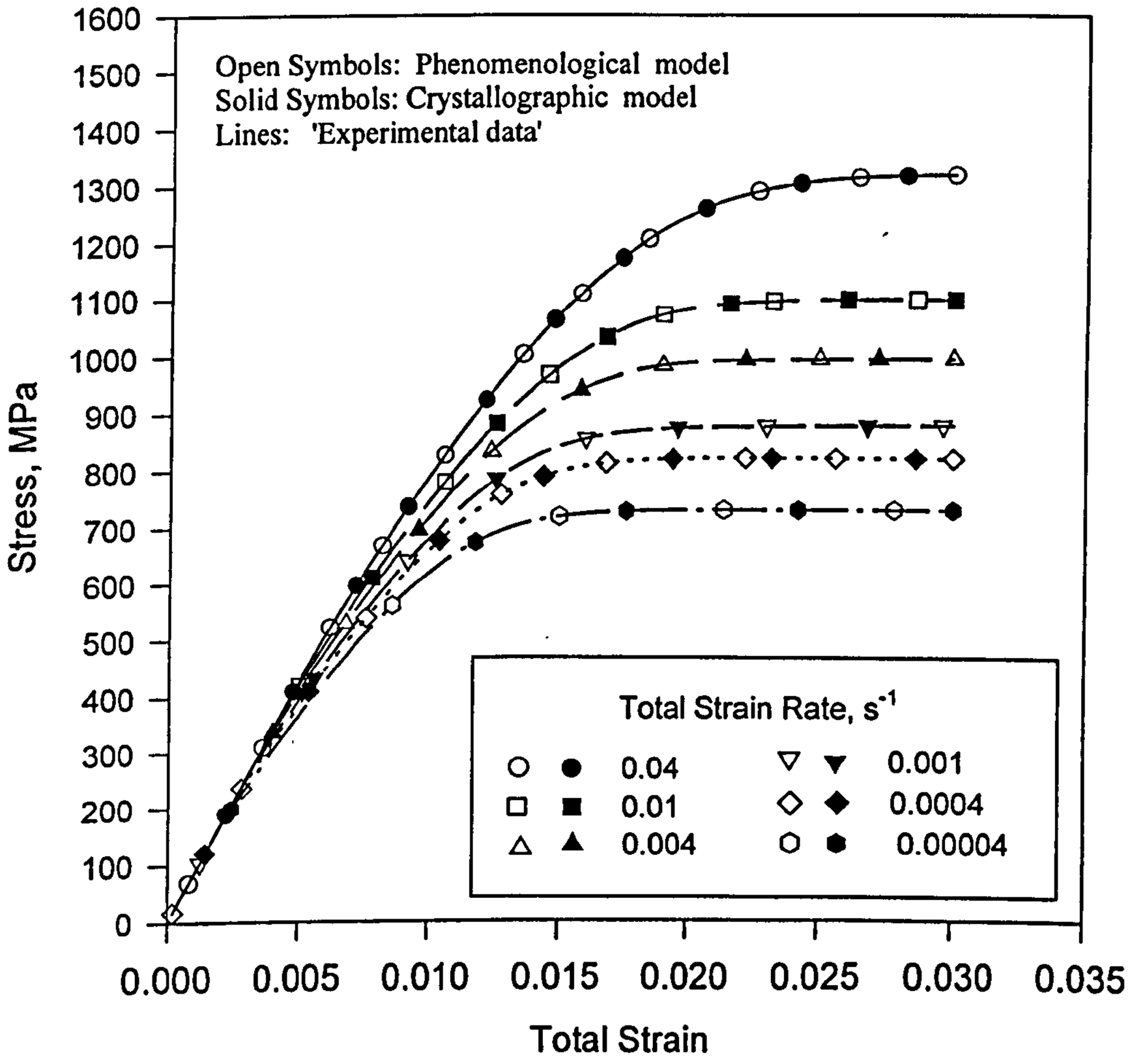

Fig.3.3a Stress and Strain Curves for Different Strain Rates ([001] Orientation)

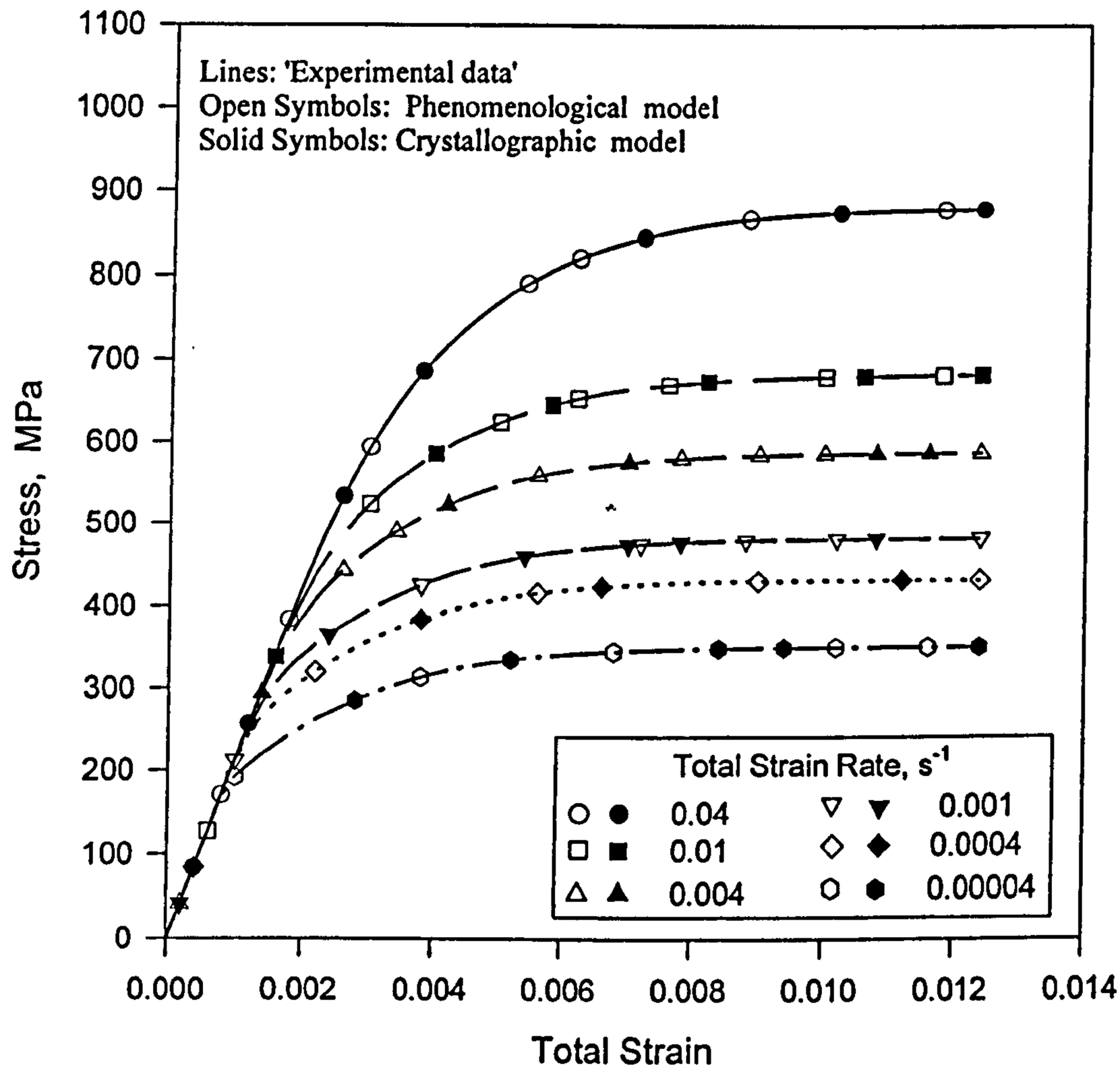

Fig.3.3b Stress and Strain Curves for Different Strain Rates ([111] Orientation)

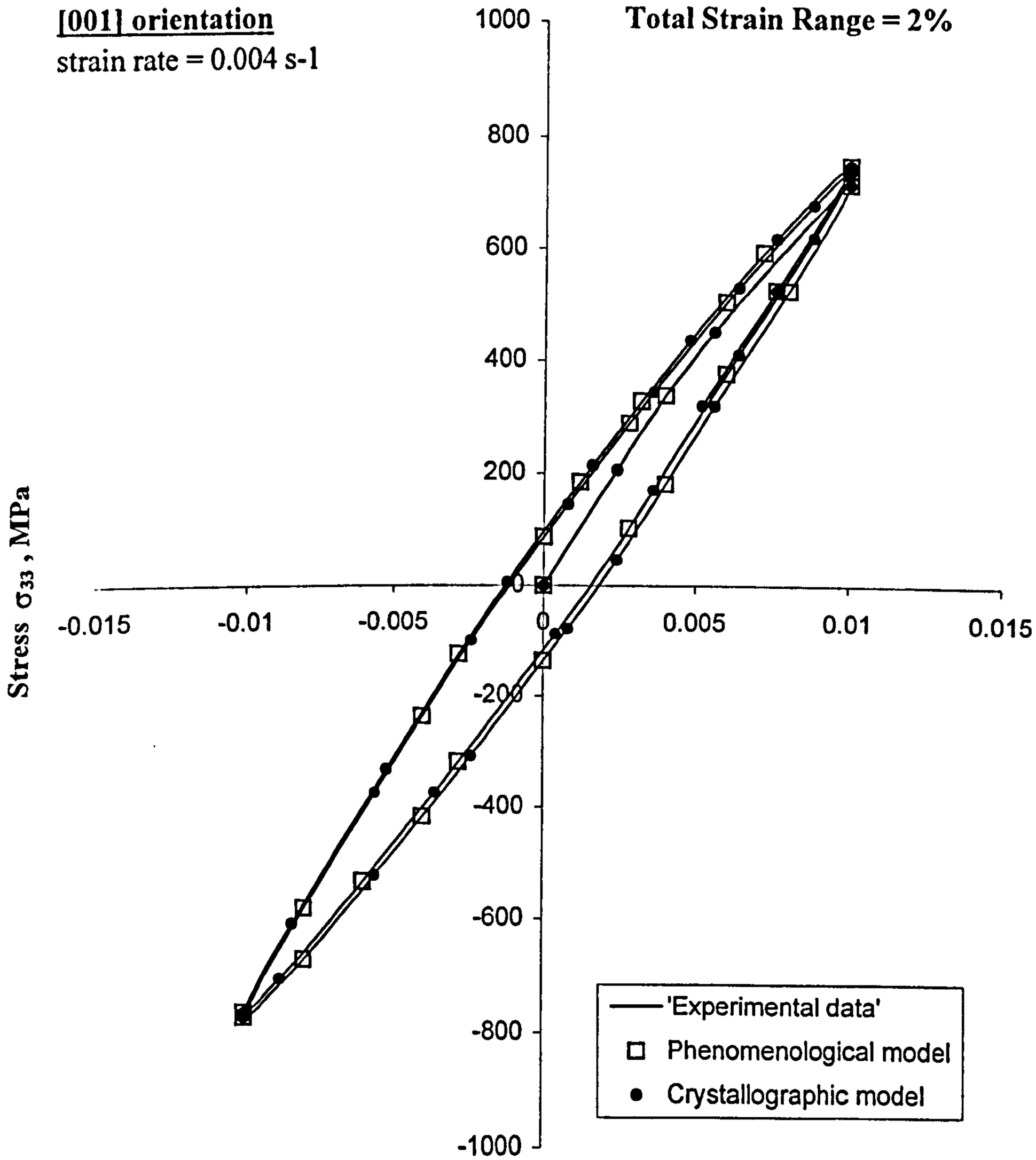

Fig.3.4a Initial Stress and Strain Response of the [001] Orientation

[111] orientation

strain rate = 0.004 s^{-1}

Total Strain Range = 0.8%

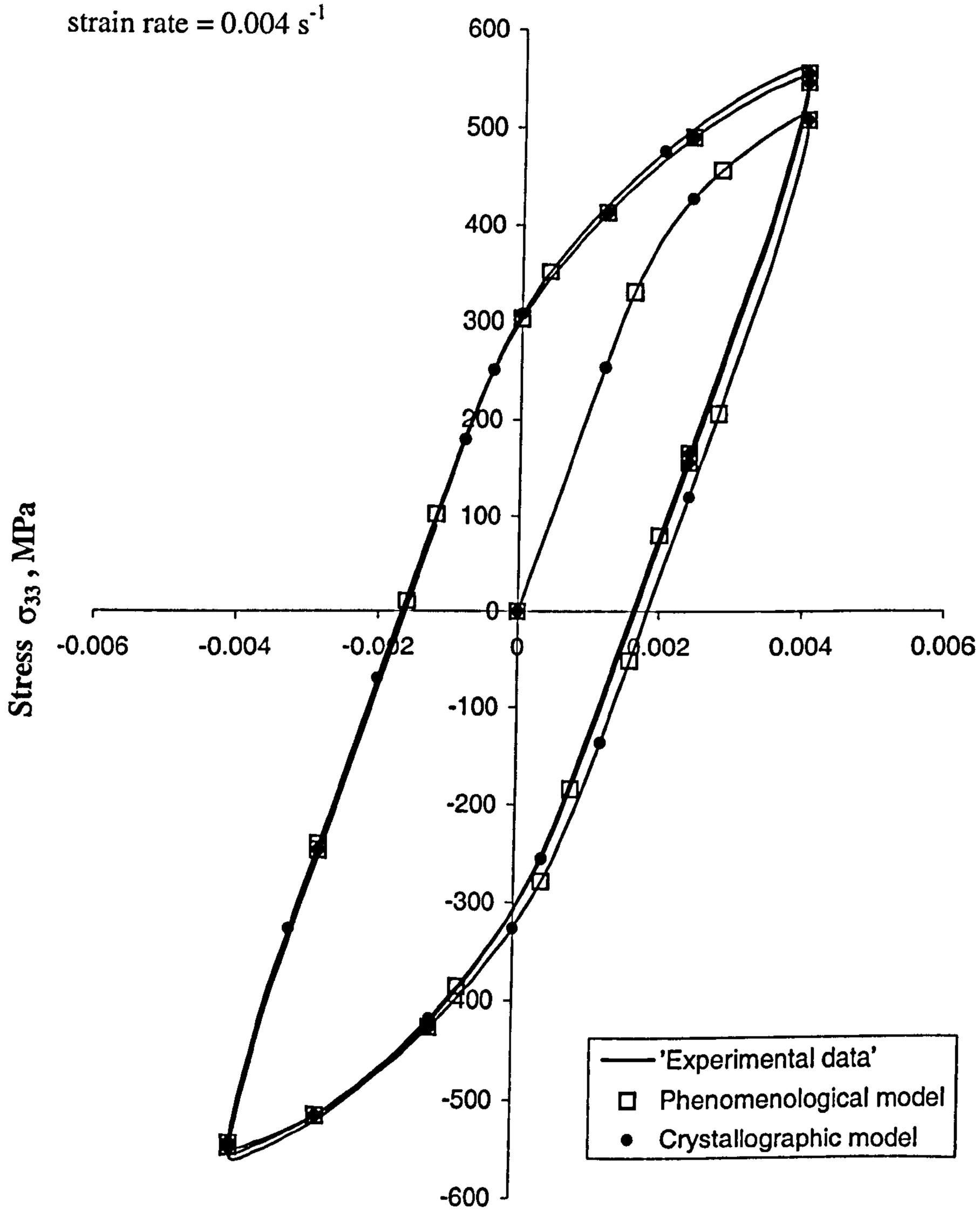

Fig.3.4b Initial Stress and Strain Response for the [111] Orientation

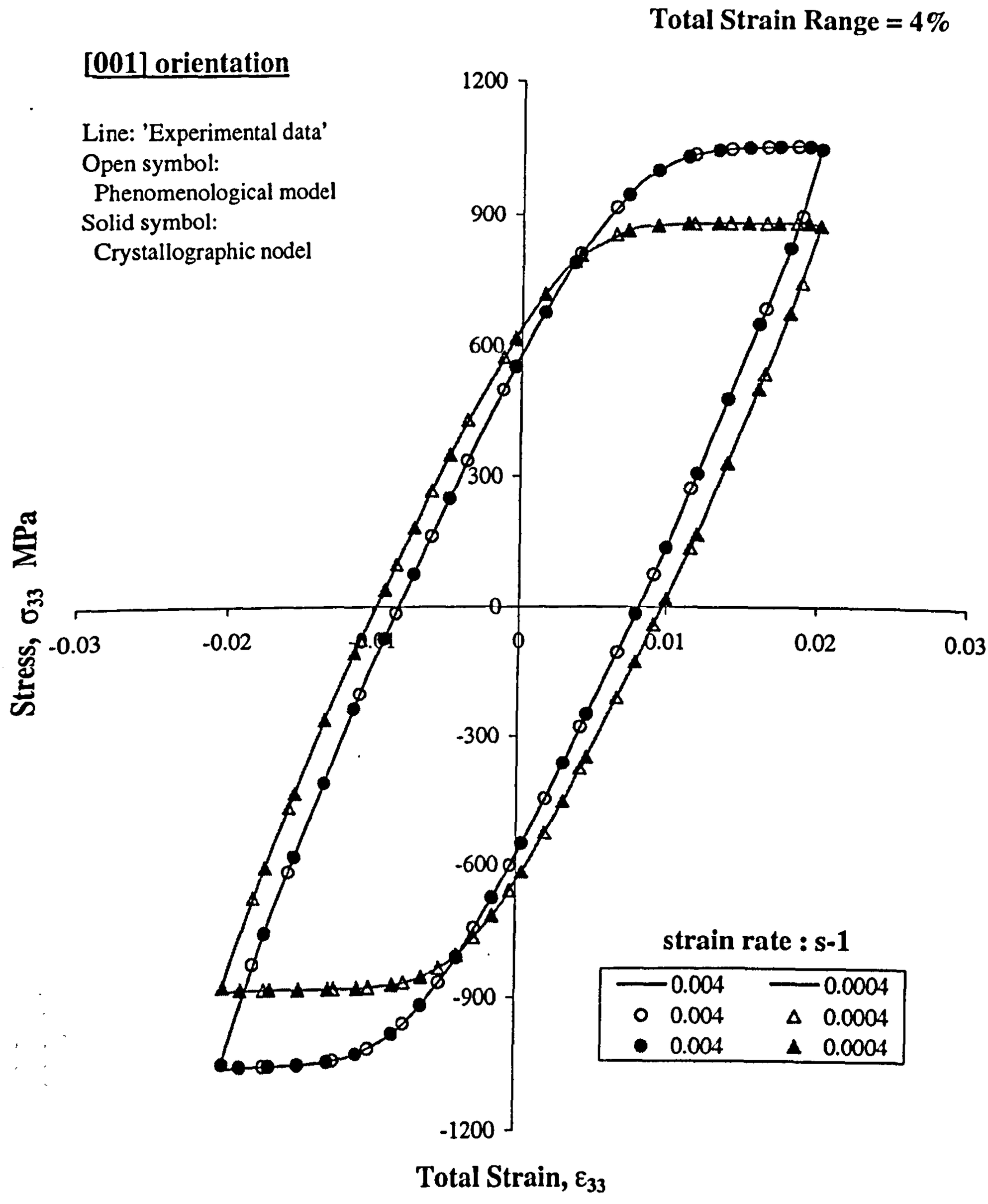

Fig.3.4c Stable Cyclic Stress and Strain Response of the [001] Orientation

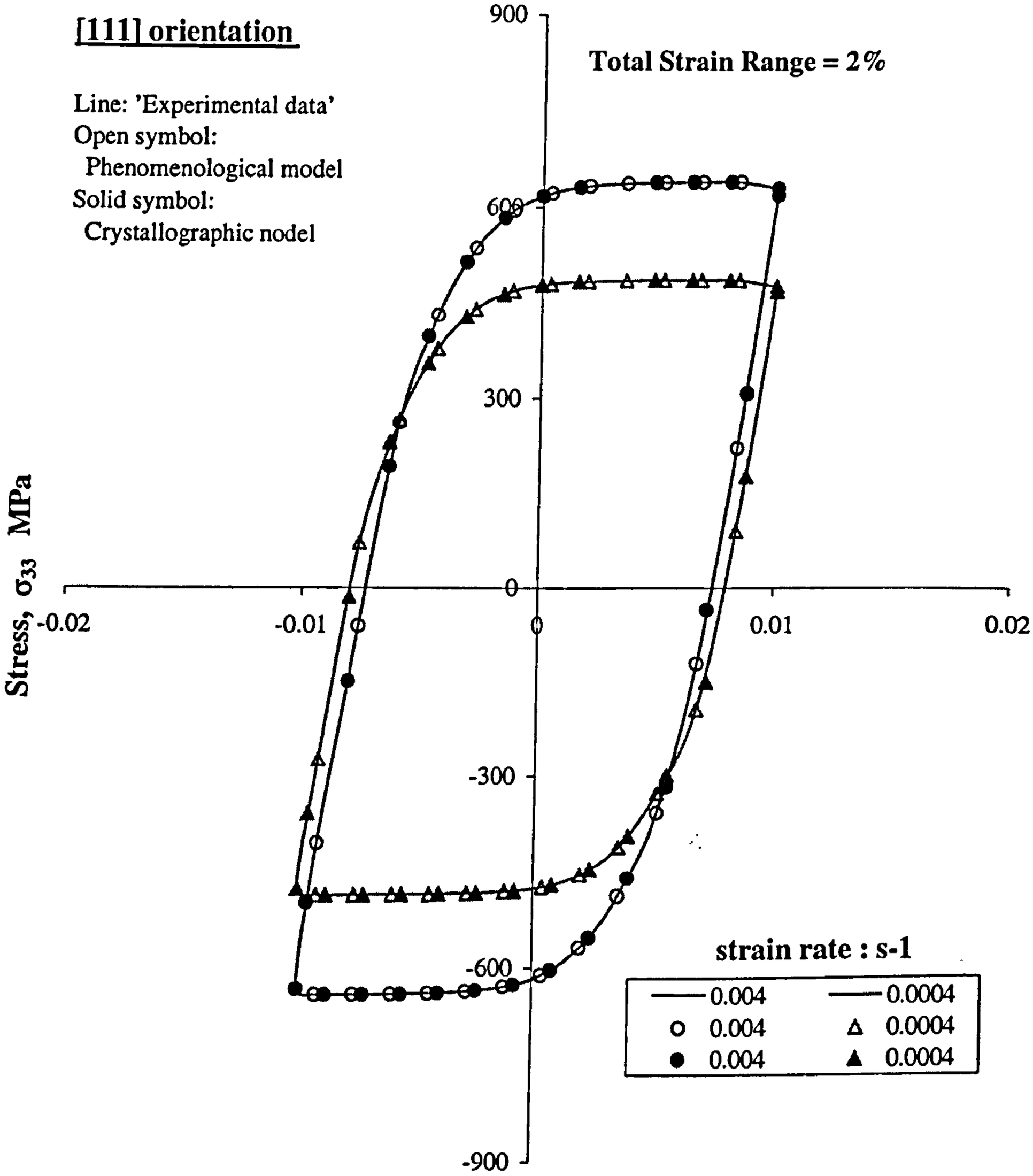

Fig.3.4d Stable Cyclic Stress and Strain Response of the [111] Orientation

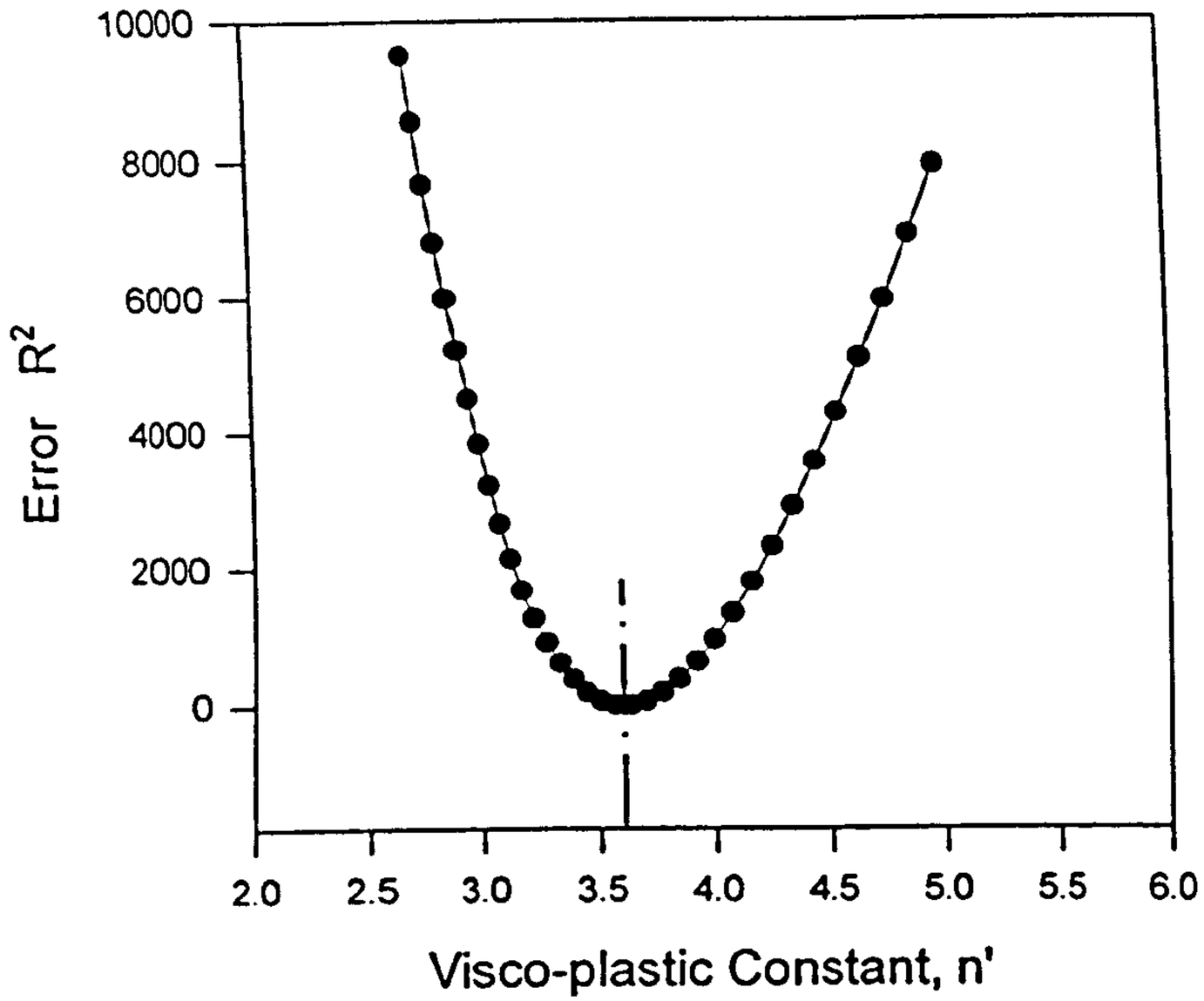

3.5a. Variation of Square Error R^2 with n' Values

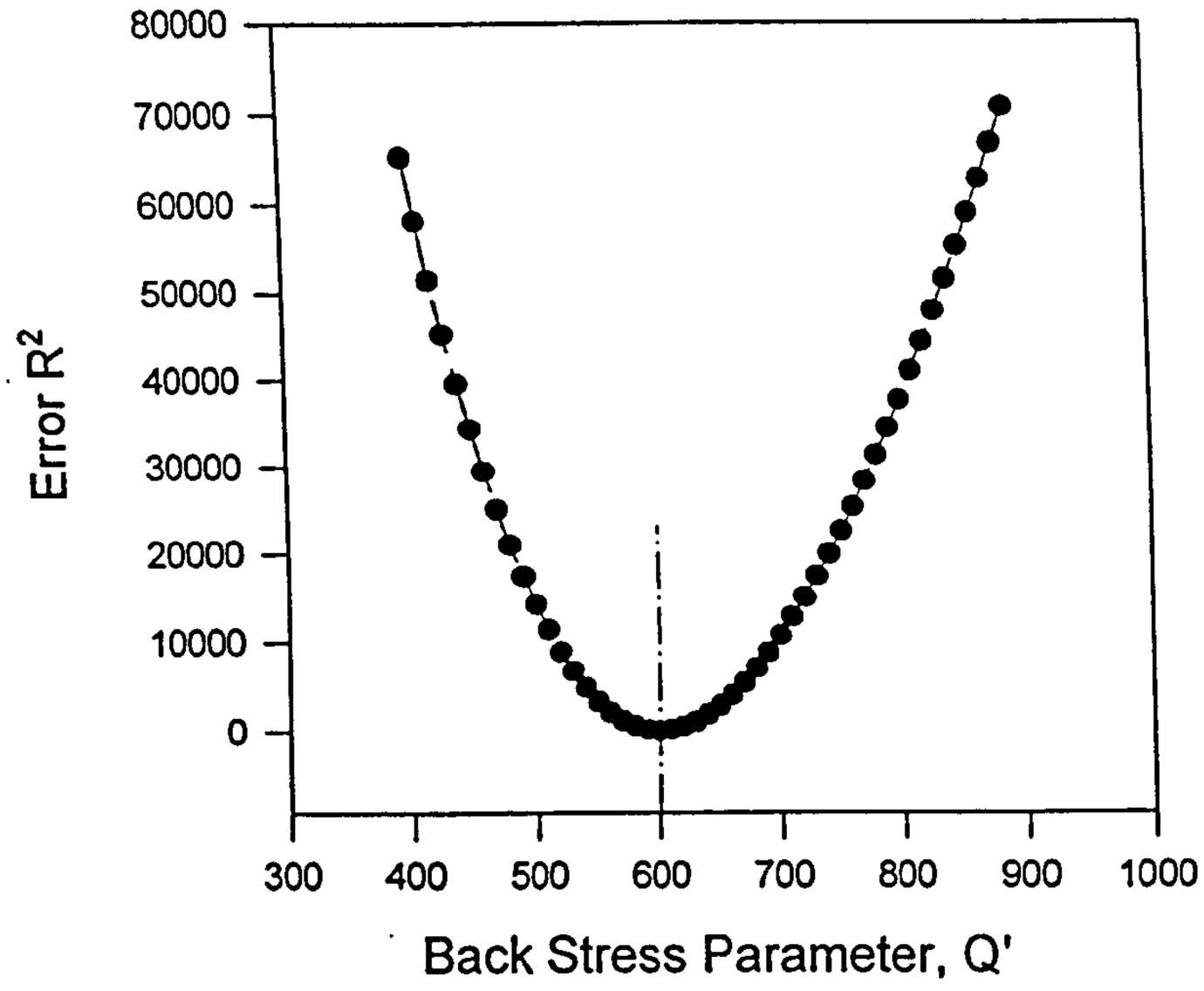

3.5b. Variation of Square Error R^2 with Q' Values

Fig.3.5 Evaluation of Non-linear Regression Errors

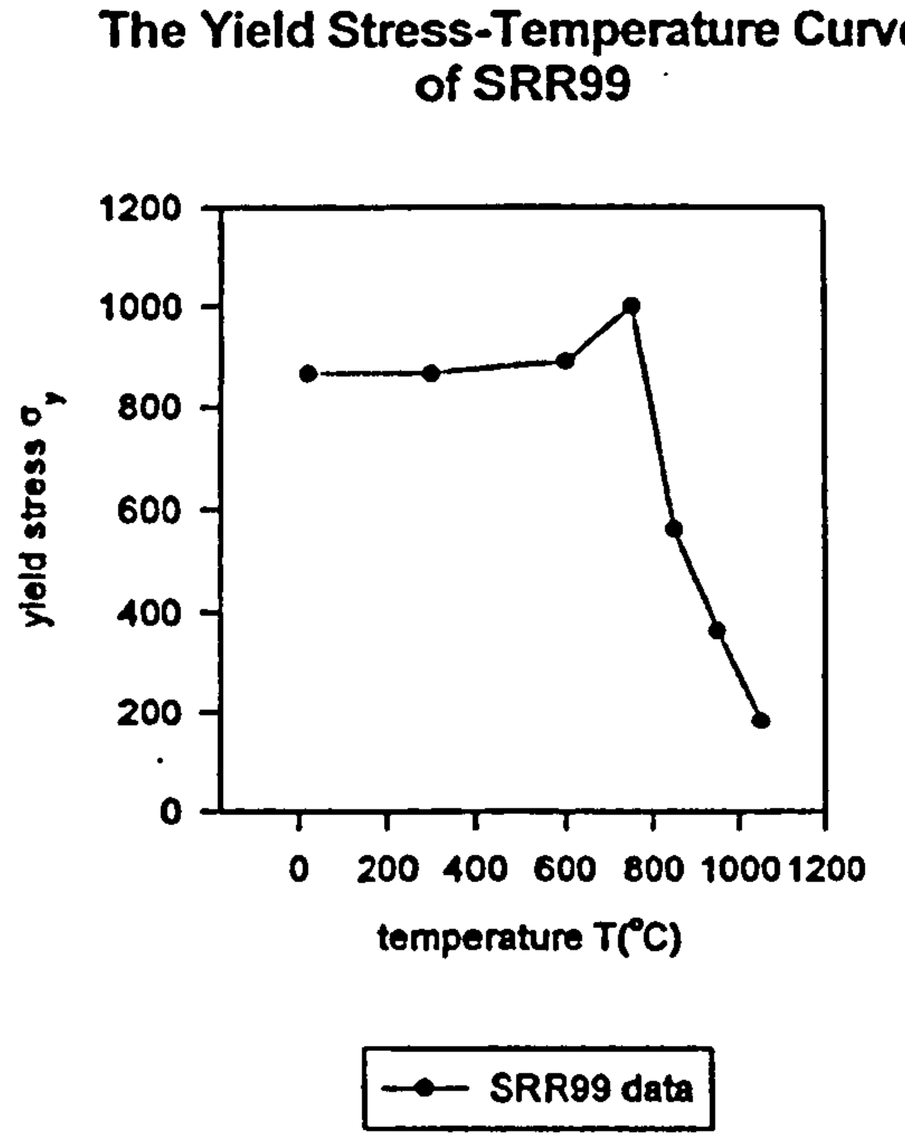

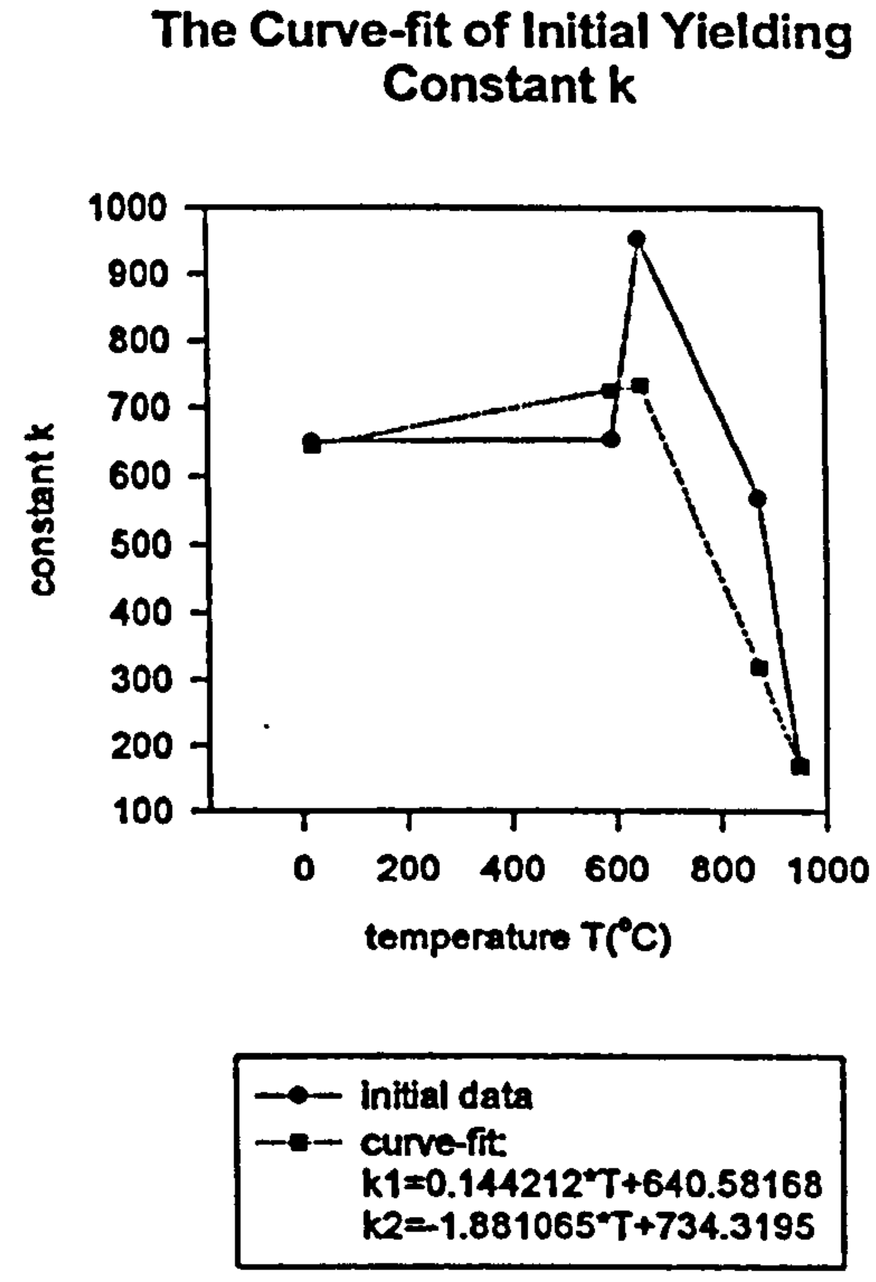

Fig.3.6a The Curve-fit of Yielding Parameter As a Function of Temperature

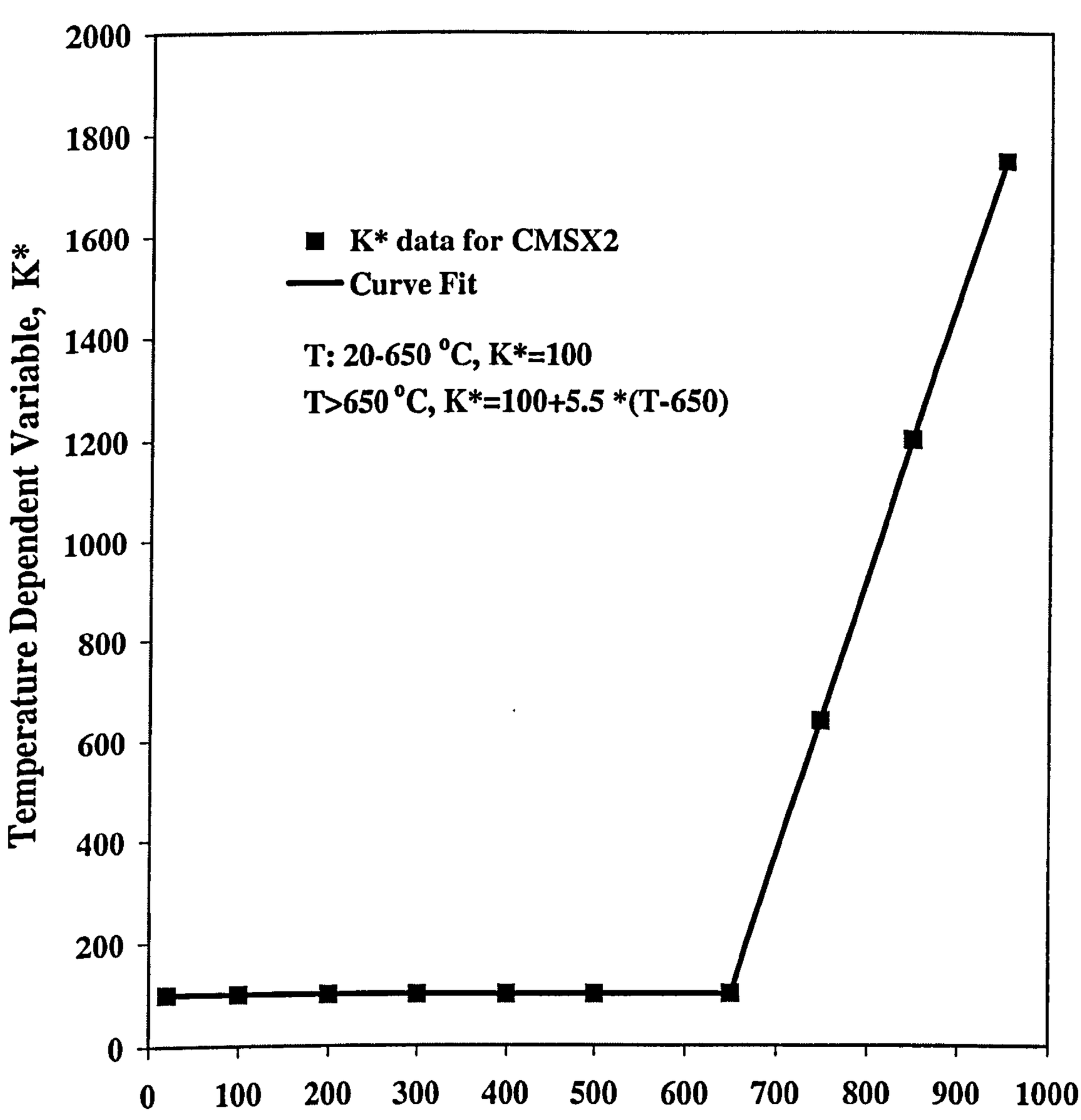

Fig.3.6b Data and Curve Fit of Viscosity Constant K*
(Single Crystal CMSX2)

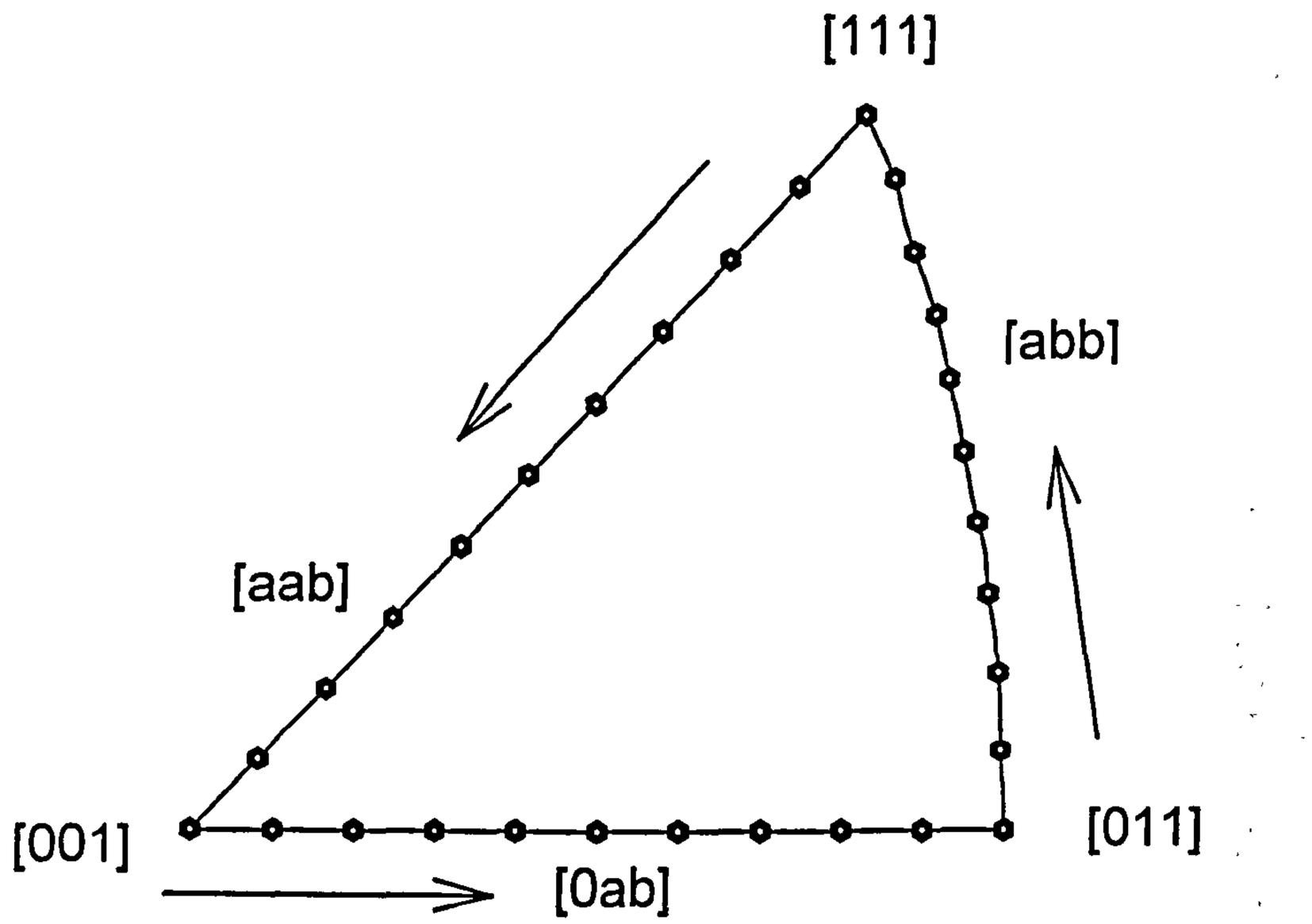

Fig.3.7. Crystal Orientations used in the Simulations

3.8a. Phenomenological Model

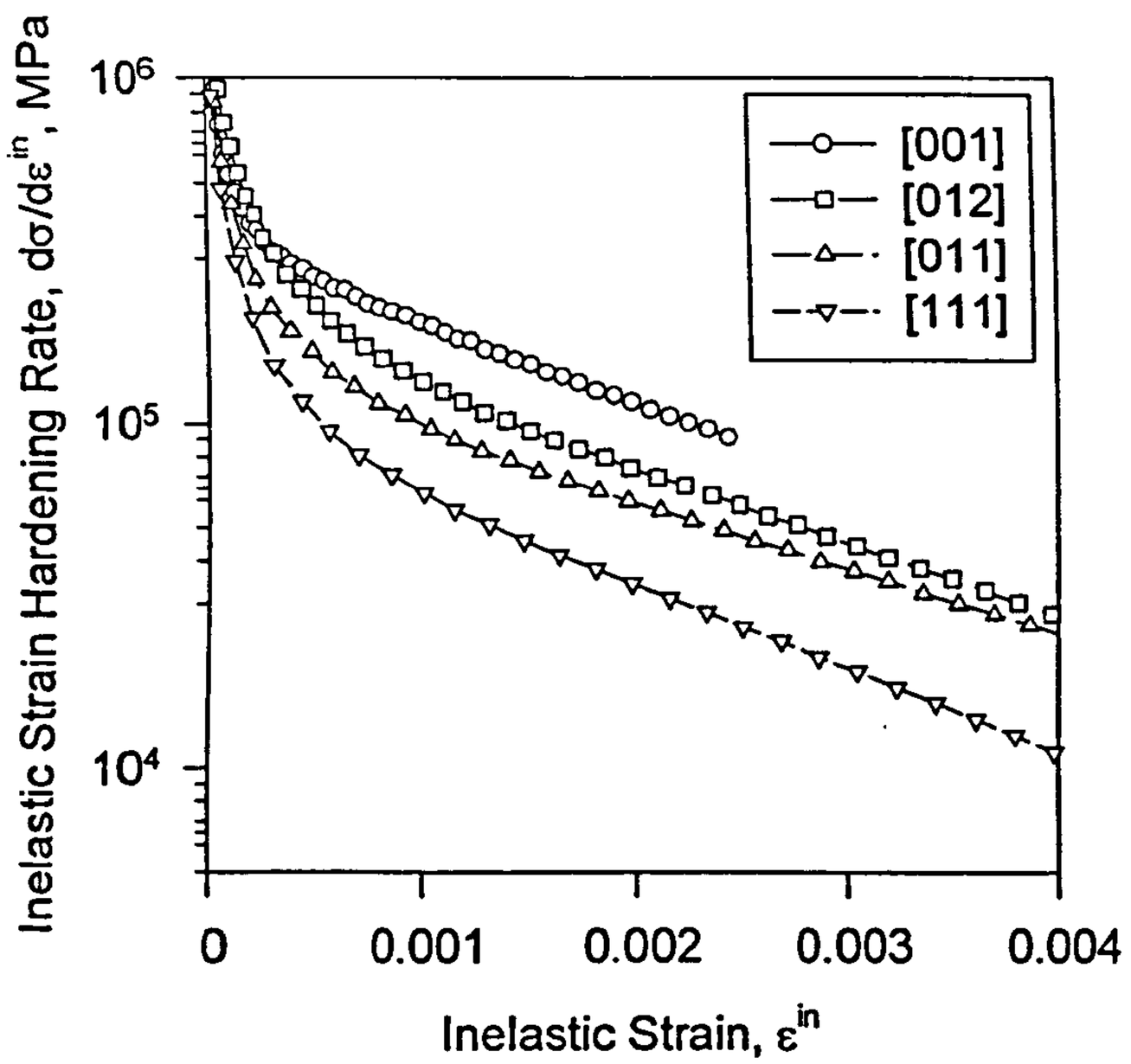

3.8b. Crystallographic Model

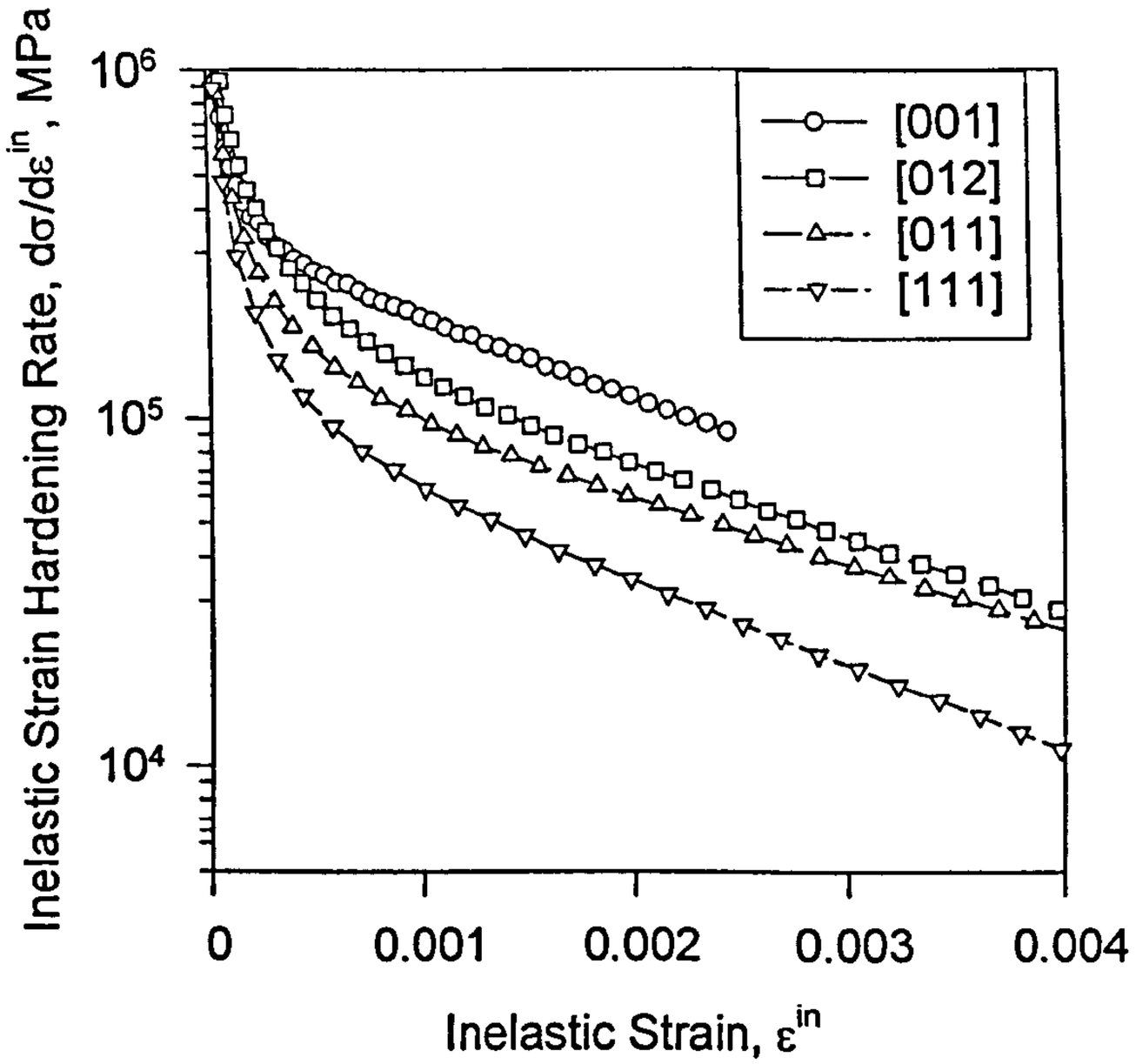

Fig.3.8. Comparison of Inelastic Strain Hardening Rate of Different Orientations

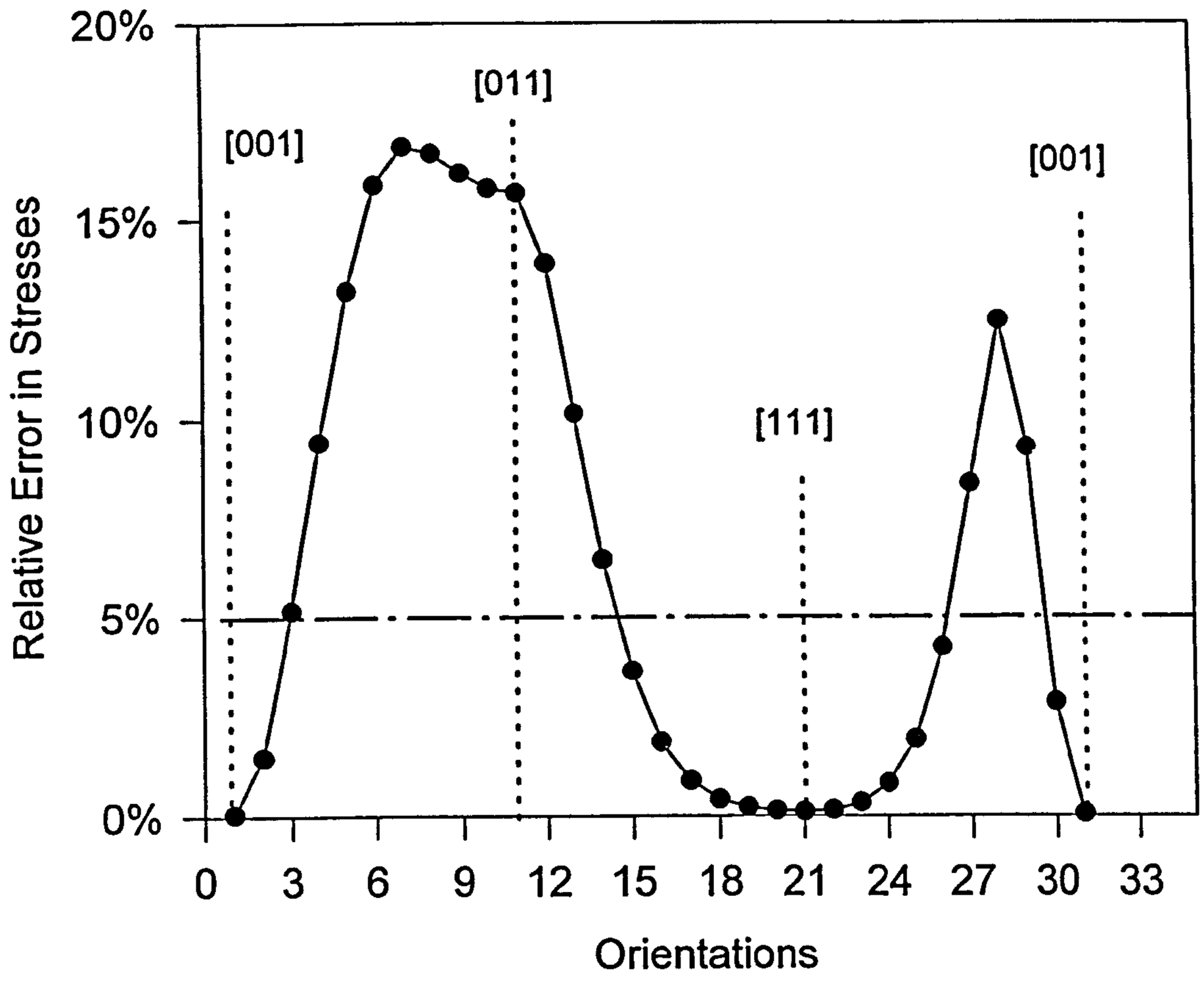

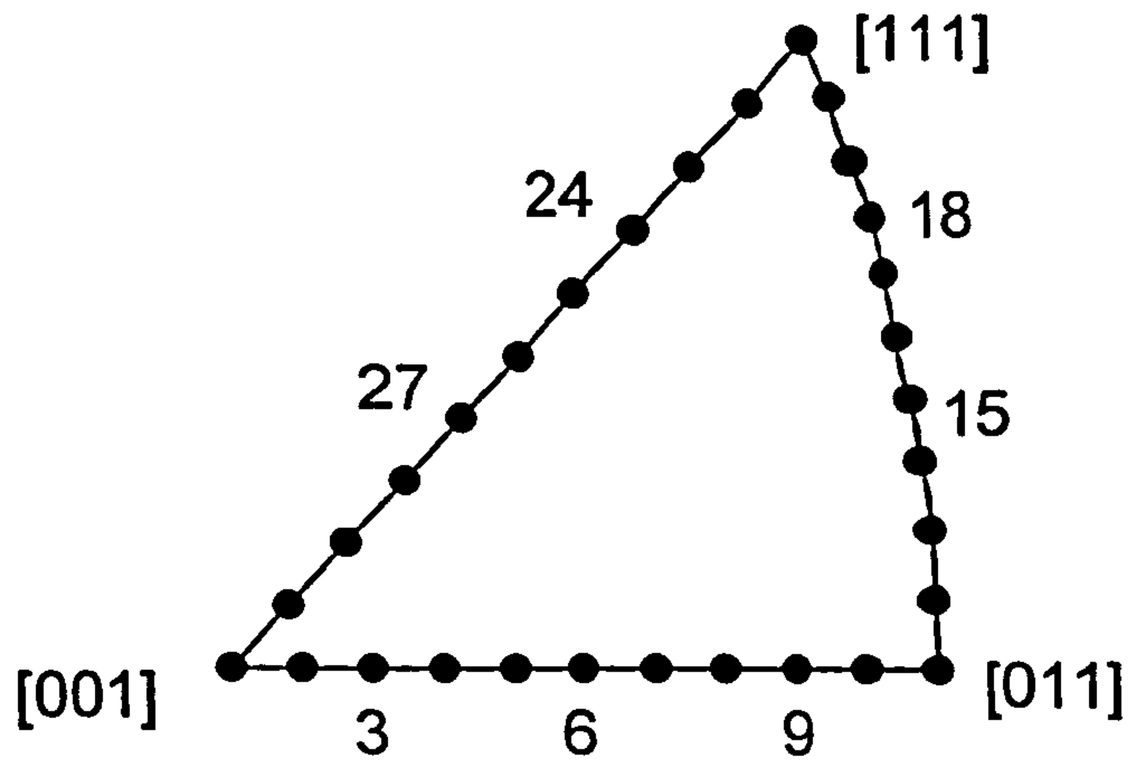

Fig.3.9 Relative Error in Peak Stresses from the Two Models

(a) Crystallographic Model

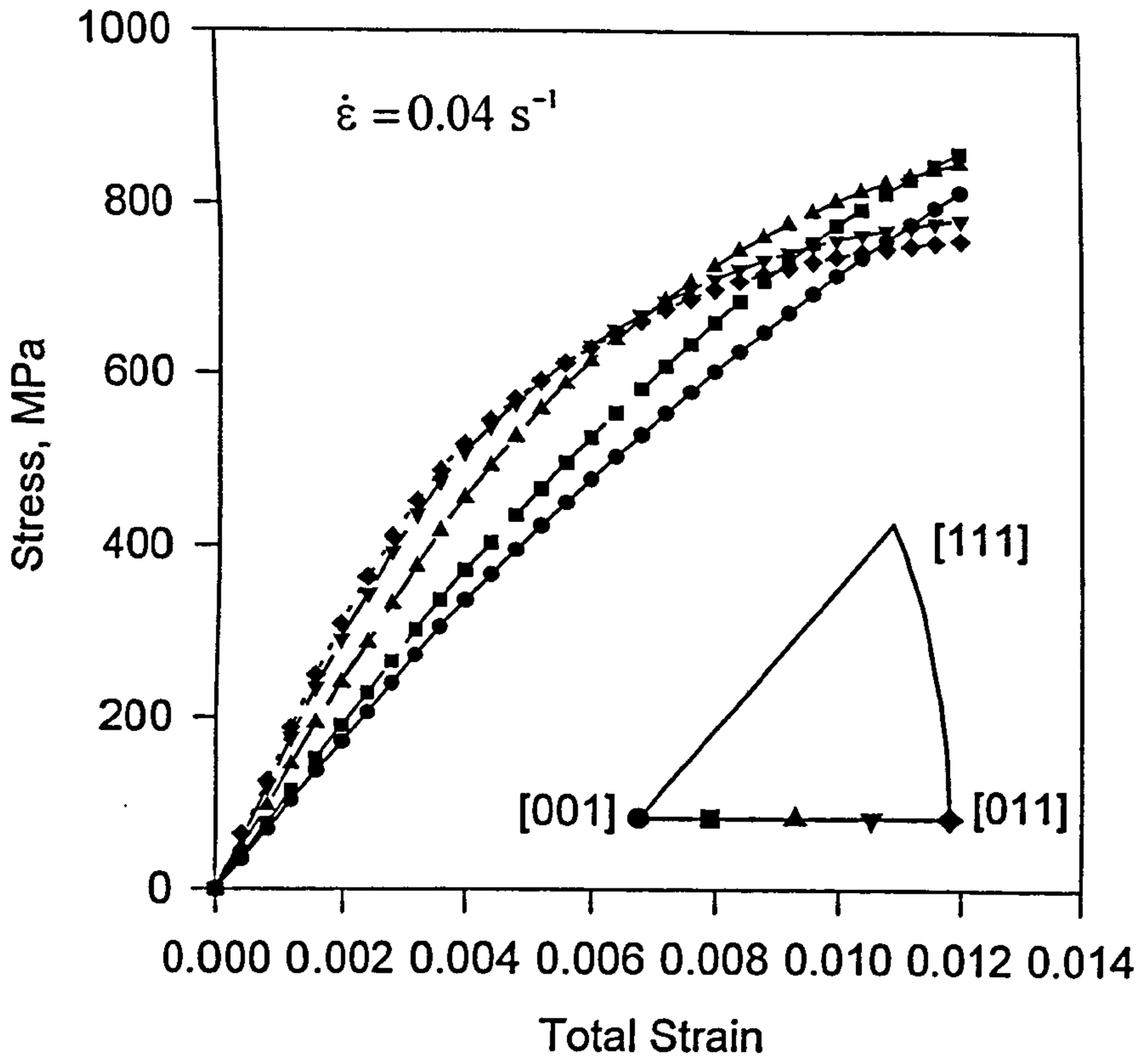

(b) Phenomenological Model

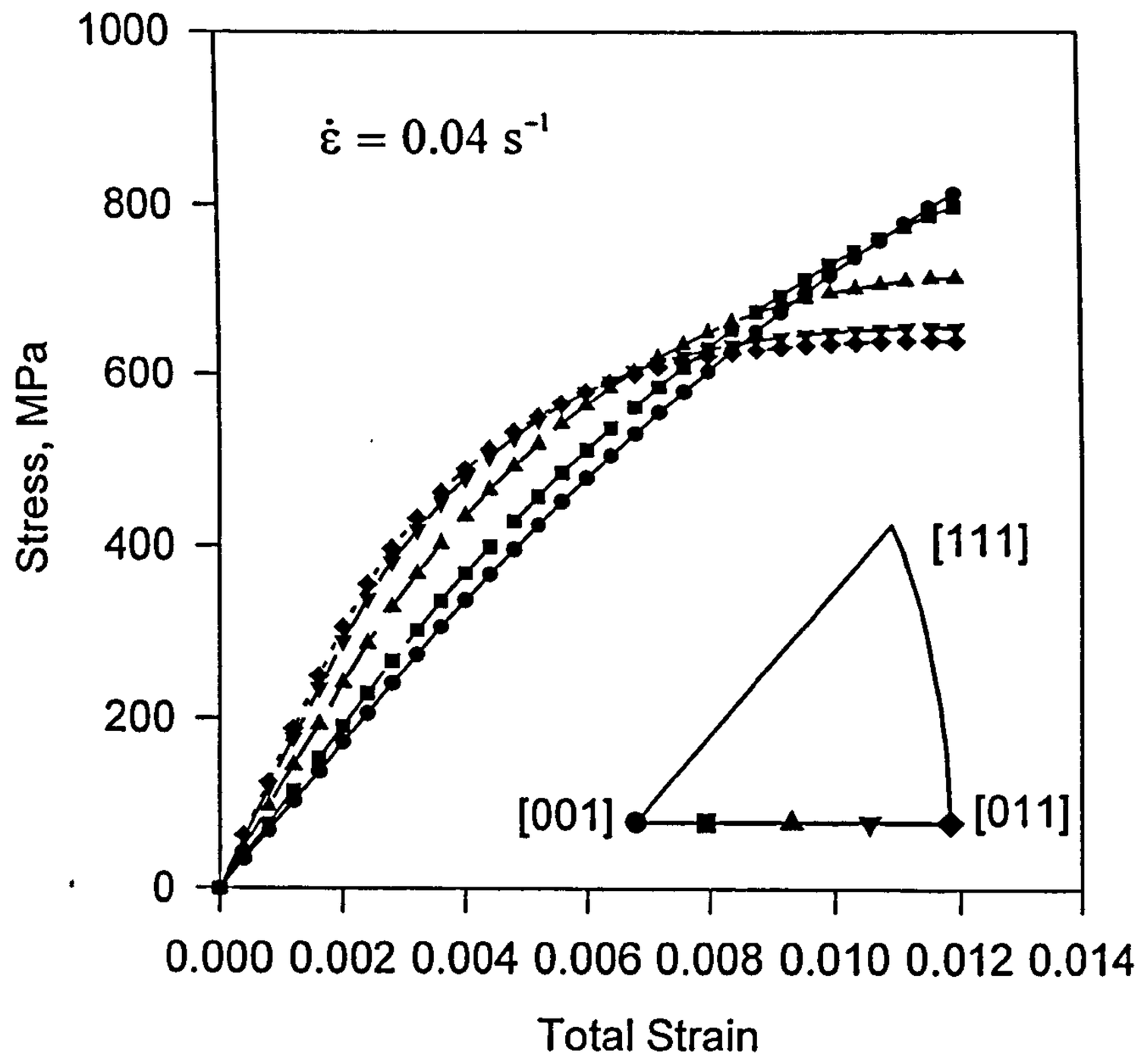

Fig.3.10a Comparison of Stress and Strain Response on the [001]-[011] Side

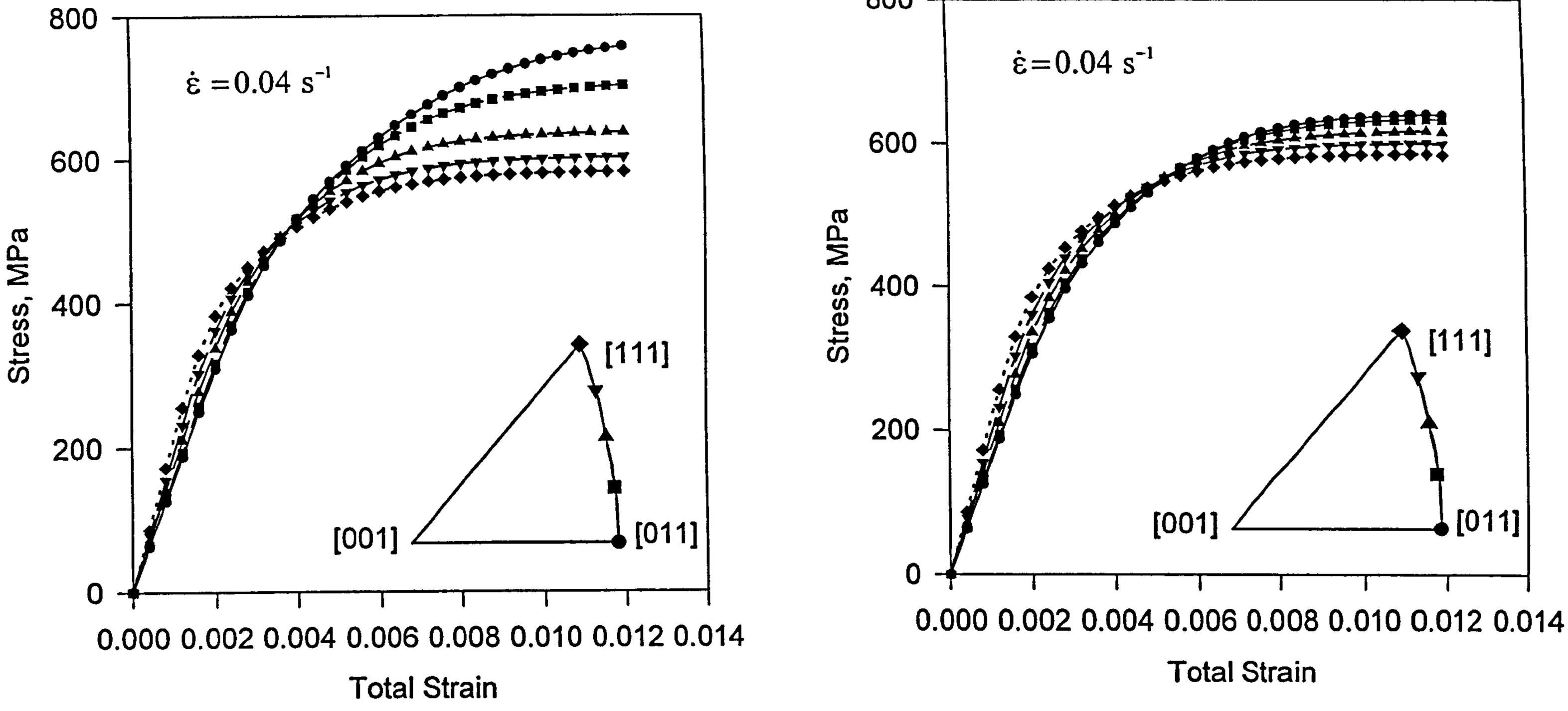

Fig.3.10b Comparison of Stress and Strain Response on the [011]-[111] Side

(a) Crystallographic Model

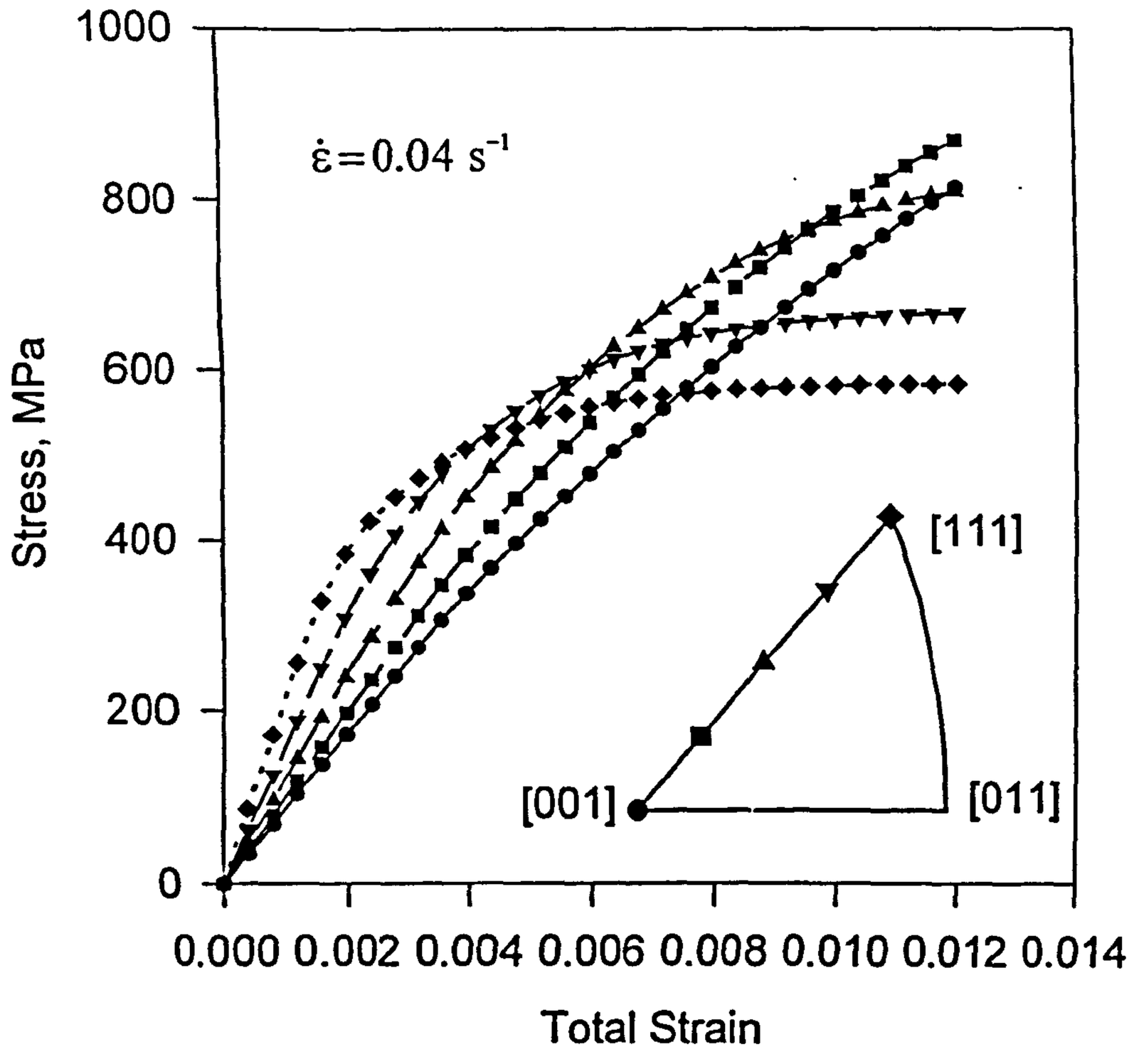

(b) Phenomenological Model

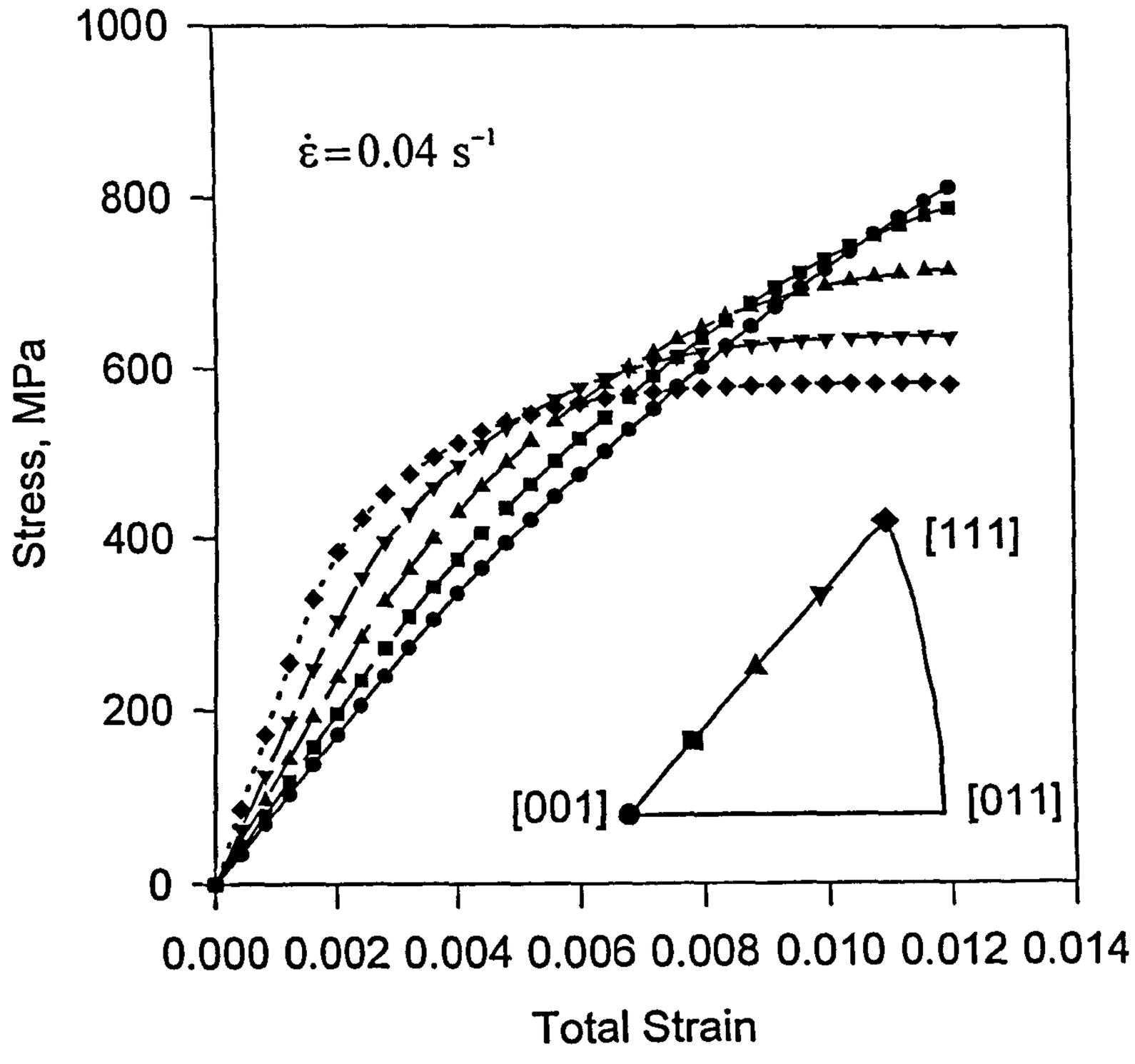

Fig.3.10c Comparison of Stress and Strain Response on the [001]-[111] Side

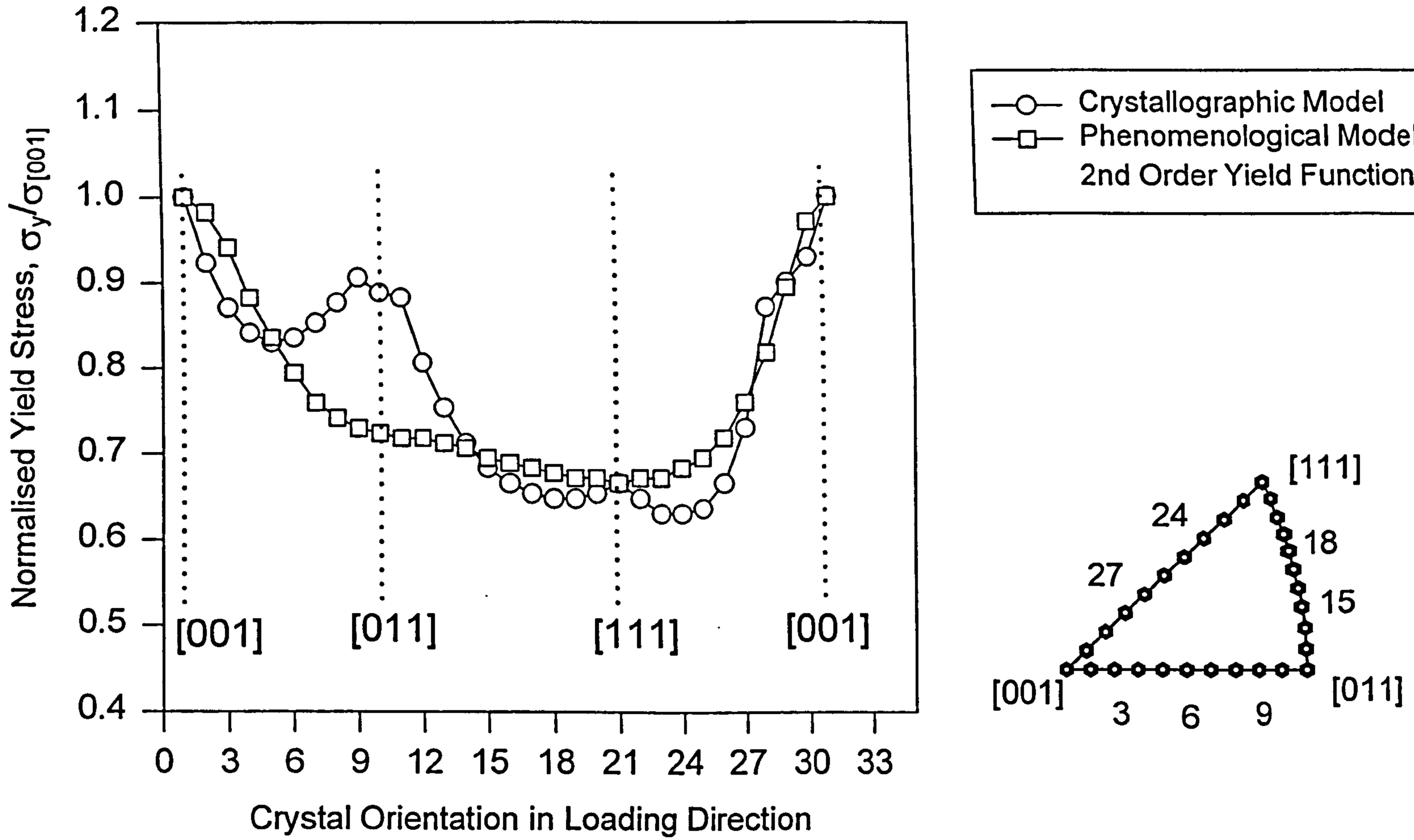

Fig.3.11 Comparison of Yield Stresses under Uniaxial Loading

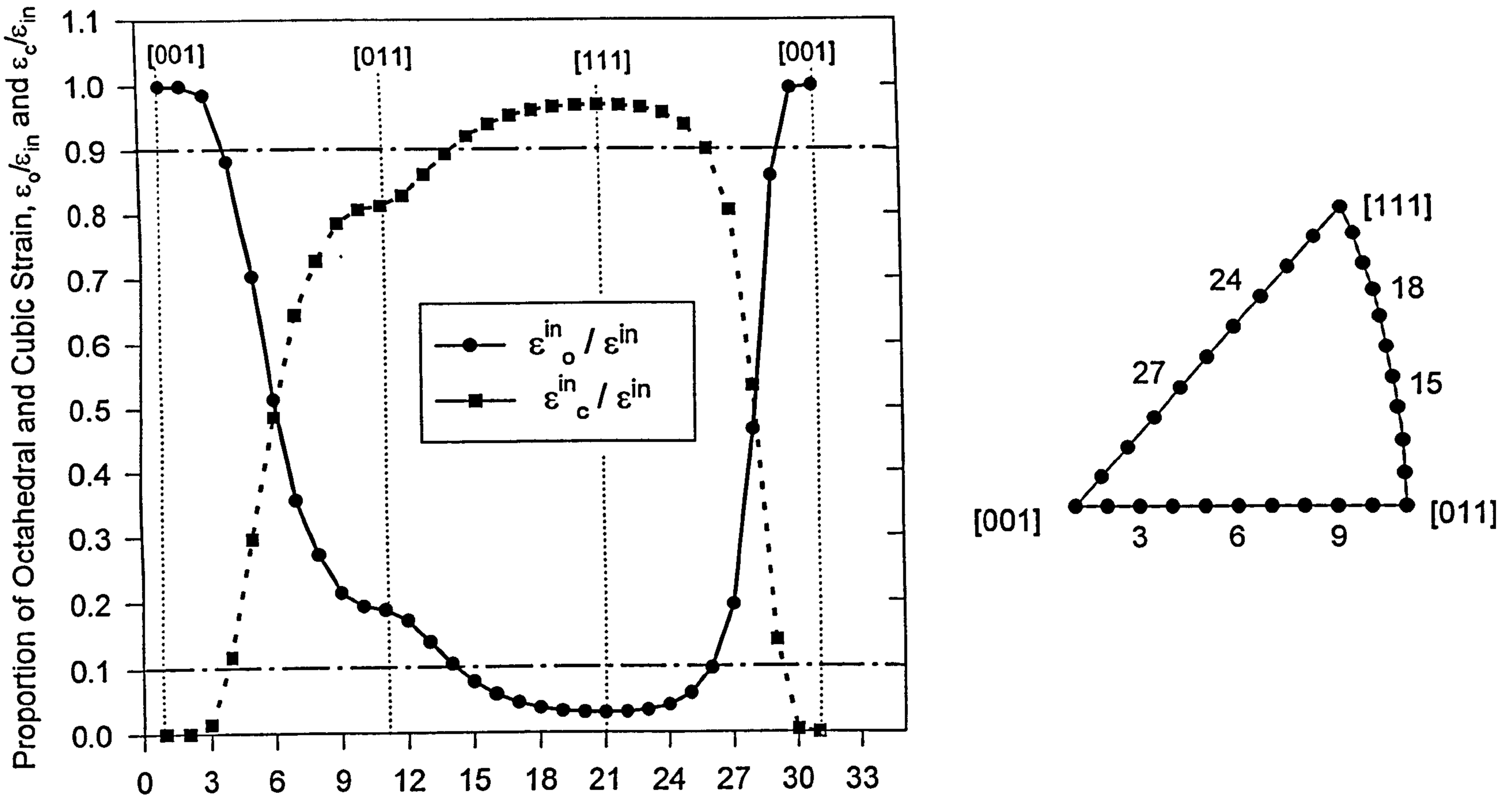

Fig.3.12. Inelastic Strain Ratio of Cubic and Octahedral Deformation Based on the crystallographic Model

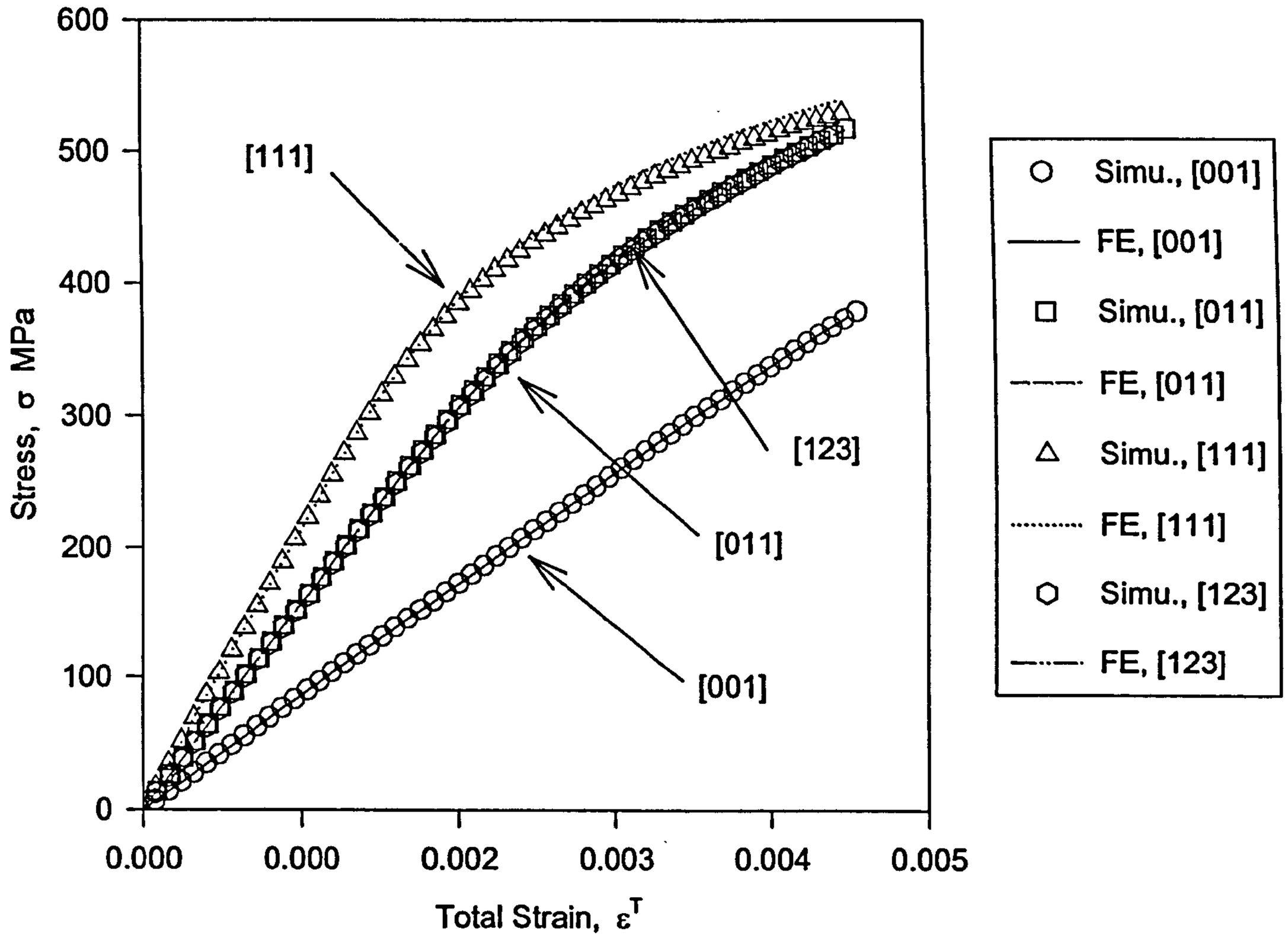

Fig.4.1 Comparison of Stress and Strain Response for Different Orientations between FE and Theoretical Simulation Results

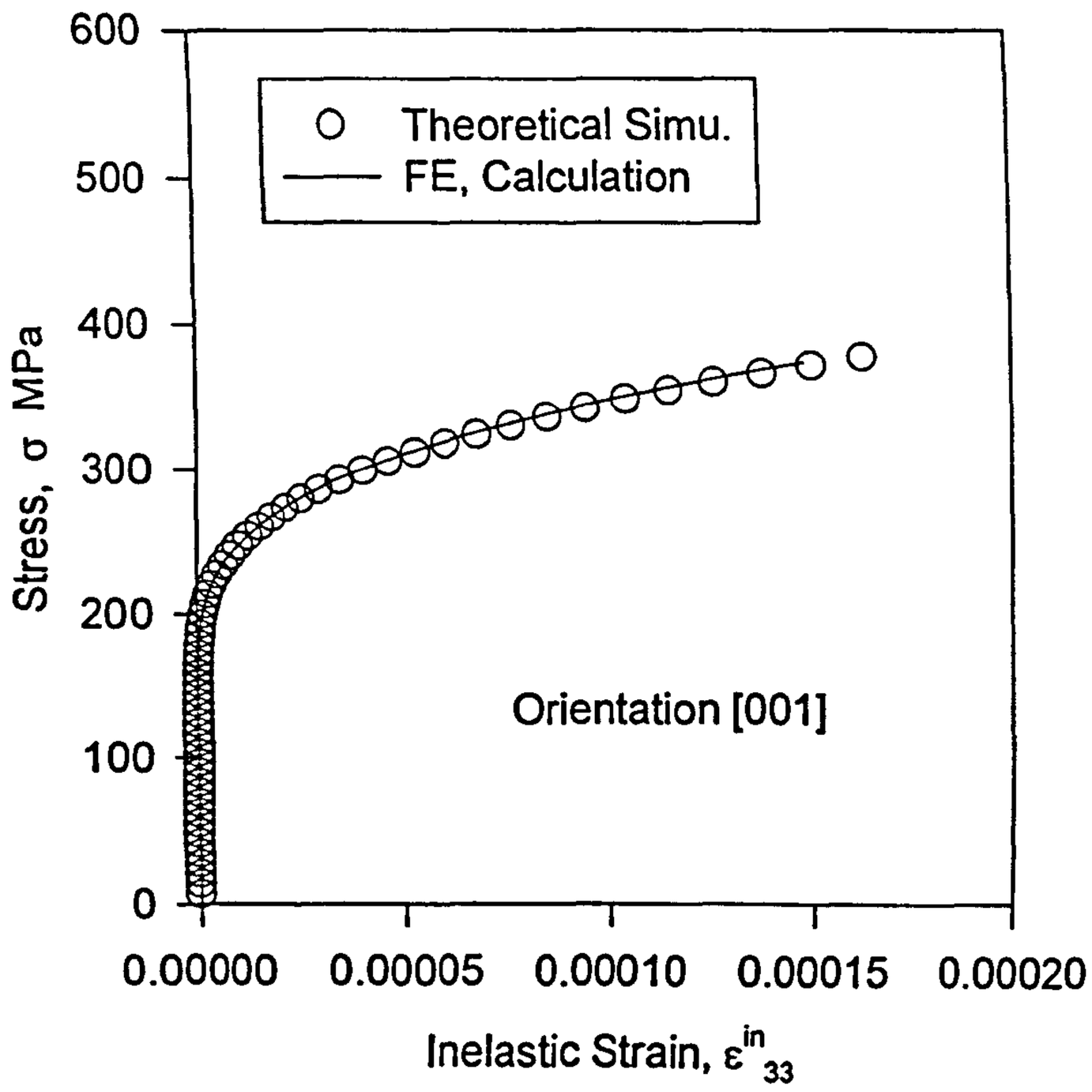

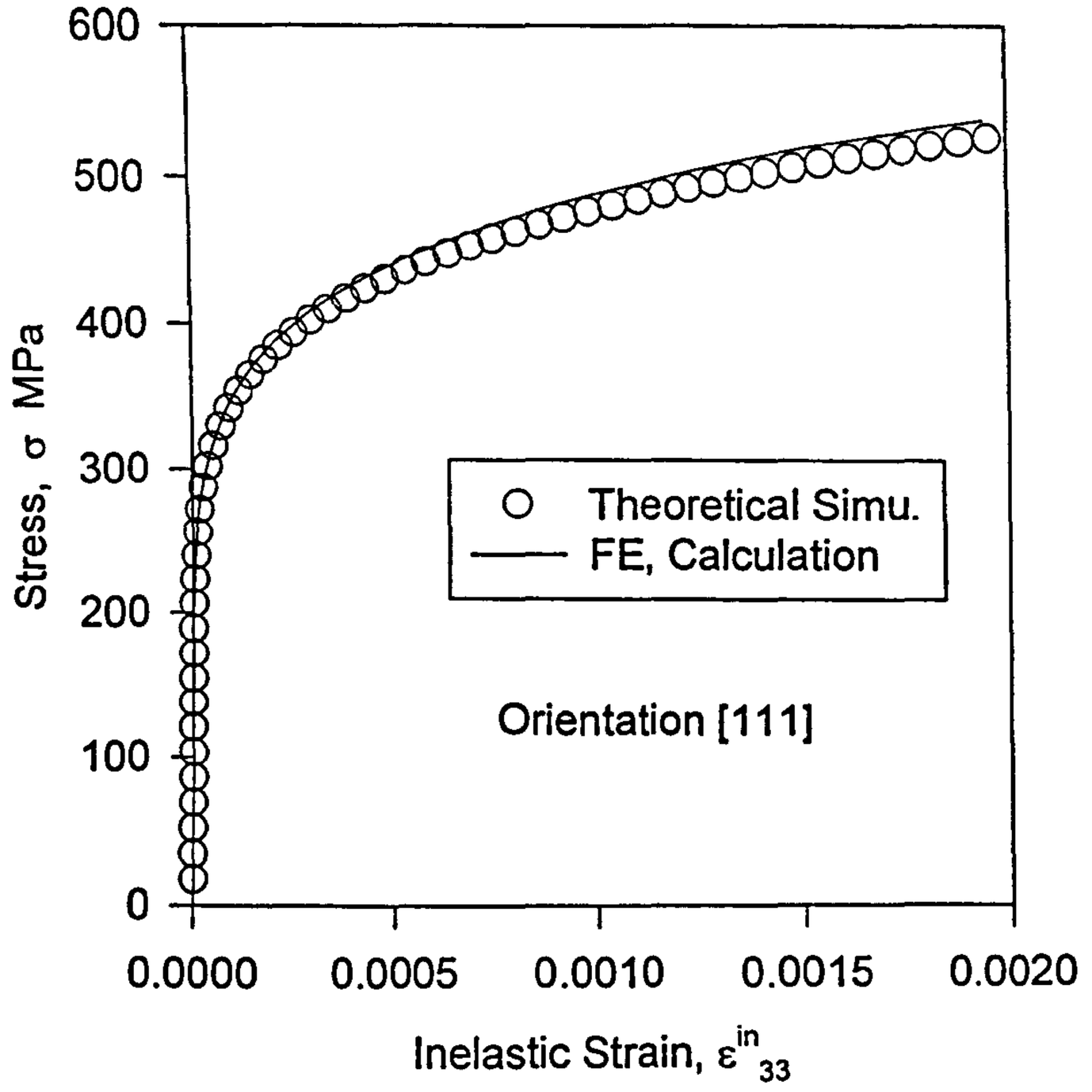

Fig.4.2a Stress and Inelastic Strain Response for [001] and [111] Comparison of FE and Theoretical Simulation Results

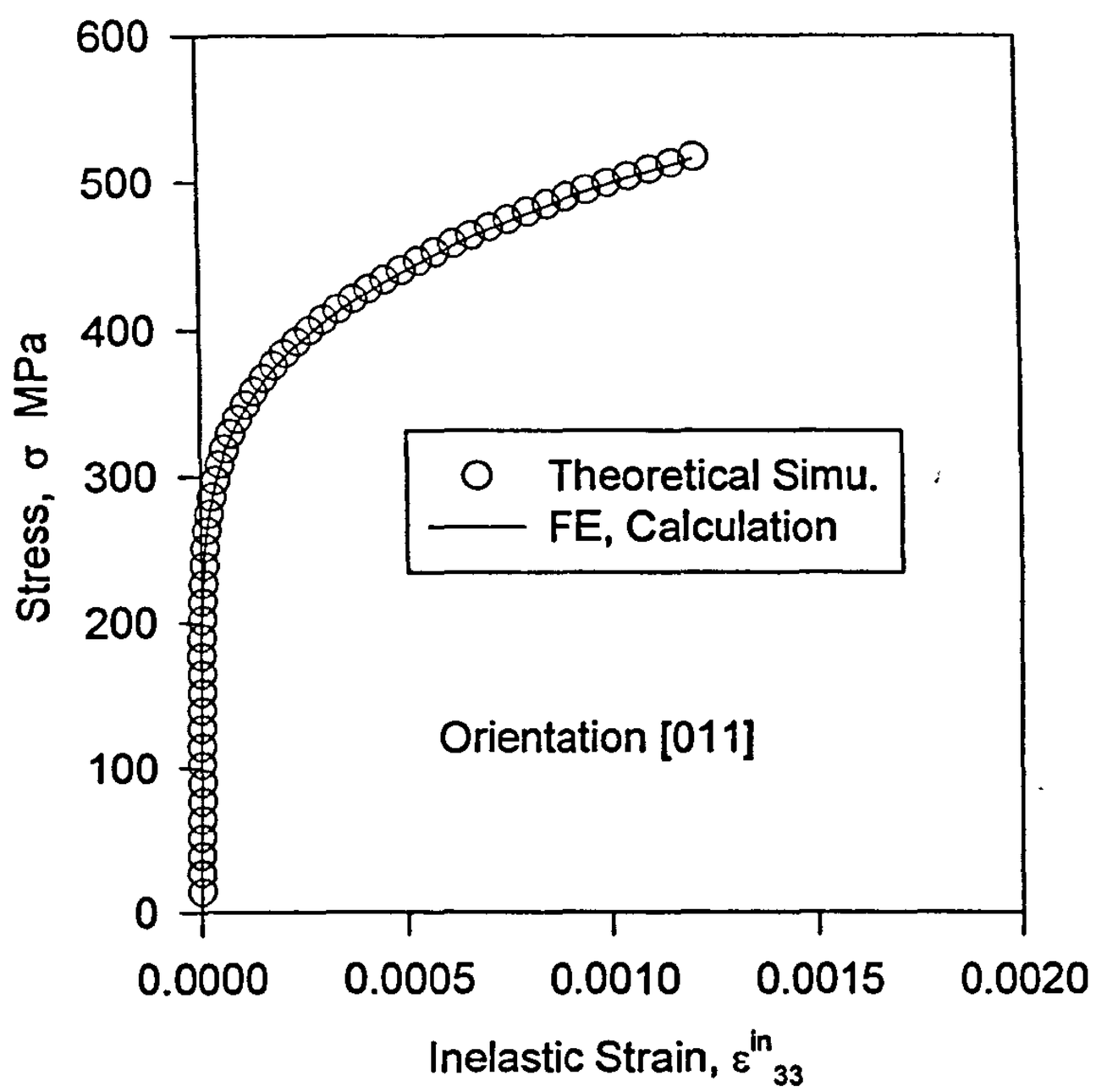

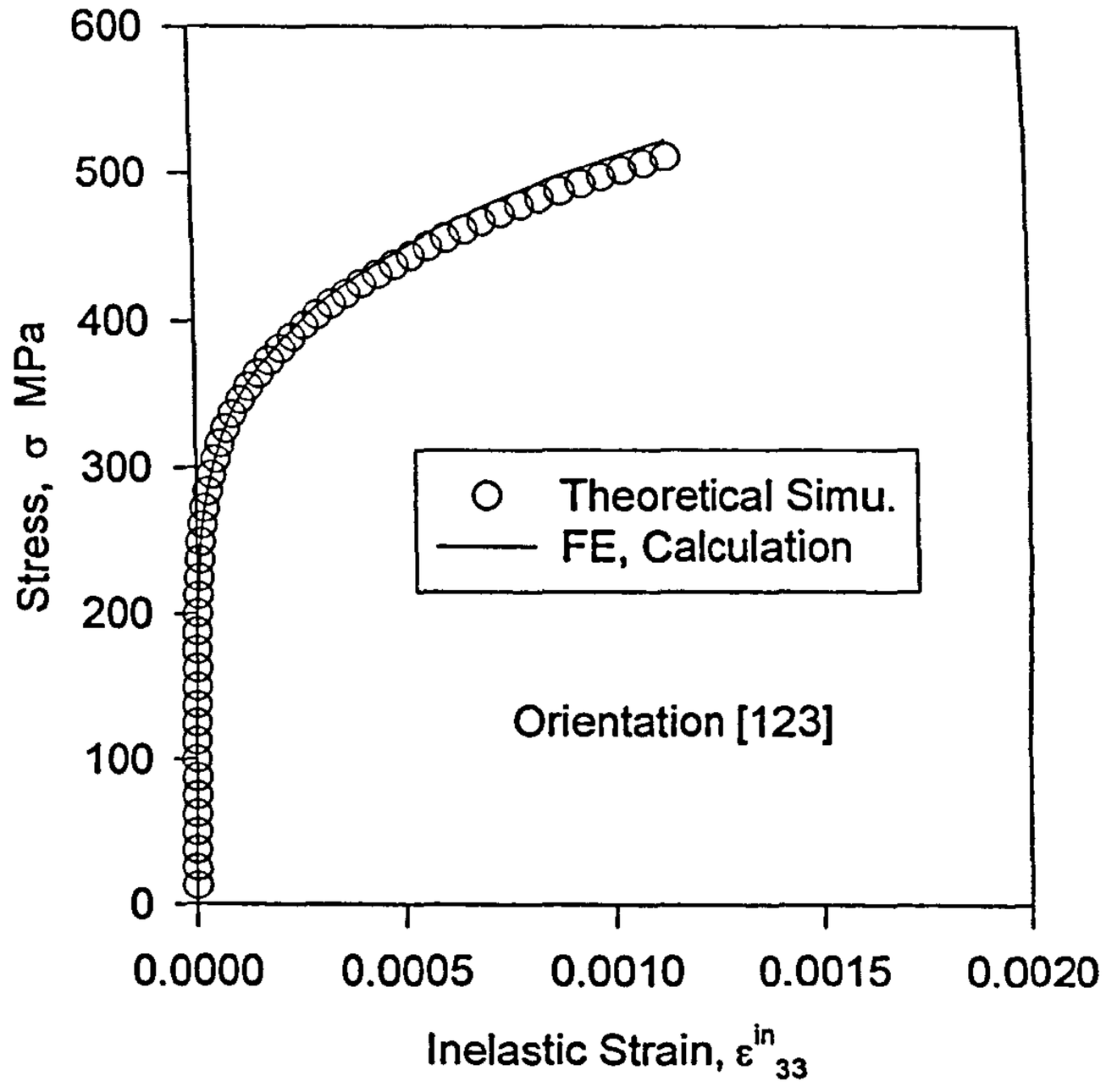

Fig.4.2b Stress and Inelastic Strain Response for [011] and [123] Comparison of FE and Theoretical Simulation Results

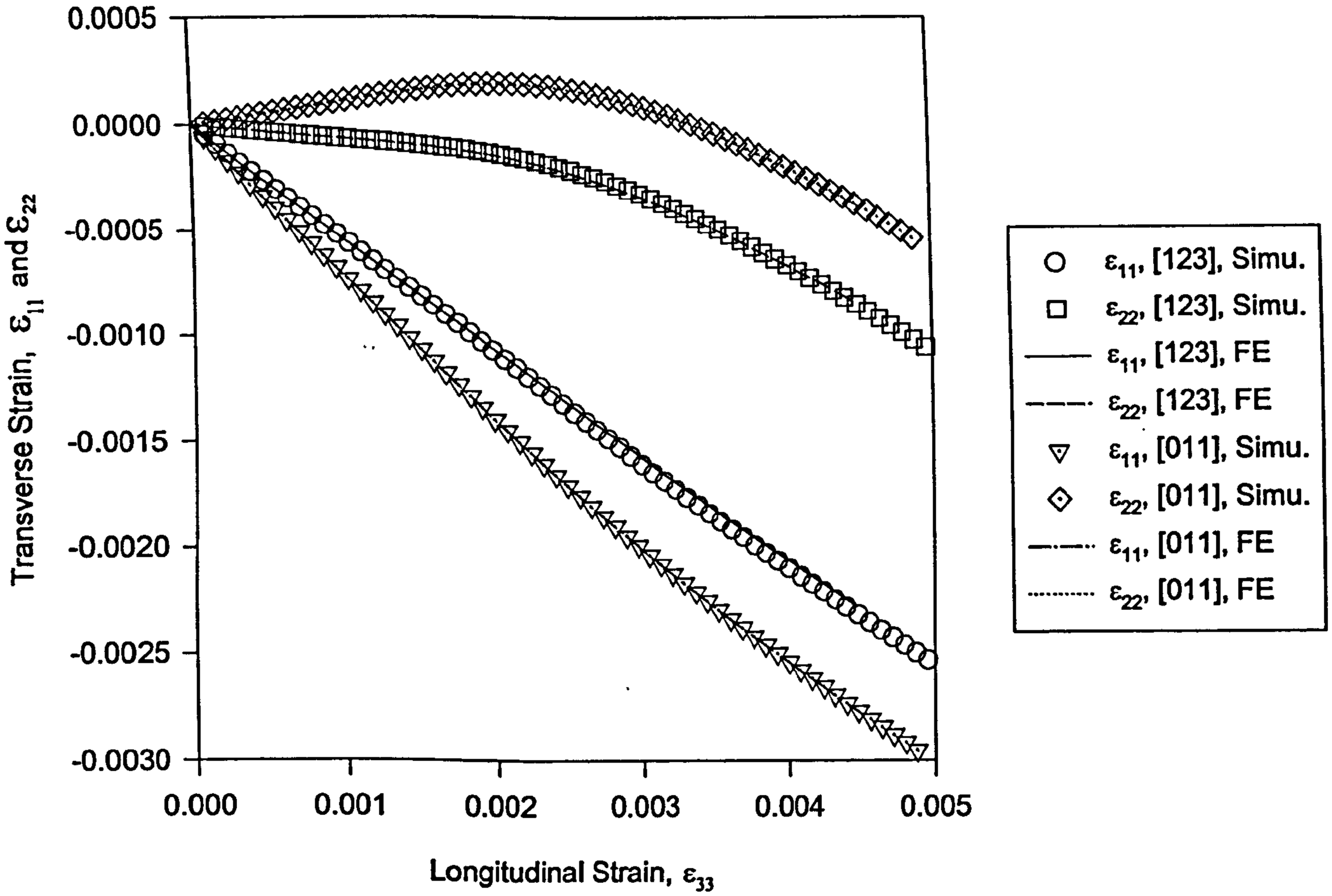

Fig.4.3a Comparison of Transverse Strain Response for the [123] and [011] Orientations

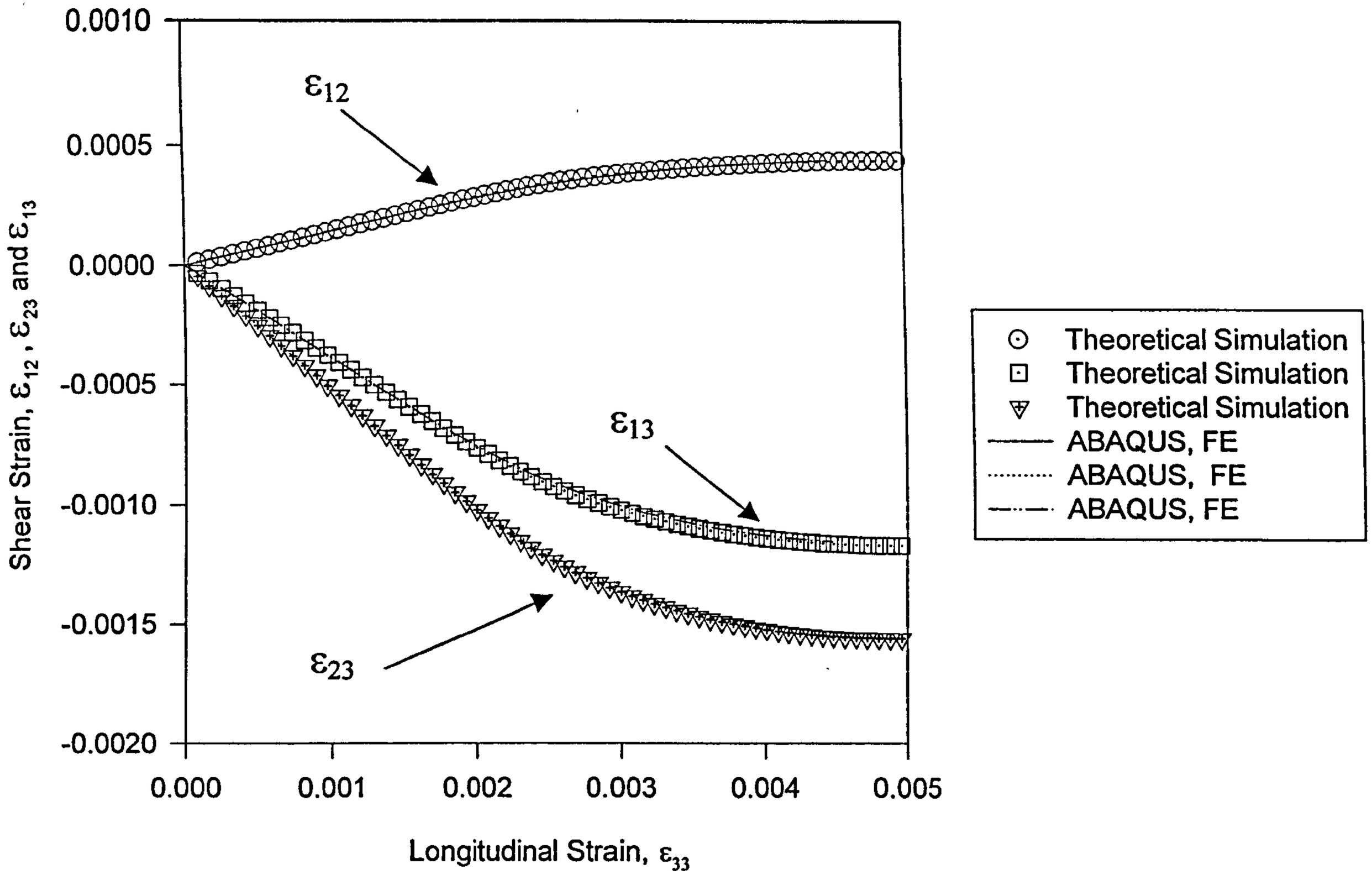

Fig.4.3b Comparison of Shear Strain Response Obtained from Different Calculations for Orientation [123]

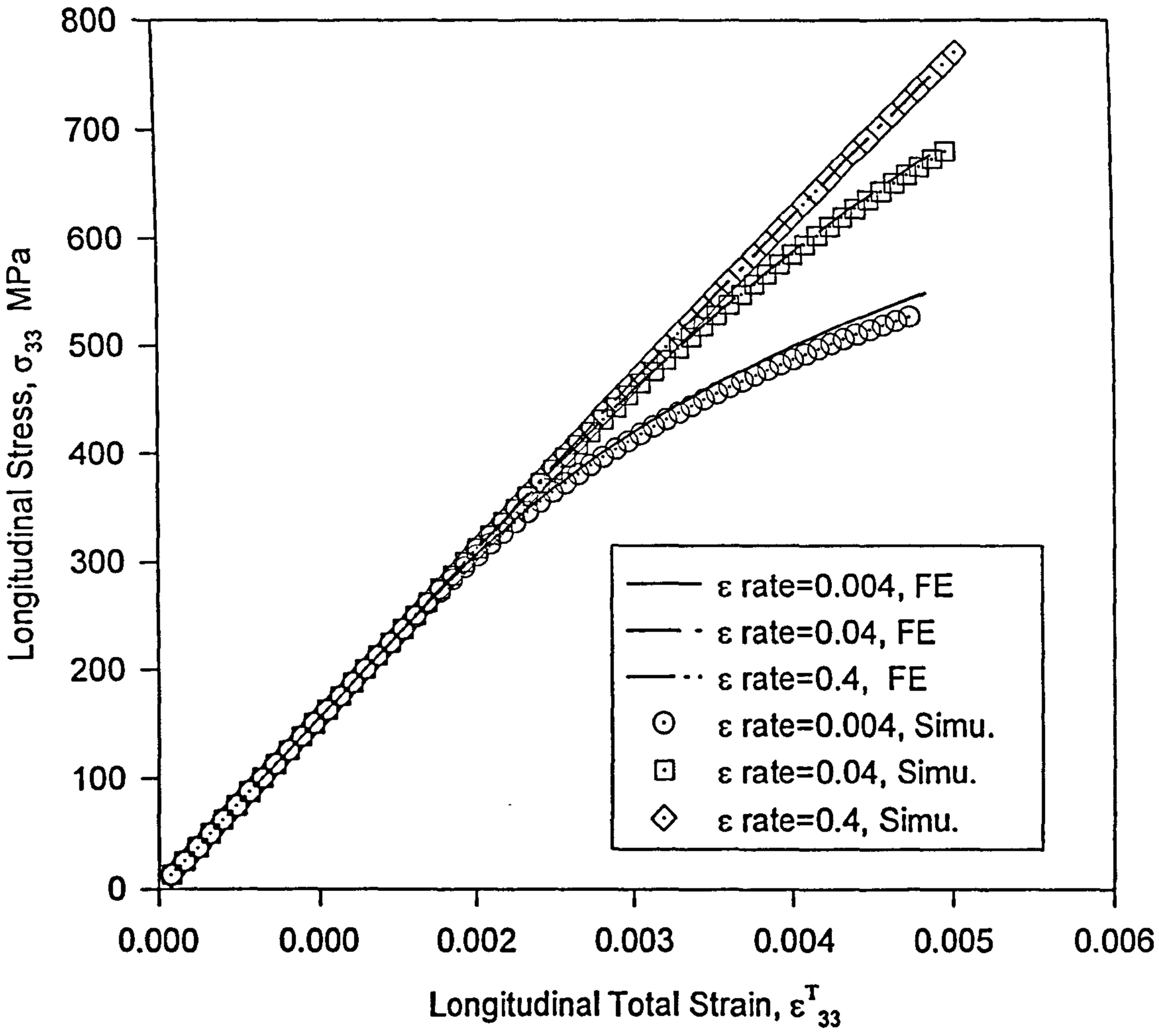

Fig.4.4a Strain Rate Effect on Stress and Strain Response of Orientation [123]

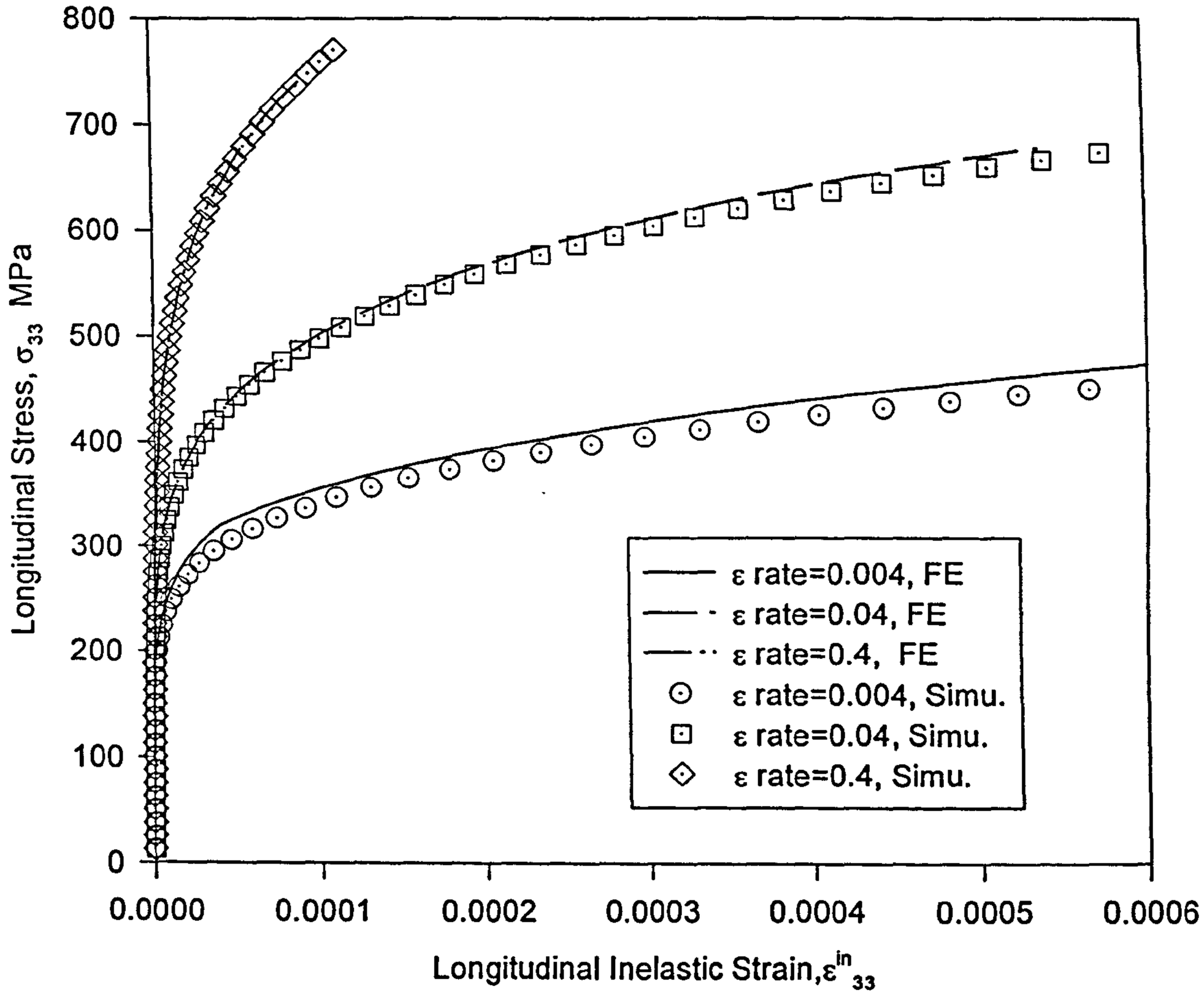

Fig.4.4b Strain Rate Effect on Stress and Inelastic Strain Response of Orientation [123]

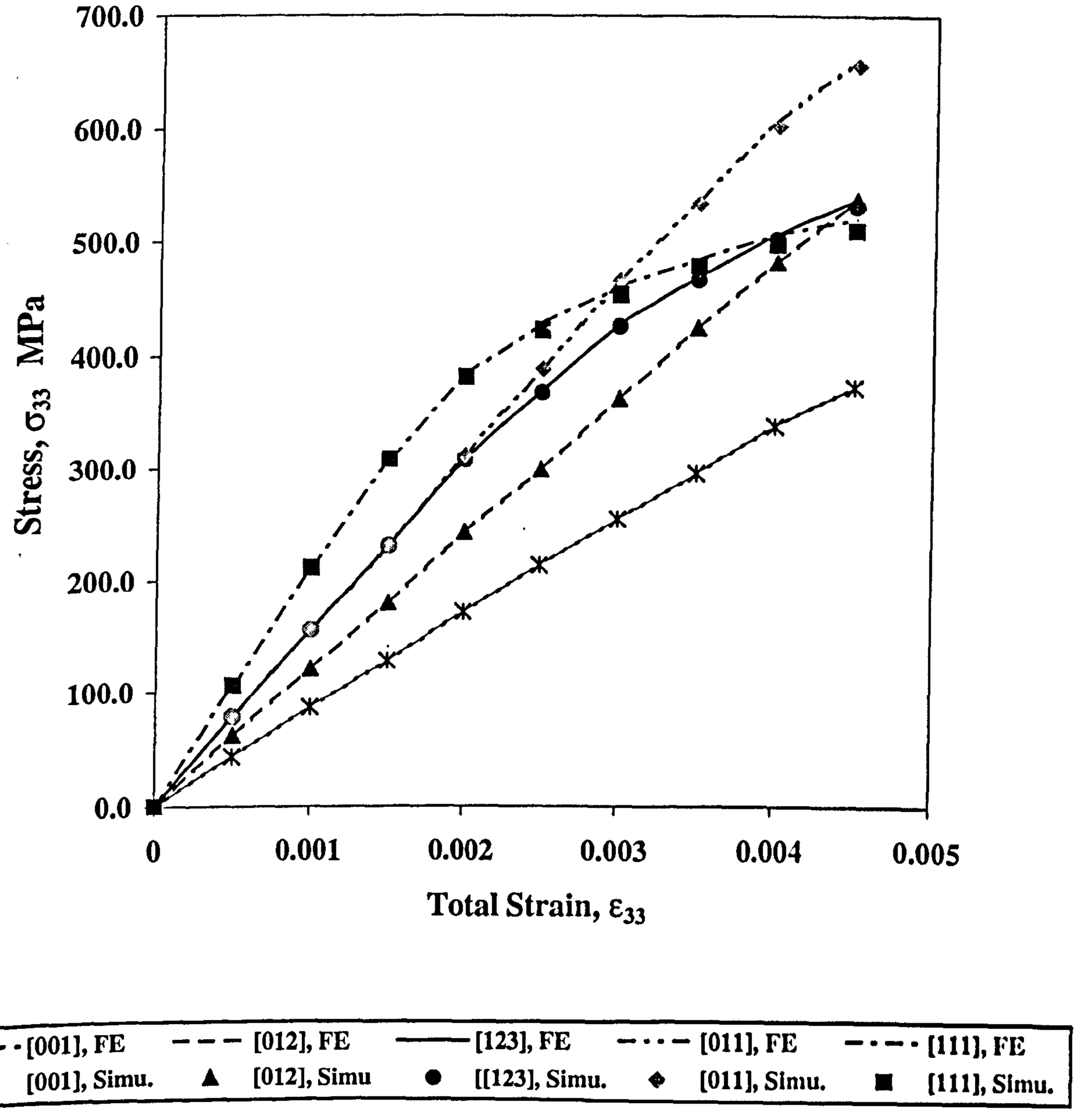

Fig.4.5 Orientation Dependent Stress and Strain Response Predicted by the Crystallographic Model

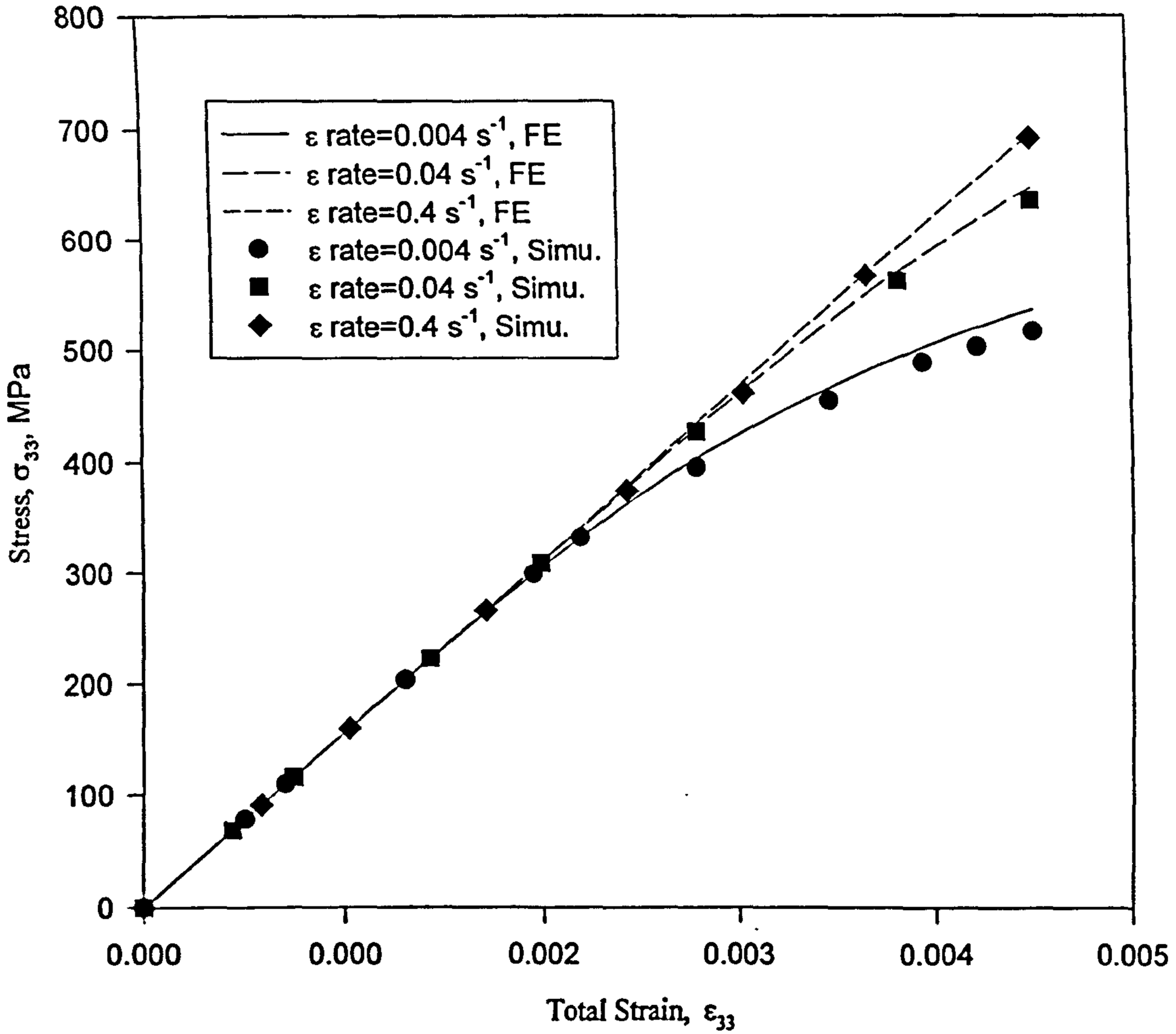

Fig.4.6a The Strain Rate Effect on Stress and Total Strain Response of Orientation [123] (Crystallographic Model)

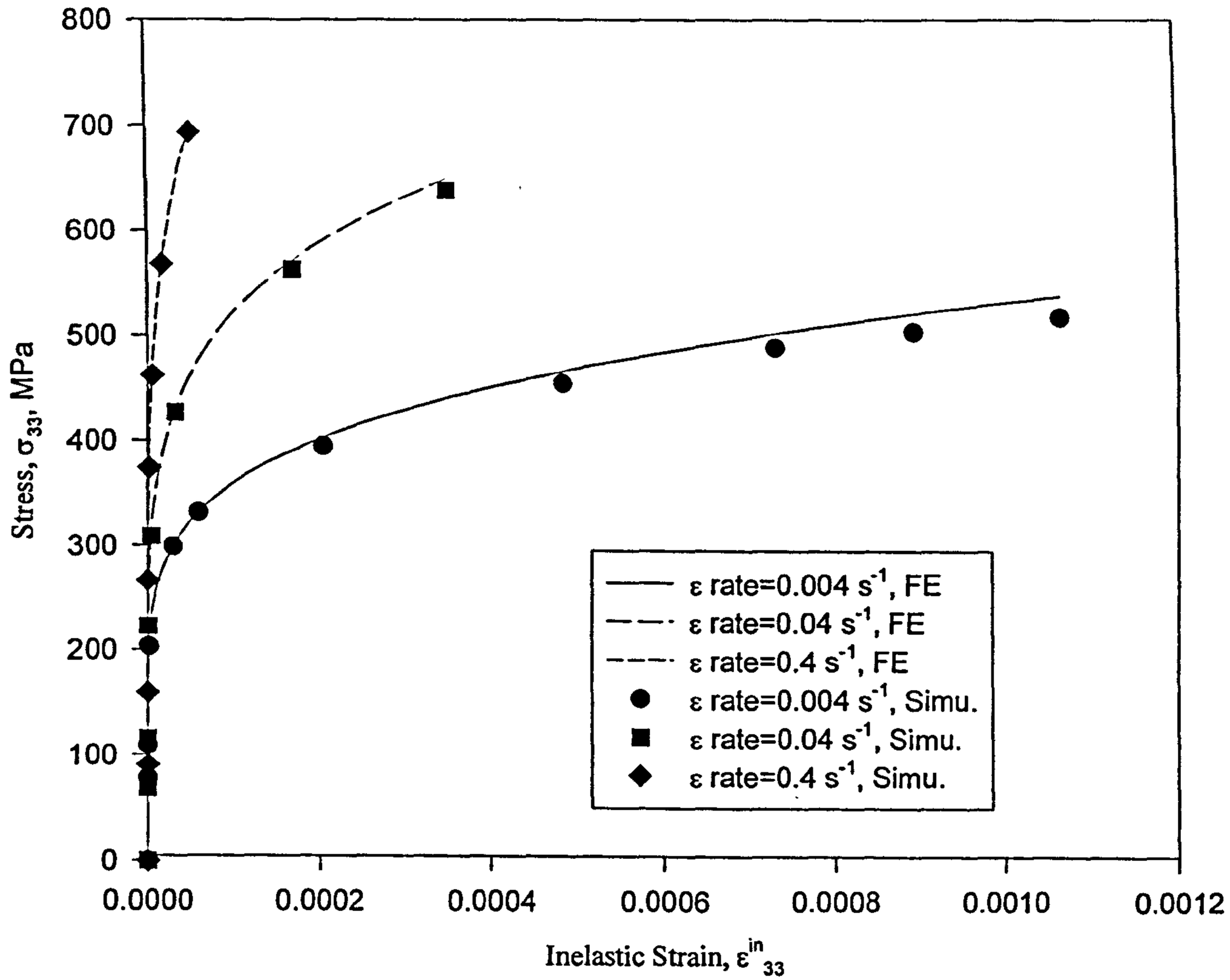

Fig.4.6b The Strain Rate Effect on Stress and Inelastic Strain Response of Orientation [123] (Crystallographic Model)

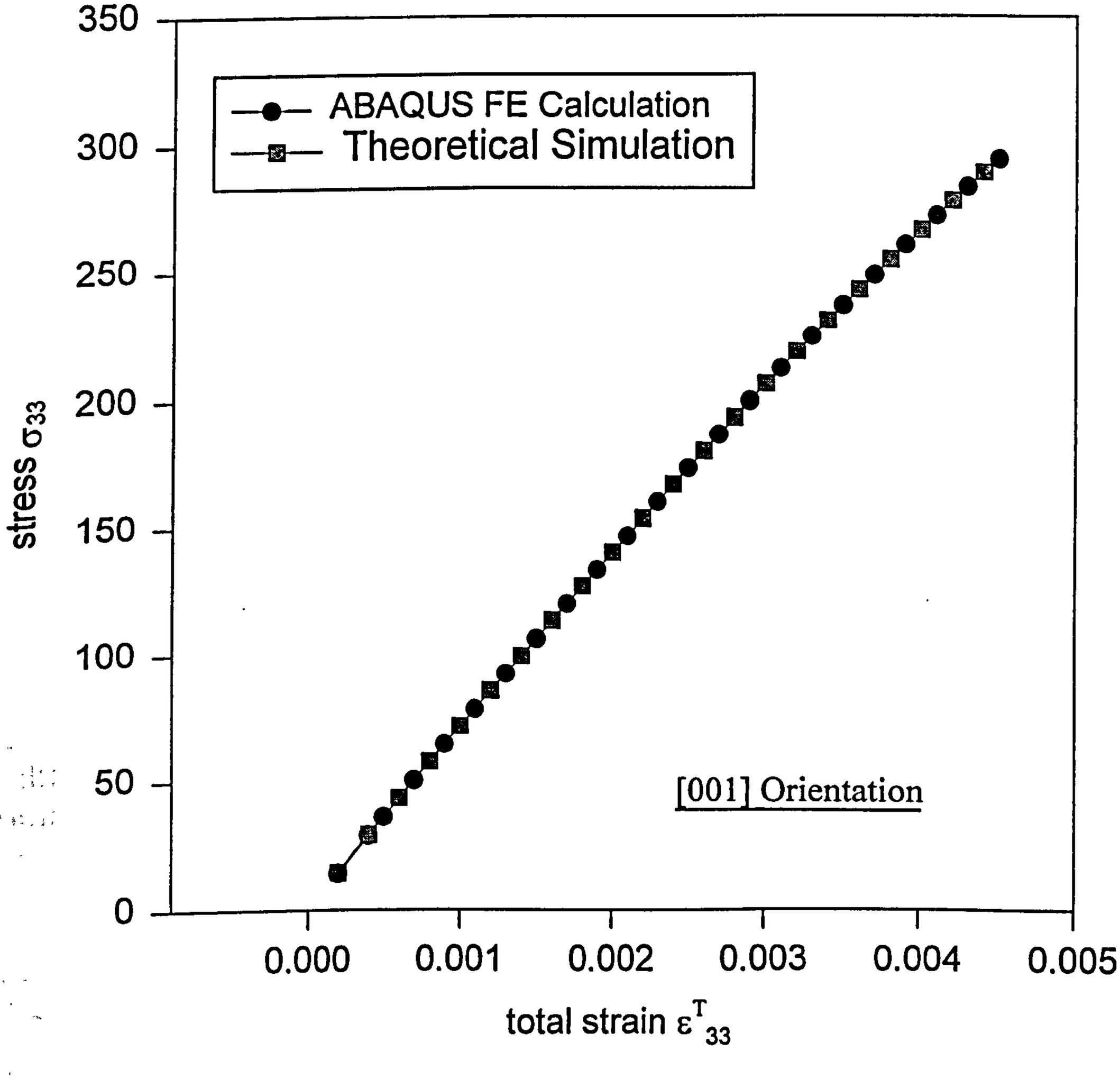

Fig.4.7 Comparison of Stress-Strain Response under Thermal-Mechanical Loading for [001] Orientation

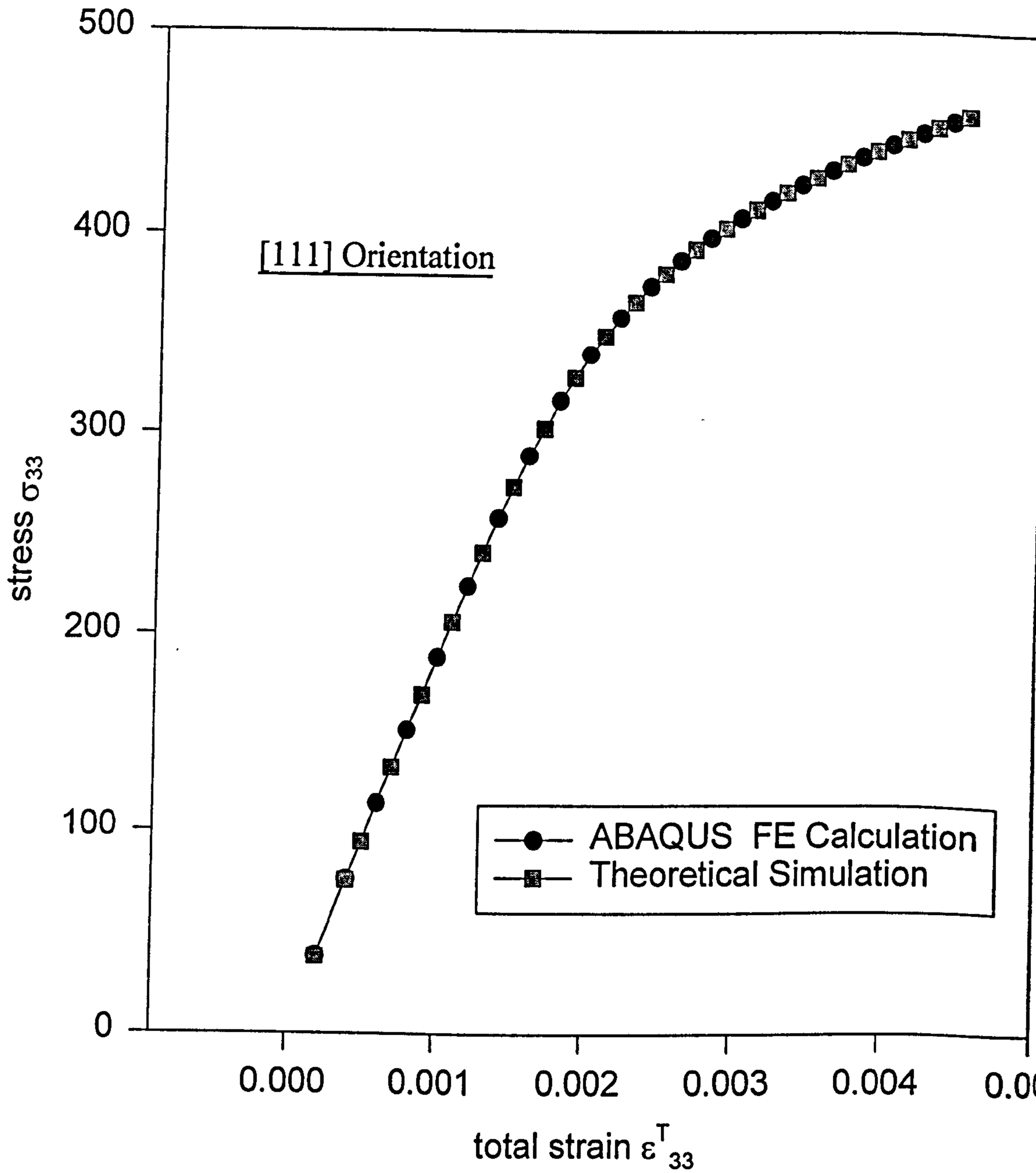

Fig.4.8 Comparison of Stress-Strain Response under Thermal-Mechanical Loading for [111] Orientation

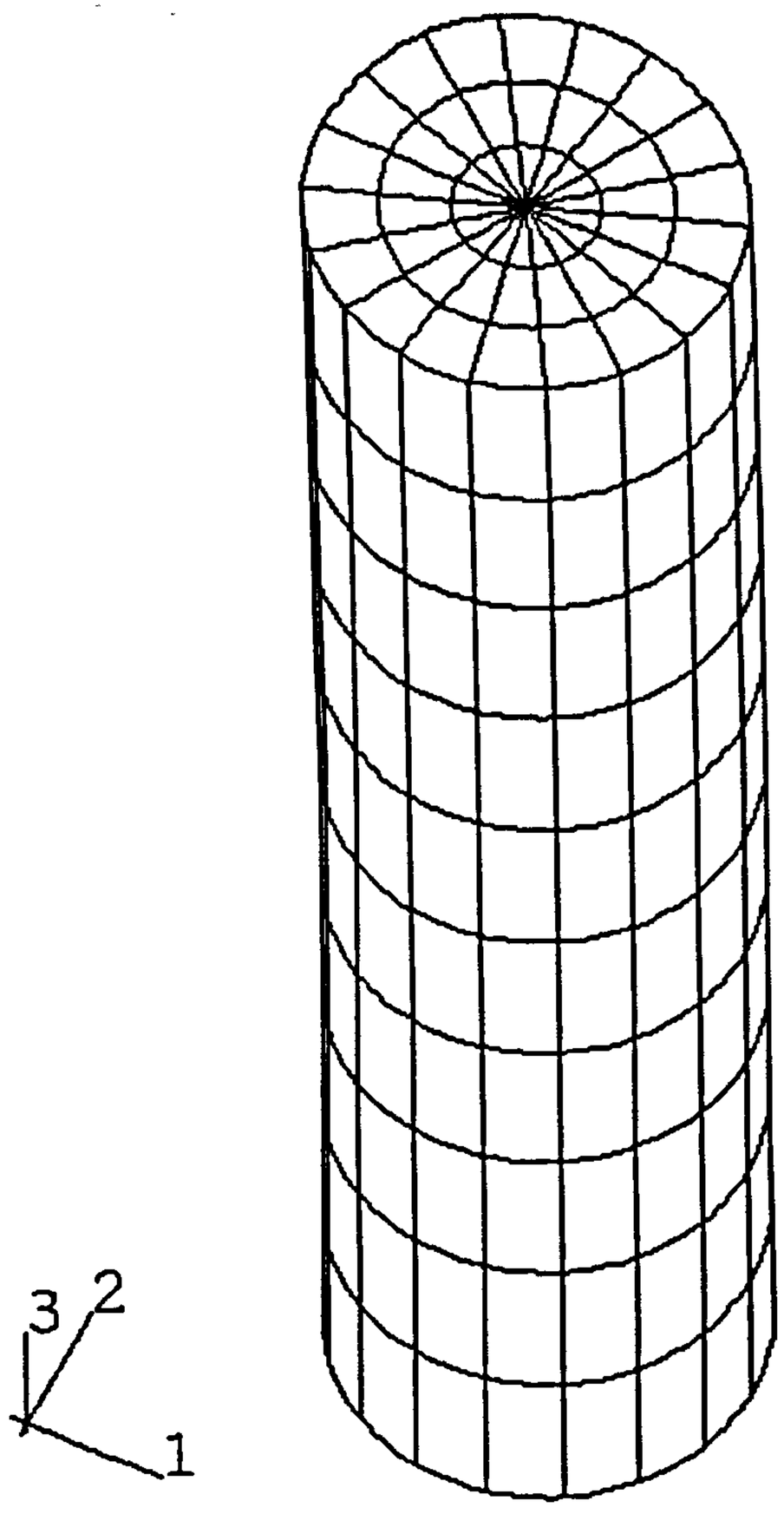

(1a) Cylindrical Bar

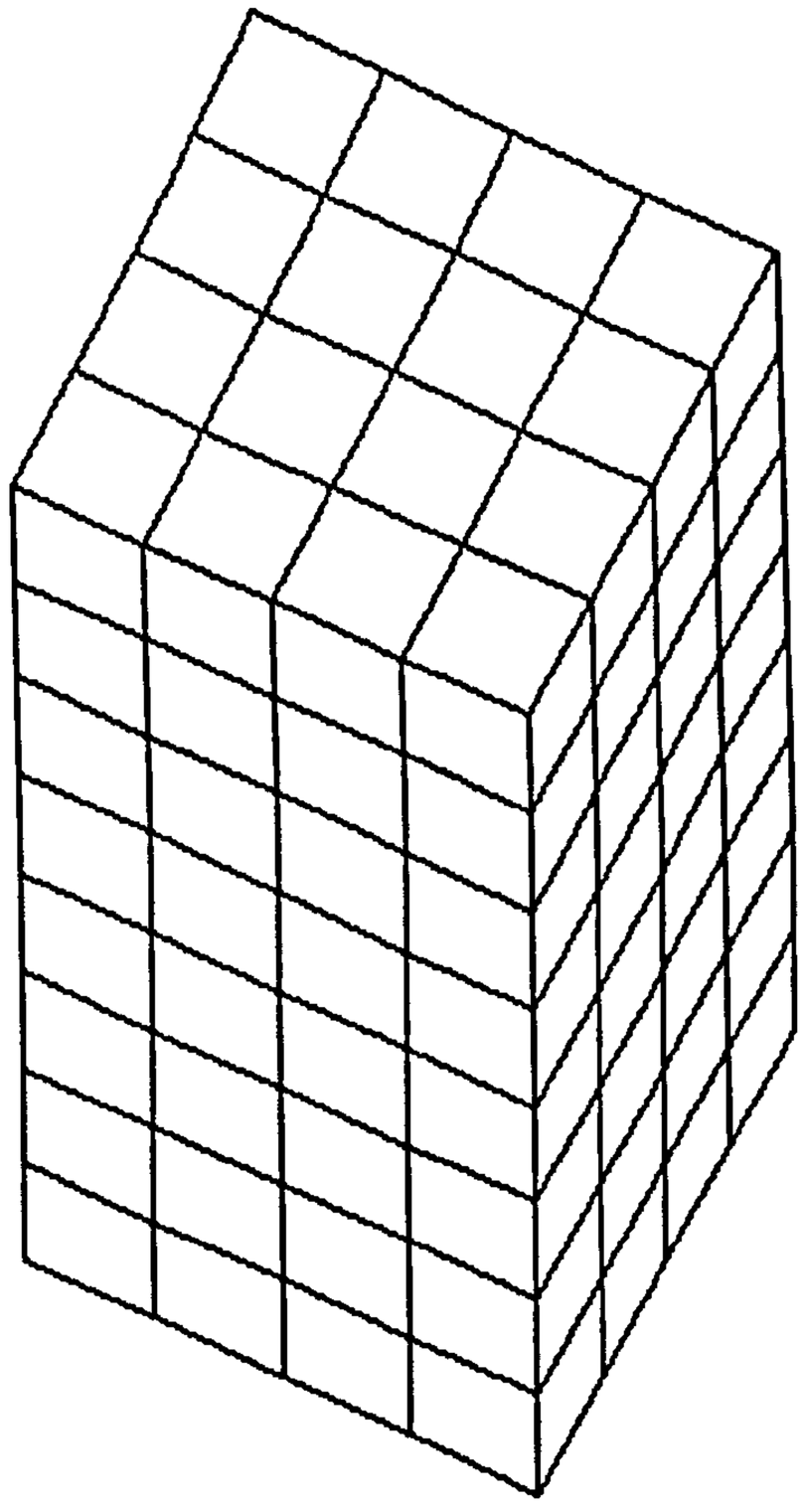

(1b) Column Bar

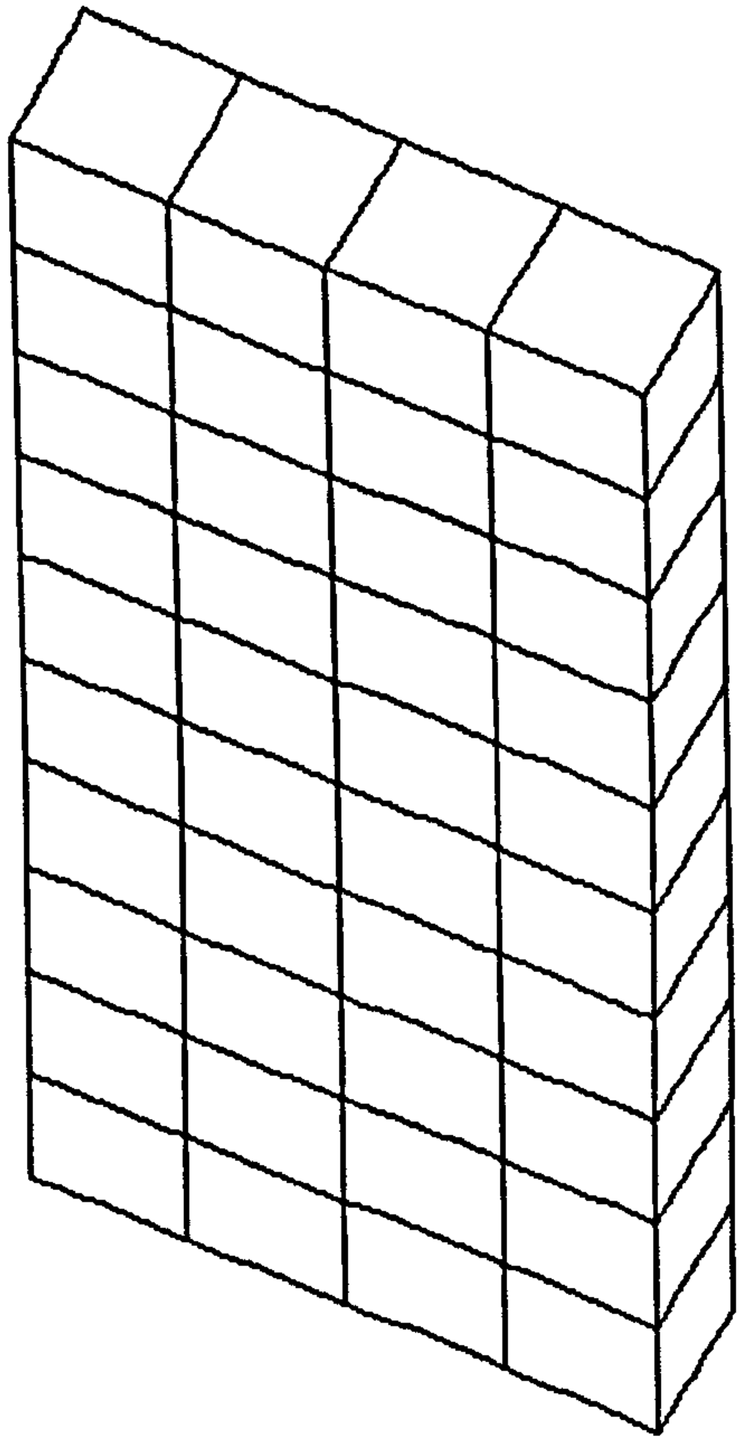

(1c) Rectangular Plate

Fig.5.1 Original Mesh for Different Solid Specimens Used in the FE Calculations

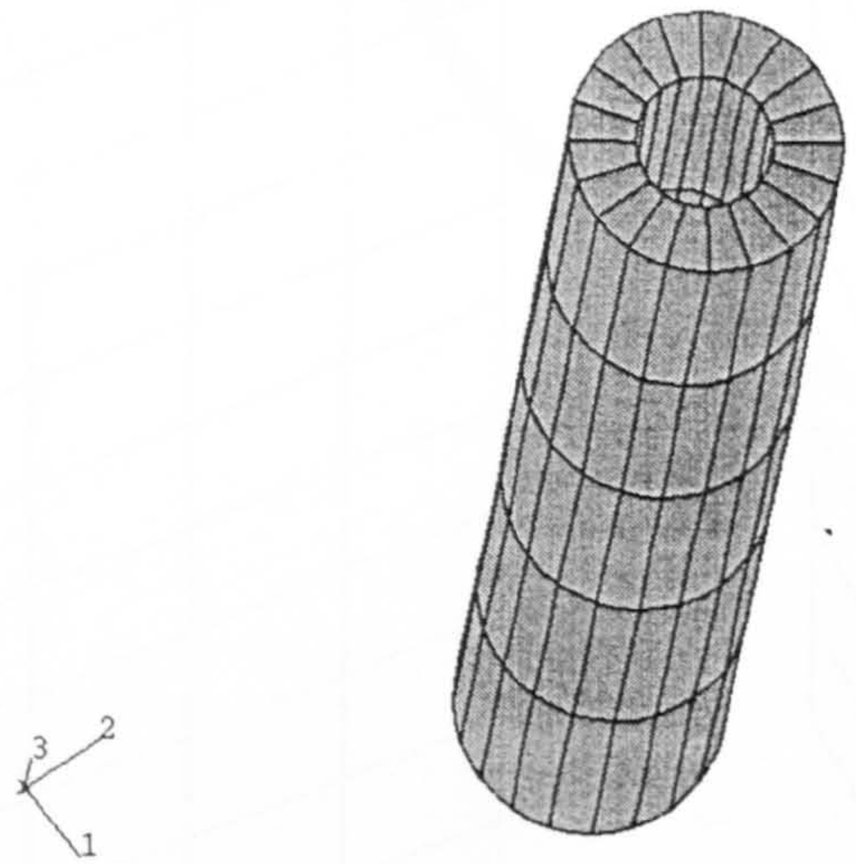

(5.2a)

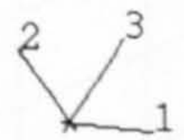

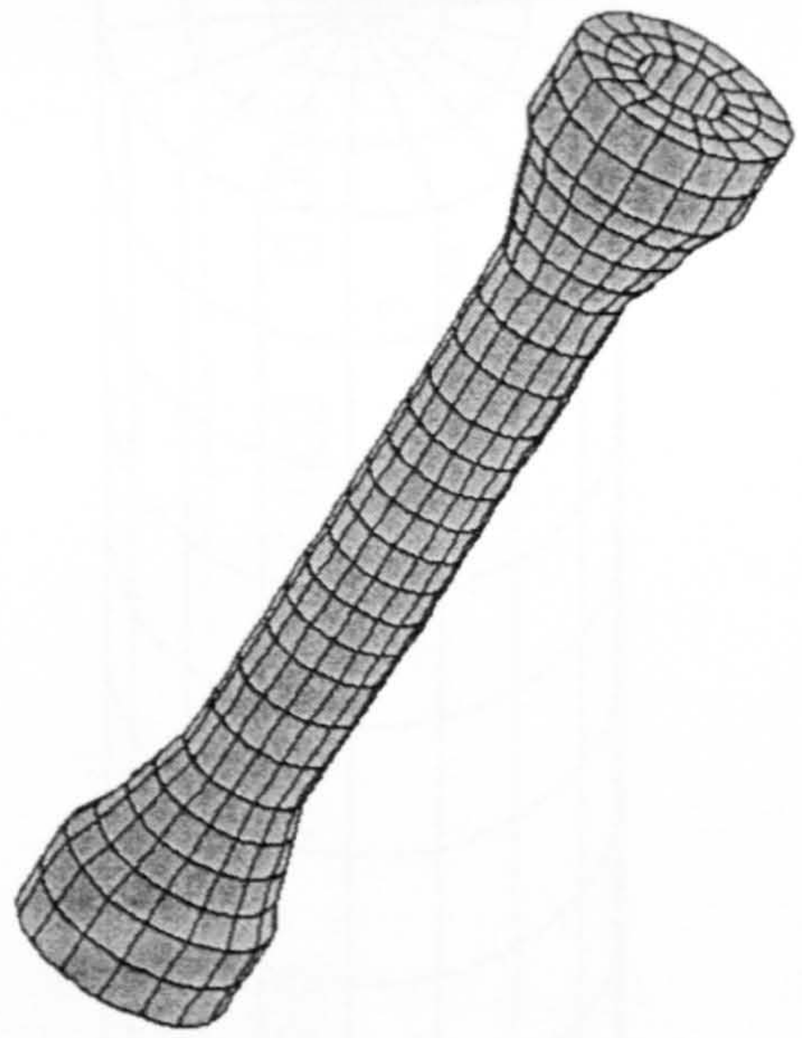

(5.2b)

Fig.5.2 Original Meshes for Different Tube Specimens Used in the FE Calculations

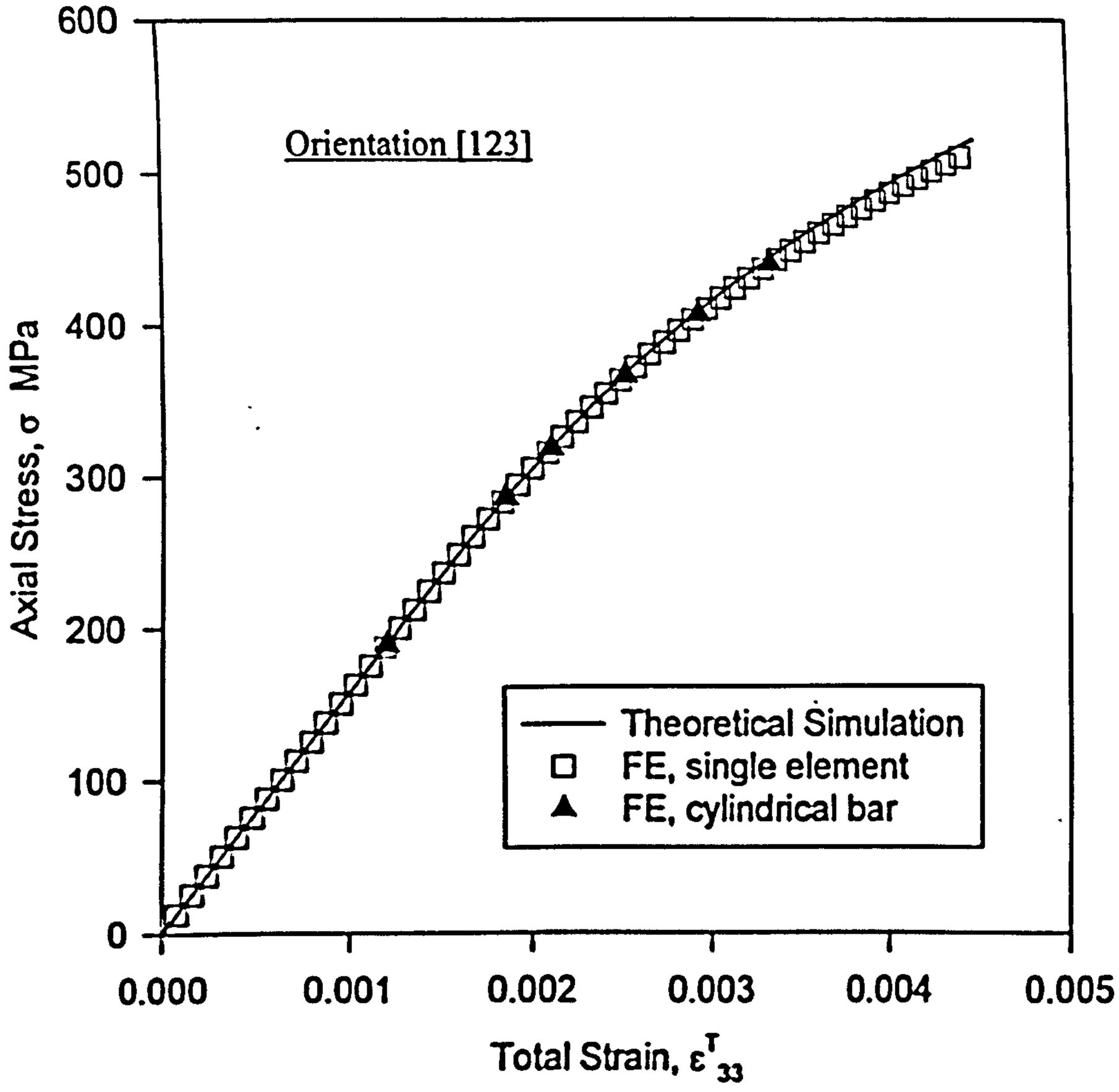

Fig.5.3. Comparison of Stress and Strain Responses Obtained from Different Calculations

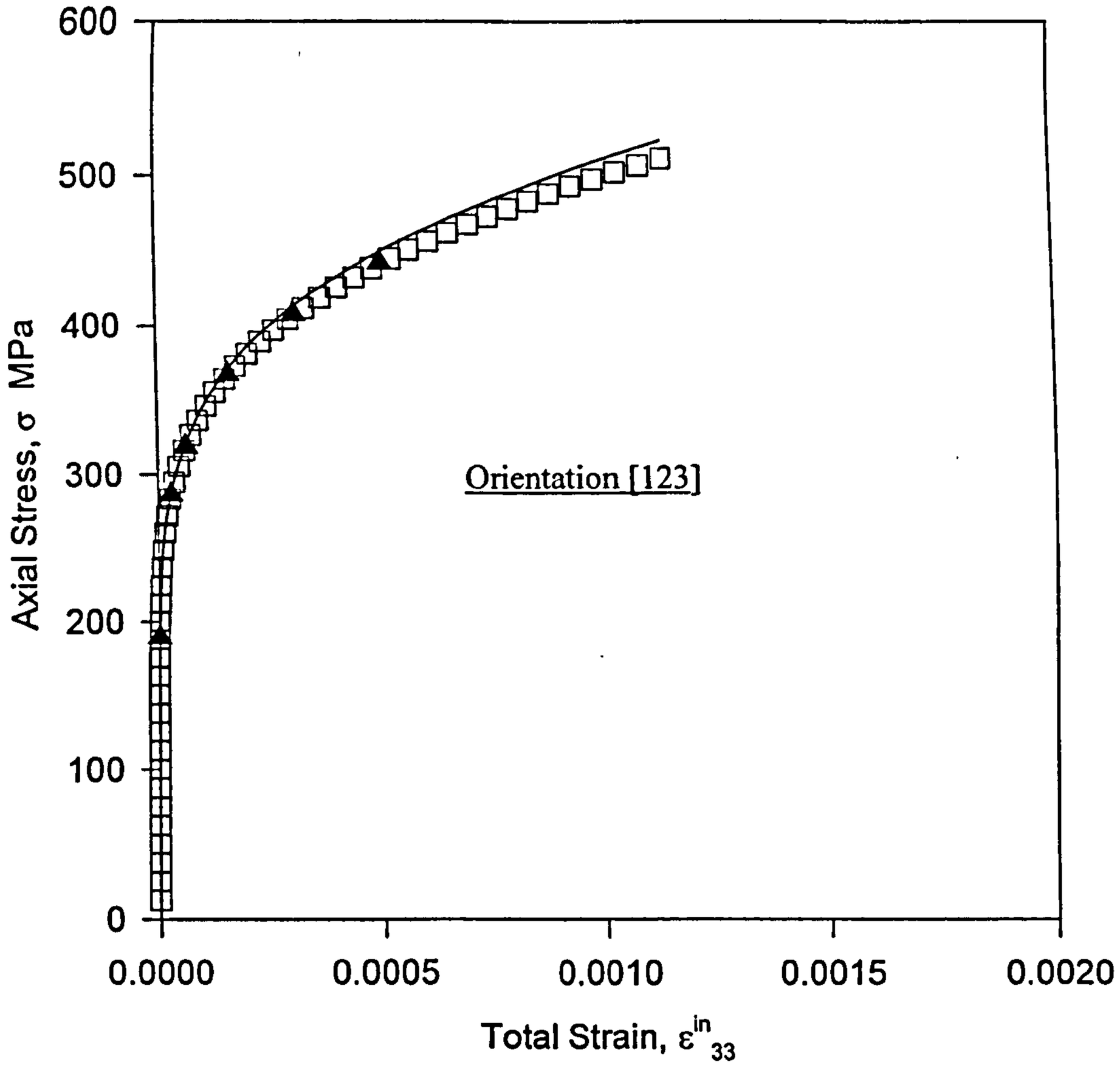

Fig.5.4 Comparison of Stress and Inelastic Strain Responses Obtained from Different Calculations

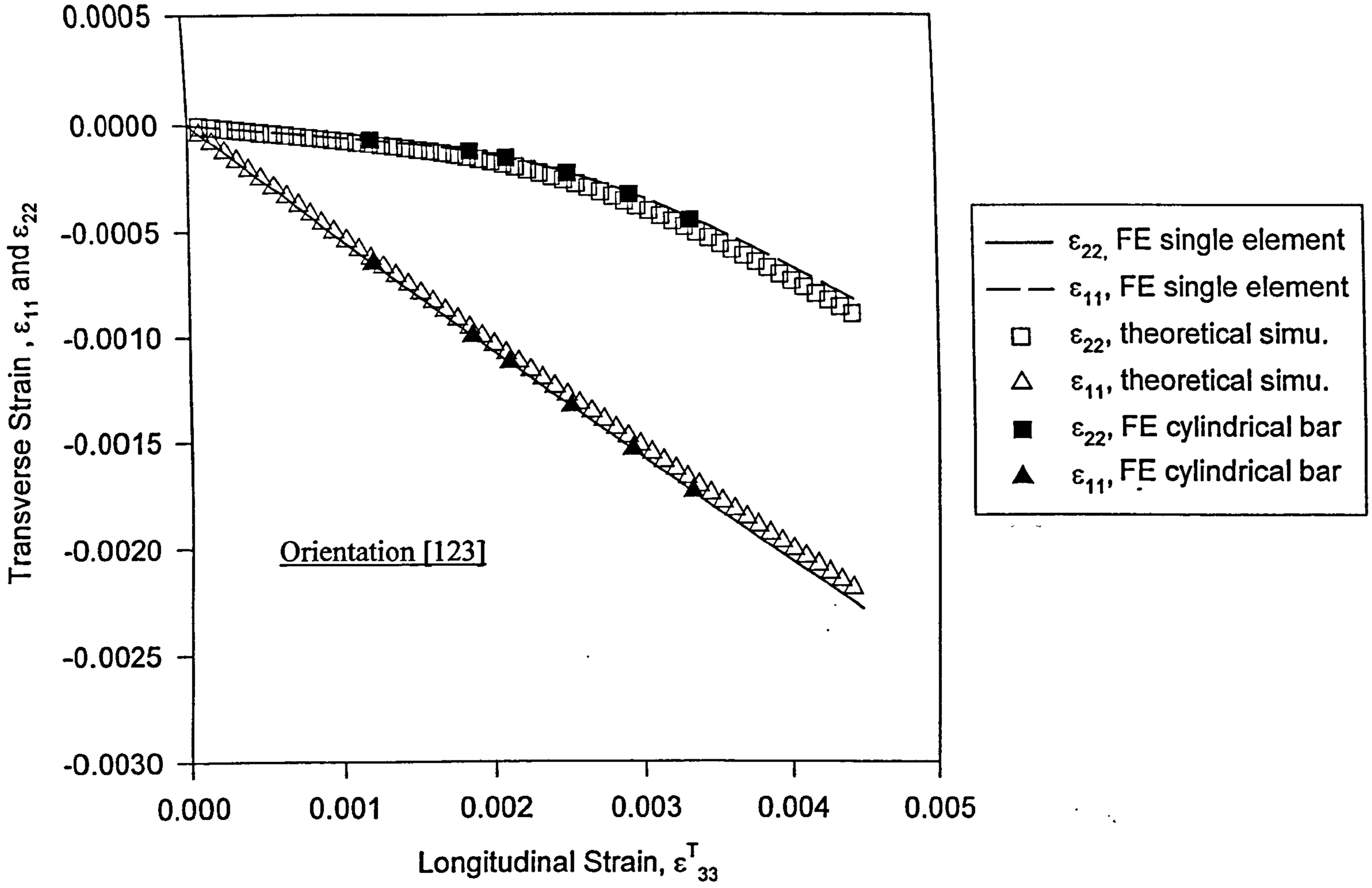

Fig.5.5 Comparison of Transverse Strain Response Obtained from Different Calculations

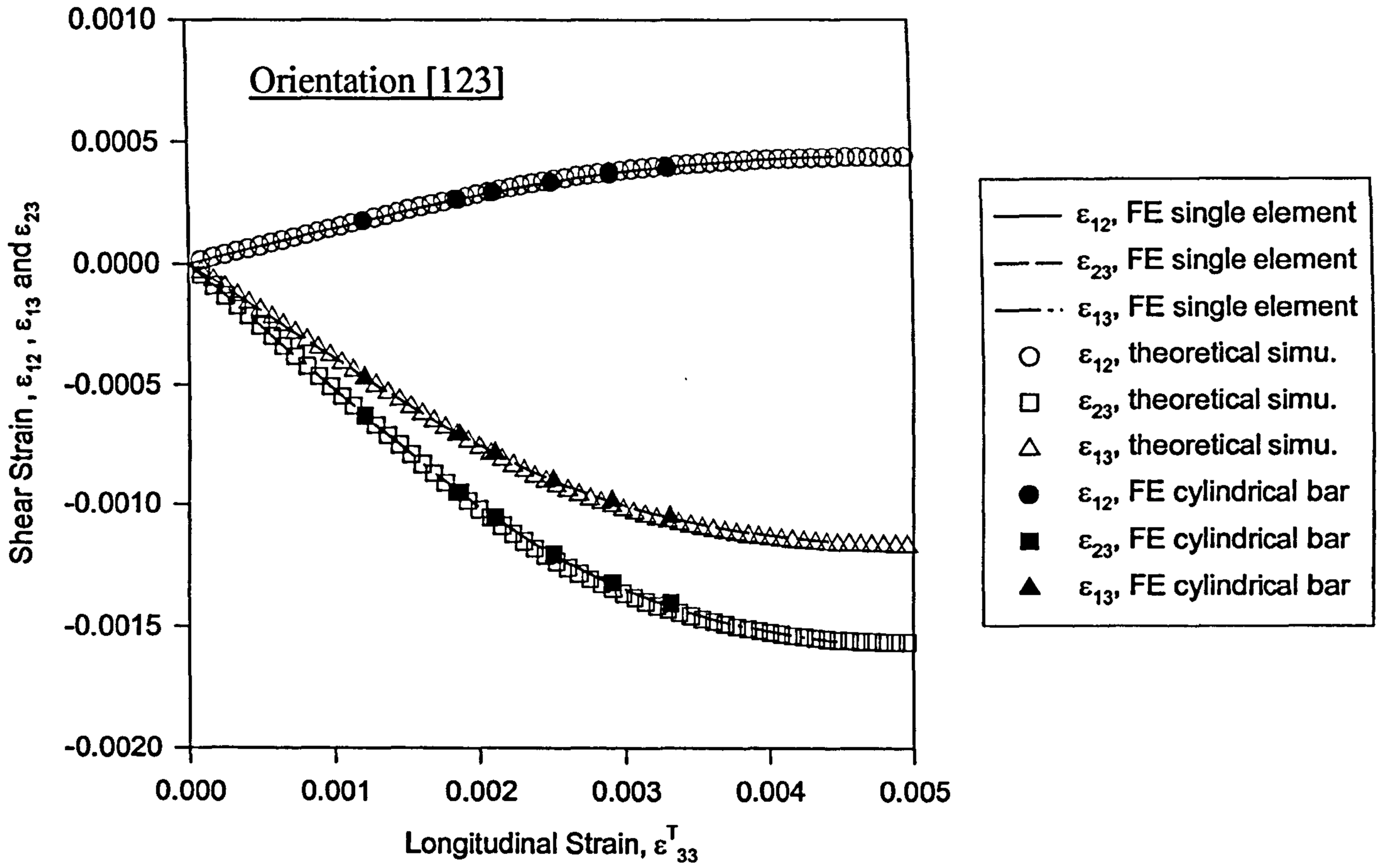

Fig. 5.6 Comparison of Shear Strain Responses Obtained from Different Calculations

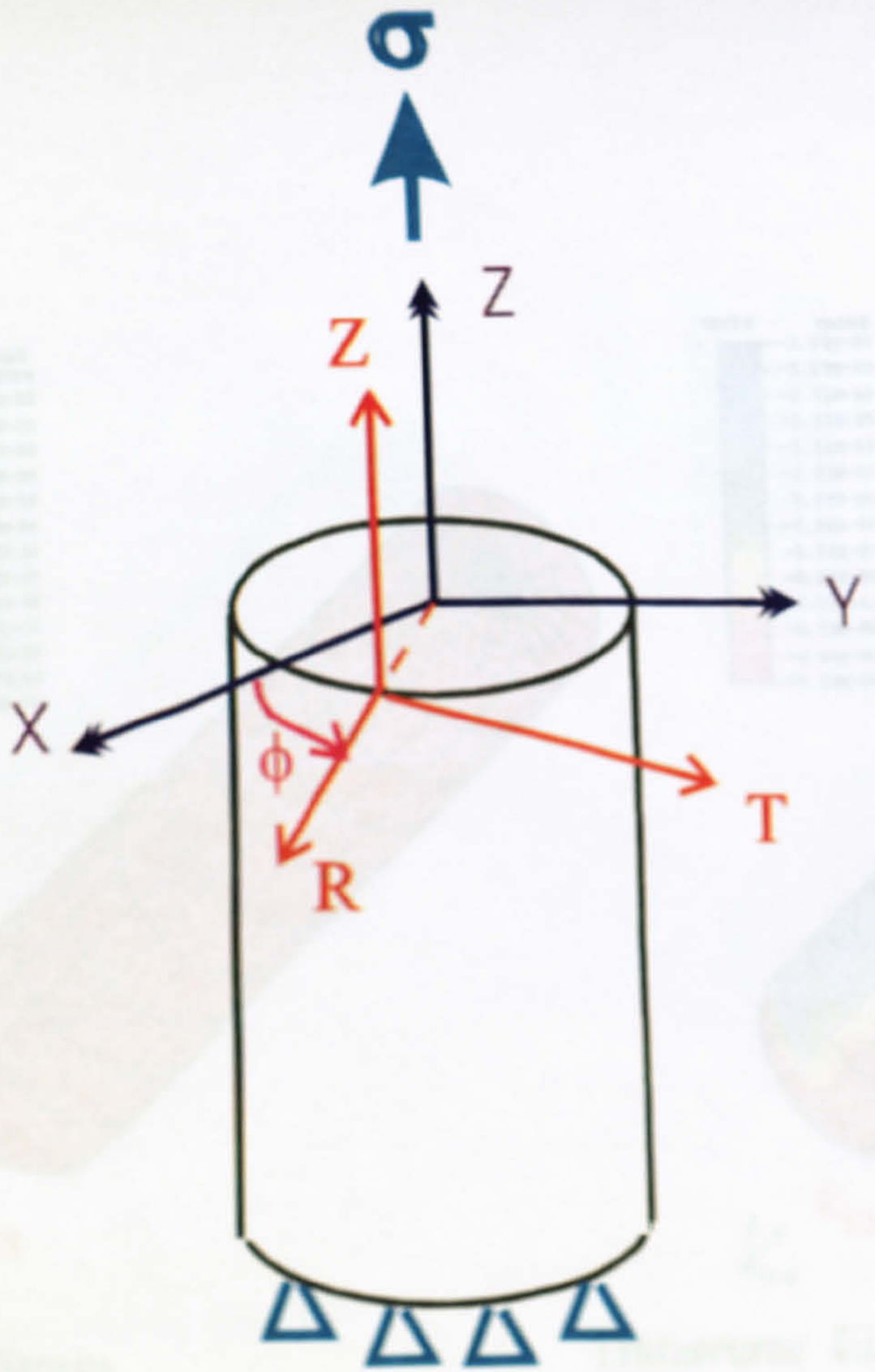

X-Y-Z:
global coordinate system

R-T-Z:
local cylindrical system

ϕ: rotation angle of local system
in X-Y plane of global system

Fig.5.7 Coordinate Systems for Strain Transformation of Cylindrical Bar Specimen

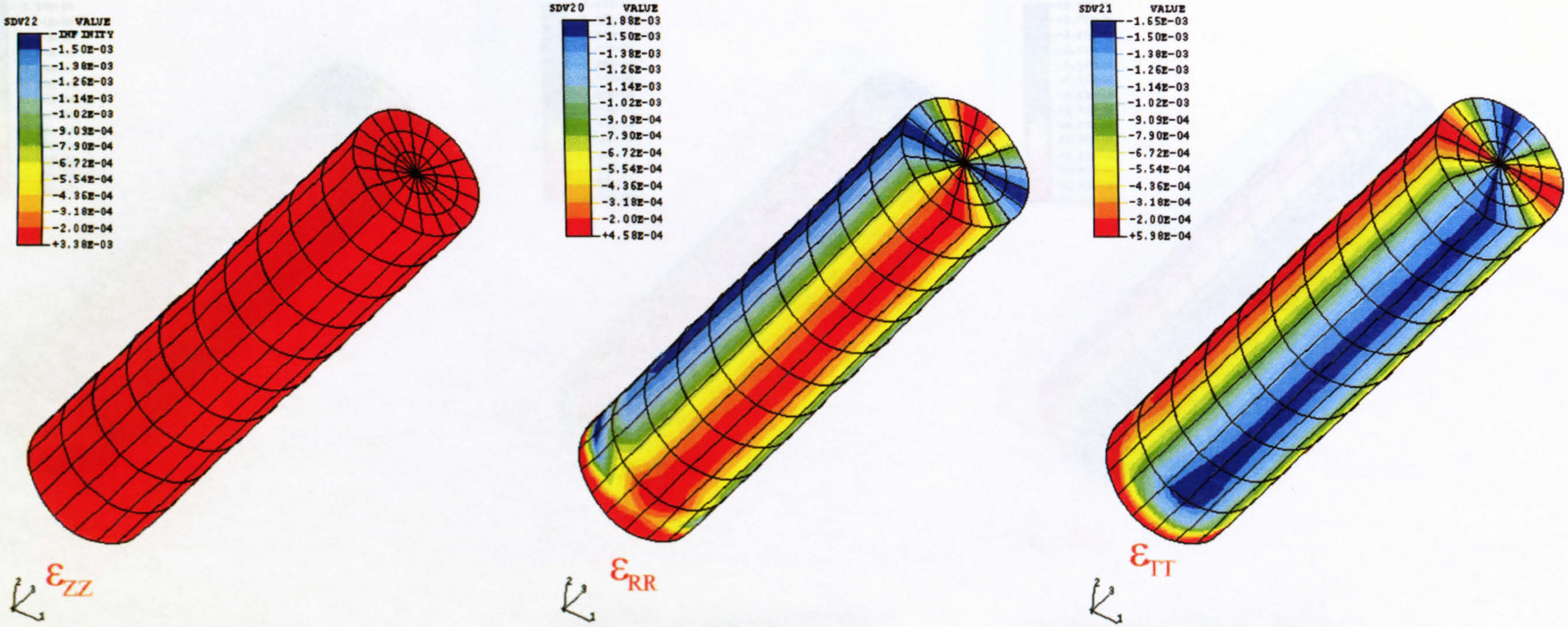

Axial Elastic Strain

Transverse Elastic Strain

Transverse Elastic Strain

Fig.5.8 Axial and Transverse Elastic Strain Distribution Contour of Cylindrical Bar Under Uniaxial Loading in [123](phenomenological model)

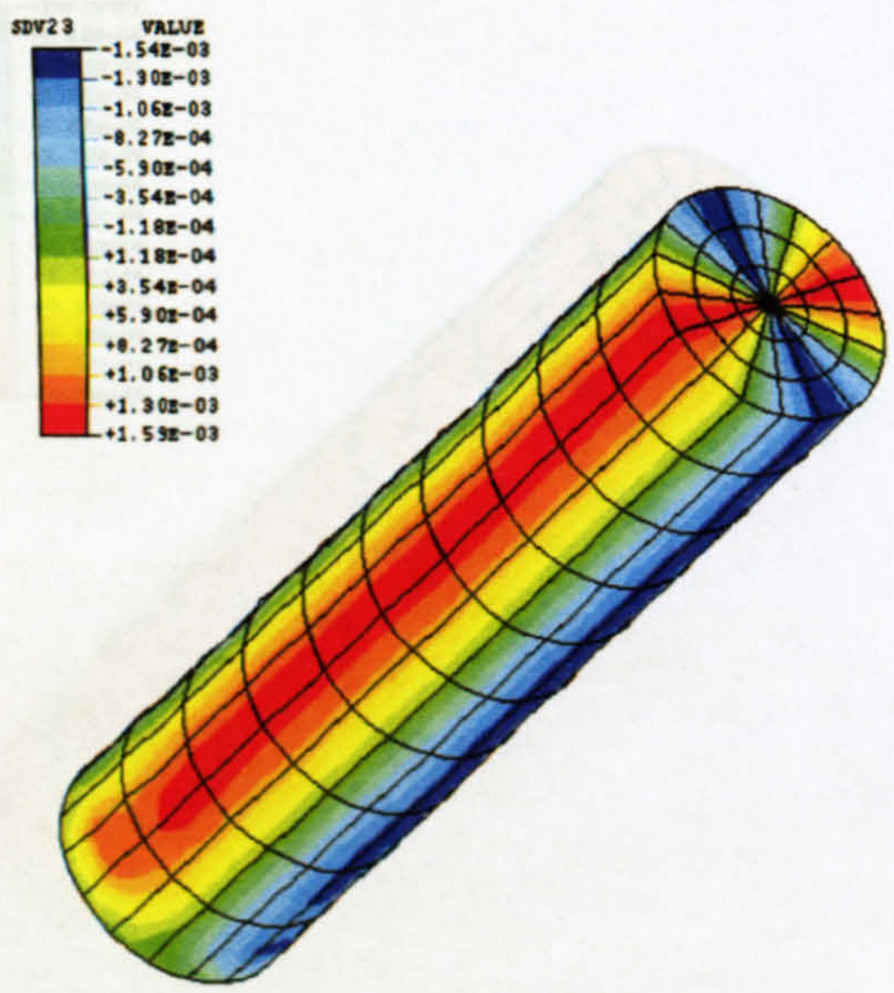

Transverse Shear Elastic Strain

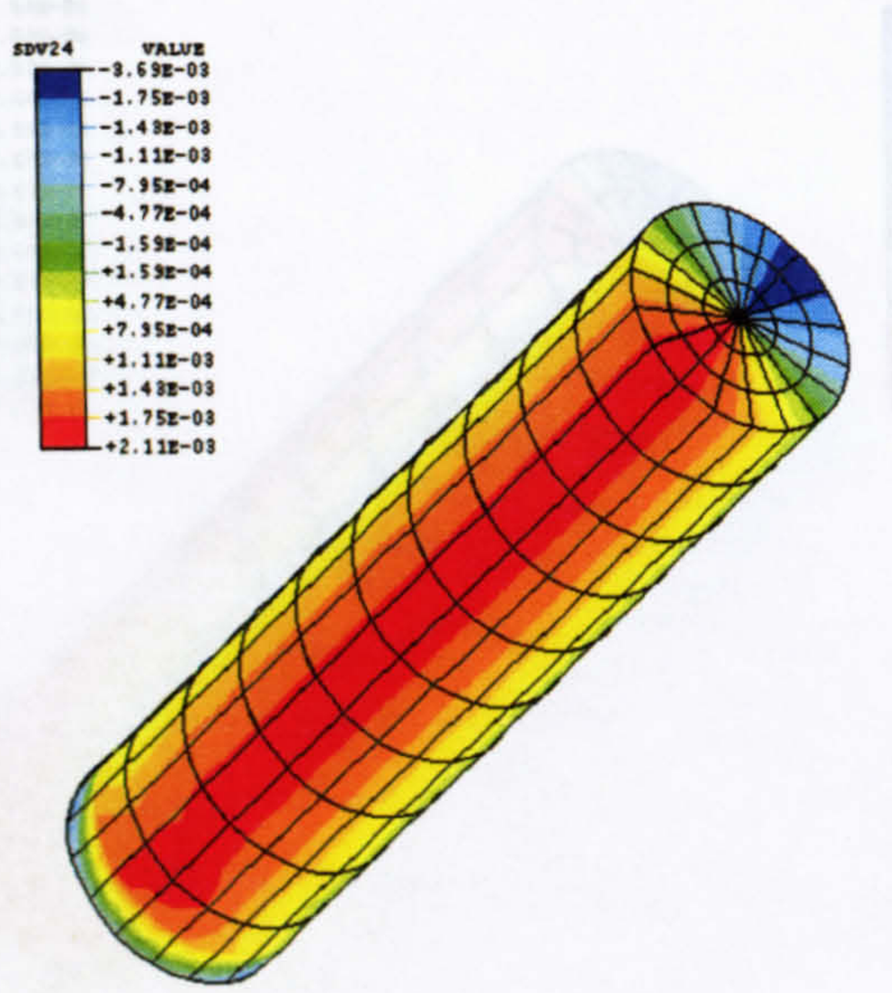

Axial Shear Elastic Strain

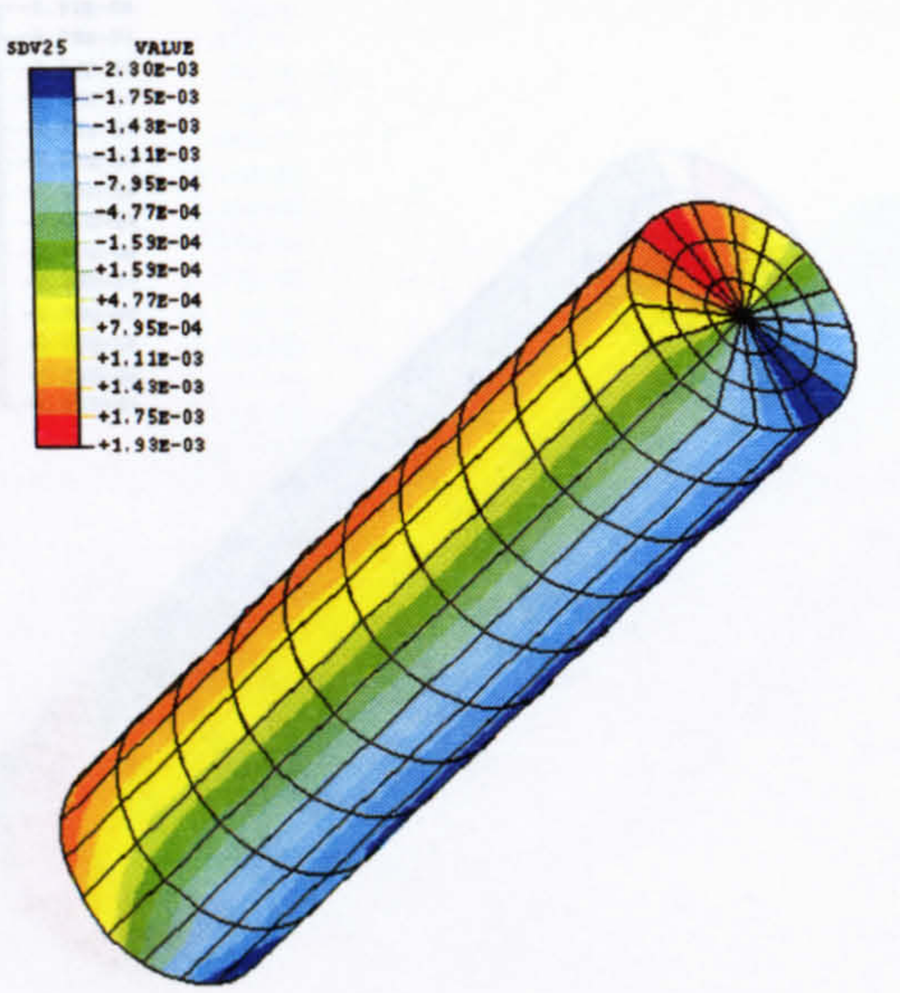

Axial Shear Elastic Strain

Fig.5.9 Shear Elastic Strain Distribution Contour of Cylindrical Bar Under Uniaxial loading in [123] (phenomenological model)

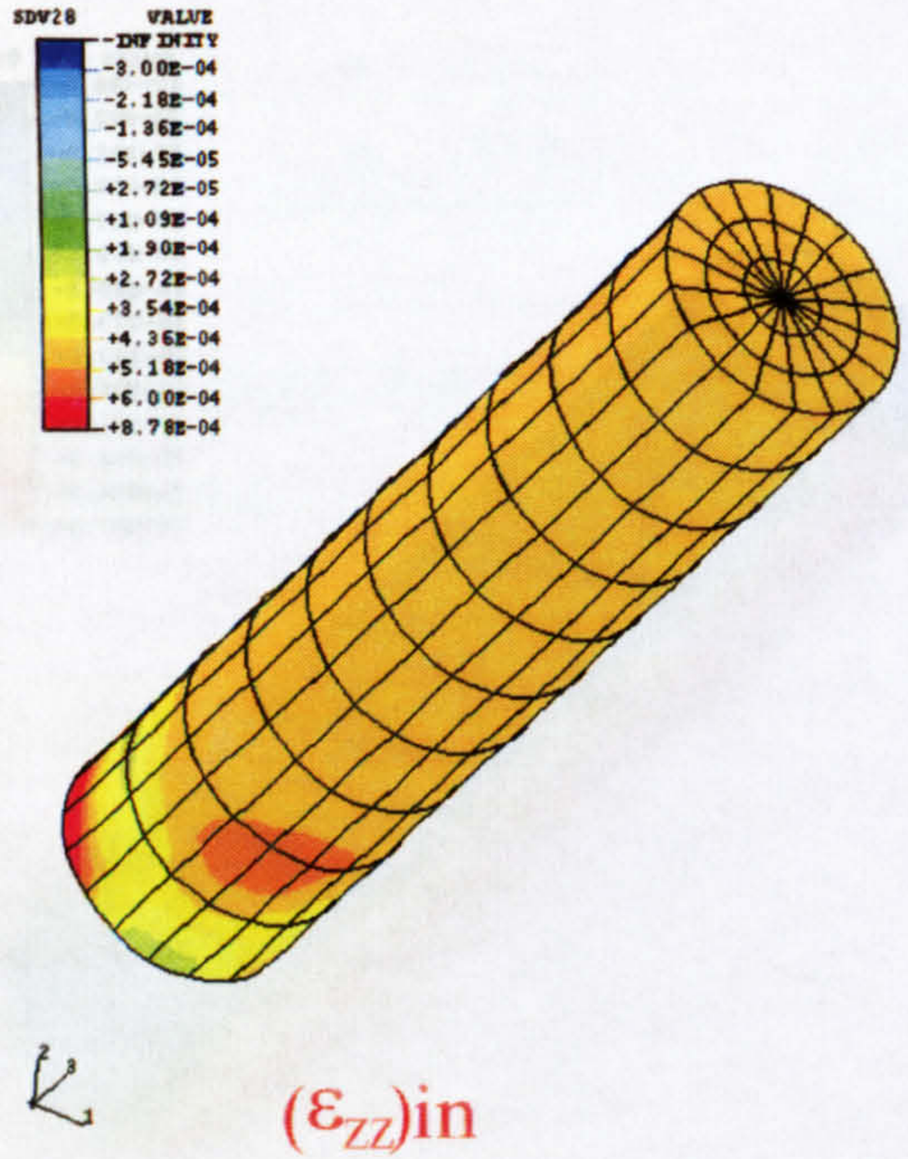

$(\varepsilon_{ZZ})in$

Axial Inelastic Strain

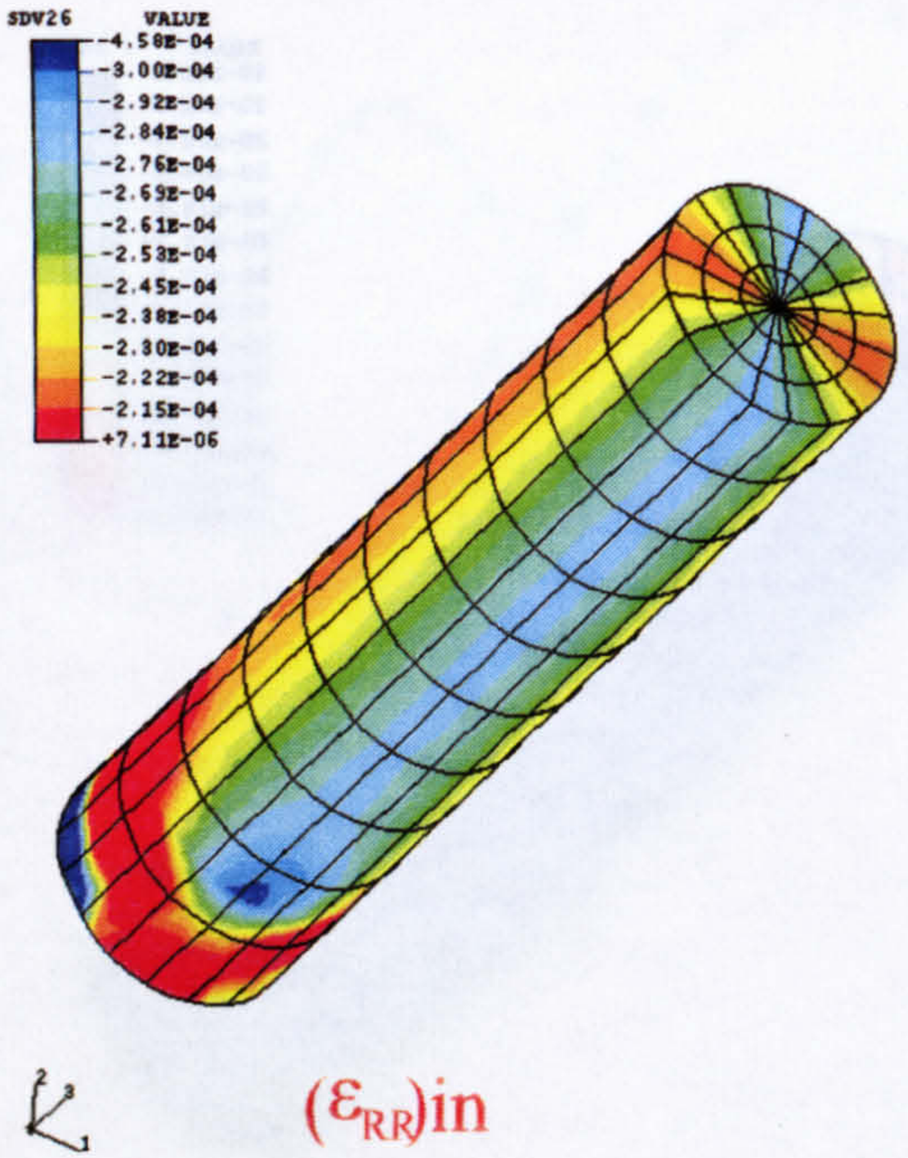

$(\varepsilon_{RR})in$

Transverse Inelastic Strain

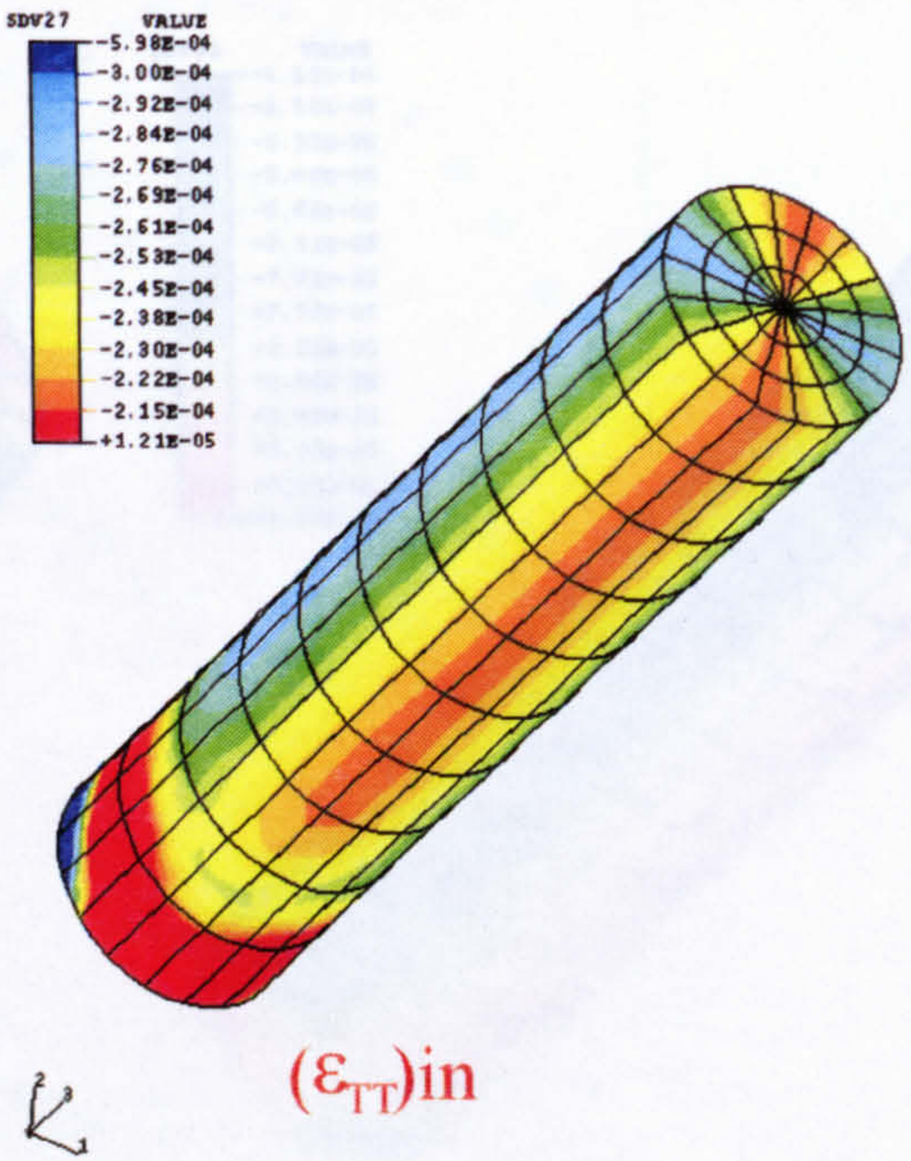

$(\varepsilon_{TT})in$

Transverse Inelastic Strain

Fig.5.10 Inelastic Axial and Transverse Strain Distribution Contour of Cylindrical Bar Under Uniaxial Loading (phenomenological model)

ABAQUS

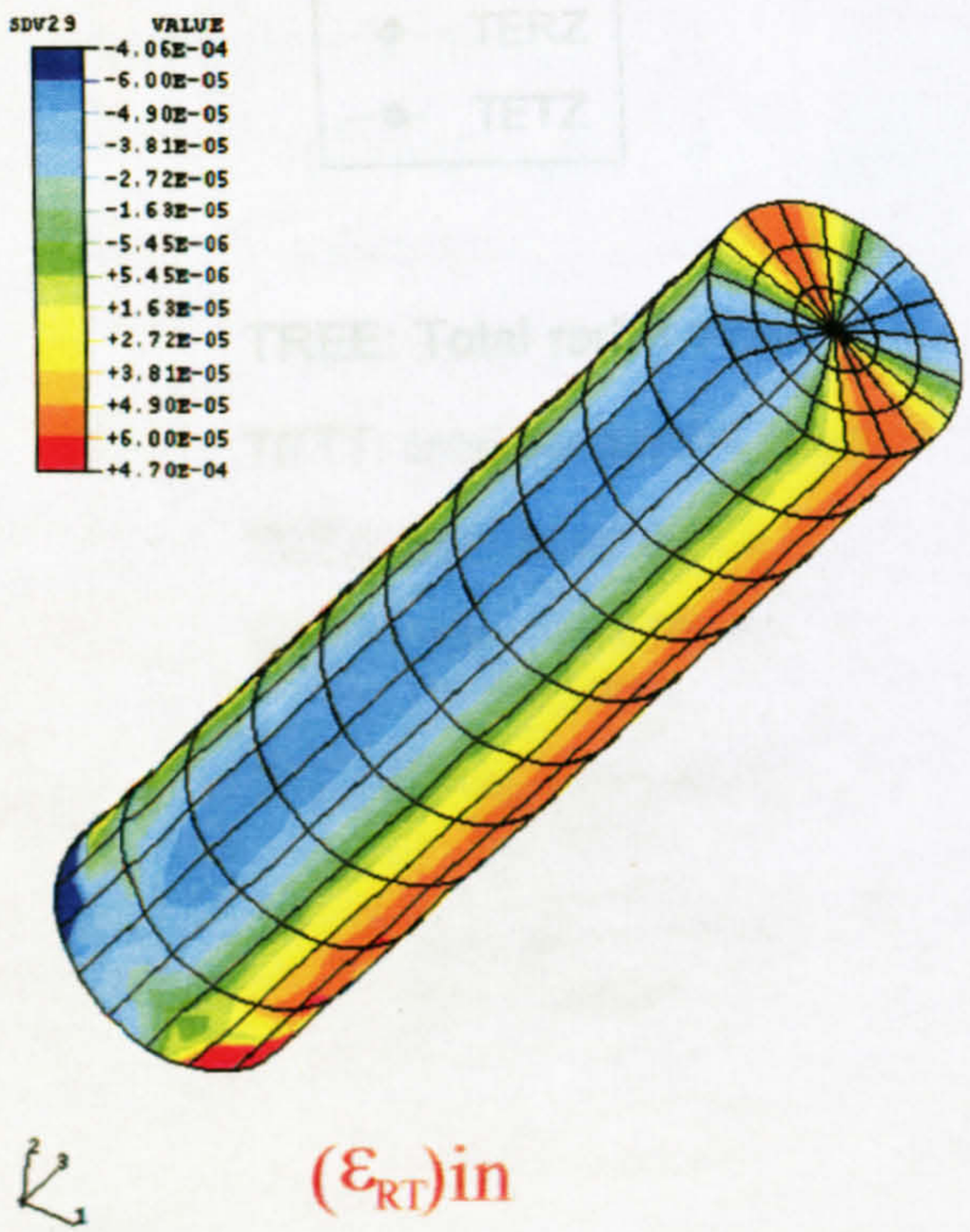

$(\varepsilon_{RT})in$

Transverse Inelastic Shear Strain

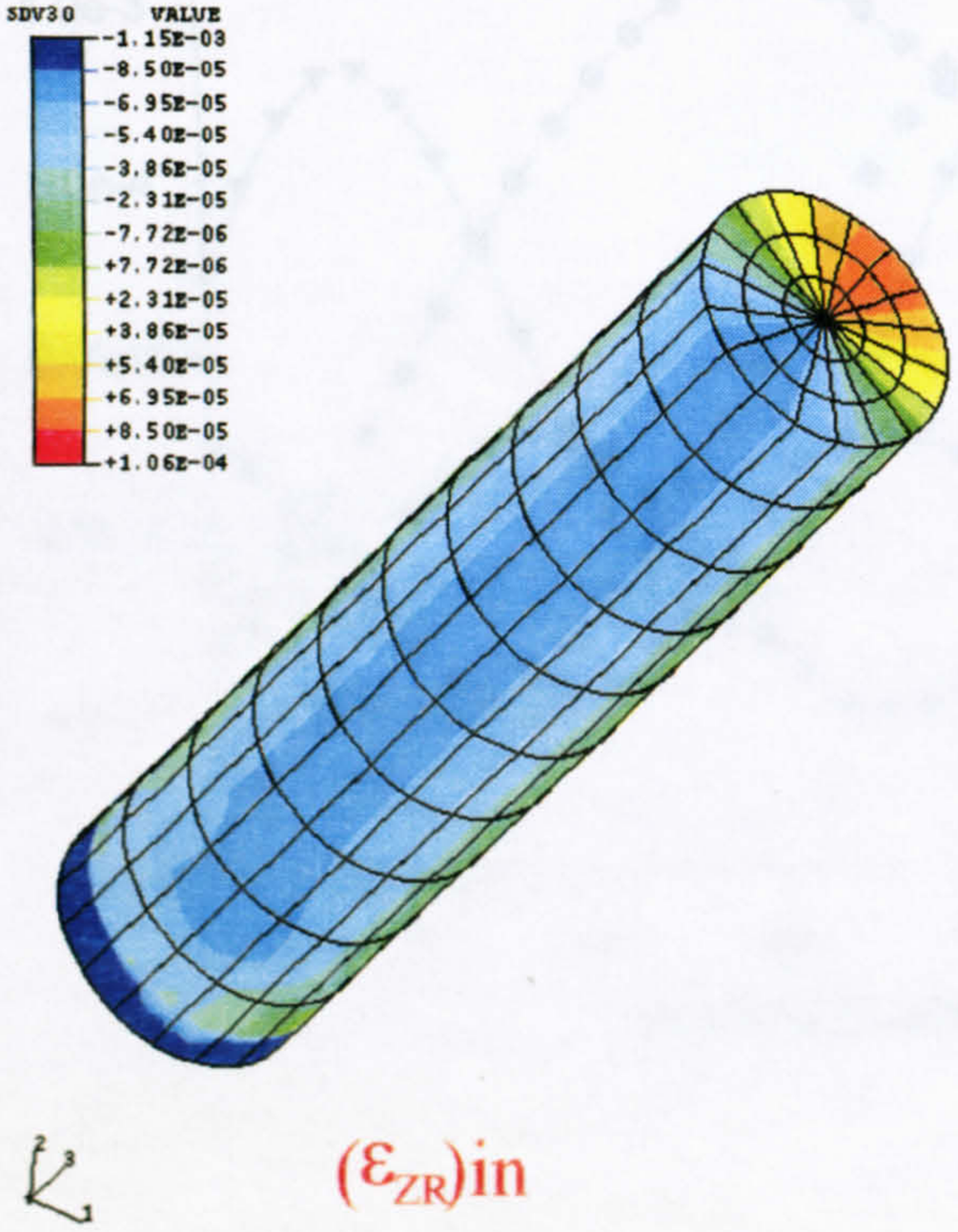

$(\varepsilon_{ZR})in$

Axial Inelastic Shear Strain

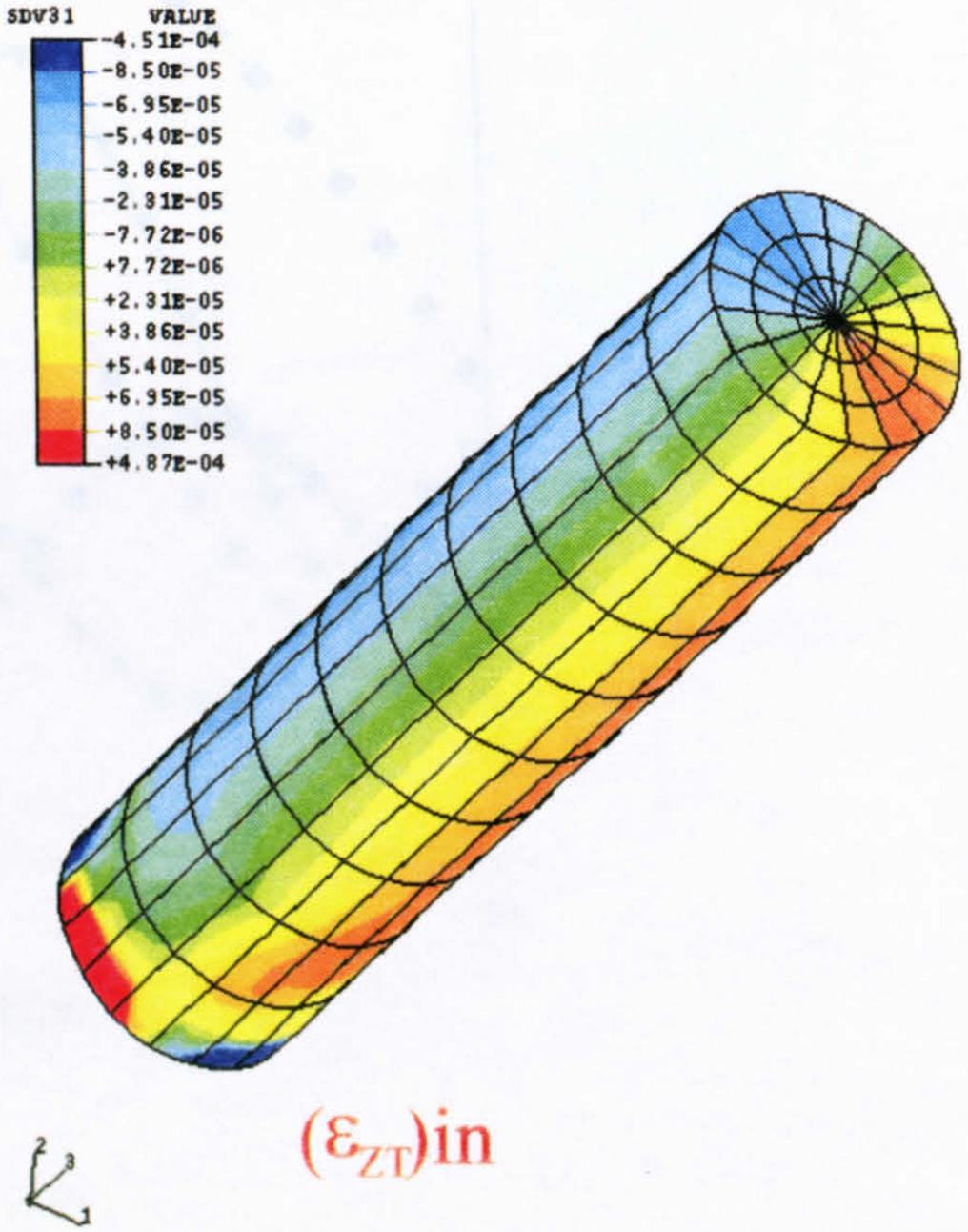

$(\varepsilon_{ZT})in$

Axial Inelastic Shear Strain

Fig.5.11 Inelastic Shear Strain Distribution Contour of Cylindrical Bar Under Uniaxial Loading (phenomenological model)

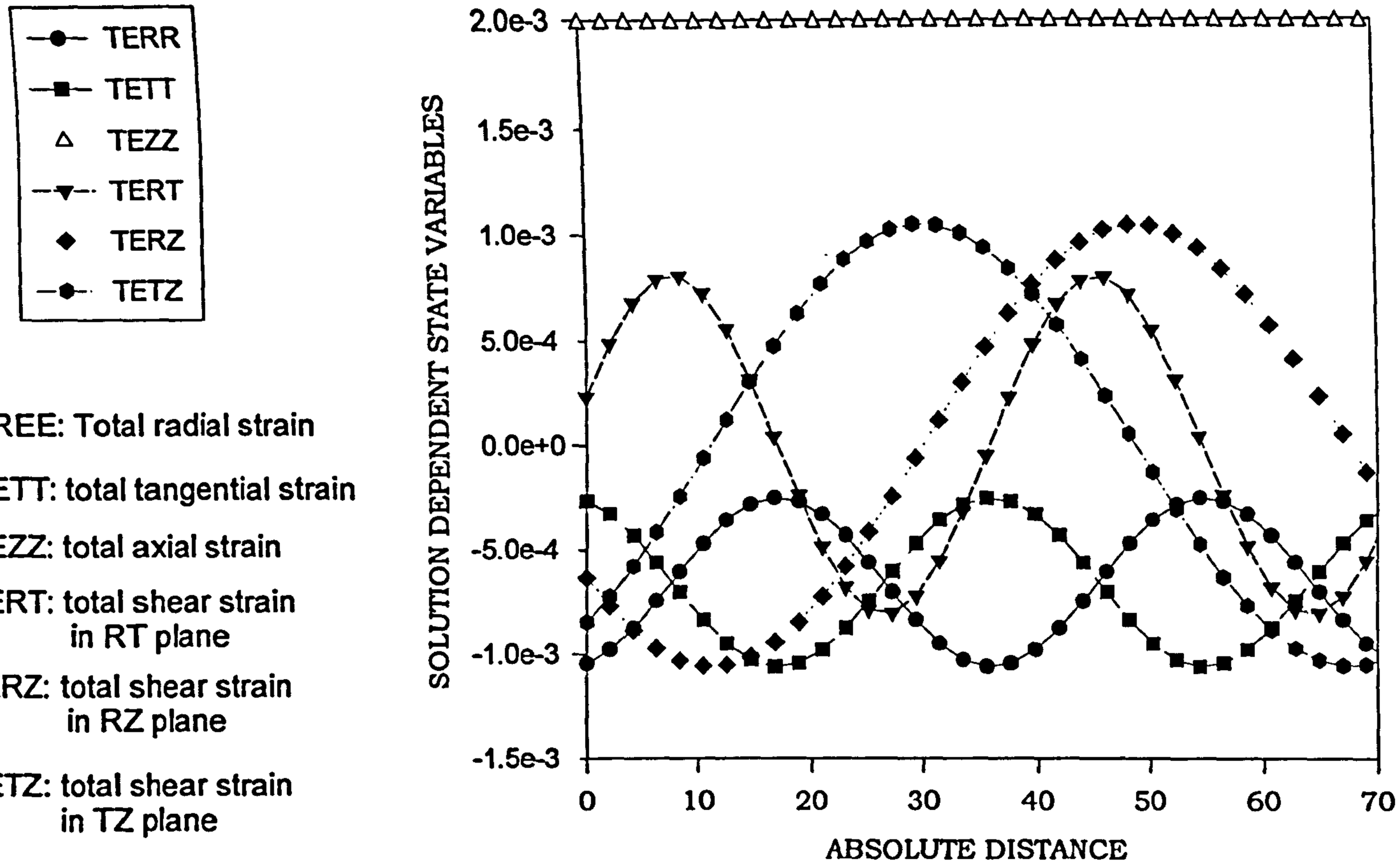

TREE: Total radial strain

TETT: total tangential strain

TEZZ: total axial strain

TERT: total shear strain in RT plane

TERZ: total shear strain in RZ plane

TETZ: total shear strain in TZ plane

Fig.5.12 The Distribution of Total Strain along a Circle (nodes 1001 to 1036) for Loading in [123] (phenomenological model)

TEXT BOUND INTO

THE SPINE

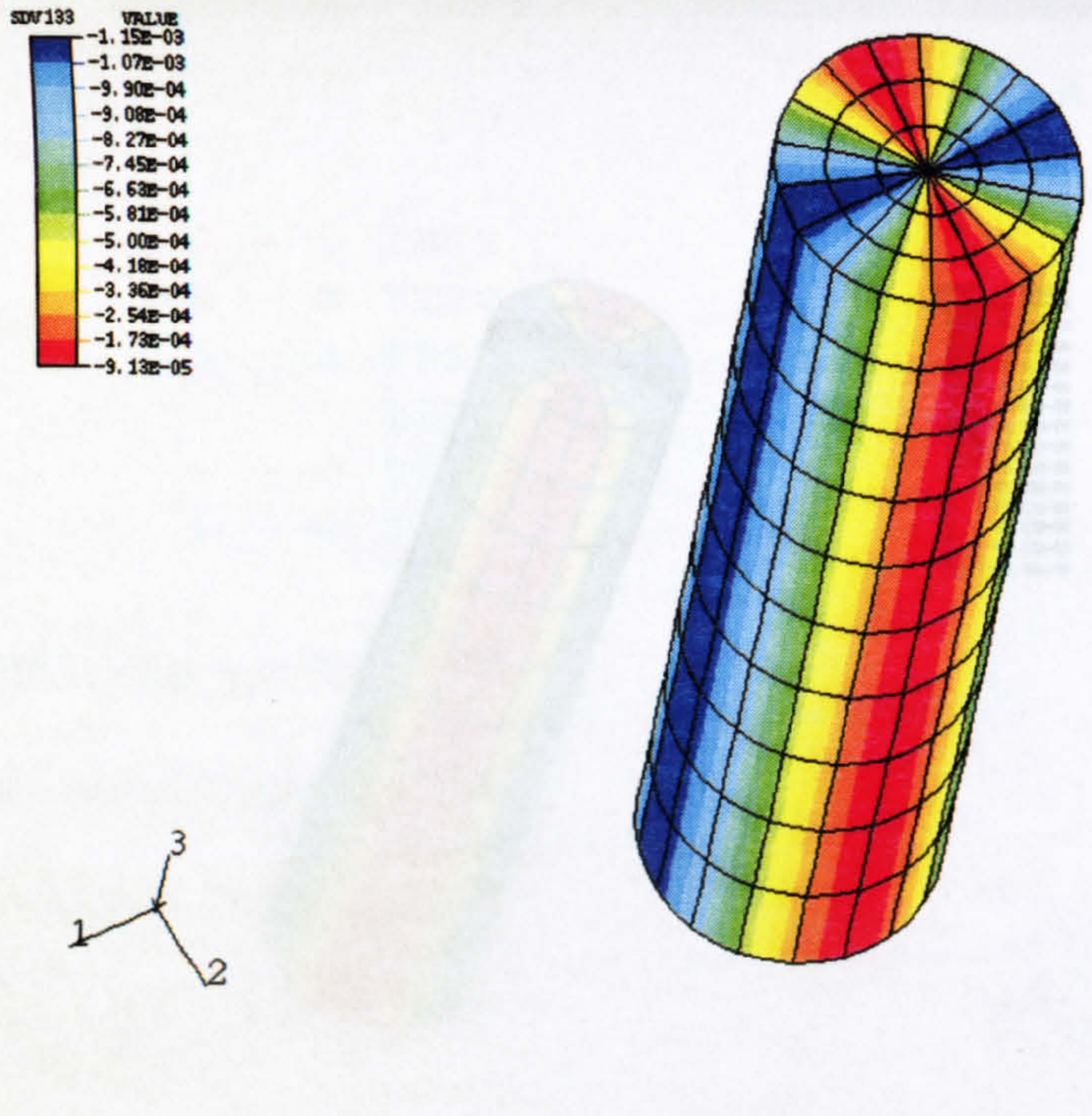

ε_{RR}

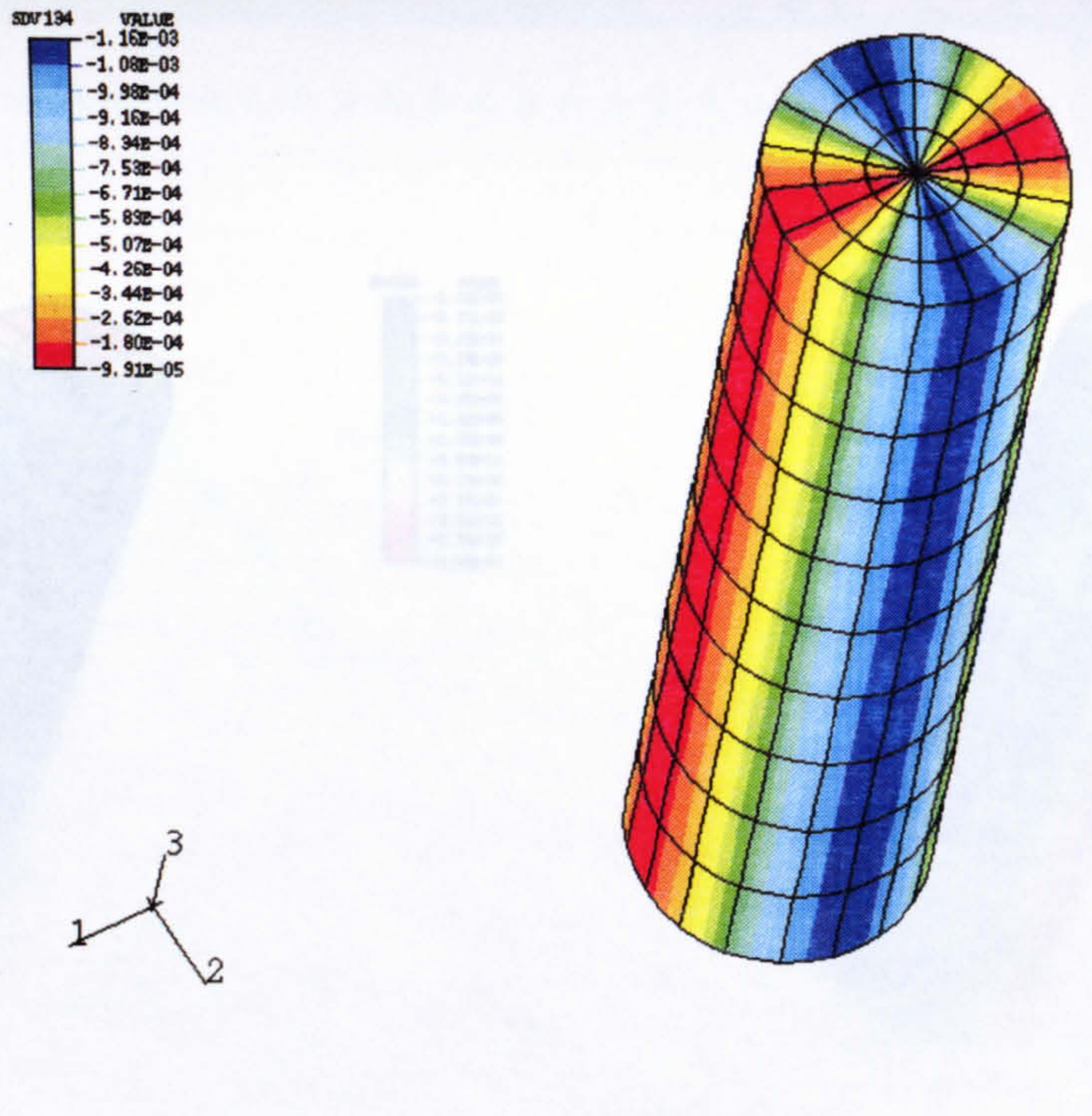

$\varepsilon_{\theta\theta}$

Fig.5.14 The Transvers Strain Distribution Contour of Cylindrical Bar Under Uniaxial Loading in [123] (crystallographic model)

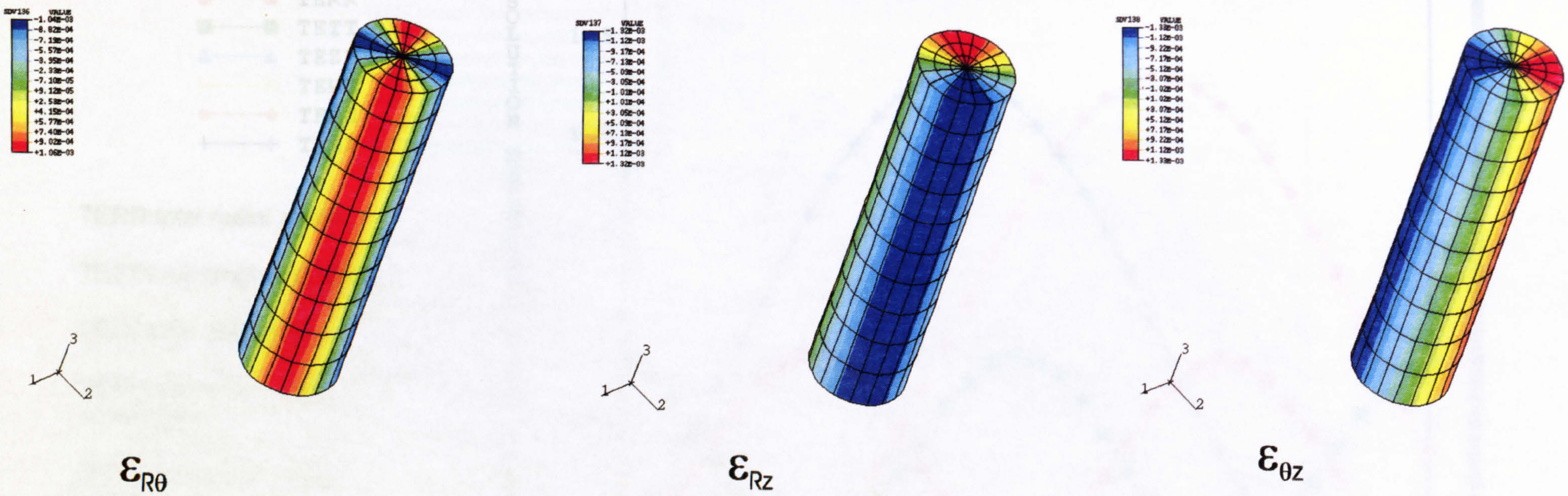

Fig.5.15 The Shear Strain Distribution Contour of Cylindrical bar Under Uniaxial Loading in[123] (crystallographic model)

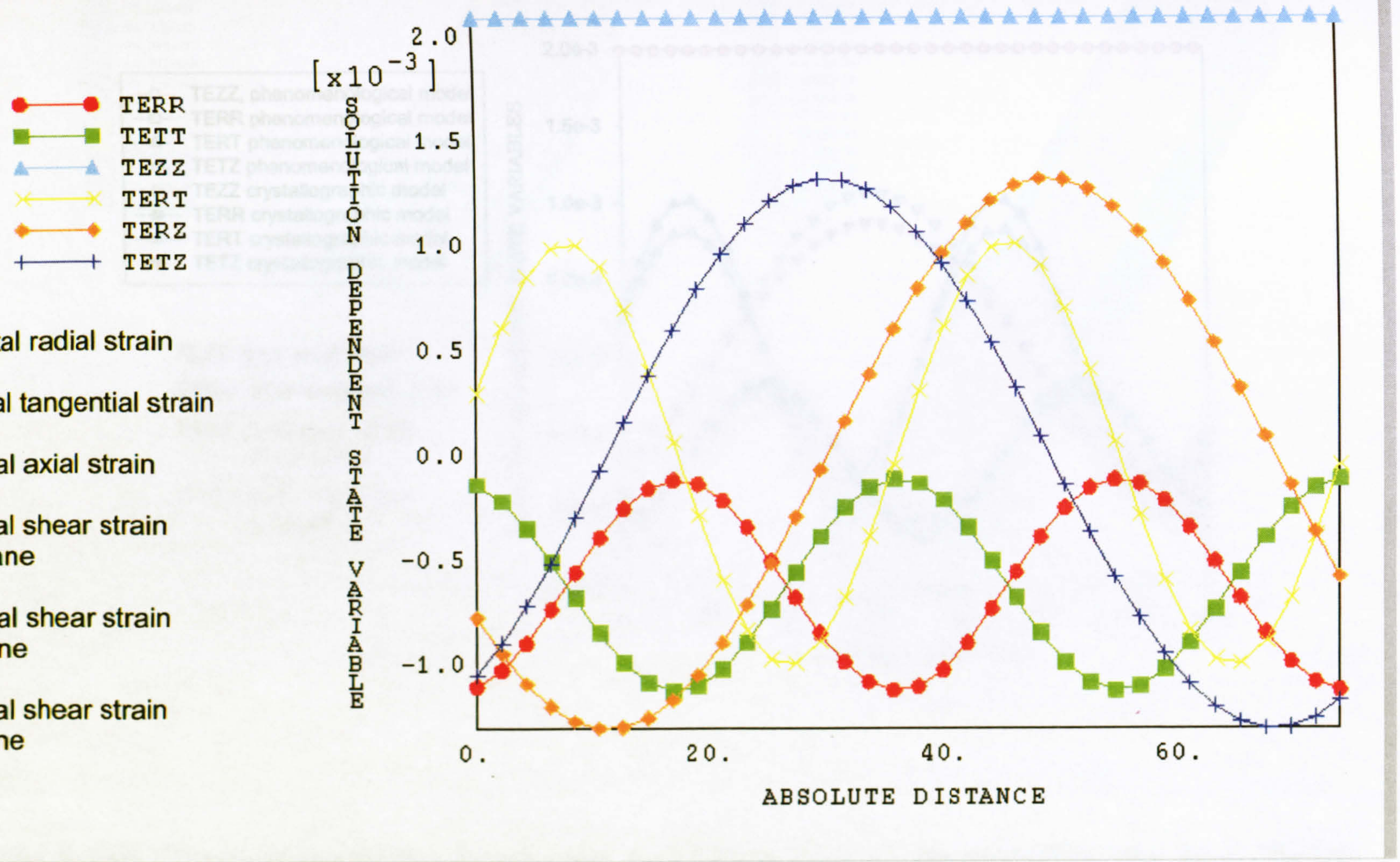

TERR:total radial strain

TETT:total tangential strain

TEZZ:total axial strain

TERT:total shear strain in RT plane

TERZ:total shear strain in RZ plane

TETZ:total shear strain in TZ plane

Fig.5.16a The Distribution of Total Strain along a Circle(nodes 1001 to 1036) for Loading in [123] (crystallographic model)

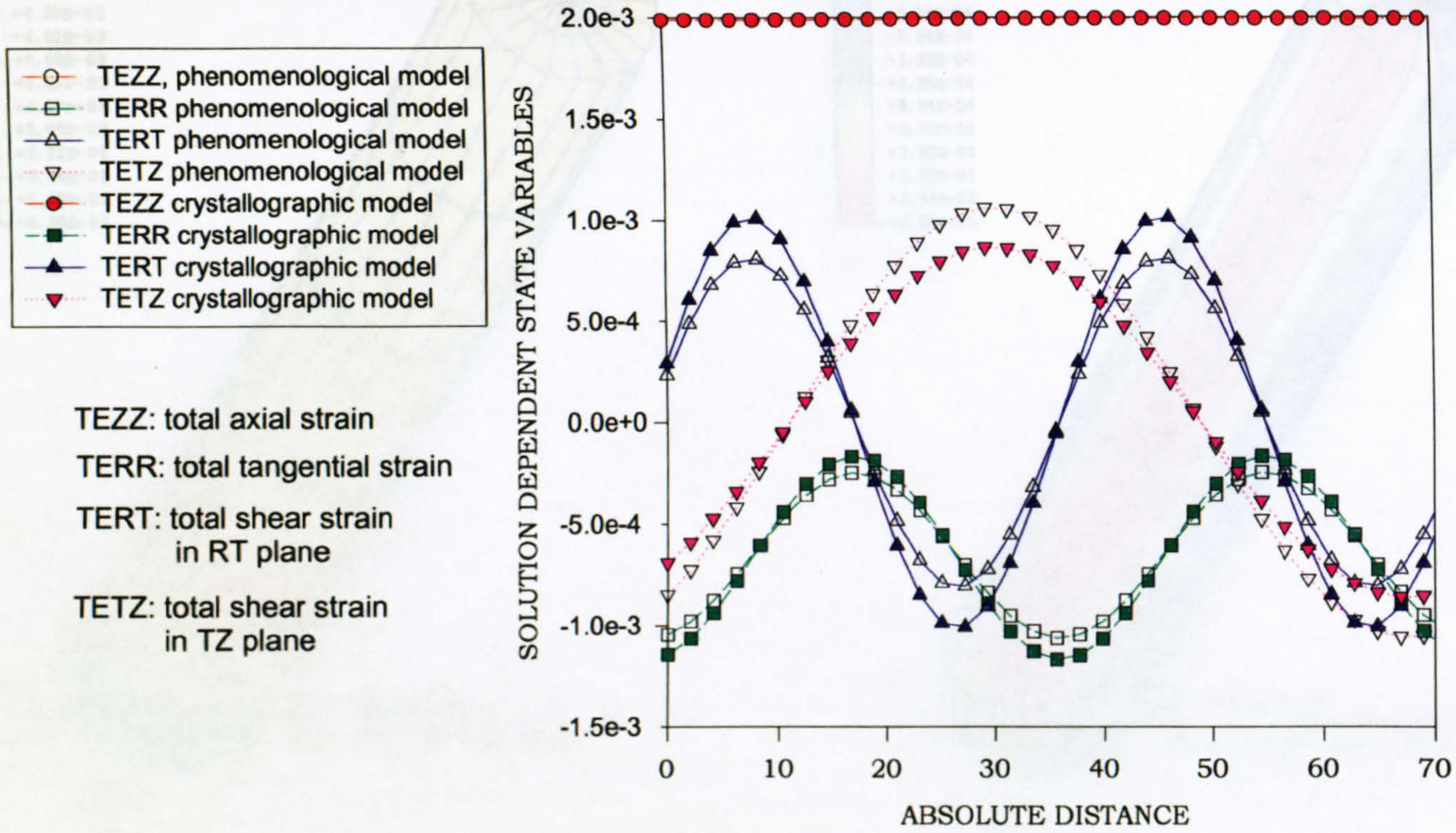

Fig.5.16b Comparison of the Tangential and Shear Strains Predicted by the Two Models Along the Circle of a Cylindrical Bar for Loading in [123]

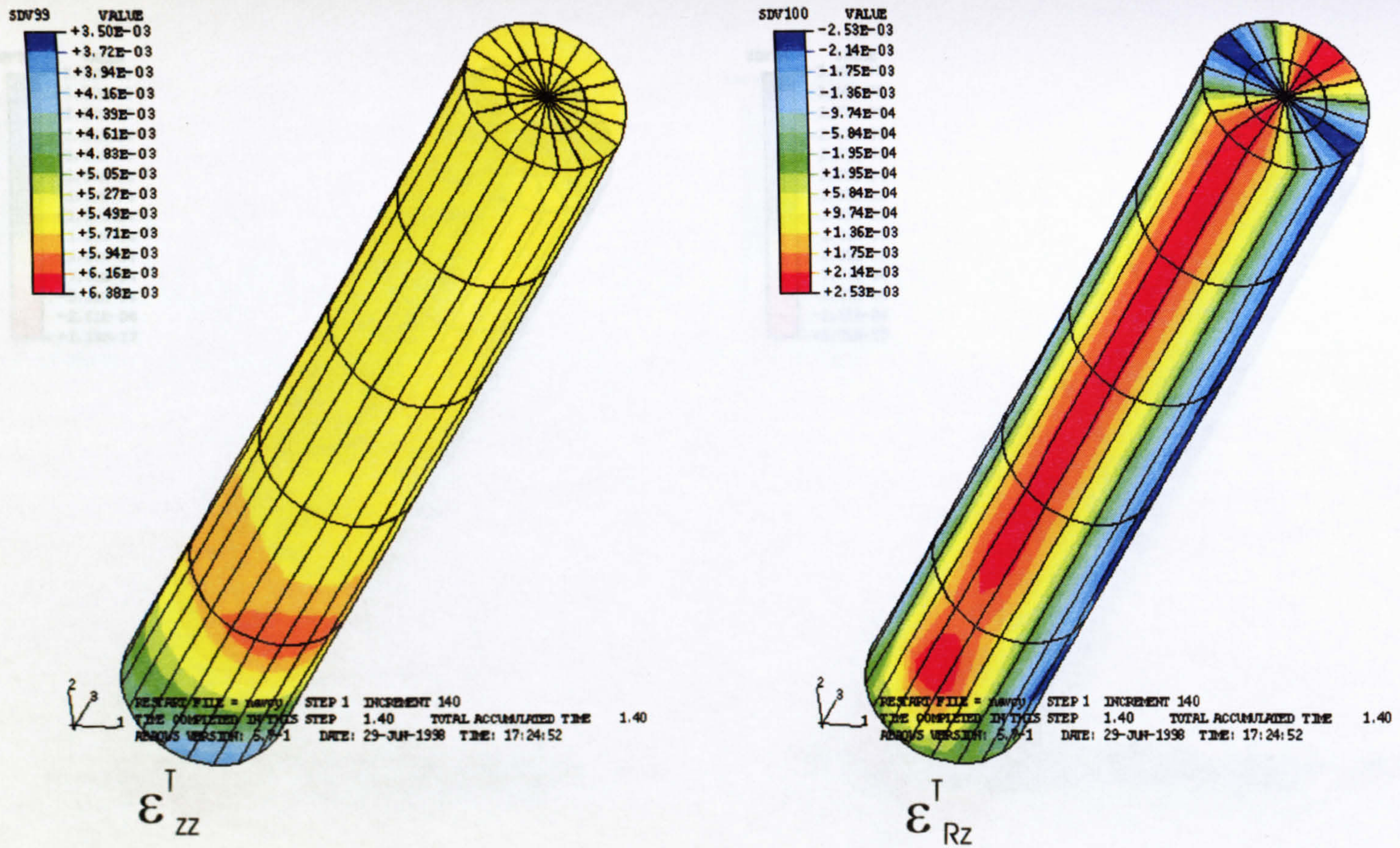

Fig.5.17a Total Strain Distribution Contour of Cylinder Under Uniaxial Loading in [011] (Crystallographic model)

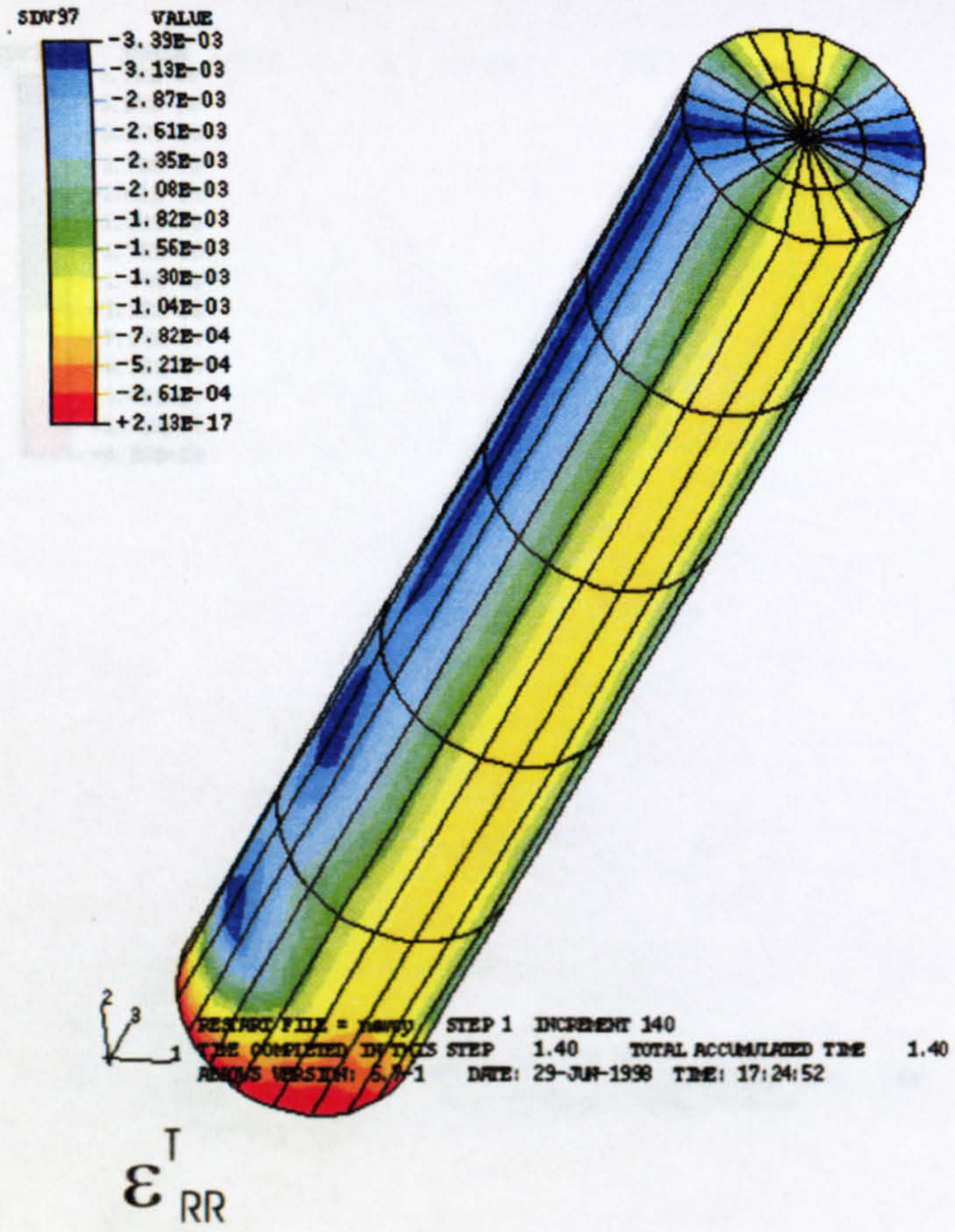

ε^{T}_{RR}

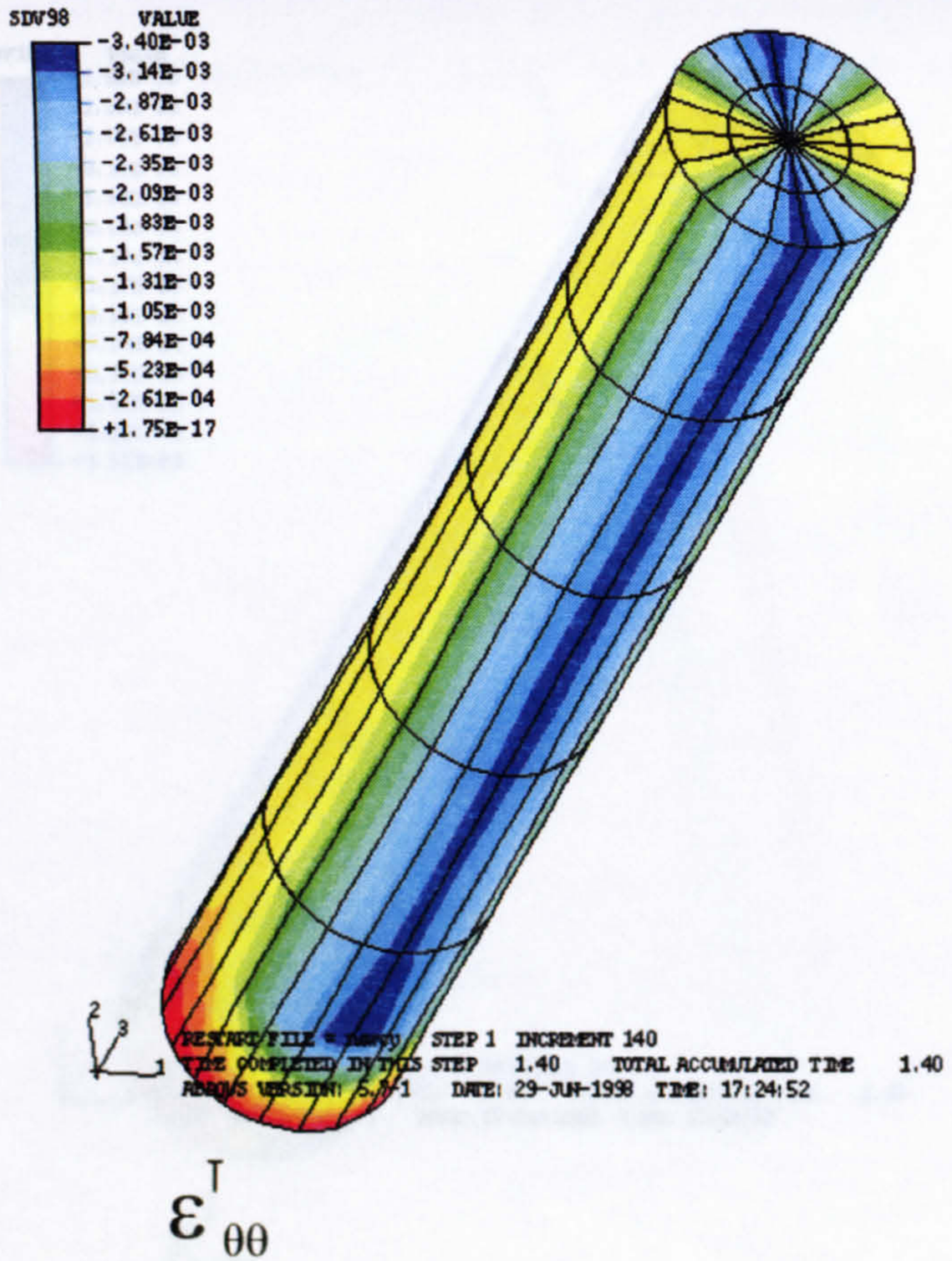

$\varepsilon^{T}_{\theta\theta}$

Fig.5.17b Total Strain Distribution Contour of Cylinder Under Uniaxial Loading in [011] (Crystallographic model)

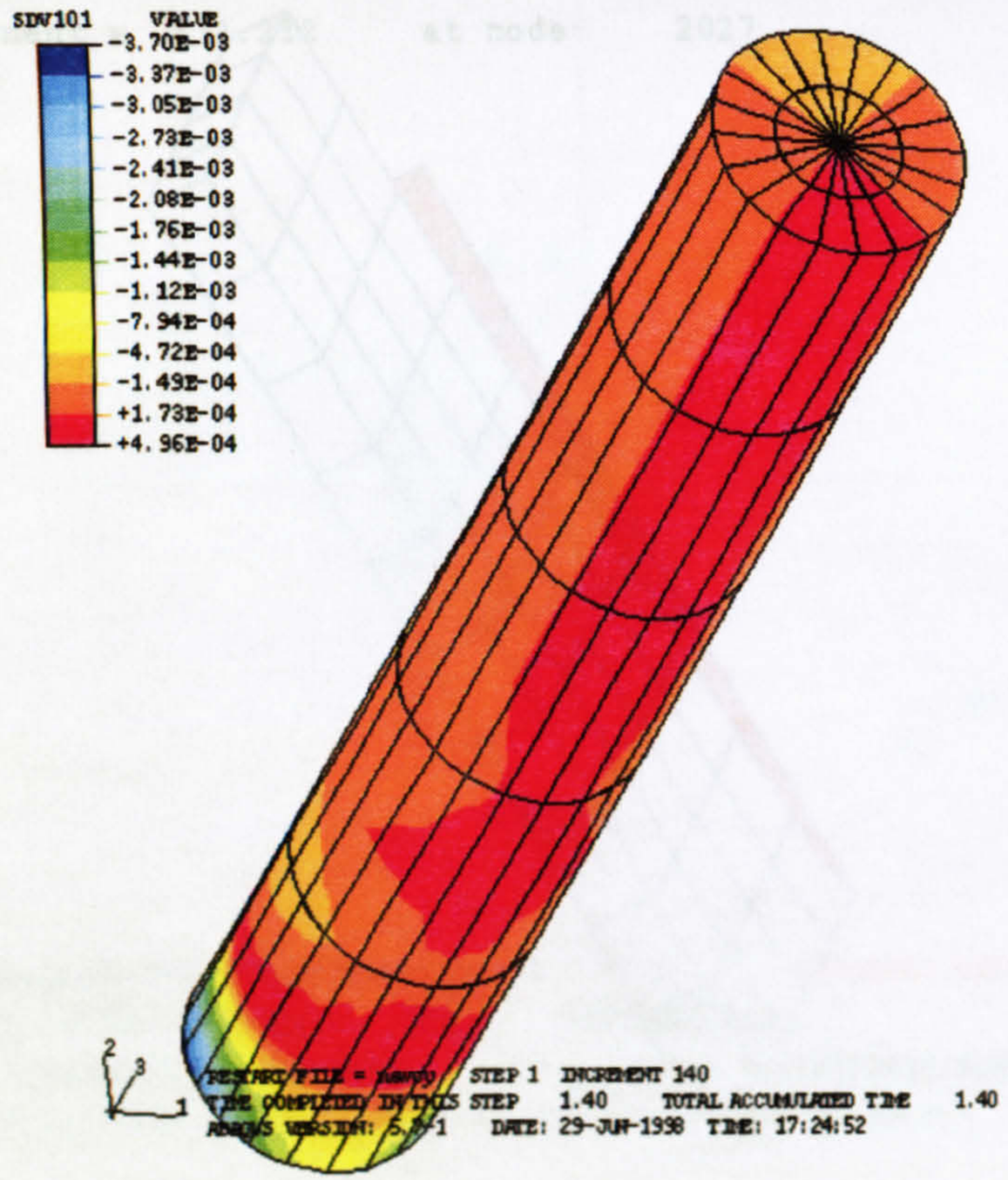

$\varepsilon^{T}_{R\theta}$

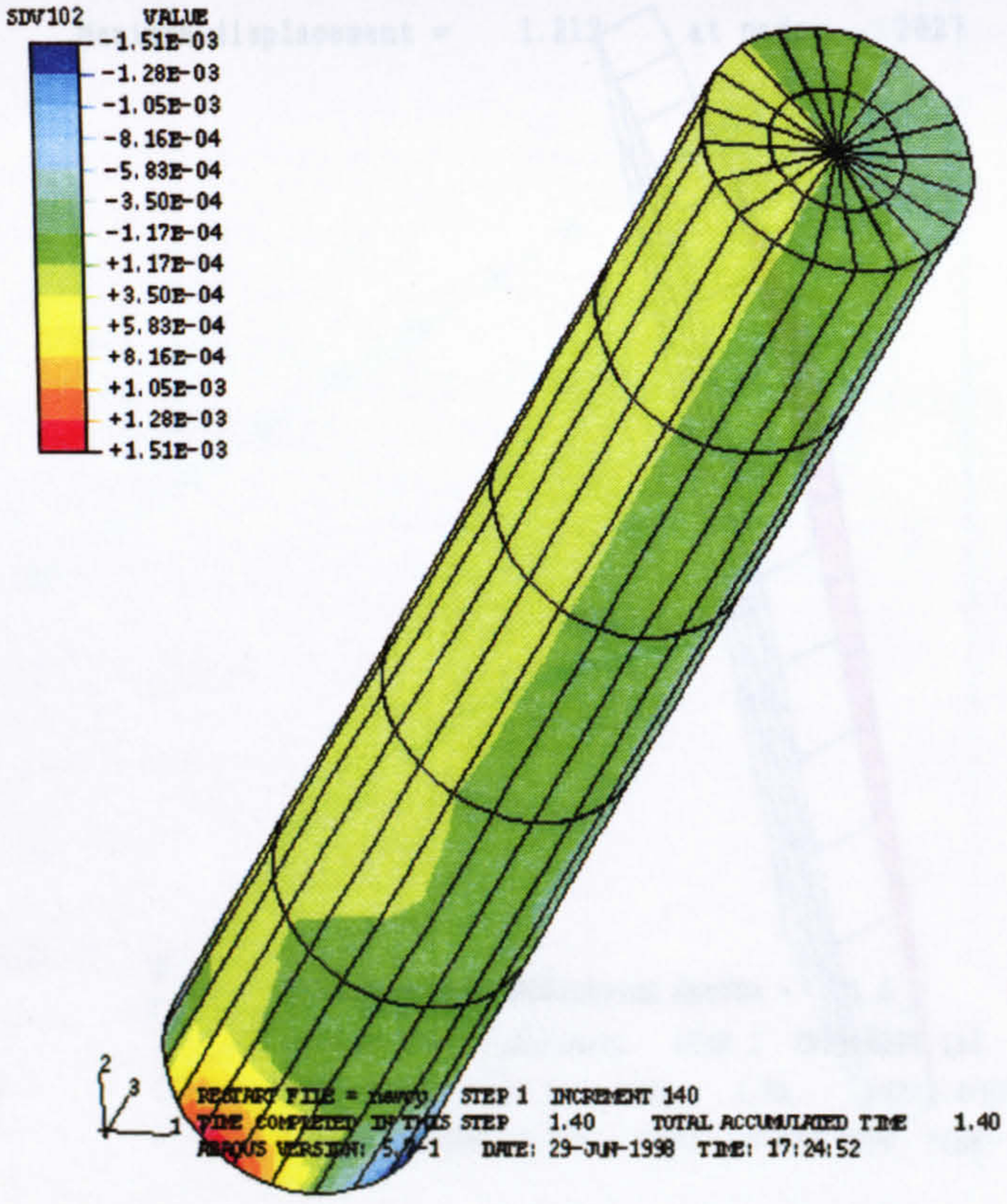

$\varepsilon^{T}_{\theta Z}$

Fig.5.17c Total Strain Distribution Contour of Cylinder Under Uniaxial Loading in [011] (Crystallographic model)

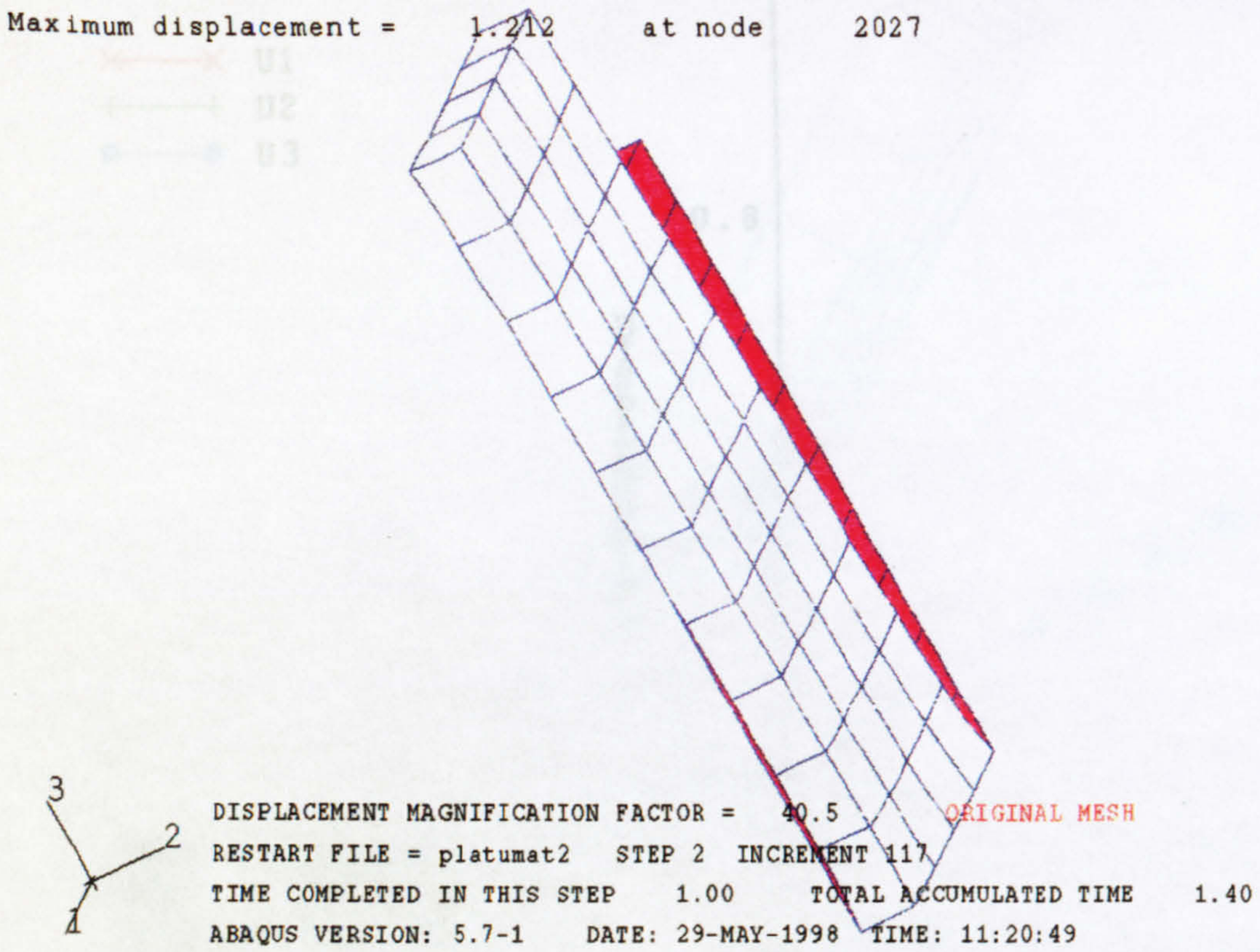

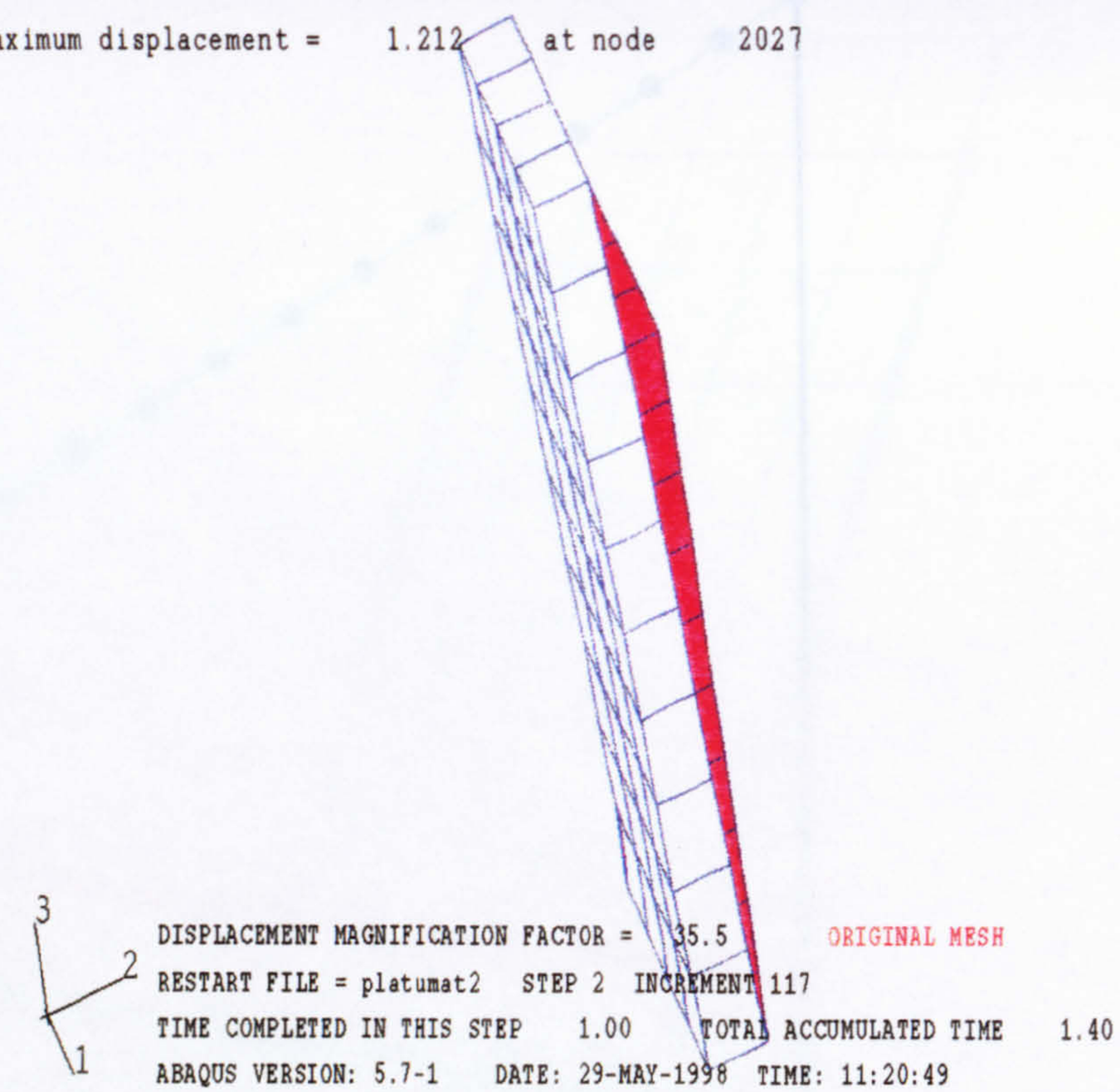

Fig.5.18 The Displacement of Plate Under Tension Loading in [123] Orientation

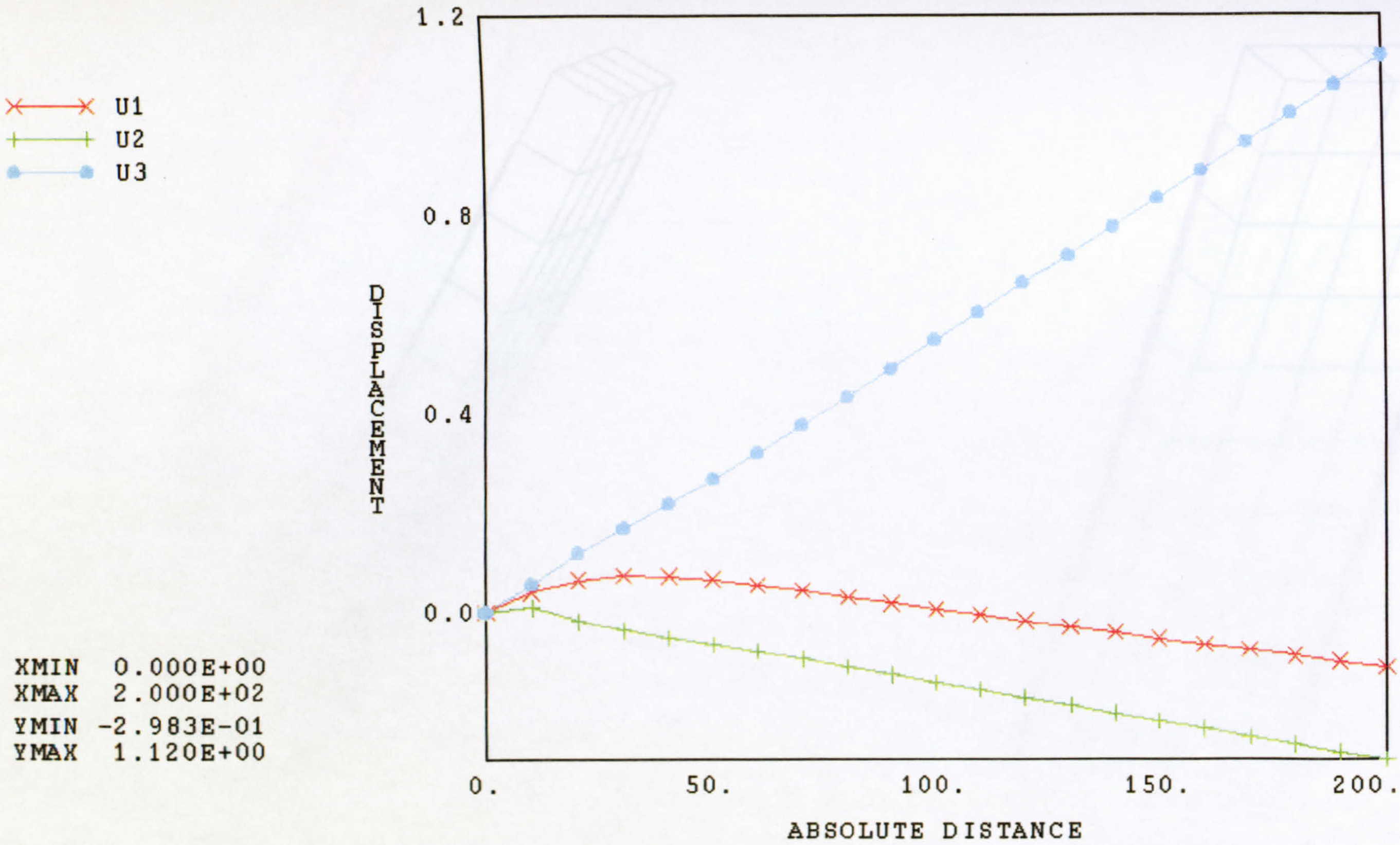

Fig.5.19 The Distribution of Displacement Along a Longitudinal Side of Plate (loading in [123])

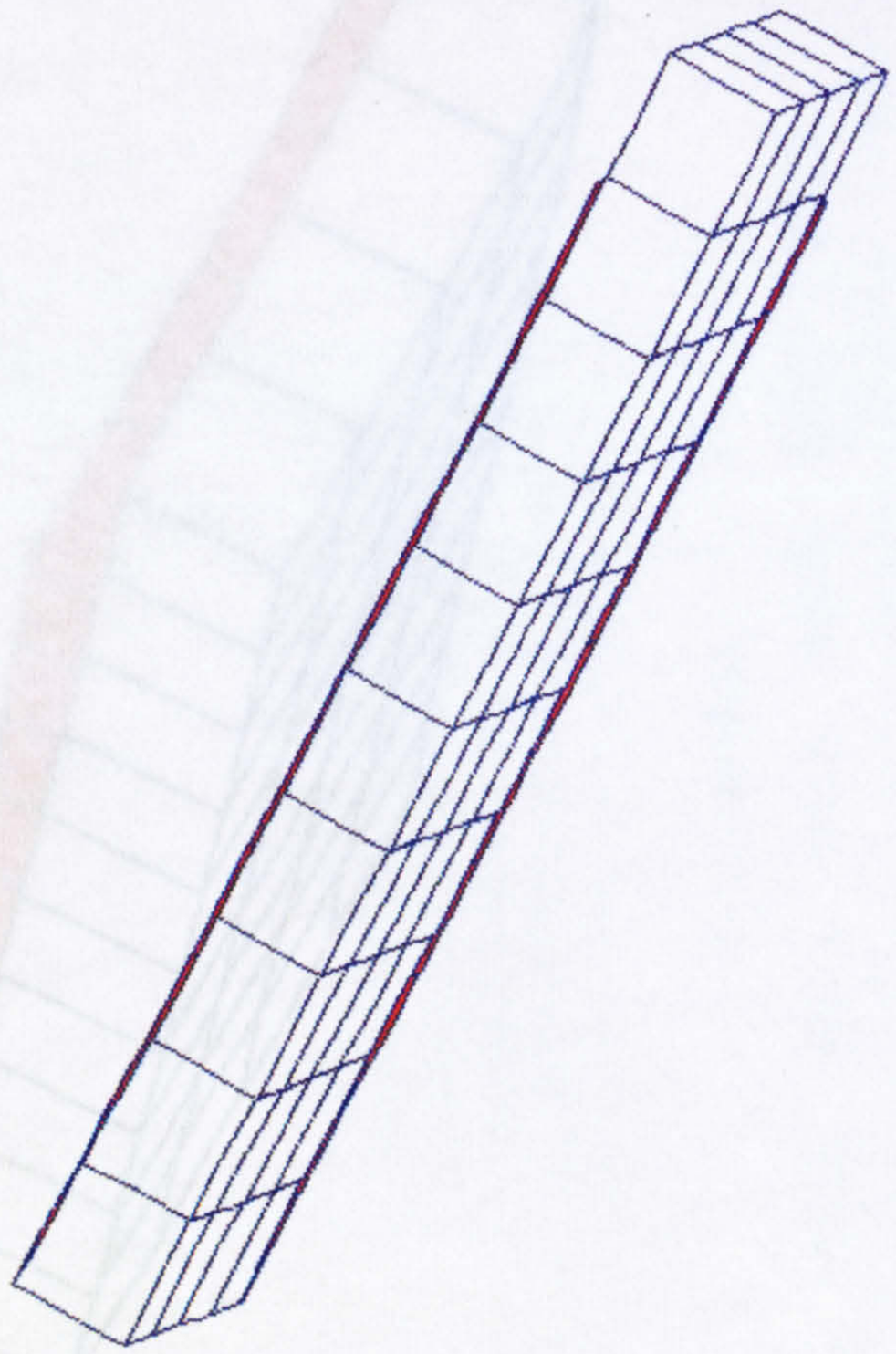

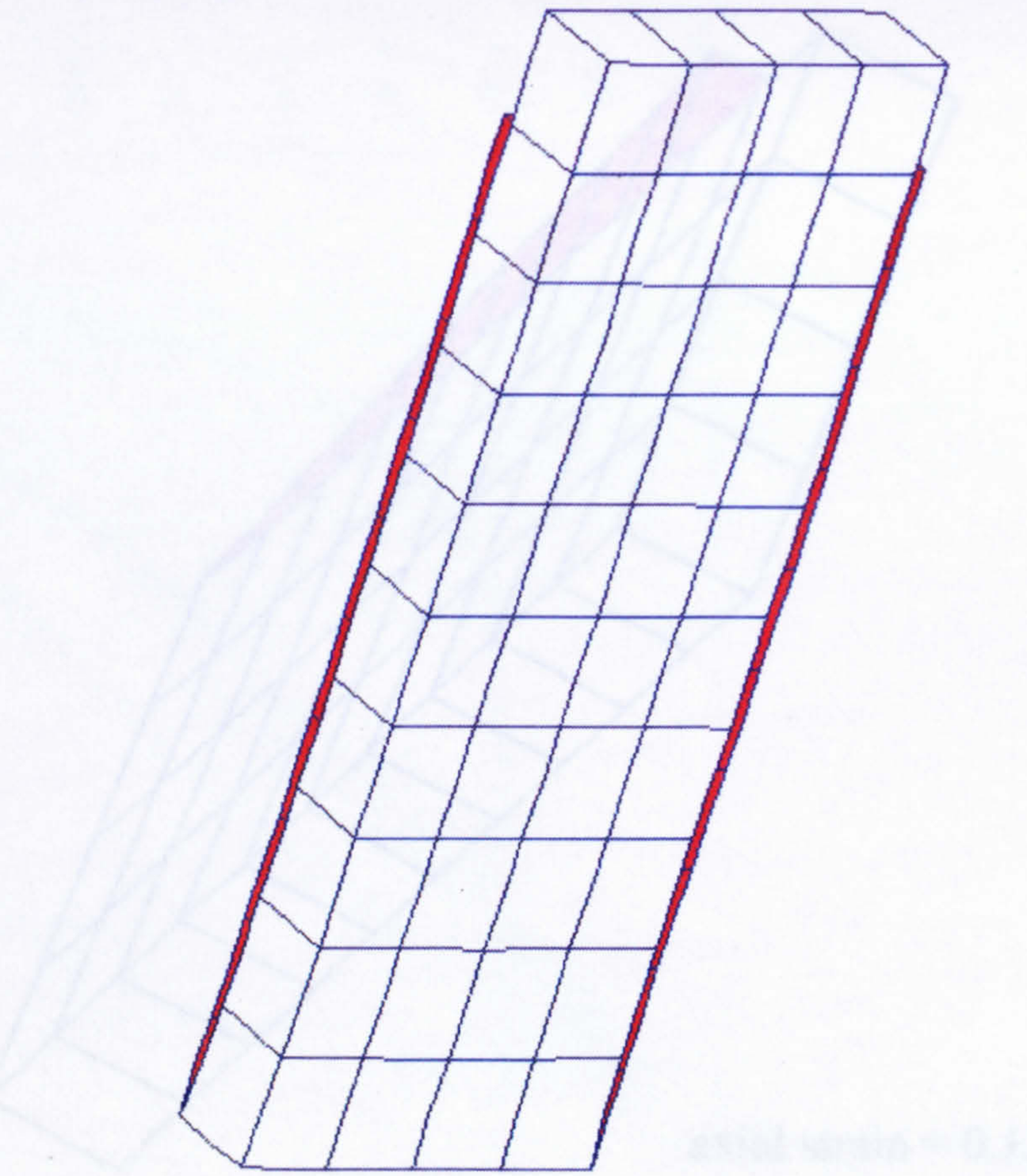

Fig.5.20 The Displacement of Plate Under Tension Loading in the [001] Orientation

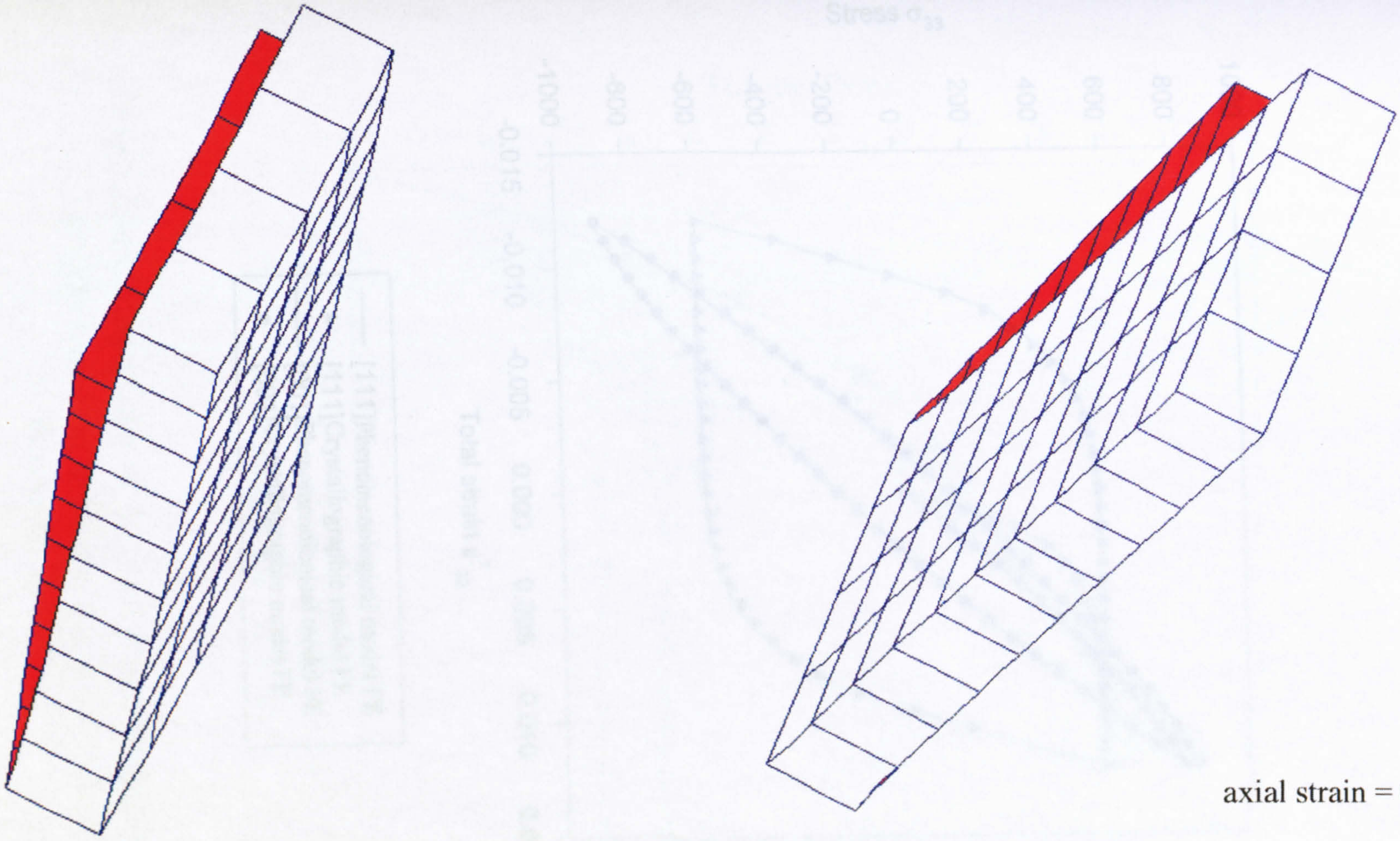

axial strain = 0.12%

Fig.5.21 Disorder Deformation Induced from Material Anisotropy of Single Crystal for a Plate Specimen with Orientation 10 Degree Away From [001]

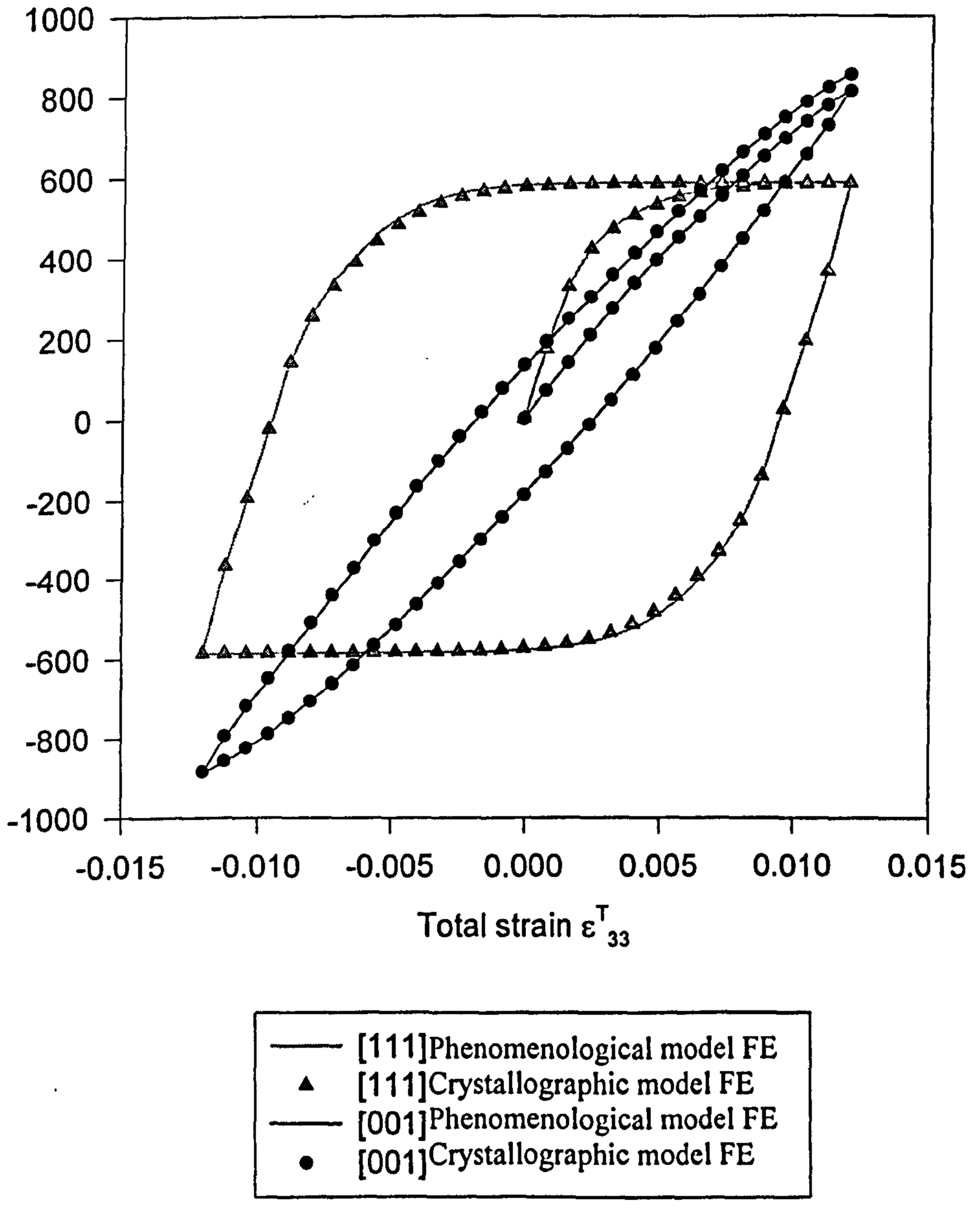

Fig.5.22 Comparison of Stress-Strain Response under Cyclic Loading between the Two Models

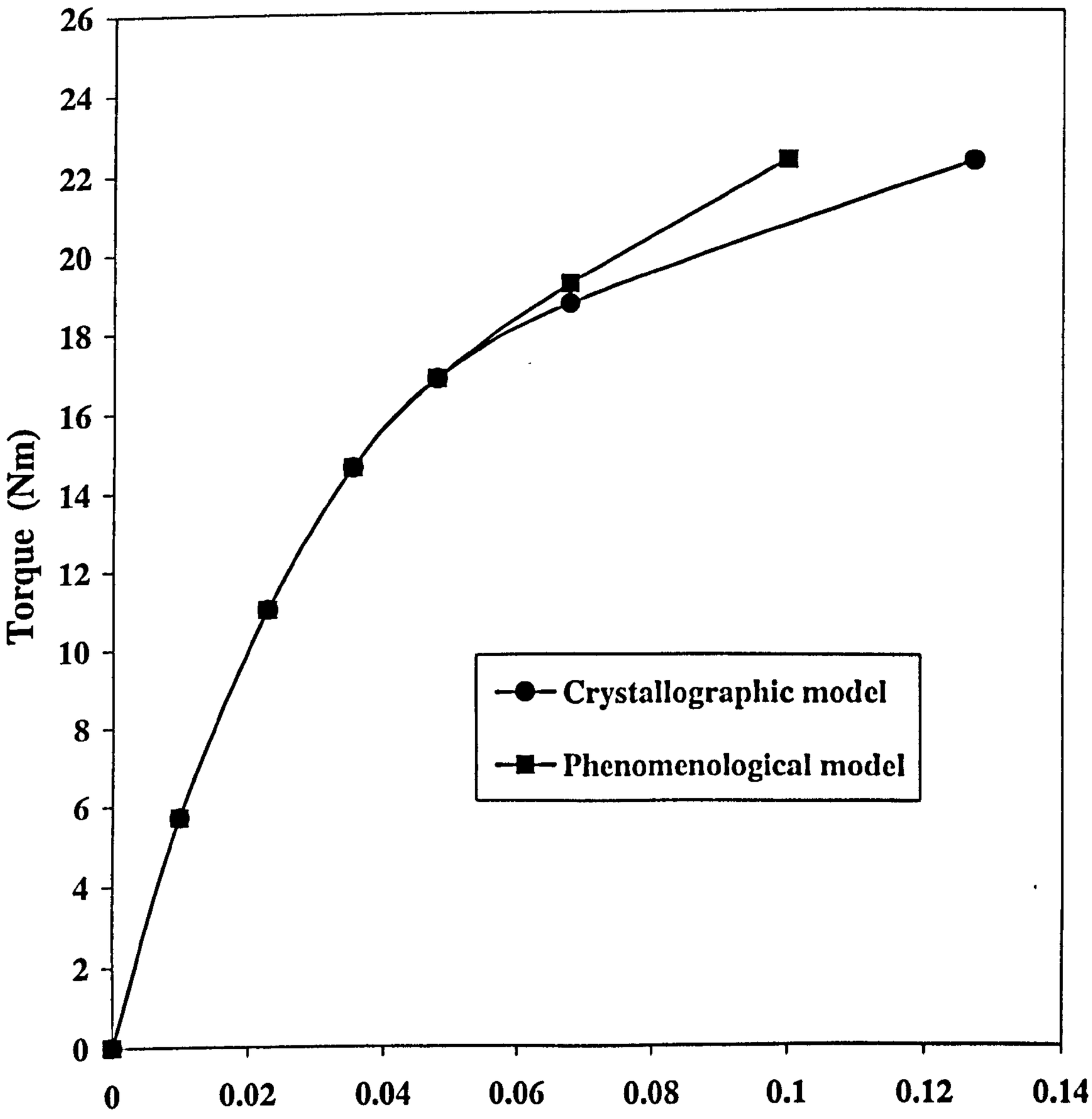

Fig.5.23a Comparison of Angle-Torque Response for Torsion Loading between the Two Models (stress control)

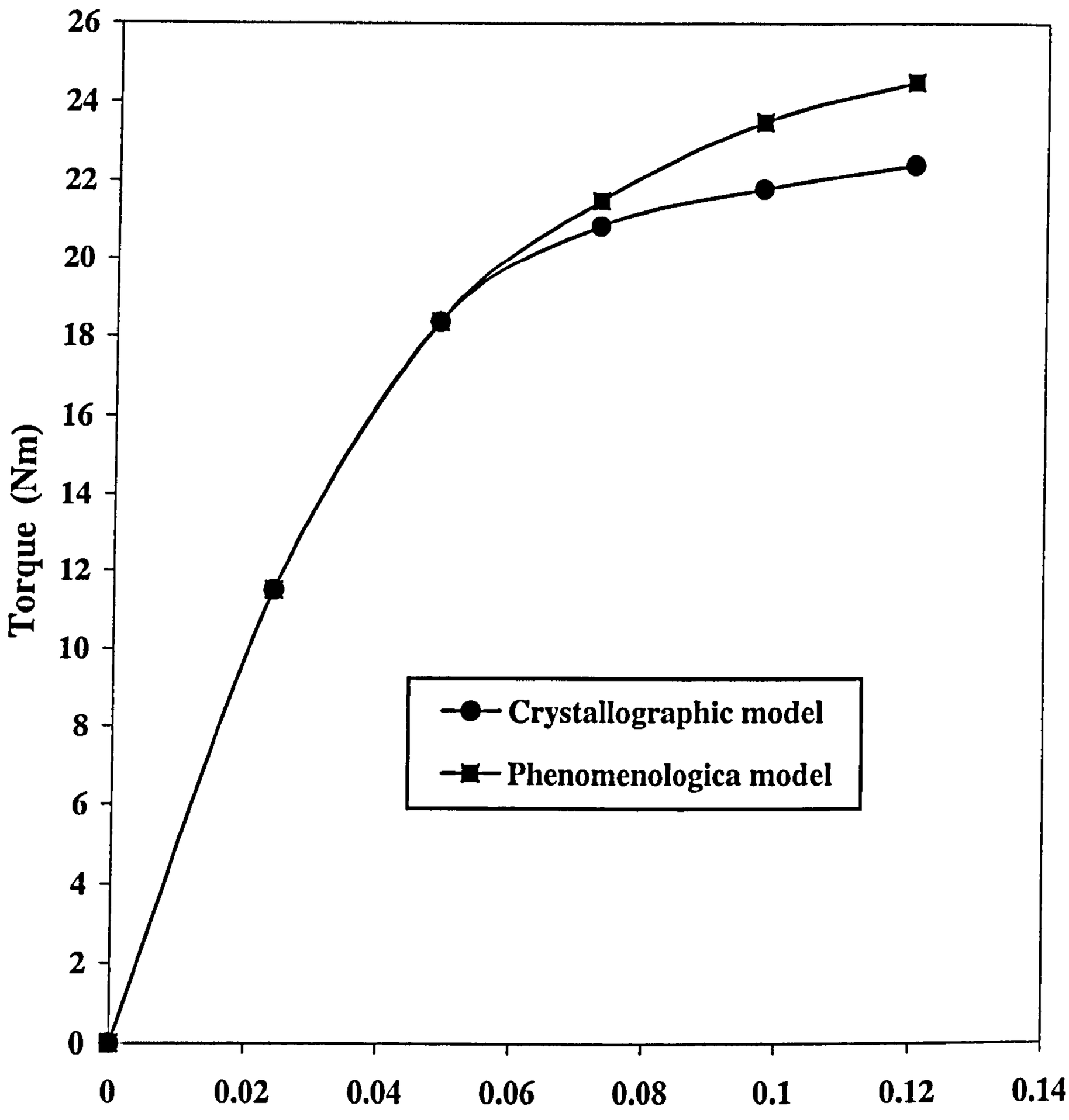

Fig.5.23b Comparison of Angle-Torque Response for Torsion Loading between the Two Models (strain control)

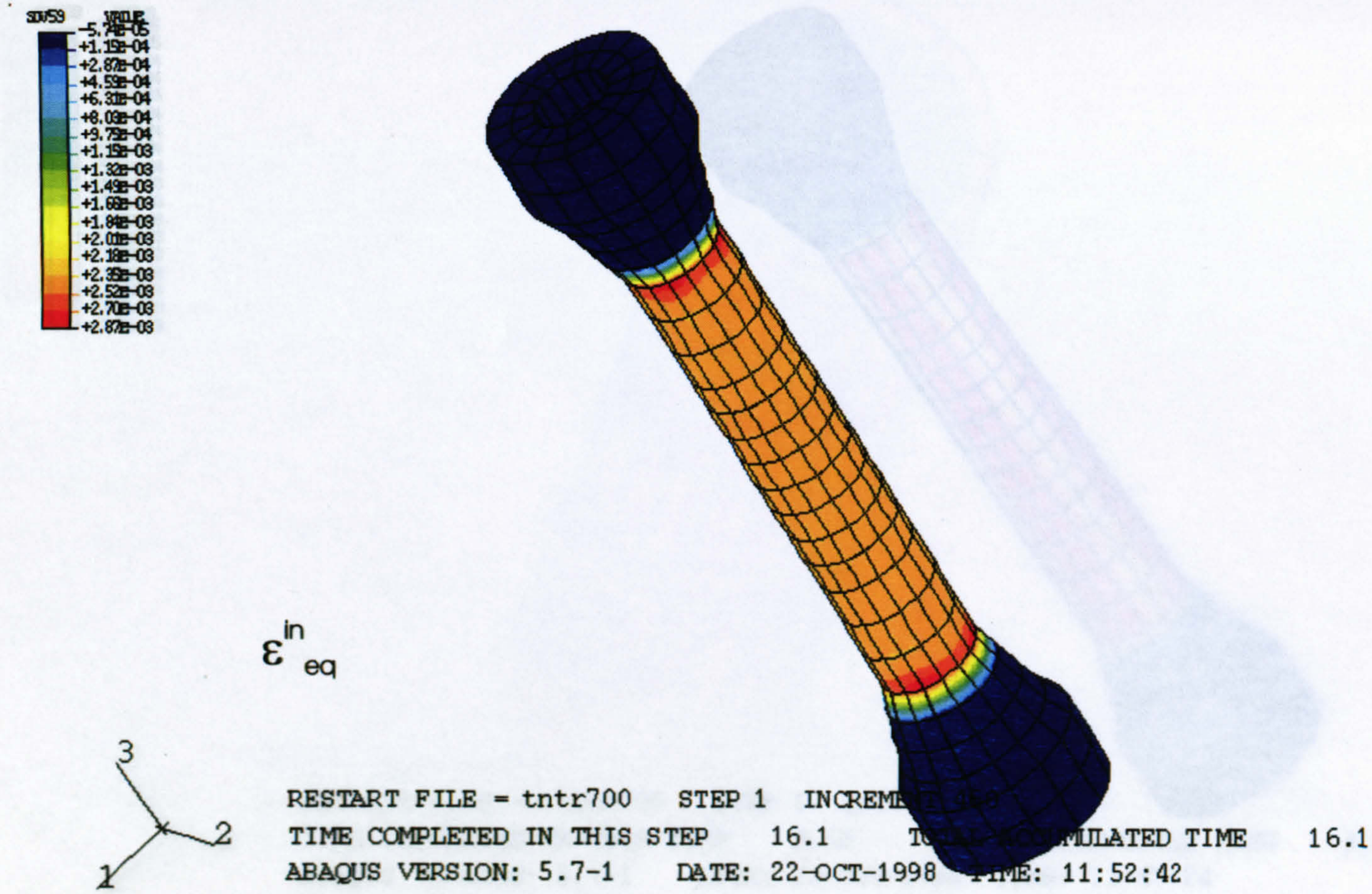

Fig. 5.24a The Distribution of Equivalent Inelastic Strain Predicted by For Pure Torsion Loading (Phenomenological Model)

Fig.5.25a Contours of Equivalent Viscoplastic Strain in the Tube Under Torsion (phenomenological model, twist around [001])

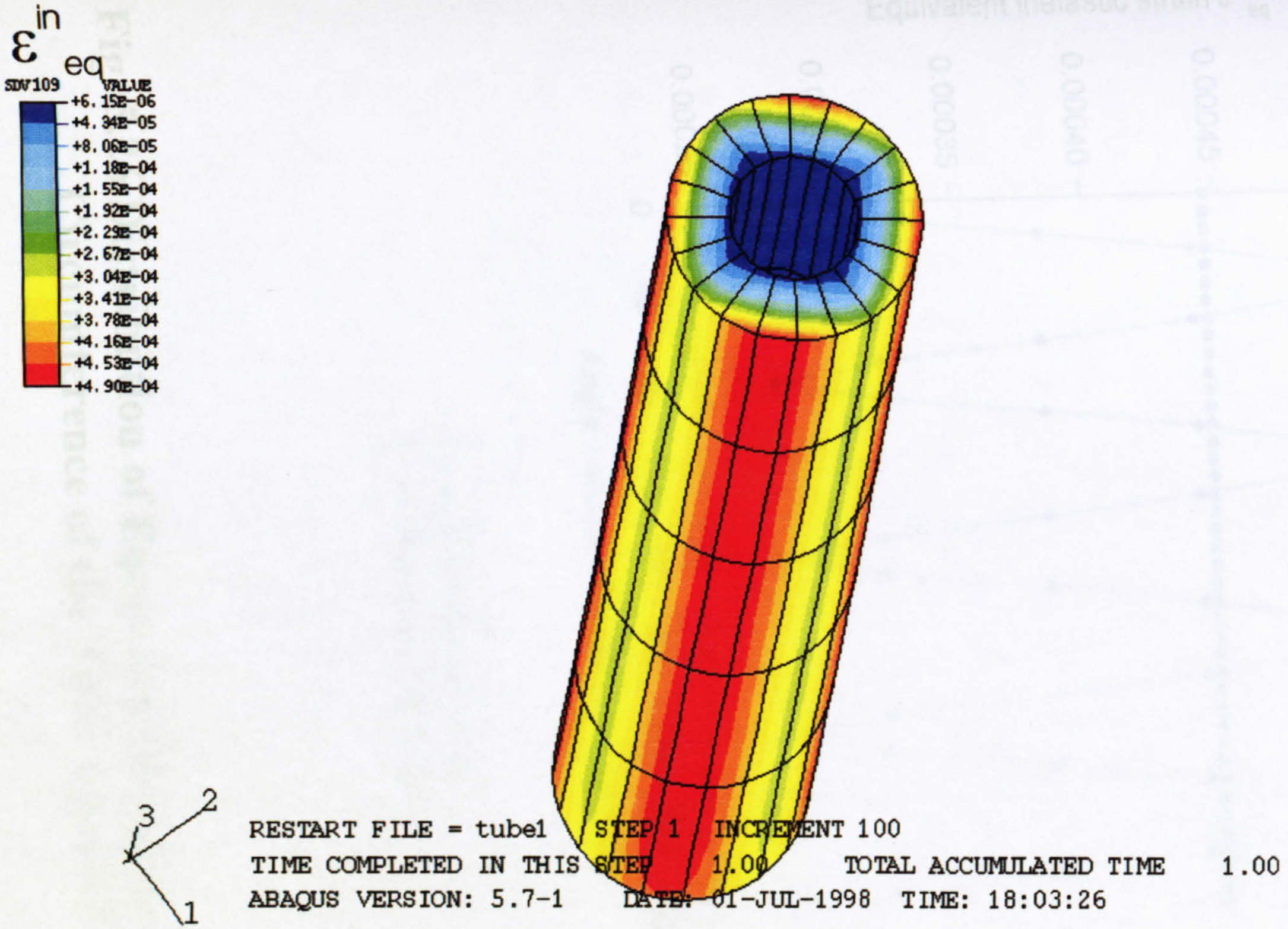

Fig.5.25b Contour of Equivalent Viscoplastic Strain in the Tube Under Torsion (Crystallographic model,twist around [001])

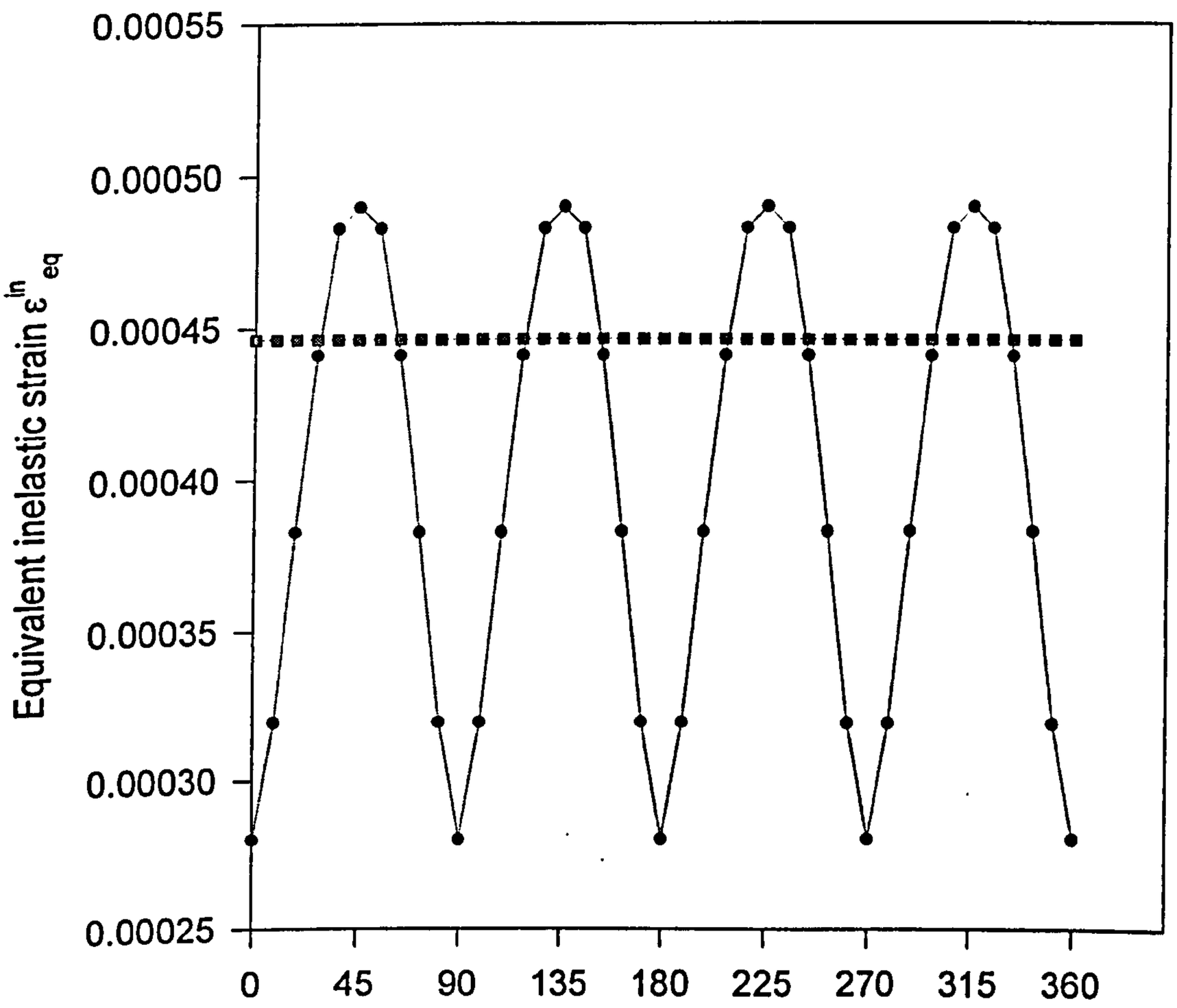

Fig. 5.26 Distribution of Equivalent Inelastic Strain around Circumference of the Tube under Torsion

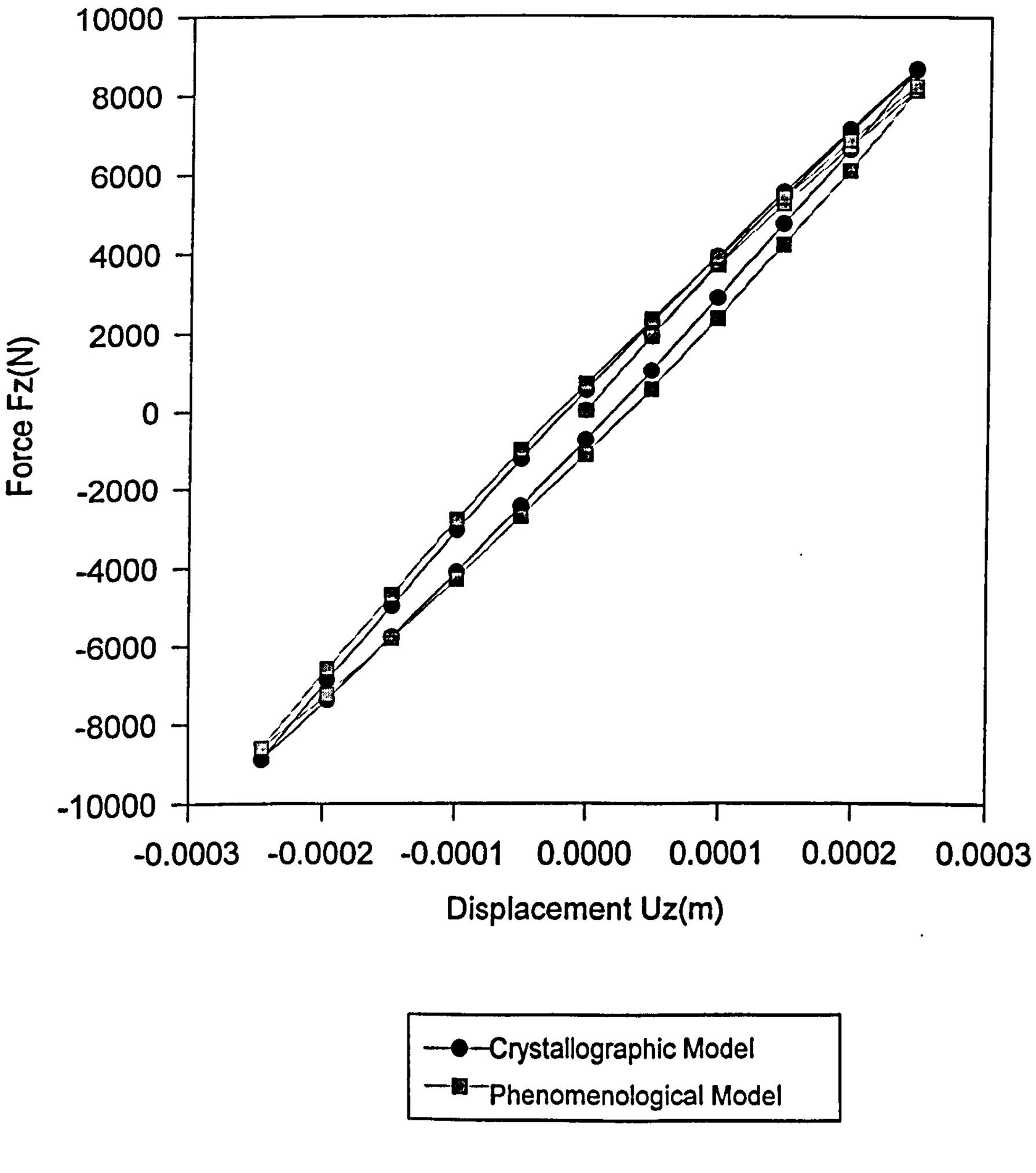

Fig.5.27a Comparison of Displacement – Force Responses between the Two Models for Tension-Torsion Loading

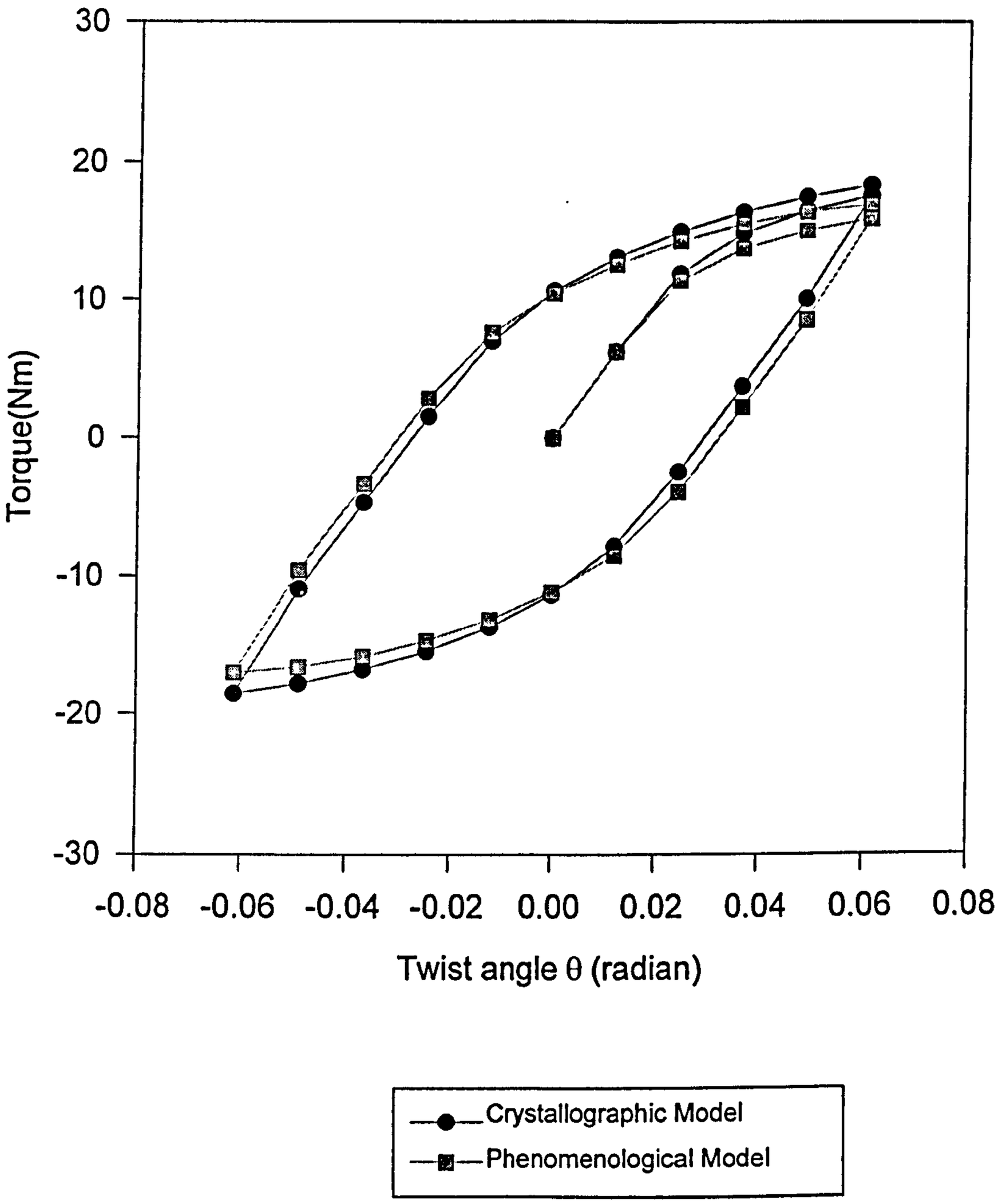

Fig.5.27b Comparison of Angle-Torque Responses between the Two Models for Tension-Torsion Loading

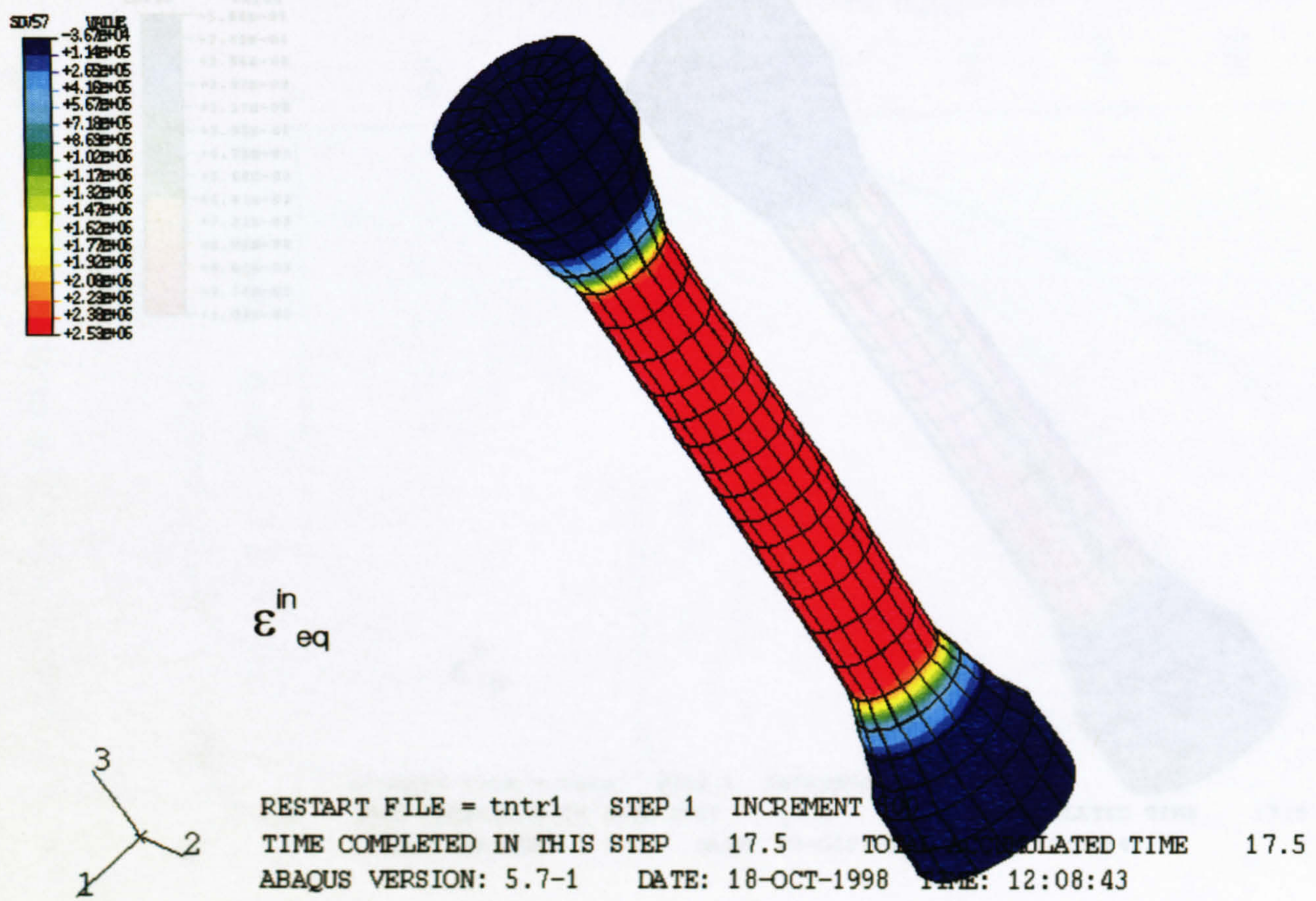

Fig.5.28 The Distribution of Equivalent Inelastic Strain Predicted by For Tension-Torsion Combined Loading (Phenomenological Model)

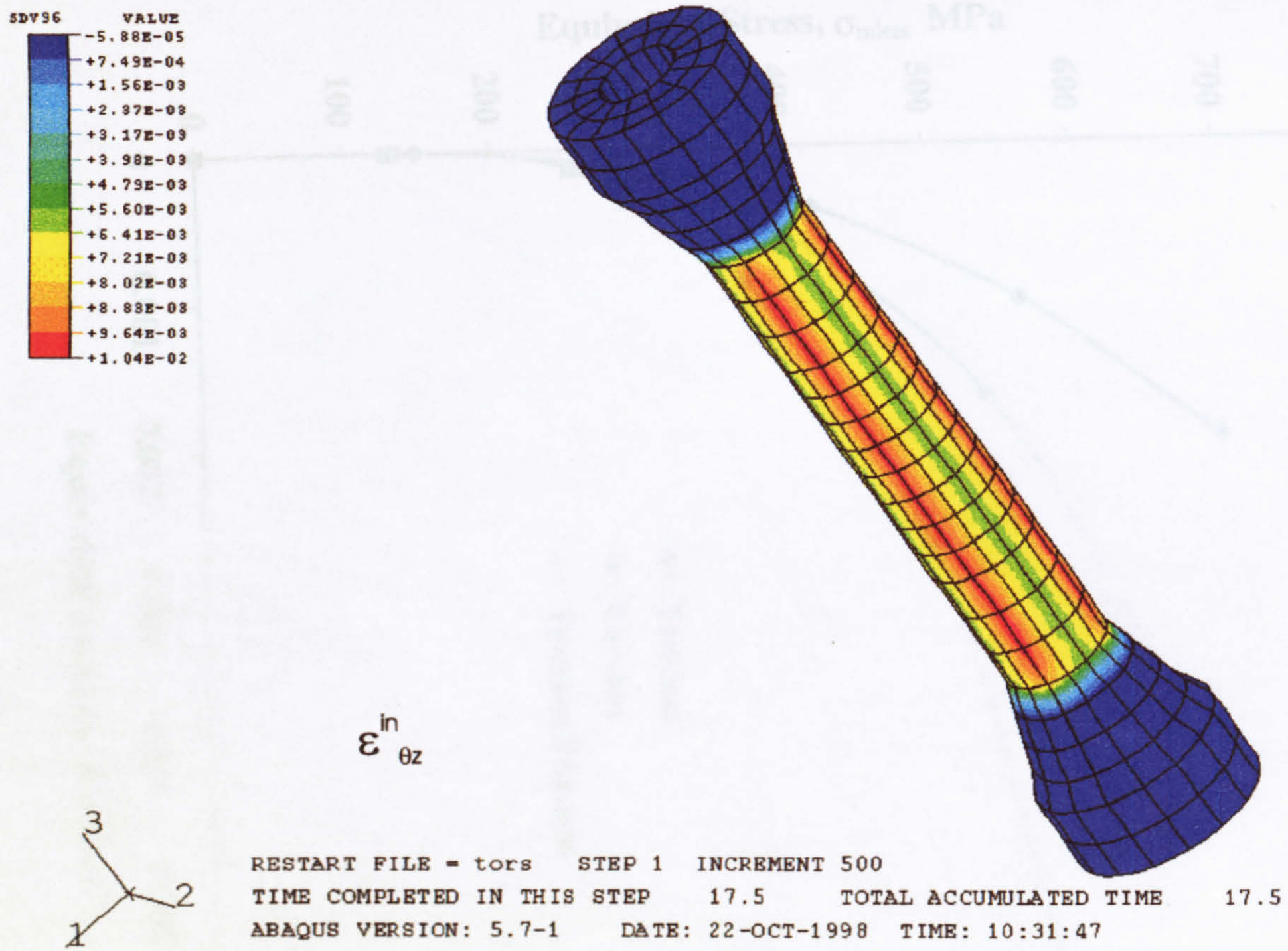

Fig.5.29 The Distribution of Inelastic Shear Strain Predicted by For Tension-Torsion Combined Loading (Crystallographic Model)

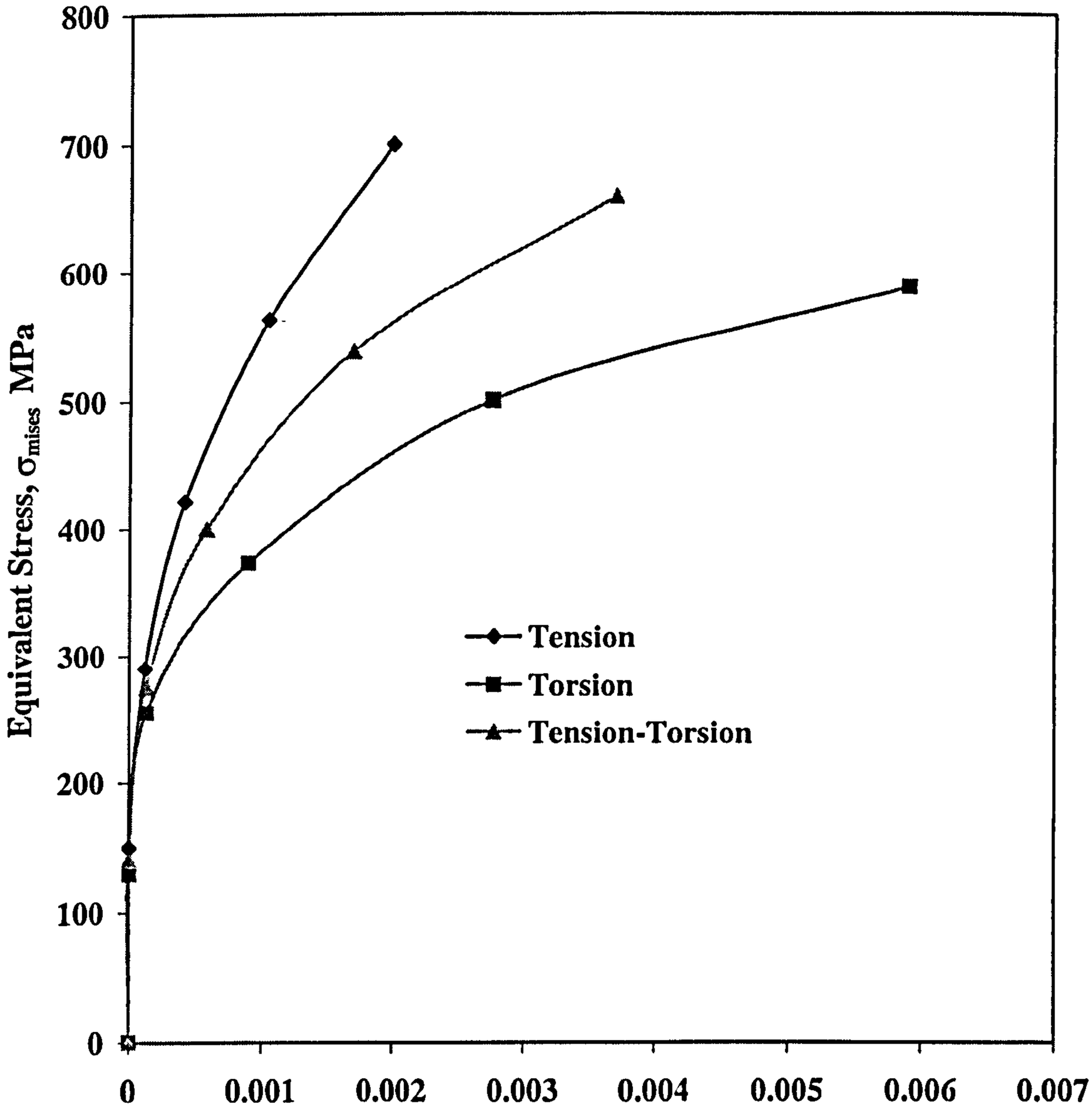

Fig.5.30 Comparison of Equivalent Stress and Inelastic Strain Curves between Different Lonading Conditions
(phenomenological model)

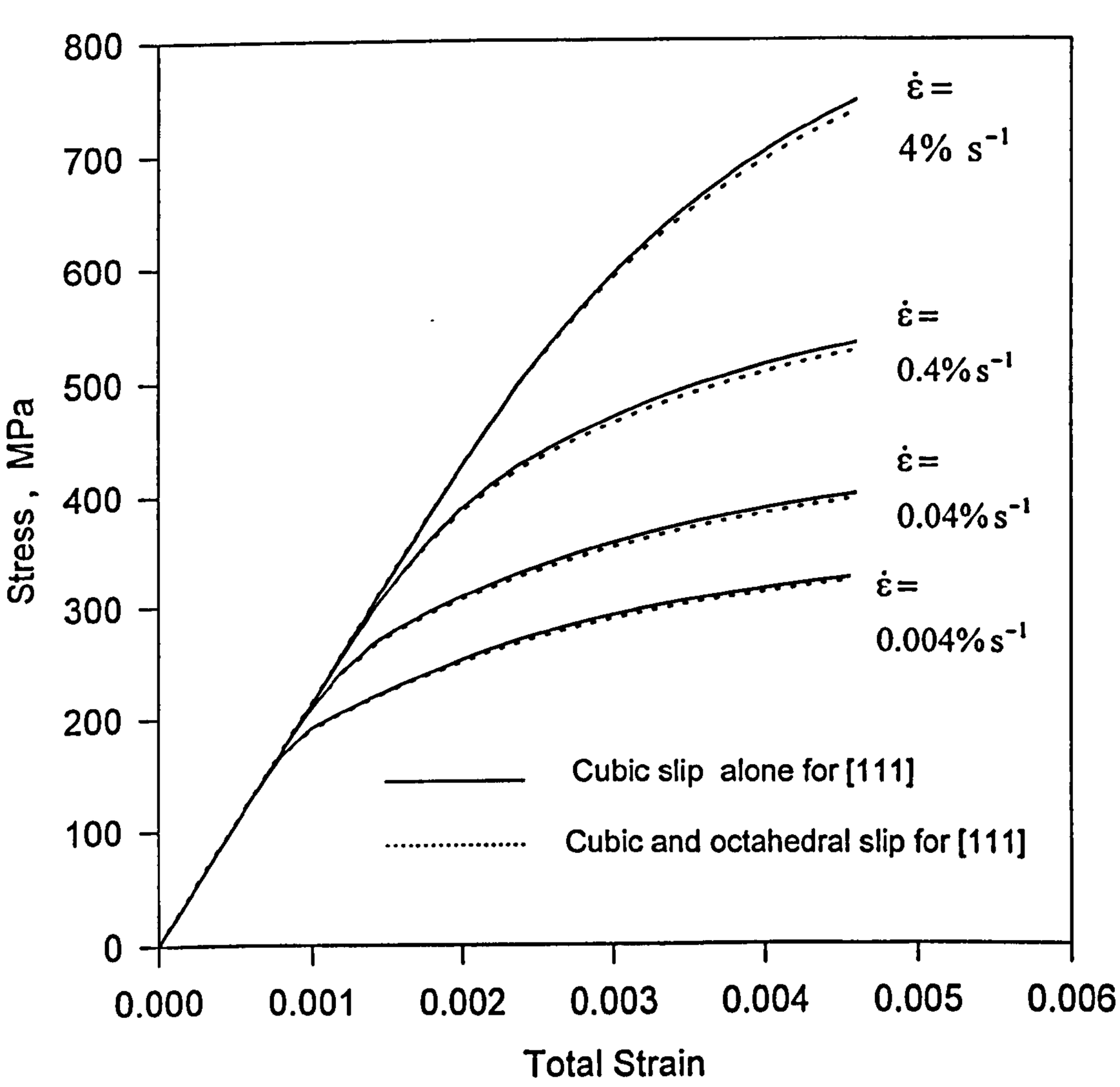

Fig.6.1. Comparison of Simulation Results from Crystallographic Model with and without Assumption

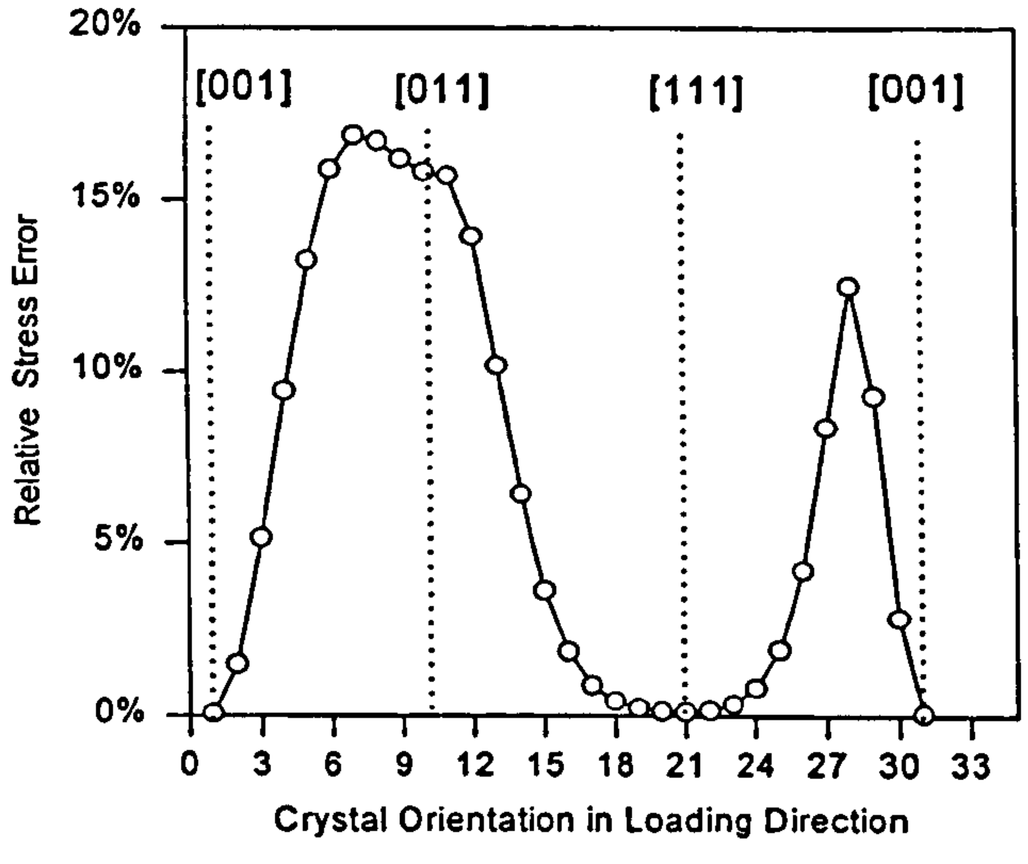

(a) Relative Error in Peak Stresses Between the Two Models

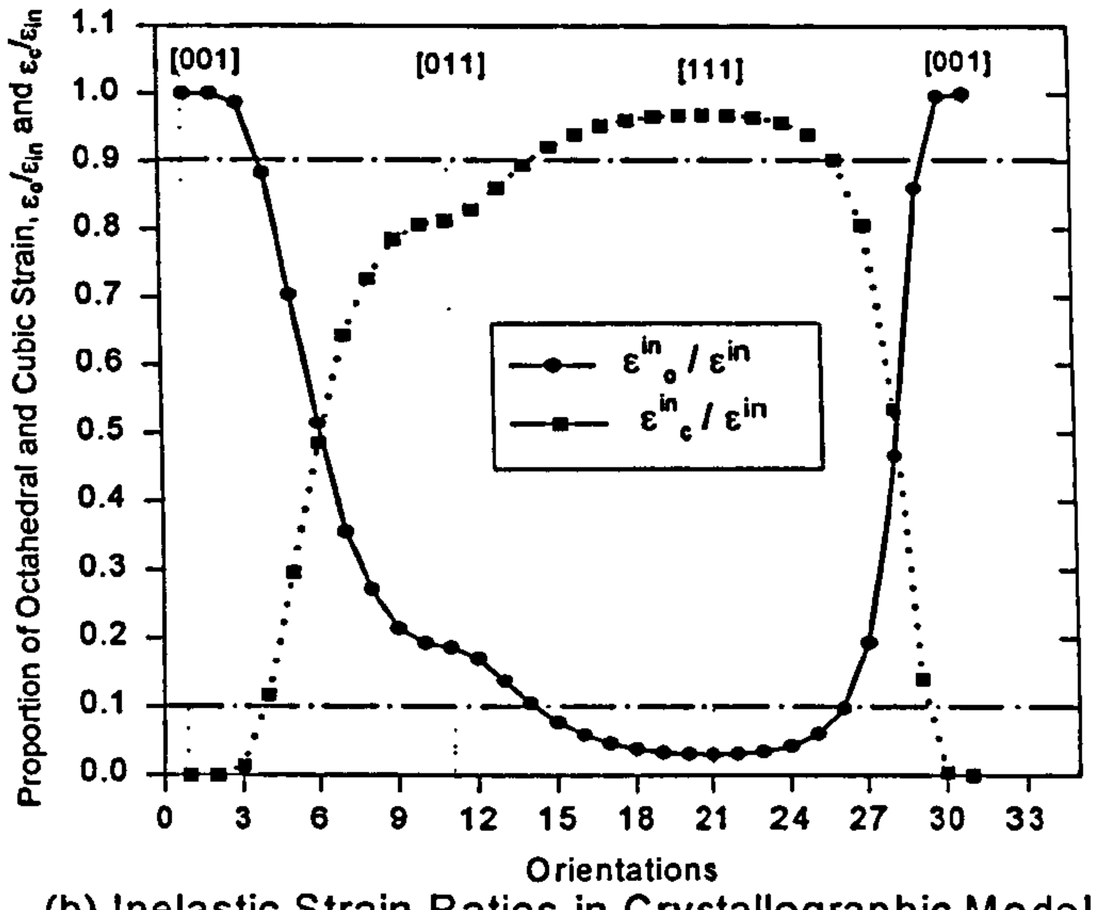

(b) Inelastic Strain Ratios in Crystallographic Model

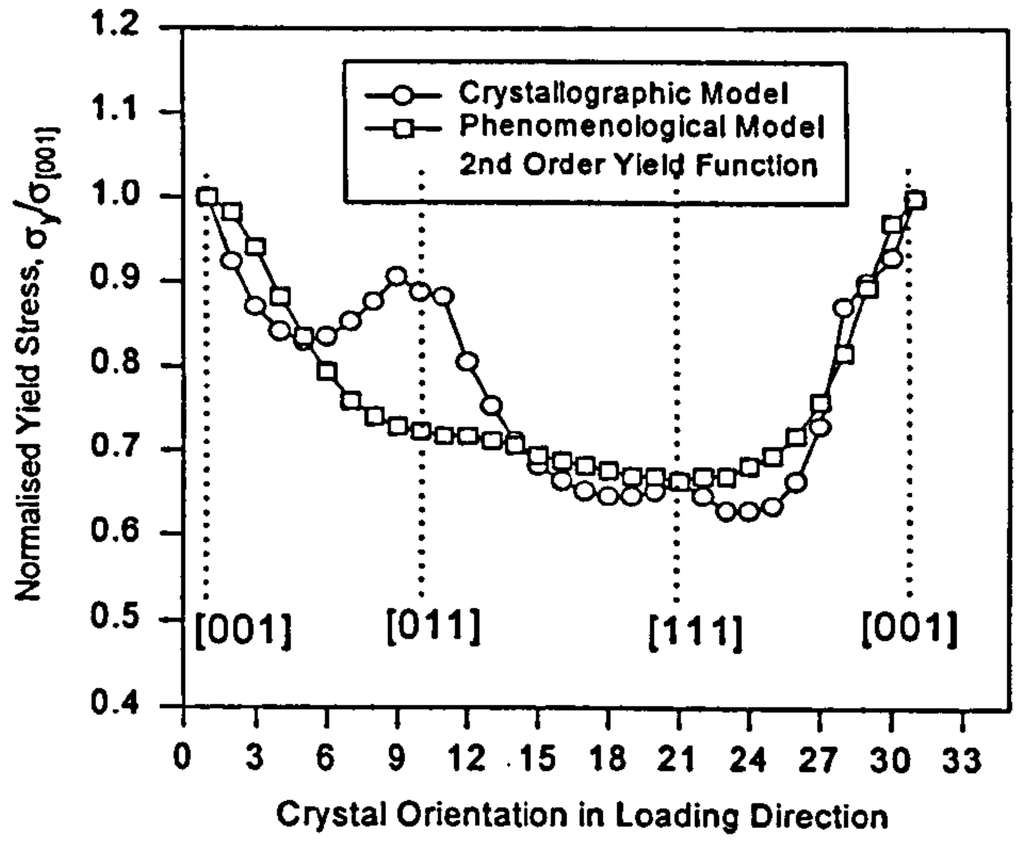

(c) Compasrison of Yield Stresses Under Uniaxial Loading

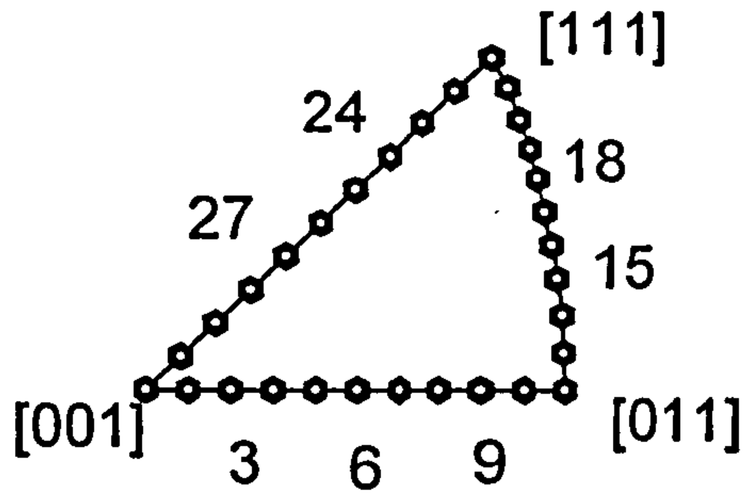

Fig.6.2 Comparison of the Deformation Characteristics of the Two Models

Fig.6.3. Illustration of Different Crystal Orientation Regions

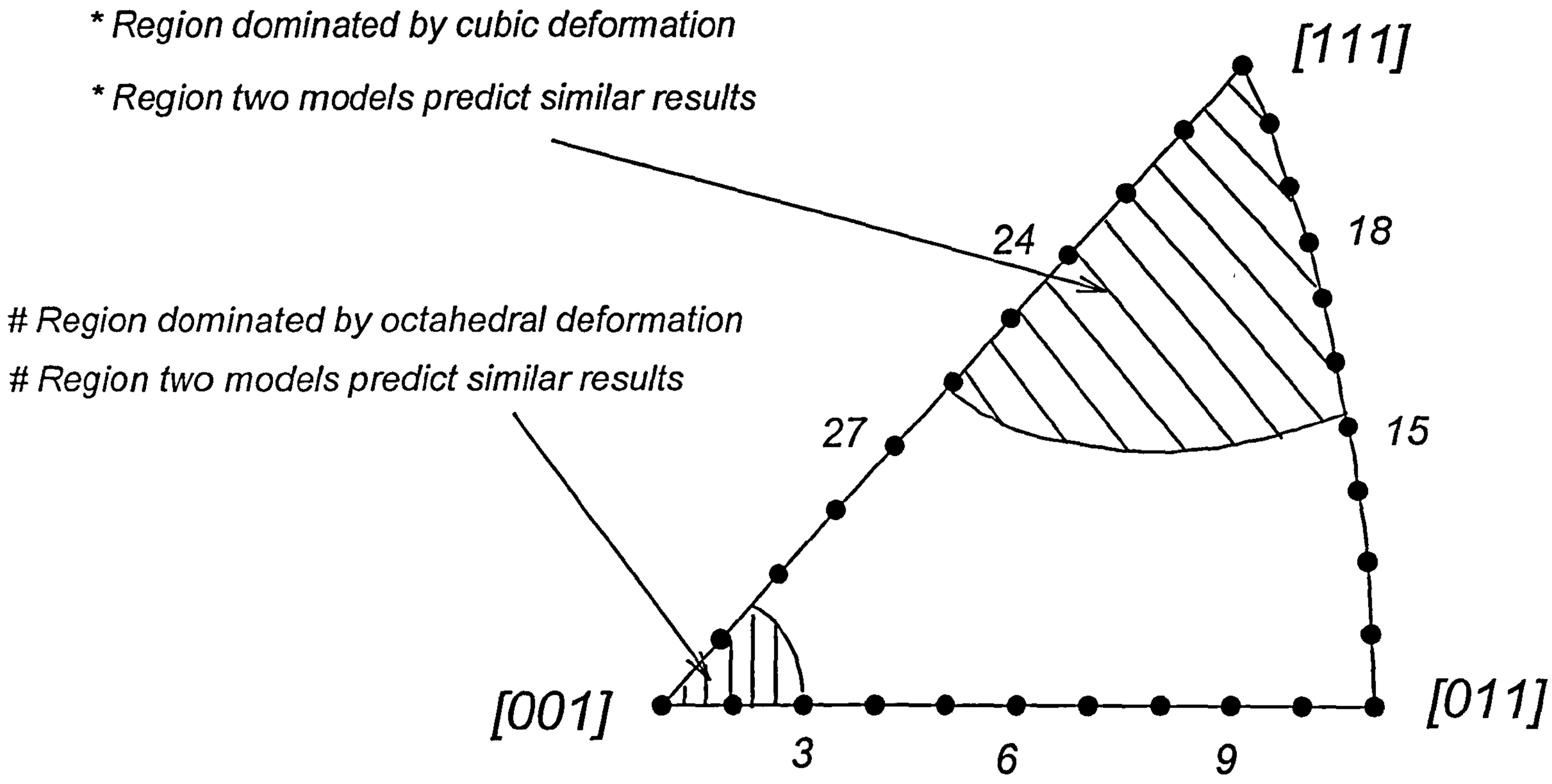

Fig.6.4. Comparison of Yield Stresses for Different Models

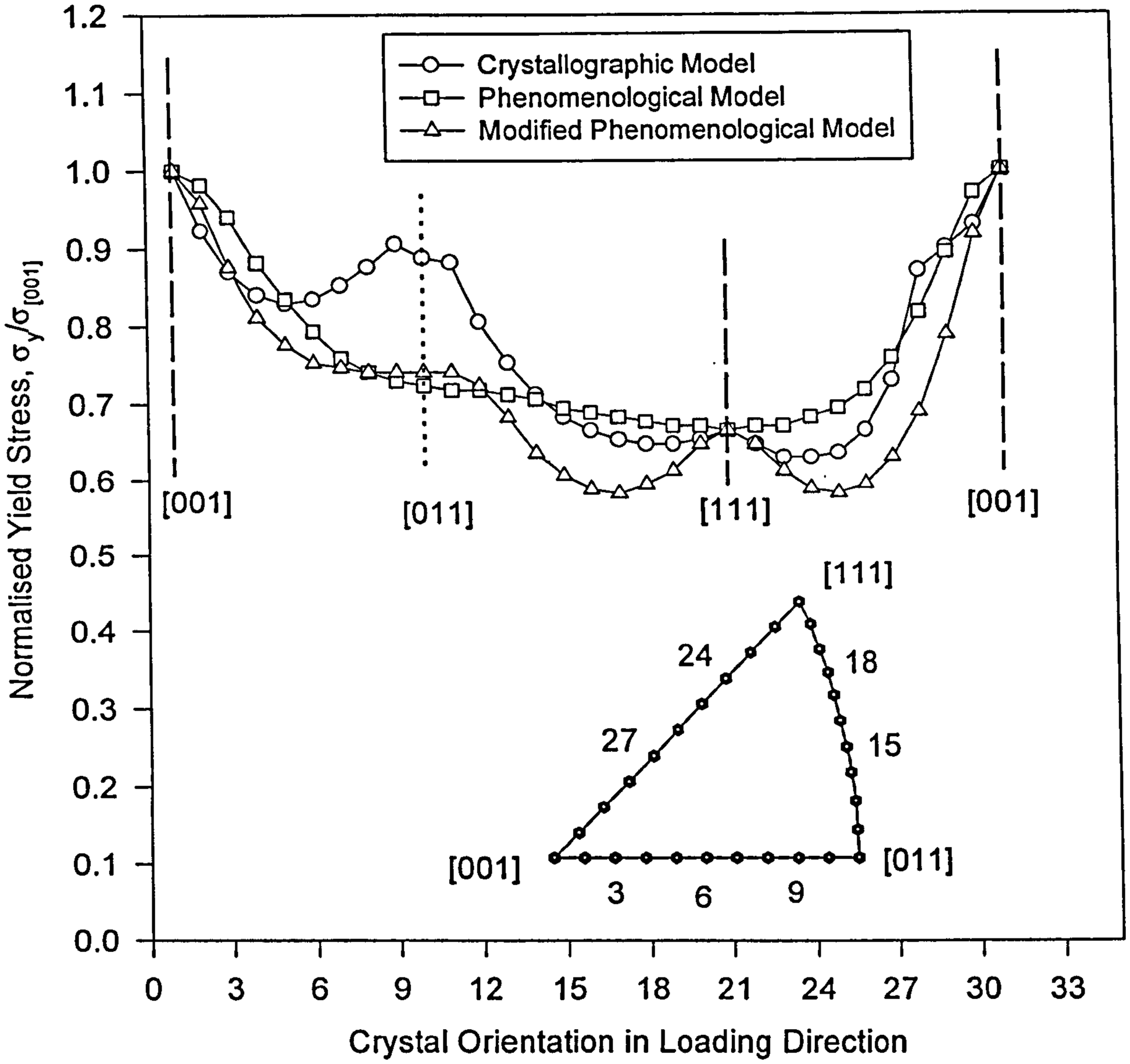

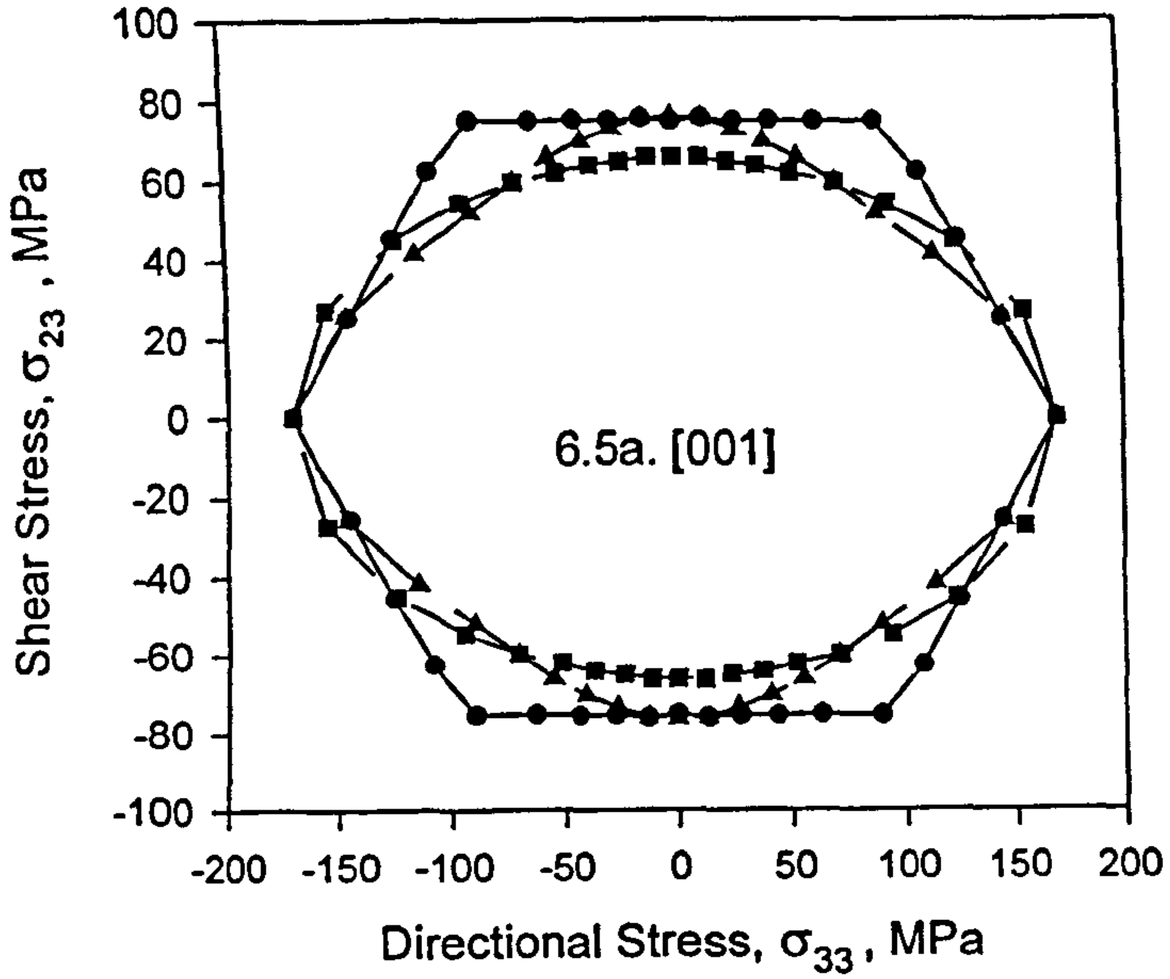

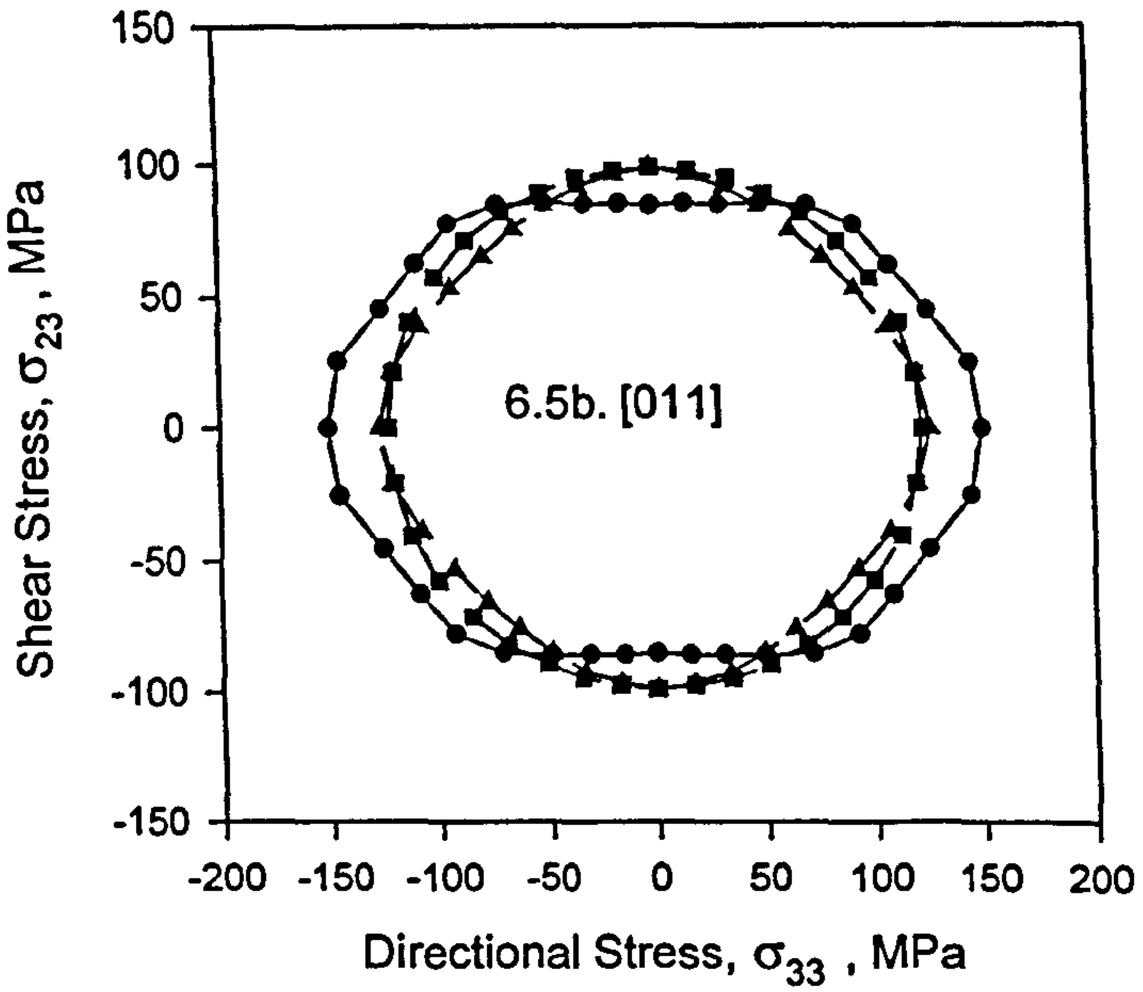

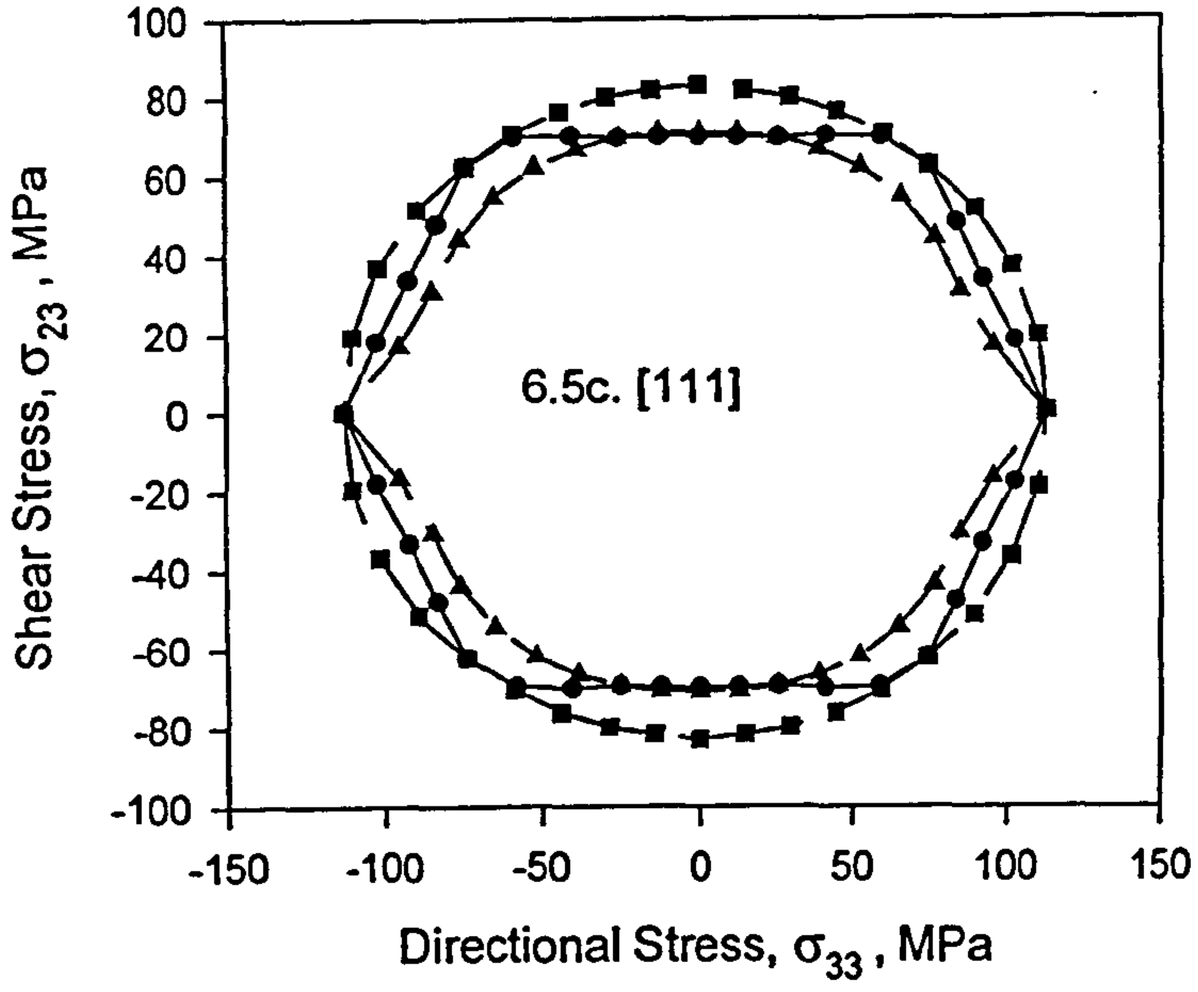

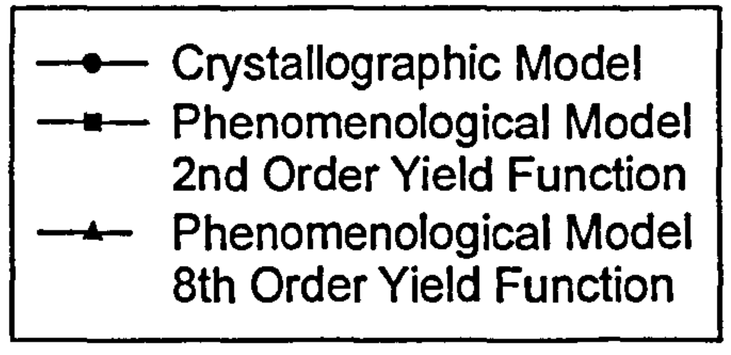

Fig. 6.5. Comparison of Yield Loci Under Tension-Torsion

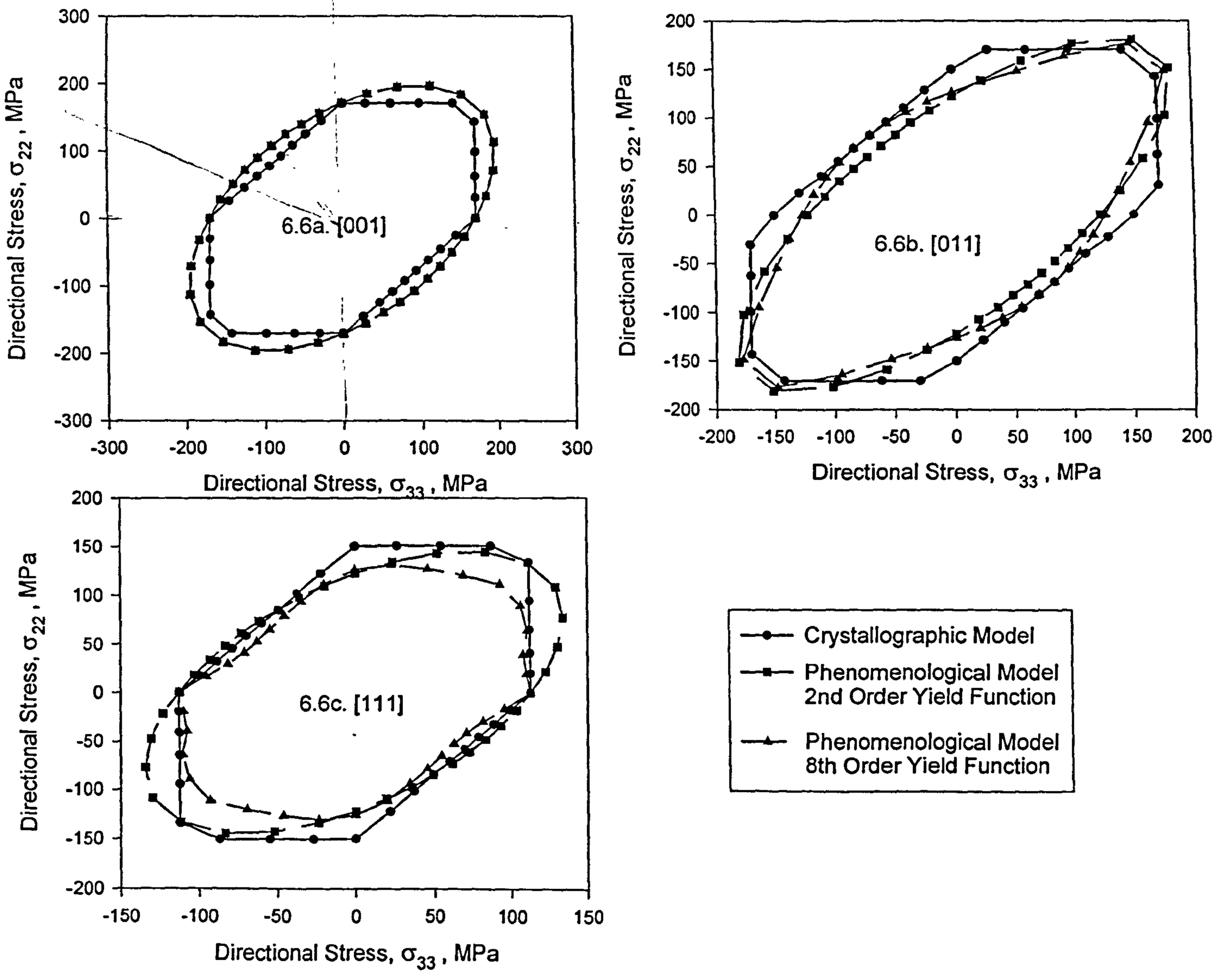

Fig. 6.6. Comparison of Yield Loci Under Tension-Tension

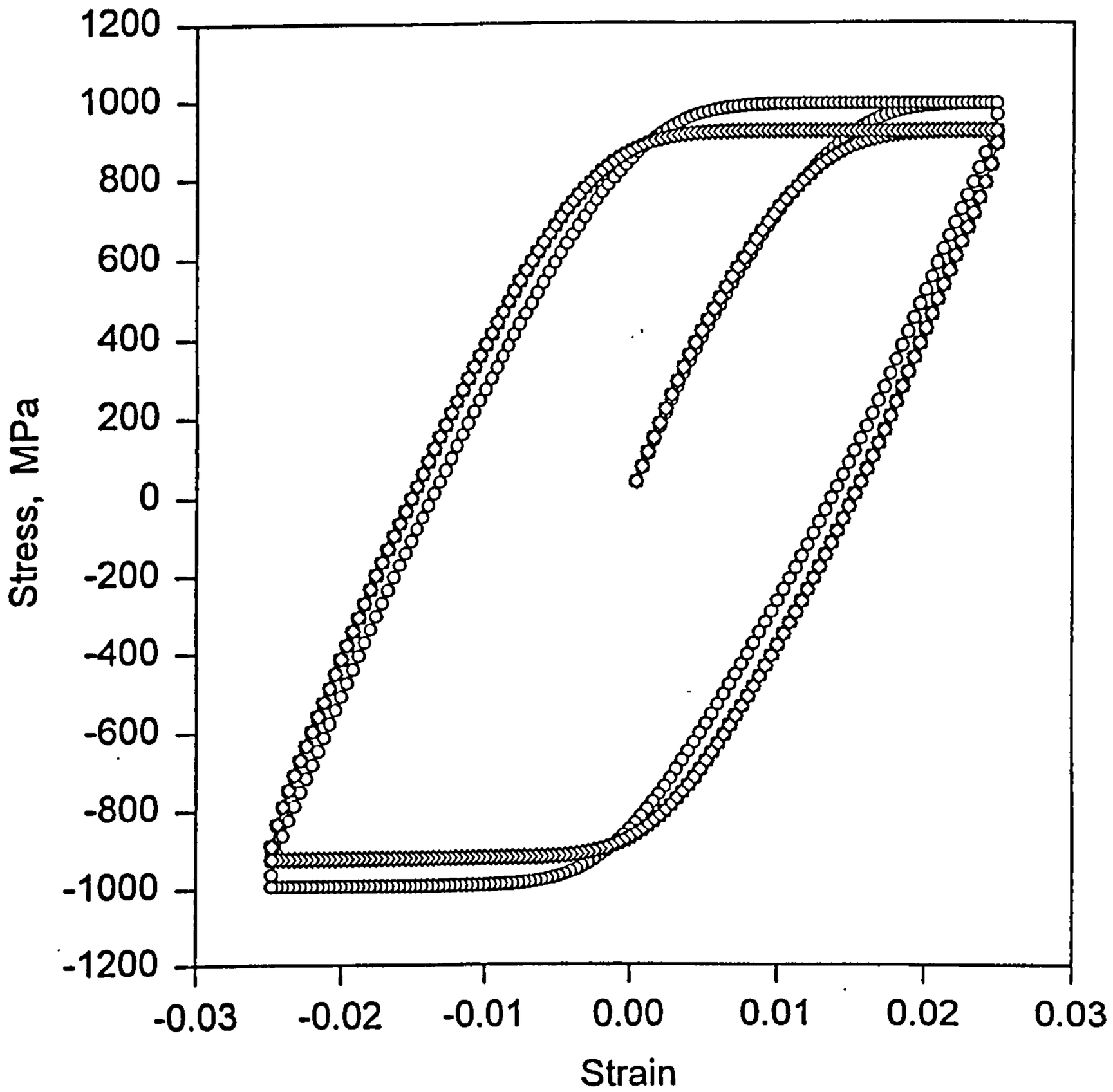

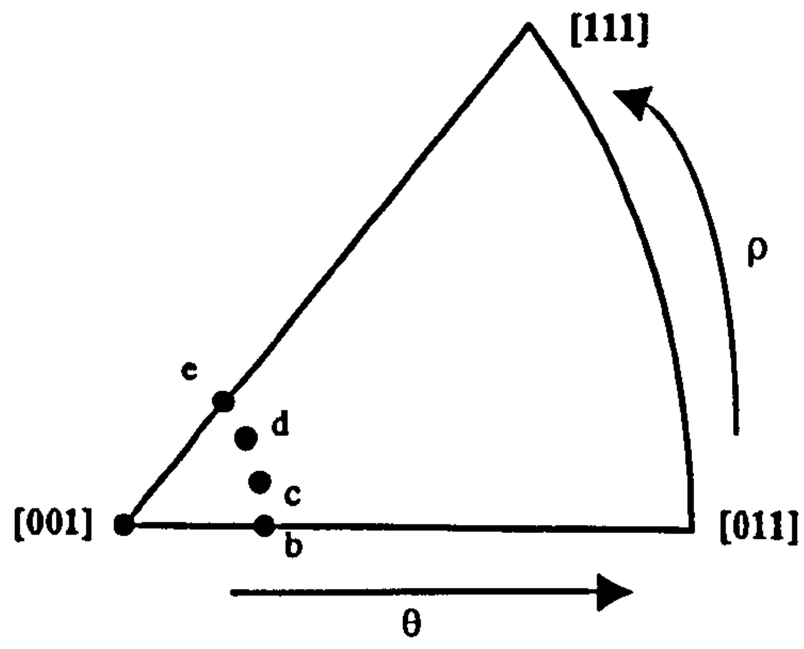

Fig.6.7 Stress-Strain Curves of Orientation Around [001]
(θ = 10 degree, misorientation effect)

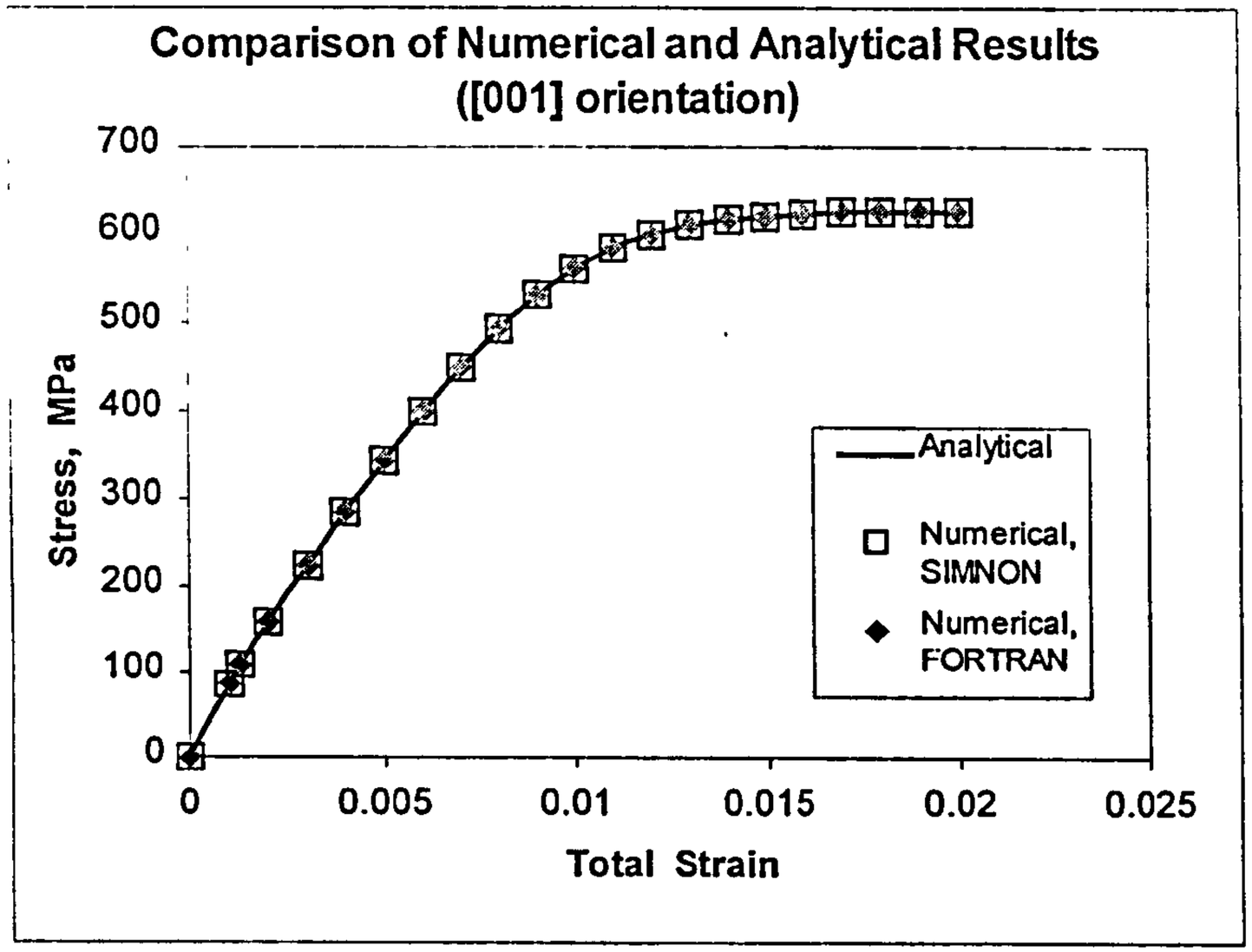

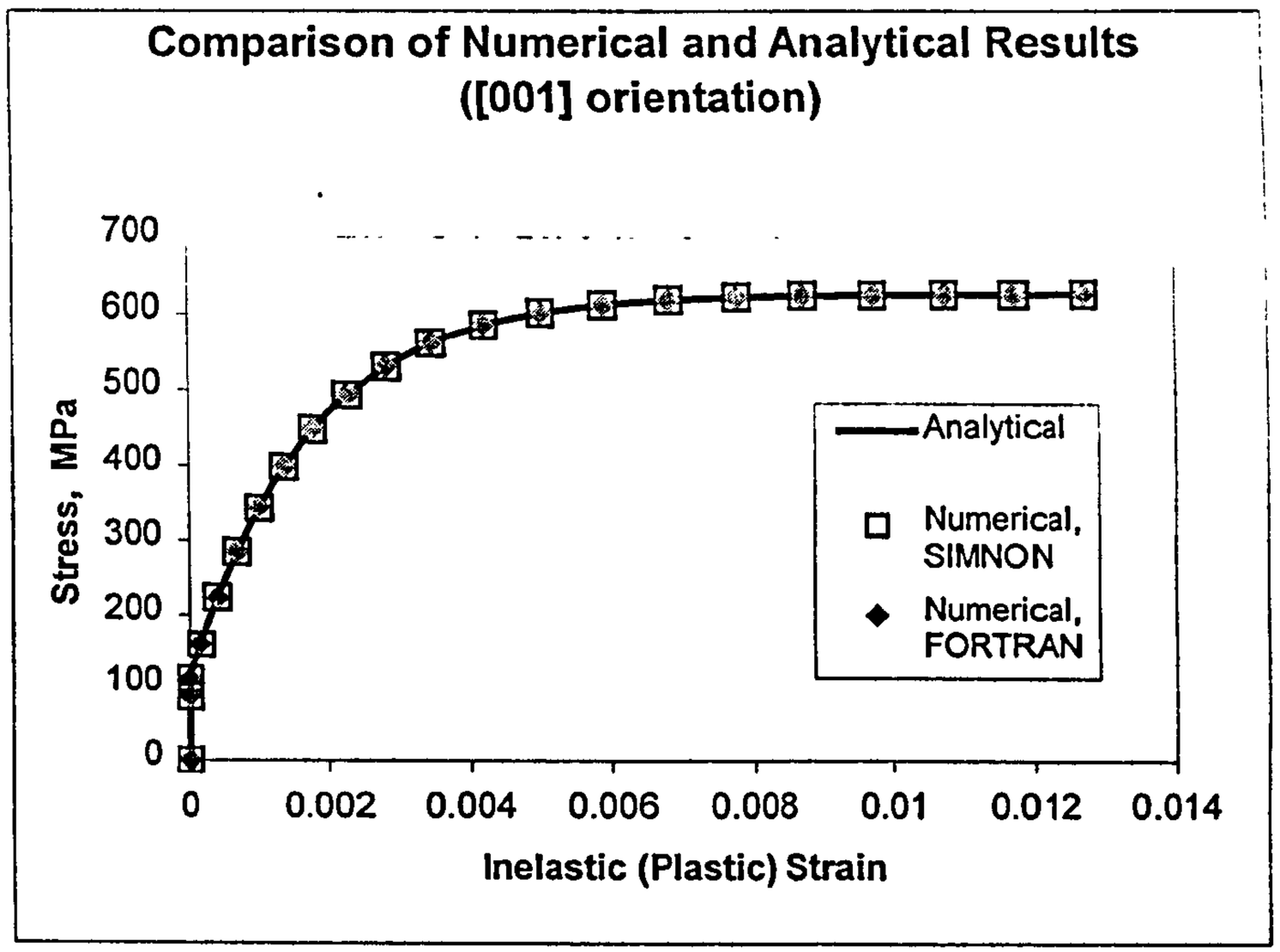

Fig. 6.8 Comparison of Numerical and Analytical Results for [001] Orientation

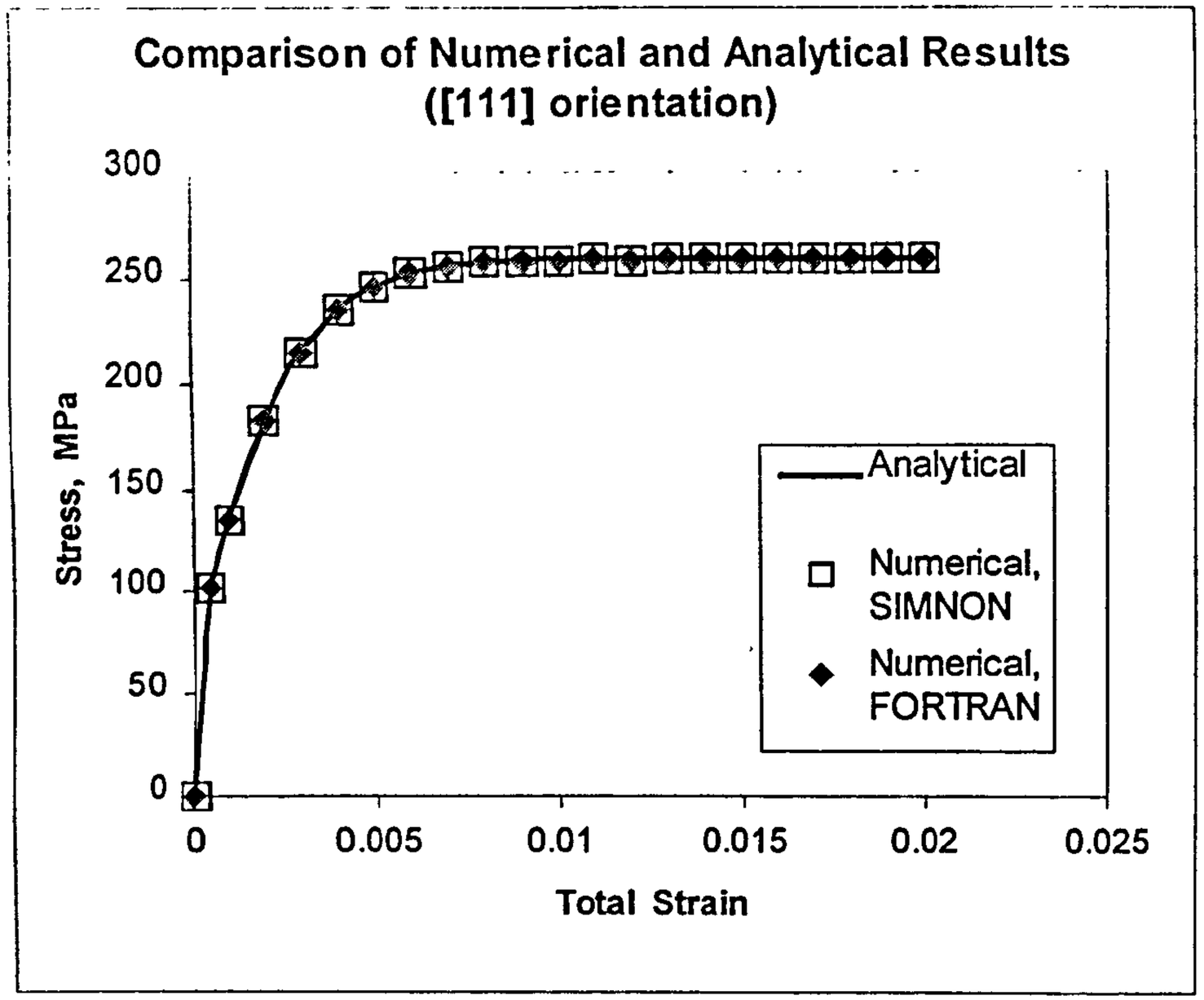

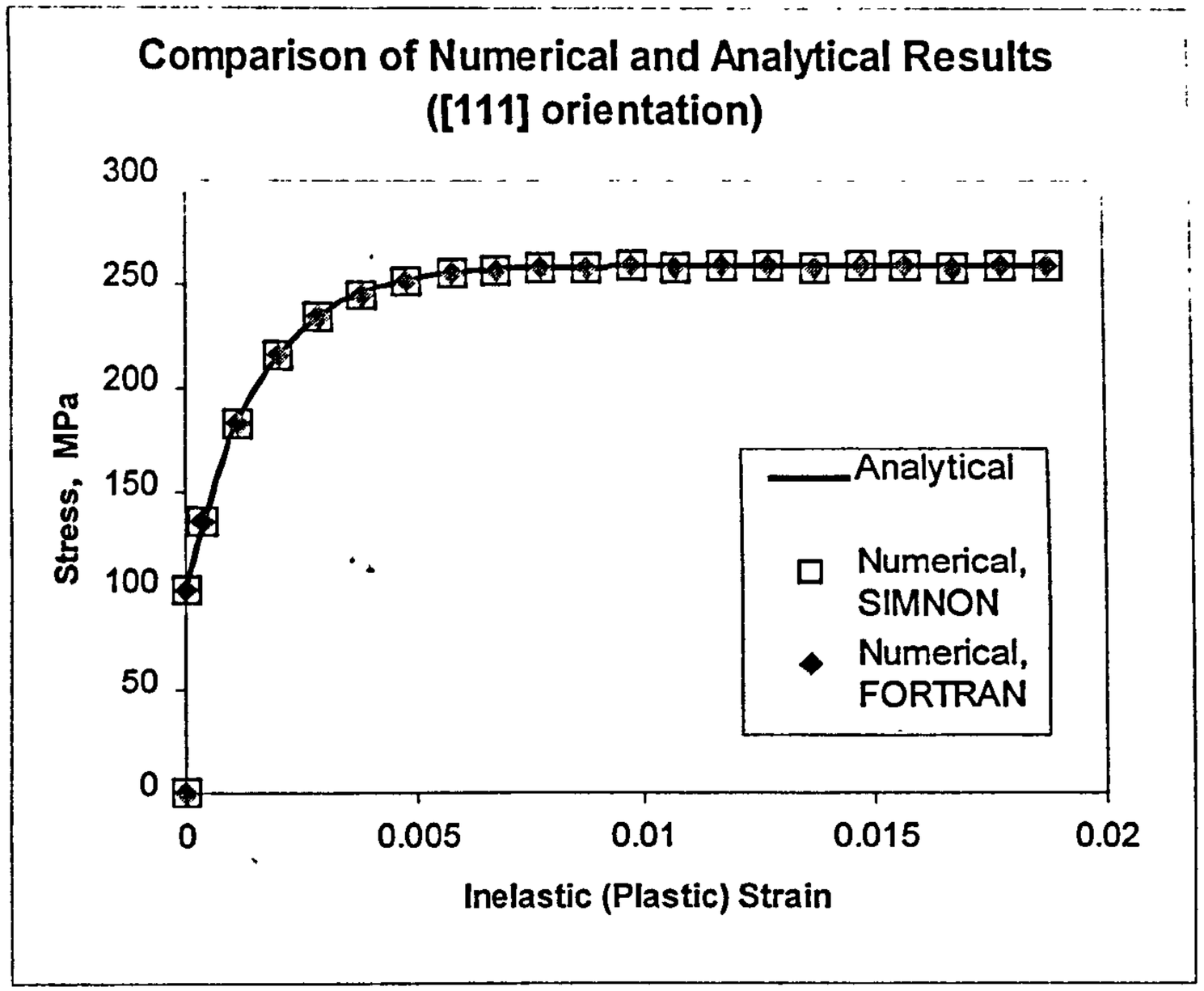

Fig. 6.9 Comparison of Numerical and Analytical Results for [111] Orientation

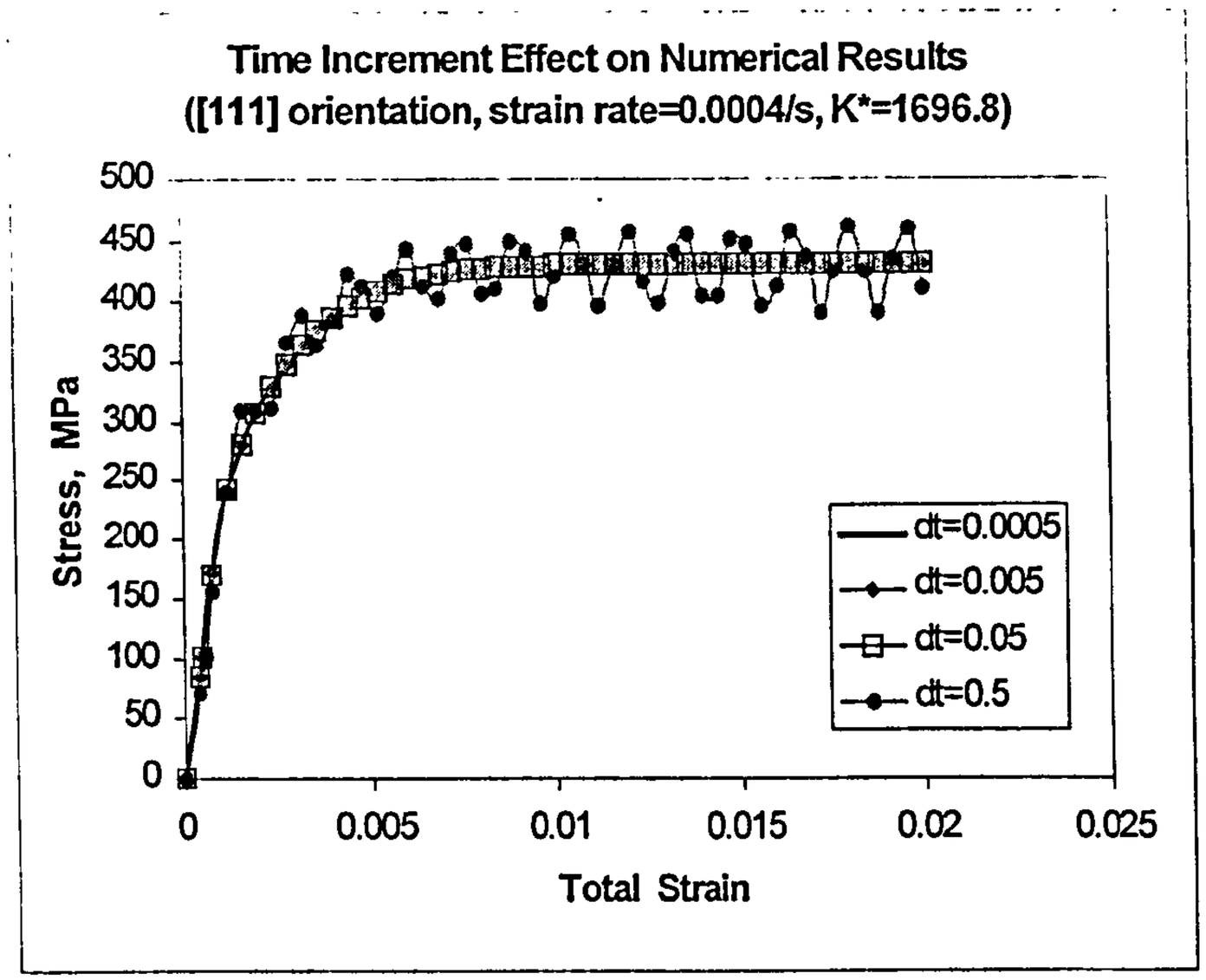

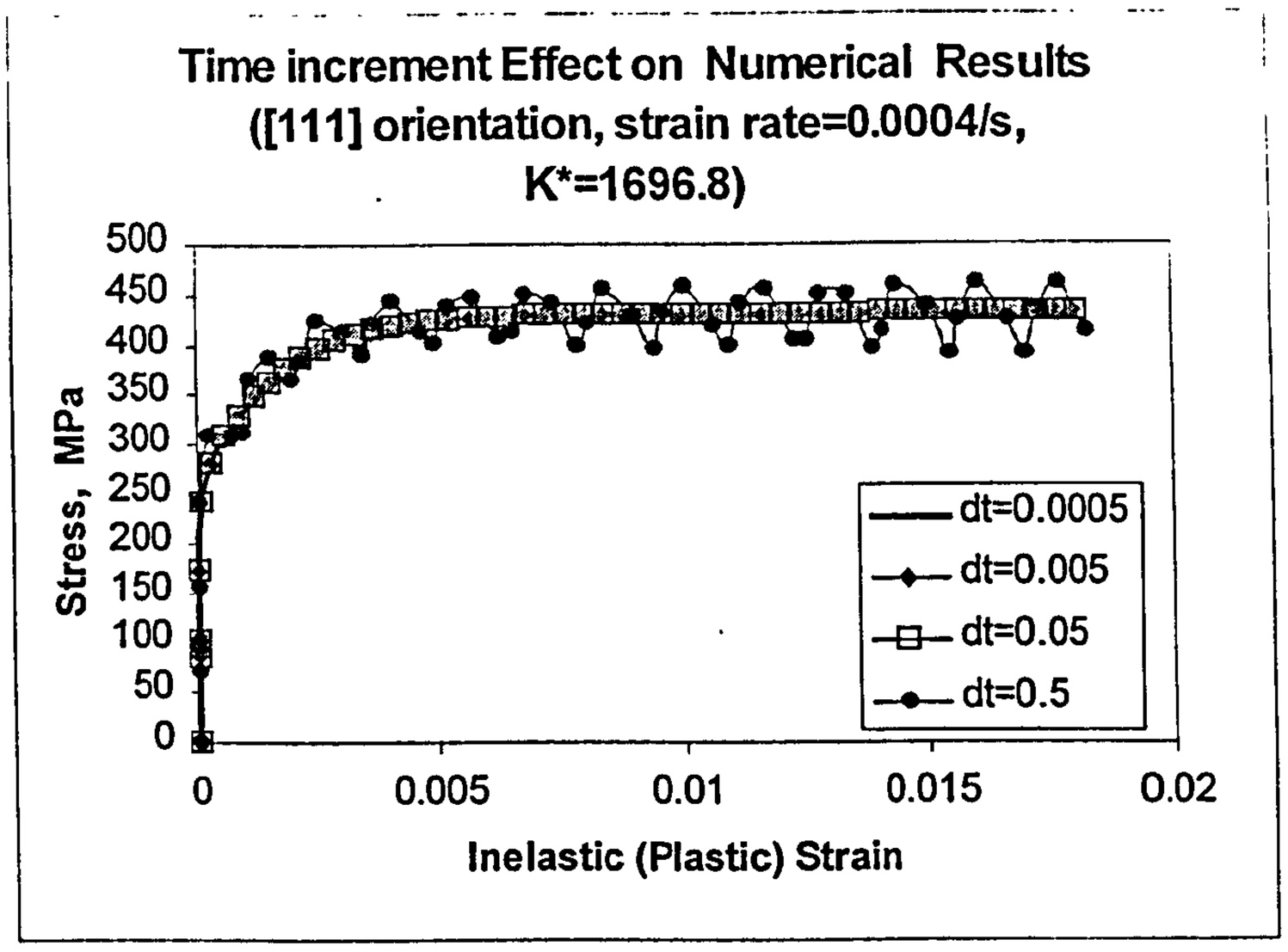

Fig.6.10 Time Increment Effect on the Numerical Simulation Results

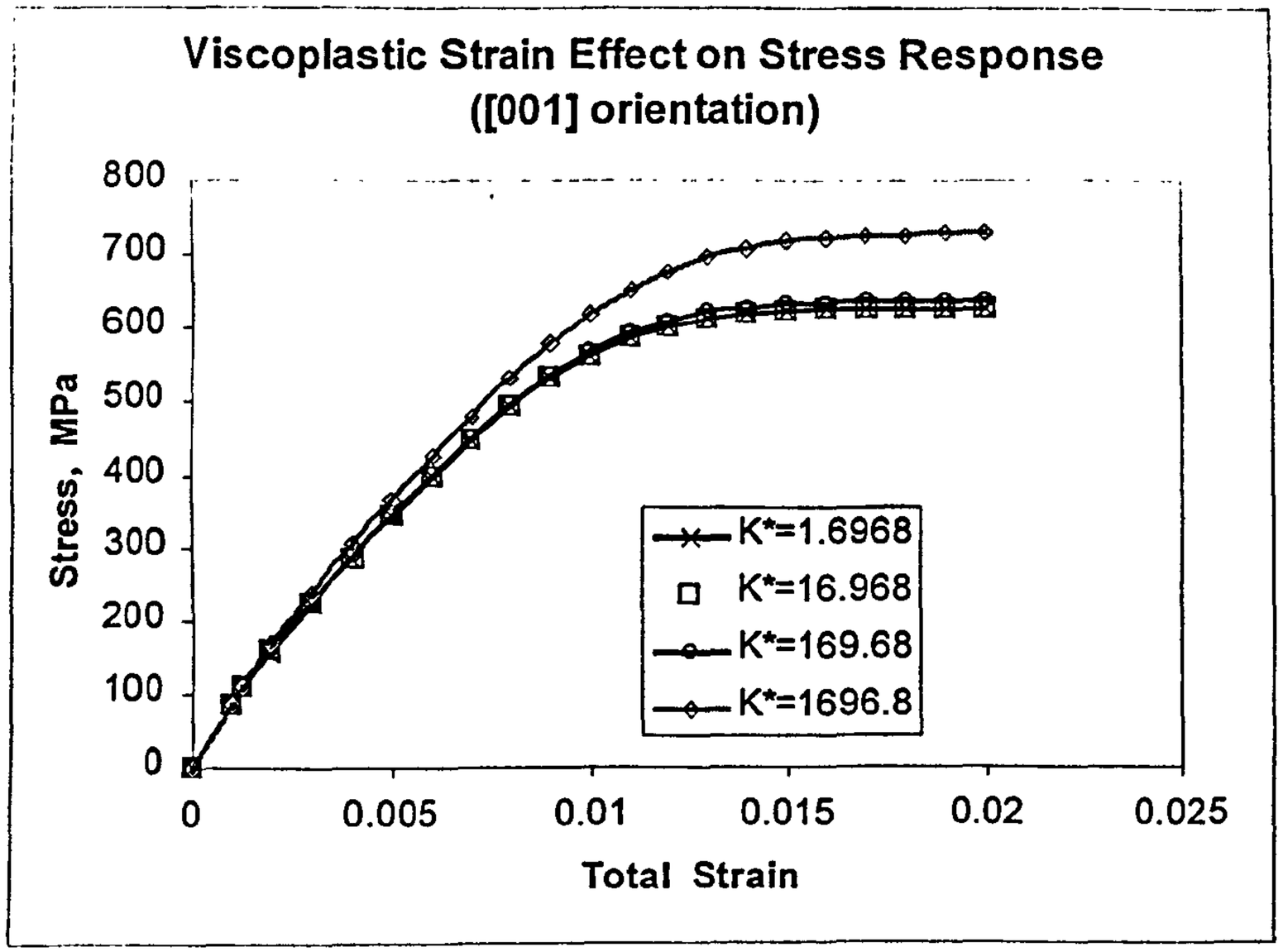

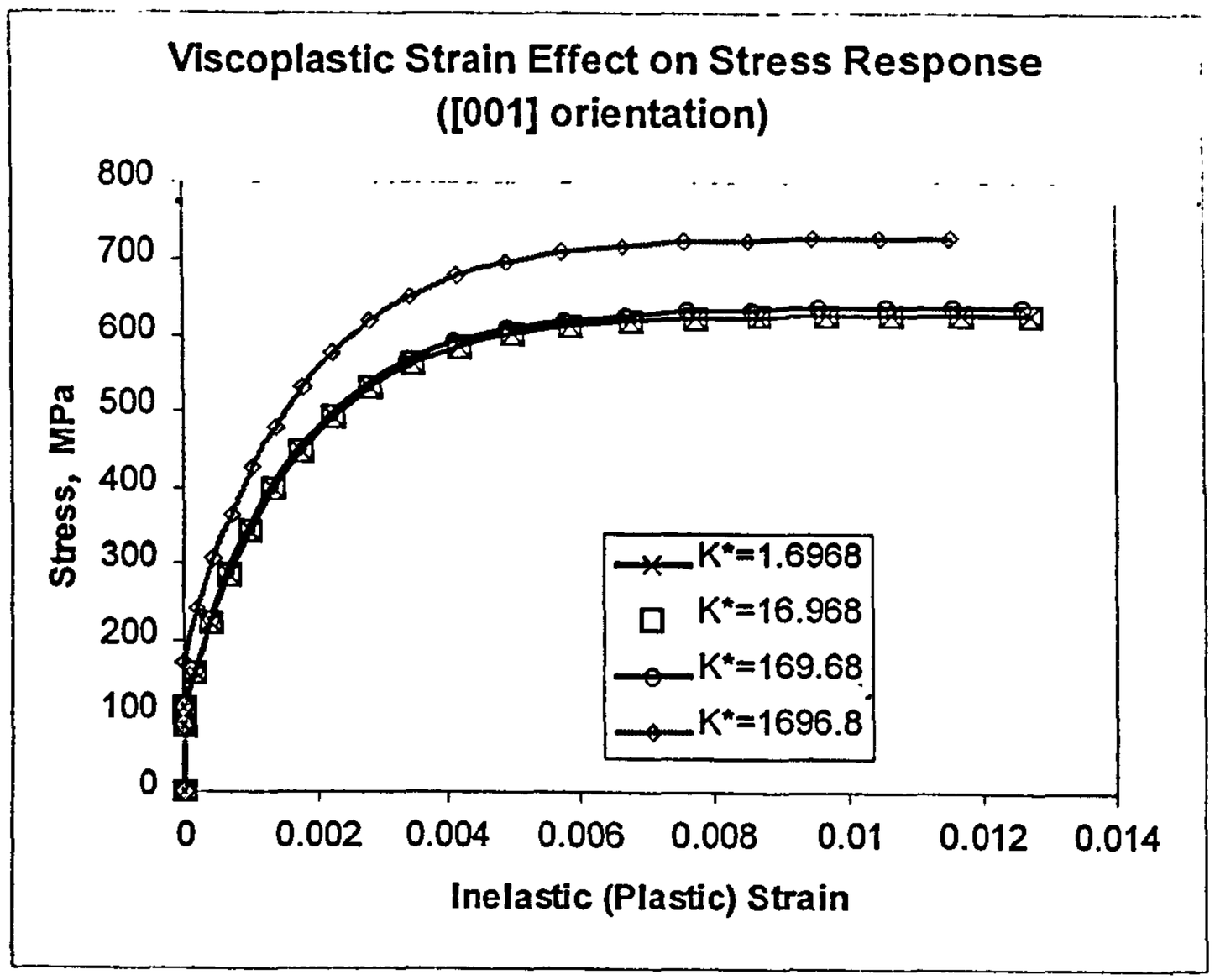

Fig.6.11 Viscoplastic (Time Dependent) Strain Effect on Stress Response of [001] Orientation

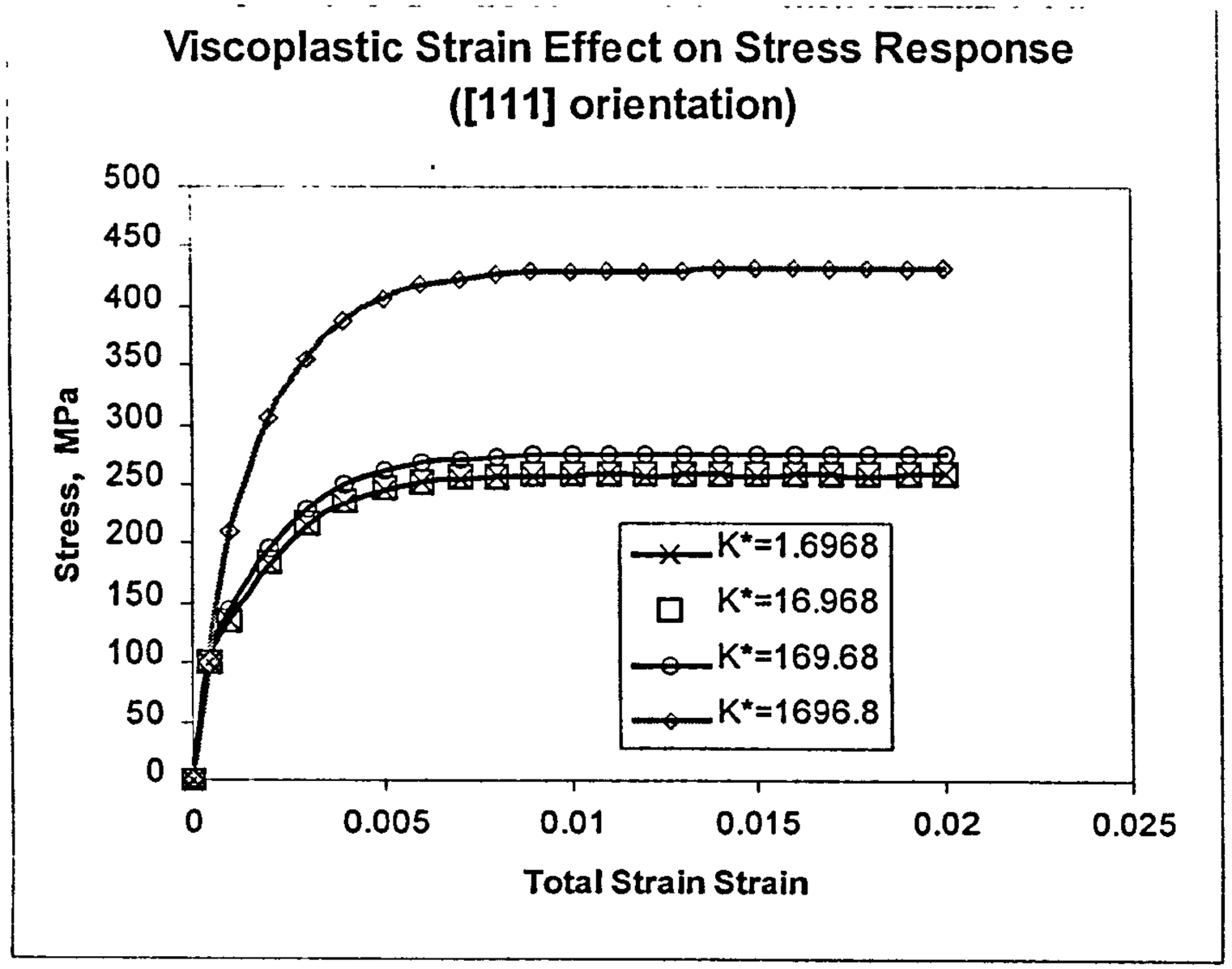

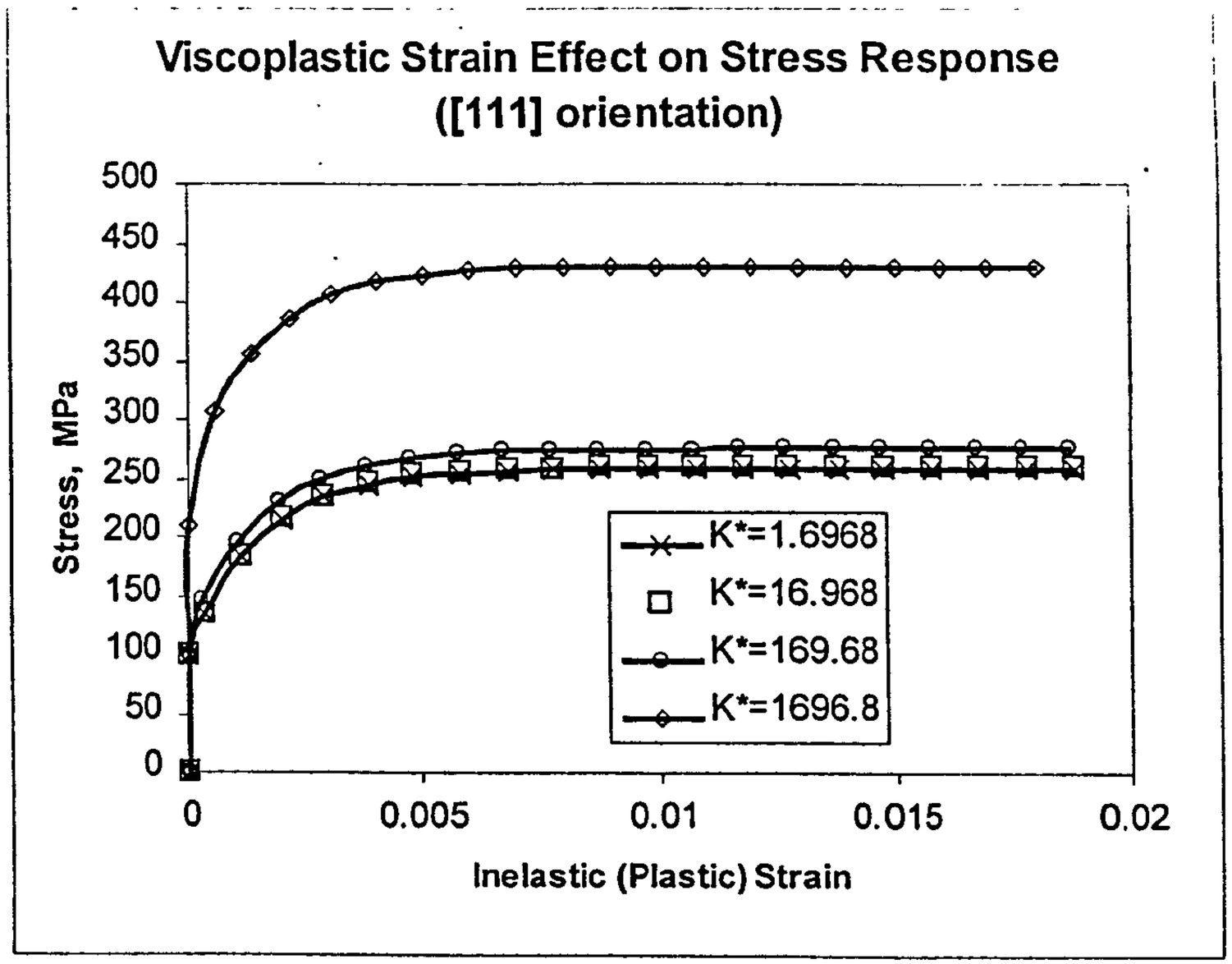

Fig.6.12 Viscoplastic (Time Dependent) Strain Effect on Stress Response of [111] Orientation

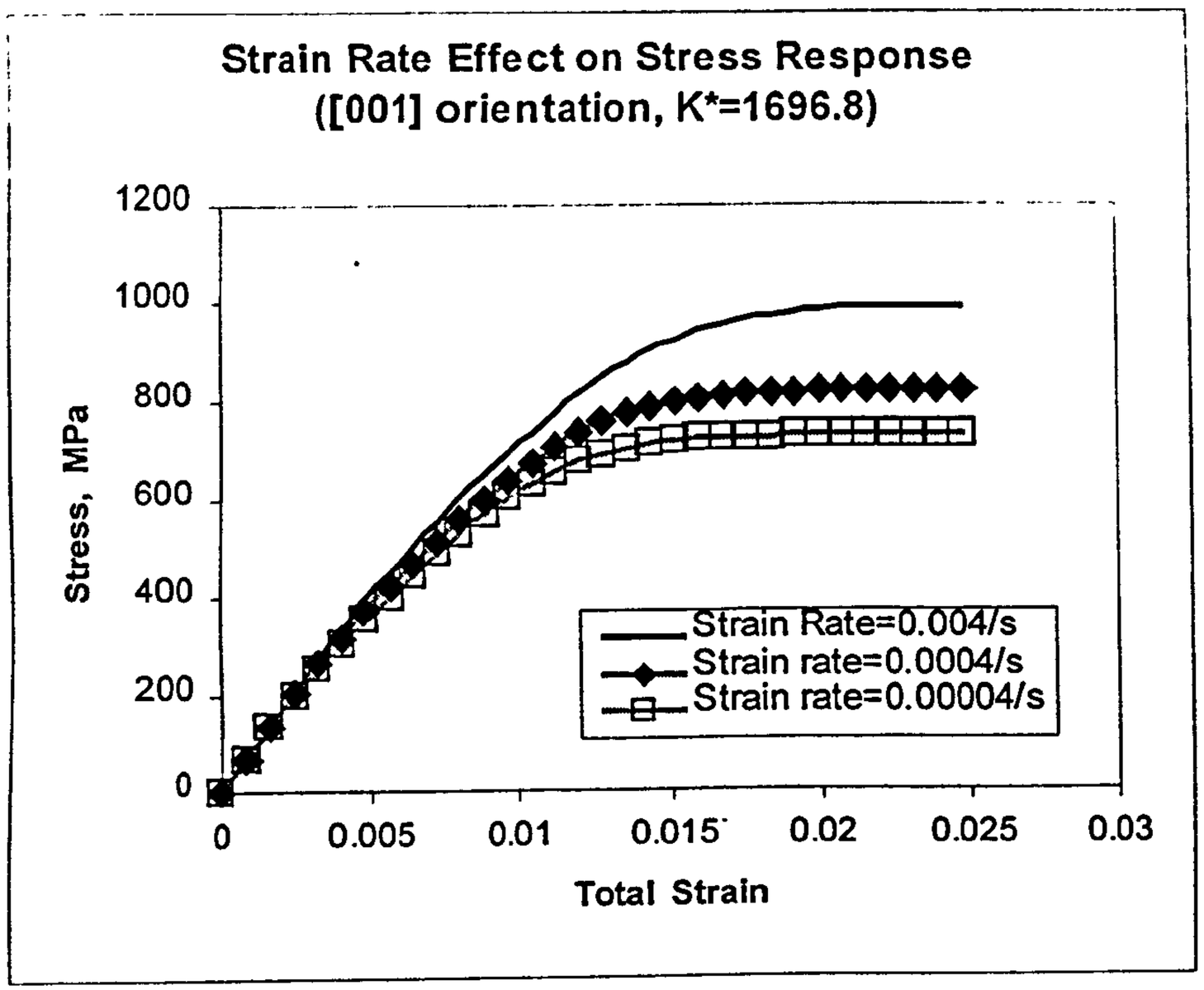

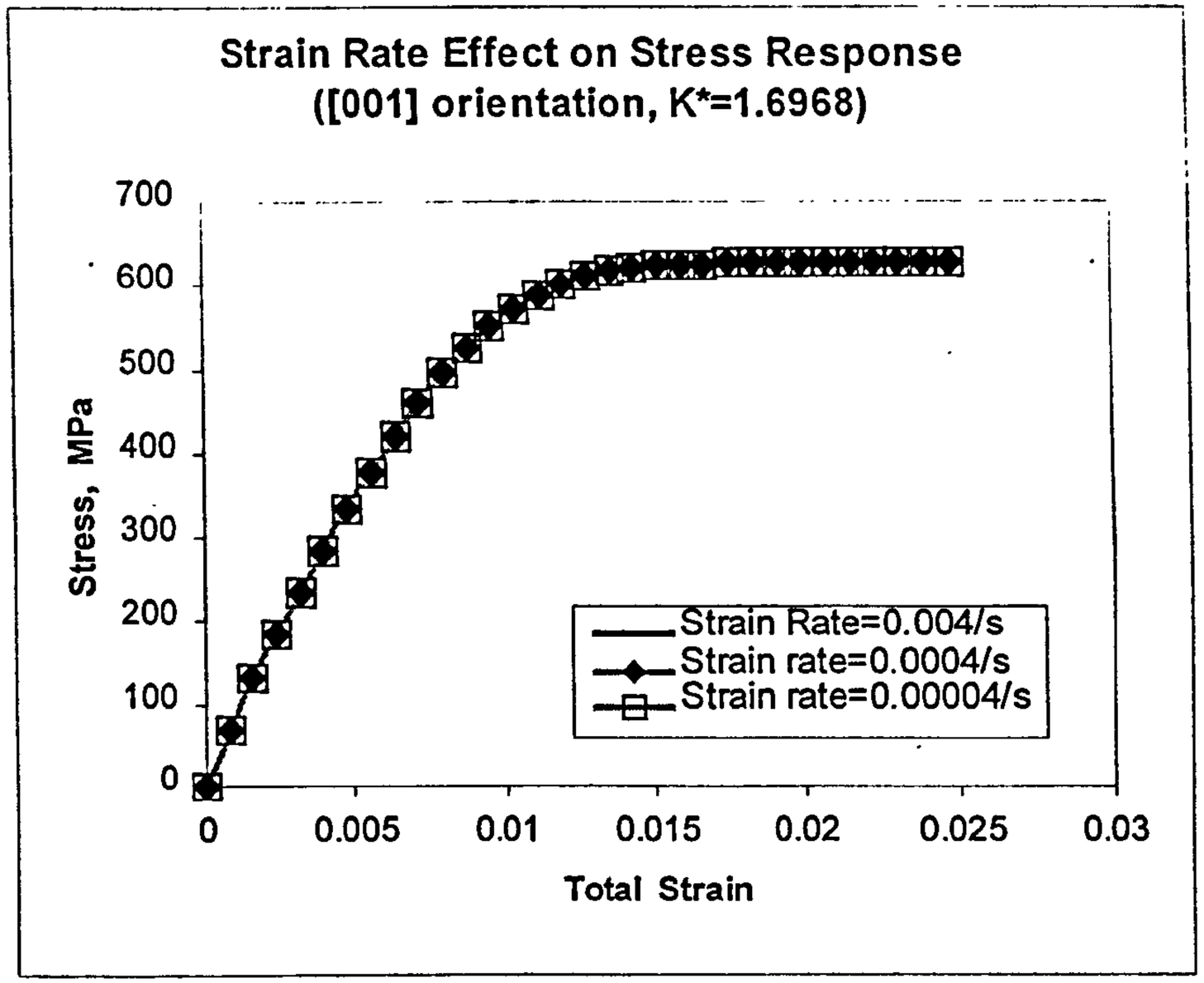

Fig.6.13 Simulation Results of Strain Rate Effect on Stress Responses of [001] Orientation

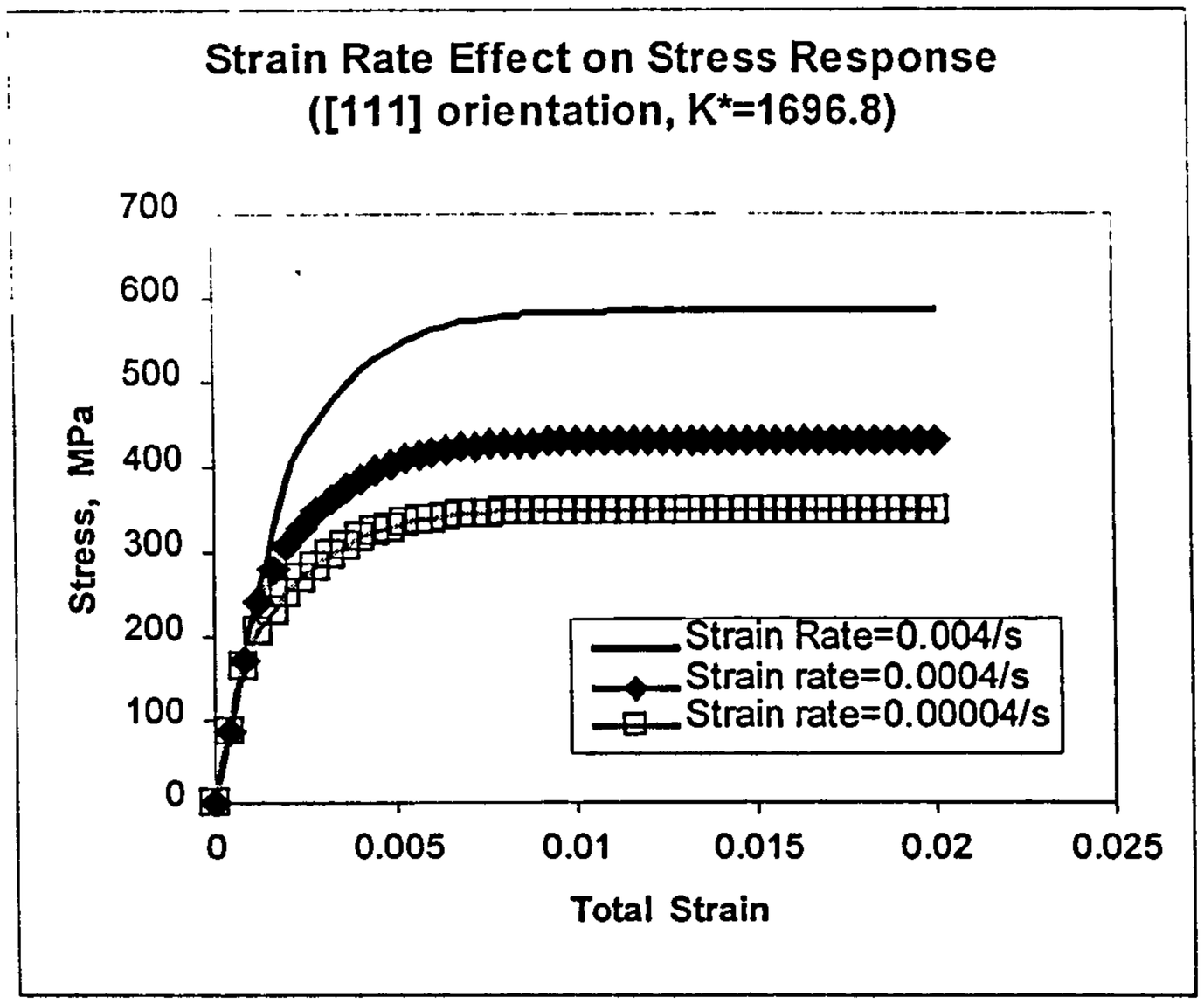

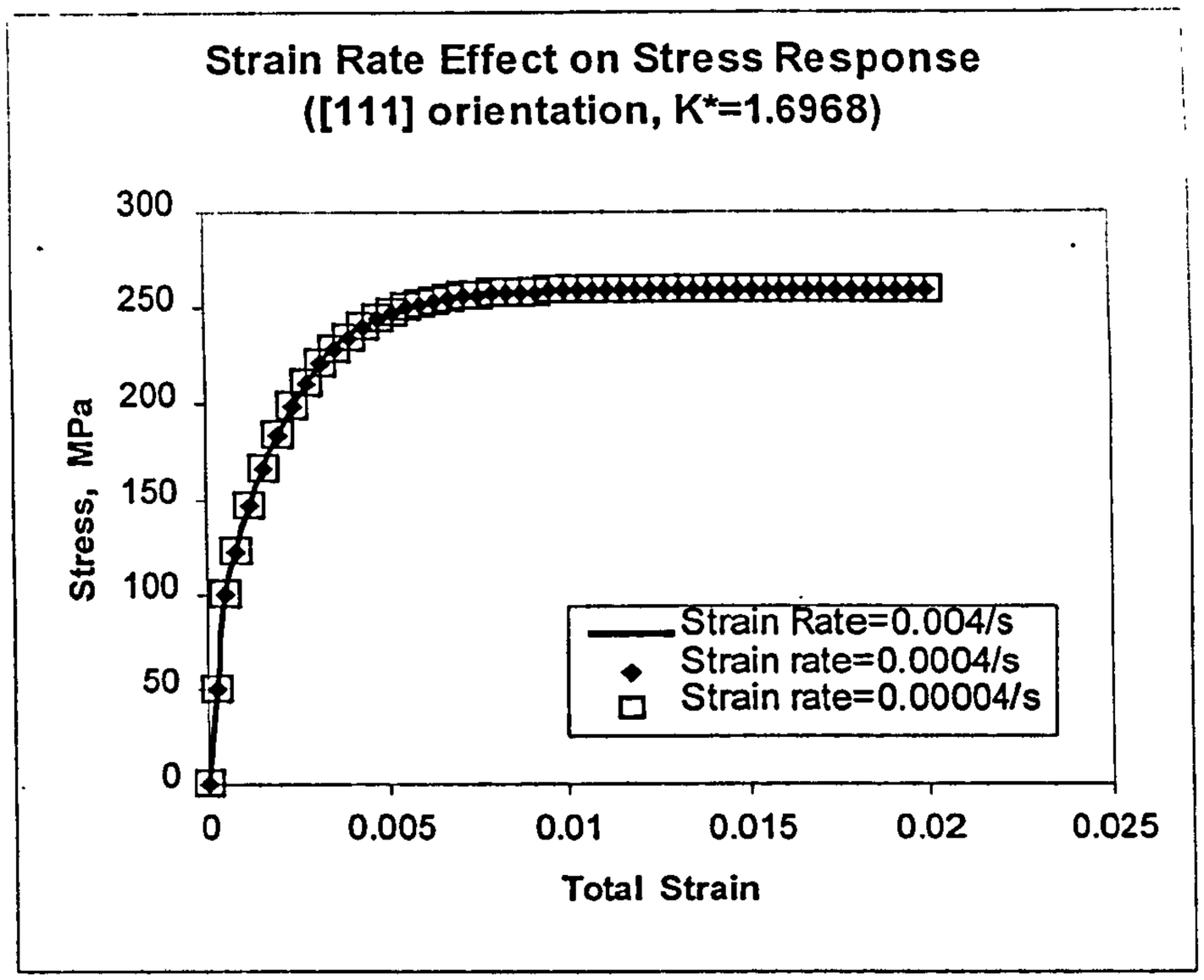

Fig.6.14 Simulation Results of Strain Rate Effect on Stress Responses of [111] Orientation

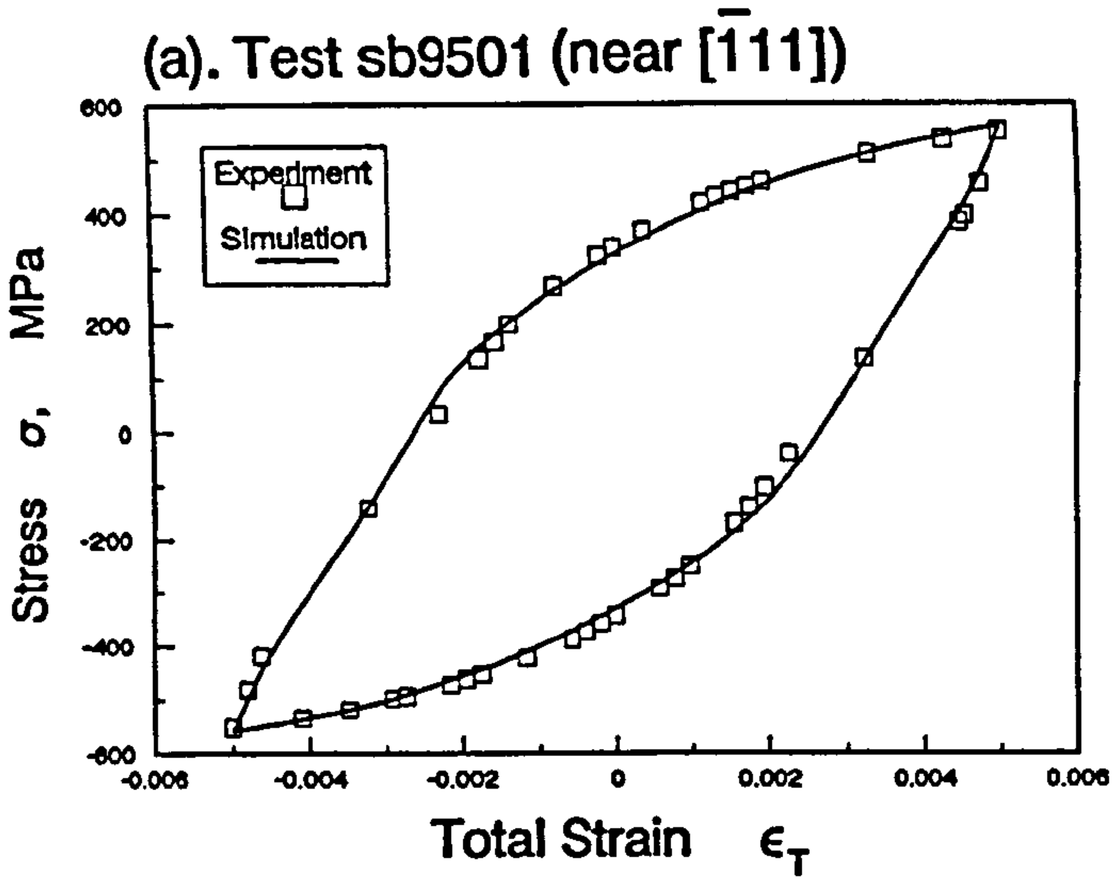

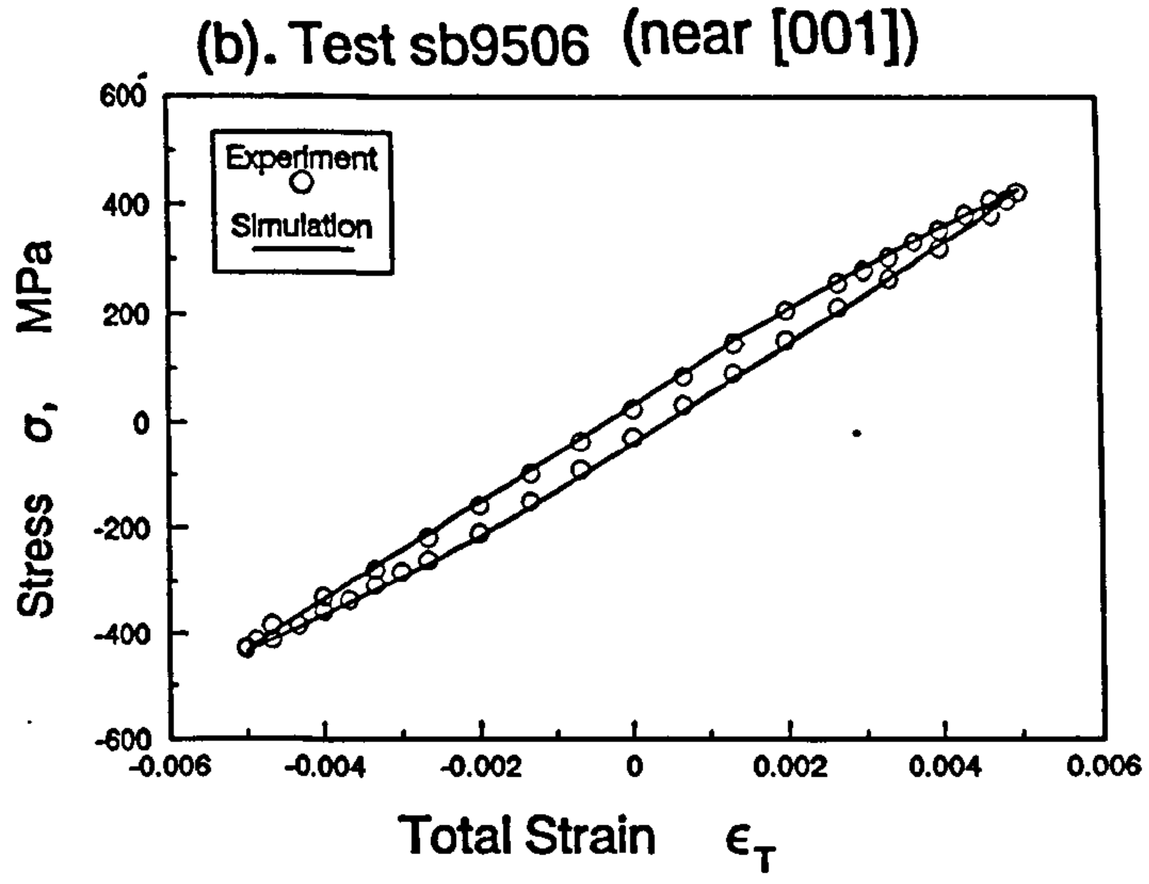

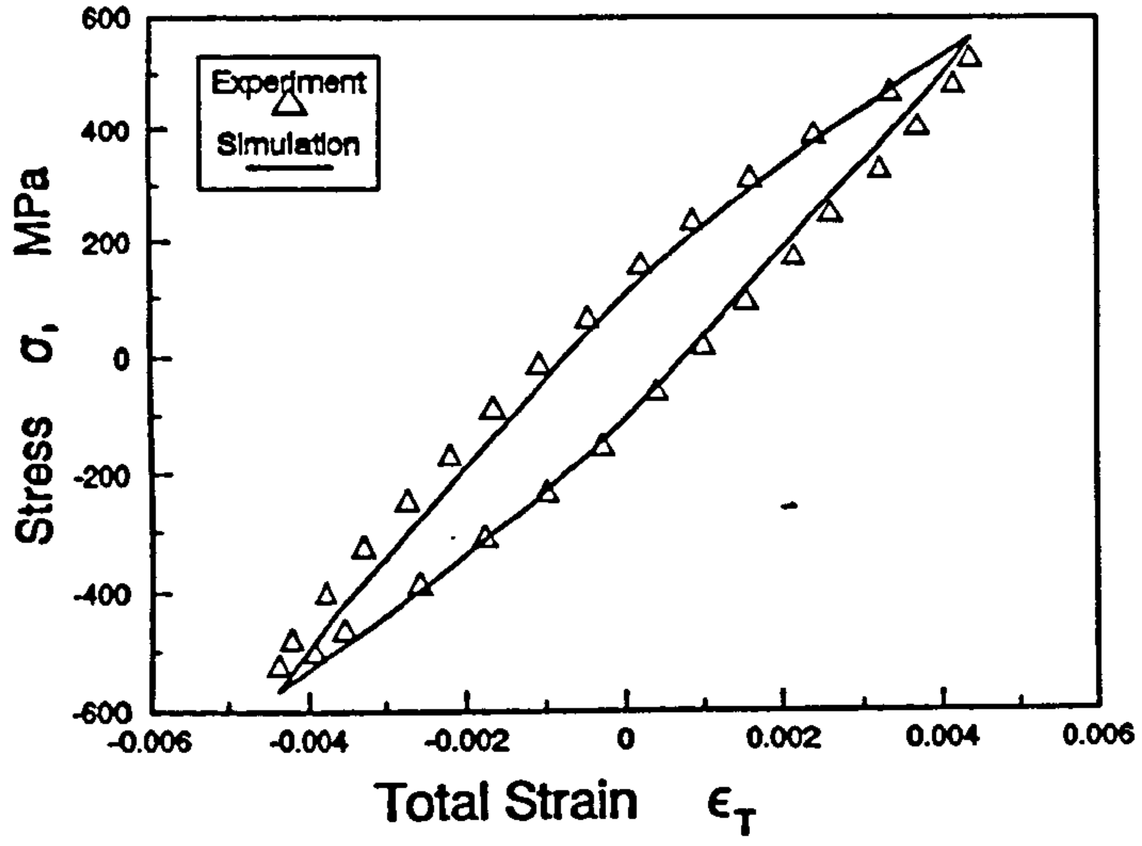

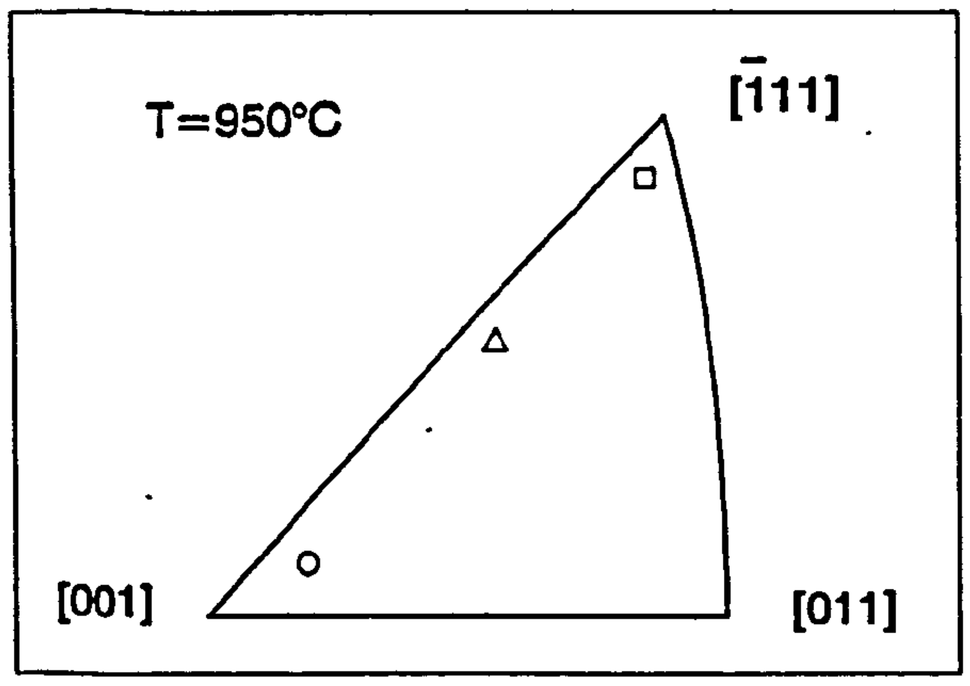

Fig.6.15. Comparison of the cyclic stress-strain responses between simulation and experimental results (continuous cyclic tests)

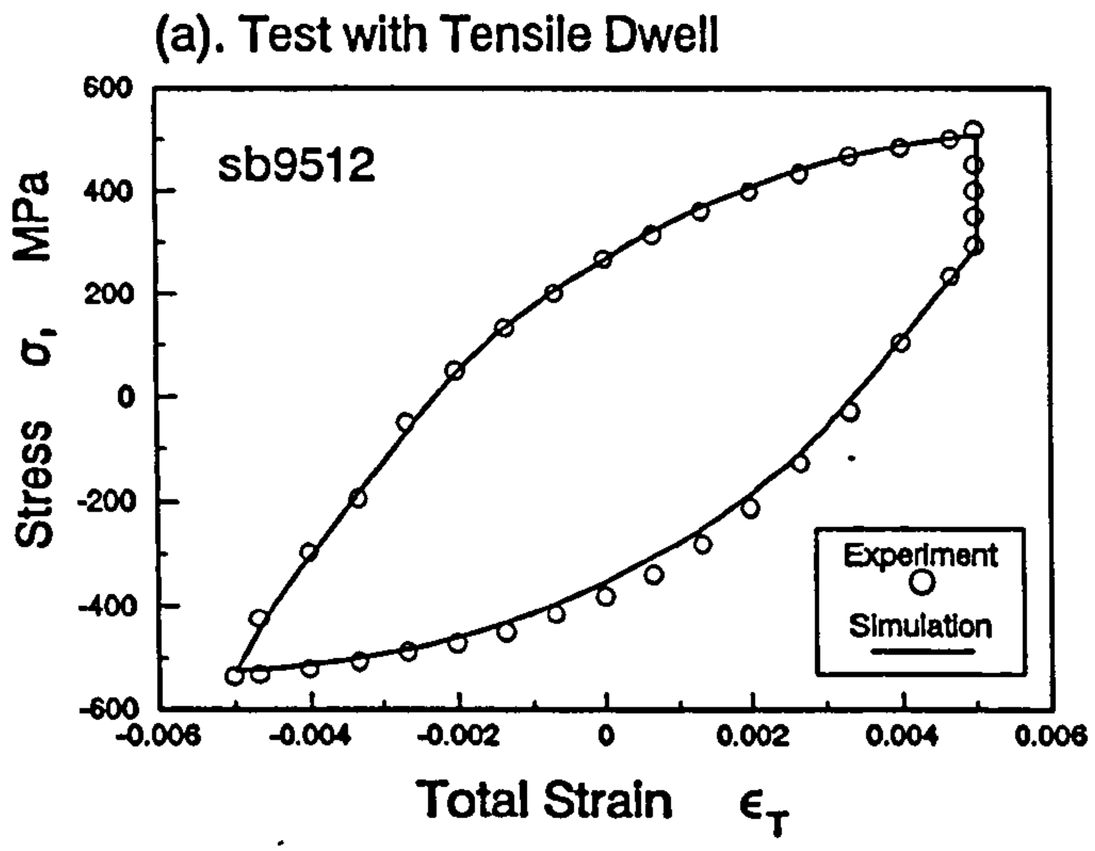

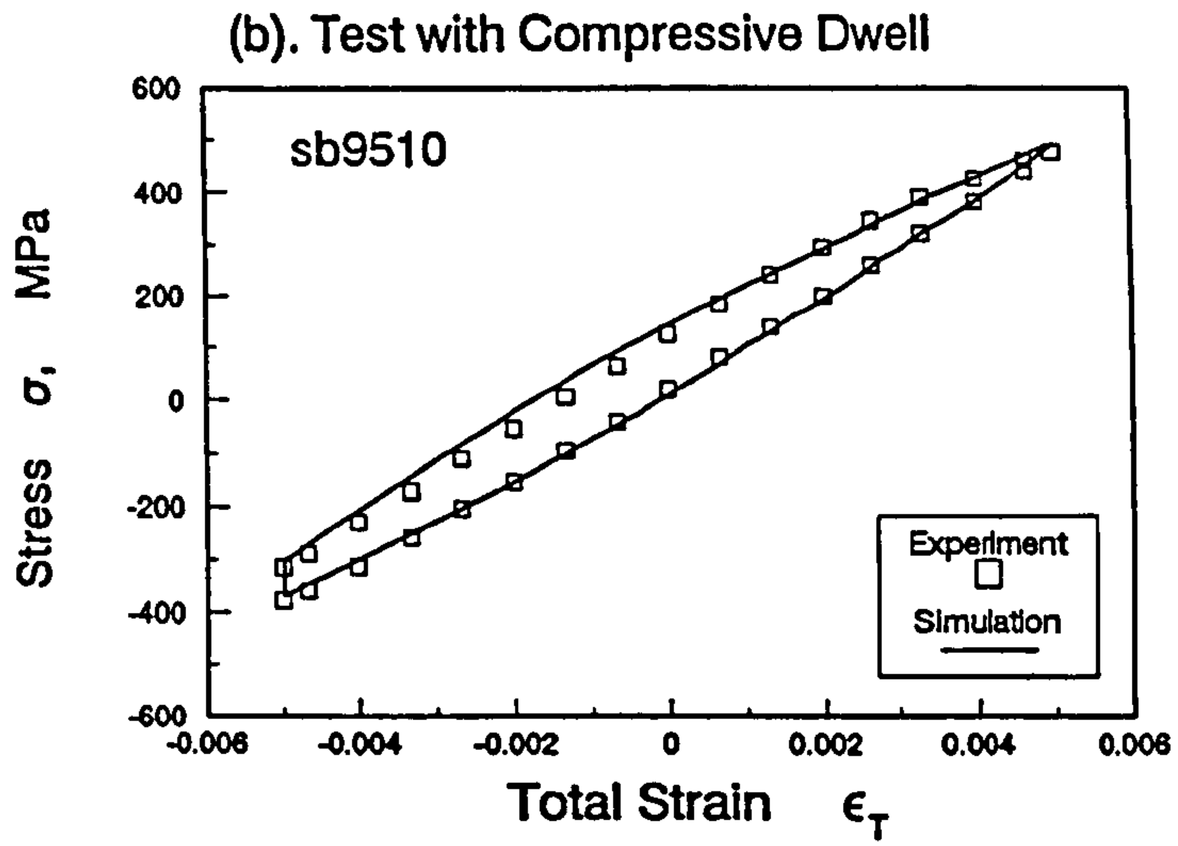

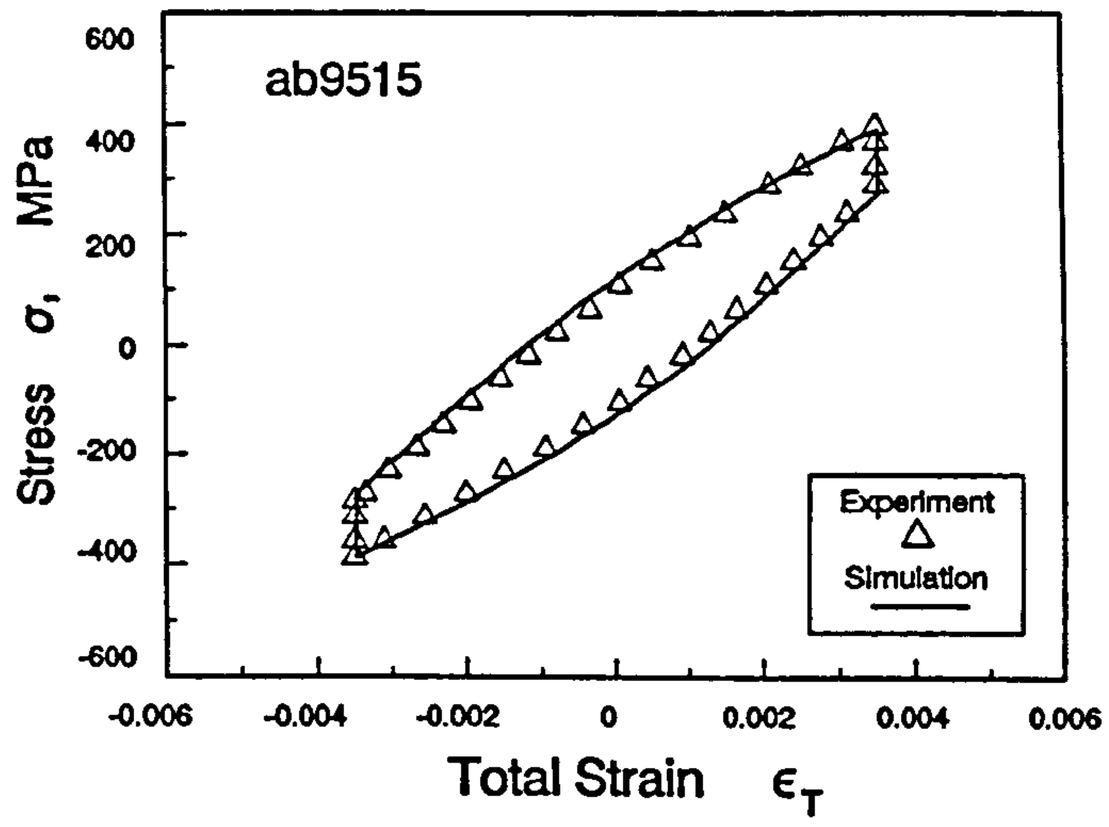

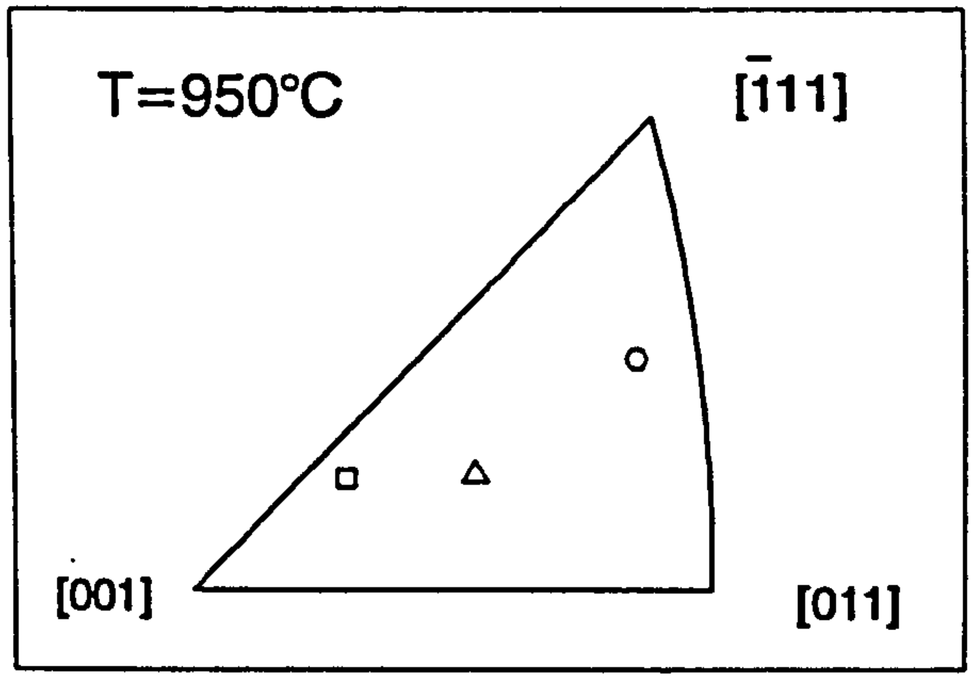

Fig.6.16. Comparison of the cyclic stress-strain responses between simulation and experimental results (cyclic tests with dwells)

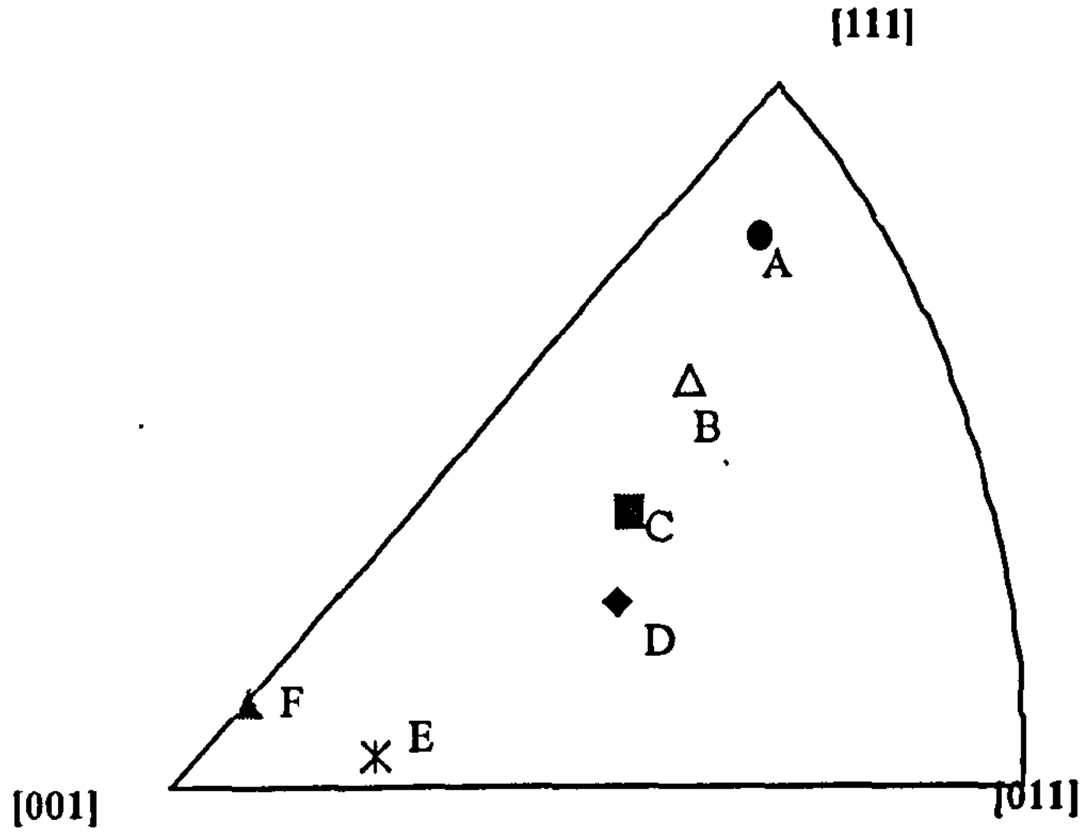

Fig. 6.17 Specimen Orientations Used in Experiments and FE Calculations

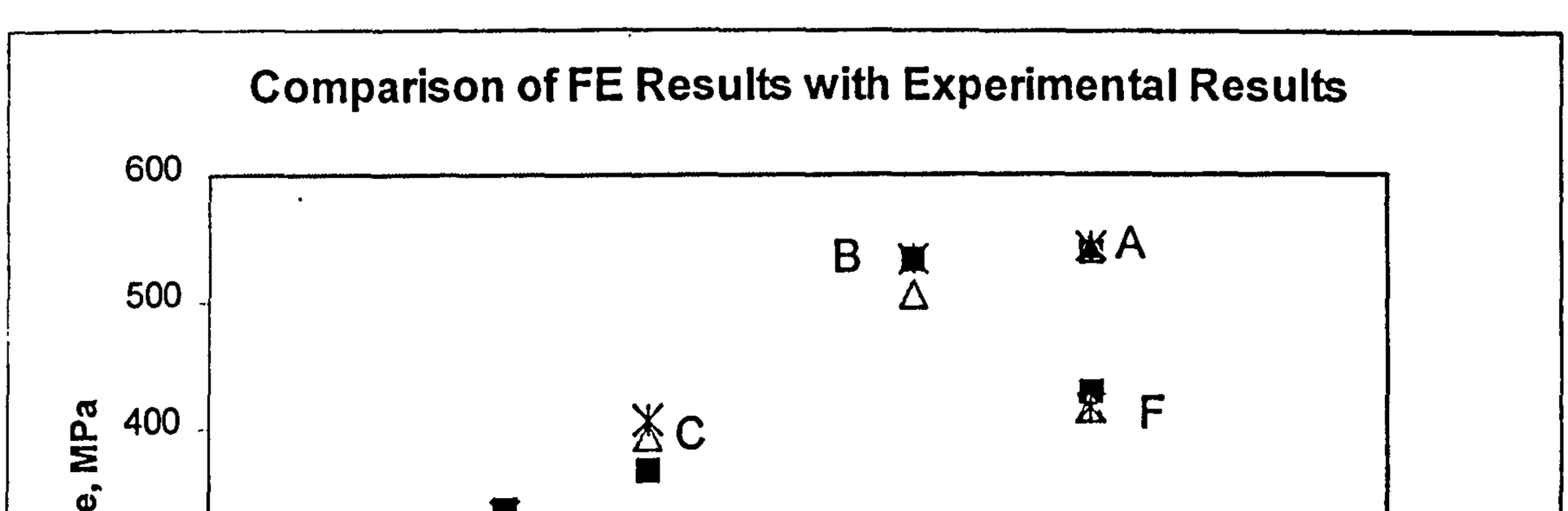

Fig.6.18 Comparison of FE Calculation and Experimental Results

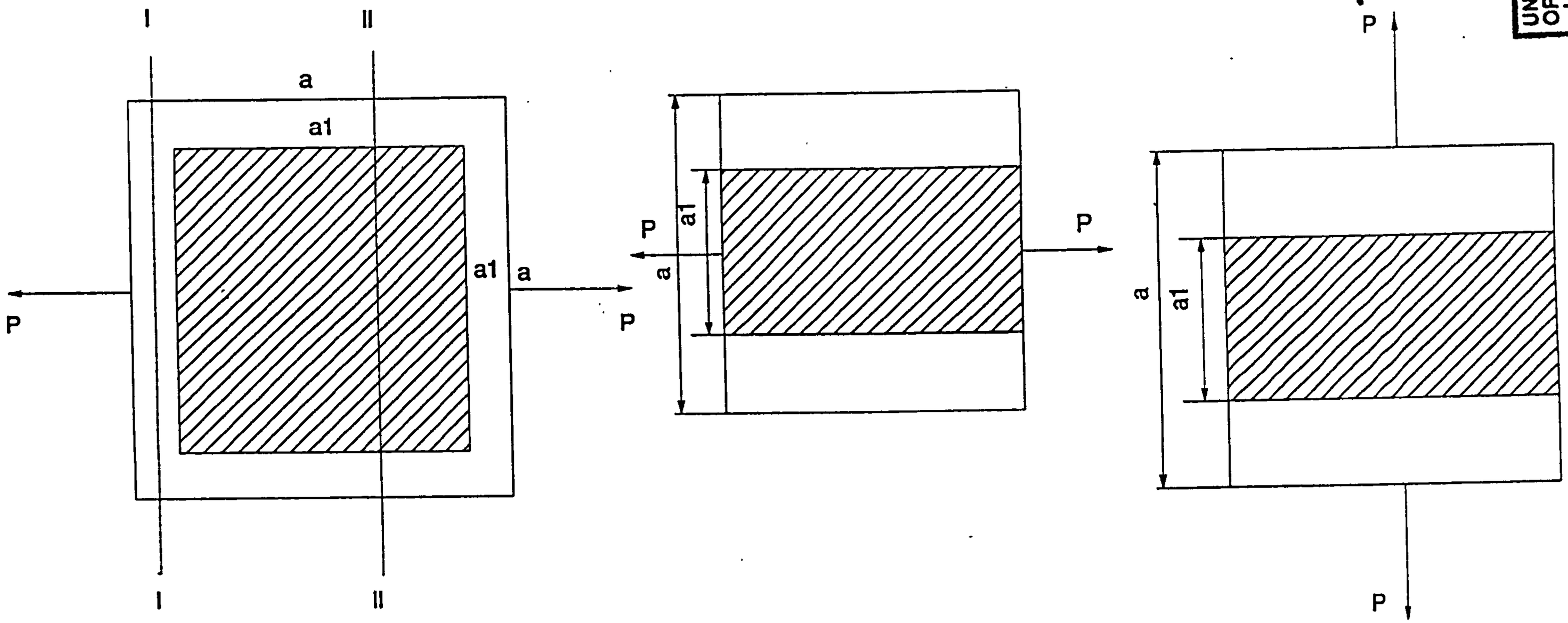

(a) Original Structure (b) Rafting Structure, α Case (c) Rafting Structure, β Case

Fig.A7.1 Schematic of the Original and Rafting Structures